NATIONAL AND KAPODISTRIAN UNIVERSITY OF ATHENS

SCHOOL OF SCIENCES

FACULTY OF GEOLOGY AND GEOENVIRONMENT

DEPARTMENT OF GEOPHYSICS AND GEOTHERMY

Appraisal of the self-organization and evolutionary dynamics of seismicity based on (non-extensive) statistical physics and complexity science methods

PhD THESIS

Angeliki Efstathiou

Geologist, Msc.

ATHENS

December 2018

ΕΘΝΙΚΟ ΚΑΙ ΚΑΠΟΔΙΣΤΡΙΑΚΟ ΠΑΝΕΠΙΣΤΗΜΙΟ ΑΘΗΝΩΝ

ΣΧΟΛΗ ΘΕΤΙΚΩΝ ΕΠΙΣΤΗΜΩΝ

ΤΜΗΜΑ ΓΕΩΛΟΓΙΑΣ ΚΑΙ ΓΕΩΠΕΡΙΒΑΛΛΟΝΤΟΣ

ΤΟΜΕΑΣ ΓΕΩΦΥΣΙΚΗΣ ΚΑΙ ΓΕΩΘΕΡΜΙΑΣ

Μελέτη της αυτο-οργάνωσης και εξέλιξης της σεισμικότητας με χρήση μεθόδων στατιστικής φυσικής και επιστήμης πολυπλοκότητας

ΔΙΔΑΚΤΟΡΙΚΗ ΔΙΑΤΡΙΒΗ

Αγγελική Ευσταθίου

Γεωλόγος, Msc.

ΑΘΗΝΑ

Δεκέμβριος 2018

PhD THESIS

Appraisal of the self-organization and evolutionary dynamics of seismicity based on (non-extensive) statistical physics and complexity science methods

Angeliki Efstathiou

SUPERVISOR: Andreas Tzanis, Associate Professor of Geophysics & Geothermy, UoA

THREE-MEMBER ADVISORY COMMITTEE:

Andreas Tzanis, Associate Professor of Geophysics and Geothermy, UoA

Nikolaos Voulgaris, Professor of Geophysics and Geothermy, UoA

Filippos Vallianatos, Professor of Geophysics and Seismology, TEI of Crete

SEVEN-MEMBER EXAMINATION COMMITTEE

Andreas Tzanis,
Associate Professor UoA

Nikolaos Voulgaris,
Professor UoA

Filippos Vallianatos,
Professor TEI of Crete

Eleutheria Papadimitriou,
Professor AUTh

Panagiotis Papadimitriou,
Professor UoA

Georgios Drakatos,
Research Director GEIN NOA

Gerasimos Papadopoulos,
Research Director GEIN NOA

Examination Date 14/12/2018

ΔΙΔΑΚΤΟΡΙΚΗ ΔΙΑΤΡΙΒΗ

Μελέτη της αυτο-οργάνωσης και εξέλιξης της σεισμικότητας με χρήση μεθόδων στατιστικής φυσικής και επιστήμης πολυπλοκότητας

Αγγελική Ευσταθίου

ΕΠΙΒΛΕΠΩΝ ΚΑΘΗΓΗΤΗΣ: Ανδρέας Τζάνης, Αναπληρωτής Καθηγητής ΕΚΠΑ

ΤΡΙΜΕΛΗΣ ΕΠΙΤΡΟΠΗ ΠΑΡΑΚΟΛΟΥΘΗΣΗΣ:

Ανδρέας Τζάνης, Αναπληρωτής Καθηγητής ΕΚΠΑ

Νικόλαος Βούλγαρης, Καθηγητής ΕΚΠΑ

Φίλιππος Βαλλιανάτος, Καθηγητής, ΤΕΙ Κρήτης

ΕΠΤΑΜΕΛΗΣ ΕΞΕΤΑΣΤΙΚΗ ΕΠΙΤΡΟΠΗ

Ανδρέας Τζάνης,
Αναπληρωτής Καθηγητής ΕΚΠΑ

Νικόλαος Βούλγαρης,
Καθηγητής ΕΚΠΑ

Φίλιππος Βαλλιανάτος,
Καθηγητής ΤΕΙ Κρήτης

Ελευθερία Παπαδημητρίου,
Καθηγήτρια ΑΠΘ

Παναγιώτης Παπαδημητρίου,
Καθηγητής ΕΚΠΑ

Γεώργιος Δρακάτος,
Διευθυντής Ερευνών Γ.Ι. ΕΑΑ

Γεράσιμος Παπαδόπουλος,
Διευθυντής Ερευνών Γ.Ι. ΕΑΑ

Ημερομηνία εξέτασης 14/12/2018

ABSTRACT

A fundamental challenge in many scientific fields is to define norms and laws of higher-order in relation to the existing knowledge about phenomena of lower-order. It has been long suggested that the active tectonic grain comprises a self-organized complex system, therefore its expression (seismicity) should be manifested in the temporal and spatial statistics of energy release rates, and exhibit memory due to long-range interactions in a fractal-like space-time. Such attributes can be properly understood in terms of Non-Extensive Statistical Physics (NESP) In addition to energy release rates expressed by the magnitude M, measures of the temporal and spatial interactions are the time (Δt) and hypocentral distance (Δd) between consecutive events. Recent work indicated that if the distributions of M, Δt and Δd are independent so that the joint probability $p(M, \Delta t, \Delta d)$ factorizes into the probabilities of M, Δt and Δd, i.e. $p(M U \Delta t U \Delta d) = p(M)\, p(\Delta t)\, p(\Delta d)$, then the frequency of earthquake occurrence is multiply related, not only to magnitude as the celebrated Gutenberg – Richter law predicts, but also to interevent time and distance by means of well-defined power-laws consistent with NESP. The present work applies these concepts to investigate the dynamics of seismogenetic systems along the NE – N boundary of the Pacific and North American plates and the seismogenic zones of Greece – Western Turkey. The analysis is conducted to full and declustered (reduced) catalogues where the aftreshocks are removed by the stochasting declustering method of Zhuang et al., 2002.The statistical behaviour of seismicity suggests that crustal seismogenetic systems along the Pacific–North American plate boundaries in California, the seismogenic zones of Greece – Western Turkey, Alaska and the Aleutian Arc are invariably sub-extensive; they exhibit prominent operative long-range interaction and long-term memory, therefore they are self-organized and possibly critical. The degree of sub-extensivity is neither uniform, nor stationary but varies dynamically between systems and may also vary with time, or in cycles. The only sub-crustal system studied herein (Aleutian Subduction) appears to be Poissonian. The results are consistent with simulations of small-world fault networks in which free boundary conditions at the edges, (i.e. at the surface) allow for self-organization and criticality to develop, and fixed boundary conditions within, (i.e. at depth), do not. The results indicate that NESP is an excellent natural descriptor of earthquake statistics and appears to apply to the seismicity observed in different seismogenetic environments. The NESP formalism, although far from having answered questions and debates on the statistical physics of earthquakes, appears to be an effective and insightful tool in the investigation of seismicity and its associated complexity.

SUBJECT AREA: Non – Extensive Statistical Physics,

KEYWORDS: Tsallis entropy, complexity, non-extensivity, statistical seismology

ΠΕΡΙΛΗΨΗ

Θεμελιώδης πρόκληση σε πολλά επιστημονικά πεδία αποτελεί ο καθορισμός κανονικοτήτων και νόμων ανωτέρας κλίμακας σε σχέση με την υπάρχουσα γνώση για φαινόμενα κατωτέρας κλίμακας. Είναι πλέον αποδεκτό ότι ο ενεργός τεκτονικός ιστός αποτελεί ένα κρίσιμο πολύπλοκο σύστημα, αν και δεν έχει ακόμη οριστικοποιηθεί αν είναι στατικό, δυναμικό/εξελικτικό, ή ένας χρονικά εξαρτημένος συνδυασμός αμφοτέρων. Σε κάθε περίπτωση, τα κρίσιμα συστήματα χαρακτηρίζονται από μορφοκλασματική ή πολυ-μορφοκλασματική κατανομή των στοιχείων τους, ισχυρές αλληλεπιδράσεις μεταξύ των κοντινών και μακρινών γειτόνων και διακοπτόμενη (ασυνεχή) έκφρασή τους. Οι ιδιότητες αυτές μπορούν να μελετηθούν με όρους Μη Εκτατικής Στατιστικής Φυσικής (ΜΕΣΦ). Πέραν του ρυθμού έκλυσης ενέργειας που εκφράζεται μέσω του μεγέθους (M), μέτρο των πιθανών συσχετίσεων αποτελεί ο παρέλθων χρόνος (Δt) και η υποκεντρική απόσταση (Δd) μεταξύ αλλεπάλληλων σεισμών πάνω από ένα κατώφλι μεγέθους σε μια περιοχή. Πρόσφατες έρευνες έδειξαν ότι, εάν οι κατανομές μεγέθους (M), χρονικής (Δt) και χωρικής (Δd) εξάρτησης μεταξύ διαδοχικών σεισμών θεωρηθούν ανεξάρτητες έτσι ώστε η από κοινού πιθανότητα $p(M, \Delta t, \Delta d)$ να παραγοντοποιείται σε $p(M U \Delta t U \Delta d) = p(M)\, p(\Delta t)\, p(\Delta d)$, τότε η συχνότητα εμφάνισης ενός σεισμού εξαρτάται πολλαπλώς όχι μόνο από το μέγεθος όπως πρόβλεπει ο νόμος Gutenberg – Richter αλλά και από τη χρονική και χωρική εξάρτηση διαδοχικών σεισμών. Αυτό, με τη σειρά του, σημαίνει ότι η αυτο-οργάνωση της σεισμικότητας θα πρέπει να εκδηλώνεται μέσω μιας συγκεκριμένης στατιστικής συμπεριφοράς της χρονικής και χωρικής εξάρτησης της (κατανομές νόμων δύναμης). Στην παρούσα διατριβή θα επιχειρηθεί η περιγραφή της σεισμικότητας με όρους ΜΕΣΦ, σε σεισμογενετικά συστήματα κατά μήκος του ορίου πλακών του ΒΑ-Β Ειρηνικού και της Βορείου Αμερικής, καθώς και στο σεισμογενετικό σύστημα του ελλαδικού χώρου-Δυτικής Τουρκίας. Η ανάλυση πραγματοποιείται σε πλήρης και ομαδοποιημένους καταλόγους σεισμών, όπου οι μετασεισμοί έχουν αφαιρεθεί με τη στοχαστική μέθοδο απομαδοποίησης του Zhuang et al., (2002). Η στατιστική συμπεριφορά της σεισμικότητας υποδεικνύει ότι η επιφανειακή σεισμικότητα των συστημάτων που μελετώνται είναι υποεκτατική, χαρακτηρίζεται από μακράς εμβέλειας συσχετίσεις και για το λόγο αυτό είναι αυτο-οργανωμένη και πιθανόν κρίσιμη. Ο βαθμός της υπο-εκτακτικότητας δεν είναι ομοιόμορφος, ούτε σταθερός, αλλά διαφέρει δυναμικά από σύστημα σε σύστημα, ενίοτε διαφέρει στη χρονική εξέλιξη και μπορεί να παρουσιάζει κυκλικότητα. Το μόνο σύστημα βαθειάς δομής (σεισμικότητα σε μεγάλα εστιακά βάθη) που εξετάζεται εδώ - η Αλεούτια ζώνη υποβύθισης- φαίνεται να παρουσιάζει στατιστική που περιγράφεται με όρους κατανομής Poisson (απουσία συσχέτισης). Τα αποτελέσματα που προκύπτουν υποδεικνύουν ότι η ΜΕΣΦ αποτελεί ένα εξαιρετικό εργαλείο για την φυσική περιγραφή της σεισμικότητας σε διάφορα σεισμογενετικά περιβάλλοντα. Ο μη εκτατικός φορμαλισμός θεωρείται το κατάλληλο μεθοδολογικό εργαλείο για να περιγράψει φυσικά συστήματα που δε βρίσκονται σε ισορροπία και έχουν μεγάλη μεταβλητότητα και πολυκλασματική δομή όπως η σεισμικότητα.

ΘΕΜΑΤΙΚΗ ΠΕΡΙΟΧΗ: Μη Εκτατική Στατιστική Φυσική

ΛΕΞΕΙΣ ΚΛΕΙΔΙΑ: Εντροπία Τσάλλη, μη-εκτατικότητα, στατιστική σεισμολογία.

To my life-coach, my mother Eugenia: because I owe it all to you…

“Learning is never cumulative, it is a movement of knowing which has no beginning and no end.”

Bruce Lee (1940 – 1973)

This work was partly supported by the THALES Program of the Ministry of Education of Greece and the European Union in the framework of the project "Integrated understanding of Seismicity, using innovative methodologies of Fracture Mechanics along with Earthquake and Non-Extensive Statistical Physics – Application to the geodynamic system of the Hellenic Arc - SEISMO FEAR HELLARC"

ACKNOWLEDGEMENTS

Firstly, I would like to express my sincere gratitude to my advisor **Prof. Andreas Tzanis** for the continuous support of my Ph.D study and related research, for his patience, motivation, and immense knowledge. His guidance helped me in all the time of research and writing of this thesis. I could not have imagined having a better advisor and mentor for my Ph. D study.

Besides my advisor, I would like to thank the rest of my avdvisory committee: **Prof. Fillipos Vallianatos**, for giving me the opportunity to be a part of the THALES – SEISMO FEAR HELLARC Research programme which provided the funding for the most part of the present work. I also thank him for his encouragement but also for the hard questions which incented me to widen my research from various perspectives. I would also like to thank **Prof. Nikolaos Voulgaris** for his insightful comments on this study.

A very special gratitude goes to my colleagues from UoA, **Mr. Stelios Chailas** and **Dr. Kostas Dimitropoulos** for their support and the stimulating discussions. I would like to give special thanks to **Dr. Margarita Segou** for our insightful discussions particularly with respect to declustering.

I am grateful for my eternal cheerleaders – my parents **Kostas** and **Eugenia** who have provided me through moral and emotional support in my life, my forever interested and always enthusiastic grandparents **Ludmila** and **Anatoliy** who are always keen to know what I was doing and how I was proceeding. I am grateful to my sibling **Fotis**, although we are far away from each other, he is always there for me. I am also grateful to my other family members and friends who have supported me along the way.

And finally, last but by no means least, I owe thanks to a very special person, my husband, **Ioannis** for his continued and unfailing love, support and understanding during my pursuit of Ph. D degree that made the completion of thesis possible. You were always around at times I thought that it is impossible to continue, you helped me to keep things in perspective. I greatly value his contribution and deeply appreciate his belief in me.

Thank you all for your encouragement!

Angeliki Efstathiou

PUBLICATIONS

Most of the results obtained in this thesis have been published in a series of conferences announcements and research papers in International Journals:

Book chapter contribution:

Tzanis, A., **Efstathiou, A**. and Vallianatos, F., 2018. Are seismogenetic systems random or organized? A treatise of their statistical nature based on the seismicity of the north-northeast Pacific Rim. In Chelidze, T., Vallianatos, F. and Telesca, L. (eds), Complexity of Seismic Time Series, Elsevier, eBook ISBN: 9780128131398, Paperback ISBN: 978012813138

Peer Reviewed Papers in International Scientific Journals

1. **Efstathiou A**. and Tzanis A, 2018. An examination of the nature and dynamics of seismogenesis in South California, USA, based on Non-Extensive Statistical Physics. Physics of the Earth and Planetary Interiors, In Press, Available online 1 September 2018. https://doi.org/10.1016/j.pepi.2018.08.013
2. **Efstathiou A**., Tzanis A, Vallianatos F, 2017. On the nature and dynamics of the seismogenetic systems of North California, USA: An analysis based on Non-Extensive Statistical Physics. Physics of the Earth and Planetary Interiors 270 (2017) 46–72, http://dx.doi.org/10.1016/j.pepi.2017.06.010
3. **Efstathiou A**., Tzanis A., Vallianatos F., 2015. Evidence of Non-Extensivity in the evolution of seismicity along the San Andreas Fault, California, USA: An approach based on Tsallis Statistical Physics. Physics and Chemistry of the Earth Parts A/B/C; doi:10.1016/j.pce.2015.02.013

Workshop Attendance

Workshop Earthquakes: Nucleation, triggering, and relationship with aseismic processes. Cargese, Corsica, 3-10 November 2014, supported by CNRS, LABEX OSUG@2020, NSF, EGU, Université de Savoie. Presentation at special session: **Efstathiou A**., 2014. Variation of entropic indices and fractal dimension before large earthquakes along the San Andreas Fault system, California.

Oral Presentations in International Conferences

1. **Efstathiou A**., Tzanis A, Vallianatos F., 2016. On the nature and dynamics of the seismogenetic system of South California, USA: an analysis based on Non-Extensive Statistical Physics. Bulletin of the Geological Society of Greece, vol. L, 2016. Proceedings of the 14th International Congress, Thessaloniki, May. 2016
2. **Efstathiou A**., Tzanis A., Vallianatos F., 2014. An analysis of Greek seismicity based on Non-Extensive Statistical Physics: The interdependence of magnitude, interevent time and interevent distance. EGU General Assembly, 2014 (Vienna – Austria, 27 April-02 May 2014).
3. Tzanis A., Vallianatos F., **Efstathiou A**., 2013. On the Universality of Generalized multidimensional earthquake frequency distributions consistent with Non-Extensive Statistical Physics: the interdependence of magnitude, interevent time and interevent distance. 13th International Congress of the Geological Society of Greece, (Chania, Crete- Greece, 05 – 08 September 2013).ONLINE pdf
4. Tzanis A., Vallianatos F., **Efstathiou A**., 2013. Generalized multidimensional earthquake frequency distributions consistent with Non-Extensive Statistical Physics: an appraisal of Universality in the interdependence of magnitude, interevent time and interevent distance. EGU General Assembly 2013, (Vienna – Austria, 07 – 12 April 2013).

TABLE OF FIGURES

LIST OF TABLES

TABLE OF CONTENTS

INTRODUCTION

Over the last decades, complexity science has been approached by a fast-growing number of studies (Bak et al, 1988; Jensen H.J., 1998; Dimri V.P., 2005; Donner & Barbosa, 2008; etc) and is becoming more and more important in various fields of research.

Complex systems are all around us. They are seen in the way that migrating birds organize themselves into flocking formations and that ants communicate to successfully forage. They are seen in the way in which humans form social networks, and in the patterns of communication, social capital, and reputation that emerge from these networks. They are seen in the emergent power-law or fractal structures of plants, snowflakes, landslides, and galaxies, as well as in similar structural patterns of wealth and income distribution, stock market fluctuations, population distributions between cities, and patterns of urban development.

The most famous quote about complex systems comes from Aristotle who said that “wholes are more than the sum of their parts", wholes whose behavior cannot be understood without looking at the individual components and how they interact. In this context, complex systems are featured by several characteristics such as nonlinearity, criticality, long-range interactions, scaling, self-similarity, fractality/multifractality in space and time, high sensitivity to small impacts etc., which are ubiquitous in nature from the subnuclear scale to cosmology.

Seismogenetic systems are generally thought to comprise a mixture of processes that express the continuum of tectonic deformation (*background process*) and a large population of aftershocks that express the short-term activity associated with the occurrence of significant earthquakes (*foreground process*). Seismogenetic systems may serve as an example for complex systems, where earthquakes interact over a wide range of spatial and temporal scales exhibiting scale-invariance and fractality (Sornette, 2000; Turcotte, 1997; Turcotte et al., 2009). The first evidence of complexity in seismicity was observed by Omori (1894), who obtained the first empirical power law for aftershock rate decay in time. Then, the empirical law of Gutenberg and Richter (1954) for earthquake magnitude distribution reinforced such a view of seismic processes as complex; a concept that found its mathematical basis in the fractal geometry of nature (Mandelbrot, 1967)

leading to many investigations focused on the fractal and multifractal analysis of earthquake spatial and temporal distributions.

The question as to whether seismogenetic systems are **random** or **organized**, has been a subject of an ongoing debate. The question originates in a long-standing discourse between the two principal schools of thought (and epistemological paradigms) developed in the process of studying earthquake occurrence and quantifying the expectation of seismic activity. Accordingly, far from being purely academic the problem of understanding the proper statistical nature of seismicity is also practical: the answer can have significant repercussions on forecasting intermediate term earthquake hazard.

Although, progress has been made in understanding the foreground process, the statistical physics of background seismicity, hence the nature of seismogenetic system remains ambiguous. There are two general theoretical frameworks to describe the statistics of (background) seismicity. The first, and currently most influential, postulates that the expression of the background process is *Poissonian* in time and space and obeys additive Boltzmann-Gibbs thermodynamics. In consequence, it expects background earthquakes to be statistically independent and while it is possible for one event to trigger another, it submits that this occurs in an unstructured way and does not to contribute to the long-term evolution of seismicity. Thus, according to the “Poissonian viewpoint”, seismogenesis should be a *memoryless* process. The most influential realization of the Poissonian paradigm is the ETAS model (Epidemic-Type Aftershock Sequence, e.g. Ogata, 1988, 1998; Zhuang et al, 2002; Helmstetter and Sornette, 2003; Touati et al, 2009; Segou et al, 2013), which essentially is a self-excited conditional Poisson process (Hawkes, 1972; Hawkes and Adamopoulos, 1973; Hawkes and Oakes, 1974). ETAS posits that randomly occurring background earthquakes trigger aftershocks, and aftershocks trigger their own aftershocks, thus spawning a short-term proliferation of clustered foreground events (aftershock sequences) whose number decays according to the Omori-Utsu power-law (e.g. Utsu et al., 1995). Proxy-ETAS models (Console and Murru, 2001), as well as point process models to address the problem of intermediate to long-term clustering have also been developed, such as EEPAS (Each Earthquake is a Precursor According to Scale, e.g. Rhoades & Evison, 2006, Rhoades 2007) and PPE (Proximity to Past Earthquakes, e.g. Marzocchi and Lombardi, 2008).

At this point, it is important to point out that Poissonian models are mainly concerned with the statistics of time and distance between events. The size (magnitude) distribution of

both background and foreground processes is still thought to be governed by the time-honoured frequency – magnitude (F-M) relationship of Gutenberg and Richter. However, the scale-free grading between earthquake frequency and magnitude implied by the F-M relationship is a power-law that *cannot* be derived from the Boltzmann-Gibbs formalism. Likewise, the Omori-Utsu formula is a Zipf-Mandelbrot power-law, therefore inconsistent with the Boltzmann-Gibbs formalism. The heavy reliance of Poissonian seismicity worldviews and models on irrefutable, yet evidently non-Poissonian empirical laws is an apparent contradiction (self-inconsistency) with no theoretical resolution; it shows that Poissonian seismicity models are effectively *ad hoc* conceptual constructs that try to reconcile the (inherited) Poissonian worldview of statistical seismology with the obviously non-Poissonian dynamics of fault formation and clustering.

The second framework also comprises different classes of models and proposes that the seismogenetic system is complex. A well-studied class of models generically known as Self-Organized Criticality (SOC) proposes that seismicity is the expression of a non-equilibrating, fractal active fault network that continuously evolves toward a stationary critical state with no characteristic spatiotemporal scale, in which events develop spontaneously and any small instability has a chance of cascading into global failure (e.g. Bak and Tang, 1989; Sornette and Sornette, 1989; Olami et al., 1992; Sornette and Sammis, 1995; Rundle et al., 2000; Bak et al, 2002; Bakar and Tirnakli, 2009, etc.). According to Hanken (1983), the macroscopic properties of a self-organized system may change with time due to perturbations in its possible microscopic configurations, but the system as a whole will remain in, or continuously try to reach the critical state. The advantage and allure of SOC is that it is consistent both with itself and with several observed properties of earthquake occurrence: the Gutenberg-Richter law, the Omori-Utsu law and other power-law distributions of parameters pertaining to the temporal and spatial expression of a simulated fault network emerge *naturally* during the evolution of simulated fault networks. A variant of Self-*Organized* Criticality is Self-*Organizing* Criticality leading to Critical Point behaviour at the end of an earthquake cycle (e.g. Sornette and Sammis, 1995; Rundle et al., 2000; Sammis and Sornette, 2001; many others). This has been influential during the late 1990's and early 2000's but is no longer pursued as it made specific predictions (acceleration of seismic release rates) that could not be verified experimentally. In the context of Criticality, the dependence between successive earthquakes (faults) is known as *correlation*; it involves long-range interaction

and endows the seismogenetic system with memory that should be manifest in power-law statistical distributions of energy release, temporal dynamics and spatial dependence.

A number of authors have investigated for signs of correlation in earthquake catalogues with the use of stochastic models with memory that consider the non-random character of magnitude and time occurrence, such as Markov models that have been employed for seismic hazard assessment since the late 80's (Anagnos and Kiremidjian, 1988). In a more recent development, Votsi et al (2012) introduced a Markov model extension, i.e. a semi-Markov model (SMM) in continuous time for the description of seismicity patterns in time domain in the Northern Aegean Sea (Greece); Panorias et al., (2016) applied SMM to study the earthquake occurrences in Japan finding model's limiting behaviour for which is sufficient an interval of time of seven years. An application of Poisson hidden Markov Models revealed changes in seismicity rate in Ionian Sea, while also used for identifying the unobservable stress level controlling the evolution of the strong seismicity ($M \geq 6.5$) in Greece and the broader area (Orfanogiannaki et al., 2010; Votsi et al., 2013; 2014). Bountzis et al., (2018), applied Markovian Arrival Process as a candidate model to describe the time-varying earthquake activity in Corinth Gulf in Greece and demonstrate a high index of burstiness for the earthquake generation i.e. long quiescent periods alternate with short ones of intense seismic activity in the eastern part of the Gulf.

A few authors have also investigated models with alternative complexity mechanisms that do not involve criticality yet maintain the fault system in a state of non-equilibrium: a list can be found in Sornette (2004) and a comprehensive discussion in Sornette and Werner (2009). In a more recent development, Celikoglu et al., (2010) applied the Coherent Noise Model (Newman, 1996) based on the notion of external stress acting coherently onto all agents of the system without having any direct interaction with them. The CNM was shown to generate power-law behaviour in the temporal expression of its agent interevent time distributions but has a rather weak point: it does not include some geometric configuration of the agents and it is not known how this would influence the behaviour of the system.

The Poissonian and Complexity/Criticality viewpoints agree that the foreground process comprises a set of dependent events but the former assigns only local significance to this dependence, while Criticality considers them to be an integral part of the regional seismogenetic process. In practice, the fundamental difference between the two approaches is in their understanding of the background process. The former assumes

that there is no correlation (interaction) between random background events and argues that their statistical manifestations should best be described with the exponential and Gaussian distributions (consistent with the Boltzmann-Gibbs thermodynamic formalism). Criticality requires short and long-range interactions (correlation) between near or distal background/ background, background/ foreground and foreground/ foreground events, leading to power-law distributions of its temporal and spatial dynamic parameters. Moreover, non-critical complexity models cannot develop power-law distributions unless they evolve in non-equilibrium states, meaning even in this case correlation is unavoidable. It is therefore clear that if it is possible to identify and remove the foreground process (aftershocks), it would also be possible to clarify the nature and dynamics of the background process by examining its spatiotemporal characteristics for the existence of correlation. It should also be apparent that in order to successfully pursue this line of inquiry one must have a *natural* self-consistent general theoretical framework on which to base their search for the existence of correlation (and not model-based or *ad hoc* conceptual constructs). One also requires effective measures of correlation in the temporal and spatial expression of seismicity, as well as effective methods to separate the background and the foreground processes. As it turns out, there are (nearly) satisfactory answers to all three requirements.

Non-Extensive Statistical Physics (NESP) is a fundamental generalized conceptual framework to describe non-additive (non-equilibrating) systems in which the total (systemic) entropy is not equal to the sum of the entropies of their components. The concept has been introduced by Constantino Tsallis (Tsallis, 1988, 2001; 2009; Tsallis and Tirnakli, 2010) as a generalization of the Boltzmann-Gibbs formalism of thermodynamics. As such, it comprises an appropriate tool for the analysis of complexity evolving in a fractal-like space-time and exhibiting scale invariance, long-range interactions and long-term memory (e.g. Gell-mann and Tsallis, 2004).

Let X be a seismicity parameter (e.g. energy, interevent time etc.) and $p(X)dX$ the probability of finding its value in $[X, X+dX]$, such that $\int_W p(X)dX = 1$, where W is the support of X and expresses the total number of microscopic configurations of the system. Non-equilibrium states in systems with complex behaviour can be described by the Tsallis (1988) entropic functional:

$$S_q = k\frac{1}{q-1}\left[1-\int_W p^q(X)dX\right] \quad (1)$$

where *k* is the Boltzmann constant and *q* the *entropic index*. The latter is a measure of the *non-extensivity* of the system and for the particular case *q* = 1 Eq. 1 reduces to the Boltzmann–Gibbs entropy

$S_{BG} = -k\int_W p(X)\ln(p(X))dX$.

The Tsallis entropy shares properties with the Boltzmann-Gibbs entropy, including concavity and fulfilment of the H-theorem. However, it is *pseudo-additive* in the sense that it is not proportional to the number of the elements of the system as is S_{BG}. Thus, for a composite of two statistically independent systems, *A* and *B*,

$S_q(A, B) = S_q(A) + S_q(B) + (1-q)\, S_q(A)\, S_q(B)$,

leading to *super-additivity* for $q<1$, *additivity* for $q=1$, i.e. Gibbs-Boltzmann statistics, and *sub-additivity* for $q>1$. NESP predicts power-law cumulative probability distributions in non-additive (non-extensive)[1] systems, which reduce to the exponential cumulative distribution in the limiting case of additive (extensive/ random/ point) processes.

NESP has already been applied to the statistical description of seismicity with noteworthy results. It has also been shown to generate the Gutenberg-Richter frequency-magnitude distribution from first principles (Sotolongo-Costa and Posadas, 2004; Silva, 2006; Telesca, 2011, 2012). In conclusion, NESP provides a general, complete, consistent and model-independent context in which to investigate the nature and dynamics of seismogenetic processes.

A definite indicator of correlation (interaction) between faults is the lapse between consecutive earthquakes above a magnitude threshold and over a given area: this is referred to as *interevent time*, *waiting time, calm time*, *recurrence time* etc. Understanding the statistics of earthquake frequency vs. interevent time is apparently essential for understanding the dynamics of the active fault network. For that reason, the frequency – interevent time (F-T) distribution has been studied by several researchers. Almost every hitherto study has focused on foreground and mixed background/foreground processes. Empirical F-T distributions generally exhibit power-law characteristics and fat tails. For that reason, in the context of statistical seismology they have been analysed with tailed standard statistical models reducible to power laws in some way or another. Examples of

[1] The term “extensive” (full/ complete according to Merriam-Webster’s definition), was used by Tsallis (1988) to designate systems that are equilibrating, as opposed to those that are not (incomplete, i.e. non-extensive). The terms “additive” and “non-additive” are probably more appropriate but for consistency, we adopt Tsallis’s terminology.

this approach are the gamma distribution and the Weibull distribution (e.g. Bak et al., 2002; Davidsen and Gold, 2004; Corral, 2004; Martinez et al, 2005; Talbi and Yamazaki, 2010). Some researchers, working from a statistical physics vantage point, proposed *ad hoc* mechanisms for the generation of power laws by a combination of correlated aftershock and uncorrelated background processes (e.g. Saichev and Sornette, 2013; Hainzl et al, 2006; Touati et al, 2009). Nevertheless, Molchan (2005) has shown that for a stationary point process, if there is a universal distribution of interevent times, then it must be an exponential one!

A second measure of fault interaction is the *hypocentral distance* between consecutive earthquakes above a magnitude threshold and over a given area (*interevent distance*). The statistics of the frequency – interevent distance (F-D) distribution should be related to the *range of interaction* over that area; unfortunately, it is not fully understood as it has been studied by less than a handful of researchers (e.g. Eneva and Pavlis, 1991; Abe and Suzuki, 2003; Batak and Kantz, 2014; Shoenball et al., 2015). A third criterion of correlation, (albeit not commonly acknowledged as one), is the *b* value of the Gutenberg–Richter frequency – magnitude (F-M) distribution which expresses the scaling of the size-space of active faults over a given area (fault hierarchy) and conveys information about their distribution in space and the homogeneity of the domain they occupy. The F-M distribution is *static* and does not say much about the dynamics of the fault network, nor about correlations in the energy released by successive earthquakes. Nevertheless, this undisputable empirical relationship is a standard against which to compare and test any physical and statistical description of the scaling of earthquake sizes and as such will be used herein.

The present work is an attempt to examine the dynamics of seismogenesis by studying the local and regional statistical characteristics of earthquake occurrence in different seismogenetic areas. Accordingly, the main goals are:

1) To empirically validate the possibility to describe the seismogenesis in the context of NESP.

2) To investigate correlation in seismicity (organization) by studying the **entropic indices predicted by NESP,** in seismogenetic systems of regional and global scales.

3) To investigate the evolution of seismicity and search for signs of randomness or (self-) organization in the probability distributions of event size, interevent time and interevent distance

In order to ensure the rigour of the analysis, instead of considering only one-dimensional earthquake frequency distributions of the as almost all hitherto studies have done, I will focus on *multivariate* distributions that express the joint probability of observing an earthquake larger than a given magnitude, after a given lapse time and beyond a given distance, thereby introducing additional mutual constraints on the permissible variation of the relevant parameters. Based on the above, the present work is organized as follows:

Chapter 1 presents the theoretical frameworks which describe the statistics of seismicity. It includes an overview of the basic - and currently most influential- (Poissonian) models in seismicity, as well as an introduction in the concepts of self-Organised Criticality, SOC models, non-statistical mechanics, non-equilibrium thermodynamics and their usefulness in the investigation of phenomena exhibiting fractality and long-range interactions such as earthquake activity is provided.

Chapter 2 gives a brief exposé of NESP approach to earthquake statistics and focuses on the construction of multivariate earthquake frequency distribution and NESP – based modelling which comprise a significant part of our analysis procedure. Chapter 2 also presents an overview of the stochastic declustering procedure (Zhuang et al, 2002) so as to separate the foreground and background processes and discuss the validation tests which defined base values of the temporal entropic index, above which it is safe to assume non-Poisson processes.

Chapters 3, 4 and 5 are the focal points of this thesis. They present NESP application to various seismogenetic environments such as: **a)** the transformational boundaries of California (San Andreas Fault – Sierra Nevada Range – Walker Lane fault systems), the large transformational zone of Greece and Western Turkey (from the North Anatolian Fault – North Aegean Trough to Evia, Attica, NW Peloponnesus up to the Cephalonia Transform Fault) and the transformational boundaries of Queen Charlotte – Fairweather and Denali faults in Alaska, **b)** the Mendocino Triple Junction in California, **c)** various seismogenetic zones of Greece – Western Turkey and **d)** the Alaskan – Aleutian convergence plate boundary and Continental Alaska . With reference to the latter, crustal and sub-crustal earthquakes are examined so as to inquire whether environmental or/and boundary conditions affect the dynamics of a fault network.

Finally, **Chapter 6** includes a recapitulation of the basic concepts, techniques and procedures utilized in the data analysis; results are discussed and interpreted through a series of useful observations.

Summarizing, the present thesis is a continuation of a systematic pursuit to examine the seismic processes by implementing such tools of complexity theory as the Non – Extensive Statistical Physics approach. The knowledge and application of such modern tools as NESP will contribute in understanding the basic rules governing the dynamics of seismogenesis. The key scientific challenge is how to use the information in such fields as earthquake hazard analysis.

CHAPTER 1

LITERATURE OVERVIEW

1. BASIC CONCEPTS IN STATISTICAL SEISMOLOGY

Over the last two decades seismicity modelling with increasing component of physical reasoning has been attracting attention. Statistical seismology comprises a useful tool which aims to bridge the gap between physics-based models without statistics, and statistics-based models without physics. Although progress has been made, seismicity has proved a difficult subject to deal with and make breakthroughs. The seismogenetic system is generally thought to comprise a mixture of processes that express the continuum of tectonic deformation (background process) and a large population of aftershocks that express the short-term activity associated with the occurrence of significant earthquakes (foreground process). Although, progress has been made in understanding the foreground process, the statistical physics of background seismicity, hence the nature of seismogenetic system remains ambiguous with significant repercussions for problems such as hazard analysis and long-term forecasting.

A number of factors have contributed in the development of what we call statistical seismology. The first one is based on the attempts to follow the example of success of classical models in statistical mechanics, thermodynamics etc. Although progress has been made, seismology has proved a difficult subject in which to make a breakthrough. Appealing analogies such as the approach to a phase change can be made, and general models such as self-organized criticality (SOC) can provide valuable insights into the processes at work. From a physical point of view there have been many attempts to model the processes of rupture and fault propagation. There have been many variations in earthquake models in order to fit a variety of seismological and geodetic data. Such models may represent faults as dislocations surfaces in surrounding elastic solid or block and slider models with similar function. From a statistical point of view an important impulse has been the development of the theory of stochastic point process.

In the last decades, the development of effective procedures and techniques of combining both physical and statistical sides have led the research into two main categories: the one that quests modeling and methodological issues and the other that primarily deals with observational studies and incorporates statistical models for the data interpretation. The seismogenetic system is complex, thus when modeling the observed earthquake phenomenology, we must take into account considerable amount of uncertainty. This is

typically done using either stochastic dynamics with a few variables or deterministic dynamics in a highly heterogeneous system with many degrees-of freedom.

Many studies have been published with subjects from both categories. For example Shcherbakov et al., (2005) combine the Gutenberg-Richter, modified Omori and Baths law in order to give a relation of the aftershock decay rate, Zöller et al., (2005) show that realistic aftershock sequences with space-time characteristics compatible with observations are generated by a model consisting of brittle fault segments separated by creeping zones, Botiglierri et al., (2011) compare stochastic branching models for seismicity by developing a procedure to maximize log likelihood of the different models. Rhoades and Evison, (2004) developed a forecasting model based on the idea of self-similarity for their analysis of the Japanese earthquake data; their model was one of the first to combine self-similarity within an explicit stochastic model that can be fitted to data. Iwata and Young (2005) applied the analysis of b-value for acoustic emissions monitored at the Underground Research Laboratory in Canada. Zhuang et al.,2002 analyzed data provided by the China Seismological Bureau on low-frequency electrical signals as potential earthquake precursors.

In most of the aforementioned analyses, the problems demand seismological and statistical interaction. Of course, there are still many unresolved issues that require more extent and vigorous investigation; therefore, the entire field evolves rapidly with application of pioneering techniques in statistical analysis and data processing, making the field of Statistical Seismology even more challenging.

1.1. STOCHASTIC MODELS

As was mentioned above statistical seismology is closely associated with the application of stochastic modeling to existing data. A fundamental difference between a physical, a deterministic and a stochastic model is that a physical model seeks to understand and predict a process fully while a stochastic model takes into account that some aspects of the physical process are out of range and must be replaced in the model by some unknown (random) process. In deterministic models the output of the model is fully determined by the parameter values and the initial conditions while stochastic models possess some inherent randomness. The same set of parameter values and initial conditions will lead to an ensemble of different outputs. Obviously, the natural world is buffeted by stochasticity. But stochastic models are considerably more complicated, so why to inhere uncertainties into the models? An important reason is that by building

uncertainties into a model, it becomes possible to quantify the variability in the predicted outcomes.

The resulting stochastic model should reproduce those aspects of the physical phenomenon which are relevant to measurements. However, just because a stochastic model treats some aspects of the process as random, that does not mean it is not consistent with the physical parameters. When it comes to classical physics, uncertainties in a model are usually attributed to observational errors, while in quantum physics they reflect a fundamental characteristic of the universe. Uncertainties in geophysics lie somewhere in the middle; they are associated with observational errors which are due to indirect observations on the physical processes that take place within the earth's crust. The processes themselves are complex. Stochastic models of earthquake occurrence must somehow marry the limited physical theory to the limited data that bears directly on questions such as the initiation of a rupture and its development into a large-scale earthquake. Under such circumstances, one of the major goals is to be able to quantify the uncertainties in the model predictions. For this reason, it is important for the produced stochastic models to reflect the physical picture at least in a more limited way. The underlying question however remains: how the observations and the physical picture could be extended to allow a better quantification of the variability.

Of course, the answer is not that simple, especially if we consider the different roles of stochastic models across their diverse fields of application. For example, in statistical mechanics stochastic model plays an integral role in understanding the physical processes themselves, while in other applications it is used as a basis for prediction or decision-making. In all cases, it is crucial for the model to be fully fitted to the available data.

1.1.1. Basic mathematical concepts

An earthquake is the vibration of the Earth's surface that follows a release of energy in the Earth's crust. This energy which accompanies the movement or fracture of faults can be generated by a sudden dislocation of segments of the crust or the upper mantle. The point information available for each earthquake refers to the origin, hypocenter and magnitude. In most cases earthquakes are treated as points in time and space; this way they can be study by using point process models.

In mathematical terms (commonly in statistics and probability theory) a point process is a type of random process for which any one realization consists of a set of isolated points

either in time or geographical space, or in even more general spaces. A point process can be generally regarded as a type of stochastic model which defines probabilistic rules of the occurrence of points in space and time. The realizations of such process can be represented as a family of delta-functions in space or time or both.

Let *E* be an Euclidean space, with Borel *σ*-algebra *Ɛ*. Let *ß* denote the ring of bounded Borel sets. A *point measure μ* on *E* is a measure that $\mu(\mathrm{A}) \in \mathrm{N}$ and $\mu(A) < \infty$ for every *A*∈ ß.

The fundamental point measures are the point δ_x defined by $\delta x(A) = 1(x \in A) = \begin{cases} 1, & \text{if } x \in A, \\ 0, & \text{if } x \notin A \end{cases}$,

where δ_x is commonly called *Dirac measure.*

A point measure μ can be decomposed as $\mu = \sum_{\mathrm{i}=1}^{K} \alpha_{\mathrm{i}} \delta_{\mathrm{i}}$,

Where $0 \le K \le \infty$, α_{i} are positive integrals and the x_i are distinct points in *E*.

If $\alpha_{\mathrm{i}} = 1$ for each *i,* the point measure is called *simple point measure*.

Let (Ω, *F, P*) be a probability space. A *point process* on *E* is a measurable mapping *N* of (Ω, *F*) into (M_p, M_p) where M_p is the set of all the point measures in *E* and M_p is the *σ*-algebra. For a random measure *M* and *A*∈ *Ɛ*, the random variable *M (A*) is termed as the number of points falling into *A*, and for a function C_K, the integral $N(f) = \int_E f(x) N(dx)$

The most important point process model is the Poisson process, which is a simple point process *N* such that the number of points in any set follows a Poisson distribution and the numbers of points in disjoint sets are independent. That is, *N* is a Poisson process if

$N(A_1)$, ..., $N(A_k)$ are independent Poisson random variables, for any disjoint, measurable subsets A_1, ..., A_k of S. The behavior of a simple temporal point process N is typically modeled by specifying its ***conditional intensity***, *λ(t)*, which represents the infinitesimal rate at which events are expected to occur around a particular time *t*, conditional on the prior history of the point process prior to time *t*. Formally, the conditional intensity associated with a temporal point process N may be defined via the limiting conditional expectation

$$\lambda(t) = \lim_{\Delta t \to 0} E\left\{ N\left[t, t + \Delta t\right) / Ht \right\} / \Delta \mathrm{t}$$

provided this limit exists, where Ht is the history of the point process *N* over all times strictly prior to time *t*.

A point process N may be called self-exciting if *cov{N(s,t), N(t,u)} > 0 for s < t < u*. N is self-correcting if instead this covariance is negative. Thus, the occurrence of points in a self-exciting point process causes other points to be more likely to occur, whereas in a self-correcting process, the points have an inhibitory effect. By definition, a Poisson process is neither self-exciting nor self-correcting. Self-exciting point process models are often used in seismology to model events that are temporally clustered. A commonly used example is the Hawkes process, where the conditional intensity is given by $\lambda(t) = \mu(t) + \sum_{i:\tau i<t} \nu\left(t-\tau i\right)$

Where *μ(t)* is the deterministic background rate and the function *v* governs the clustering density.

Self-correcting models are used in ecology, forestry and other fields to model occurrences that are well-dispersed. Such models may be useful in describing births of species, for example, or in seismology for modeling earthquake catalogs after aftershocks have been removed. An important example is the Markovian point process model (so called because the conditional rate obeys the Markov property) where

$$\lambda(t) = g\left\{t, N\left[0,t\right)\right\}$$

For example, the function *g* may be selected so that *λ* takes the form $\lambda(t) = \exp\left\{\alpha + \beta\left(t - \rho N\left[0,t\right)\right)\right\}$,

where α, β, and ρ are constants. The parameters α and β govern the background rate and trend in the occurrences, while the product *βρ* represents the decrease in conditional rate of future events caused by each event, which may be due to diminished fuel load in the case of wildfire modeling, for instance, or the release of strain energy in the seismological case.

Several studies also make an important use of models for space – time point process which allow at least some elements of the physical processes to be incorporated into the *conditional intensity function* which controls the evolution of the point process.

Accordingly, *λ(t)* is uniquely associated with any analytic space-time point process (Daley and Vere-Jones, 2003) and can be defined as the frequency with which events are

expected to occur around a particular location in time and space, conditional on the prior history Ht of the point process up to time t:

$$\lambda(t,x,y)=\lim_{\Delta t,\Delta x,\Delta y\downarrow 0}\left(E\left[N\left\{(t,t+\Delta t)\times(x,x+\Delta x)\times(y,y+\Delta y)\right\}\mid Ht\right]/(\Delta t\Delta x\Delta y)\right)$$

An example of one of the most well-studied point processes models is the Epidemic Type Aftershock Sequence (ETAS) model suggested by Ogata (1988) which over the years has played an increasingly important role as a base-line model because of its built-in clustering. Detailed description of the ETAS model is given in section 1.2.

1.2 BASIC MODELS OF SEISMICITY

1.2.1 Size-Frequency distribution of earthquakes

Formulas of quantifying the size of earthquakes by a logarithmic measure were first developed in the late 1930's. The size distribution of earthquakes in a seismogenic area was described over a range of magnitudes by a power law (Ishimoto and Iida, 1939; Gutenberg and Richter, 1944):

$$\log_{10}N(M)=a-bM$$

where N (M) is the cumulative umber of earthquakes with magnitude ≥ M and a and b are constant parameters. The parameter 'a' describes the productivity of a volume, and b, the slope of the frequency-magnitude (F-M) distribution, describes the relative size distribution of events. An example is shown in Fig. 1.1 where the *a*, *b* and *M* were estimated for southern California, period 1980 - 2017.

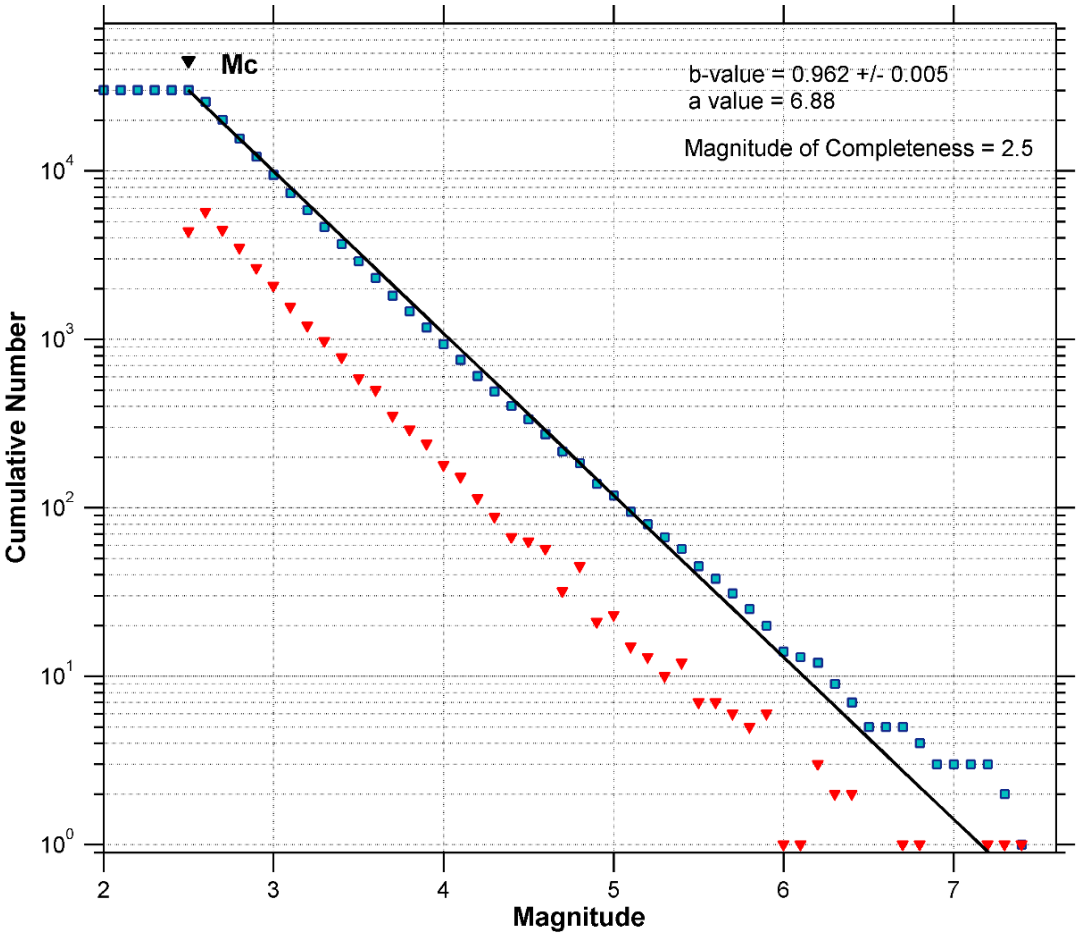

Figure 1.1 Frequency – magnitude (F-M) distribution of Southern Californian seismicity for the period 1968-2017; red triangles denote the incremental distribution and blue squares the cumulative distribution.

Numerous studies focus mostly on the *b-value* parameter. For example, a series of papers address *to b-value* computation uncertainties (Aki, 1965; Utsu, 1965; Hamilton, 1967; Page, 1968; Utsu, 1982; Bender, 1983; Tinti and Mulargia, 1987; Kijko and Sellevoll, 1989; Utsu 1992; Zuniga and Wyss, 1995; Gibowicz and Lasocki, 2001). Other studies address to temporal variations of b-value (Patane et al., 1992; Wiemer and Benoit, 1996; Wiemer and McNutt, 1997; Wiemer and Wyss, 1997; Wiemer and Katsumata, 1999; Wyss and Lee, 1973; Wyss et al., 1997; Wyss et al., 2000; Zobin, 1979) or its spatial variability according to scale (Frohlich and Davis, 1993; Gerstenberger et al., 2001; Jolly and McNutt, 1999; Mori and Abercrombie, 1997; Ogata et al., 1991; Ogata and Katsura, 1993; Wiemer and Benoit, 1996; Wiemer and Wyss, 1997; Wiemer et al., 1998; Wiemer and Katsumata, 1999; Wyss et al., 2001a,b; Wyss and Wiemer, 2000), while several studies relate *b-value* to physical properties such as pore pressure, material

homogeneity, stress etc (Lockner and Byrlee, 1991; Mogi, 1962; Scholz, 1968; Shaw, 1995; Warren and Latham, 1970; Wyss, 1973).

There have been quite a few papers that deal with the implications of power law scaling in such concepts as fractality and chaotic behavior (Bak and Tang, 1989; Hirata, 1989; Ito and Matsuzaki, 1990; Okuda et al., 1992; Papadopoulos et al., 1993; Main, 1995; Main, 1996; Amelung and King, 1997; Sammis et al., 2001). Many of these studies denote that the relationship between the size of an earthquake and its frequency of occurrence obeys fractal statistics. Given that very large earthquakes are rare events and very small earthquakes are very frequent (seismically active regions can register hundreds of small earthquakes per day, then the G-R formulation is a power law relationship between the number of large and small events in a given region per unit time. Pioneers in this field, Bak and Tang (1989) refer to the common phenomena of power law in nature and critical behavior in dynamic systems which can be directly linked to spatiotemporal distribution of earthquakes. Such terms as fractality, criticality and complexity are discussed in Sections 1.4 and 1.5.

1.2.2. Poissonian Models

As already discussed above, in probability theory, a Poisson process is a simple and widely used stochastic process for modeling the times at which arrivals enter a system. It is in many ways the continuous-time version of the Bernoulli process (which is a discrete – time stochastic process).

The Poisson process forms the basis for most of the present probabilistic seismic hazard analysis (Cornell 1968) and has been also known as the model of complete randomness (self-exciting point process). Thus, it naturally serves as the null model in many hypothesis tests to clarify whether systematic structure is contained in the observations. An example is the discussion by Gardner and Knopoff (1974) as to whether the seismicity in California is Poissonian or not after the removal aftershock sequences.

If N (a, b) is the number of events in a point process N that fall in the time interval (a,b), then the Poisson process is stationary if the system is characterized by the following conditions (Zhuang et al, 2012):

The numbers of events occurring in two disjoint time intervals are independent of each other.

$$\Pr\left\{N(a,b)=m, N(c,d)=n\right\} = \Pr\left\{N(a,b)=m\ \right\}, \Pr N(c,d)=n\right\}$$

for all non-negative integers m, n and any interval pairs $(a,b)\cap(c,d)=\varnothing$

There is never an occasion that two or more events occur simultaneously (Simplicity).

The probability distribution of the number of events falling in a time interval only depends on the length of the time interval (Stationarity).

A point process is a non-stationary Poisson process if it satisfies the independent increments and simplicity conditions but violates the stationarity condition. Consequently, the Poisson process has a rate that is a function of time, denoted by λ(t).

Given the definition $\Lambda(t)=\int_0^t \lambda(x)dx$ and $\Lambda(t+s)=\int_0^{t+s}\lambda(x)dx$, the probability of observing *n* events in the interval $[t,t+s]$ is

$$\Pr\{N[t,t+s)=n\}=\frac{e^{-(\Lambda(t+s)-\Lambda(t))}\left[\Lambda(t+s)-\Lambda(t)\right]^n}{n!}$$

That is, $N[t,t+s)$ is Poisson distributed with expectation value $\int_0^{t+s}\lambda(u)du$ where $\lambda(t)$ is the time dependent intensity.

a) Temporal Models

A number of temporal models have been developed to describe, analyze and forecast the probabilities of earthquake occurrences. An overview of the basic temporal models has been discussed by Zhuang et al., (2012) who provided a general framework of the models as important tools for time-independent and time-dependent seismic hazard analysis in order to understand the various seismic patterns. Here we briefly present the basic temporal models starting from simple one-dimensional models to more complex models such as ETAS model, EEPAS and the alternative BASS model.

Recurrence – Renewal models

In general, earthquake recurrence refers to the time between subsequent rupturing on a given segment of fault, hence to the period of the loading cycle. The term may be also used to indicate the mean time between earthquakes within a specified region in which many active faults may be present.

Although the latter represents a statistical concept useful in earthquake hazard analysis, the data that can be used to study earthquake recurrence are quite limited. The main reason is that recurrence times are generally large (a hundred years or more), while recording seismometers have been in existence for only a little more than a century, and

in many tectonically active regions reliable historical records cannot be obtained for periods earlier than about a hundred years before that. In addition, many remote areas lack of historical records are available. As a result, for many areas of the world, one complete seismic cycle has not been documented yet, and for others only one is known, which does not carry any information about periodicity.

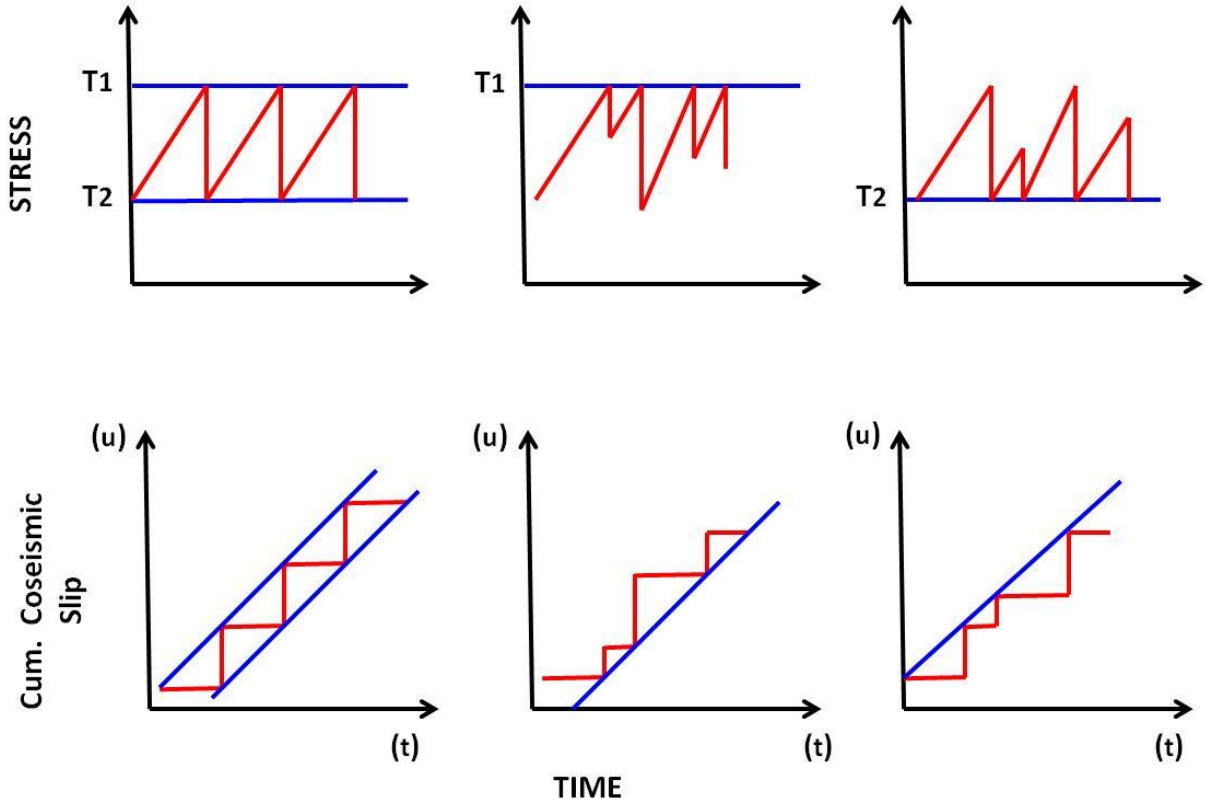

Figure 1.2 Simple earthquake recurrence models: (a) Reid's perfectly periodic model; (b) time predictable model; (c) slip-predictable model. The time-predictable model is motivated by the observation of the Nankaido earthquakes. (Shimazaki and Nakata, 1980).

A renewal process is simply a generalization of the Poisson process. It is basically an idealized stochastic model for events that occur randomly in time and it is defined as a point process with the *waiting times* having a more general distribution, which is not necessarily exponential distribution. These models are widely used in seismicity and seismic hazard analysis. For example, in his study, Field (2007) summarizes the estimations of the recurrence probabilities of large earthquakes on Californian major fault segments using recurrence models that produced the official California seismic hazard map (http://pubs.usgs.gov/of/2007/1437/).

The elastic rebound theory initially proposed by Reid (1910) in the context of his study of the great San Francisco, 1906 earthquake, sometimes sustain the above models.

According to his theory stresses which cause earthquakes are slowly built up by plate movements until the stress or deformation energy reaches a critical value, at which a rupture occurs. Later on, with the formulation of plate tectonics theory, the idea of the seismic gap of first kind[2] was initially introduced by Mogi (1968), and elaborated by Schwartz and Coppersmith, (1984) and Wesnousky, (1994). According to their model large earthquakes tend to repeat themselves along the same fault or plate boundary. The occurrence of a characteristic earthquake ruptures the entire segment and relieves tectonic stress within the segment. Therefore, the characteristic earthquake hypothesis cannot be taken independently of its implications on the time occurrence of earthquakes. In fact, if one assumes a constant average slip rate between two plates along their boundary, and a fairly constant slip and stress drop released by each characteristic earthquake on a fault, the regularity of the inter-event time is just a simple physical consequence. According to this hypothesis, the earthquake hazard is small immediately following the previous large earthquake and increases with time since the latest event on a certain fault or plate boundary. Hence, the earthquake occurrence can be regarded as a quasi-periodic process (Mc Cannet al., 1979; Nishenko and Buland, 1987; Shimazaki and Nakata, 1980).The controversy whether quasi-periodic or uniform inter-event time distributions apply to individual faults has been going on many years, and the choice affects not only earthquake probabilities and seismic hazard calculations, but also our understanding of the physics of earthquakes. This debate was partly developed through discussions by Nishenko and Sykes (1993), Kagan and Jackson (1991) and Kagan and Jackson (1995). The controversy did not have a clear conclusion and is ongoing.

Most recently, in the debate on the preference between a characteristic earthquake hypothesis and a simpler time-independent hypothesis, Parsons and Geist (2009) applied a simulator-based model. Their simulations showed that the Gutenberg–Richter distribution can be used as a model for earthquake occurrence on sub-segments of different sizes on individual faults in probabilistic earthquake forecasting.

[2] A seismic gap of the first kind is a segment of plate boundary, for which the time elapsed since its latest rupture is significantly long relatively to that of the neighboring segments. According to a very popular and intuitive view, a seismic gap is likely to rupture again generating a large earthquake in the near future.

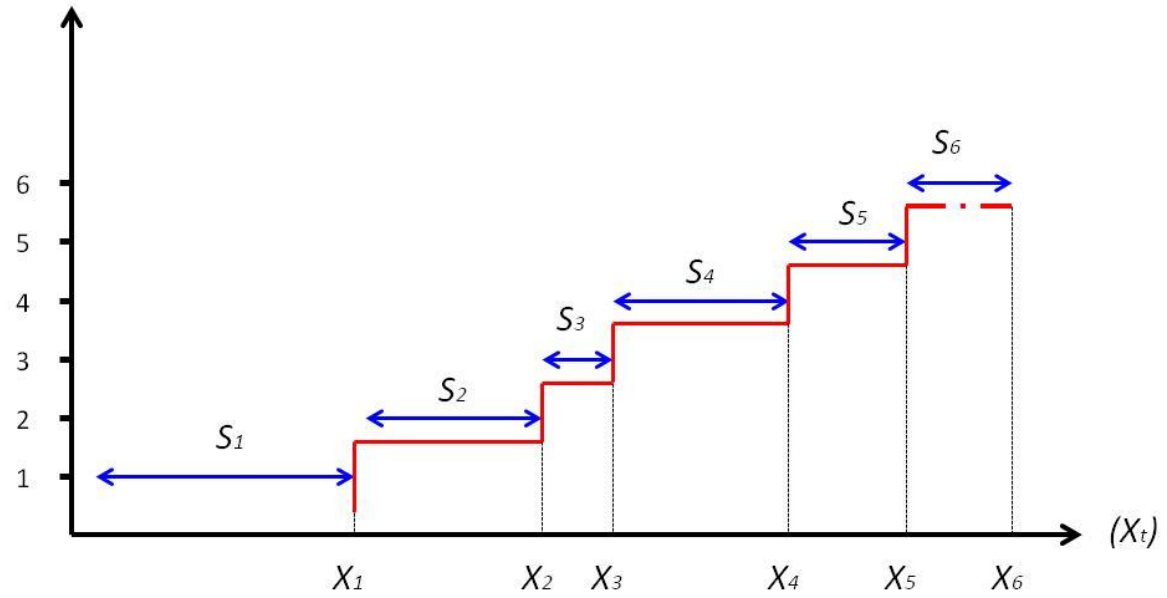

Figure 1.3 Schematic sample evolution of a renewal process with waiting times S_i and jump times X_j.

The conditional intensity of the renewal process can be derived as follows: suppose that the time interval between any two adjacent events is independent from other intervals. This means that the occurrence of the next event depends only on the time of the last event but not on the full history. Thus, the conditional intensity function is

$$\lambda(t) = \frac{f(\mathrm{t} - \mathrm{t}_{N(\mathrm{t}\_)})}{1 - F(t - \mathrm{t}_{N(\mathrm{t}\_)})},$$

Where $t_{\mathrm{N}(t\_)}$ is the occurrence time of the last event is before *t* and *F* is the cumulative probability function of *f*. In their study Zhuang et al, (2012) reports the probability functions that are often chosen as the renewal densities which are:

1) The gamma density

$$f(u;k;\theta) = u^{k-1}\frac{e^{-u/\theta}}{\theta^k \Gamma(k)}, \qquad \text{for } u \geq 0 \text{ and } k, \theta > 0,$$

with a hazard function $h(u;k;\theta) = \dfrac{u^{k-1}e^{-\frac{u}{\theta}}}{\theta^k \Gamma_{\frac{u}{\theta}}\left(k, \frac{u}{\theta}\right)},$

Where θ is the scale parameter, k the shape parameter and Γ and Γ_α are the gamma and the incomplete gamma functions, respectively defined by

$\Gamma(x)=\int_0^\infty t^{x-1}e^{-t}dt$ and $\Gamma_\alpha(x)=\int_0^\infty t^{x-1}e^{-t}dt$

2) The log normal density function

$$f(u;\mu,\sigma)=\frac{1}{u\sigma\sqrt{2\pi}}e^{-\frac{(\ln(u)-\mu)^2}{2\sigma^2}}, \qquad \text{for } u\geq 0$$

with a hazard function

$$h(u;\mu,\sigma)=\frac{2}{u\sigma\sqrt{2\pi}}\frac{e^{-\frac{(\ln(u)-\mu)^2}{2\sigma^2}}}{1-erf\left[\frac{\ln(u)-\mu}{\sigma\sqrt{2}}\right]}$$

where u and μ are the mean and standard deviation of the variable's natural logarithm[3] and erf is the error function.

3) The Weibull distribution

In probability theory and statistics, the Weibull distribution is a continuous probability distribution which was described in detail by Wallodi Weibull (1951). The pdf of a Weibull random variable is:

$$f(u;\mu,k)=\begin{cases}\frac{k}{\mu}\left(\frac{u}{\mu}\right)^{k-1}e^{-(u/\mu)^k} & u\geq 0\\ 0\end{cases}$$

where $k>0$ is the shape parameter and $\mu>0$ is the scale parameter of the distribution. Its cumulative distribution function is a stretched exponential function $F(u;\mu,k)=1-e^{-(u/\mu)^k}$

and its hazard function $h(u;k,\mu,k)=\frac{k}{\mu}\left(\frac{u}{\mu}\right)^{k-1}$

[3] If X is a normal random variable with mean μ and variance σ^2, then Y = expX has a log-normal distribution with a density of $f(u;\mu,\sigma)$.

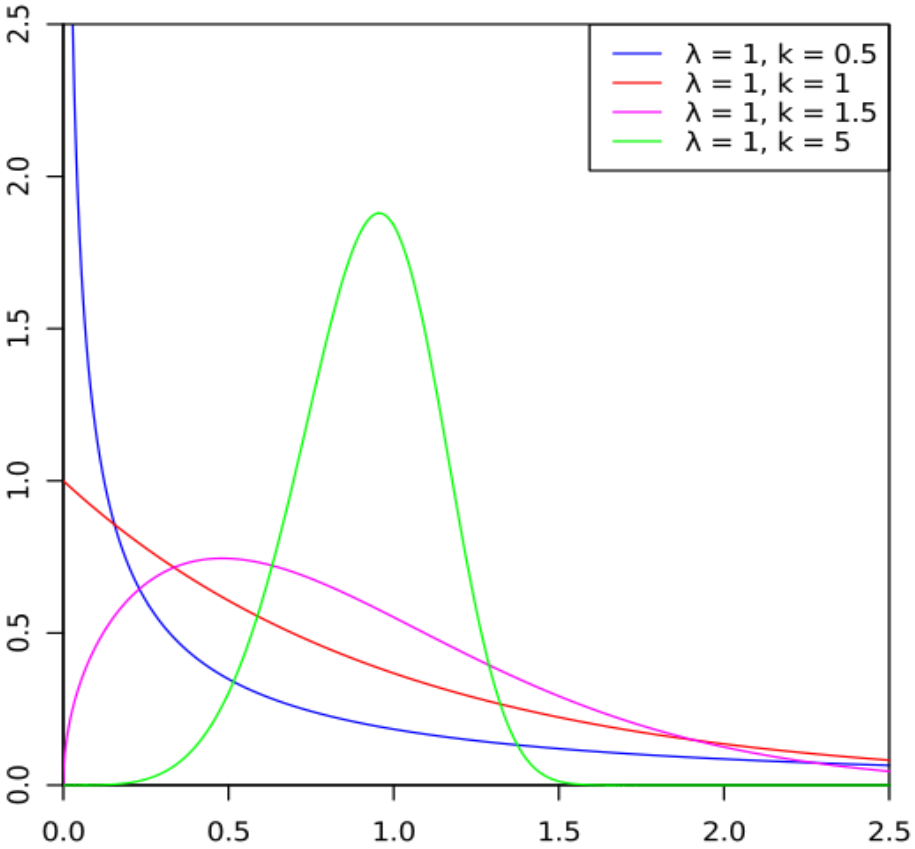

Figure 1.4 Weibull (2-parameter) density function

4) Brownian Passage - Time (BPT) Model

This model was originally introduced by Ellsworth et al., (1999) and Matthews et al., (2002) to provide a physically-motivated renewal model for earthquake recurrence. It is based on the properties of the Brownian relaxation oscillator (BRO). A Brownian passage-time model considers an event as a realization of a point process in which a new earthquake will occur when a state variable (or a set of them) reaches a critical failure threshold (χ_f) and at which time the state variable returns to a base ground level (χ_0). Adding Brownian perturbations to steady loading of the state variable produces a stochastic load-state process. An earthquake relaxes the load state to the characteristic ground level and begins a new cycle. In the conceptual Model of Matthews et al (2002) the loading of the system has two components: (1) a constant-rate loading component λt, and (2) a random component, $\sigma W(t)$, that is defined as a Brownian motion (where W is a standard Brownian motion and σ is a nonnegative scale parameter). Standard Brownian motion is simply integrated stationary increments where the distribution of the increments

is Gaussian, with zero mean and constant variance. The Brownian perturbation process for the state variable χ_t is defined as:

$$X(t) = \lambda t + \sigma W(t)$$

An event will occur when $\chi(t) \geq \chi_f$. The BRO are a family of stochastic renewal processes defined by four parameters: the drift or mean loading (λ), the perturbation rate (σ^2), the initial stress state (χ_0), and the failure state (χ_f). On the other hand, the recurrence properties of the BRO (repose times) are described by a Brownian passage-time distribution which is characterized by two parameters: (1) the *mean time* or period between events, (μ), and (2) the aperiodicity of the mean time, α, which is equivalent to the familiar coefficient of variation. The probability density for the Brownian passage-time model is given by:

$$f(t) = \left(\frac{m}{2\pi\alpha^2 t^3} \right)^{1/2} \exp\left[\frac{-(t-m)^2}{2m\alpha^2 t} \right]$$

This distribution has the following noteworthy properties: (1) the probability of immediate rerupture is zero; (2) the hazard rate increases steadily from zero at t = 0 to a finite maximum near the mean recurrence time and then decreases asymptotically to a quasi-stationary level, in which the conditional probability of an event becomes time independent; and (3) the quasi-stationary failure rate is greater than, equal to, or less than the mean failure rate because the coefficient of variation is less than, equal to, or greater than $1/\sqrt{2} \approx 0.707$.

Stress Release Models

The elastic rebound theory proposed by Reid, in the early 20th century is one of a few classical models for earthquake mechanisms. It indicates that elastic stress is concentrated in a seismogenic environment due to plate motions and is released when the stress exceeds the strength of the medium. These models have been utilized in long-term prediction, suggesting that a large earthquake should be followed by a calm period. However, the behavior of earthquake sequences is far more complicated; in reality strong earthquakes can be followed by a period of “activation” or more precisely a period of triggering earthquakes of similar magnitude outside of the immediate aftershock zone.

The stress field within a region can be extracted from a variety of information; however temporal variations of seismic activity may most directly reflect the nature of earthquake

generating stress. In the past few years there have been many studies towards this direction. Knopoff (1971) developed a stochastic (Markov) model for the occurrence of earthquake sequences while Vere-Jones (1978) introduced the stress release model (SRM), a stochastic version of the elastic rebound theory which was developed afterwards by a series of papers (see, e.g., Zheng and Vere-Jones 1991, 1994). The SRM assumes that the stress level in a certain region is gradually built up, linearly with time by tectonic movements, and drops down suddenly coinciding with earthquakes. This can be written:

$$X\left(t\right)=X\left(0\right)+\rho t-S(t)$$

where X(0) is the initial stress level, is the constant loading rate from the tectonic movements, and S(t) is the accumulated stress release from earthquakes in the period [0; t), and can be written $S(t)=\sum_{i:t_i<t} s_i$.

Usually, three types of distributions for *S* are considered:

1) the Pareto distribution of *S* corresponds to the case where the magnitude distribution follows the G-R (F-M) law, i.e. the exponential distribution; the pdf is

$$\xi\left(s\right)=\frac{k-1}{S_o}\left(\frac{s}{S_o}\right)^{-k}; \qquad s\geq S_o,\ k>1,$$

where *k* is lined with the G-R *b*-value by $k=\frac{4}{3}b+1$.

2) The truncated (or bounded) Pareto distribution corresponds to the case where the magnitude distribution follows the truncated G-R law, with PDF

$$\xi\left(s\right)=\frac{k-1}{S_0\left[1-\left(\frac{S_u}{S_0}\right)\right]}\left(\frac{s}{S_0}\right)^{-k}; \qquad S_o\leq s\leq S_u,$$

where Su and S0 are the upper and lower thresholds respectively.

3) The tapered Pareto distribution or also called the Kagan distribution has a CDF

$$\Xi\left(s\right)=1-\left(\frac{s}{S_0}\right)^{k-1}\exp\left(\frac{S_0-s}{S_c}\right), \qquad S_o\leq s\leq\infty$$

and a density

$$\xi(s)=\left(\frac{k-1}{s}+\frac{1}{S_c}\right)\left(\frac{s}{S_0}\right)^{k-1}\exp\left(\frac{S_0-s}{S_c}\right), \qquad S_o \leq s<\infty$$

where Sc is a parameter governing the strength of the exponential taper affecting frequency of large events.

Linked stress release model

The SRM has been applied to the statistical analysis of several historical earthquake catalogs from various areas (Vere-Jones and Deng, 1988; Zheng and Vere-Jones, 1991, 1994). A noteworthy observation from the above studies was that significant earthquakes where followed by large events in longer distances (far-field) than the immediate aftershock zone. These observations have led to more recent studies which are focusing on non-linear aspects of earthquake dynamics.

Obviously, stress transfer and interaction cannot be considered in the simple stress release model, and the earlier analyses concentrated on dealing with regional differences. Zheng & VereJones (1994) found that large geographical regions give better fits to the stress release model when broken down into subunits, and further noted some hints of clustering relating to some form of action at a distance, i.e. stress transfer and interaction. Although Zheng & Vere-Jones (1991) investigated various multivariate extensions to the model, the natural and elegant extension that we shall next outline was not considered until Shi et al. (1998) and Liu et al. (1998). The evolution of stress $X_i(t)$ in the i^{th} region can be rewritten as $X_i(t)=X_i(0)+\sum\theta_{ij}S^{(j)}(t)$

where $S_{(j)}(t)$ is the accumulated stress release in region *j* over the period (0, t), and the coefficient θ_{ij} measures the fixed proportion of stress drop initiated in region j which is transferred to region *i*. Here, θ_{ij} may be positive or negative, resulting in damping or excitation, respectively. It is convenient, in dealing with a declustered catalogue (i.e. with aftershocks removed), to set θ_{ij} = 1 for all i. The new version we shall call a linked (or coupled) stress release model (LSRM).

If θ_{ij} = 0 for all i = j, the model is reduced to an independent aggregation of simple forms as in eq. (1). Liu et al, (1999) use a slightly different form, replacing $S_{(j)}(t)$ by $S_i^{(j)}(t)=S^{(j)}\left\{\max\left[t_k^{(i)}:\mathrm{t}_k^{(i)}<1\right]\right\}$

where $\{t^{(i)}_k\}$ are the occurrence times in region i. Thus, events in other regions j have no transfer effect on region i until the occurrence of a subsequent event in region i. In a

somewhat similar fashion and in order to reduce periodic-type behavior, Imoto et al. (1999) introduce a time delay into the transfer by replacing $S_{(j)}(t)$ by $S_D^{(j)}(t) = S^{(j)}(t - t_d)$

The LSRM has been proposed for the analysis of spatial interaction of earthquake occurrences through stress transfer within large area of Earth's crust. It has also served as a basis for a stochastic model of aftershocks (Borovkov & Bebbington 2003). Having one 'region' generate mainshocks, and second generating aftershocks, reproduced the result of Dieterich (1994) for the aftershock decay rate, with the additional property that, as with the stress release model generally, the parameters could be fitted statistically to the data.

The sensitivity of the model to regionalization, magnitude errors, catalogue incompleteness, catalogue size and declustering/magnitude cut-off is then considered in detail with reference to data from north China. The latter data were also used to illustrate the model evaluation techniques introduced earlier. In more recent studies (Mangira et al., 2017; Mangira et al., 2018) application of LSRM and restricted LSRM were used to model the earthquake occurrence of moderate earthquakes ($M \geq 5.2$) in the Corinth Gulf and Central Ionian Islands (Greece).

b) Temporal / Spatiotemporal clustering models

Seismicity is considered to be clustered in space and time. Clusters of earthquakes are commonly addressed in terms of swarms incorporating the concepts of foreshocks and aftershock sequences that are highly related to a mainshock of large magnitude (Cho et al, 2010). The above terms lack of precise definition and often are used loosely in a large number of studies. The occurrence of aftershocks in close spatial and temporal proximity (short –field and short – term period) is commonly due to local static and dynamic stress changes induced by another earthquake (main shock). However, some aftershocks may occur at very large distances (far-field) beyond the influence of static stress changes from the main shock. These events are more likely to be triggered by transient dynamic stresses generated by a main shock, and for this reason they are often referred to as remotely triggered earthquakes (Gomberg, et al. 2011; Peng et al, 2010; Brodsky, 2006; Prejan et al., 2004, Brodsky et al., 2000).

Aftershock Properties

Before proceeding to the description of some of the widely used temporal-spatiotemporal seismicity models, we make a short note on the aftershock properties. It is well known

that the magnitude, the duration and the spatial distribution of aftershocks strongly depends on the magnitude of the main shock. In several studies of aftershock time-space dependence it has been found that the properties of aftershock sequences generally conform to four fundamental empirical models:

a) **G-R relationship**: the Frequency – Magnitude (F-M) distributions of aftershocks follows the G-R relationship which implies that the frequency of aftershock occurrence diminishes by about a factor 10 for each progressively higher magnitude unit.

b) **Bath's Law**: correspondingly the average difference between the main shock magnitude and its largest aftershock is about 1.2 magnitude units, independent of the magnitude of the main shock;

(c) **Omori's law**: aftershock frequency decays temporally according to Omori‟s law, which states that frequency decreases in proportion to the reciprocal of the time since the mainshock;

(d) aftershock geographic density decreases in proportion to the reciprocal of distance from the mainshock (Felzer and Brodsky, 2006; Marsan and Lengline, 2010). That is, aftershocks are most common immediately after and in the immediate vicinity of the main shock.

Although G-R law describes the distribution of the expected number of earthquakes with respect to magnitude, there is no constraint on when earthquakes of different magnitudes occur. Earthquake magnitudes are therefore distributed randomly throughout the aftershock sequence and large aftershocks are equally likely late in the aftershock sequence as they are early in the sequence. In addition, the ordered occurrence of aftershocks with passing time from the mainshock only differs from mainshock earthquakes in that we expect them to occur (Hough and Jones, 1997).

A number of short – term statistical seismicity models have been developed in the last century. Among them are the widely used Omori-Utsu formula and the Epidemic Type Aftershock Sequence (ETAS) model, which emphasize the evolutionary nature of a developing earthquake cluster. Herein we give a brief description of the two models without the spatial component, i.e. assuming that the spatial area is sufficiently small so that any given event can conceivably interact with all following events, regardless of their spatial locations.

Omori-Utsu

Almost one hundred years ago Omori (1894a, b) proposed a formula to represent the decay of aftershock activity with time. This formula and its modified version have been extensively used as one well - established empirical laws in seismology. This law is unique for its power law dependence on time which implies the long-lived nature of activity in contrast to the exponential function appearing in most decay laws in physics.

The equation that describes the number of aftershocks occurring each day is the following:

$$n(t) = K\,(t + c)^{-1}$$

where t is the time from the occurrence of the mainshock, K and c are constants.
In 1957 Utsu postulated that the decay of the aftershock numbers could vary, and he modified the Omori formula as follows: $n(t) = K(t + c)^{-p}$

The above formula yielded better fitting results and from then on it is called the modified Omori-Utsu law. In the study of Utsu et al. (1995), where approx. 200 aftershock sequences are reviewed, p-value varies from 0.5 to 2.6; however, there was no clear relationship between mainshock magnitude and p-values.

In the context of statistical seismology, we usually make use of (1.2) in the form of a conditional intensity function, given by $\lambda(t) = \dfrac{K}{(t+c)^{p}}$

When the magnitude distribution of the aftershocks is also considered, the conditional intensity for the full model is written as $\lambda(t,m) = \dfrac{Ks(m)}{(t+c)^{p}}$

where *s(m)* is the magnitude probability density function and usually takes the form of the Gutenberg-Richter magnitude-frequency relation. This model has been used by Reasenberg and Jones for forecasting aftershock activity (see, e.g., Reasenberg and Jones 1989, 1994). Therefore, some researchers also call the Reasenberg-Jones model.

The typical aftershock decay is represented by the Modified Omori function. This formula remains the most widely used model for typical aftershock rate decay. Typically, the Modified Omori formula holds for quite a long period in the order of some tens of years or more, depending on the background seismicity rate in the neighboring area (Utsu et al.,1995; Ogata & Shimazaki, 1984). As we consider small aftershocks, however,

occurrence time clustering of the events within the sequence becomes apparent. Thus, aftershock activity is not always best predicted by the single Modified Omori function, especially when it includes conspicuous secondary aftershock activities of large aftershocks (Guo and Ogata, 1997; Ogata et al., 2003a). Indeed, cascading complex features of aftershocks such as interactively triggered aftershocks including those among off-fault regions, are often observed (Felzer et al., 2002).

Epidemic Type aftershock sequence (ETAS)

The Epidemic Type Aftershock Sequence model (ETAS) originally proposed by Ogata (1988; 1992) entails the parameters of time and space, thus it is not a pure temporal model and it is often described as a spatiotemporal model.

As was mentioned above it is well known that numerous aftershocks follow after the occurrence of a large earthquake. Forecasting the aftershock activity is considered to be a scientific challenge of great importance for reducing the seismic risks. In the past two decades there has been a significant development in probabilistic earthquake forecast (Reasenberg and Jones, 1989; Kagan and Jackson, 2000; Helmstetter et al., 2006); however there is a number of primary difficulties to suit the forecast model to each aftershock sequence at its early stage (Ogata, 1983; Utsu et al., 1995; Enescu et al., 2007). As a result a number of studies have used the data from a period prior to main shock in order to estimate the forecast model (Marzocchi and Lombardi, 2009; Nanjo et al., 2012; Marzocchi et al., 2012). Such an approach possibly makes biased prediction, considering significant diversity of statistical properties of an aftershock sequence. Hence, the forecast model should be optimized somehow based on the available data of an ongoing aftershock sequence. Therefore, sensible and robust estimation of the forecast model based on an early aftershock sequence is strongly required. The Omori – Utsu (O-U) aftershock decay formula is the simplest model which can be applied in forecasting aftershock activity; however, the O-U formula is not always appropriate, especially as data increases in a longer period, because an aftershock sequence generally features hierarchical cascading such as the secondary aftershocks, third-order aftershocks, and so on. Even though possible triggering events could be determined through residual analysis, separating triggering quakes has proved to be a complicated procedure. For this purpose, Ogata (1988) generalized the O-U model by overcoming the distinction between triggering and other events; in other words, he proposed that each event, irrespectively of its magnitude size can in principle trigger its own offspring. This generalized model which represents the natural extension of the O-U formula is widely

known as the Epidemic Type Aftershock Sequence (ETAS) model and is one of the earliest point-process models created for clustered events. Ogata named the model based on an analogy with the spread of epidemics.

In terms of temporal conditional intensity, the ETAS model can be defined as (Zhuang et al., 2012): $\lambda(t,m) = s(m)\left[\mu + \sum_{i:t_i<t} \kappa(m_i)\, g(t-t_i)\right]$

where $s(m) = \beta e^{-\beta(m-m_0)}, m \geq m_0$ is the PDF form of the G-R relation, m_0 the magnitude threshold, $\kappa(m) = \mathrm{A}\exp\left[\alpha\left(m-m_0\right)\right]$ is the mean number of events directly triggered by an event of magnitude m and $g(u) = (p-1)(1 + t/c)^{-p}/c$ is the probability density function (PDF.) of the time difference between the parent event and its children, i.e., the PDF form of the O-U formula.

In data analysis an important condition that justifies whether estimated parameters are reliable or irrational and is essential for the stability of the ETAS model, is that the process must be subcritical. A supercritical system specified by model parameters may lead to overestimates of seismicity risks especially on long-term conditions. In general, the stability of the ETAS model or more general branching models is closely related to such concepts as criticality (see details in Section 1.3) and branching ratio.

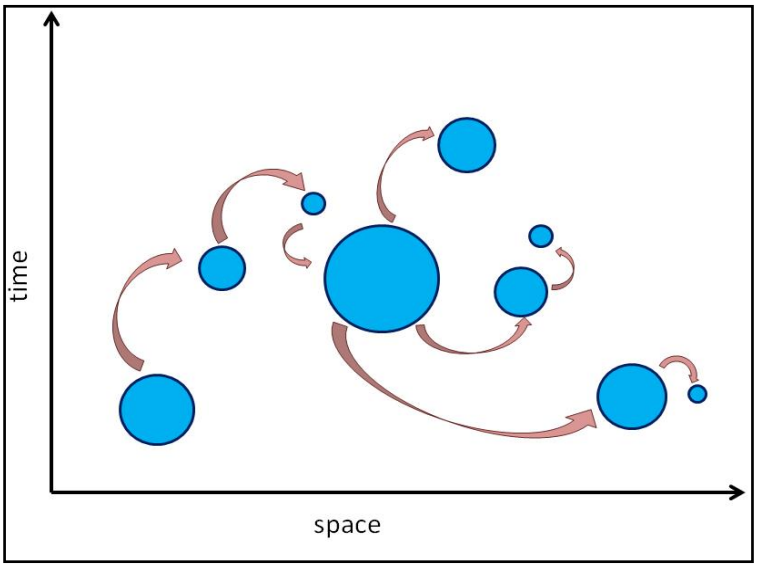

Figure 1.5 Schematic illustration of the triggering effect based on the ETAS model basic concept

From a spatiotemporal point of view there have not been many models to describe seismicity. The basic reason is the complicated and heavy numerical computations during the implementation. The spatiotemporal ETAS model has been extensively studied in the context of marked branching properties with immigration and although it is based on empirical statistical laws, it is suggested as the best model especially for describing short-term seismicity (Console et al., 2007; Iwata, 2010).

Initially, space –time diffusion clustering where used to analyze seismicity (Musmeci & Vere-Jones, 1992). The conditional intensity of these kind of models have the common form:

$$\lambda(t,x,y) = \mu(x,y) + \sum_{i:t_{i<t}} g_\phi\left(t-t_i, x-x_i, y-y_i, m_i\right),$$

where $g_\phi\left(t,x,y,m\right) = A\frac{e^{am_i e^{-ct}}}{2\pi\sigma_x\sigma_y t}\exp\left\{-\frac{1}{2t}\left(\frac{x^2}{\sigma_x{}^2}+\frac{y^2}{\sigma_y{}^2}\right)\right\}$ and ***A, α, σ_x, σ_y*** are constants.

Ogata (1998) generalized the temporal ETAS model to spatiotemporal model which had the same general form with Eq.2, but different definition of g_ϕ which was defined as:

$$g_\phi\left(t,x,y,m\right) = \kappa(m)g(t)\,f\,(x,y\,|\,m)$$

Where ***k(m)*** is the expected number of aftershocks generated from a main shock of magnitude *m*, ***g(t)*** is probability density function of the lagged time distribution of aftershocks and ***f(x, y| m***) is the density function of the aftershock locations from a main shock at the origin with magnitude *m.*

Outline of the common forms of ETAS models:

1. The ETAS model assumes that each primary aftershock (parent event) may trigger its own secondary aftershocks (offspring or child event) based on the same law, the secondary aftershocks may trigger their own and so on, creating a cascading effect. This way each event produces its own offspring events independently of the others.

2. The expected number of direct offspring events is assumed to depend on the magnitude m of the parent event and is expressed by the member $\kappa(m)$ of Eq. 5 which is called productivity[1].

3. The occurrence rate of background events in the branching process is assumed to be a function of space and magnitude while it is independent of time.

4. Based on the probability distribution of time that functions as a time lag until the occurrence of the child event and its independence of magnitude, the pdf of time is assumed to have the following expression: $g(t|\tau) = g(t-\tau)$, where τ is the occurrence time of the parent event and t is the occurrence time of the child event.

5. The probability distribution of location (ψ,ω) and magnitude (m) of the parent event and the correspondingly the probability distribution of location (x,y) and magnitude M of the child event are strongly dependent, while the pdfs are expressed as $f(x-\psi, y-\omega|M)$ and $s(m|M)$ respectively.

6. The magnitudes of all the events, including background events and their child events, are independent random variables drawn from the same $s(m)$.

Based on the above assumptions the conditional intensity for the spatiotemporal ETAS model can be expressed as :

$$\lambda(t,x,y,m) = s(m)\left[\mu(x,y) + \sum_{\{k:t_k<t\}} \kappa(m_k)\, g(t-t_k)\, f(x-x_k, y-y_k; m_k)\right]$$

In the above equation, $\mu(x,y)$ is the background intensity function, which is assumed to be independent of time. The functions $g(t)$, $f(x,y;m_k)$ and $s(m)$ are respectively the normalized response functions (i.e., probability density functions) of the occurrence time, the location, the magnitude of an offspring from an ancestor of magnitude m_k.

The ETAS model uses three empirical laws as direct inputs (Gutenberg-Richter law, Omori's law and aftershock productivity law). In the ETAS model, a main event of magnitude m triggers its own primary aftershocks (considered as point processes)

according to the following distribution in time and space

$$\phi_m(r,t)\,drdt = K10^{a_u m}\frac{\theta c^{\theta}dt}{(t+c)^{1+\theta}}\frac{\mu d^{\mu}dr}{(r+d)^{1+\mu}}$$

where *r* is the spatial distance to the main event. The spatial regularization distance d accounts for the finite rupture size. The power law kernel in space with exponent μ quantifies the fact that the distribution of distances between pairs of events is well described by a power-law.

ETAS model represents the seismicity as a nonstationary Poisson process in which the instantaneous rate, or intensity, is modulated by the past of the process itself, and perhaps of other processes evolving with it. Such a representation opens up a route both to incorporating at least rudimentary physical ideas, and to fitting, testing and simulating the models.

Other spatiotemporal models

Many spatiotemporal seismicity models such as EEPAS (Every Earthquake is a Precursor According to Scale, Rhoades and Evison 2004) model, BASS (Branching Aftershock Sequence) model and the double branching models (Marzocchi and Lombardi 2008) have aspects in common with the ETAS model, i.e., using the ETAS model as the standard clustering component.

i) Every Earthquake is a Precursor According to scale model (EEPAS)

The EEPAS (Every Earthquake a Precursor According to Scale) model (Rhoades and Evison, 2004, 2005) is a space–time model of earthquake occurrence that incorporates many aspects of scale-invariance. It is constructed around the phenomenon of the precursory scale increase (**Ψ**), an increase in the rate and magnitude of seismicity that has been retrospectively recognized to occur as a long-term precursor of earthquakes from several seismically active areas such as California, New Zealand, Italy, Greece, NW Turkey, and northern Mexico.

The basic features of the Ψ-precursory are the magnitude M_P of the largest precursory earthquakes, the time T_P between the onset and the major earthquake, and the area A_P occupied by the precursor, mainshock and aftershocks all scale with mainshock magnitude M_m. Hence M_P could in principle be used to predict the major earthquake via linear regressions of M_m, logT_P and logA_P on M_P, provided that the Ψ –phenomenon could be recognized in advance of the major earthquake. In the EEPAS model, the problem of

recognizing the Ψ -phenomenon in advance is set aside, and every earthquake is treated as a precursor, according to scale, of larger earthquakes to follow it in the long term.

In the EEPAS model, the rate intensity *λ (t, m, x, y)* of an earthquake is defined for any time *t*, magnitude *m* and location (*x, y*) with *m* above a magnitude threshold *mc*, and x, y is a point in a region of surveillance R. Each earthquake *(t, m, x, y)* contributes a transient increment *λ (t, m, x, y* to the future rate density in its vicinity, given by $\lambda_i(t,m,x,y) = w_i f1_i(t) g1_i(m) h1_i(x,y)$

where w_i is a weighting factor that may depend on other earthquakes in the vicinity, and $f1_i$; $g1_i$ and $h1_i$ are densities of the probability distributions for time, magnitude and location, respectively. The total rate density is obtained by summing over all past occurrences and including a term that allows for the possibility of earthquakes occurring without precursors, as follows: $\lambda_i(t,m,x,y) = \mu\lambda_0(t,m,x,y) + \sum_{t_i \geq t_0} \eta(mi)\lambda_i(t,m,x,y)$

where λ_0 is a baseline rate density (which also takes the role of a null hypothesis) such as that of the stationary Poisson model, t_0 is the time of the beginning of the catalogue, μ is a parameter and η a function of magnitude. The parameter μ can be interpreted as the failure-to predict rate, i.e., the proportion of earthquakes that occur without an appreciable sequence of precursory shocks.

ii) Proximity to Past Earthquakes (PPE)

The PPE model was initially formulated by Jackson and Kagan (1999) and named by Rhoades and Evison (2004). It is a Poisson model with a specific method of estimating the seismicity rate, i.e., it is a smoothed seismicity baseline model. It can play the role of a spatially varying reference model against which the performance of time varying models can be compared. For this reason, it is adopted in this study as the reference model. The Relative Intensity (RI) model by Nanjo (2010, 2011) and the Simple Smoothed Seismicity (Triple-S) model by Zechar and Jordan (2010), also belong to this category, the only difference being how the seismicity rate is estimated. The PPE model is used as a forward likelihood method to estimate the seismicity rate function (see also Chiodi and Adelfio, 2011), i.e., it has a conditional intensity (seismicity rate) of the form

$$\lambda_i(t,x,y,m) = \frac{s(m)}{t-t_0} \sum_{t_i<t} \left(\frac{a}{d^2 + (x-xi)^2 + (y-yi)^2} + \varepsilon \right), \qquad m \geq m_c$$

where *i* includes all events before *t* (possibly including events outside the study region), *t0* is the starting time, *α*, *d*, and *ε* are model parameters, and *s*(*m*) represents the p.d.f. form of the G-R magnitude-frequency relation for earthquake magnitudes larger than the magnitude threshold *m*c, i.e., $s(m) = \beta e^{-\beta(m-m_c)}$, $m \geq m_c$

with β linked to the b-value by β= b ln 10. Such a formulation enables us to maximize the likelihood estimate of the seismicity rate. Given an earthquake catalog, which is recorded as a list in the form *{(ti, xi , yi, mi) : i = 1, · · · , N* } from spatial region S and time interval [0, T], the likelihood has the standard form (see, e.g., Ogata, 1988; Daley and Vere-Jones, 2003; Zhuang et al., 2012)

iii) Branching Aftershock Sequence Model (BASS)

The BASS model is an alternative to the ETAS model. It recognizes that each earthquake is associated with a sequence of aftershocks. In this way each main shock produces a sequence of primary aftershocks, each of these aftershocks, in turn, produces second-order aftershocks and so forth. Statistically, a primary aftershock can be larger than the initial main shock. In this case the initial main shock becomes a foreshock, and the larger primary aftershock becomes the main shock of the sequence. In principal, a higher-order aftershock could be the main shock. The probability of this occurring, however, is extremely small. The BASS formulation comprises some of the common forms of an ETAS–based spatiotemporal model. In particular:

a) The F-M distribution of each order of aftershocks satisfies the G-R relation as follows:

$$\log 10\left[N_d(\geq m_d)\right] = a_d - b_d m_d$$

where m_d is the magnitude of a child event, $N_d(\geq m_d)$ is the number of child events with magnitudes greater than or equal to m_d, and a_d and b_d are the *a* and *b*-values of the distribution, respectively, with b_d for each sequence not necessarily equal to the b-value of all aftershocks, due to the superposition of many generations of aftershock sequences for each parent earthquake. Modifications by Scherbakov & Turcotte (2004) and Holliday et al., (2008) led to the form:

$$N_{dT} = N\left(\geq m_{\min}\right) = 10^{b_d\left(m_p - \Delta m^* - m_{\min}\right)}$$

where *Δm** is a fixed value with *m* less than the *m* of parent event. The above relation is the essential feature of the BASS model. Respectively the CBA P_{Cm} for the magnitudes of the child events is: $P_{Cm}(m_d > m_p) = 10^{-b_d \Delta m^*}$

b) For the time occurrence of child events, the model satisfies a general form of Omori's law (Shcherbakov et al., 2004): $R(t_d) = \frac{dN_d}{dt} = \frac{1}{\tau(1+t_d/c)^p}$

where $R(t_d)$ is the rate of aftershock occurrence, t_d is the time delay and p, c, τ are the parameters. The number of child events that occur after the time t_d is: $N_d(\geq t_d) = \int_{t_d}^{\infty} \frac{dN_d}{dt} = \frac{c}{\tau(p-1)(1+t_d/c)^{p-1}}$

When t_d=0 → $N_{dT} = \frac{c}{\tau(p-1)}$ (total number of child events). Accordingly, the CDF for time occurrences is $P_{Ct} = \frac{N_d(\geq t_d)}{N_{dT}} = \frac{1}{(1+t_d/c)^{p-1}}$. For 0<$P_{Ct}$<1 →$t_d = c(P_{Ct}^{-1/(p-1)} - 1)$

c) The location of each child event is specified relatively to its parent event. A power law dependence of the radial position in direct analogy to Omori's law is assumed (Felzer & Brodsky, 2006). Based on this the CDF for the radial distance is:

$$P_{Cr} = \frac{N_d(\geq r_d)}{N_{dT}} = \frac{1}{(1+r_d/(d\times 10^{0.5m_p}))^{q-1}}$$

The primary difference of the ETAS and BASS models is the way in which the number of child events is specified. The ETAS model incorporates in its formula two constants a and k which must be specified. The BASS formulation utilizes the modified form of Bath's law while the general ETAS formula does not satisfy Bath's law. In terms of time and locations of child earthquakes the two models are based on the same formulations (Omori's law and radiation positions).

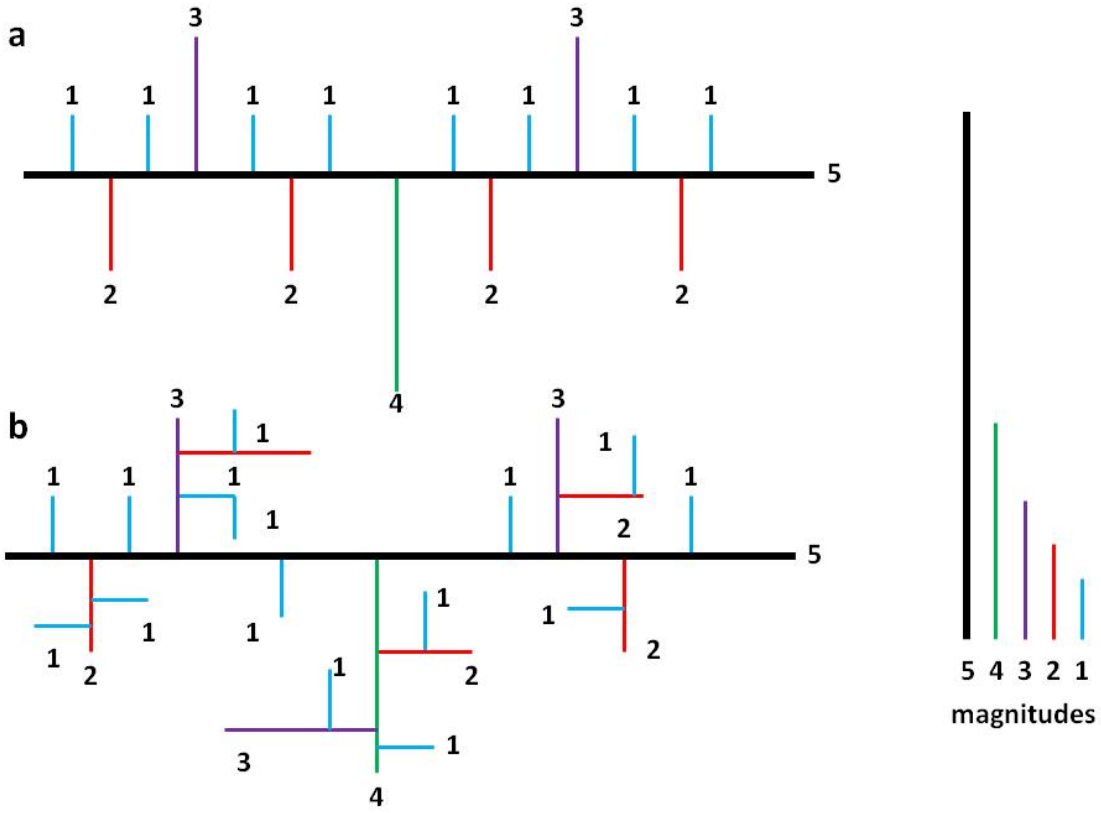

Figure 1.6 Illustration of the BASS model (after Holliday et al., 2008): a) The primary family of aftershocks is a generator for the fractal construction; b) the structure of side-branching aftershocks.

iv) Short Term Earthquake Probability Model (STEP)

The "Short – Term Earthquake Probability" or STEP model produced by USGS is a relatively simple method of predicting the rate of aftershock production based on empirical statistical parameters of aftershock distribution in California. This method is a "one-generation" aftershock model, meaning that aftershocks are not allowed to produce their own aftershock sequences as in the ETAS model described later in the paper, and the sequence is assumed to be independent of any seismicity prior to the mainshock. The STEP model is also not specific to the times, locations and magnitudes of aftershocks as they occur. Empirical coefficients of the Gutenberg-Richter magnitude-frequency relationship, Omori's time-decay law, and the distance-decay relationship have been calibrated to California region, although the general method can be applied to other regions by using appropriate region-specific parameters.

1.2.3 MARKOV Models

Stochastic earthquake occurrence models can be divided to memoryless (Poissonian) and the ones with memory. One of the most known stochastic models with memory. One of the well-known models with memory is the Markov chain which describes the dependency between observations collected in successive time intervals. The Markovian property predicts that in aprocess with a series of known past states, the next state depends only on the current state of the process but not on the previous ones.

Markov models have been employed since the late 80's (Anagnos and Kiremidjian, 1988). There are many applications of Markov models on seismicity problems such as seismic hazard assessment. In their study, Tsapanos and Papadopoulou (1999) applied a discrete-time Markov model for earthquake occurrences, in one of the most seismically active regions of the world, the area of Alaska and Aleutian Islands. Another example is the study of Herrera et al., (2006) who compared the application of direct and *mixed Markov chain* method to the area of Japan for probablities of occurrence of a system state for $M \geq MM\ r$ on the basis of the observed state for $M \geq M^m_r$ in the previous Δt. Ünal et al., (2011), also applied direct Markov chain to estimate risk hazaed in the area ofTurkey. An extension of Markov and renewal models, the semi-Markov model (SMM), allows the consideration of dependencies on both the magnitude and the elapsed time of the last event. In a more recent development Votsi et al., (2012) introduced a Markov model extension, i.e. a semi-Markov model (SMM) in continuous time for the description of seismicity patterns in time domain in the Northern Aegean Sea (Greece); Panorias et al., (2016) applied SMM to study the earthquake occurrences in Japan finding model's limiting behaviour for which is sufficient an interval of time of seven years.In a more recent development Pertsinidou et al., (2017) applied a SMM to study the seismicity of the central Ionian Islands in terms of the occurrence probabilities and found that the time window obtained the time windows obtained by the destination probabilities include 72.9% of the observed earthquake occurrence times (for all M) and 71.4% for $M \geq 6.0$.

In recent years, a few applications of Hidden Markov Models (HMM) on earthquake problems have also been published. Similarly, to Markov chains, HMM consist of a set of states, a set of initial probabilities and a transition probability matrix although in this case the state is unobserved. In addition, each state in HMM is associated with a probability distribution to which the unobserved state refers. An application of Poisson hidden Markov Models revealed changes in seismicity rate in Ionian Sea, while also used for

identifying the unobservable stress level controlling the evolution of the strong seismicity (M ≥ 6.5) in Greece and the broader area (Orfanogiannaki et al., 2010; Votsi et al., 2013; 2014). Petsinidou et al., (2017) applied hidden semi-Markov models (HSMMs) for strong (M ≥ 5.5) earthquake occurrence in the areas of North and South Aegean Sea, considering that the real stress field in an area associated with earthquake generation which cannot be directly observed, constitutes the hidden process. The optimal HSMM provided an alarm period for 70 out of 88 events.

Finally, Bountzis et al., (2018), applied Markovian Arrival Process as a candidate model to describe the time-varying earthquake activity in Corinth Gulf in Greece and demonstrate a high index of burstiness for the earthquake generation i.e. long quiescent periods alternate with short ones of intense seismic activity in the eastern part of the Gulf.

1.3 THE CONCEPT OF SELF ORGANISED CIRITICALITY (SOC)

When Bak, Tang and Wiesenfeld introduced in 1987 the concept of Self-Organized Criticality (SOC) it worked as an attempt to explain an unexpected observation of scale invariance and link the multitude of complex phenomena observed in nature to physical laws and / or one underlying process. It was the basis of a theory of the internal interactions of large systems. Specifically, the concept of SOC stated that large interactive systems will self-organize into a critical state. In this state small perturbations result in chain reactions, which can affect any number of elements within the system.

The history of SOC revolves around a significant number of computer models, many of which are not intended to model much except themselves in the hope that they display a certain aspect of SOC in a particularly clear way (Gisiger et al., 2001). Therefore the term SOC shall be used in its original meaning (Bak et al., 1987) to be assigned to systems: a behaviour that could appose to a phase transition in which there is a singular critical point where the system experiences a breakdown of symmetry and long – range spatial and temporal correlations in non-equilibrium can be generally summarized as (power law) scaling (Widom, 1965; Stanley, 1971). A paradigmatic example is the *Ising model*[4], a two-dimensional square – lattice model for ferromagnetism which displays scaling only at a certain temperature, the value of which depends on the size of the lattice (Fig.1.7).

Of course, in many systems which exhibit critical phenomena, there exist adjustable parameters which have to be finely tuned in order for the system to reach the critical point. In the Ising model, one needs to adjust both two essential parameters in order to achieve critical behavior: the temperature and the external magnetic field values. If the system is initially prepared such that the temperature and the external magnetic field are far from their critical values, the system will not show critical behavior even if other parameters

[4], A mathematical model of ferromagnetism in statistical mechanics, named after the physicist Ernst Ising. The model consists of discrete variables that represent magnetic dipole moments of atomic *spins* that can be in one of two states (+1 or −1). The spins are arranged in a graph, usually a lattice, allowing each spin to interact with its neighbors. The model allows the identification of phase transitions, as a simplified model of reality. The two-dimensional square-lattice Ising model is one of the simplest statistical models to show a phase transition. This type of model, as derived from the Burridge and Knopoff (1967) model, is a direct one, where the initial conditions are given, as well as the transition rules (which depends on the control parameter), and it is iterated several times for analyzing its behavior. The parameters of interest (magnetization, for example) are calculated as averages (macroscopic magnitudes), and the particular state of the cell in each time is not important, but the properties of the whole system are of interest. They have been used to successfully describe the macroscopic behavior of the seismicity, such as the Gutenberg-Richter law, the temporal and spatial clustering of the hypocenters (Carlson and Langer, 1989b, a, Christensen and Olami, 1992; Nakanishi, 1990, 1991; Olami et al., 1992; Otsuka, 1972; Bak and Tang, 1989; Bak et al., 1988; Barriere and Turcotte, 1991; Rundle, 1988; Rundle et al., 2002).

are changed, or if the system is perturbed. Since most systems with phase transitions exhibit the above behavior, it would seem reasonable to guess that critical phenomena can be triggered only if all relevant parameters have been fine tuned.

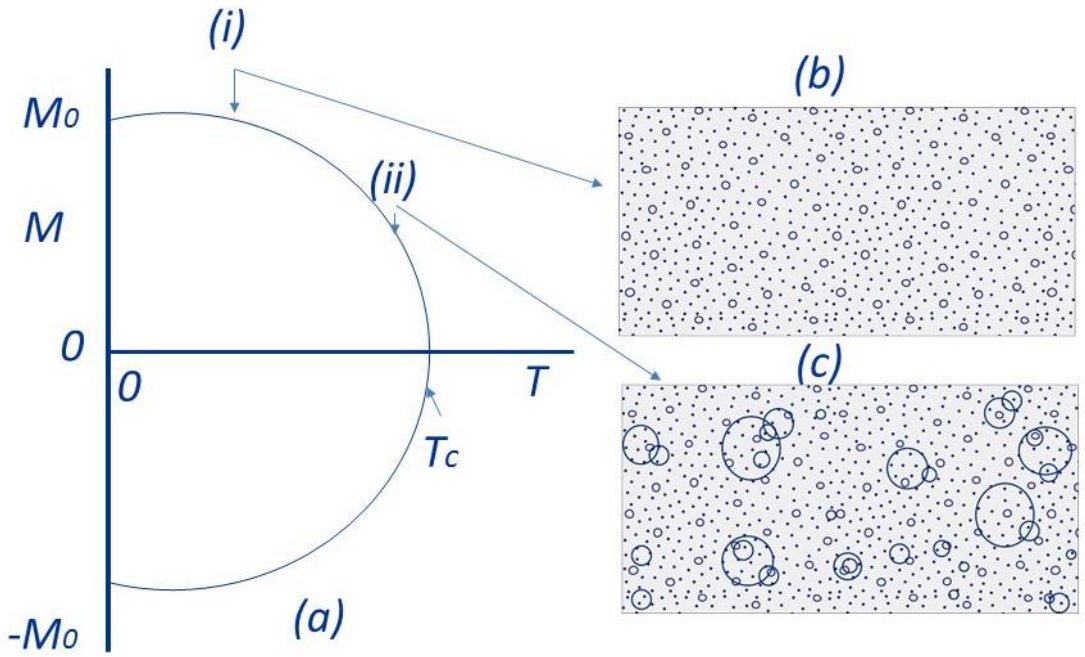

Figure 1.7 a) Dependence of the magnetic moment *M* on temperature *T* for the Ising model; **(b)** Exponential frequency-area distribution of patches of negative magnetization at point (i) in (a); **(c)** Power-law frequency area distribution of patches of negative magnetization at point (ii) in (a) as the second-order critical point at $T=T_c$ is approached (from Rundle et al , 2000).

1.3.1 The BTW Model

Bak et al., (1987) found a simple model which seemed to develop into a non-trivial scale invariant state, displaying long – range spatiotemporal interactions and self-similarity without the need of fine tuning the control parameter to critical value. The so called BTW model or also known as the *sandpile model* contained the hypothesis that, systems consisting of many interacting constituents may exhibit some general characteristic behavior. In particular, under very general conditions, dynamical systems organize themselves into a state with a complex but rather general structure. The systems are complex in the sense that no single characteristic event size exists (there is not just one time and one length scale that controls the temporal evolution of these systems). Although the dynamical response of the systems is complex, the simplifying aspect is that the statistical properties are described by simple power laws. Moreover, some of the

exponents may be identical for systems that appear to be different from a microscopic perspective.

The BTW model displayed spatial and temporal power laws and scale invariance, without controlling the external parameters. In this model the sand is slowly dropped onto a surface, forming a pile. As the pile grows, avalanches occur, which carry sand from the top to the bottom of the pile. The slope of the pile becomes independent of the rate at which the system is driven by dropping sand. The system evolves in a way that it spontaneously moves towards a critical point (critical slope). Because of this, the critical behavior exhibited by this model was termed as self-organized criticality.

1.3.2. Basic design elements of a SOC model

Phenomena in very diverse fields of science soon have been claimed to exhibit SOC behavior, such us earthquakes, forest fires, electric breakdown, motion of magnetic flux lines in superconductors, water droplets on surfaces, dynamics of magnetic domains, and growing interfaces, economics, as well as in biological evolution. In all cases, the basic design elements of a SOC model can be summarized as follows:

Many interacting degrees of freedom: Complex systems are characterized by many degrees of freedom. Sites for which the local degree of freedom is below a certain threshold are said to be stable, those for which the local degree of freedom is above the threshold are called active or unstable.

A local energy or force is required to "trigger" the model - A slow external drive and thresholds triggering*:* The models are subjected to an external drive/ driving which changes/charges the local variables, continuously or discretely everywhere or at one particular point (*point driving* or *boundary driving*). The external driving plays two different roles: on the one hand it acts as a loading mechanism which allows the system to response strongly or sensitively to an external perturbation and on the other hand it acts like such a perturbation, triggering a potential large response. Once the external charges trigger the threshold interaction occurs which leads the threshold being triggered at neighboring sites.

A fast-internal relaxation mechanism giving rise to "avalanching": The relaxation process is defined by the microscopic dynamics following a set of update rules which specifies how degrees of freedom are updated as they interact. The totality of such interaction is called an "avalanche". Avalanching is the archetypical relaxation mechanism in SOC models and is often considered as the signature of metastability, i.e.

the system is not at the lowest energy state. Among all the metastable states some are of particular importance where the system is neither asymptotically stable nor unstable: it is marginally stable.

Scale invariance*:* Bak, Tang, and Wiesenfeld originally envisaged the marginally stable states as characterized *by the lack of any typical time or length scale*. This is precisely the case for the configurations of a thermodynamic system at the critical temperature. The lack of a typical scale leads to algebraic correlation functions. One finds, as anticipated, that the distribution functions describing the frequency with which various events occur in the SOC state exhibit *power laws*[5].

Universality*:* Universality is the observation made in the context of ordinary critical phenomena that certain universal quantities are independent of many details of a system. If SOC were generally to be found across a large class of systems, then universality would unify these systems and their internal interactions could be identified and studied. Hohenberg and Halperin (1977) were first to introduce universality in non- equilibrium systems, i.e. systems lacking detailed balance.

1.3.3. SOC and earthquakes

SOC applies to the class of phenomena occurring in driven out of equilibrium systems made of many interactive components, which possess the following fundamental properties: 1) a highly non-linear behavior, 2) a very slow driving rate, 3) a globally stationary regime, characterized by stationary statistical properties, and 4) power-law distributions of event sizes and fractal geometrical properties. According to Sornette & Sornette (1989) and Bak & Tang (1989), the crust obeys these four conditions; the above studies were the first to suggest the understanding of the spatio-temporal complexity of earthquakes in this perspective. For example, Sornette and Sornette (1989) was one of the first to suggest that the concept of self-organized criticality is particularly well suited for rationalizing observations on occurrences and magnitudes of earthquakes and explored the idea that, if earthquakes are the natural consequences of the stationary dynamical state of the crust submitted to steady increasing stresses, they also organize the crust in a self-consistent way.

[5] A common feature of a nonlinear dynamical process. It is a mathematical pattern in which the frequency of an occurrence of a given size is inversely proportionate to some power (n) of its size $y(x)=x^{-n}$ or it can be expressed in its "linear form": $log10(y)=-n*log10(x)$, where the coefficient *n* represents the fractal dimension. Power laws are an important tool to express self-similarity of large and small patterns, i.e. to unite different sizes and lengths within a system.

The expectation that earthquakes can be interpreted in terms of SOC has been a subject of observations and studies for many decades (Scholz 1990, 1991; Sornette 1991).

- The Gutenberg – Richter law for the distribution of energy release in earthquakes is found to follow a power law behaviour. If *E* is the energy released during an earthquake, then the probability for an earthquake of that size is given by $P(E) \sim E^{-B}$, where the exponent B exhibits some geographical dependence and is found to be in the interval from about 1.8 to 2.2.
- The morphology of the faults exhibits features characteristic of fractals.
- The temporal frequency of aftershocks following in the wake of a major earthquake decays with a power law known as the Omori law (Omori 1895).
- Earthquakes exhibit a broad range of responses, and their spatial and temporal behavior may best be described in terms of fractals and power laws. However, there appear to exist characteristic scales for earthquakes (Scholz 1990, 1991).

The Olami-Feder-Christensen (OFC) Model

One of the first models that was soon recognized to reproduce fundamental statistical properties of real earthquakes, the G-R law, the occurrence of large periodic events, as well as the occurrence of foreshocks and aftershocks according to Omori's law was the Olami-Feder-Christensen (OFC) model (Olami et al., 1992). In this context, it was also found that the foreshock and aftershock sequences of the model reproduce several further important statistical properties of real seismicity such as the increase of the number of foreshocks with the mainshock size and some kind of aftershock diffusion (Helmstetter et al., 2004).

The OFC model is based on the Burridge-Knopoff spring-block model (Burridge and Knopoff, 1967) and has been conjectured to be an example of self-organized criticality where local exchange dynamics are not conservative. It refers to a square lattice with N ×N blocks where each site is interconnected by springs with its four nearest neighbours and with a rigid driving plate moving at constant velocity (Figure 1.8). Through analogy with the Burridge-Knopoff model, what is being simulated is a fault, where one of the lattice's dimensions is the flaw depth and the other one follows the flaw.

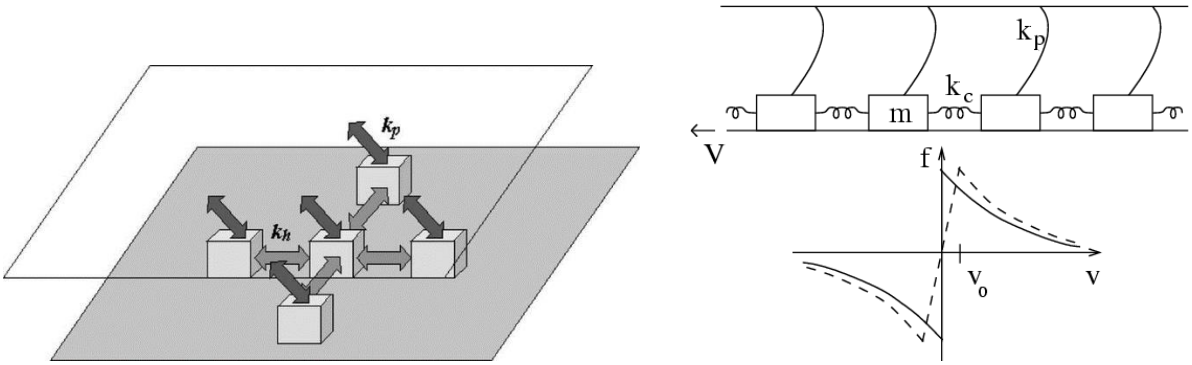

Figure 1.8 The OFC model: Let S be square lattice with N ×N sites and let $K_{mn} \geq 0$ be the tension at site (m,n). The sites with tension greater than 1 are called critical and go through a relaxation step where their tension spreads to their neighbours.

Despite the original claims of the authors and subsequent claims of other authors such as Lise & Paczuski (2000; 2001) whether or not the model is self-organized critical remains an open question. The emergence of criticality in the non-conservative regime has been debated from the very beginning (Olami et al., 1992; Grassberger, 1994; de Carvalho and Prado, 2000; Christensen et al., 2001; de Carvalho and Prado, 2001; Drossel, 2002; Miller and Boulter, 2002, 2003; Wissel and Drossel, 2006). A number of studies indicate that the SOC behavior of the model is destroyed upon introducing some small changes in the rules of the model from example replacing open boundary conditions with periodic boundary conditions (Pérez et al., 1996), introducing frozen noise in the local degree of dissipation (Mousseau, 1996) or in its threshold value (Jánosi and Kertész, 1993), including lattice defects (Ceva, 1995). Despite these findings as well as others which show, that it is insufficient to account for certain aspects of the spatiotemporal clustering of seismicity (Peixoto and Davidsen, 2008), the OFC model appears to show many features found in real earthquakes including temporal correlations between foreshocks, aftershocks and asperity events. As far as earthquake predictability (Pepke and Carlson, 1994) or Omori's law (Helmstetter et al., 2004; Hergarten and Neugebauer, 2002) is concerned, the OFC models appear to be closer to reality than others (Wissel and Drossel, 2006).

The analysis on the dissipative OFC model on a small world topology considering avalanche (earthquake) size differences performed by Caruso et al (2007) showed that when criticality appears, the probability density functions for the avalanche (earthquake) size differences at different times where characterized by fat tails with a *q*-Gaussian shape. This behaviour did not depend on the time interval adopted and was also found

when considering energy differences between real earthquakes. This led to a further support to the hypothesis that seismicity can be explained within a dissipative self-organized criticality scenario when long-range interactions are considered. The analysis by Caruso et al also indicated that although temporal and spatial correlations among earthquakes do exist and a certain degree of statistical predictability is likely possible, it is rather unlikely to predict the magnitude of seismic events.

In his study of the correlation functions in simulations of an earthquake model, the critical properties of the system, Ramos O. (2010) performed simulations in a more realistic modification[6] of the OFC model of earthquakes and resulted in uncorrelated avalanches distributed following a power-law with weak signs of foreshocks and aftershocks. The analysis of the correlation length had shown that power-law distributed events do not necessarily imply criticality of the system, defined in terms of the divergence of the correlation length, calculated from the correlation function averaged over the entire simulation. The lack of criticality was mainly a consequence of the low value of the exponent of the power-law in the distribution of earthquakes (Gutenberg and Richter, 1956) which gives the proportion between small and large events. It was also an indication that the farther a system is from the critical state (averaged over all the states in the system), the better the conditions for prediction. The occurrence of “critical slowing down” in temporal windows can be an indication of an upcoming large event; this, according to Ramos, leads to the necessity of analysing data that evolve continuously with time.

Main & Naylor (2008) explored the connection between Maximum Entropy Production (MEP) and SOC in model and natural seismicity. They defined entropy production in terms of the ratio of strain energy flux and a ‘temperature term’ not related to heat (particle velocity), but instead to fluctuations in the local strain energy field on a fixed lattice Main & Naylor (2008), then applied this to the non-conservative OFC numerical model for earthquakes, which includes an additional degree of freedom in terms of local stress

[6] The simulations take place on a lattice of L×L sites (L=128, 256, 512) with open boundary conditions, where a few modifications to the original OFC model make the system more realistic (Ramos et al., 2006). The spring-block model consists of a two-dimensional array of blocks on a flat surface. Each block is connected by means of springs with its four nearest neighbours, and in the vertical direction, to a driving plate which moves horizontally at velocity v. When the force acting on a block overcomes the static friction of the surface, the block slips. A redistribution of forces then takes place in the neighbours that eventually triggers new displacements. In this model the force on each block is stored in a site of the lattice, and the static friction thresholds are distributed randomly following a Gaussian centred at 1.0 with a standard deviation equal to 0.001.

dissipation, and used it to show that MEP occurs strictly in a state of self-organized subcriticality, consistent with all of the key aspects of natural seismicity quoted above, as well as the general observation b ≈1. A few year later, Main & Naylor (2010) derived an expression for the entropy-production rate for the OFC model for earthquake populations using Dewar's formulation, including both flux and source terms. The results showed that the MEP solution exhibits the universally observed Gutenberg–Richter b value of around 1 in frequency-magnitude data. In this state, the model stress field organizes into coherent domains, providing a physical mechanism for retaining a finite memory of past events, with quasi-periodic saw-wave fluctuations in the macroscopic strain, implying a finite degree of predictability, albeit strongly limited theoretically by the proximity to criticality and practically by the difficulty of directly observing the Earth's stress field at an equivalent resolution.

The critical theory/ critical point approach

Another important contribution to SOC ideas was the *critical point* theory. The critical point hypothesis for earthquakes has been proposed to understand important empirical scaling laws in seismology, since the scaling properties of earthquake populations, show remarkable similarities to those observed among the critical phenomena of other composite systems in statistical physics such as magnetic phenomena. In the last three decades many researchers have attempted to model seismogenetic processes by analogy with the statistical mechanics of critical phenomena.

A pioneering attempt was conducted by Vere Jones (1976; 1977) with pilot studies of space time correlations for microearthquakes and statistical behaviour of crack propagation. Almost a decade later, Allégre et al., (1982), proposed a percolation model of rupture prior to an earthquake emphasizing on the multiscale nature of the rupture prior to a critical point, while Sornette and Sornette (1990) proposed the consequence of the point model of Allégre with the goal of verifying the scaling laws of rupture. Sykes and Jaumé (1990) performed the first empirical study to quantify the acceleration of seismicity prior to large earthquakes by using an exponential law; however, they did not discuss the concept of a critical earthquake.

Sornette and Sammis (1995) were the first to re-interpret all the previous studies and present a model in which the occurrence of large earthquakes is examined as critical point phenomenon in the framework of the statistical physics of critical phase transitions. The above model invoked a more general self – organization of the stress prior to large

earthquake; moreover, the power law description of the accelerated seismicity was generalized by considering complex scaling exponents which resulted in log-periodic corrections to the scaling (such a generalized power law was used to describe the increase of the energy release of a rock as it undergoes fracturing).

Earthquakes have been considered as an example of critical phenomena due to the fact that large events are frequently observed to be preceded by accelerating seismicity occurring over a region much larger than the rupture zones. Bowman et al., (1998) presented a systematic procedure to test the accelerating seismicity predicted by the critical point model and to identify the region approaching criticality, based on a comparison between the observed cumulative energy (Benioff strain) release and the power-law behaviour predicted by theory. In their model the cumulative seismic strain release increased as a power-law time-to failure before the final event; this method was used to find the critical region before all earthquakes along the San Andreas system since 1950 with earthquake magnitudes $M \geq 6.5$. Zoller et al., (2001) developed a combined approach based on numerical modelling and data analysis in order to understand seismicity and the emergence of patterns in the occurrence of earthquakes. Their interpretation of seismicity in terms of statistical physics led to the concept of “critical states” and also provided perspectives provide perspectives for the understanding of the relevant mechanisms and developments related to time-dependent seismic hazard.

Since earthquakes represent a release of accumulated stress, the critical point theory of earthquakes would therefore predict that main shock and its aftershocks would be associated with a strongly correlated spatial region of high stress that forms prior to the main shock. Indirect evidence for the existence of such correlated regions of high stress has been reported, for example in the appearance of time-dependent variations in the form of the G-R relation (Jaume and Sykes, 1999; Chen, 2003), and in the correlation in seismic activity over large distances (Bowman et al., 1998; Zöller et al., 2001). A self-organising spinodal (SOS) model was also proposed by Rundle et al., (2000) in order to describe time-dependent variations in the Frequency-Magnitude statistics which indicated changes in correlation length of earthquake fault systems. The SOS model was a description of a first-order phase transition leading in proximity to the observation of scaling; the spinodal behaved like a line of critical points (Klein et al., 1997; Rundle et al., 2000b). It was suggested that the behaviour of the earth’s crust can be understood in terms of the physics of a first-order phase transition, aka self-organizing spinodal (SOS)

behaviour. This type of behaviour was similar to the intermittent criticality model of Sornette and Sammis (1995). Rundle et al, considered the time evolution of seismicity in the earth's crust prior to a major earthquake, which is a consequence of the fault reaching its limit of stability, or spinodal, and referred to this earthquake as the characteristic earthquake in a region.

Although the power-law behaviour of accelerating seismicity is in most studies considered as a consequence of a system approaching a critical point, King and Bowman (2003) and Mignan et al., (2007) showed that power-laws can result from a variety of processes, not all of them critical phenomena. Another alternative has been proposed based on the simple concept of Elastic Rebound (Reid, 1910). The concept of Elastic Rebound in explaining AMR was first proposed by King and Bowman (2003) in the Stress Accumulation Model (note that Jaumé and Sykes (1996) approached the problem of AMR origin in a similar way, but without clearly stating the relation between power-law and stress loading. Mignan et al., (2007) proposed a new approach, slightly different from the original Stress Accumulation Model, to demonstrate that criticality is not a necessary condition for the emergence of the AMR power-law. Mignan (2008) developed this concept and referred to it as the Non-Critical Precursory Accelerating Seismicity Theory.

1.4 STATISTICAL MECHANICS & THERMODYNAMICS: THE CONCEPT OF ENTROPY

This section presents the concept of entropy in the framework of thermodynamics and statistical mechanics which is fundamental in the foundation of statistical physics. It first appeared in thermodynamics through the second law of thermodynamics. The notion of entropy has been broadened by the advent of statistical mechanics and has been still further broadened by the later advent of information theory. In order to understand how the complex concept of entropy emerged, we make a brief review towards the works of Clausius, Boltzmann and Gibbs and Planck.

1.4.1 HISTORICAL REVIEW AND CONTEMPORARY ISSUES

The concept of entropy is considered as a difficult matter of subject and frequently it is seen as very mysterious quantity. Over the past two centuries entropy has received a very large number of interpretations, explications and applications. The literature on entropy is huge and it is possible in any work on entropy to mention only a very small fraction of the already published works on the subject.

One of the first works was that of Rudolf Clausius, who is considered as one of the founders of the science of thermodynamics. Clausius published a series of papers in German on the theory of heat and its applications to engines (1850-1864) which were published all together in a book in 1872. The important result of his work was the formulation of the Second law of Thermodynamics which states that it is impossible to transform heat completely into mechanical work in a cyclic process (e.g. Carnot cycle). The impossibility for heat to pass spontaneously from a cold reservoir to a hot reservoir can be deduced from this formulation of the Second Law. Apparently, this formulation did not introduce neither the notion of non-reversible process (since the engine can work in the two directions), nor entropy. However, the formulation involved the concept of irreversibility; in a cyclic process, it is possible to transform completely work into heat when the contrary is not possible. Moreover, heat passes spontaneously from a hot reservoir to a cold reservoir while the contrary is possible only in investing work, i.e. non-spontaneously. In later studies (1854), Clausius distinguished two interdependent transformations in the Carnot cycle: a) the transfer of heat and b) the transformation of work into heat (or heat into work) and introduced the concept of the equivalent-value.

If *Q* is the heat transformed into work (or the work into the heat) from the hot reservoir at temperature T_h, the equivalent-value is (Q/T_h) (a) and if Q' is the heat transferred from one reservoir to the other the equivalent-value is Q' $(1/T_h - 1/T_c)$ (b).

Equating (a) and (b)

$(Q - Q') / Th + Q' / Tc = 0$ (1.4.1)

Generalizing to a cyclic process as the limit of infinity of elementary Carnot cycles, Clausius gets ∫dQ/T = 0 the integral being calculated along the cycle. Or, in other words, the differential

d*S* = dQ / T. (1.4.2)

The new variable *S* introduced by Clausius depended only on the state of the system and this way one can only calculate the difference of S between two different states (A and B) of the system as

$$S_B - S_A = \int_A^B dQ / T \quad (1.4.3)$$

In the case of irreversible process (not cyclic) the famous expression relating entropy variation along (not cyclic) and the integral ∫dQ/T becomes

$$S - S_0 \geq \int_{irr} dQ / T \quad (1.4.4)$$

While in an adiabatic irreversible process *dQ = 0* and one has the fundamental relation between entropy and irreversibility: In a closed system (adiabatic transformation) the entropy cannot decrease, it remains constant or increases.

Boltzmann and Gibbs entropy

Although Clausius found the connection between entropy and irreversibility he never put a question about the origin of irreversible process. However, he found a new function: the entropy as a state function depending only on the parameters defining the system. The problem of irreversibility or how to explain the origin of irreversible processes became a subject of an intense debate among scientists in the second part of the 19th century.

An important contribution to this subject was that of Ludwig Boltzmann. Boltzmann addressed to the problem of irreversibility with the H- theorem (1872) claiming that this was a general theorem which could give an explanation of irreversibility. The H- theorem

is an integro-differential equation concerning the distribution function f(**v**,t) such that f(**v**,t)d^3**v** gives the relative number of molecules of a gas between **v** and **v** + d^3**v** at time t (where v is the vector velocity).

The H-theorem states that the quantity defined as

$$H = \int f(v,t) \ln f(v,t) d^3v \tag{1.4.5}$$

decreases with time or dH/dt ≤ 0 until that dH/dt = 0 at equilibrium. The H-theorem was heavily criticized by a handful of authors (up until today) and thus H could not be considered as the entropy.

Another important contribution of Boltzmann concerns the formula based on his *H theorem* (1877) which led to a statistical - probabilistic definition of entropy. The principal point is the definition of a microstate (see section 1.4.3) A fundamental hypothesis concerning a closed system is that the probability of occurrence of a particular microstate is identical for all the microstates of the system. Consequently, the equilibrium state is that with the largest possible number of microstates since it corresponds to the largest probability for the system itself. If a closed system is not in an equilibrium state, it will evolve to states with larger and larger number of microstates until it reaches the equilibrium state with the largest number of microstates corresponding to its energy. Being in the equilibrium state, the system may pass to another macroscopic state with a smaller number of microstates. However, the probability that the system reaches such a state is very low such it is never observed. Here an important step was the introduction of the notion of the probability for the occurrence of a state of the system. Next, was the identification of the largest probability with entropy and express the proportionality of S with the logarithm of the number W of microstates

$$S \approx \ln W \tag{1.4.6}$$

Based on this the measure of disorder first provided by Boltzmann principle (known as Boltzmann entropy) is given by

$$S = k_B \ln W \tag{1.4.7}$$

where k_B is the thermodynamic unit of measurement of entropy and is known as Boltzmann constant and W the thermodynamic probability or statistical weight or "degree of disorder", i.e. the total number of microscopic complexions compatible with the macroscopic state of the system. Boltzmann entropy plays a crucial role in the connection of the nonmechanical science of thermodynamics with mechanics through statistics. In thermodynamics, two fundamental properties of Boltzmann entropy are a) its *non-decrease*: if no heat enters or leaves a system, the entropy S of the system is a monotonic increasing function of "degree of disorder" W, that is, S (W) ≤ S (W +1) and b) its *additivity*: the entropy is assumed to be an additive function for two statistically independent systems with degrees of disorder W1 and W2, respectively. The entropy of two systems, taken together, is the sum of their separate entropies $S\left(W_1 \times W_2\right) = S\left(W_1\right) + S\left(W_2\right)$.

Another important concept of the entropy is the distinction of microstates and the parameter which defines different microstates. Boltzmann proposed to make the energy a discrete quantity characterized by energy steps Δ. In this case, two microstates are different if their energies were different at least by Δ. It resulted that the number of microstates W and consequently the entropy depend on the choice of Δ. In the case of particles with continuous values of the coordinates indicating their continuous values of their positions and of their momenta, if the famous formula (1.4.7) can be used only in a world of discrete quantities, is it possible to calculate quantity like entropy by discretization? The answer was lying in Quantum Mechanics where, in a limited volume, the relevant quantities are discrete. In his study Maxwell Planck succeeded in finding the correct expression for the density of energy for the black body emission by discretization of the energy. By using the method of microcanonical ensemble (see Appendix 1) he was able to calculate the number of possible states with a given energy paving the way to the development of Quantum Mechanics.

A conceptual difference between Boltzmann and Gibbs entropy is that Boltzmann entropy *S* is defined for a macroscopic state whereas Gibbs entropy is defined over a statistical ensemble and can be expressed in terms of the probability distribution of the observational states of the system. Gibbs considers a very large number of identical systems, the ensemble and supposes that each system in the ensemble is in a particular situation i.e. that in each system the particles are in different positions with different momenta or in a different microstate.

Let us consider a collection of subsystems of N molecules within a volume V, each of which is part of the larger construction, the totality of which is known as *the system Ω*.

Then let ω_i the occupation number, denote the number of subsystems from this collection that are in the same thermodynamic state. These occupations will thus take on a large value in the thermodynamic limit and they obey a sum rule

$$\sum_i \omega_i = \Omega \quad (1.4.8)$$

Next, we consider the following formula as a combination of equations (1.4.7) and (1.4.8):

$$S_e = k \ln W\{\omega\} = k \ln \frac{\Omega!}{\omega_1! \omega_2! \ldots} \quad (1.4.9)$$

where W{ω} is the number of ways in which the set of occupations {ω} may be arranged consistent with the given macrostate. The quantity S_e may be identified with the thermodynamic entropy of the ensemble of systems at equilibrium, with each systems entropy given by $S = \frac{S_e}{\Omega}$. Necessarily, the expression involves the logarithm in order to make entropy an extensive property. The connection between the $S=k \ln W$ and the Gibbs entropy (Eyring et al, 1964; McQuarrie et al, 1997) is given by:

$$S_e = k\left\{\Omega \ln \Omega - \Omega - \sum_i \omega_i \ln \omega_i + \sum_i \omega_i\right\} \quad (1.4.10)$$

By substituting $\omega_i = \Omega p_i$ the system's entropy can be written as:

$$S = -k \sum_i p_i \ln pi \quad (1.4.11)$$

where p_i is the probability of finding a system in a given state, which can be invoked for any equilibrium ensemble and associated state probabilities. The Gibbs entropy is an entirely general definition specifying the relationship between the partition function for any equilibrium ensemble and the associated characteristic thermodynamic function. As can be seen, it is a direct consequence of the statistical entropy formula, $S = k \ln W$, in conjunction with the Gibbs construction of an ensemble that contains a large number of macroscopic subsystems, each consistent with the desired thermodynamic variables; *W* gives the number of possible realizations within the Gibbs construction for the ensemble under consideration.

Some of the advantages of Gibbs entropy over the Boltzmann entropy is that Gibbs entropy is defined directly from the distribution of microstates, thus avoiding the

identification of a microstate. Secondly, it defines entropy for systems which are not large which is very important since it helps in the partition of a system into small subsystems. And finally, it defines entropy for systems which are not in thermal equilibrium but have been perturbed in some way or are undergoing some irreversible process.

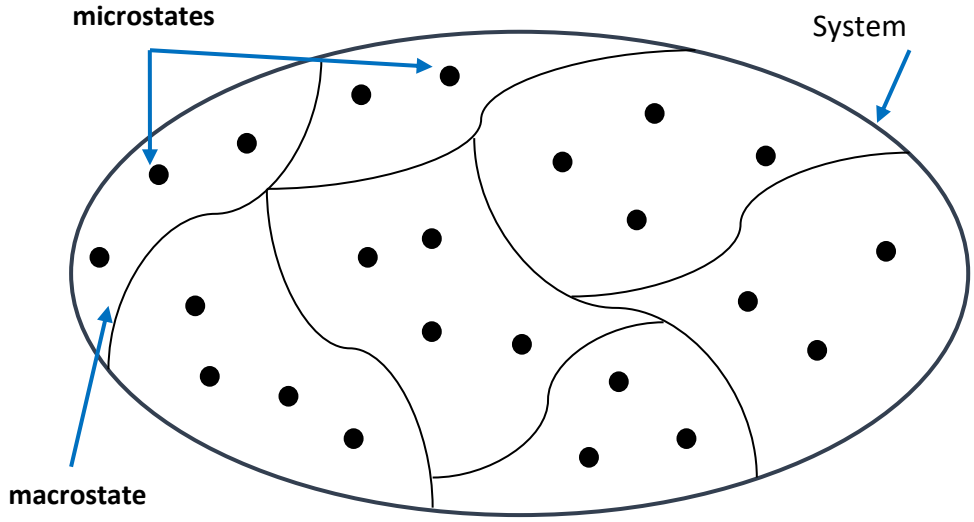

Figure 1.9 Ω is partitioned into a finite number of regions corresponding to macrostates, with each microstate belonging to one macrostate.

1.4.2 ENTROPY IN QUANTUM MECHANICS

In both discrete and continuous cases that we have addressed above, we were considering classical systems in the sense that all physical observables are real quantities and not operators. However, for intrinsically quantum systems, we must generalize the concept. In that case, the *BG* entropic form is to be written (introduced by von Neumann) in the following manner:

$$S = -k_B \sum \rho_n Ln\rho_n = Tr\left[\rho Ln\rho\right] \tag{1.4.12}$$

where k_B is the Boltzmann and ρ is the density matrix, constant acting on a W-dimensional Hilbert vectorial space (typically associated with the solutions of the Schroedinger equation with the chosen boundary conditions).

According to Landau and Lifshitz (1968; 1969; 1980) one considers a very large system isolated from the external surrounding in equilibrium. This closed system is divided into a large number of subsystems with the same volume: they are all identical and large enough to be considered as macroscopic bodies. It is possible to see these subsystems as a physical realization of a canonical ensemble. They have all the same temperature and the same volume, but the energy fluctuates from one subsystem to another.

In Quantum Mechanics, the state of a system is defined by its wave function (Ψ) and its energy. The wave functions of one of the subsystems are denoted as ψn(q) where q indicates the coordinates and the index n the state and En, the energy of the state. At a given time for one subsystem, the distribution probability dependent on the energy En, from which the mean values of the various important quantities can be calculated. If the number of quantum states with energy less than a given value E is described by the function Γ(E), the number of states between E and E + dE is given by (dΓ(E)/dE)dE. Thus, the probability that the energy of the system is between the values E and E + dE is the product of the probability w(E) by the number of states with energy between E and E + dE

$$W(E)\,dE = [d\Gamma(E)/dE]\,w(E)\,dE$$

with condition $\int W(E)dE=1$.

The function W(E) is in general peak shaped, since the macroscopic value of the energy given by its average Eav is also equal to the most probable value Em or Em= Eav .

It results that the function W(E) has values different from zero only in the vicinity of the peak value. This gives the possibility to define a width ΔE of the function as given by the product

$$W(Em)\,\Delta E = 1$$

where Em is the value of E at the maximum of W(E).

Consequently,

$$W(Em) = [d\Gamma(Em)/dE]\,w(Em)$$

$$W(Em)\,\Delta E = [d\Gamma(Em)/dE]w(Em)\,\Delta E$$

$$= w(Em)\Delta\Gamma = 1$$

where ΔΓ is defined as

$$\Delta\Gamma = [d\Gamma(Em)/dE]\,\Delta E = [d\Gamma(Eav)/dE]\,\Delta E$$

The derivative [dΓ(Em)/dE] gives the number of states around Em and ΔΓ is the number of states in the interval ΔE in which the probability function W(E) has values different from zero. Thus, ΔΓ is a measure of the spread of the energies of the microstates of one subsystem around the most probable value.

The entropy is defined as $S = k_B \,\mathrm{Ln}\,\Delta\Gamma$

The distribution probability function w(E) is that given by the canonical ensemble, i.e. Ln w(E) is linear with the energy. Thus, one has Ln w(E) = α + βE

Now considering the ensemble of the subsystems, one can take the average values of different quantities. The average of Ln w(E) is [Ln w(E)]av = α + βEav = Ln w(Eav)

Since w(Em)ΔΓ = 1 and recalling that Em = Eav one gets Ln ΔΓ = - [Ln w(E)]av

or S = - kB Σ wn Ln wn = - kB Tr(wo Ln wo)

One recovers again the preceding formula namely that the entropy is the average of the logarithm of the distribution probability. The definition of the entropy S = kB Ln ΔΓ is equivalent to the expression of Gibbs Φ_0 = [Ln(dV/dε)]0 with the exception of the quantity ΔE which does not appear in the Gibbs's expression. But this quantity ΔE is important since it introduces the notion of spreading of the energies.

1.4.3 BOLTZMANN-GIBBS STATISTICAL MECHANICS AND THERMODYNAMICS

In many studies the Boltzmann- Gibbs (B-G) entropy is introduced as *the generalization of Boltzmann entropy*. The entropic forms (1.4.7) and (1.4.11) correspond to the case where the microscopic states of the system are discrete. However, in cases where the appropriate variables are continuous, the entropy takes the form

$$S_{BG} = -k \int dx p(x) \ln\left[\sigma p(x)\right] \tag{1.4.13}$$

with $\int dx p(x) = 1$

where $x/\sigma \in \mathbb{R}^D$, $D \geq 1$ being the dimension of the full space of microscopic states (called Gibbs Γ phase-space for classical Hamiltonian systems), with x and σ carrying physical units. For the case of *equal probabilities* (i.e., $p(x) = 1/\Omega$, where Ω is the hypervolume of the admissible *D*-dimensional space), we have

$$S_{BG} = k \ln\left(\Omega / \sigma\right) \tag{1.4.14}$$

The BG statistical mechanics can be briefly reviewed as follows: let us consider a quantum Hamiltonian system constituted by *N* interacting particles under specific boundary conditions, and denote by $\{E_i\}$ its energy eigenvalues.

a) Microcanonical ensemble/ isolated system: the micorcanonical ensemble corresponds to an isolated *N*-particle system whose total energy *U* is known within some precision δU (to be in fact taken at its zero limit at the appropriate mathematical stage).

The number of states *i* with U ≤ Ei ≤ U + δU is denoted by W. Assuming that the system is such that its dynamics leads to ergodicity at its stationary state (thermal equilibrium), we assume that all such states are equally probable, i.e., pi = 1/W, and the entropy is given by Eq. (1.4.6). The temperature T is introduced through

$$\frac{1}{T}=\frac{\partial S_{BG}}{\partial U}=k\frac{\partial \ln W}{\partial U}$$

b) Canonical Ensemble – Thermostat: The canonical ensemble corresponds to an *N*-particle system defined in a Hilbert space whose dimension is noted W, and which is in thermal contact with a (infinitely large) thermostat at temperature T. Its exact energy is unknown, but its mean energy *U* is known since it is determined by the thermostat. By optimizing the entropy given by Eq. S_{BG}=-k$\sum_{i=1}^{W} p_i\, lnp_i$ with the norm constraint

$\sum_{i=1}^{W} p_i = 1$, and with the energy constraint $\sum_{i=1}^{W} p_i E_i = U$

where $p_i=\frac{e^{-\beta E_i}}{Z_{BG}}$ with the partition function given by $Z_{BG}=\sum_{i=1}^{W} e^{-\beta E_i}$

The Lagrange parameter *β* being related with the temperature through *β* ≡ 1/(*kT*).

c) The grand-canonical ensemble refers to the physical situation where the system may be exchanging with the thermostat not only energy, but also particles, so that also the chemical potential is fixed by the reservoir. This and other similar physical situations can be treated along the same path, as shown by Gibbs. Some other important physical systems which constitute what is referred to as *B-G* statistical mechanics are for example *bosons* (leading to Bose–Einstein statistics) and *fermions* (leading to Fermi–Dirac statistics).

Basic Properties of S_{BG}

Non – negativity. If the state of the system is known, then: $p_{i_0}=1$ and *pi* =0, ∀ *i* = i_0. Then it follows that S_{BG} = 0, where we have taken into account that $\lim_{x\to 0}(x \ln x) = 0$. In any other case, we have p_i < 1 for at least two different values of *i*. We can therefore write Eq. (1.1) as follows:

$$S_{BG}=-k\left\langle \ln p_i \right\rangle = k\left\langle \ln\frac{1}{p_i}\right\rangle \qquad (1.4.15)$$

where $\langle ... \rangle \equiv \sum_{i=1}^{W} p_i (...)$ is the standard mean value

Since ln $(1/p_i) > 0$ $(\forall_i)$, it clearly follows that SBG is positive.

Expansibility. Adding to a system new possible states with zero probability should not modify the entropy; S_{BG} satisfies the above statement if we take into account the property $\lim_{x\to 0}(x \ln x) = 0$, so that $S_{BG}(p_1, p_2 \ldots p_W, 0) = S_{BG}(p_1, p_2 \ldots p_W)$.

Additivity. Let $\mathcal{Q}$ be a physical quantity with a given system, while A and B two probabilistically independent subsystems. If and only if $\mathcal{Q}(A+B) = \mathcal{Q}(A) + \mathcal{Q}(B)$ the term additive, can be used. If *A* and *B* are independent, i.e. if their joint probability satisfies $p_{ij}^{A+B} = p_i^A p_j^B (\forall(ij))$, then $S_{BG}(A+B) = S_{BG}(A) + S_{BG}(B)$. Therefore, S_{BG} is *additive*.

Concavity. Let us assume two arbitrary and different probability sets $\{p_i\}$ and $\{p'_i\}$ associated with a single system having *W* states. An intermediate probability is defined as follows:

$$p_i'' = \lambda p_i + (1-\lambda) p_i' \qquad (\forall_i; 0 < \lambda < 1) \tag{1.4.16}$$

The functional $S_{BG}(\{p_i\})$ is concave if and only if

$S_{BG}(\{p''_i\}) > \lambda S_{BG}(\{p_i\}) + (1-\lambda) S_{BG}(\{p'_i\})$, which is indeed satisfied by S_{BG}

Maximal at equal properties. The BG entropy, which in some sense represents the concept of energy in a system, depends on the total number of possible microscopic configurations of the system, however it is insensitive to its specific physical support, taking into account the probabilistic information on the system. Let us consider a spin that can be up or down, a coin that comes head or tail, a computer bit which can be 0 or 1; these are all equivalent for the concept of entropy. Consequently, entropy is expected to be a functional which is invariant with regard to any permutations of the states. Indeed, expression (1.4.11) exhibits this invariance through the form of a sum. Consequently, if $W > 1$, the entropy must have an extremum (maximum or minimum), and this must occur for equal probabilities. The identification that it is a maximum (and not a minimum) becomes obvious since S_{BG} is a concave functional.

Composability. The entropic form $S(\{p_i\})$ is said to be *composable*, if the entropy S corresponding to a system composed of two independent subsystems A and B can be expressed in the form: $S(A + B) = F(S(A), S(B); \{\eta\})$, where $F(x, y; \{\eta\})$ is a function which, besides depending symmetrically on (x, y), depends on a typically small set of universal indices $\{\eta\}$. In other words, it does *not* depend on the microscopic configurations of *A* and *B*. Equivalently, we are able to macroscopically calculate the entropy of the composed

system without any need of entering into the knowledge of the microscopic states of the subsystems. This property appears to be a natural one for an entropic form if we desire to use it as a basis for a statistical mechanics which would naturally connect to thermodynamics.

Although S_{BG} enjoys universal acceptance, the formal manners for obtaining *B-G* entropy and its associated distribution for thermal equilibrium are not derived from first principles. This was one of Boltzmann's main scientific goals which was not accomplished due to difficulties that are so heavy even to these days. An example is a series of studies by Fisher et al., (1964; 1965; 1966; 1970) which proved for a class of short-range-interacting many-body Hamiltonians that the thermal equilibrium physical quantities are computable within standard B-G statistical mechanics. Although clearly there is no reasonable doubt today that the B-G approach is the correct one, back then however such a proof, no matter how precious it was, did not prove also that the B-G statistics indeed provided the correct description at thermal equilibrium.

Similarly, for the case of long-range-interacting Hamiltonians (e.g., infinitely-long-range interactions), the standard B-G calculations can still be performed through convenient renormalizations of the coupling constants. The possibility of computability does by no means prove, that B-G statistics is the correct description. And certainly, it does not enlighten us on what the necessary and sufficient first-principle conditions could be for the B-G description to be the adequate one. After 130 years of impressive success, there can be no doubt that B-G concepts and statistical mechanics provide the correct connection between microscopic and macroscopic laws for a vast class of physical systems in equilibrium state.

For the case of non-equilibrium phenomena, the general formalism is far from having been completely developed, although individual formalisms been suggested many of which require some additional assumptions or excessive information. For example, Onsager's kinetics (Onsanger, 1931) requires linearization, while the theory of dynamical response (Grandy W.T 1988; 2008), employing the convolution with a response function besides initial and boundary conditions requires the knowledge of the past evolution of a process during some time interval. An interesting approach was suggested by Abaimov S. (2009). In his study, Abaimov considered the classical Gibbs approach for states and found it ineffective for non-equilibrium phenomena because it is based on a distribution of probabilities indirectly. Based on this assumption he developed a path formalism which

is directly based on the distribution of probabilities and therefore significantly simplifies the analytical approach. The suggested formalism requires generalizing the ‘static’, state quantities of a system, like entropy or free energy potential, to their path analogues. For the distribution of probabilities, he obtained a functional dependence where the role of a Hamiltonian is played by the state entropy. For the production of the state free energy he illustrated a significant dependence on the type of system’s connectivity.

It becomes clear that the general formalism for non-equilibrating systems if would be developed, should inherit the mathematical beauty and simplicity of the Gibbs approach of equilibrium statistical mechanics. Non-equilibrium thermodynamics is a work in progress, not an established edifice and the mathematically precise qualification of this class remains an open question.

1.5 NON-EQUILIBRIUM THERMODYNAMICS, NON-EXTENSIVE STATISTICAL PHYSICS APPROACH: TSALLIS ENTROPY

The concept of “entropy” has been long used as a measure of disorder and is expressed by one of the most famous formulas in physics, proposed by Ludwig Boltzmann and J. Willard Gibbs. For more than 20 years, however, the Greek-born physicist Constantino Tsallis, has been arguing that entropy is in need of some refinement. According to Tsallis, entropy – as defined by Boltzmann and Gibbs – works perfectly, but only within certain limits. If a system is out of equilibrium or its component states depend strongly on one another, he believes an alternative definition should take over.

As has already been discussed in the previous sections, Boltzmann’s formula ($S=k \log W$) – shows that entropy increases logarithmically with the number of microstates. It also tends to class entropy as an “extensive” property i.e., a property, like volume or mass, whose value is proportional to the amount of matter in a system, unlike an “intensive” property such as temperature, which remains the same no matter how large or small the system. However, Boltzmann’s formula is not, the final word on entropy. A more general Boltzmann–Gibbs formula is used to describe systems containing microstates that have different probabilities of occurring. For example, in a piece of metal placed in a magnetic field, the spins of the electrons inside are more likely to align parallel than antiparallel to the field lines. In this scenario, where one state (parallel alignment) has a much higher probability of occurring than the other (anti-parallel alignment), the entropy is lower than in a system of equally likely states; in other words, the alignment imposed by the magnetic field has made the system more ordered. Nonetheless, the entropy here is still extensive: double the electrons, double the entropy.

Unfortunately, according to Tsallis it is not always possible to keep entropy extensive when calculating it with the B-G formula. Systems in which the B-G formula does not keep entropy extensive include those that are out of equilibrium, or where the probability of a certain microstate occurring depends strongly on the occurrence of another microstate – in other words, when the elements of a system are “strongly correlated”.

There are many examples in the physical world of strong correlations affecting entropy, such as magnetic systems, Quantum Hall systems, conventional superconductors etc. And it turns out that in any system with strong correlations, the number of possible microstates, W, no longer increases exponentially with the number of elements, N,

instead, it follows a power of N such as $W=N^X$. In other words, entropy is no longer proportional to N; it is forced to be non-extensive.

1.5.1 Generalization of BG entropy – Tsallis entropy

In 1988, Constantino Tsallis introduced an entropic functional as a result of generalization of BG statistics which could describe non-equilibrium states in systems with complex behaviour. The generalization of BG statistics derives from a metaphor of the ordinary differential equations $\frac{dy}{dx}=0$

(y (0) = 1), $\frac{dy}{dx}=1$

(y (0) = 1), and $\frac{dy}{dx}=y$

(y (0) = 1)

Whose solution is $y=e^x$ (1.5)

The above equations can be unified by just considering $\frac{dy}{dx}=a+by$ (y (0) = 1).

It is also possible to unify the above equations with only one parameter when *out of linerarity:*

$\frac{dy}{dx}=y^q$ $(y(0)=1; q\in\mathbb{R})$.Its solution is $y=\left[1+(1-q)x\right]^{1/(1-q)}\equiv e_q^x$

$\left(e_1^x=e^x\right)$

Its inverse is $y=\frac{x^{1-q}-1}{1-q}\equiv \ln_q x \qquad \left(x>0; \ln_1 x=\ln x\right)$ (1.5.1)

and satisfies the following property:

$\ln_q\left(xAxB\right)=\ln_q xA+\ln_q xB+(1-q)(\ln_q xA)(\ln_q xB)$.

The above two functions are commonly referred as the *q-exponential* and the *q-logarithm*, respectively and have played an important role through the entire theory. Figures 10 a, b, c, illustrate typical representations of the *q-exponential* function.

Through the above metaphor the equation a generalization of Eq (1.4.7) can be postulated as follows: $Sq=k\ln_q W$ ($S1=S_{BG}$) (1.5.2)

S_{BG} can be also written as the mean value of ln(1/p_i), a quantity that is refered as *surprise* or *unexpectedness* (Watanabe S., 1969; Barlow H., 1990). Indeed, when there is a certainty that something will happen, i.e p_i=1, then there is no surprise; on the opposite when something is very unexpected (p_i = 0), if it eventually happens, it will be a surprise. It then appears as quite natural to postulate the simultaneous generalization of Eqs. (1.5.1) and (1.5.2) as follows:

$$S_q = k\left\langle \ln_q\left(1/\ p_i\right)\right\rangle \tag{1.5.3}$$

If we use the definition (1.5.1) in this expression, we obtain

$$S_q = k\frac{1-\sum_{i=1}^{W} p_i^q}{q-1} \tag{1.5.4}$$

This is precisely the form postulated in the study by Constantino Tsallis (1988) as a possible basis for generalizing B-G statistical mechanics (Fig.1.10– 1.11).

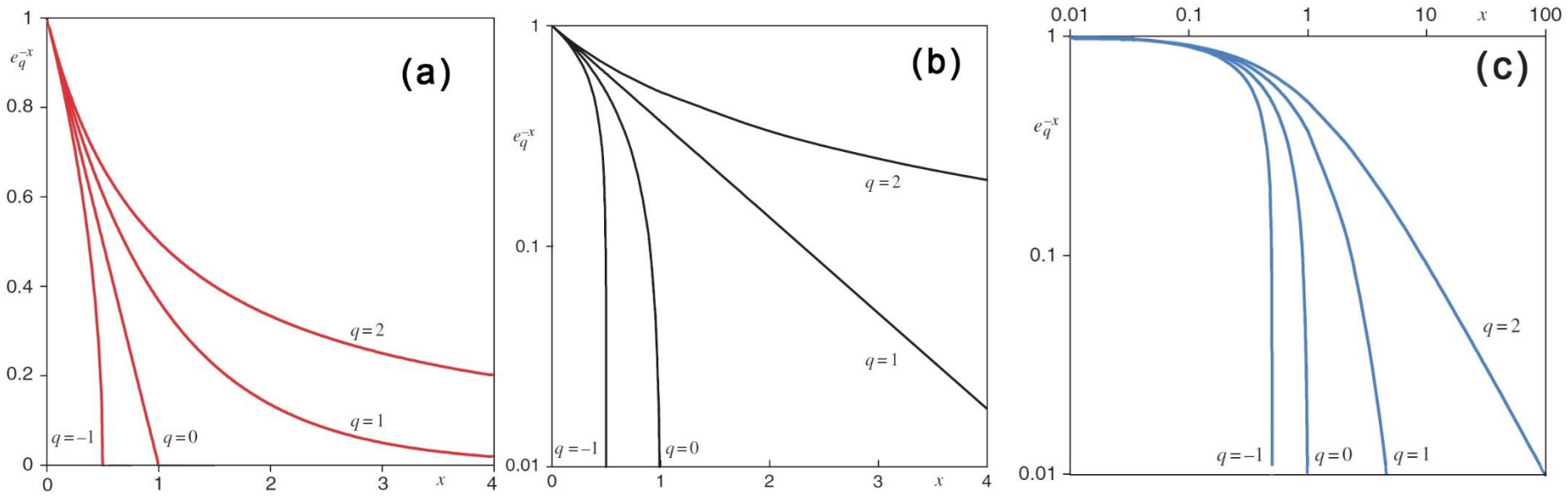

Figure 1.10 The *q*-exponential function e_q^{-x} for typical values of *q:* **a)** linear–linear scales. *For* q > *1,* it vanishes like $[(q-1)x]^{-1/(q-1)}$ for x →∞. For *q* < *1*, it vanishes for x > $(1-q)^{-1}$ (cutoff); **b)** log–linear scales. It is convex (concave) if *q* > *1 (q* < *1).* For *q* < *1,* it has a vertical asymptote at x = *(1* − q*)−1;* **c)** log–log scales. For *q>1,* it has an asymptotic slope equal to *−1/(q* − *1).*

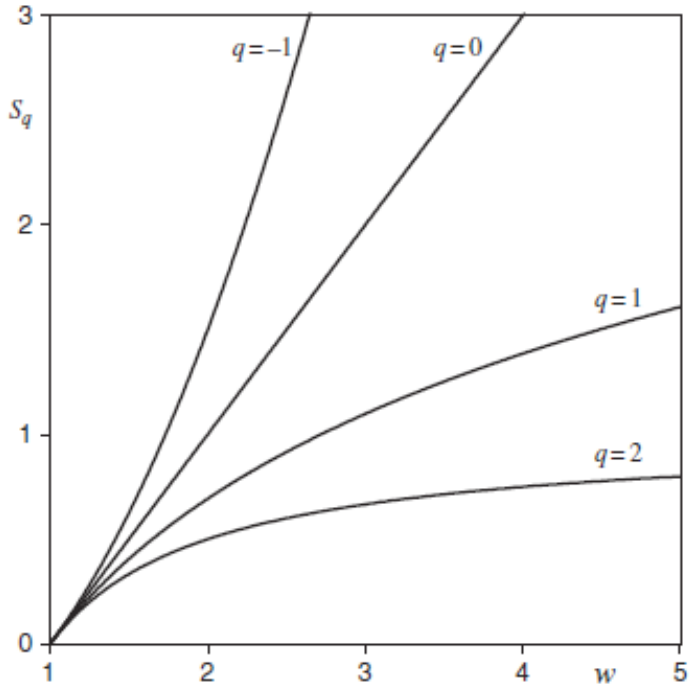

Figure 1.11 The equiprobability entropy *Sq* as a function of the number of states W (with k = 1), for typical values of *q.* For $q > 1$, *Sq* saturates at the value $1/(q-1)$ if $W \to \infty$; for $q \leq 1$, it diverges. For $q \to \infty (q \to -\infty)$, it coincides with the abscissa (ordinate).

Basic Properties of non- extensive S_q

I shall next address the properties of *Sq.* But before doing that, let us clarify a point which has a generic relevance. If $q > 0$, then expression (1.5.4) is well defined whether or not one or more states have *zero* probability. Not so if $q < 0$. In this case, it must be understood that the sum indicated in Eq. (1.5) runs *only* over states with *positive* probability.

Non-negativity. If we have certainty about the state of the system then $p_i=1$, and all the others vanish. Consequently, the entropy S_q vanishes for all q. If we do not have certainty, at least two of the probabilities are smaller than unity. Therefore, for those, $1/p_i > 1$, hence $\ln_q(1/p_i) > 0$, $\forall i$.Consequently, using Eq. (1.5.3), it immediately follows that $S_q > 0$, for all q.

Expansibility. S_q is expansible $\forall q$ since $S_q(p_1, p_2, ..., p_w, 0) = S_q(p_1, p_2, ..., p_w)$

Nonadditivity. Unlike BG entropy, the generalized form of S_{BG}, is *pseudo-additive* ($q \neq 1$) in the sense that unlike the S_{BG}, it is generally not proportional to the number of the elements of the system. This leads to *super-additivity* if $q<1$, *additivity* when $q=1$, (that is Gibbs-Boltzmann statistics), and *sub-additivity* if $q>1$.

Sensitivity to the Initial Conditions

Let us now consider a one-dimensional nonlinear dynamical system (characterized by the variable *x*) whose Lyapunov exponent *λ1* vanishes (e.g., the edge of chaos for typical unimodal maps such as the logistic one). The sensitivity to the initial conditions ξ is conjectured to satisfy the equation

$$\frac{d\xi}{dt} = \lambda_q \xi^q \quad (1.5.5)$$

Whose solution is given by

$$\xi = e_q^{\lambda_q t} \quad (1.5.6)$$

The paradigmatic case corresponds to $\lambda_q > 0$ and q <1. In this case we have

$$\xi \propto t^{1/(1-q)} \quad (t \to \infty) \quad (1.5.7)$$

and it refers as weak chaos, in contrast to strong chaos, associated with positive *λ1.* To be more precise, Eq. (1.5.6) has been proved to be the upper bound of an entire family of such relations at the edge of chaos of unimodal maps. For each specific (strongly or weakly) chaotic one-dimensional dynamical system, we generically expect to have a couple (q_{sen}, λq_{sen}) (where sen stands for sensitivity) such that we have

$$\xi = e_{q_{sen}}^{\lambda_{q_{sen}} t} \quad (1.5.8)$$

Clearly, strong chaos is recovered here as the particular instance q_{sen} = 1. Let us now address the interesting question of the *Sq* entropy production as time *t* increases. By using *Sq* instead of S_{BG}, one could attempt the definition of a *q-generalized* Kolmogorov–Sinai entropy rate. We will not follow along this line, but we shall rather *q-generalize* the entropy production *K1*[7] (as introduced in Tsallis, 2009). By defining

$$K_q \equiv \lim_{t\to\infty} \lim_{W\to\infty} \lim_{M\to\infty} \frac{S_q(t)}{t} \quad (1.5.9)$$

Tsallis *conjectured* that generically a unique value of *q* exists, noted q_{ent} (where *ent* stands for *entropy*) such that (the upper bound of) K_{qent} is *finite* (i.e., positive), whereas K_q

[7] K1 is the entropy production per unit time defined as $K1 = \lim_{t\to\infty} \lim_{W\to\infty} \lim_{M\to\infty} \frac{SBG(t)}{t}$. By using the Pesin-like identity for large classes of dynamical systems $K1 = \sum_{r=1}^{d+} \lambda_{1^{(r)}}$

vanishes (diverges) for $q > q_{ent}$ ($q < q_{ent}$). Further he conjectured for one-dimensional systems that

$$q_{ent} = q_{sen} \tag{1.6.0}$$

and that

$$K_{q_{ent}} = K_{q_{sen}} = \lambda_{q_{sen}} \tag{1.6.1}$$

Strong chaos is recovered as a particular case, and we obtain the Pesin-like identity $K1 = \lambda 1$. Conjectures (1.5,8), (1.6,0), and (1.6.1) were first introduced in Tsallis et al, 2007, and have been analytically proved and/or numerically verified in a considerable number of examples (Costa et al, 1997; Lyra et al, 1998; da Silva et al, 1999; Baldovin et al, 2003; Tirkanli et al, 1999; 2001; Borges et al, 2002; Baldovin & Robledo, 2002; Ananos & Tsallis, 2004; Baldovin & Robledo, 2004).

If the weakly chaotic system has ν positive q-generalized Lyapunov coefficients $\lambda_{q(1)_{sen}}, \lambda_{q(2)_{sen}}, \ldots\ldots, \lambda_{q(\nu)_{sen}}$, it is expected that

$$\frac{1}{1-q_{ent}} = \sum_{k=1}^{\nu} \frac{1}{1-q_{sen}^{(k)}} \tag{1.6.2}$$

This yields, if all the $q_{sen}^{(k)}$ are equal,

$$q_{ent} = 1 - \frac{1-q_{sen}}{\nu} \tag{1.6.3}$$

If v=1, the Eq.1.6.0 is recovered. If $q_{sen} = 0$ we obtain

$$q_{ent} = 1 - \frac{1}{\nu} \tag{1.6.4}$$

TABLE 1.1 Comparative table of selected properties of S_{BG} and S_q (with k=1):

$S_{BG} = -k\sum_i p_i \ln pi$ and $S_q = k\frac{1-\sum_{i=1}^{w} p_i^q}{q-1}$

ENTROPY	**S_{BG}**	**S_q**
Additive $\left(\forall_q \neq 1\right)$	YES	NO
$q<1$ exists such that S is extensive for special global correlations	NO	YES
Concave $\left(\forall_q > 0\right)$	YES	YES
Lesche stable $\left(\forall_q > 0\right)$	YES	YES
$q<1$ exists such that entropy production per unit time is finite	YES	YES
$\hat{S}$ exists, $\forall_q \neq 1$ such that *$\hat{S}$ and S=($\hat{S}$)* obeys for independent events the same composition law	YES	YES
$\hat{S}$ exists, $\forall_q \neq 1$ such that $\hat{S}(\hat{p}^{-1})$ *has the same functional form as S(p_i=1/W)*	YES	YES
Same functional form for both $Z_q(\beta F_q)$ and $[Z_q\, p\,(E_i)]$, $\forall_q \neq 1$	YES	YES
Optimizing distribution $\forall_q \neq 1$	exp	*q*-exp

1.5.2 Non-Extensive Approach to the Statistical Physics of Earthquakes

The knowledge of the microscopic dynamics is essential for the implementation of the entire theory from first principles. Indeed, it is only in principle that the microscopic dynamics contains all the ingredients enabling the calculation of the index (or indices) q. It is still necessary to be able to calculate, in the full phase-space, quantities such as the sensitivity to the initial conditions or the entropy production. This calculation can be extremely hard. But, once q is known, it becomes possible to implement the thermodynamical steps of the theory. This is to say, we can in principle proceed and calculate the partition function of the system, and, from this, calculate various important thermodynamical quantities such as specific heat, susceptibility, values of energy, seismic moment and entropy increase as a function of temperature and others. Naturally, the difficulty of this last step of the calculation should not be underestimated. In a full q-statistical calculation, we have to deal typically with interactions at all distances (or related conditions) and power-law weights.

As a mathematical exercise, the q-statistics of simple systems such as the ideal gas and the ideal paramagnet are available in the literature. However, these calculations only provide some mathematical hints with modest physical content. Indeed, thermal equilibrium in the absence of interactions mandates $q = 1$. Further, and extremely powerful, hints are also available from the study of non- thermodynamical systems. However, no matter how useful these systems might be, they do *not* have energy associated, and are therefore useless in order to illustrate the thermostatistical steps of the full calculation, and their connection to thermodynamics itself.

Critical complex (non-equilibrating) systems such as seismogenetic systems, evolving in a fractal-like space-time are considered to be characterized by long-range interactions and long-term memory which, at least at a regional scale, should be manifested by correlations and power-law distributions observable in the statistical behaviour of their energy release, temporal dependence and spatial dependence. However, there is no clear picture of the essential conditions under which SOC behaviour arises. Connected with the lack of SOC definition is the lack of a mathematical formalism. Despite numerous studies in many different fields, SOC still lacks a well-established mathematical framework; a formalism that could work as a mathematical foundation and is equivalent to the partition function and the free energy in equilibrium statistical mechanics is emerging.

The *q-statistical* theory and functional forms have been successfully applied to earthquakes in many occasions (Franca et al., 2007; Kalimeri et al., 2008; C. Papadimitriou et al., 2008; Balasis et al., 2008; Darooneh & Dadashinia, 2008; Tirkanli & Abe, 2004; U. Tirkanli, 2005 etc). Successive earthquakes in a given geographic area occur with epicenters distributed in a region just below the Earth surface. We note r the successive distances (measured in three dimensions). It has been verified by Abe & Suzuki, (2003) that, in California and Japan, this distribution, *p(r),* happens to be well represented by a *q-exponential* form. More precisely, the corresponding accumulated probability is given by the Abe–Suzuki distance law

$$P(>r) = e_q^{-r/r_0} \qquad (0 < q < 1; r_0 > 0)$$

Consequently $p(r) = -\frac{dP(>r)}{dr} = \frac{1}{r_0} e_Q^{-r/[r_0(2-Q)]}$ with $Q \equiv 2 - \frac{1}{q} < q$

Moreover, between successive events within an area, there are calm or “wainting” times (τ) and defined through a fixed threshold magnitude. It has been verified that in California and Japan, the calm distribution is *p(τ)* happens to be represented by a *q- exponential distribution*. The accumulated probability is given $P(>\tau) = e_q^{-\tau/\tau_0}$ $(q > 1; \tau_0 > 0)$

Another important feature of earthquakes is the aging which occurs within the nonstationary regime called Omori regime, the set of aftershocks that follow a big event. The correlation functions of typical earthquakes in South California inside and outside the Omori Regime have shown that whenever aging is observed, data collapse can be obtained through rescaling. The connection with *q-statistics* comes from the fact that the type of dependence appears to be of the *q-exponential* form.

Other models for earthquakes have been discussed by Trikanli U (2005) and Tirkanli & Abe (2004); these are the Newman model (coherent noise model) and Olami–Feder–Christensen models. Both earthquake models yielded virtually the same result, namely that the rescaled correlation function is of the *q-exponential* form with q ≈ 2.98.

Let us address now the most classical quantity for earthquakes, namely the probability of having earthquakes of magnitude M (Gutenberg–Richter law). A nontrivial result (generalizing in fact the classical Gutenberg–Richter law) has been analytically obtained by Sotolongo & Posadas (2005) along this line for the cumulative probability G(> m) involving two parameters, *q* and *a* (*a* is the constant of proportionality between the released relative energy *E* and the linear dimension r of the fragments of the fault plates).

Finally, let us focus on the histograms of the avalanche size differences (Fig. 1.12). In particular, such probability distributions have been calculated in a dissipative Olami–Feder–Christensen model, and also for real earthquakes. The results for the OFC model have been calculated in both a small-world lattice (referred to as the critical case) and a regular lattice (referred to as the noncritical case). The conclusion is highly interesting: at criticality *q- Gaussian-like* distributions are obtained, whereas something close to a Gaussian on top of another (larger) Gaussian is obtained out of criticality.

The (analytic) connection between the various *qs* that have been presented here for earthquakes remains an open worthwhile question. Along this line, some hint might be obtained from the following observation. Series corresponding to thirteen earthquakes have been analysed in the study of Darooneh and C. Dadashinia (2008). It is claimed that the cumulative distribution of the distances between the epicentres of successive events is well fitted by a *qs*-exponential (where *s* stands for spatial); analogously, the cumulative distribution of the time intervals between successive events was also well fitted by a *qt*-exponential (where *t* stands for temporal).

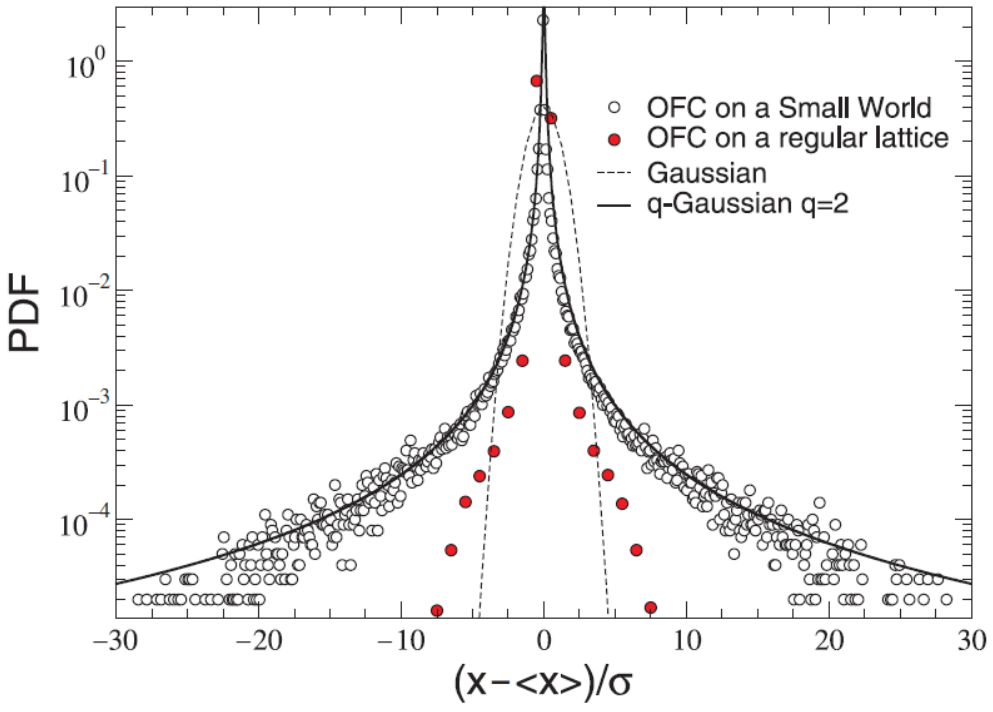

Figure 1.12 Probability distribution of the avalanche size differences (returns) *x(t) = S(t +1)−S(t)* for the OFC model on a small-world topology (critical state, open circles) and on a regular lattice (noncritical state, full circles). For comparison, a Gaussian and a *q-Gaussian* (with *q* = 2) are indicated as well. All the curves have been normalized so as to have unit area. For further details see Caruso et al., (2007).

CHAPTER 2

MODELING PROCEDURES & METHODS OF ANALYSIS

2.1 NON-EXTENSIVE APPROACH TO THE STATISTICAL PHYSICS OF EARTHQUAKES

2.1.1 Brief exposé of NESP.

In statistical mechanics, an *N*-component dynamic system may have $W=N!/\Pi_i N_i!$ microscopic states, where *i* ranges over all possible conditions (states). In classical statistical mechanics, the entropy of that system *S* is related to the totality of these microscopic states by the Gibbs formula $S=-k\sum_i p_i \ln(p_i)$, where *k* is the Boltzmann constant and p_i is the probability of each microstate. Furthermore, if the components of the system are all statistically independent and uncorrelated to each other, (non-interacting), the entropy of the system factorises into the product of *N* identical terms, one for each component; this is the Boltzmann entropy $S_B=-Nk\sum_i p_i \ln(p_i)$. It is easy to see that one basic property of the Boltzmann-Gibbs formalism is *additivity* (*extensivity*): the entropy of the system equals the sum of the entropy of their components. In the past few decades it has been widely appreciated that a broad spectrum of non-equilibrating natural and physical systems does not conform to this requirement. Such *non-additive* systems, which are also commonly referred to as *non-extensive* after Tsallis (1988), include statistically dependent (*interacting*) components, in consequence of which they acquire memory and can no longer be described with Boltzmann-Gibbs (B-G) statistical physics.

An appropriate thermodynamic description of non-extensive systems has been pioneered by Tsallis (1988, 2009), who introduced the concept of Non-Extensive Statistical Physics (NESP) as a direct generalization of Boltzmann-Gibbs statistical physics. Letting *x* be some dynamic parameter, the non-equilibrium states of non-extensive systems can be described by the Tsallis (1988) entropic functional:

$$S_q(p)=\frac{k}{q-1}\left[1-\int_0^{\infty} p^q(x)dx\right] \tag{2.1}$$

where $p(x)dx$ is the probability of finding the value of *x* in $[x, x+dx]$ so that $\int_W p(x)dx = 1$, and *q* is the *entropic index*. In the limiting case $q \rightarrow 1$, Eq. (2.1) converges to the Boltzmann–Gibbs functional

$$S_{BG}=-k\int_W p(x)\ln\left(p(x)\right)dX\ , \tag{2.2}$$

Like the Boltzmann-Gibbs, the Tsallis entropy is concave and fulfils the *H*-theorem but is

not additive when $q \neq 1$. For a mixture of two statistically independent systems *A* and *B*, the Tsallis entropy satisfies

$S_q(A, B) = S_q(A) + S_q(B) + (1-q)\, S_q(A)\, S_q(B)$.

This property is known as *pseudo-additivity* and is further distinguished into *super-additivity* (*super-extensivity*) if $q < 1$, *additivity* when $q \to 1$ (i.e. Boltzmann-Gibbs statistics) and *sub-additivity* (*sub-extensivity*) if $q > 1$. Accordingly, the entropic index is a measure of *non-extensivity* in the system.

An additional feature of NESP is the generalization of the expectation value in accordance with the generalization of entropy. Thus, the *q-expectation* value of *x* is defined as

$$\langle x \rangle_q = \int_0^\infty x \cdot p_q(x) dx \,, \tag{2.3}$$

where

$$p_q(x) = \frac{[p(x)]^q}{\int_0^\infty [p(x')]^q dx'} \,. \tag{2.4}$$

is an *escort distribution*. The concept of escort distributions has been introduced by Beck and Schloegl (1993) as a means of exploring the structures of (original) distributions describing fractal and multi-fractal non-linear systems: the parameter *q* behaves as a microscope for exploring different regions of $p(x)$ by amplifying the more singular regions for $q > 1$ and the less singular for $q < 1$.

Maximization of the Tsallis entropy yields the probability density function (PDF):

$$\hat{p}(x) = \frac{1}{Z_q} \exp_q \left[-\frac{\lambda}{I_q} \left(x - \langle x \rangle_q \right) \right], \tag{2.5}$$

$$Z_q = \int_0^\infty \exp_q \left[-\frac{\lambda}{I_q} \cdot \left(x - \langle x \rangle_q \right) \right] dx \,,$$

$$I_q = \int_0^\infty [\hat{p}(x)]^q dx$$

where λ is an appropriate Lagrange multiplier associated with the constraint on the *q*-expectation value and $\exp_q(.)$ denotes the *q-exponential* function

$$\exp_q(z) = \begin{cases} \left(1 + (1-q)z\right)^{\frac{1}{1-q}} & 1 + (1-q)z > 0 \\ 0 & 1 + (1-q)z \leq 0 \end{cases}, \tag{2.6}$$

that comprises a generalization of the exponential function: for $q \to 1$, $\exp_q(z) \to e^z$.

Eq. (2.5) is a *q-exponential distribution* and as evident from the definition of Eq. (2.6), it is a power-law if $q > 1$ corresponding to *sub-extensivity* (*sub-additivity*), an exponential if $q = 1$ corresponding to *extensivity* (*additivity*), and a power-law with cut-off if $0 < q < 1$ corresponding to *super-extensivity* (*super-additivity*); in the last case the cut-off appears at

$$x_c = \frac{x_0}{1-q}, \qquad x_0 = I_q \lambda^{-1} + (1-q)\langle \mathrm{x} \rangle_q \,. \tag{2.7}$$

Using the definitions of x_0 from Eq. (2.7) and the q-expectation value from Eq. (2.4), the probability $\hat{p}(x)$ can be expressed as

$$\hat{p}(x) = \frac{\exp_q \left(x/x_0 \right)}{\int_0^\infty \exp_q \left(x'/x_0 \right) dx'} \tag{2.8}$$

In the NESP formalism, the theoretical distribution to be fitted to the observed (empirical) distribution of x is not the original stationary distribution $\hat{p}(x)$ but the escort probability $\hat{p}_q(x)$. Accordingly, the *cumulative* probability function (CDF) becomes:

$$\hat{P}(> x) = \int_x^\infty \hat{p}_q(x') dx' \,. \tag{2.9}$$

By substituting Eq. (2.8) in Eq. (2.4) and evaluating the integral, Eq. (2.9) reduces to:

$$\hat{P}(> x) = \exp_q \left(-\frac{x}{x_0} \right) = \left[1 - (1-q) \left(\frac{x}{x_0} \right) \right]^{\frac{1}{1-q}} \tag{2.10}$$

which also is a q-exponential distribution that for $q > 1$, defines a CDF of the Zipf-Mandelbrot kind.

Fig. 2.1 illustrates the behaviour of a q-exponential CDF (Eq. 2.10) for different values of q. For $q > 1$ the CDF has a tail that becomes increasingly longer (fatter) with increasing q: this translates to increasing correlation (interaction) between its components and long-term memory. For $q \to 1$, the power law converges to the common exponential distribution so that the system comprises an uncorrelated and memoryless point (random) process. For $0 < q < 1$, the CDF is a power-law exhibiting a cut-off whenever the argument becomes negative, i.e. $\hat{P}(> x) = 0$, and is characterized by a bounded correlation radius.

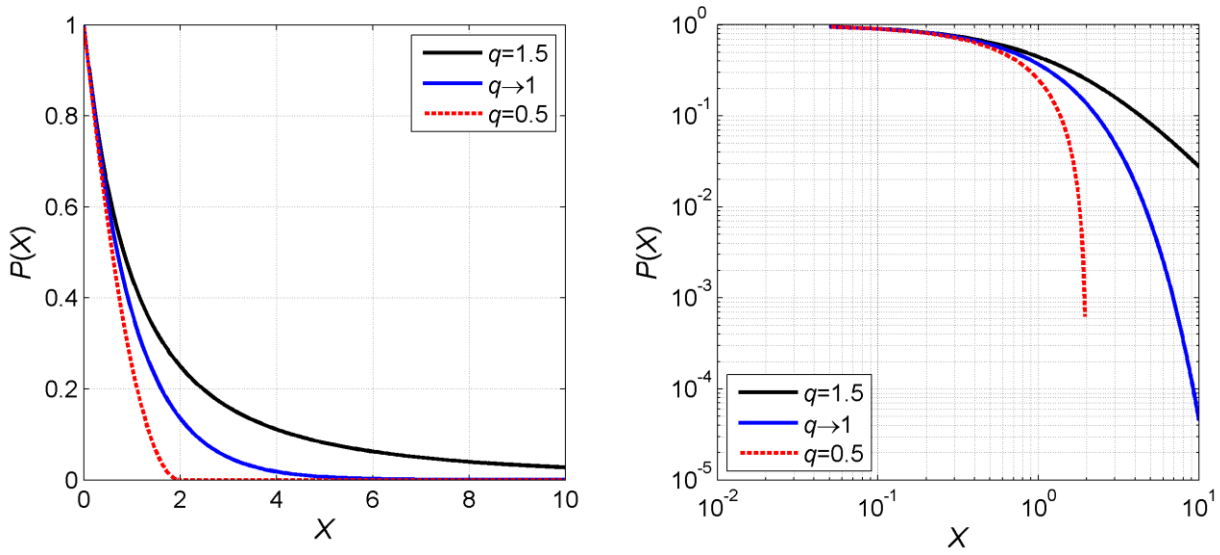

Figure 2.1. Three realizations of the *q*-exponential CDF for $q < 1$ (red line), $q = 1$ (blue line) and $q > 1$, plotted in linear (left) and double-logarithmic scale (right).

2.1.2 Seismicity and NESP: An overview

During the past several years, Non-Extensive Statistical Physics (NESP) has enjoyed increasing attention with several researchers studying the properties of the F-T and F-M distributions (e.g. Vallianatos and Telesca, 2012). This includes studies of simulated *q*-exponential distributions emerging from critical seismicity models (e.g. Caruso et al., 2007; Bakar and Tirnakli, 2009), non-critical models, (e.g. Celikoglu et al., 2010), and rock fracture experiments (e.g. Vallianatos et al., 2012a). It also includes empirical studies of interevent time statistics based on the *q*-exponential distribution specified by Eq. 2.10 (e.g. Abe and Suzuki, 2005; Carbone et al., 2005; Vallianatos et al., 2012b; Vallianatos et al., 2013; Vallianatos and Sammonds, 2013; Papadakis et al., 2013, 2015; Michas et al., 2013, 2015; Antonopoulos et al., 2014). A recent review of NESP applications over a broad spectrum of scales, from tectonic plates to country rock fractures and laboratory fragmentation experiments is given by Vallianatos et al., (2016).

Non-extensive analysis of the F-M distribution has been undertaken by Sotolongo-Costa and Posadas (2004), Silva et al. (2006) and Telesca (2011, 2012). These authors proposed NESP generalizations of the Gutenberg-Richter law based on physical models that consider the interaction between two rough fault walls (asperities) and the fragments filling space between them (*fragment-asperity model*); this interaction is supposed to modulate earthquake triggering. In this model, the generalized Gutenberg-Richter law is approached by considering the size distribution of fragments and asperities and the

scaling of size with energy. The transition from size to energy and magnitude distributions depends on how energy scales with size and with magnitude.

Sotolongo-Costa and Posadas (2004) assumed that the energy stored in the asperities and fragments scales with their linear characteristic dimension r ($E \propto r$) or, equivalently, with the square root of their areas σ ($E \propto \sigma^{1/2}$); they also assumed that the magnitude scales with energy as $M \propto \log(E)$. Darooneh and Mehri (2010) expand on the same model but assume that $E \propto \exp(\sigma^{1/a})$ and $M \propto \ln(E)$. We propose that the above assumptions are not compatible with the empirical laws of energy – moment and moment – magnitude scaling in particular (e.g. Scholz, 2002; Lay and Wallace, 1995). Silva et al., (2006) revisited the fragment-asperity model and expressed Eq. (2.10) as

$$\hat{p}(\sigma) = \left[1 - \frac{1-q}{2-q}\left(\sigma - \langle\sigma\rangle_q\right)\right]^{\frac{1}{1-q}}. \tag{2.11}$$

Assuming that the energy scales with the characteristic volume of the fragments ($E \propto r^3$), so that $E \propto \sigma^{3/2}$ because σ scales with r^2, it is easy to see that $(\sigma - \langle\sigma\rangle_q) = (E/\alpha)^{2/3}$ with α being a proportionality constant between E and r. This yields the energy density function

$$\hat{p}(E) = \left(\frac{2}{3}\cdot\frac{E^{-1/3}}{\alpha^{2/3}}\right)\cdot\left[1 - \frac{(1-q)}{(2-q)}\frac{E^{2/3}}{\alpha^{2/3}}\right]^{-\frac{1}{1-q}}$$

so that $\hat{P}(>E) = N(>E)N_0^{-1} = \int_E^{\infty}\hat{p}(E)dE$, where N ($>E$) is the number of events with energy greater than E and N_0 is the total number of earthquakes. If the magnitude scales with energy as $M \propto \frac{1}{3}\log(E)$, for $q > 1$,

$$\hat{P}(>M) = \frac{N(>M)}{N_0} = \left(1 - \frac{1-q_M}{2-q_M}\cdot\frac{10^{2M}}{\alpha^{2/3}}\right)^{\left(\frac{2-q_M}{1-q_M}\right)} \tag{2.12}$$

Eq. (2.12) has been used to investigate the seismicity of different tectonic regions (Telesca, 2010a, 2010b; Telesca and Chen, 2010; Scherrer et al., 2015, Esquivel and Angulo, 2015). Finally, assuming $E \propto r^3$ but that the magnitude scales with energy as $M \propto \frac{2}{3}\log(E)$, Telesca (2011, 2012) has introduced a modified version of Eq. (2.12):

$$\hat{P}(>M) = \frac{N(>M)}{N_0} = \left(1 - \frac{1-q_M}{2-q_M}\cdot\frac{10^{M}}{\alpha^{2/3}}\right)^{\left(\frac{2-q_M}{1-q_M}\right)}. \tag{2.13}$$

Here it is suggested that this model, by postulating that the energy released in the form

of seismic waves scales with the effective area of the fault (fragments and asperities), is consistent with the empirical laws of energy–moment and moment–magnitude scaling and is also compatible with the well-studied rate-and-state friction laws of rock failure. In consequence, our analysis will be based on the F-M distribution specified by Eq. (2.13).

2.2. MULTIVARIATE EARTHQUAKE FREQUENCY DISTRIBUTIONS: CONSTRUCTION AND NESP-BASED MODELLING

One of the main goals is to investigate whether seismicity is a Poissonian or Complex/Critical process by using the NESP formalism to search for the presence (or absence) of correlation in time, size and space. This can be done by determining the values and variation of the relevant entropic indices. To ensure rigour in our analysis, instead of considering only one-dimensional frequency distributions as almost all hitherto studies have done, we focus on *multivariate* earthquake frequency distributions thereby introducing additional mutual constraints on the permissible variation of the empirically determined entropic indices. The most general multivariate earthquake frequency distribution is one that expresses the joint probability of observing an earthquake larger than a given magnitude, after a given lapse time and beyond a given distance. This would require the construction and analysis of *tri-variate* frequency – magnitude – interevent time – interevent distance (F-M-T-D) distributions which live in a four-dimensional realm and would be more difficult to manage and interpret. Accordingly, the easier to handle *bivariate* Frequency – magnitude – interevent time (F-M-T) distributions was used in order to focus on correlations in earthquake size and time of occurrence. However, because this may not extract explicit information about the range of possible correlations, the *interevent distance* was also used as a spatial filter by which to separate and study the temporal correlation of *proximal* and *distal* earthquakes. The rationale behind this approach is that if distal earthquakes are correlated in time, then they have to be correlated in space via long-distance interaction and vice versa.

A bivariate F-M-T distribution can be constructed as follows: A *threshold* (cut-off) magnitude M_{th} is set and a bivariate frequency table (histogram) representing the empirical *incremental* distribution is first compiled. The empirical *cumulative* distribution is then obtained by backward bivariate summation, according to the scheme

$$N_{m\tau} = \sum_{j=D_T}^{\tau} \sum_{i=D_M}^{m} \left\{ H_{ij} \Leftrightarrow H_{ij} \neq 0 \right\}, \quad \tau = 1,\ldots D_T, \quad m = 1,\ldots D_M \tag{2.14.}$$

where H is the incremental distribution, D_M is the dimension of H along the magnitude axis and D_T is the dimension of H along the Δt axis. In this construct, the cumulative

frequency (earthquake count) can be written thus: $N(\{M \geq M_{th},\ \Delta t : M \geq M_{th}\})$. Then, the empirical probability $P(>\{M \geq M_{th},\ \Delta t : M \geq M_{th}\})$ is simply

$$\frac{N\left(>\{M \geq M_{th},\ \Delta t : M \geq M_{th}\}\right)}{N_0}, \qquad N_0 = N(M = M_{th}, 0) = \left\|N\right\|_{\infty}. \tag{2.15}$$

An empirical cumulative F-M-T distribution constructed according to Eq. (2.14) is presented in Fig.2.2: It is based on a subset of 3,653 events extracted from the NCSN earthquake catalogue published by the North California Earthquake Data Center, using a threshold magnitude M_{th} = 3.4 over the period 1975-2012 and excluding the Mendocino Fracture Zone. The distribution is shown in linear (Fig. 2.2a) and logarithmic (Fig. 2.2b) frequency scales and comprises a well-defined surface in which the end-member ($M \geq M_{th}$, Δt=0) is the one-dimensional empirical Gutenberg – Richter law and the end-member ($M = M_{th}$, Δt) is the one-dimensional frequency – interevent time (F-T) distribution.

Assuming that magnitudes and interevent times are statistically independent, namely that the hierarchy of the active fault network does not influence the sequence of events, the joint probability $P(M \cup \Delta t)$ factorizes into the probabilities of M and Δt in the sense $P(M \cup \Delta t) = P(M)\ P(\Delta t)$. Then, by implicitly *identifying* the empirical and escort probabilities we obtain

$$\frac{N\left(>\{M \geq M_{th},\ \Delta t : M \geq M_{th}\}\right)}{N_0} = \left(1 - \frac{1-q_M}{2-q_M} \cdot \frac{10^M}{\alpha^{2/3}}\right)^{\left(\frac{2-q_M}{1-q_M}\right)} \cdot \left(1 - (1-q_T) \cdot \frac{\Delta t}{\Delta t_0}\right)^{\frac{1}{1-q_T}}, \tag{2.16}$$

where q_M and q_T are the entropic indices for the magnitude and interevent times respectively and Δt_0, is the *q-relaxation time*, analogous to the relaxation (characteristic) time often encountered in the analysis of physical systems. On taking the logarithm and setting $a = \log(N_0)$, Eq. (2.16) becomes

$$\log N\left(>\{M \geq M_{th},\ \Delta t : M \geq M_{th}\}\right) = \\ = a \quad + \quad \left(\frac{2-q_M}{1-q_M}\right) \cdot \log\left(1 - \frac{1-q_M}{2-q_M} \cdot \frac{10^M}{\alpha^{2/3}}\right) \quad + \quad \frac{1}{1-q_T} \log\left(1 - \Delta t_0^{-1}(1-q_T)\Delta t\right) \tag{2.17}$$

Eq. (2.17) is a generalized (bivariate) law of the Gutenberg – Richter kind in which

$$b_q = \frac{(2-q_M)}{(q_M - 1)} \tag{2.18}$$

is the NESP *generalization* of the *b* value (also see Telesca, 2012). Accordingly, Eq. (2.17) is the general model to be implemented in the ensuing analysis.

The logarithmic form of the distribution shown in Fig. 2.2b can be approximated with Eq. (2.17) using non-linear least-squares. Because the parameters are all positive and the entropic indices are bounded, we implemented the *trust-region reflective* algorithm (e.g. Moré and Sorensen, 1983; Steihaug, 1983), together with *least absolute residual* (LAR) minimization so as to suppress possible outliers. The result is shown in Fig. 2.3a. The quality of the approximation is excellent with a correlation coefficient (R^2) of the order of 0.99. The magnitude entropic index q_M = 1.51 so that $b_q \approx 1$, which compares well with b values computed with conventional one-dimensional techniques for the same data set. The temporal entropic index q_T is approximately 1.3 and indicates moderate sub-extensivity. Fig. 3b presents a succinct statistical appraisal of the result, performed by fitting a normal location-scale distribution (dashed line) and a Student-t location-scale distribution (solid line) to the cumulative probability of the sorted residuals (r). Approximately 85% of the residual population, for which $|r| \leq 0.1$, is normally distributed. The short-truncated tail forming at $r < -0.1$ consists of 39 residuals (~16% of the population) and does not deviate significantly from normality. The long tail forming at $r > 0.2$ is fitted with neither the normal nor the t-location-scale distribution; however, it consists of only 7 residuals (2.87%) and represents *outliers effectively suppressed* by the LAR procedure.

It is interesting to note that outliers are mainly observed at the intermediate and larger magnitude scales and longer interevent times. They frequently arise from minor flaws of the catalogue, (e.g. omitted (sequences of) events, glitches in magnitude reporting etc.), but in some cases they may comprise true exceptions to the continuum of the regional seismogenetic process: for instance, they may correspond to rare, externally triggered events. Herein, we shall not be concerned with such details, but it is interesting to point them out. The existence of outliers has compelled us to introduce a significant constraint in the construction of the F-M-T distribution: according to Eq. (2.14), the cumulative distribution is formed by stacking only the populated (non-zero) bins of the incremental distribution. Regardless of the origin of the outliers, their inclusion in the summation would have generated a *stepwise* function in which the unpopulated bins (unknown probability densities) lying between the outliers and the populated bins would appear as patches of equal earthquake frequency (uniform probability), as illustrated in Fig. 2c and 2d. In this case, the high probability zones of the empirical bivariate distribution would comply with well specified laws, but the lower probability zones would, for some “unknown” reason, include uniform patches. In one-dimensional distributions this effect may not influence

parameter estimation by a significant factor and is often neglected. In multivariate distributions however, in addition to the obvious absurdity, it would be numerically detrimental.

In a final note, in order to distinguish between proximal and distal earthquakes and assess their correlation, I apply the above modelling procedure to subsets of the catalogue in which earthquakes are grouped by interevent distance according to the rule

$$C \supset \{C_D\colon\ M > M_{th} \wedge \Delta d_L \leq \Delta d \leq \Delta d_U\}, \tag{2.19}$$

where C is the catalogue, C_D is the subset catalogue, Δd is the interevent distance and Δd_L, Δd_U are the upper and lower group limits. This is equivalent to constructing and modelling the *conditional* bivariate cumulative distribution

$$P(\ >\{M \geq M_{th},\ \Delta t\ :\ [M \geq M_{th} \wedge \Delta d_L \leq \Delta d \leq \Delta d_U\ ]\}) \tag{2.20}$$

as a proxy of the *trivariate* F-M-T-D distribution.

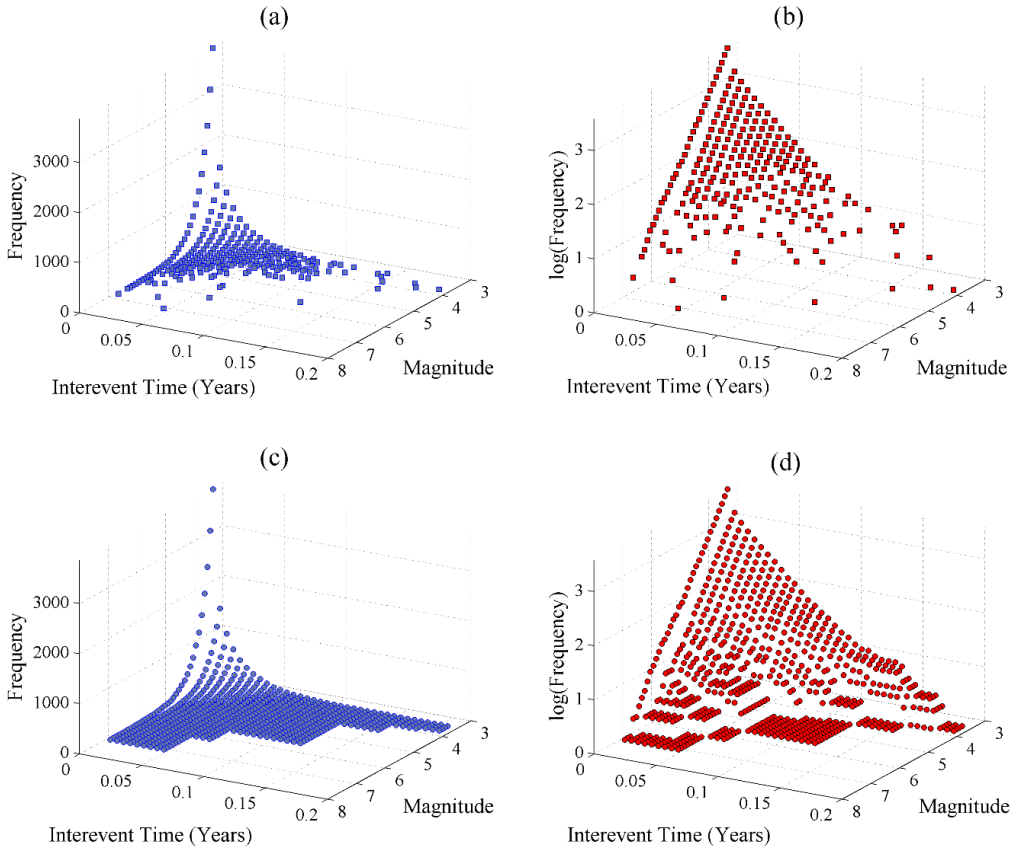

Figure 2.2. (a) Bivariate cumulative frequency – magnitude – interevent time (F-M-T) distribution constructed according to Eq. (2.14) on the basis of 3,653 events with $M_L \geq 3.4$ extracted from the NCSN earthquake catalogue; see text for details. **(b)** As per (a) but in logarithmic frequency scale. **(c)** As per (a) but including unpopulated bins in the summation, i.e. using the scheme $N_{m\tau} = \sum_{j=D_T}^{\tau} \sum_{i=D_M}^{m} H_{ij}$ instead of Eq. (2.14). **(d)** As per (c) but in logarithmic frequency scale.

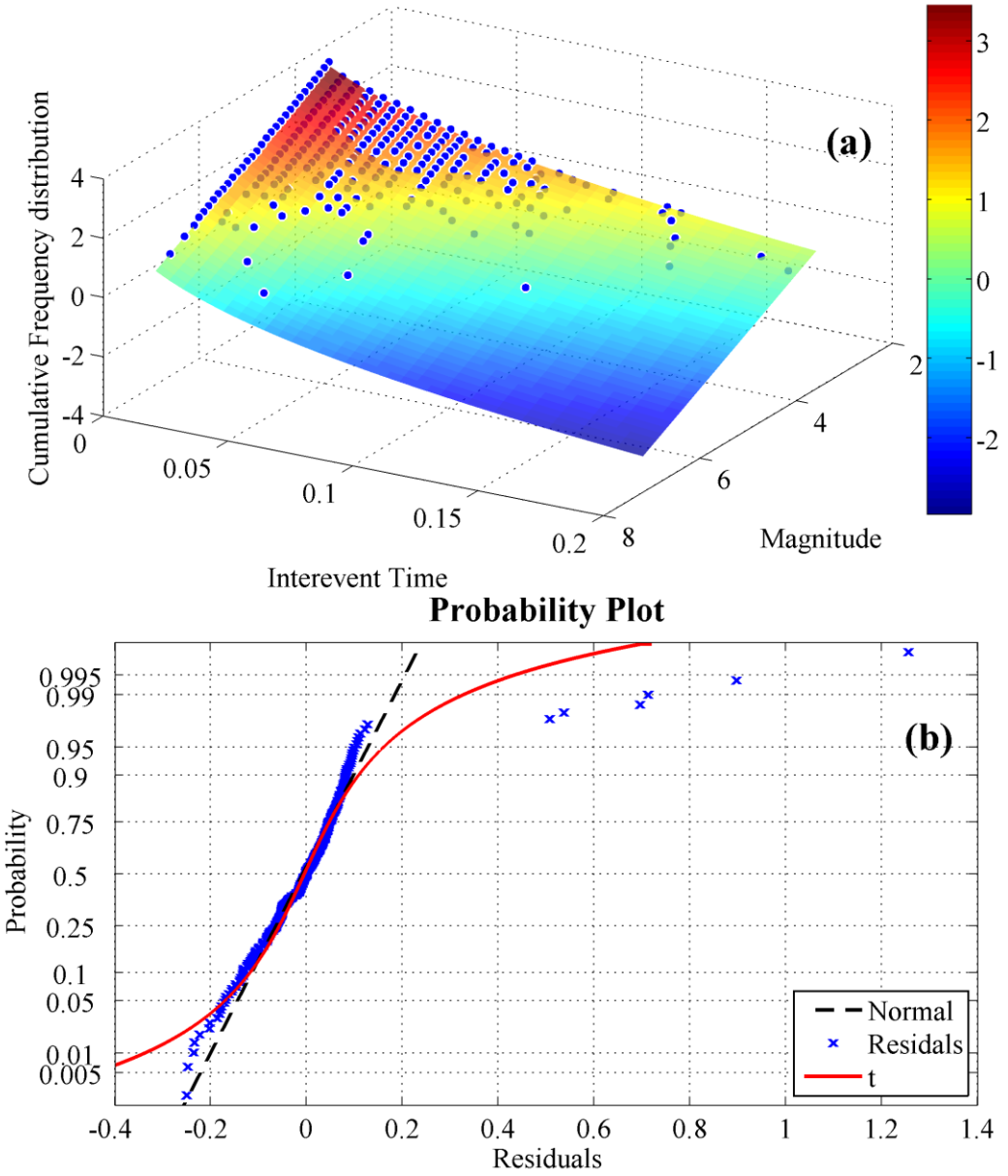

Figure 2.3. (a) The logarithmic scale F-M-T distribution of Fig. 2b together with the model fitted using Eq. (2.17); the colorbar represents the number of events in logarithmic (frequency) scale. **(b)** Probability analysis of the residuals.

2.3 DECLUSTERING

The question of whether the background seismogenetic process is fundamentally random or correlated is open to debate and can be answered by analysing reduced versions of the earthquake catalogues, in which the aftershock sequences have been eliminated in an optimal as possible way. The process of reducing an earthquake catalogue so as to separate background and foreground events is referred to as *declustering*.

Declustering is often required before analysing earthquake catalogues, especially when testing some hypotheses of seismicity associated with tectonic environments, for temporal clustering of foreshocks, aftershocks, and swarms always complicate the analysis. However, there is no accepted physical mechanism separating aftershocks from mainshocks that would lead to a unique method of discrimination. In fact, declustering is often motivated by attempts to constrain such a mechanism by the statistical properties of main shocks e.g. their frequency-magnitude relationship (Knopoff, 2000). Therefore, declustering methods have been devised that identify aftershocks based on belonging to a set of earthquakes defined by a space-time window around presumed mainshocks (Utsu, 1969; Gardner and Knopoff, 1974, Helmstetter, 2003) or by a link-based method Reasenberg (1985); Hainzl et al., (2006) etc.

Declustering and modelling should be equivalent or at least consistent since declustering is an expression of some belief about seismicity relations that are captured by the model. The use different models for predicting and declustering, for instance, only makes sense if the two are consistent with each other. This approach was followed by Kagan (1991) and Zhuang and co-authors (Zhuang et al., 2002; 2004) because an available likelihood model could be fit to the catalogue to estimate the probability of independence of a given value.

An excellent review of declustering methods and their evolution from deterministic (e.g. Gardner and Knopoff, 1974; Reasenberg, 1985) to stochastic (e.g. Zhuang et al., 2002; Marsan and Lengliné, 2008), is given in van Stiphout et al, (2012). The deterministic methods identify foreground events on the basis of temporal and spatial windows that scale with the magnitude of the main shock while ignoring aftershocks triggered by aftershocks (higher order events). The stochastic methods allow for multiple generations of aftershock triggering within a cluster and use Omori's law as a measure of the temporal dependence of aftershock activity. Both approaches ignore fault elongation and assume circular (isotropic) spatial windows. Stochastic declustering was introduced by Zhuang et

al., (2002); their approach improves on previous methods because it optimizes the temporal and spatial window in which to search for aftershocks by fitting an ETAS model to the earthquake data. Furthermore, instead of assigning aftershocks to arbitrarily chosen main shocks, it assigns each earthquake in the catalogue with a probability that it is an aftershock of its predecessor so that all earthquakes may be possible main shocks to their short-term aftereffects. Marsan and Lengliné (2008) carried stochastic declustering one step forward by introducing a generalized triggering process that does not require some underlying earthquake occurrence model; nevertheless, they still assume that background earthquakes occur at constant and spatially uniform rate.

Herein we have chosen to implement the method of Zhuang et al., (2002) because it has an additional and significant for our objectives advantage: it is a *paradigmatic* realization of the self-excited Poisson process. Thus, if the background seismicity obeys Boltzmann-Gibbs statistics, this method should be able to extract a nearly random background process against which to test the alternative hypotheses. If it is does not, the argument in favour of non-Poissonian background would be stronger.

The Zhuang et al., (2002) method utilizes the following form of the normalized probability that one event will occur in the next instant, conditional on the history of the seismogenetic process:

$$\lambda\left(t,x,y,M \mid H_t\right)=\mu\left(x,y,M\right)+\sum_{i:t_i<t}\kappa\left(M_i\right)\cdot g\left(t-t_i\right)\cdot f\left(x-x_i,y-y_i \mid M_i\right)\cdot j(M \mid M_i)$$

where λ is the conditional intensity on the history of observation H_t until time t, $\mu(x, y, M)$ is the background intensity, $\kappa(M)$ is the expected number of foreground events triggered by a magnitude M main shock and $g(t)$, $f(x,y|M_i)$ and $j(M|M_i)$ are respectively the probability distributions of the occurrence time, the location and the magnitude events triggered by a main shock of magnitude M_i. If the catalogue is arranged in chronological order, then the probability of an event j to have been triggered by an event $i < j$ can be estimated from the occurrence rate at its occurrence time and location as

$$p_{i,j}=\frac{\kappa(M_i)\cdot g(t_j-t_i)\cdot f(x_j-x_i,y_j-y_i \mid M_i)}{\lambda(t_j,x_j,y_j \mid H_t)}$$

and the probability that event j is aftershock is given by

$$p_j=\sum_{i=1}^{j-1}p_{i,j}$$

Conversely, the probability that event j is background is given by

$$\phi_j = 1 - p_j = \frac{\mu(x_j, y_j \mid H_t)}{\lambda(t_j, x_j, y_j \mid H_t)}$$

The algorithm runs iteratively through the catalogue and by assigning probabilities $p_{i,j}$, p_j and ϕ_j to the j^{th} event, generates the foreground sub-process associated with the i^{th} event (i.e. its aftershock sequence). It thus separates the catalogue into a number of sub-processes whose initiating events comprise the background. As a general rule, events with $\phi_j \leq 50\%$ are considered to be foreground.

Since the output of stochastic declustering is not unique, it is useful to use the probabilities $p_{i,j}$ and ϕ_j to generate different realizations of the declustered catalogue at different probability levels and use them to test hypotheses associated with background seismicity and/or aftershock clustering. Our analysis herein will be based on the assumption that events with probability $\phi_j \geq 70\%$ are likely to be background. Results obtained from NESP analysis of higher probability levels will not be shown herein because they do not offer significant additional information with respect to the objectives of this paper.

The results of our declustering exercise are summarized in the corresponding Tables for each study area. In general, as will be seen in the following chapters, all catalogues declustered at the $\phi \geq 70\%$ level are *almost* free of the time-local rate jumps that indicate the presence of aftershock sequences; therefore, they are fairly representative of the background process. It should be noted, however, that they are not always completely smooth and exhibit small fluctuations because a small portion of the remaining events are residuals of the foreground process.

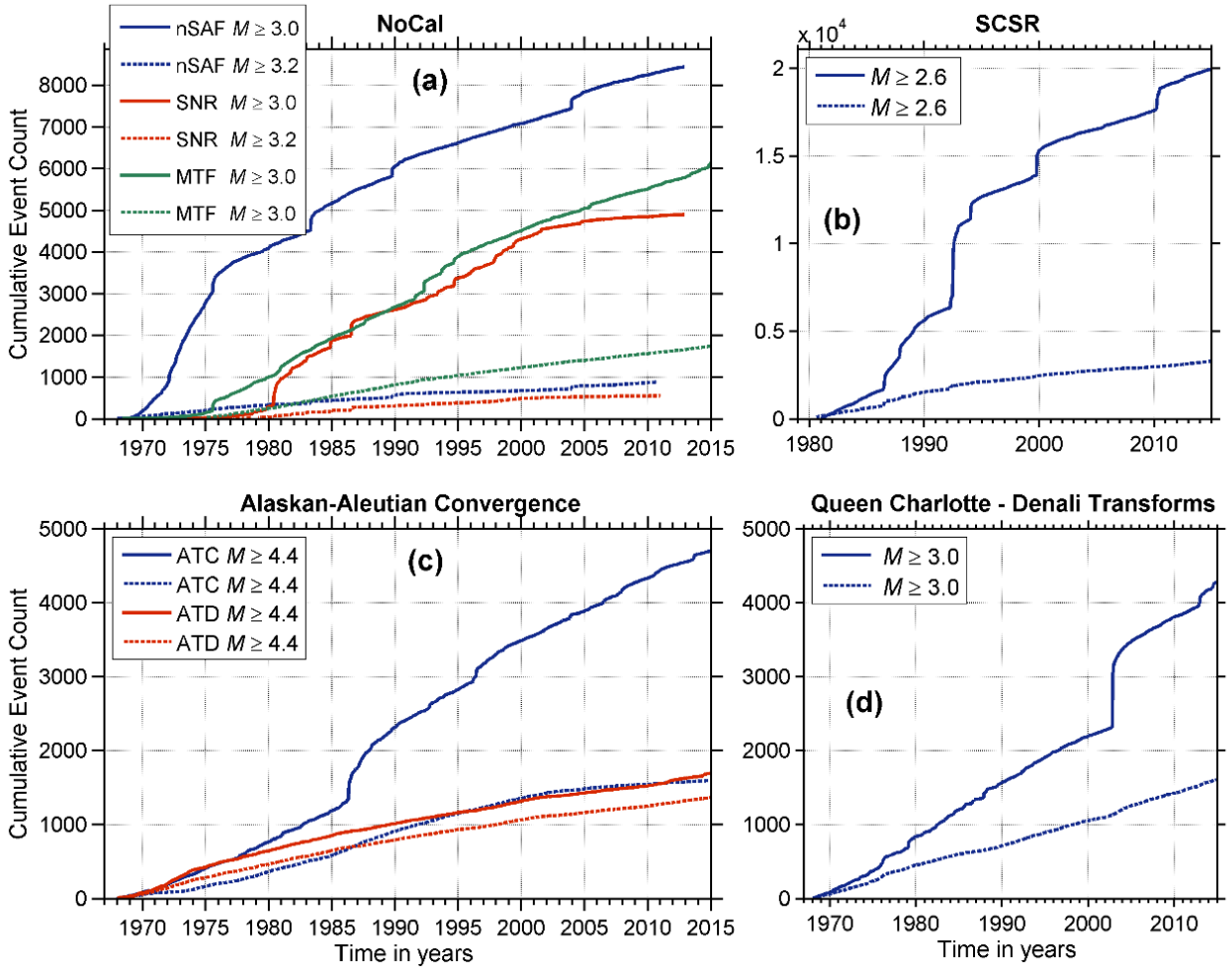

Figure 2.4. An example of cumulative event counts for the full (solid lines) and declustered (broken lines) earthquake catalogues used in this study (in the following chapters). **a)** Full and declustered sub-catalogues of North California (NoCal); **b)** As per (a) for the South California Seismic Region (SCSR). **c)** As per (a) for the crustal (ATC) and sub-crustal (ATD) catalogue subsets of the Aleutian Arc and Trench. **d)** As per (a) for the Queen Charlotte – Fairweather and Denali zone of transform faults (Alaska).

2.4. DETERMINATION OF RANDOMNESS THRESHOLDS

In order to determine a threshold value above which it is safe to conclude that the temporal entropic index (q_T) indicates non-extensive seismogenetic processes, I apply Eq. (2.17) to the analysis of several background catalogues generated on the basis of the ETAS model: each of those catalogues should yield temporal entropic indices with an expectation value of unity. The synthetic catalogues were generated with the stochastic ETAS aftershock simulator program “AFTsimulator” of Felzer (2007). The program uses the Gutenberg-Richter and Omori-Utsu laws to simulate the statistical behaviour background and foreground seismicity, and Monte Carlo methods to simulate background earthquakes as well as multiple generations of aftershocks. Known main shocks can be included as point or planar sources and background earthquakes are chosen randomly

from observed or contrived spatial distributions (grids) of earthquake rates. This facilitates the generation of realistic synthetic background catalogues, consistent with the known long-term seismotectonic characteristics of a given area (for details see Felzer et al., 2002 and Felzer and Brodsky, 2006). In my implementation of the AFTsimulator I have used the ETAS parameterizations for North and South California obtained (fitted) by declustering the NCSN and SCSN catalogues. I have also assumed a uniform background seismicity rate such that b = 1 and have set the maximum expected magnitude to be M_L = 7.2, approximately the same as the maximum magnitudes observed in California during the 47-year period 1968-2015 (the Loma Prieta and Landers earthquakes of 1989 and 1992 respectively).

Fig. 2.5 illustrates results from NESP analysis of 40 synthetic background catalogues, 20 of which were compiled for the SCSR source area and 20 for the whole of North California (NoCal ≡ nSAF + SNR + MFZ). Both sets of catalogues span a period of 47 consecutive years. Fig. 8a illustrates the variation of the mean values $\langle q_T \rangle$ and $\langle q_M \rangle$ computed from the analysis of the synthetic catalogues, together with their associated 3σ error margins, as a function of the threshold (cut-off) magnitude M_{th}. It is apparent that all $\langle q_T(M_{th}) \rangle$ are consistently lower than 1.1 without exception, so that $\max[\langle q_T(M_{th}) \rangle + 3\sigma] < 1.15$. Likewise, all $\langle q_M(M_{th}) \rangle$ exhibit an almost imperceptible variation around 1.5, so that $b_q \approx 1$, consistently with the assumption on which the synthetic ETAS catalogues were constructed. It is also apparent that the populations $\{q_T(M_{th})\}$ and $\{q_M(M_{th})\}$ from which $\langle q_T(M_{th}) \rangle$ and $\langle q_M(M_{th}) \rangle$ have been derived are remarkably consistent: the 3σ error bars are generally very small and, in many cases, smaller than the size of the symbols representing the expectation values! Fig. 8b illustrates the variation of entropic indices computed by grouping the earthquakes of the synthetic catalogues according to interevent distance (Eq. 2.19) and modelling the conditional probability function expressed by Eq. (2.20). All results have been derived by considering earthquakes above a threshold magnitude M_{th} = 3.0. As above, the figure shows mean values $\langle q_T(\Delta d) \rangle$ and $\langle q_M(\Delta d) \rangle$ with their associated 3σ error margins. All $\langle q_T(\Delta d) \rangle$ are consistently low for all interevent distance groups, so that $\max[\langle q_T(\Delta d) \rangle + 3\sigma] \leq 1.2$, while $\langle q_M(\Delta d) \rangle$ are also very stable and exhibit small fluctuations around 1.5, so that $b_q \rightarrow 1$ as expected.

The above exercise was conducted with several random background catalogues generated on the basis of the ETAS model. In consequence, it can be concluded that the analytical procedure described in Sections 2.2 and 2.3 yields stable magnitude entropic

indices and proxy *b-values* (b_q) absolutely consistent with the assumptions on which the synthetic ETAS catalogues were constructed. More importantly, however, the results establish that the systematic observation of experimental values $q_T(M_{th}) \geq 1.15$ and $q_T(\Delta d)\rangle > 1.2$ would be compelling evidence of non-extensive seismogenetic dynamics.

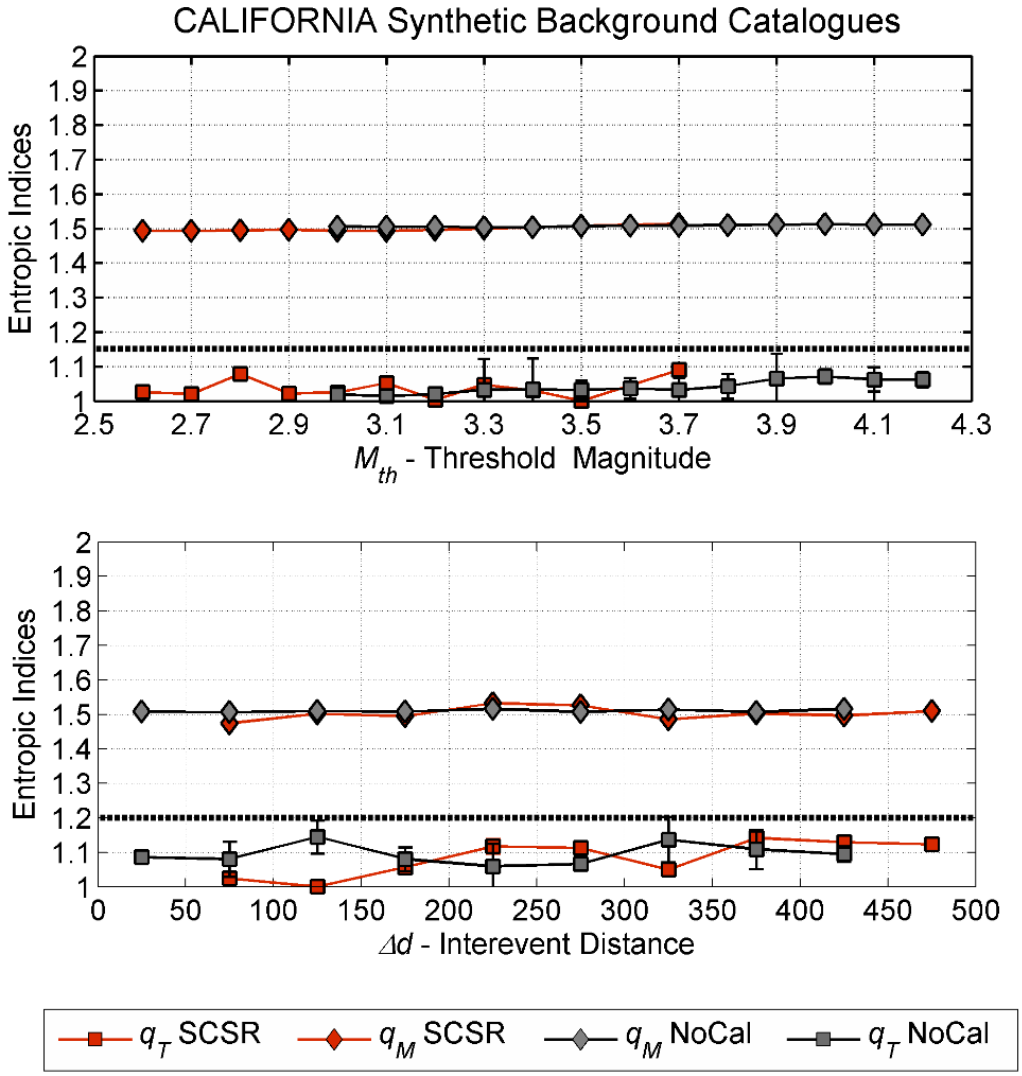

Figure 2.5. NESP analysis of 20 ETAS synthetic background catalogues constructed with the characteristics of South Californian (SCSR) and 20 constructed with the characteristics of North Californian seismicity (NoCal). Both catalogues span a period of 47 consecutive years. **(a)** Mean values $\langle q_T(M_{th})\rangle$ and $\langle q_M(M_{th})\rangle$ of the entropic indices and associated 3σ error margins, computed for different threshold magnitudes (M_{th}). The horizontal dashed line at q_T = 1.15 marks the threshold above which $q_T(M_{th})$ can be *safely* assumed to indicate non-Poissonian processes. **(b)** Mean values $\langle q_T(\Delta d)\rangle$ and $\langle q_M(\Delta d)\rangle$ with associated 3σ error margins computed for different interevent distance groups Δd. The horizontal dashed line at q_T = 1.2 marks the threshold above which $q_T(\Delta d)$ can be *safely* assumed to indicate non-Poissonian processes.

2.5 COMPLETENESS AND HOMOGENEITY OF EARTHQUAKE CATALOGUES

A critical issue to be addressed before any scientific analysis, is to assess the quality, consistency, and homogeneity of the data. The accuracy and reliability of seismic hazard assessment depends on the kind of seismicity data being used. Catalogue incompleteness has been a subject of discussion for many years. The level of incompleteness mostly occurs in different time segments from pre-historic (palaioseismological) and historic and instrumental data sets. The completeness of historical earthquake data depends on the local intensity of a historical event as well as on various other factors such as the population density, interest and motivation of chronologists to note down the event, social and political circumstances and other natural disasters distracting attention from earthquakes (Gutdeutsch and Hammerl 1997; 1999). The incompleteness of instrumental data, however, may be due to the geometry and coverage of the seismic network, or malfunction of seismic stations. A thorough assessment of the data completeness is therefore a prime prerequisite for any hazard evaluation.

The minimum magnitude of complete recording, M_c, is an important parameter for most studies related to seismicity. It is well known that M_c changes with time in most catalogues, usually decreasing, because the number of seismographs increases, and the methods of analysis improve. The spatial and temporal completeness is essential, for the estimation of seismic hazard parameters, like the activity rate, λ, relationship ($b = \beta \log e$), the maximum magnitude, Mmax, expected to occur in a target area and the b-value of the G–R (frequency - magnitude).

Space and temporal variations of the *b-value* have been employed in numerous seismicity studies. At small magnitudes, significant deviations of b-values may imply artifacts due to catalogue incompleteness (small earthquakes not as numerous); at large earthquakes this problem may be associated with inhomogeneity in the way magnitudes are measured and/or with the length of available catalogues with missing large earthquakes. High-quality results can be achieved, with the use the maximum number of events available. This comes as a contradiction with the fact that in many cases one has to use a single overall M_c cutoff that is high, in order to guarantee completeness.

To demonstrate all the above constraints, I use as an example the F-M distribution for the Hellenic network (compiled from the ISC catalogue) for the period 1964-2015, as well as for the Aleutian Arc – Trench system during the period 1968-2015 (Figure 2.6). As can

be seen, in both cases the catalogues clearly are not complete to values of Mc 4.1 and 4.4 respectively, suggesting that the heterogeneity of *Mc* caused the nonlinearity of the F-M distribution. In such statistical techniques as NESP, a population of events below *Mc* threshold may result in doubtful interpretations of the modeling process and the model itself (Figure 2.7).

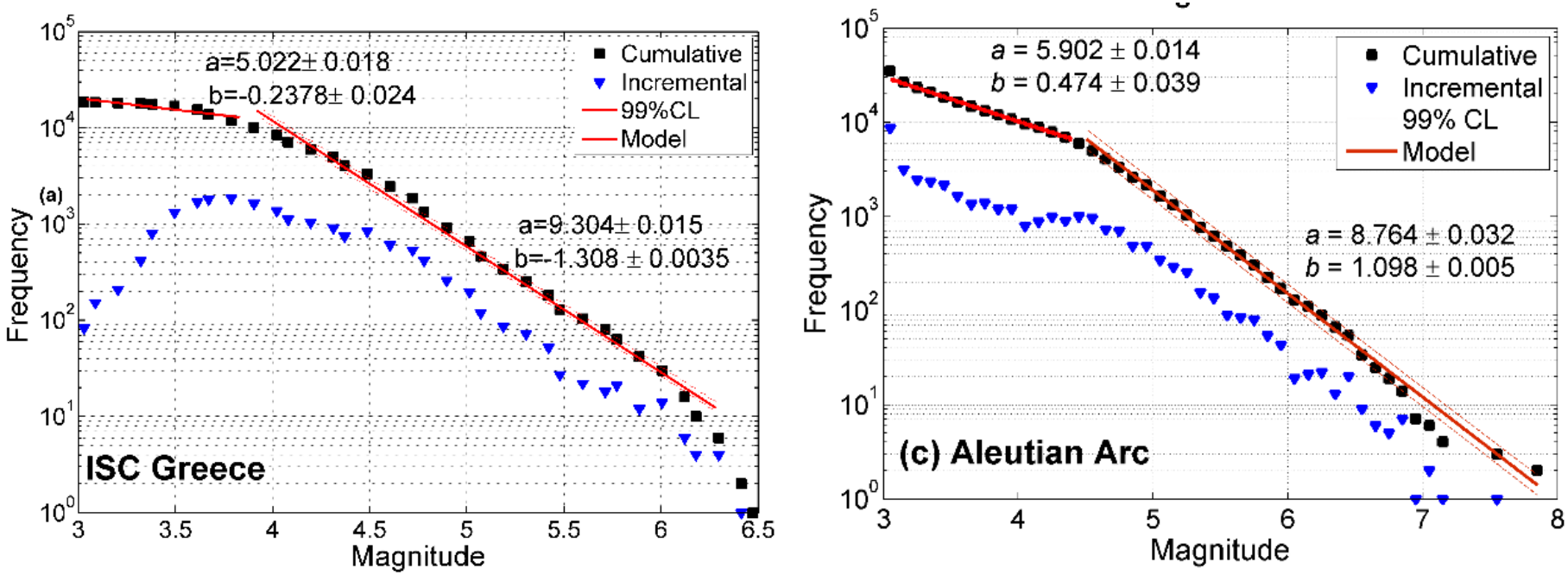

Figure 2.6 Cumulative FMD of all earthquakes of the Hellenic network (1964-2015) and the Aleutian Arc-Trench system (1968-2015). The origin of this bimodal distribution might be natural, (different physical mechanisms operating at small and intermediate-large magnitude scales), although *b values* as low as 0,24 and 0.47 over so broad an area are not easy to explain. Also, for the Aleutian Arc, in the incremental distribution (downward pointing triangles) the escalation of frequency is faltering between *ML* = 3.9 and 4.3 (events missing) and there is a rather suspicious leap of about 5500 events between *ML* = 3.0 and 3.1 (event surplus), which is also difficult to explain naturally.

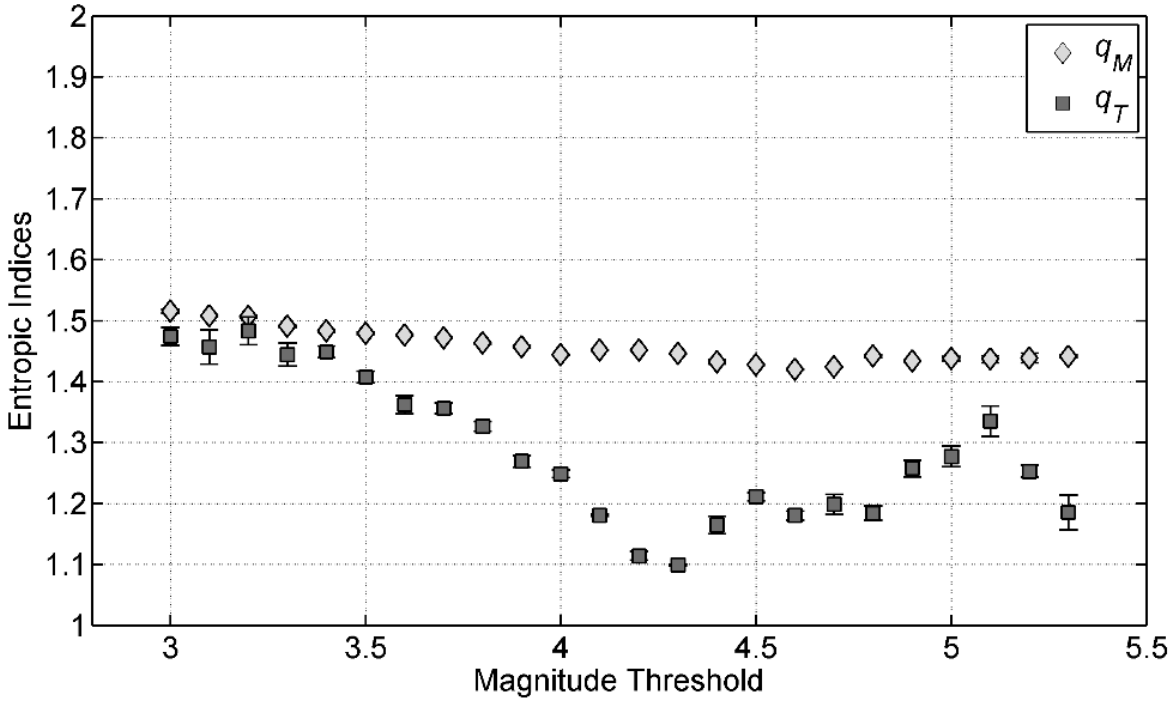

Figure 2.7 NESP realization of the entropic indices *qM* and *qT* with respect to magnitude threshold (*Mb*) for the Greek seismicity, period 1964-2015, compiled from ISC catalogue. The results imply a change in the scale, but this output clearly represents an artifact due to catalogue incompleteness.

As a conclusion, a careful estimate of the so-called artifacts in the catalogues, such as (1) changes in Mc as a function of time; (2) mixing heterogeneous population of events, for example, explosions and tectonic earthquakes, or volcanic earthquake families and tectonic earthquakes; and (3) spatially heterogeneous is essential when drawing conclusions about the dynamics of seismicity. Over the next chapters, I examine the nature of seismogenetic system of Californian and Continental Alaskan transformational plate margins, as well as the Alaskan – Aleutian convergent plate margin. These areas were chosen not only for their long-standing, reliable earthquake monitoring services and seismological catalogues, but mainly because they comprise three different seismotectonic contexts in which there is: a) lithospheric seismogenesis along transform faults, b) lithospheric seismogenesis along a convergent margin and, c) large-scale deep focus seismogenesis in and around a major subducting slab. The Alaskan and Alaskan – Aleutian systems are both crustal and sub-crustal. Along with the seismogenetic systems of California which are all crustal will constitute a differential study that will also provide the opportunity to begin an inquiry as to whether environmental conditions (e.g.

temperature, pressure), or/and boundary conditions (free at the surface vs. fixed at depth), have a role in the dynamic expression and evolution of the seismogenetic fault network. The nature of the Greek crustal seismogenetic system is also investigated by considering the complex seismotectonic environment; the subset areas are defined with respect to the stress field computed by inverting a total number of 930 focal mechanisms.The comparison of results from such exercises may afford –for the first time– evidence as to the existence of differences between crustal and sub-crustal seismogenesis and, in case of an affirmative answer, as to the origin of the differences and the cause of Complexity/Criticality thereof.

CHAPTER 3

CASE STUDY 1:
CALIFORNIAN SEISMOGENETIC SYSTEM

THE SEISMOGENETIC SYSTEM OF CALIFORNIA

One of the most seismically active systems of the world and the most intensely studied is the Californian seismogenetic system, USA, (32°32′ N to 42° N, 114°8′ W to 124°26′ W) partly due to its reliable earthquake monitoring services and seismological catalogues and partly because Californian seismicity is a test bed for the development of seismogenetic models, therefore an appropriate place to conduct this type of research.

The history of seismicity in California is closely related not only to the many major earthquakes that have occurred on the SAF but also to those on other significant members of the California faulting system. The large amount of data set has allowed an advanced level of research in terms of geotectonic regime of the area. Several lines of evidence support that SAFS is part of the transform boundary between the Pacific Plate and North America Plate and is bounded by the Sierra Nevada-Great Valley (SNGV) microplate to the east which moves subparallel to the motion of the Pacific Plate relative to North America and the the Cascadia Subduction Zone to the north. Moreover, geodetic and geological studies indicate that South California straddles the boundary between the Pacific and North American plates.

Discrepancies in GPS velocities, sress data, tectonic setting and other attributes of the SAFS and Sierran Micorplate have led many scientists to subdived the system into several domains where various parts are not parallel to the Pacific- Sierran plate movement (Figure 3.1). This relative plate motion is distributed on faults across the Western US and their displacement along the north-west striking SAFS takes the major portion of the motion. Most of the remaining transform motion has been found on similar trending zone of faults that strikes through Mojave Desert and the eastern boundaries of Sierra Nevada, referred as the Walker Lane (WL) and East California Shear Zone (ECSZ) (Wesnousky et al., 2005). Many studies indicate that the velocity field within this area is oriented sub-parallel to the northwest motion of the Sierra Nevada microplate, and oblique to its eastern margin which is the deformation zone boundary indicating that the ECSZ–WL is a zone of transtensional non-plane strain involving a combination of shear and extension (Hammond et al., 2012; Argus and Gordon 2001, Bennett et al., 1999; Dixon et al,. 2000; McClusky et al., 2001).

To the contrary, the largest blocks of SNGV between SAFS and ECSZ–WL and the eastern Basin and Range, have shown permanent strain of only a few nannostrain per year, indicating a relatively stable behavior and reffered as a rigid microplate (McCaffrey

2005). The reason for this is not as yet clear and several hypotheses have been offered. One hypothesis that was based on the Landers Earthquake in 1992 is that the plate boundary may be shifting eastward, away from the San Andreas to the Walker Lane (Becker et al., 2005).

According to Atwater and Stock (1998) the change in Pacific-North America plate motion from NNW to WNW at 7-8 Ma caused the Pacific plate to move approximately parallel to the North America plate margin. This inhibited North America extension and reorganized the North America deformation; the extension in the South Basin and Range was constrained while the SNGV block changed its motion from WNW to NNW (Wernickie et al., 1988), nearly parallel to Pacific-North America relative motion. This block motion developed an interior shear zone, the eastern California-Walker Lane shear zone, which has accommodated ~cm/yr of right-lateral shear strain during the last 7 Ma.

The most prominent and well-studied seismogenetic feature of California is the San Andreas Fault (SAF). This comprises a NW to NNW oriented, 1300 km long, right-lateral transformational boundary between the Pacific plate to the west and the North American plate to the east and has generated several large (M > 7) earthquakes during the past two centuries (e.g. 1857, 1906, 1989, 1992 and 1999). The SAF system (main and "sibling" faults) is generally thought to comprise three major segments: a) **The Mojave segment** in South California, between Salton Sea (approx. 33.36°N, 115.7°W at the SE corner of California) and Parkfield, Monterey County (approx. 35.9°N, 120.4°W); b) **the central segment** between Parkfield and Hollister (approx. 36.85°N, 121.4°W) and, finally, c) **the northern segment** between Hollister and through the San Francisco bay area up to the Mendocino Fracture Zone (offshore, approx. 40.36°N, 124.5°W).

The two largest earthquakes in 1857 (M=7.9) and 1906 (M=7.8) ruptured SAF north and central sections. To the contrary the South section has not experienced such great earthquakes at least the last 200 years. According to Fialko Y. (2006) the reasons for the absence of great historic earthquakes on the south SAF is the significantly lower slip rate in South SAF (25± 3 mm/yr) than the rate in the rest of the SAF (30-40 mm/yr) or the fault may undergo a substantial creep, at least near the surface, although slip rates in the area of South California have been the subject of debate, with Becker et al., (2005) to propose 15 to 23 $mmyr^{-1}$.

Differences between the various parts of the Californian seismogenetic system(s) can be detected in the expression of seismicity. For example, the Mendocino Triple Junction

includes one of the most seismically active parts of the California (Yeats, 2013) and according to Dengler et al., (1995) the north coastal region accounted for about 25% of the seismic energy released in California in a 50 year period. The Mendocino Fracture Zone (MFZ) is a W-E right-lateral transformational plate boundary between the Pacific and Gorda plates, off the coast of Cape Mendocino in northern California (e.g. Dickinson and Snyder, 1979a; Furlong and Schwartz, 2004). It extends westward from its transform–transform–trench junction with the San Andreas Fault and the Cascadia subduction zone (Mendocino Triple Junction), to the southern end of the Gorda Ridge at approx. (40.4°N, 128.7°W); it then continues on as an inactive segment for several hundred kilometres.

The SAF accommodates only about 75% of the total motion between the North American and Pacific plates. The rest is accommodated by NNW-SSE right-lateral deformation in an area east of the Sierra Nevada mountain range, called the Walker Lane or Eastern California Shear Zone (Wesnousky, 2005; Guest et al., 2007). The Walker Lane terminates between the Pyramid Lake in Nevada and Lassen Peak in California, approx. at (40.3°N, 120.6°W) where the Honey Lake Fault Zone meets the transverse tectonic zone forming the southern boundary of the Modoc Plateau and Columbia Plateau with the Great Basin. Pease (1965) observed that the alignment of that transverse zone and the MFZ suggests that the former might have once been the continental terminus of the MFZ. The highly seismically active SAF has experienced some notable earthquakes (1857, 1906, 1989) while the ECSZ-WL is also considered to be a seismically active system.To the contrary the interposing SNGV and the Basin and Range Province behave as a semi-rigid microplate while often its interior is described as rigid with respect to the absence of significant fautls and internal seismicity (Saleebi et al., 2009; Hammond et al., 2012), geodetic measurments, patterns of topography and structure (Goter et al., 1994; Dixon et al., 2000; McCaffrey 2005)

To further complicate things, California is geologically divided into North and South by the SW-NE left-lateral Garlock fault which extends for approx. 250 km between its junction with the East California Shear Zone (ECSZ) at the north-eastern edge of the Mojave Desert (approx. 35.6°N, 116.4°W) and its junction with the SAF at Tejon Pass (approx. 34.8°N, 118.9°W). This major tectonic boundary is believed to have developed in order to accommodate the strain differential between the almost W-E extension of the Great Basin eastwards of the ECSZ (e.g. Wernicke et al., 1988), and the NW-SE right lateral

transformation of the ECSZ and SAF. Thus, the right-lateral motion on the SAF and ECSZ locks up in the area of the Garlock, where local variations in the mode of deformation and earthquake focal mechanisms are observed (e.g. Jones, 1988; Hardebeck and Hauksson, 2001; Fialko, 2006; Becker et al., 2005). Between 37.7°N and 35.1°N, the left-lateral motion of the Galrlock fault generates a restraining bend and a broad S-shaped westward displacement of the SAF, known as the “Big Bend”; there the strike of the fault rotates from N40°W to N70°W. Moreover many studies have indicated that the stress changes from reverse to normal faulting earthquakes at Mojave –San Bernardino boundary. In particular the Mojave segment is characterized by a mixture of reverse and strike slip solutions and the reverse give way to normal faulting in San Bernardino. To the north at Parkfield area, almost right lateral strike slip solutions predominate near SAF while reverse faulting is present at greater distances (i.e in Coalinga). Regarding the Walker Lane, there is deformational stage which is characterized by a generally WNW trending extension direction. The present day strike-slip stress regime has produced strike-slip, normal oblique-slip, and normal dip-slip faulting. (Bellier & Zoback, 1995).

The Garlock Fault

Another significant segment of the SAF system is a 250 km long strike-slip fault known as the Garlock Fault Zone(GFZ) that intersects the SAF from the east. Unlike most of the other faults in California, the Garlock Fault has been described as a left-lateral slip fault;. this means that the terrain north of the fault is moving westward relative to the terrain south of the fault, which is moving relatively eastward. According to Walker and Glazner (1999), GFZ is a major boundary between the Basin and Range Province and Mojave Desert and is believed to have developed to accommodate the strain differential between the extensional tectonics of the Great Basin crust and the right lateral strike-slip faulting of the Mojave Desert crust. McGill et al., (2009) have analysed three tectonic models that may explain its relation with the SAF by incorporating paleoseismic evidence and indicated that a slip rate of at least 5.3 mm/yr for the western GFZ while for eastern part the slip rate is lower, while block rotation may play a major role in slip on the eastern Garlock fault and in absorbing the termination of left slip near the eastern end of the fault.

The southern margin of the study area is taken to be northward of the ENE-WSW oriented, left-lateral Garlock Fault Zone (GFZ). This is a major boundary between the Great Basin (extending to the east of Walker Lane), and the Mojave Desert extending to the south and southwest; it is characterized by a mixture of left-lateral strike-slip and

reverse focal mechanisms and is believed to have developed in order to accommodate the strain differential between the dominantly extensional tectonics of the semi-rigid Great Basin microplate and the right lateral strike-slip faulting of the Mojave Desert's crust. The intersection of the Garlock and San Andreas faults begets a restraining bend located approx. between 34.5°N and 35.5°N (Big Bend), where the strike of the SAF and the mode of deformation are notably different from that experienced in either side of the bend (e.g. Jones, 1988; Hardebeck and Hauksson, 2001). Studies based on slip rates, focal mechanisms etc. indicate that the GFZ is the area where the SAF and the East California Shear Zone lock up in Southern California and a tectonic boundary forms between north and south California, delimiting the central/north and south segments of the SAF (e.g. Fialko, 2006; Becker et al., 2005). However, the GFZ is not included in the present analysis as I consider that it must be studied separately: it is a significant feature whose geodynamic characteristics clearly distinguish it from the nSAF and SNR. Accordingly, the source areas to be considered in the present analysis are outlined below and shown in Figure 3.3.

Relation of plate tectonics to magmatism at the Western US

Another significant characteristic of Californian geodynamic regime is the magmatic activity at the Western US which is evident through the existence of one of the largest batholiths in North America, that can be traced 600 km along the Sierra Nevada mountain range in California and is adjacent to the Garlock fault (Fig.3.2) and also through the presence of numerous volcanic centers to the north (at the Cascades). Forming the core of the moutain rangre and varying in width between ~80 and 120 km the Sierra Nevada batholith comprises mainly subduction-related intermediate to felsic intrusive rocks and associated metamorphic screens and pendants (Cecil et al., 2012 and references therein). Although it is classified as a single mega-plutonic complex, major lateral W to E changes in the age and compostion (Kistler and Peterman, 1973,1978; Stern et al., 1981; Chen and Moore, 1982) of the batholith have long been recognized. These changes are largely attributed to the flaring and migration of magmatism across heterogeneous crustal and upper mantle domains.

The origin of Sierra batholith from heating as the Farallon Plate subducted below the North American Plate is accepted by most indicating that the last 150 Ma, magmatic activity at the Western US is related to plate tectonic processes and especially to subduction. However, this aspect of magmatitic evolution remains ambiguous and in

some regards much of the magmatic activity is related to processes not typically thought of as plate tectonic in nature. According to Humphreys (2009) such non -plate tectonic activities include for example dynamic downwarping and strong contraction caused by slab sinking on North America; regional increases in lithospheric buoyancy; loss of lithospheric strength; small-scale convection and the resulting loss of strength and density; thermal-mechanical effects of the asthenosphere flow around the edge of sinking Gorda-Juan de Fuca slab; and mantle flow driven by processes related to Yellowstone.

The above outlined tectonic setting results in four distinct earthquake source areas (from South to North):

a. Opposite to their distinct nature north of the Garlock Fault, the SAF and ECSZ converge and are not as easy to distinguish to south of the fault. In consequence, I will consider that area (southern SAF segment and ECSZ) to comprise an integral seismogenetic entity and henceforth refer to it as the South California Seismic Region (SCSR). The north boundary of the SCSR is the WNW-ESE oriented Santa Ynez and Garlock Fault zones; it begins at the western terminus of the Santa Ynez Fault Zone – Pacific Section which is a virtual extension of the Garlock fault (34.5°N, -120.5°E); then it runs south of Tejon Pass and parallel to the Garlock Fault up to approximately (35.5°W, -116.3°E) the past its eastern terminus (Mojave Desert). It then turns south and runs eastward of the South Bristol Mts. Fault (34.6°N, -115.6°E), to approximately (32.0°N, -114.5°E) in the Gran Desierto de Altar (Sonora, Mexico), north of the head of the Gulf of California. It continues westwards to approx. (32°N, -117°E), which is south of Tijuana, Mexico, and then to (32°N, -119°E) off the west coast of Mexico. Finally, it turns north and runs parallel to the coastline and west of the San Clemente and Santa Cruz Islands up to 34.5°N.

b. The Central Valley and Sierra Nevada Range, up to and including the Walker Lane (henceforth SNR). This extends northward of the Garlock Fault and behaves as a semi-rigid microplate (Sierran microplate) whose interior (Central Valley) is characterized by the absence of significant faults and large earthquakes (Hammond et al., 2012; Saleeby et al., 2009; McCaffrey 2005; Dixon et al., 2000; Goter et al, 1994). In this study, the geographic boundaries of SNR are defined to the north by the line joining the Battle Creek Fault and the northern termini of the Butt Creek and Almanor fault zones (roughly 44.5°N, 121.2°W) and then up to 116°W; to the east by the 116°W meridian; to the south by the

Garlock Fault and to the west by the White Wolf and Kern Gorge fault zones, the Foothills Fault system and the Battle Creek Fault.

c. The central and northern SAF segments (henceforth **nSAF**), north of the Garlock Fault between Parkfield and the MFZ. For the purpose of this study, the geographic borders of nSAF are defined to the north by the line joining the northern terminus of the SAF/Shelter Cove section (40.2°N, 124.3°W), the northern terminus of the Bartlett Springs Fault System (Lake Mountain fault) and the Battle Creek Fault (40.5°N, 121.9°W); to the east by the Battle Creek Fault, the Foothills Fault system (roughly 39.3°N, 118.8°W) and the Kern Gorge fault and White Wolf fault zone (35.3°N, 118.6°W) and to the West by an imaginary line running offshore parallel to the Pacific Coast.

d. The Mendocino Fracture zone (henceforth **MFZ**), bounded by the coordinates 40°N to 43°N and 123°W to 128°W.

In this framework and based on the above attributes I shall examine the seismicity along the subset areas of California by applying Non-Extensive Statistical Physics.

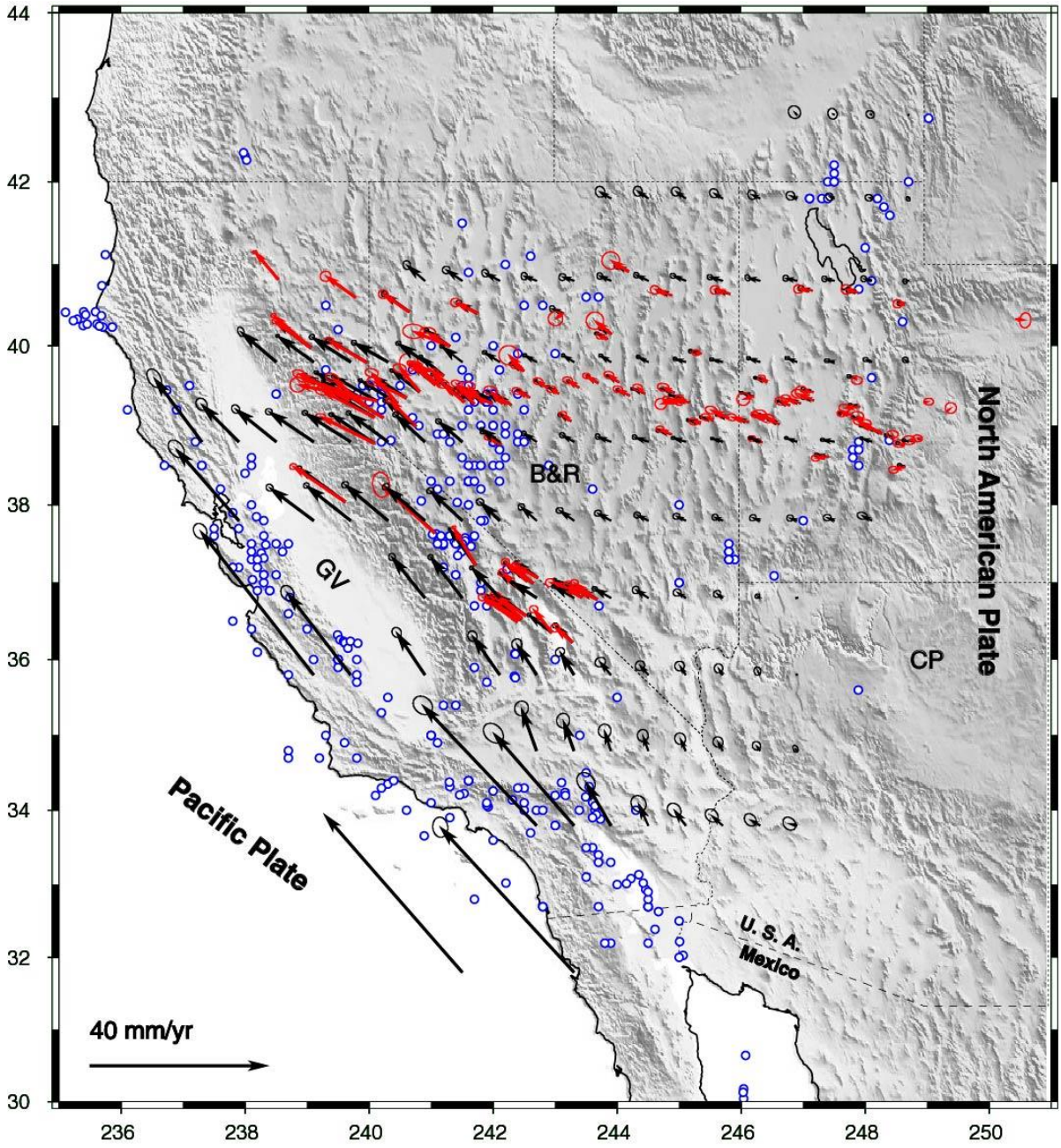

Figure 3.1 A self-consistent, continuous velocity field solution (black arrows) Shen-Tu et al., (1999) determined using GPS and VLBI data (red arrows) (Bennett et al., 1999; Thatcher et al., 1999) Quaternary fault data (Jennings, 1994; Peterson and Wesnousky, 1994), and imposed NUVEL-1A plate motion (DeMets et al., 1994). Ellipses represent a 95% confidence limit. Blue dots represent seismicity recorded from 1850-1998. (GV = Great Valley, B&R = Basin and Range, CP = Colorado Plateau, SAF = San Andreas Fault, SN = Sierra Nevada, GB = Great Basin). Longitude and latitude are given in degrees west and north.

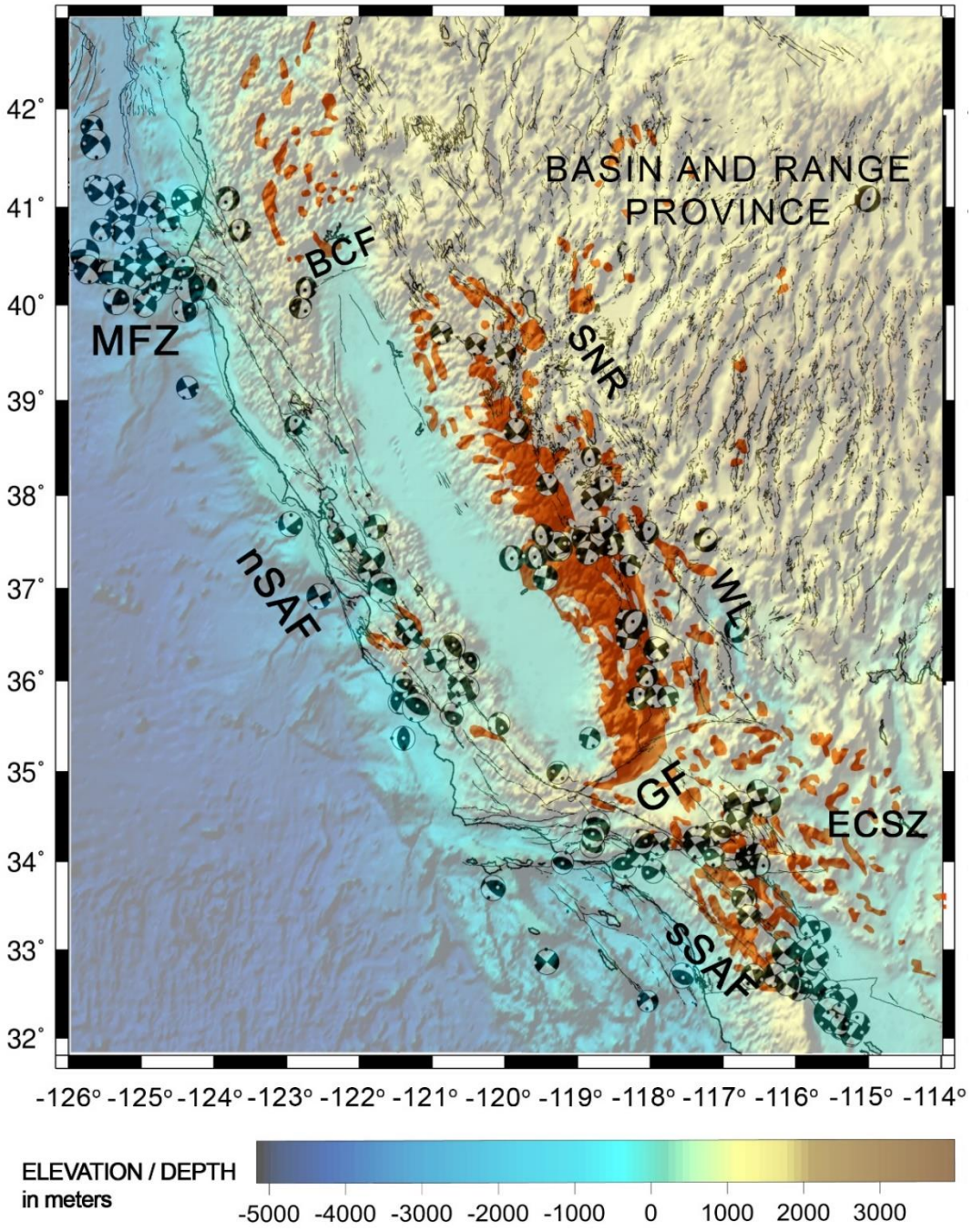

Figure 3.2 The tectonic grain of California. The Sierra Nevada batholith is illustrated with light orange. Active faults shown in solid lines: **nSAF**, north segment of the San Andreas Fault; **sSAF**, south segment of the San Andreas Fault; **GFZ**, Galrock Fault; **ECSZ,** East California Shear Zone; **MFZ**, Menodcino Fracture Zone.

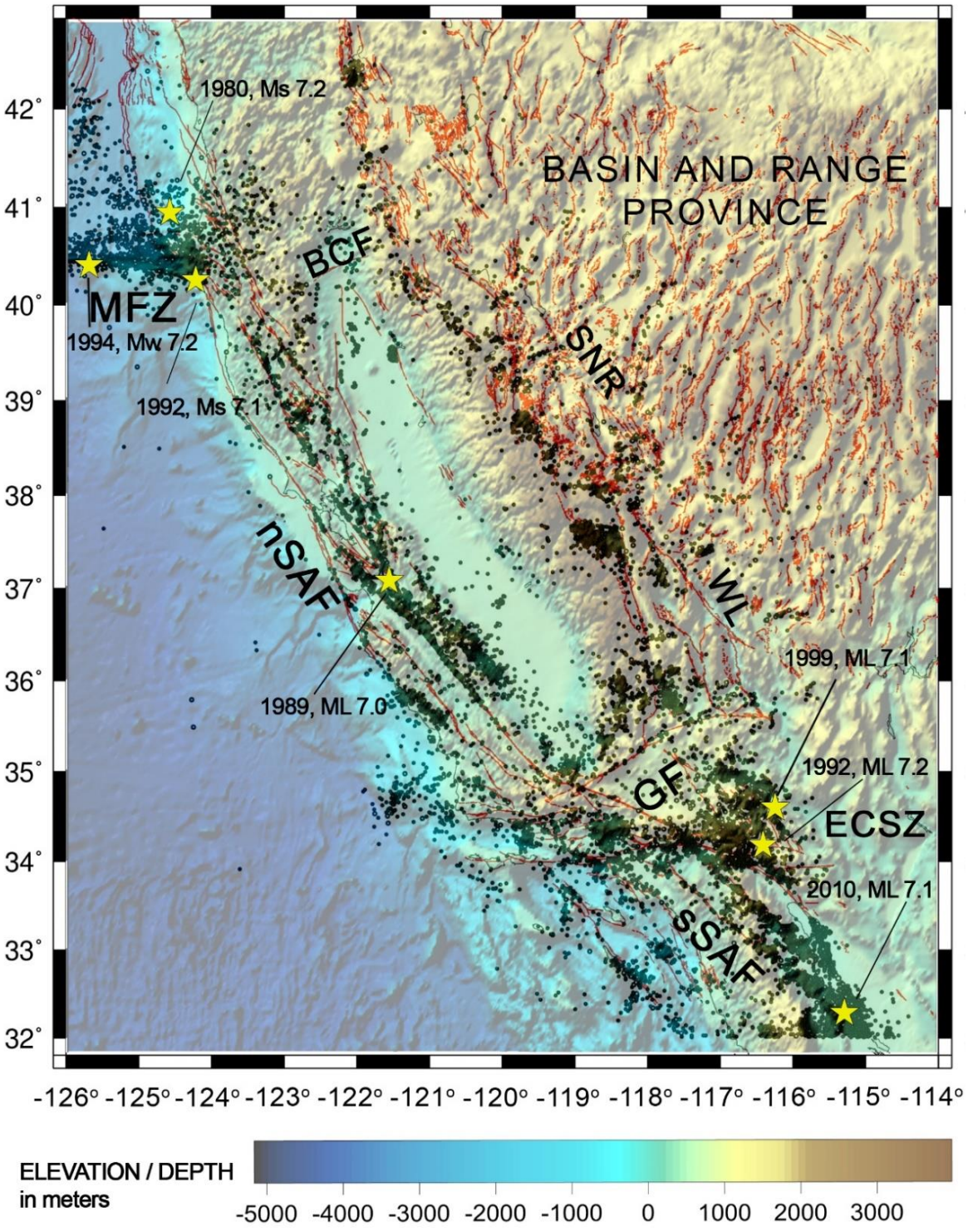

Figure 3.3 The seismicity of California as illustrated by mapping the epicentres of earthquakes included in the full NCSN and SCSN catalogues for the period 1968–2015.

3.1. SOUTH CALIFORNIA

I shall now focus on the seismicity of the broader area of southern California, USA, as above mentioned the SCSR area. SCSR is characterized by several major faults and numerous branches that create a complex landscape of seismic activity. Different earthquake source areas are included in the analysis, as illustrated in the composite seismicity map of Figure 3.4 and elaborated below:

a) The southern part of the East California Shear Zone (ECSZ) extends south of the Garlock Fault and runs across the Mojave Desert, terminating upon the San Andreas Fault system between Salton Lake and the San Bernardino Mts. It is a zone of strike-slip faults that accommodates approximately 25% of the total motion between the North American and Pacific plates (Dixon et al., 2000; Miller et al., 2001) and has generated some of the largest earthquakes of South California, such as the 1992 Landers earthquake (M_w=7.3) and the 1999 Hector Mine earthquake (M_w=7.1). The eastern expanse of the ECSZ is delimited by the diffuse extensional deformation of the Basin and Range province. Although the origin of the ESCZ is still open to debate, it has been suggested that it was formed by northward propagation of the plate boundary in the Gulf of California due to the northward motion of the Baja California microplate (Faulds et al., 2005; McCrory et al., 2009). According to Plattner et al., (2010) and Li and Liu (2006), the geometrical complexity of the San Andreas fault system along with the accommodation of shear strain from Baja–North America collision is a key component of this zone's formation.

b) The Inner Continental Borderland region (ICB) contains several faults and extends offshore and to the west of the southern California mainland, from Point Conception to the Vizcaíno Peninsula in Baja California. The area comprises a complex tectonic system in which seismicity appears to be more diffuse than in the mainland even for events associated with main-shock sequences, although this may be an artefact of lopsided network geometry and structural heterogeneity (Astiz and Shearer, 2000; references therein). The area can be divided into four major sub-parallel groups of dextral faults which, from east to west are: i) the Newport–Inglewood (NIF) and Rose Canyon (RCF) faults that make landfall at San Diego and perhaps connect with the Vallecitos and San Miguel faults in Baja California; ii) the Palos Verdes (PVF) – Coronado Bank (CBF) fault that makes landfall near Ensenada, Mexico; iii) the Santa Cruz – Santa Catalina – San Diego Trough – Bahia Soledad (SDTF) fault that makes landfall south of Punta, Mexico; iv) the Santa Cruz – San Clemente – San Isidro fault zone (SCF). During the past 50

years, several moderate (M_L 5 to 6) earthquakes have occurred in the region, kinematically consistent with the right-lateral deformation of the local Pacific–North American plate boundary and the regional tectonics of the San Andreas Fault system (e.g., Weldon and Humphreys 1986). Some of those, however, had significant dip-slip components including the largest recorded offshore event, the 1951 San Clemente Island earthquake (M_L=5.9).

c) Sandwiched between the ECSZ and the ICB is the southern San Andreas Fault system (sSAF). This is a trilateral system of large sub-parallel faults comprising the southern segment of the San Andreas Fault in the east, its sibling San Jacinto fault (SJF) in the centre and the Elsinore fault (EF) in the west. The San Jacinto fault is considered to be one of the youngest and most active faults in South California as it accounts for 75% of the slip rate between the Pacific and North America plates and has generated moderate to large earthquakes in the past. The Elsinore fault, which is the second major fault in the southland, runs parallel to the San Jacinto fault and has been considerably less active in historic times. To the north, the sSAF system terminates against the left-lateral Garlock fault, a major tectonic boundary believed to have developed in order to accommodate the strain differential between the almost W-E extension of the Great Basin eastwards of the ECSZ (e.g. Wernicke et al., 1988), and the NW-SE right lateral transformation of the ECSZ and SAF. Thus, the right-lateral motion on the SAF and ECSZ locks up in the area of the Garlock, where local variations in the mode of deformation and earthquake focal mechanisms are observed (e.g. Jones, 1988; Hardebeck and Hauksson, 2001; Fialko, 2006; Becker et al, 2005). Between 37.7°N and 35.1°N, the left-lateral motion of the Galrlock fault generates a restraining bend and a broad S-shaped westward displacement of the SAF, known as the “Big Bend”. The southern boundary of the sSAF, if any, is not clearly defined. The eponymous fault terminates at southeast corner of the Salton Sea but is thought to connect with the Imperial Fault though the extensional Brawley Seismic Zone (BSZ). The San Jacinto and Elsinore faults are also thought to extend to the SE, with San Jacinto also terminating against the Imperial Fault and Eslinore continuing into Mexico as the Laguna Salada Fault (LSF), in which the M7.2 Baja California of 2010 has occurred. It is interesting to point out that there is a zone of perfectly aligned earthquake activity that appears to commence at the terminus of sSAF at Salton Sea, run in an average N220° direction parallel to the south coast of Salton Sea, pass along a N40° zone of short fault strands associated with the San Jacinto fault – Superstition Hills segment (active in historic times), then pass between the N220°

oriented left-lateral Yuha Wells fault (active in the Late Quaternary) and the “unnamed faults north of Coyote Wash” of unspecified kinematics but active in the last 15ka (e.g. Jennings, 1994), and continue south-westward crossing the coastline just north of Ensenada, Mexico. This “*Unnamed Seismic Zone*” is better observed with the 2016 upgrade of the relocated catalogue of Hauksson et al., (2012); because horizontal motion there can only be left-lateral, one is tempted to *ponder* whether it actually comprises a *zone* analogous to the Garlock fault and serves as a barrier against the right-lateral motion of the Laguna Salada and Imperial faults, thus delimiting the southward extent of the SCSR as a whole.

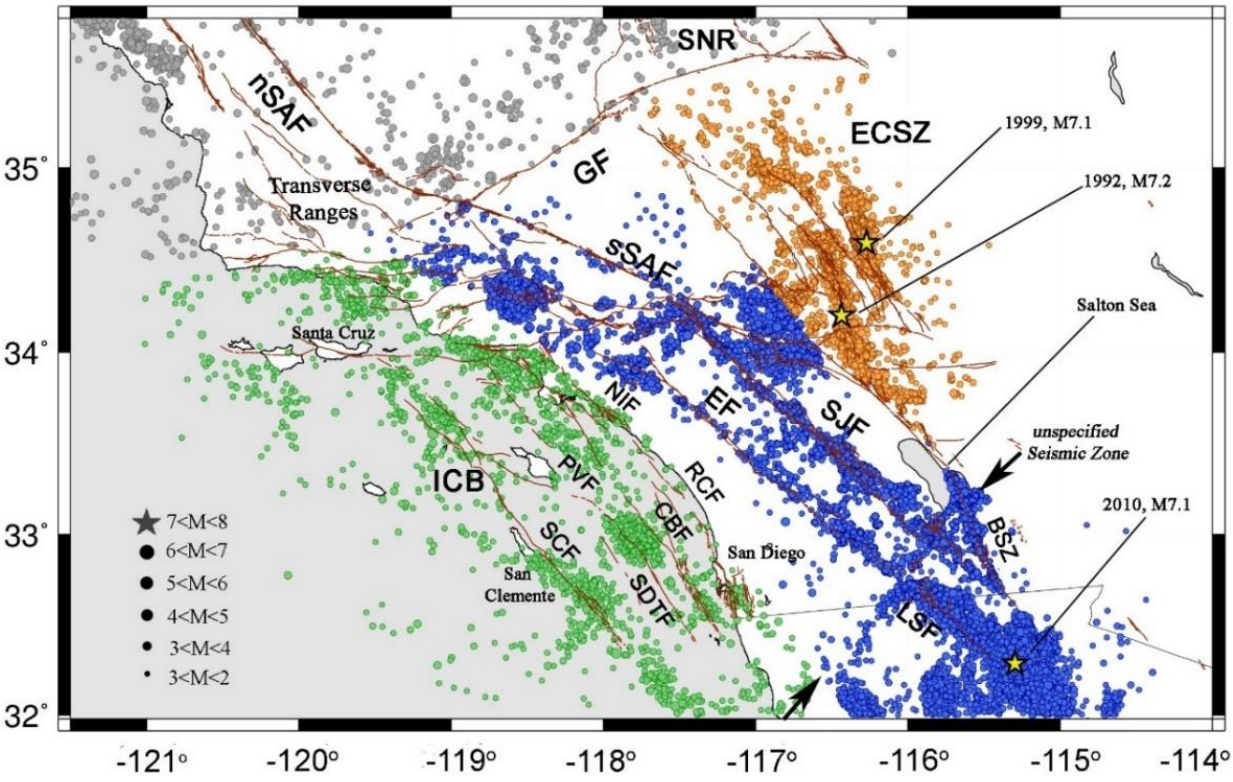

Figure 3.4 South California earthquake epicenters and major faults. **GF:** Garlock Fault; **ECSZ:** south segment of Eastern California Shear Zone; **nSAF:** north segment, San Andreas Fault; **SNR:** north segment of ECSZ; **sSAF:** south segment, San Andreas Fault; **SJF:** San Jacinto Fault; **EF:** Elsinore Fault; **BSZ:** Brawley Seismic Zone; **LSF:** Laguna Salada fault; **PVF:** Palos Verdes Fault; **NIF:** Newport-Inglewood fault; **RCF:** Rose Canyon fault. Offshore faults include the Coronado Bank Fault (**CBF**), San Diego Trough Fault (**SDTF**) and San Clemente Fault (**SCF**). The Transverse Ranges include the San Gabriel Fault, the San Cayetano Fault, the Oak Ridge Fault, and Santa Ynez Fault. The stars indicate the epicentres of the major 1992 Landers, 1999 Hector Mine and 2010 Baja earthquakes (M >7).

3.1.1 South California Earthquake Data

The earthquake data utilized in this study was extracted from the regional earthquake catalogue of the South California Earthquake Data Centre (SCEDC @ http://www.data.scec.org) for the area 36ºN to 32ºN and -122ºE to -114ºE and period 1968-2017. As reported by Hutton et al., (2010), as of the early 1930's and up to the early 1970's the SCSN network was sparse and consisted of about 49 stations. As a result, the epicentral distribution maps compiled for the broader area of South California projected an image of diffuse seismicity. During the 1980's and early 1990's the network and its products improved qualitatively and quantitatively: more than 100 additional stations were installed by the USGS/Caltech collaboration, while past events were relocated, and magnitudes re-determined. With denser network and modern data processing, it became clear that the distribution of earthquakes was mainly clustered along and around the large active faults of the Late Quaternary (Fig. 3.4).

As can be seen in Fig. 3.5a, the sustainable magnitude of completeness (M_c) was approximately 3.0 during the early to mid-1970s and decreased after 1975 so as to attain a sustainable level of approximately 2.5 as of the early 1980's. The spiky fluctuations observed in Fig. 3.5a correspond to time-local instabilities caused by major aftershock sequences and should not be viewed as temporary changes in the detection threshold. In the SCSN catalogue most earthquakes are reported in the M_L and M_w magnitude scales while there is a considerable number of events reported in the duration (M_d) and amplitude (M_x) scales. Eaton (1992) has calibrated M_d and M_x against the M_L scale and has shown that they are within 5% of the M_L scale for magnitudes in the range 0.5 to 5.5, as well as virtually independent of the distance from the epicentre to at least 800 km. In consequence, M_d and M_x are practically equivalent to M_L. For the purpose of the present analysis M_w magnitudes were converted to M_L using the empirical formula of Uhrhammer et al., (1996): $M_w = M_L \times (0.997 \pm 0.020) - (0.050 \pm 0.131)$. Given these adjustments, for the period 1968-2017 the catalogue is complete for magnitudes $M_L \geq 3$ and comprises 10793 events (Fig. 3.5b) while for the period 1980-2017 it is complete for $M_L \geq 2.5$ and comprises 30117 events (Fig. 3.5c).

The question of whether the background seismogenetic process is inherently random or correlated is open to debate and may be answered by analysing reduced versions of the earthquake catalogue. Here I have chosen to implement the declustering method of Zhuang et al., (2002; see detailes in Chapter 2). The results of the declustering exercise are summarized in Table 3.1.1 and an example of the resulting cumulative earthquake

counts for the period 1968-2017 ($M_c \geq 3$) is given in Fig. 3.6. It is apparent that at the $\phi \geq$ 70% probability level the catalogue is *almost* free of the time-local rate jumps that indicate the presence of aftershock sequences, therefore it is fairly representative of the background process. It is natural to expect that at this probability level a small portion of events will be residuals of the foreground process which, however, are progressively eliminated at higher probability levels. Fig. 3.7 illustrates the epicentral distributions of the full and declustered catalogues used herein. Thus, Fig. 3.7a shows the epicentres of the full catalogue for the period 1968-2017 and M_c.≥3.0 and Fig. 3.7b, 3.7c and 3.7d its declustered realizations at probability levels $\phi \geq$ 70%, $\phi \geq$ 80% and $\phi \geq$ 90% respectively. Likewise, Fig. 5e shows the full catalogue for the period 1980-2017 and M_c.≥2.5 and Fig. 3.7f, 3.7g and 3.7h its declustered realizations at probability levels $\phi \geq$ 70%, $\phi \geq$ 80% and $\phi \geq$ 90% respectively. The full and declustered catalogues for the period 1980-2017 contain more events than the corresponding catalogues of the period 1968-2017 due to the lower magnitude of completeness. It is also clear that background earthquake activity is compactly distributed along the major faults of the ICB, sSAF and ECSZ source areas, a point that will be of importance in discussing and explaining the results of the analysis presented in Chapter 6.

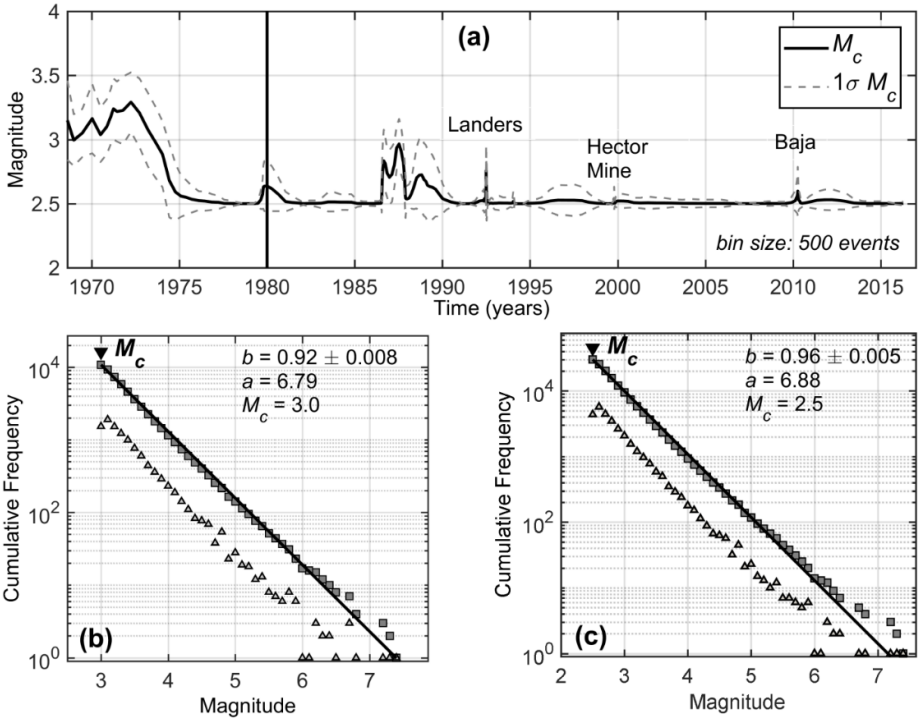

Figure 3.5 Attributes of SCSN earthquake catalogue: **a)** Magnitude of completeness (M_c) estimated as a function of time for the period 1968-2017 after Woessner and Wiemer (2005). **b)** Frequency – magnitude (F-M) distribution for the period 1968-2017; grey triangles denote the incremental distribution and grey squares the cumulative. **c)** As per Fig. 3b but for the period 1980-2017.

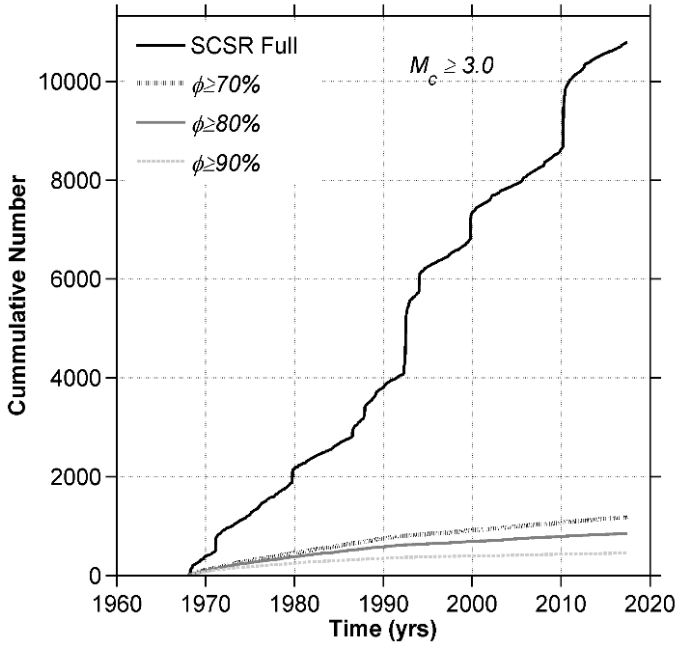

Figure 3.6 Cumulative event count of the full and declustered SCSN catalogue for the period 1968 – 2017 (magnitude of completeness $M_c \geq 3.0$).

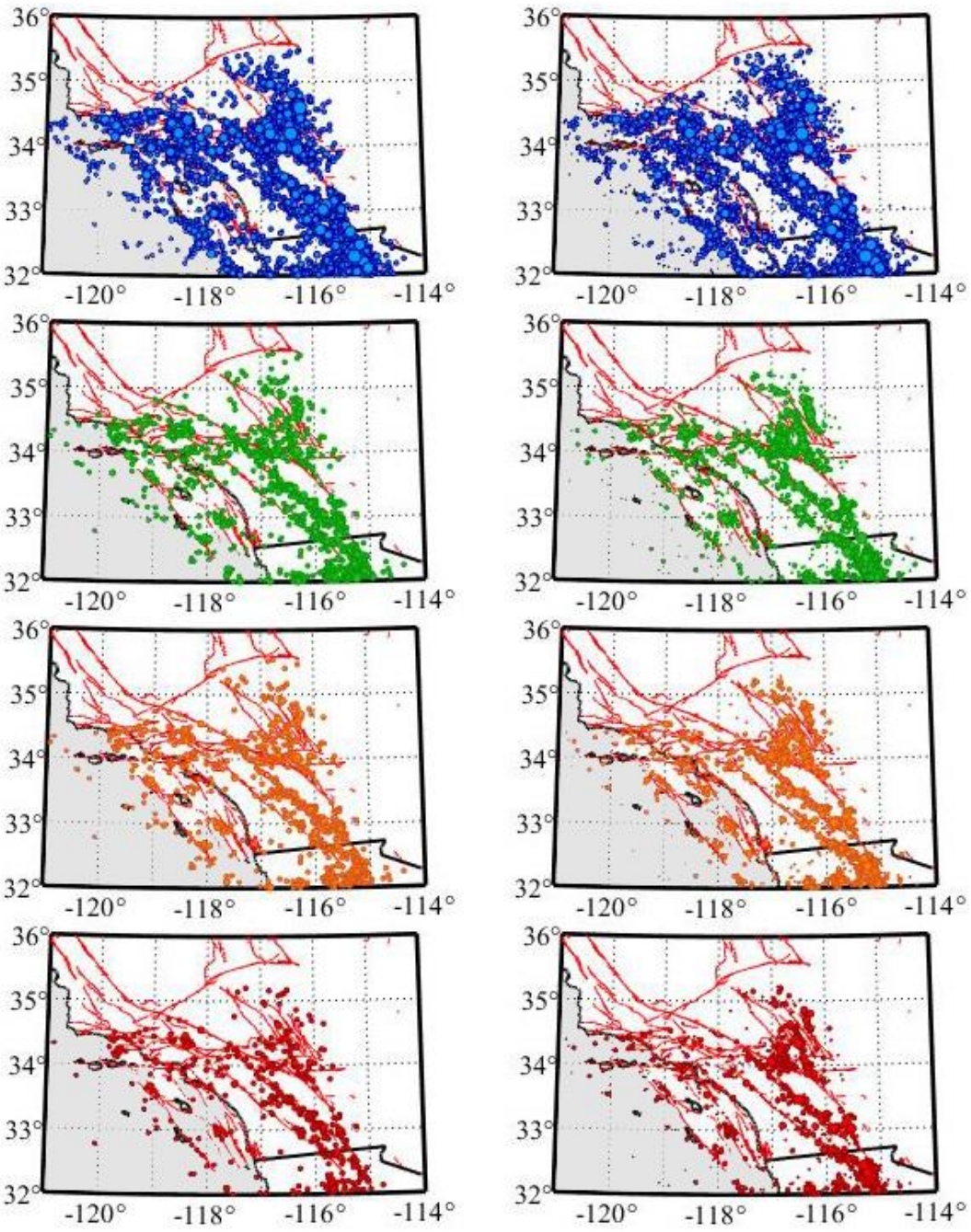

Figure 3.7 Epicentral distributions of the full and declustered versions of the SCSN catalogue. **a)** Full catalogue for the period 1968-2017 and magnitude of completeness 3.0; **(b), (c)** and **(d)** are realizations declustered at the probability levels of 70%, 80% and 90% to be background respectively. **e)** Full catalogue for the period 1980-2017 and magnitude of completeness 2.5; **(f)**, **(g)** and **(h)** are realizations declustered at the probability levels of 70%, 80% and 90% to be background respectively.

TABLE 3.1.1 Summary of South California earthquake catalogues used in the present analysis.

Source Area	Source Area Code	Period	M_{comp}	Full catalogues	Declustered catalogues ($\phi_i \geq 70\%$)	Declustered catalogues ($\phi_i \geq 80\%$)	Declustered catalogues ($\phi_i \geq 90\%$)
				№ events	№ events	№ events	№ events
South California Seismic Region	**SCSR**	1968-2017	3.0	10,793	1,182	854	< 500
		1980-2017	2.5	30,117	4,224	3,081	2,035
San Andreas Fault South Segment	**sSAF**	1980-2017	2.5	17,602	2,468	1,767	1,619
East California Shear Zone South Segment	**ECSZ**	1980-2017	2.5	8,694	1,038	733	441
Inner Continental Borderline Offshore South California	**ICB**	1968-2017	2.5	3,821	694	<500	< 300

3.1.2 NESP results for South California Earthquake Catalogues

As already discussed in Section 3.1.1, the content of the SCSN catalogue has improved significantly in response to improvements in the detection threshold of the seismological network and in analytical procedures, with particular reference to the period after 1980. Accordingly, in order to be as thorough as possible and ensure the significance of our results, I conduct comparative analyses of full earthquake catalogues for the entire SCSR, as well as for the individual source areas defined in Section 3.1, for two overlapping periods: 1968-2017 with a threshold magnitude $M_{th} \geq 3$, and 1980-2017 with a threshold magnitude $M_{th} \geq 2.5$. The analysis will focus on the variation of the entropic indices with respect to threshold magnitude, (M_{th}) and interevent distance (Δd). The results are summarized in Table 3.1.2 and illustrated in Figures 3.8 to 3.14. In order to maintain experimental rigour, estimation of the entropic indices is *not* performed for catalogue subsets containing *less than* 500 events and results are *not* considered and displayed *unless* associated with a goodness of fit (R^2) *better* than 0.97.

i.Analysis of South California Full Earthquake Catalogues

As can be seen in Fig. 3.8 magnitude entropic indices are quite stably and consistently determined. Moreover, $q_M(M_{th})$ functions computed for the SCSR, sSAF, ICB and ECSZ catalogues are very comparable between the two periods and for all threshold magnitudes. For the SCSR and sSAF catalogues, $q_M(M_{th})$ varies from 1.5 at M_{th}=2.5 (b_q=1) to 1.49 (b_q=1.04) at M_{th}=3.0, steadily increasing thereafter to 1.59 at M_{th}=4.3 (b_q=0.7). The entropic index q_M, like the b-value to which it is related, represents the scaling of the size distribution of earthquakes. Here it indicates a *sub-extensive* scale-free process associated with gradual changes in the size distribution of small-intermediate magnitude events that appears to become progressively more clustered. For the ECSZ area, $q_M(M_{th})$ is very stably determined around a mean value of 1.5 ($1.49< q_M(M_{th}) <1.53$), so that and $b_q(M_{th}) \in (0.88, 1.04)$, while for the ICB area and $M_{th}>3.0$, $q_M(M_{th})$ is estimated to be slightly higher for the period 1968-2017 ($1.51<q_M(M_{th})<1.54$) than for 1980-2017 where q_M is 1.48-1.49; given that the ICB is mainly offshore, this may actually be an effect of the post-1975 improvement of the SCSN network.

The variation of q_M with interevent distance Δd is shown in Fig. 3.9. It is again apparent that $q_M(\Delta d)$ remains stable over all interevent distances and is very consistently determined for all periods and source areas, generally varying between 1.48 and 1.53 so that $b_q(\Delta d)$ would vary between 1.08 and 0.88. Small differences of the order of 0.01–

0.03 can be observed only at short interevent distances (Δd <100 km) in the results of the SCSR and sSAF catalogues, where $q_M(\Delta d)$ is slightly higher for the period 1968-2017 (M_{th}=3.0) than for 1980-2017 (M_{th}=2.5). We consider these differences too small to be of physical consequence; they may likely be an effect of the post-1975 improvements in the detecting network. Changes in scaling analogous to those observed in Fig. 3.8 are not evident because the threshold magnitudes used in these calculations are considerably lower than the magnitude threshold of the changes.

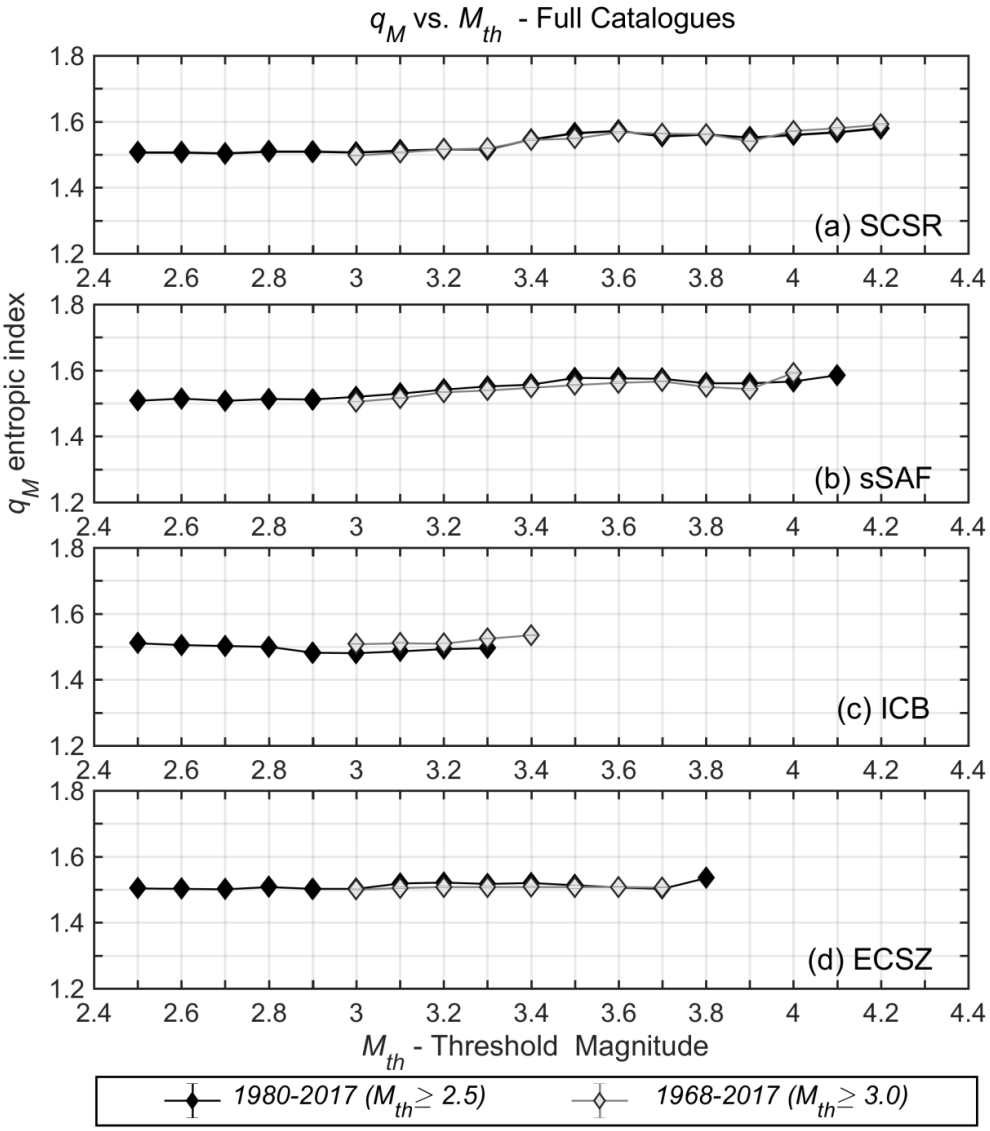

Figure 3.8 Variation of magnitude entropic indices (q_M) with threshold magnitude (M_{th}) for the full earthquake catalogues of: (a) the entire SCSR; (b) sSAF; (c) ICB, and, (d) ECSZ. 95% confidence limits are also drawn but are not always visible as they usually are smaller than the symbols.

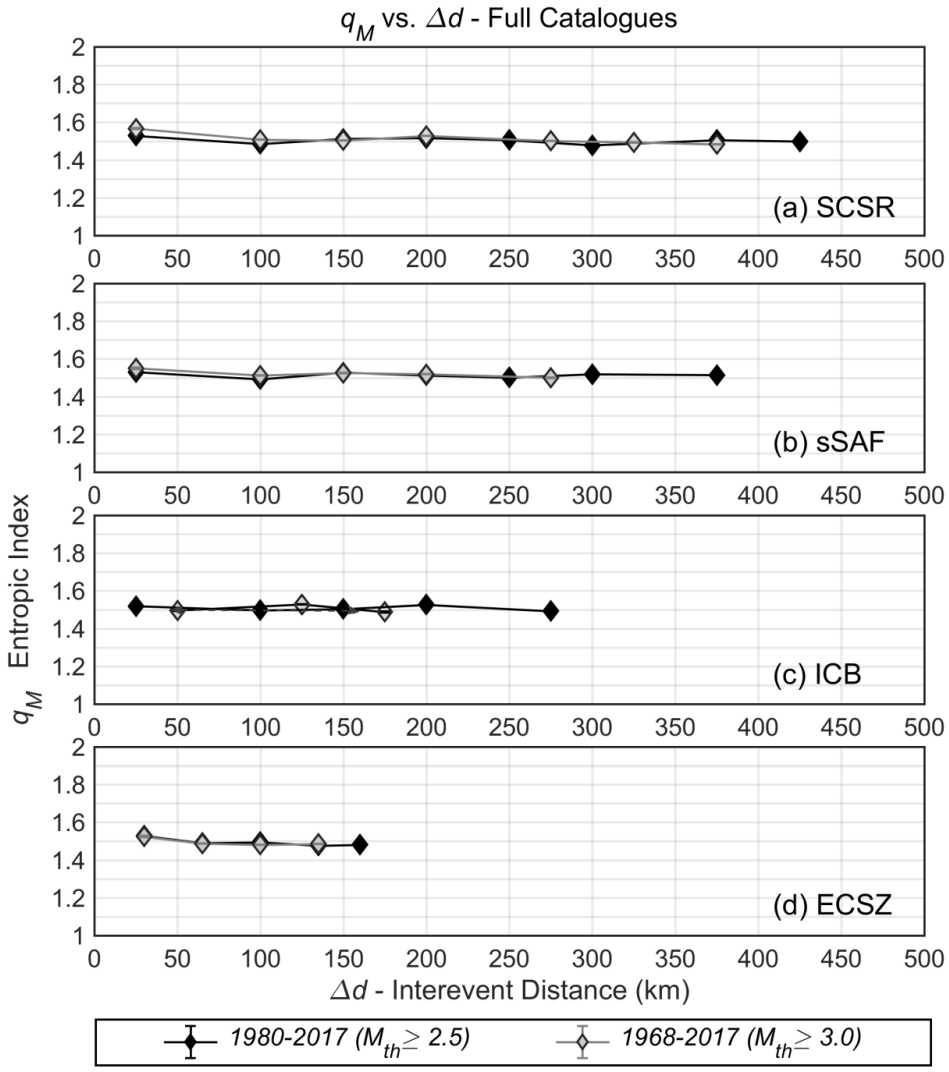

Figure 3.9 Variation of magnitude entropic indices (q_M) with interevent distance (Δd) for the full earthquake catalogues of: (a) the entire SCSR; (b) sSAF; (c) ICB, and, (d) ECSZ. Binning schemes (widths of interevent distance groups) vary and are selected so as to optimize goodness of fit. 95% confidence limits are also drawn but are not always visible as they usually are smaller than the symbols.

The variation of the temporal entropic index with threshold magnitude is shown in Fig. 3.10. To begin with the results of the full SCSR catalogues, it is apparent that for both periods $q_T(M_{th})$ is lower than 1.2 at small magnitude scales, but for M_{th} >3.6 increases steadily to above 1.6 at M_{th} > 4 (strong sub-extensivity). Taken over the *entire* SCSR area, small earthquakes appear to be uncorrelated, possibly because very small events are prolifically spawned by different parental earthquakes at distal locations of the seismogenetic area; these events have no causal relationship and when mixed and chronologically ordered in a catalogue, they may randomize the statistics of interevent times. It is also interesting to point out the increase of correlation with magnitude, which could be interpreted as an effect of the increasing interaction (correlation) radii associated

with increasingly larger events. Similar results are obtained from the sSAF full catalogues, although in this case the increase of $q_T(M_{th})$ commences sharply at M_{th}=3.6 and is apparently steeper; this may well indicate strong fault-fault interactions within the SAF system, which start and escalate rapidly beyond some critical(?) interaction radius. The ICB source area exhibits analogous behaviour and admits analogous interpretation, with the difference that the increase in correlation commences as early as M_{th} = 2.9, where $q_T \approx 1.22$, and appears to rise smoothly to the level of 1.5 at M_{th}=3.3; beyond this point earthquake numbers drop to levels that do not guarantee statistical significance. The analysis of the ECSZ full catalogues yields rather different results: $q_T(M_{th})$ is rather stably determined around a mean value of 1.8 $\pm$ 0.03 for $M_{th} \leq 3.1$ and increases up to 1.95 $\pm$ 0.03 for $M_{th} > 3.1$. The ECSZ fault system appears to be persistently sub-extensive and through correlated at very high levels; these properties render it different from the sSAF and ICB fault systems as will further be discussed below.

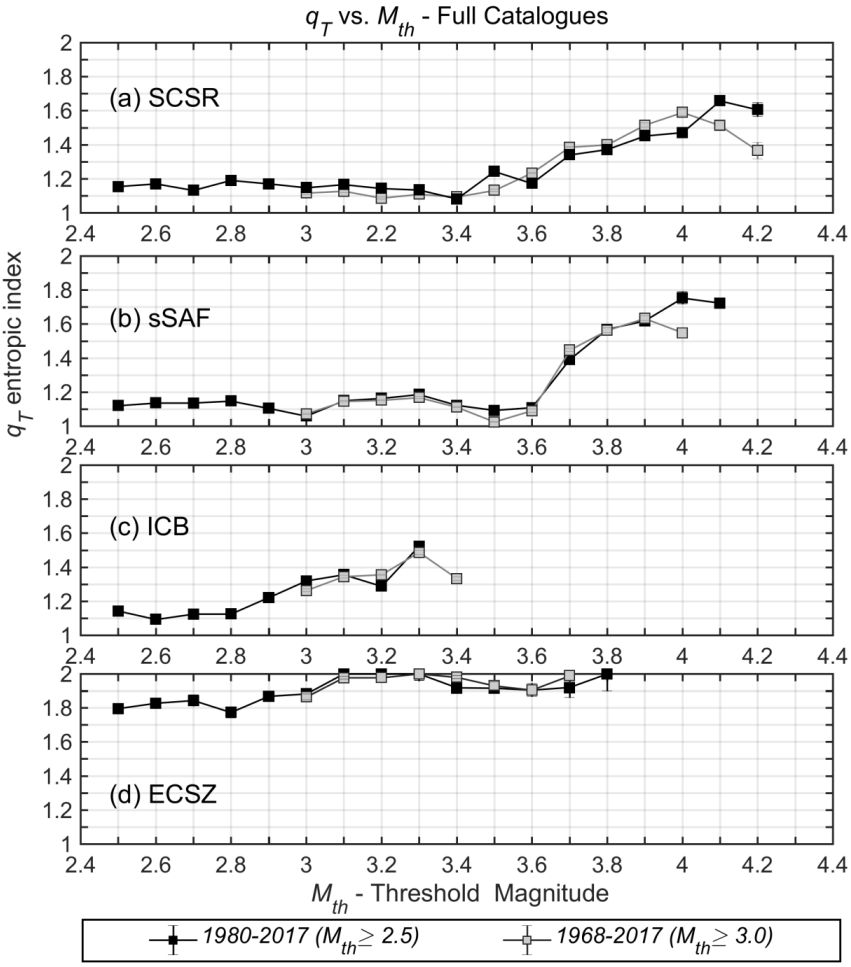

Figure 3.10 Variation of temporal entropic indices (q_T) with threshold magnitude (M_{th}) for the full earthquake catalogues of: (a) the entire SCSR; (b) sSAF; (c) ICB, and, (d) ECSZ. 95% confidence limits are also drawn but are not always visible as they usually are smaller than the symbols.

The variation of the temporal entropic index with *interevent distance* (Δd) is shown in Fig.3.11. When the analysis is carried out in this mode, it is expected that $q_T(\Delta d)$ will exhibit high values at interevent distances shorter than 100km due to the dominant effect of near field interactions, with particular reference to aftershock sequences. Such behaviour is generally observed for all $q_T(\Delta d \leq 100\text{km})$ so that $1.6 < q_T \leq 1.95$. For $\Delta d >$ 150km the results of the SCSR catalogues indicate very low correlation ($q_T < 1.2$) except for the longest interevent distances ($\Delta d >$300km). The longitudinal and latitudinal linear dimensions of the SCSR are comparable and of the order of 450km. Given the considerably smaller longitudinal dimensions of the ECSZ, sSAF and ICB, as well as the results of Fig. 10b-d, the increase in the value of q_T observed for $\Delta d >$300km may indicate interaction between faults *across* the three source areas (let alone that such interevent distances have usually nothing to do with aftershock sequences). For the sSAF catalogues, $q_T(\Delta d)$ is consistently lower than 1.15 for all $\Delta d >$100km. However, given that $M_{th} \leq 3$, it is straightforward to deduce that the results are dominated by the overwhelming majority of uncorrelated small magnitude events, consistently with the analysis of Fig. 3.10. As well in consistency with that analysis, if the threshold magnitude is increased, then the correlation increases over all interevent distances. As can be seen in Fig. 3.11a for the SCSR 1980-2017 full catalogue and $M_{th} = 3.8$, $q_T(\Delta d$=50km) increases from 1.59 to 1.81 and $q_T(\Delta d$=100km) from 1.12 to 1.7. Likewise, for Δd=100km q_T varies from 1.26 at Δd=200km to 1.16 at $\Delta d >$300km, albeit with a persistent tendency to decrease. Thus, the SCSR system can be shown to exhibit long range correlation. Unfortunately, these results cannot be repeated for higher threshold magnitudes or for the sSAF source area due to diminishing numbers of earthquakes per Δd group (and corresponding reduction in statistical significance). In the ICB source area correlation appears to increase to moderate levels (1.2 – 1.3) at long interevent distances ($\Delta d >$150km). Finally, in the ECSZ, the correlation is persistently strong ($1.54 < q_T \leq 1.73$) over all $\Delta d >$ 50km; given that the longest linear dimension of the ECSZ is of the order of 200km, the results indicate that correlation is uniformly strong over short *and* long ranges.

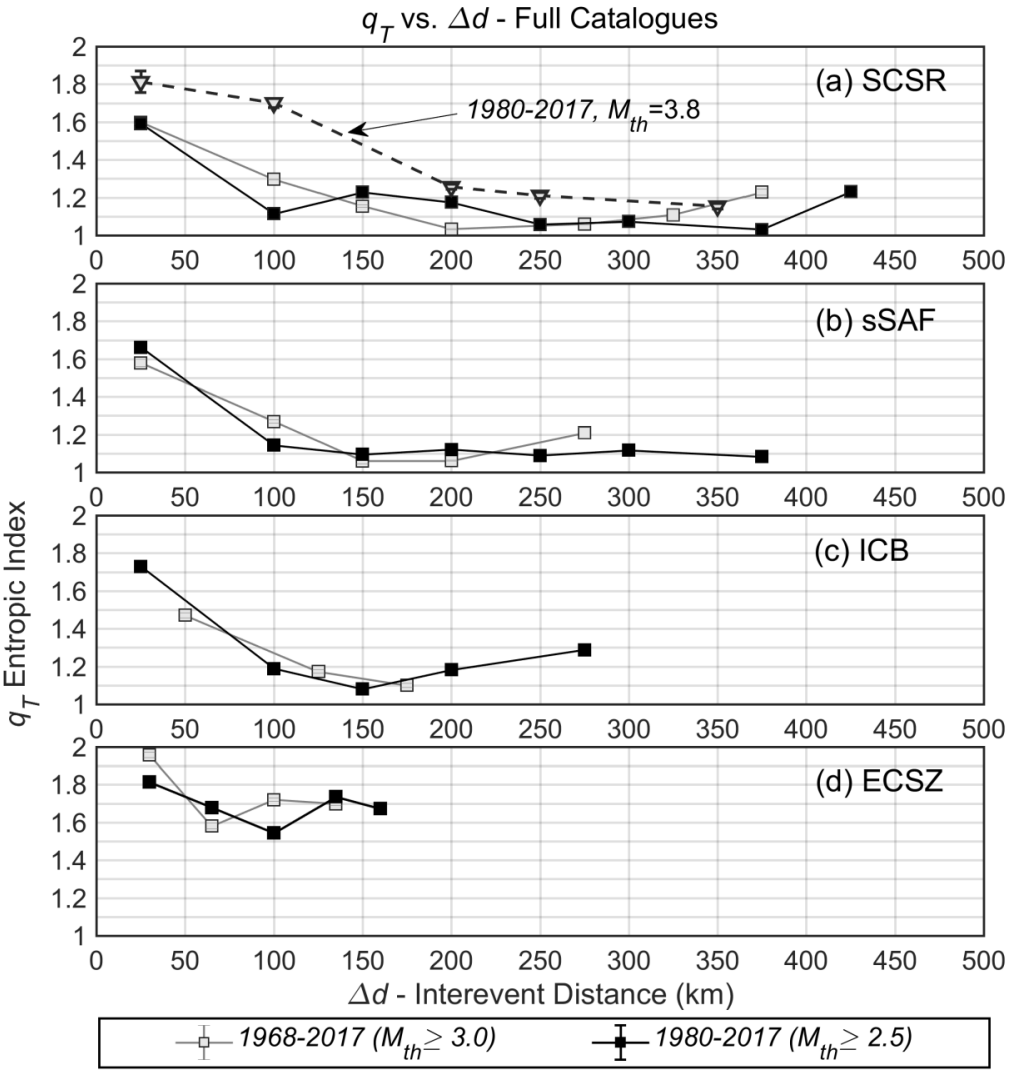

Figure 3.11 Variation of temporal entropic indices (q_T) with interevent distance (Δd) for the full earthquake catalogues of: (a) the entire SCSR; (b) sSAF; (c) ICB, and, (d) ECSZ. Binning schemes (widths of interevent distance groups) vary and are selected so as to optimize goodness of fit. 95% confidence limits are also drawn but are not always visible as they usually are smaller than the symbols

Based on the analysis of both $q_T(M_{th})$ and $q_T(\Delta d)$, it is quite apparent that the ICB and sSAF source areas (fault systems), which effectively comprise sub-parallel segments and branches of the Pacific – North American transformational plate boundary, exhibit analogous statistical behaviour and dynamics. The ECSZ system is different: it appears to exist in a state of extremely high correlation over all interevent distances (long range correlation), feature that can hardly be understood in terms other than Self-Organized Criticality. Notably, a rather similar result has been obtained for the source area of Walker Lane – Sierra Nevada Range in North California (as will be demonstrated in sections 3.2 and 3.3). It stands to reason that being a southward continuation of the Walker Lane the

ECSZ should exhibit analogous behaviour, indicative of rather unique seismogenetic dynamics. The origin of these dynamics, as well as the origin of the differences between the ECSZ and the rest of the SCSR, is open to debate and the issue will be revisited in Chapter 6 (Discussion). In a final comment, it should be noted that the results obtained for the periods 1968-2017 and 1980-2017 are absolutely compatible. Accordingly, the analysis of declustered catalogues will be based on the catalogue of the latter (1980-2017) period only, which may span a shorter interval (36.5 years instead of 48.9) but is complete for magnitudes far lower than the former (1968-2017).

ii.Analysis of South California Declustered Earthquake Catalogues

As mentioned above a primary objective of the present work is to investigate whether background seismicity is generated by non-Poissonian dynamic processes. Accordingly, I proceed to examine declustered versions of the SCSR, sSAF, ICB and ECSZ catalogues, in which aftershock sequences have been identified and removed by the stochastic declustering method of Zhuang et al (2002) at the $\phi \geq 0.7$ and $\phi \geq 0.8$ probability levels (i.e. probability greater or equal to 70% and 80% for an event to belong to the background). It must be noted that the analysis of entropic indices with respect to interevent distance will be limited to the SCSR and sSAF declustered catalogues because of the small populations of events left at interevent distances longer than 50km, which do not guarantee the statistical significance of the $q_M(\Delta d)$ and $q_T(\Delta d)$. In all other cases the analysis will focus on the study of $q_M(M_{th})$ and $q_T(M_{th})$.

Fig. 3.12 illustrates the results obtained from the SCSR catalogue. As can be seen in. Fig. 3.12a, q_M determinations do not fluctuate with M_{th} and are very consistently determined around 1.5±0.0095 and 1.51±0.006 for both probability levels, so that $b_q \approx 1$. Likewise, in Fig. 11c the determinations of $q_M(\Delta d)$ are practically featureless and stable around 1.5±0.015 and 1.51±0.0075, so that b_q is again approximately equal to unity. Interesting observations can be made only in regard to the temporal entropic index. In Fig. 3.12b, it is apparent that for probability levels $\phi \geq 0.7$, q_T is *consistently* greater than 1.4 for $2.5 < M_{th} < 3.6$, which represents a very significant increase in comparison to the correlation observed in the same magnitude range of the full catalogue (Fig. 3.10a). As per Fig. 3.10a, increase of q_T with magnitude is also observed only that here it commences as early as M_{th}=2.8 where q_T =1.44 and culminates at M_{th}=3.5 where $q_T \approx 1.8$, possibly stabilizing thereafter. By raising the probability level to $\phi \geq 0.8$, $q_T(M_{th})$ increases to values greater than 1.6 so as to average at 1.65±0.035. Given that to all intents and

purposes aftershocks have been eliminated at the 80% probability level, this can be taken to indicate a very strongly correlated seismogenetic background. It is also interesting to note that the increase of q_T with magnitude disappears and q_T fluctuates between 1.6 and 1.7, indicating a background with the same degree of correlation at all magnitude scales. Analogous observations can be made on $q_T(\Delta d)$. For $\phi \geq 0.7$, q_T cannot be determined at the required level of rigour and significance when and Δd<100km (as evident in Fig. 3.12d). However, it clearly increases from 1.64 at Δd=100km to 1.77 at Δd=250km and averages to 1.70±0.064, which represents an increase of 0.57 in comparison to the corresponding results of the full SCSN catalogue (Fig. 10a). For $\phi \geq 0.8$ and Δd<100km, q_T is 1.59±0.02, approximately the same with the corresponding determination of the full SCSR catalogue. It is therefore conceivable that strong short-range correlation (near field interaction) persists in the background. For $\phi \geq 0.8$ and $\Delta d \geq$100km, q_T rises to above 1.7 and increases to 1.9 at Δd ~250km, having an average value of 1.76± 0.04 (Fig. 3.12d). As a general conclusion, the results of both probability levels indicate sub-extensivity and very strong long-range correlation in the seismogenetic background of the entire SCSR source area.

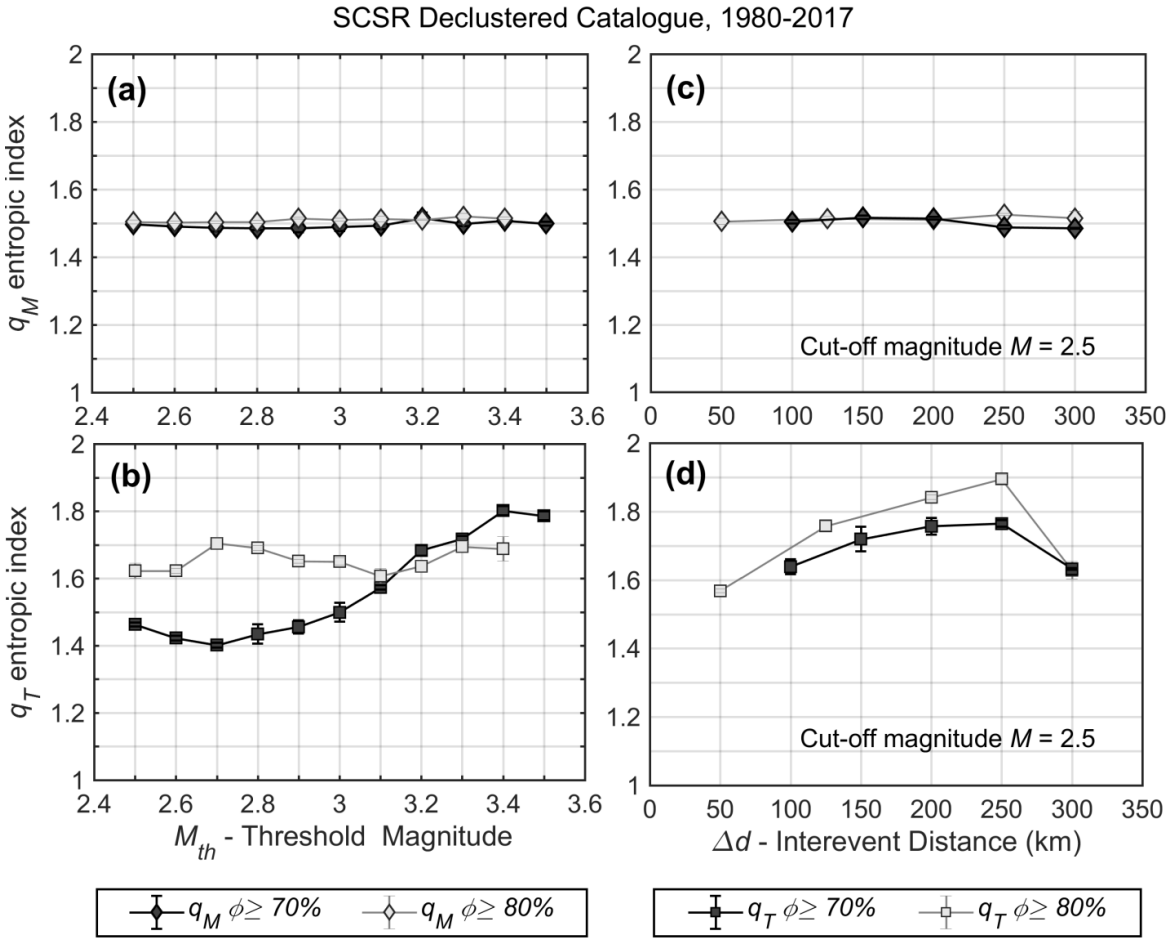

Figure 3.12 Analysis of the magnitude (q_M) and temporal (q_T) entropic indices for the catalogue of the South California Seismic Region *declustered* at probability levels 70% (dark colours) and 80% (light colours). **(a)** Variation of q_M with threshold magnitude (M_{th}); **(b)** Variation of q_T with threshold magnitude; **(c)** Variation of q_M with interevent distance (Δd); **(d)** Variation of q_T with interevent distance. In (c) and (d), binning schemes vary so as to maximize statistical rigour. Error bars represent 95% confidence limits; they are not always visible as they frequently are smaller than the symbols.

Let us, now, examine the declustered sSAF catalogue, for which results are shown in Fig. 3.13. It is immediately apparent that the variation of the entropic indices with magnitude and interevent distance are very similar to those of the declustered SCSR area. Again, q_M determinations do not fluctuate with M_{th} and are very consistently determined so that 1.52±0.009 for $\phi \geq 0.7$ and 1.51±0.004 for $\phi \geq 0.8$ (Fig. 3.13a). Perfectly analogous results are obtained for the variation of q_M with interevent distance (Fig. 3.13c). As with SCSR, interesting observations can be made only in regard to the temporal entropic index. Thus, for probability levels $\phi \geq 0.7$, q_T is *consistently* greater than 1.5 for 2.5< M_{th} <3.3 (Fig. 3.13b), which constitutes a very significant increase in comparison to the correlation observed in the same magnitude range of the full sSAF catalogue (Fig. 9a). Increase of

q_T with magnitude is once again observed with the difference that it commences at M_{th}=2.7 where q_T =1.48 and culminates at M_{th}=3.3 where $q_T \approx 1.75$. At the $\phi \geq 0.8$ probability level, $q_T(M_{th})$ increases to values greater than 1.6 and varies between 1.62 and 1.73 so as to average at 1.68±0.048; as with SCSR and Fig. 3.12b, this indicates a background with the same high level of correlation at all magnitude scales. Turning now to Fig. 3.12d, it is apparent that q_T exhibits upward trend with increasing for interevent distance. For $\phi \geq 0.7$ it steadily increases from 1.5 at Δd=50km to 1.75 at Δd=225km and averages to 1.63±0.096, which represents an increase of 0.52 in comparison to the corresponding results of the full sSAF catalogue (Fig. 3.11b). For $\phi \geq 0.8$ q_T rises from 1.62 at Δd = 50km to above 1.85 at Δd =175km and 1.79 at Δd=225km, having an average value of 1.77± 0.1. Once again, one may assert that the results of both probability levels indicate sub-extensivity and very strong long-range correlation in the background of the sSAF area which, given its relatively narrow longitudinal dimension (~100km), should mainly be attributed to processes taking place parallel to the seismogenetic faults.

The variation of the entropic indices with magnitude for the declustered ECSZ and ICB catalogues is shown in Fig. 3.14. As evident in Fig. 3.14a and Fig. 3.14c, the magnitude entropic indices are featureless and practically identical for all usable realizations of the declustered catalogues, averaging to 1.51±0.01 for ECSZ and 1.5±0.01 for ICB; in both cases b_q approach unity, consistently with the *b*-values determined by more conventional means. The temporal entropic index of the ECSZ exhibits clear increase with threshold magnitude at the $\phi \geq 0.7$ probability level, beginning with 1.63 at M_{th}=2.5 and ending with 1.78 at M_{th}=3 (Fig. 3.14b); it can also be seen to fluctuate between 1.8 and 1.9 at the $\phi \geq 0.8$ probability level, without exhibiting some trend (Fig. 3.14b). Such q_T values are very similar to those obtained from the full ECSZ catalogue in the same magnitude scales and confirm that background seismogenetic processes are thoroughly and strongly correlated in the ECSZ. The temporal entropic index of the ICB source area can be determined only for magnitude thresholds between 2.5 and 2.7 and only at the $\phi \geq 0.7$ probability level (due to diminishing earthquake populations at larger thresholds and higher probability levels). It can be observed to fluctuate between 1.6 and 1.8, averaging at 1.74 (Fig. 3.14d); when compared to the average obtained for the full ICB catalogue in the same magnitude scales, q_T can be seen to have increased by an astounding 0.62. Once again, this is compelling evidence that the background seismogenetic processes in the ICB are sub-extensive and thoroughly and strongly correlated over all magnitude scales and,

presumably, interevent distances. The analysis of catalogues declustered at the $\phi \geq 0.9$ probability level is summarized in Table 3.1 2. Results are shown only for SCSR and sSAF, as the declustered ECSZ and ICB catalogues respectively contain 441 and 290 events and cannot be reliably evaluated. For SCSR and sSAF, the determinations of $q_M(M_{th})$ and $q_M(\Delta d)$ attain values almost identical to those obtained at the 80% probability level (see above) and as well, exhibit very little variation. Likewise, the determinations of $q_T(M_{th})$ for SCSR and sSAF, as well as of $q_T(\Delta d)$ for sSAF, persist remain at the same high levels, and appear to exhibit the same type of variation as in the case of the $\phi \geq 0.8$ probability level.

In concluding this Chapter, it is important to note that as the analysis has shown, on removing aftershock sequences, the seismogenetic systems of South California exhibit very high levels of correlation (long-term memory and long-range interaction). On the basis of this evidence it is possible to infer that they are inherently non-Poissonian, as will further be discussed in Chapter 6.

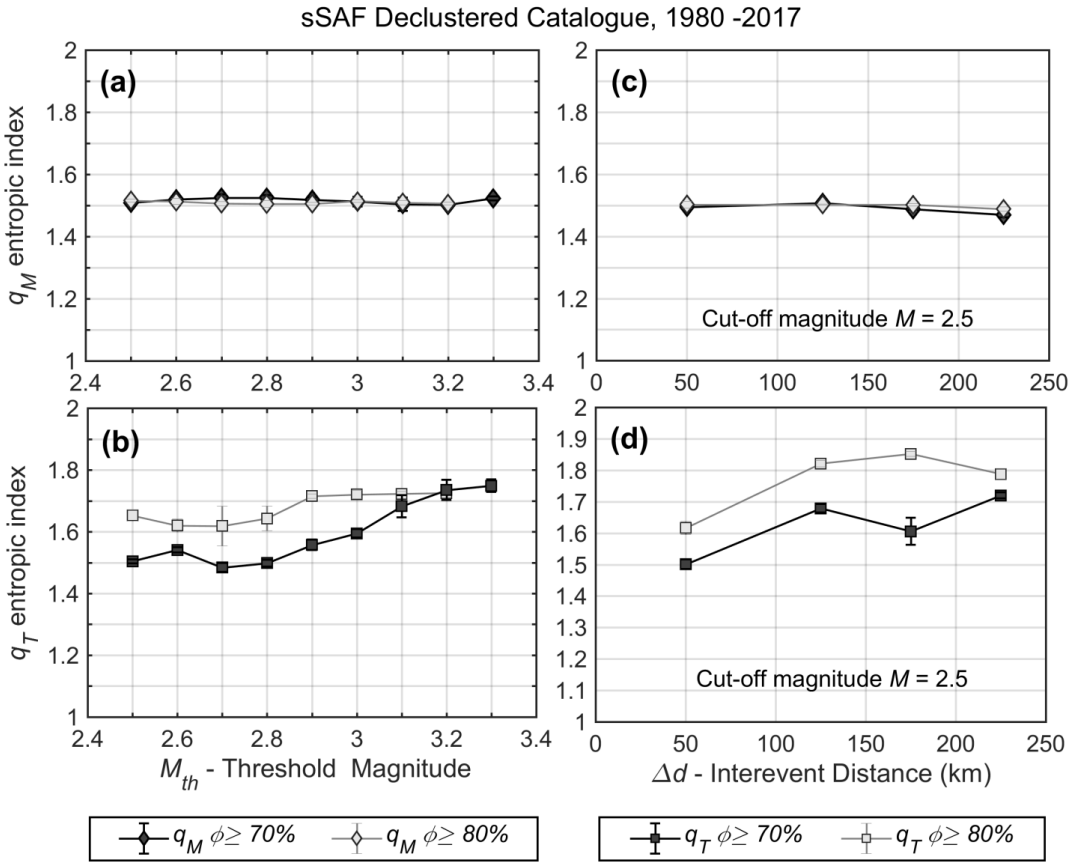

Figure 3.13 As per Fig. 3.12 but for the *declustered* catalogues of the south San Andreas Fault segment.

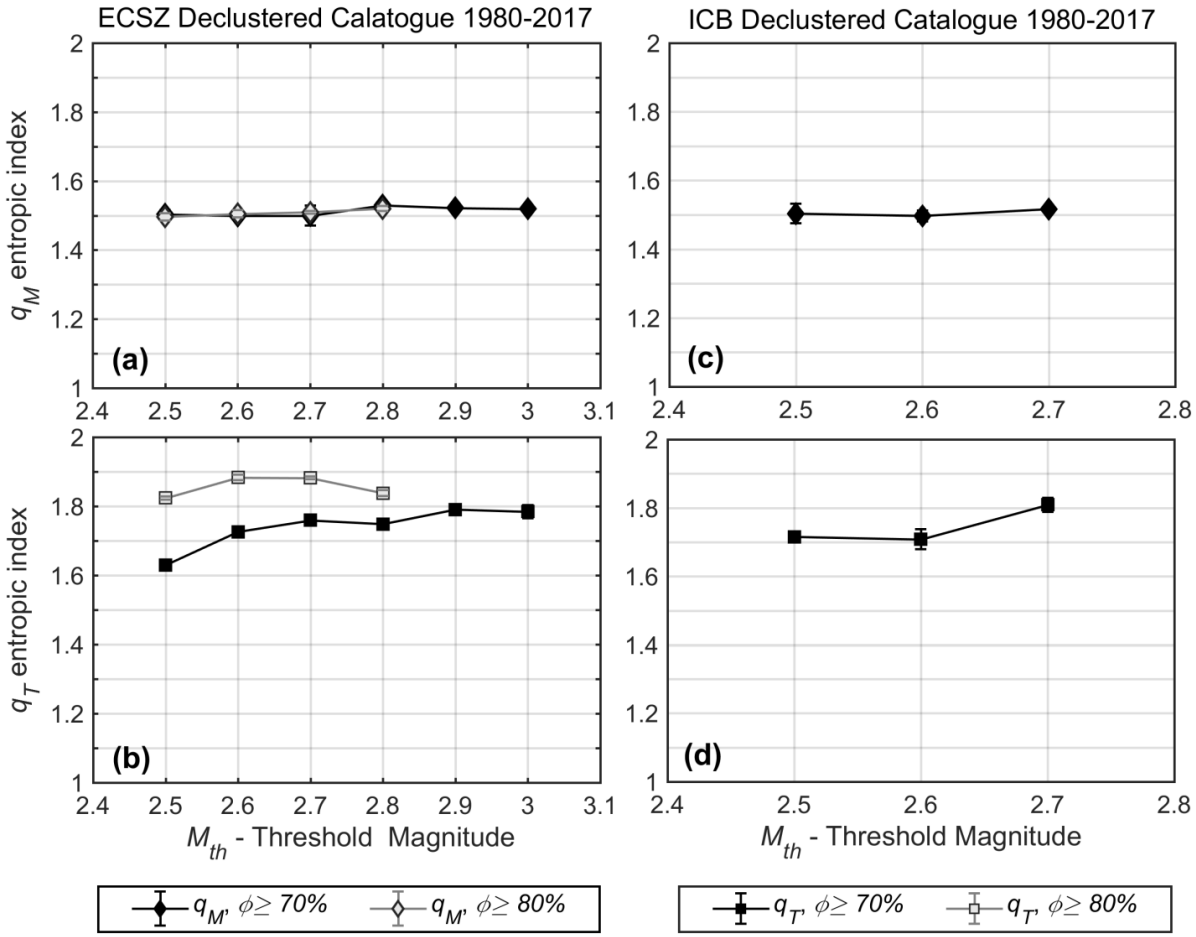

Figure 3.14 Variation of the magnitude (q_M) and temporal (q_T) entropic indices with threshold magnitude (M_{th}) for the declustered catalogues of the Eastern California Shear Zone (a, b) and the Inner Continental Borderland (c, d). Dark colours illustrate results obtained at the 70% background probability level; light colours results at the 80% probability level. Error bars represent 95% confidence limits; they are not always visible as they frequently are smaller than the symbols.

TABLE 3.1.2 Summary with the range of variation of the entropic indices obtained from the earthquake source areas of California.

		$q_T(M_{th})$ Range	$q_T(\Delta d)$ Range		$q_M(M_{th})$ Range	$b_q(M_{th})$ range	$q_M(\Delta d)$ Range	$b_q(\Delta d)$ range
			Δd<100km	Δd>100km				
FULL	**SCSR**	1.08-1.65	1.59	1.08-1.23	1.49-1.59	1.04-0.69	1.47-1.56	1.12-0.78
	sSAF	1.06-1.88	1.57-1.66	1.11-1.21	1.50-1.59	1.00-0.69	1.50-1.55	1.00-0.81
	ECSZ	1.79-1.98	1.59-1.95	1.67-1.70	1.48-1.53	1.08-0.88	1.48-1.52	1.08-0.92
	ICB	1.14-1.48	1.47-1.73	1.18-1.27	1.50-1.53	1.00-0.88	1.49-1.52	1.04-0.92
DECLUSTERED $\phi \geq 70\%$	**SCSR**	1.40-1.80	1.64	1.63-1.76	1.49-1.51	1.04-0.96	1.48-1.51	1.08-0.96
	sSAF	1.48-1.74	1.50	1.60-1.72	1.50-1.53	1.00-0.88	1.47-1.50	1.12-1.00
	ECSZ	1.62-1.79	N/A		1.49-1.52	1.04-0.92	N/A	
	ICB	1.71-1.80	N/A		1.50-1.52	1.00-0.92	N/A	
DECLUSTERED $\phi \geq 80\%$	**SCSR**	1.62-1.70	1.56	1.63-1.89	1.50-1.52	1.00-0.92	1.50-1.52	1.00-0.92
	sSAF	1.61-1.68	1.61	1.78-1.85	1.50-1.51	1.00-0.96	1.49-1.50	1.04-1.00
	ECSZ	1.83-1.88	N/A		1.50-1.52	1.00-0.92	N/A	
DECLUSTERED $\phi \geq 90\%$	**SCSR**	1.59-1.75	N/A		1.50-1.53	1.00-0.88	N/A	
	sSAF	1.64-1.75	1.61	1.82	1.52-1.54	0.92-0.85	1.51-1.54	0.96-0.85

3.2 NORTH CALIFORNIA

Next, I examine the nature of the seismogenetic system in North California, USA, by searching for evidence of complexity and non-extensivity in the earthquake record. The study area is bounded by the coordinates 34°N to 41°N and -126.0°E to -116.0°E and includes different earthquake source areas, as can be seen in the composite seismicity map of Fig 3.15. These are:

a) The broader area of the central and northern segments of the San Andreas Fault, (henceforth nSAF), where earthquake epicentres are indicated with white rectangles. This is a well-known, highly active fault system and has generated large ($M > 7$) earthquakes during the last two centuries (e.g. 1857, 1906, 1989). It extends northward of the Garlock Fault (see below), between Parkfield at approximately (35.9°N, 120.4°W) and the Mendocino Triple Junction (approx. 40.36°N, 124.6°W). For the purpose of this study, the geographic boundaries of nSAF are defined to the north by the line joining the northern terminus of the SAF/Shelter Cove section, the northern terminus of the Barlett Springs Fault System (Lake Mountain fault) and the Battle Creek Fault; to the east by the Battle Creek Fault, the Foothills Fault system and the Kern Gorge and White Wolf fault zones; to the south by the Garlock Fault and to the West by a running offshore parallel to the Pacific Coast.

b) The Central Valley – Sierra Nevada Range, up to and including the Walker Lane to the east, where epicentres are indicated with solid black circles (henceforth SNR); this fault system also extends northward of the Garlock Fault and behaves as a semi-rigid microplate (Sierran microplate) whose interior (Central Valley) is often described as rigid and is characterized by the absence of significant faults and large earthquakes (Hammond et al, 2012; Saleeby et al., 2009; McCaffrey 2005; Dixon et al, 2000; Goter et al, 1994). In this study the geographic boundaries of SNR are defined to the north by the line joining the Battle Creek Fault and the northern termini of the Butt Creek and Almanor fault zones, up to the longitude -116°E; to the east by the meridian -116°E; to the south by the Garlock Fault and to the west by the White Wolf and Kern Gorge fault zones, the Foothills Fault system and the Battle Creek Fault. **c)** The Mendocino Fracture Zone (MFZ) and Triple Junction where epicentres are indicated with light grey down triangles.

The southern margin of the study area is taken to be northward of the ENE-WSW oriented, left-lateral Garlock Fault Zone (GFZ). This is a major boundary between the Great Basin (extending to the east of Walker Lane), and the Mojave Desert extending to

the south and southwest; it is characterized by a mixture of left-lateral strike-slip and reverse focal mechanisms and is believed to have developed in order to accommodate the strain differential between the dominantly extensional tectonics of the semi-rigid Great Basin microplate and the right lateral strike-slip faulting of the Mojave Desert's crust. The intersection of the Garlock and San Andreas faults begets a restraining bend located approx. between 34.5°N and 35.5°N (Big Bend), where the strike of the SAF and the mode of deformation are notably different from that experienced in either side of the bend (e.g. Jones, 1988; Hardebeck and Hauksson, 2001). Studies based on slip rates, focal mechanisms etc. indicate that the GFZ is the area where the SAF and the East California Shear Zone lock up in Southern California and a tectonic boundary forms between north and south California, delimiting the central/north and south segments of the SAF (e.g. Fialko, 2006; Becker et al, 2005). Regarding the Mendocino Fracture Zone, we consider that it must be studied separately as it is a significant feature whose geodynamic characteristics clearly distinguish it from the nSAF and SNR. Accordingly, the source areas to be considered in the present analysis are the nSAF and the SNR as shown in Fig. 3.15, which are both characterized by NW-SE, dominantly right-lateral strike slip deformation due to pure transformational and transformational to trans-tensional stress regimes respectively.

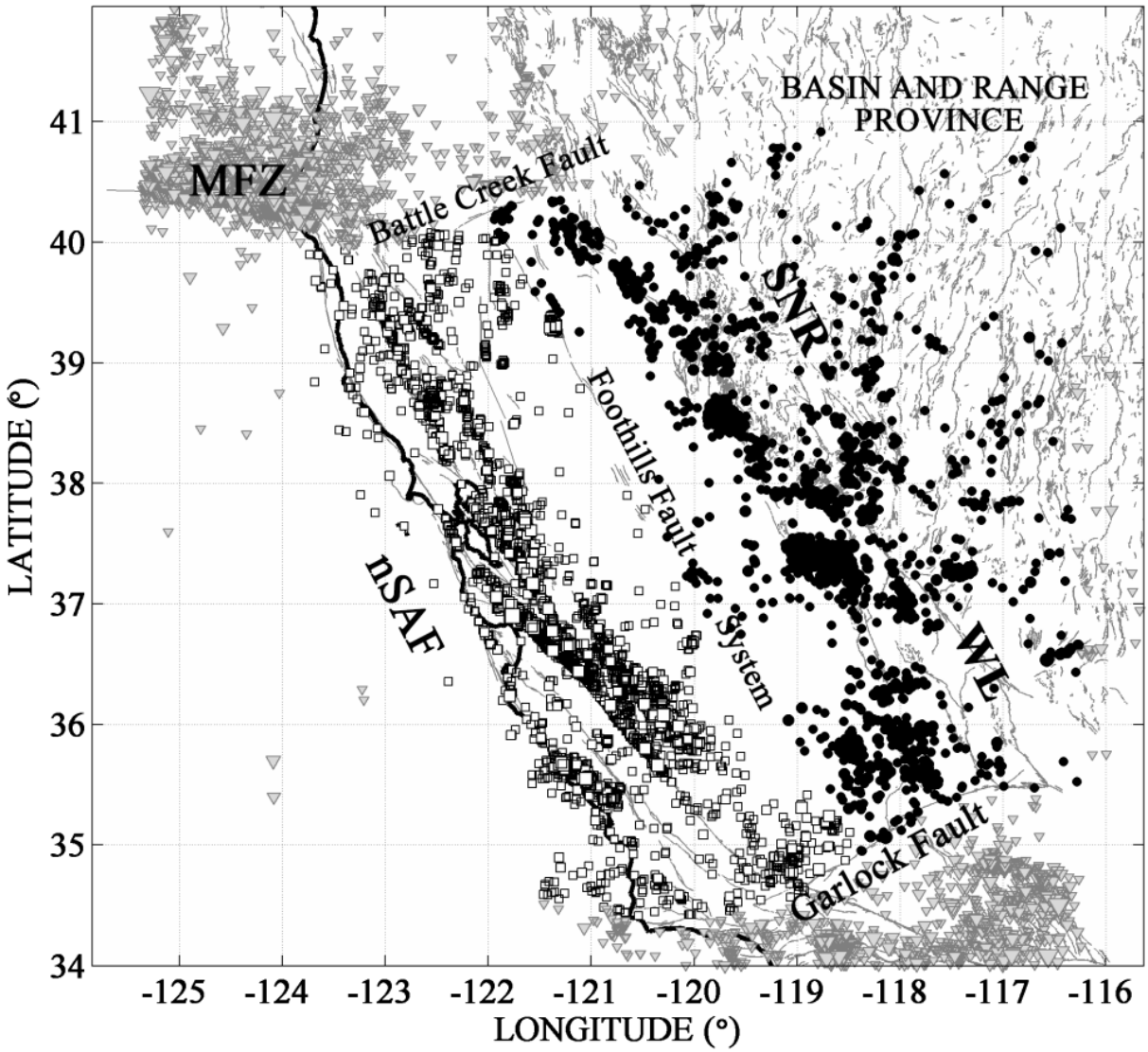

Figure 3.15 The seismicity of North California as illustrated by mapping the epicentres of earthquakes included in the full NCSN catalogue for the period 1968-2015. nSAF represents the north segment of the San Andreas Fault with earthquake epicentres depicted as white rectangles. SNR-WL represents the Sierra Nevada Range – Walker Lane system with earthquake epicentres depicted as solid black circles. The epicentres of earthquakes *not* included in the ensuing analysis (e.g. Mendocino Fault Zone – MFZ) are depicted as light grey down-pointing triangles.

3.2.1 North California Earthquake Data

The recent earthquake history of North California is summarized in two definitive catalogues published by the North California Earthquake Data Center (NCEDC, http://www.ncedc.org):

a) The original NCEDC catalogue, henceforth to be referred to as the *NCSN catalogue* (for Northern California Seismic Network). Therein, most earthquake sizes are reported in the local (M_L) and moment (M_w) magnitude scales but a considerable number of events is reported in the duration (M_d) and amplitude (M_x) scales. The latter have been exhaustively calibrated against the M_L scale: Eaton (1992) has shown that they are within 5% of the M_L scale for magnitudes in the range 0.5 to 5.5 and that they are virtually independent of the distance from the epicentre to at least 800 km. In consequence, M_d and M_x are practically equivalent to M_L. For the purpose of the present analysis M_w magnitudes were also converted to M_L using the empirical formula of Uhrhammer et al (1996): $M_w = M_L \cdot (0.997 \pm 0.020) - (0.050 \pm 0.131)$. Herein I will use a subset of this catalogue spanning the period 1968–2015 which, after homogenization of the magnitude scale was found to be complete for $M \geq 3.0$ (Fig. 3.16c and 3.16d). The epicentre distribution of this subset is shown in Fig. 3.15.

b) An updated/upgraded version of the NCEDC catalogue in which waveform cross correlation and double-difference methods were used to improve the hypocentral locations of earthquakes observed during the period 1984–2011, by up to three orders of magnitude (Waldhauser and Schaff, 2008; Schaff and Waldhauser, 2005). This is will be dubbed the *Double Difference* (DD) catalogue by reference to the relocation method. Therein, earthquakes locations are reported only for latitudes northward of 35.3°N and earthquake sizes are reported in the local magnitude scale; the catalogue is complete for $M \geq 1.8$ and for the entire period 1984-2011 (Fig. 3.16a, 3.16b) and the epicentre distribution is shown in Fig. 3.17.

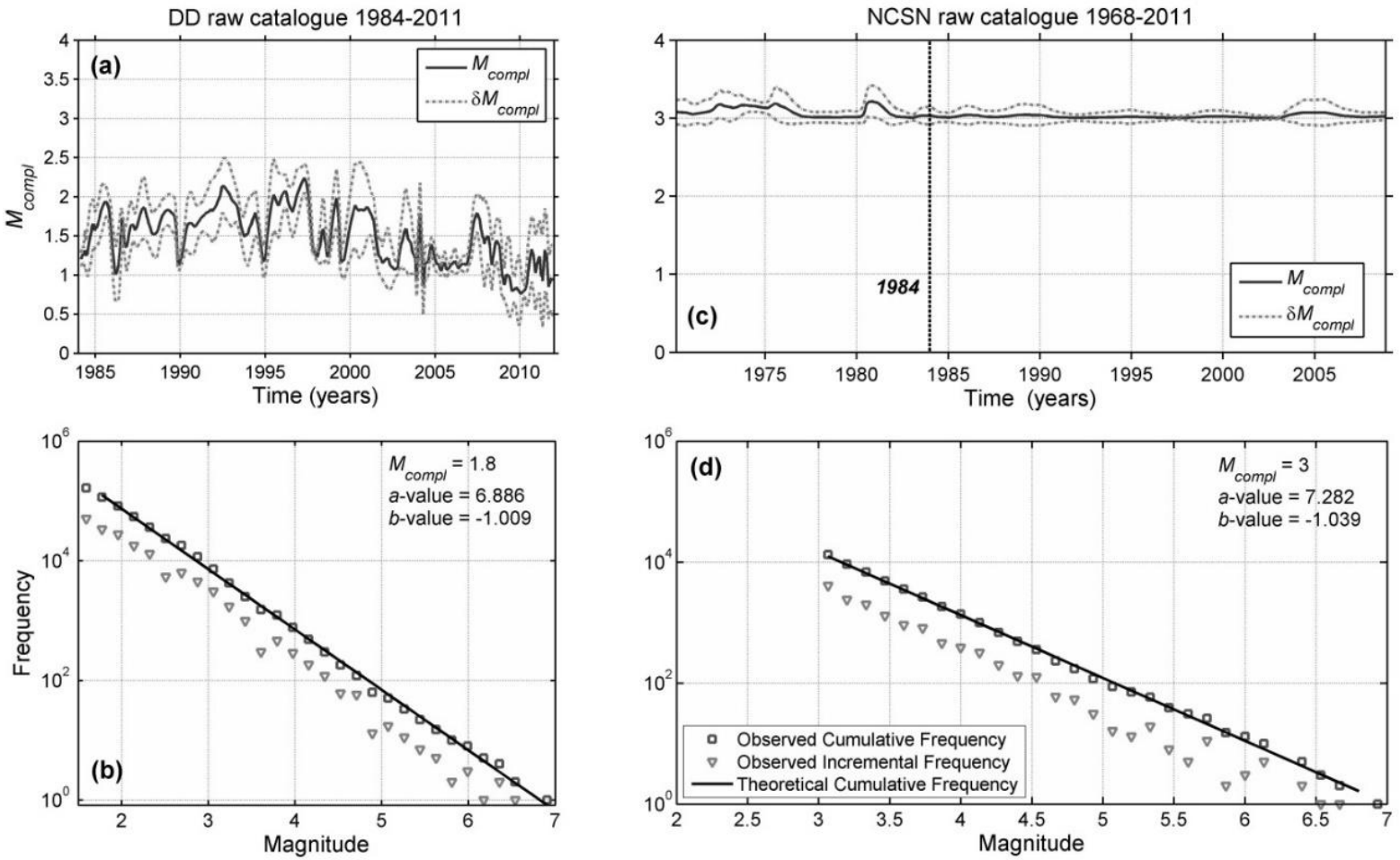

Figure 3.16 a) Variation of the magnitude of completeness (Mcompl) with time in the DD catalogue with 95% confidence limits. b) Incremental (down triangles) and cumulative (open squares) F-M distributions of the DD catalogue above the magnitude of completeness. c) Variation of Mcompl with time in the NCSN catalogue with 95% confidence limits. d) Incremental (down triangles) and cumulative (open squares) F-M distribution of the NCSN catalogue above the magnitude of completeness. Figs. 5a and 5c were prepared with the ZMAP software (Wiemer, 2001).

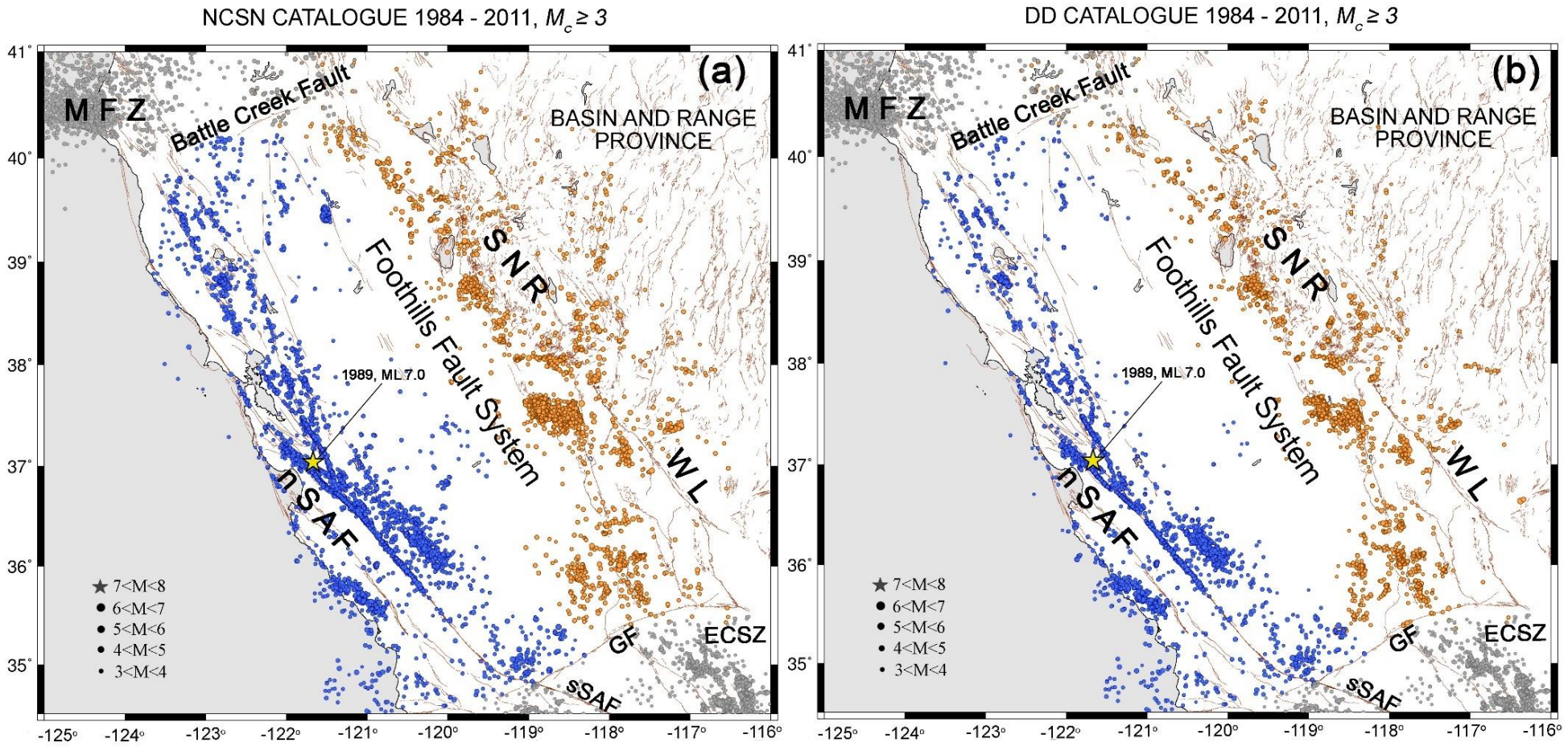

Figure 3.17. Comparative epicentre distribution of **(a)** the full NCSN and **(b)** the full DD catalogues, for the same period (1984-2011), geographical boundaries and magnitude of completeness ($M_c \geq 3$).

There are *significant* differences in the information contained in the two catalogues: when constrained by the same geographical boundaries (as per Fig. 3.17a and Fig. 3.17b), time interval (1984–2011) and magnitude of completeness ($M_c \geq 3.0$), the NCSN catalogue was found to comprise 6696 events and the DD catalogue 7465. However, the difference is *not* limited to 769 events as would appear at first sight: not only earthquakes present in the DD are missing from the NCSN catalogue, but also events present in the NCSN are missing from the DD! As evident in Fig. 3.18a, the missing events are generally interspersed with higher numbers of discrepancies clustering around larger earthquakes (main shocks) and exhibiting a very notable increase after year 2006. Thus, the total number of different events rises to an astounding 1102! As can also be seen in Fig. 3.18b, the number of discrepancies is overwhelming at the smaller magnitude scales, with a total of 839 differences at $M = 3$ and 42 – 20 differences for $M \in [3.1, 3.7]$. Even more interesting is that intermediate magnitude scales have also been affected. Finally, the sequence of missing events is completely random and unstructured: as demonstrated in Fig. 3.18c, the cumulative interevent time distribution can be almost perfectly modelled by a q- exponential function with $q \equiv 1$, or by a conventional exponential function.

The discrepancy between the two catalogues can be explained as collateral of the relocation/ magnitude re-compilation process. According to Waldhauser and Schaff (2008) some events are “re-evaluated”, and some may even be lost because of insufficient data links after the weighting function removes outliers. The analysis presented in Fig. 3.18 (and illustrated in Fig. 3.19) seems to indicate that “re-evaluation” has migrated a significant number of events with original (NCSN) magnitudes lower than 3 to eventual (DD) magnitudes ≥ 3 and a small number of events in the opposite direction, so that the DD has ended up richer in magnitude 3 events with respect to the NCSN. Moreover, it appears to have done so in a rather unsystematic (random) way with respect to the temporal sequence of events. It should also be pointed out although this explanation would appear to be straightforward for discrepancies around the magnitude of completeness ($M_c = 3$), it does not answer the question of discrepancies observed at larger magnitude scales, the origin of which remains to us uncertain (especially after 2006).

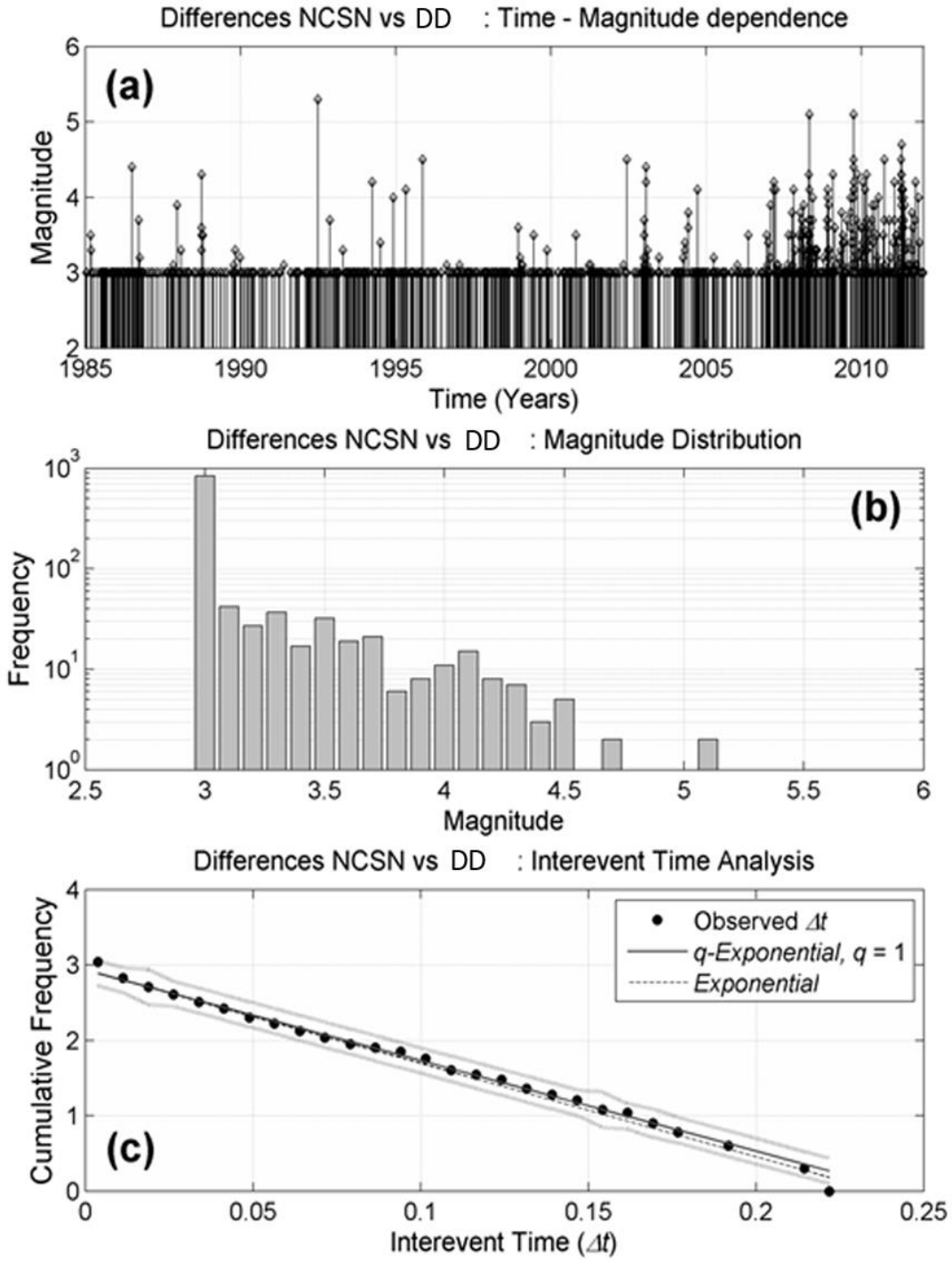

Figure 3.18 (a) Time-Magnitude diagram of the differences between the NCSN and DD catalogues. **(b)** Incremental frequency–magnitude distribution of the events shown in (a). **(c)** Black solid circles represent the empirical cumulative frequency – interevent time distribution of the events shown in (a); the distribution is almost perfectly filled by a *q*-exponential function with $q \equiv 1$ (solid line), or by a conventional exponential function (dashed line).

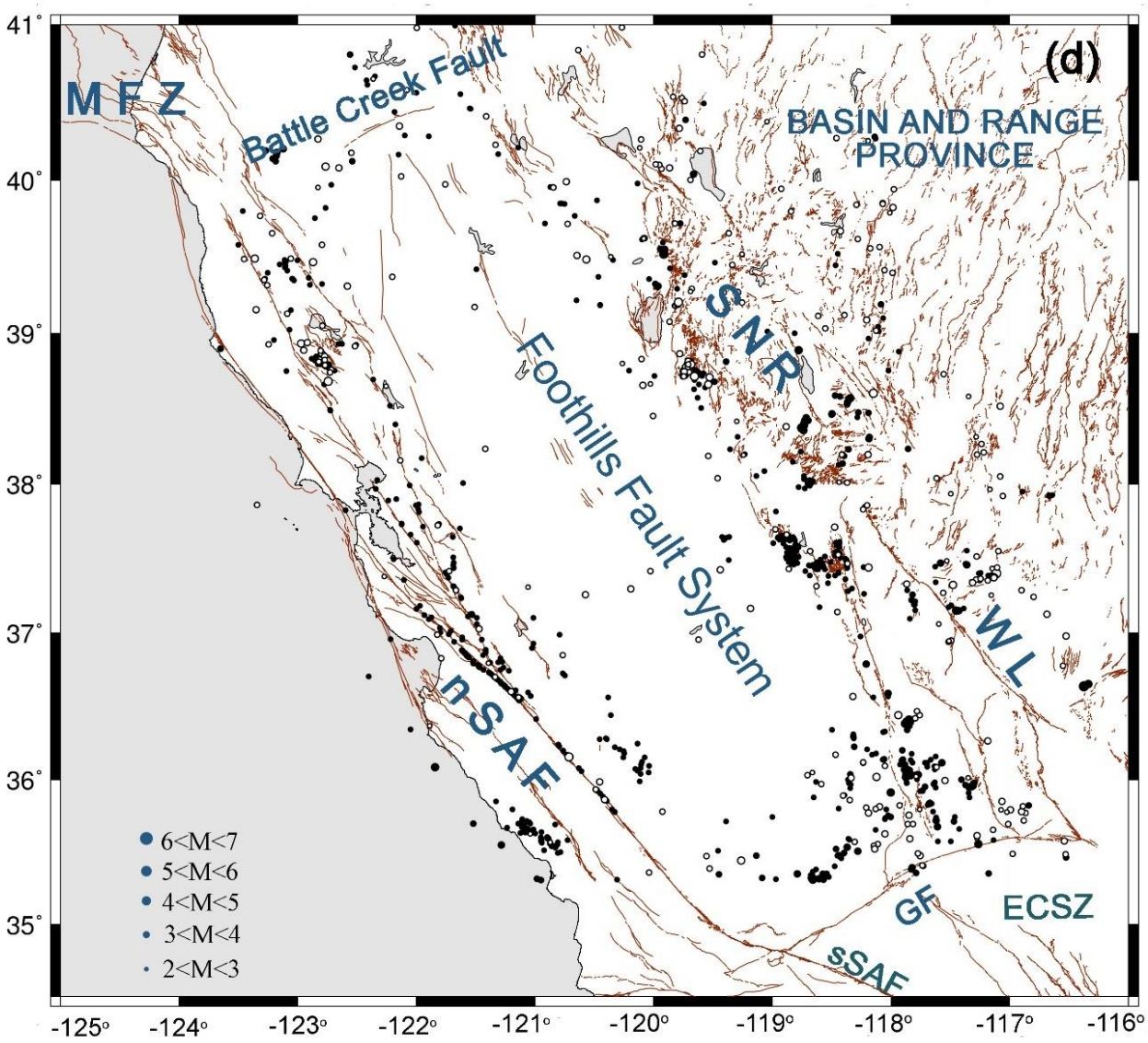

Figure 3.19 Epicentre map of the differences between the NCSN and DD earthquake catalogues for the period 1984–2011. Solid black circles represent earthquakes present in the DD catalogue but missing from the NCSN catalogue. White circles represent earthquakes present in the NCSN catalogue but missing from the DD catalogue. No discernible spatial structure or clustering of the differences can be observed.

The effect of unsystematic surplus or deficit of events in a catalogue may be significant: it not only produces outliers but is also expected to distort and possibly randomize the statistics of interevent time and interevent distance. It is therefore imperative to examine the extent to which such anomalies influence the declustering process and the estimation of the entropic indices. Accordingly, I shall first perform a comparative analysis of the NCSN and DD catalogues for events observed within identical geographical boundaries during their common interval 1984–2011 and for magnitudes equal to, or greater than a threshold of M_{th} = 3.0. The results of this exercise will expectably indicate the more

consistent catalogue, on the basis of which to evaluate the statistical mechanics of North California seismicity.

Fig. 3.20a illustrates the cumulative earthquake count of the full NCSN catalogue for the period 1968-2011 (thick black line) and its declustered versions with probability $\phi_j \geq 70\%$ (thin black line), $\phi_j \geq 80\%$ (solid grey line) and $\phi_j \geq 90\%$ (dashed grey line). The catalogue declustered at the $\phi_j \geq 70\%$ level is almost free of the time-local rate surges (jerks) that indicate the presence of aftershock sequences. Nevertheless, it is not completely smooth and exhibits small fluctuations because a portion of the remaining events are foreground residuals. Consequently, in dealing with the NCSN catalogue, I will endeavour to confirm the results obtained at the 70% probability level by studying declustered realizations with probability $\phi_j \geq 80\%$ and $\phi_j \geq 90\%$ to be background. Fig. 3.20b illustrates the corresponding cumulative count of DD catalogue realizations as per Fig 3.20a: the thick black line corresponds to the full catalogue and the thin black, solid grey and dashed grey lines to realizations declustered at $\phi_j \geq 70\%$, $\phi_j \geq 80\%$ and $\phi_j \geq 90\%$ respectively. Clearly, the full DD catalogue contains more events than the full NCSN but its declustered realizations contain significantly fewer events than the corresponding realizations of the NCSN. This could be explained as collateral of relocation: epicentres and hypocentres become compactly spaced so that the space-time distance between consecutive events decreases and their likelihood of being classified in the foreground increases. The cumulative count of the DD catalogue declustered at the $\phi_j \geq 70\%$ level is very smooth. In addition, the number of events at this level is not significantly different from the number of events remaining at higher probability levels. This indicates that to all intents and purposes, the $\phi_j \geq 70\%$ catalogue is free of foreground events. Accordingly, results based this realization, although spanning a shorter period than the corresponding declustered realization of the NCSN catalogue, will provide strong and compelling constraints on the statistical mechanics of seismogenesis in North California.

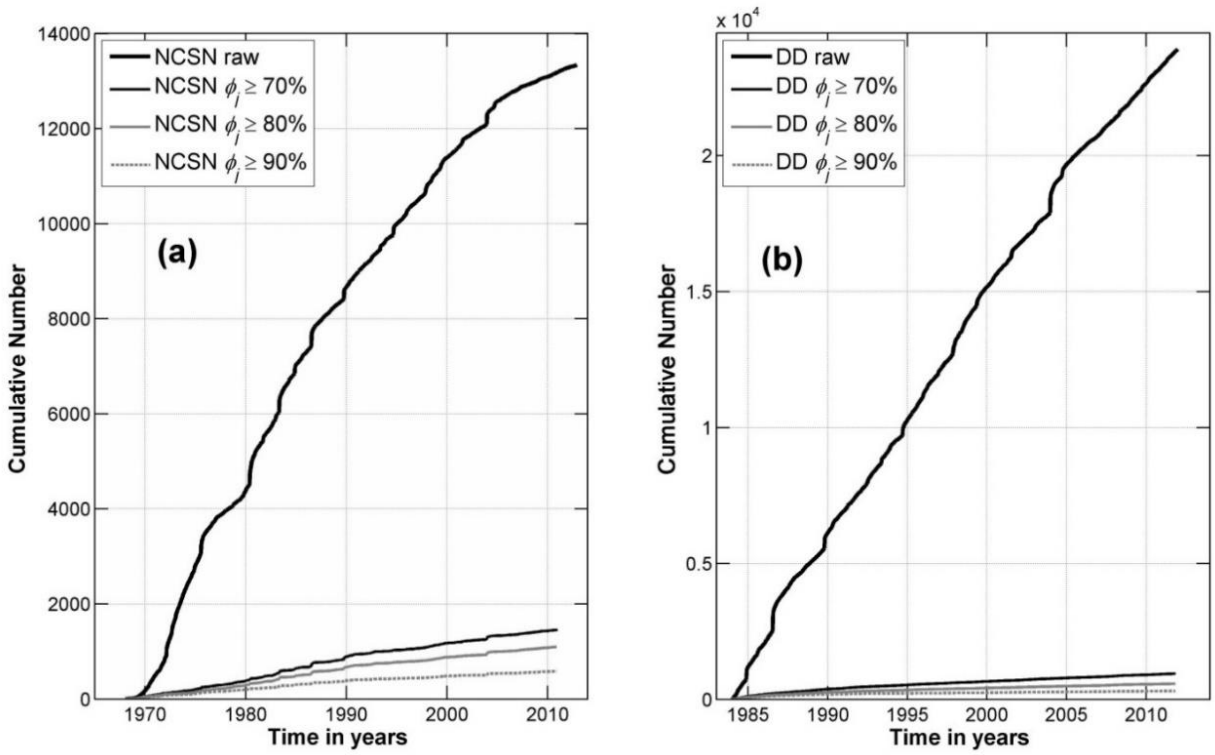

Figure 3.20 a) The cumulative earthquake count of the observed (full) and declustered realizations of the NCSN catalogue. **b)** The cumulative earthquake count of the full and declustered realizations of the DD catalogue.

TABLE 3.2.1 Summary of North California earthquake catalogues used in the present analysis.

Source Area	Source Area Code	Period	M_{comp}	Full catalogues (№ events)	M_{comp}	Declus.catalogues $\phi_i \geq 70\%$ (№ events)	Declus.catalogues $\phi_i \geq 80\%$ (№ events)	Declus catalogues $\phi_i \geq 90\%$ (№ events)
North California	**NCSN**	1968-2015	3.0	13578	3.2	1384	1218	955
		1984-2011	3.0	6,696	N/A			
		1968-1988	3.0	8,125				
		1990-2015	3.0	5092				
Double-difference Catalogue for North California	**DD**	1984-2011	3.0	7,465				
San Andreas Fault North Segment	**nSAF**	1968-2015	3.0	8,596	3.2	943	666	< 500
		1968-1988	3.0	5,738	N/A			
		1990-2015	3.0	2,615				
Sierra Nevada Range	**SNR**	1968-2015	3.0	4,982	3.2	591	< 500	
		1968-1988	3.0	2,391	N/A			
		1990-2015	3.0	2,465				

3.2.2 NESP results for North California Earthquake Catalogues

In order to conduct a comprehensive as possible study, our investigation will comprise a comparative analysis of the NCSN and DD full and declustered catalogues over the (common) period 1984–2011, as well as detailed analysis of the NCSN catalogue for the extended period 1968 – 2015 (47 years). I will also conduct a detailed comparative study of seismicity in the nSAF and -20SNR areas over the period 1968 – 2015. As in the case of South California, the analysis will focus on the properties and variation of the entropic indices with respect to threshold magnitude, (M_{th}) and interevent distance (Δd). The results are summarized in Tables 3.2.2 and 3.2.3 and displayed in Figures 3.21 to 3.32. For the sake of experimental rigour, estimation of the entropic indices is *not* performed for data sets (sub-catalogues) containing *less than* 300 events and results are *not* considered and displayed *unless* associated with a goodness of fit (R^2) *better* than 0.97.

i. Comparative study of the full NCSN and DD catalogues (1984 – 2011)

The results of this exercise are illustrated in Figures 3.21 and 3.22. As can be seen in Fig. 3.21, $q_M(M_{th})$ determinations from both catalogues are very stable and practically identical, varying smoothly from 1.49 at M_{th} = 3 to 1.57 at the M_{th} = 4.3 and exhibiting steady, quasi-linear increase with increasing threshold magnitude. The application of Eq. (18) yields $b_q(M_{th})$ estimates that respectively vary from 1.04 to 0.75. The entropic index q_M, like the b-value to which it is related, represents the scaling of the size distribution of earthquakes and clearly indicates a correlated, scale-free process, possibly associated with a gradual change in the size distribution of active faulting. As can be seen in Table 1, the determinations of $b_q(M_{th})$ are consistent with the corresponding determinations of $b(M_{th})$ which have been computed with conventional (robust least squares) methods and vary in the interval 1.1 to 0.96.

The temporal entropic indices $q_T(M_{th})$ computed from the two catalogues are systematically different by more than 0.1 for $M_{th} \leq 3.3$; this could be explained as an effect of the differences in the information content of the two catalogues which are numerous at the smaller magnitude scales and diminish with increasing earthquake size (see Fig. 3.18). Notably, the unsystematic “surplus” of small magnitude events in the DD catalogue appears to have a *randomizing* effect and renders the two catalogues *incomparable* for M_{th} < 3.5! In general terms, $q_T(M_{th})$ determinations for the NCSN catalogue are rather stable and for the most part vary between 1.2 and 1.3 so as to remain consistently greater than the “randomness threshold” of 1.2. Conversely, for the DD catalogue $q_T(M_{th})$ is not as stable a function: it is consistently lower than 1.2 for M_{th} < 3.4 and fluctuates erratically

between 1.04 and 1.33 for M_{th} > 3.6. This disparity, and more precisely the marked variability of $q_T(M_{th})$-DD, is interpreted in terms of information disruption in the DD catalogue brought on by the relocation/re-compilation procedure. This said, it should also be pointed out that both catalogues generally yield 1.1 < q_T < 1.3 and discrepancies average to 0.07, so that $\bar{q}_T$ *-NCSN* = 1.26 $\pm$ 0.04 and $\bar{q}_T$ *-DD* = 1.18 $\pm$ 0.09 (Table 1). From this point of view the results can be deemed reasonably compatible, with NCSN providing evidence of marginally correlated and DD evidence of marginally uncorrelated seismogenetic processes.

The variation of entropic indices with interevent distance is shown in Fig. 3.22. As before, the magnitude entropic indices $q_M(\Delta d)$ obtained from both catalogues are absolutely comparable with $\bar{q}_M$ *-NCSN* = 1.5 $\pm$ 0.013 and $\bar{q}_M$ *-DD* = 1.49 $\pm$ 0.016 (Table 3.2.3). The temporal entropic distances $q_T(\Delta d)$ are also very comparable for all interevent distances: for Δd up to 0-50km, $q_T(\Delta d)$ is estimated at 1.57 for the NCSN and 1.47 for the DD: these values indicate high correlation due to the overwhelming effect of near field interactions which are dominated by aftershock sequences. Conversely, for interevent distances longer than 100km, $q_T(\Delta d)$ drops to under 1.3 and fluctuates between 1.1 and 1.27 for Δd up to 350km, with mean values of 1.22 $\pm$ 0.05 for q_T*-NCSN* and 1.20 $\pm$ 0.63 for q_T*-DD*. It is rather remarkable that in spite of the differences in their information content, the behaviour of q_T with interevent distance is rather similar in *both* catalogues: this is interpreted to indicate a present albeit weak long-range effect underlying the temporal expression of earthquake occurrence which, in turn, is taken to imply non-Poissonian dynamics.

Overall, the analysis of the temporal entropic indices points toward a weakly correlated seismogenetic system verging on the limit of randomness, at least during the period 1984-2011. Moreover, a) because the results obtained from the NCSN and DD catalogues are “reasonably compatible” and, b) because of our documented concern as to the consistency of the DD catalogue and its possibly destabilizing effect, I shall focus the rest of our work on the analysis of the NCSN catalogue which not only spans a considerably longer period (47 years between 1968 and 2015), but also appears to exhibit higher internal consistency in comparison to the DD catalogue.

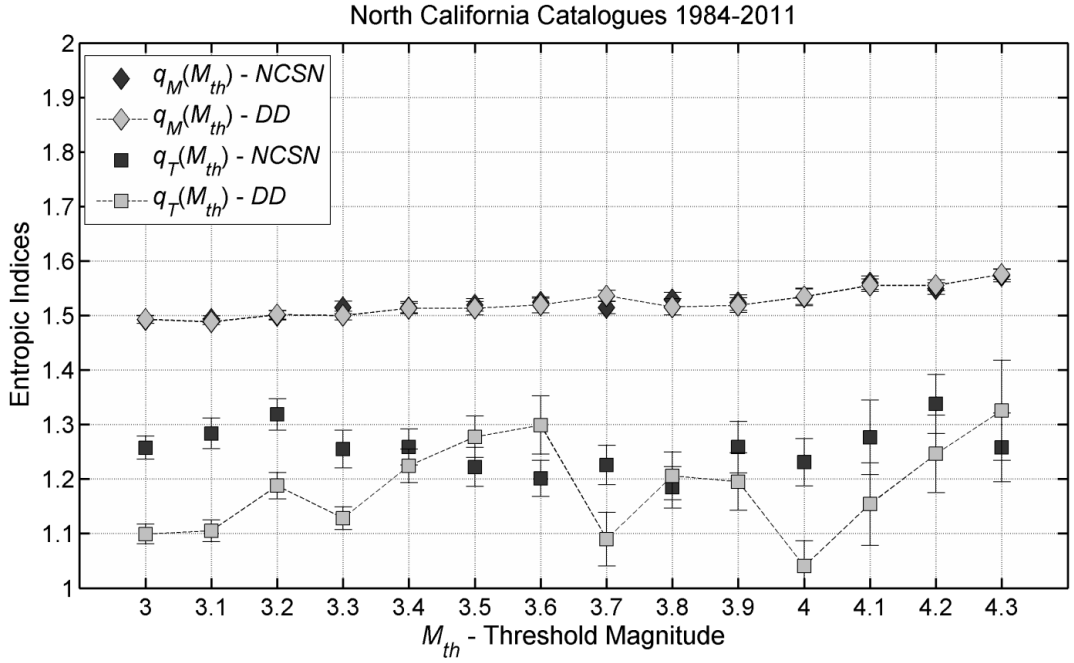

Figure 3.21 Comparative analysis of the full NCSN and DD catalogues for the dependence of entropic indices on threshold magnitude (M_{th}). Dark grey symbols represent estimates based on the NCSN catalogue and light grey symbols estimates based on the DD catalogue. Error bars represent 95% confidence intervals. Comparisons are made for the period 1984-2011.

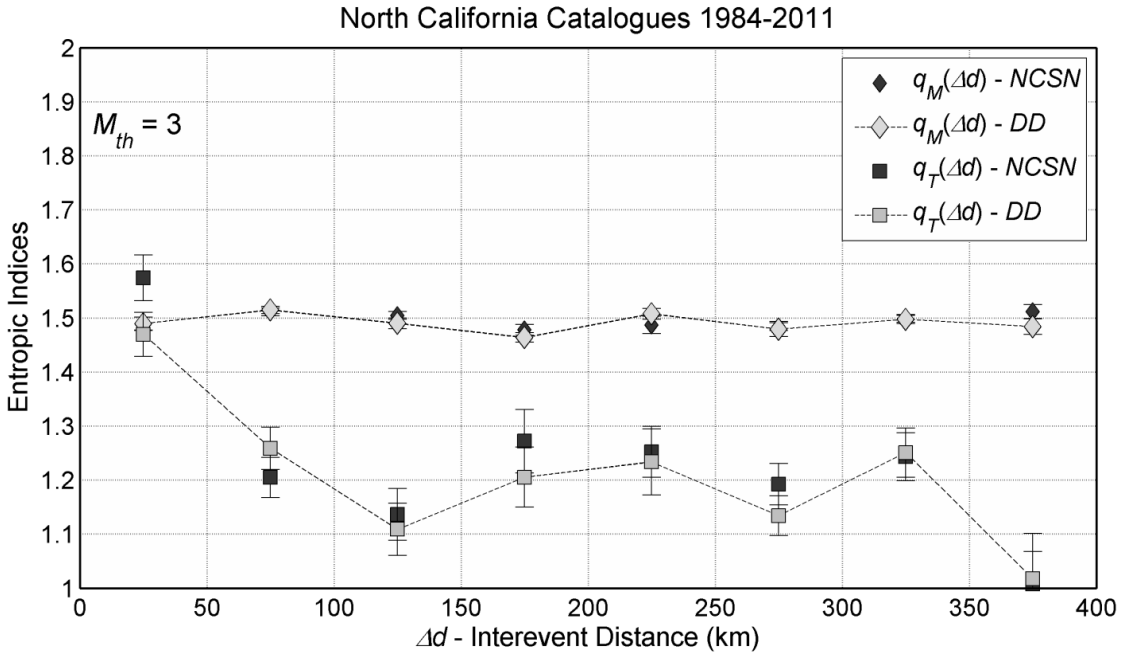

Figure 3.22 Comparative analysis of the full NCSN and DD cataloguesfor the dependence of entropic indices on interevent distance (Δd). Earthquakes are binned according to Eq. (2.19) so that each bin spans a constant 50km; symbols are plotted at the midpoint of each bin. Dark grey symbols represent estimates based on the NCSN catalogue and light grey symbols estimates based on the DD catalogue. Error bars represent 95% confidence intervals. Comparisons are made for the period 1984-2011.

ii. Analysis of Full NCSN earthquake catalogue for 1968 – 2015

The analysis of the full NCSN catalogue returns stable determinations of $q_M(M_{th})$ which vary from 1.49 to 1.56 (Fig. 3.23a) and yield b_q in the interval (1.04, 0.79), with larger the q_M (lower b_q) observed at the larger magnitude scales. As can also be seen in Fig. 3.23b, $q_M(\Delta d)$ determinations are stable in the interval (1.47, 1.53), respectively yielding b_q in the interval (1.12, 0.88). The temporal entropic indices hold a surprise: $q_T(M_{th})$ is rather consistently determined and found to vary between 1.24 and 1.42 indicating *moderate to high correlation* (Fig. 3.23a). Moreover, as evident in Fig. Fig. 3.23b, $q_T(\Delta d)$ exhibits a rather *inconsistent* variation from relatively high correlation (1.58) at short interevent distances (Δd < 100km), which is expected due to the effect of near field interaction, to *moderate correlation* (1.21 – 1.35) at intermediate interevent distances (100≤Δd < 400km) while for Δd > 400km, $q_T(\Delta d)$ rises up to 1.57 indicating high correlation at longer interevent distances.

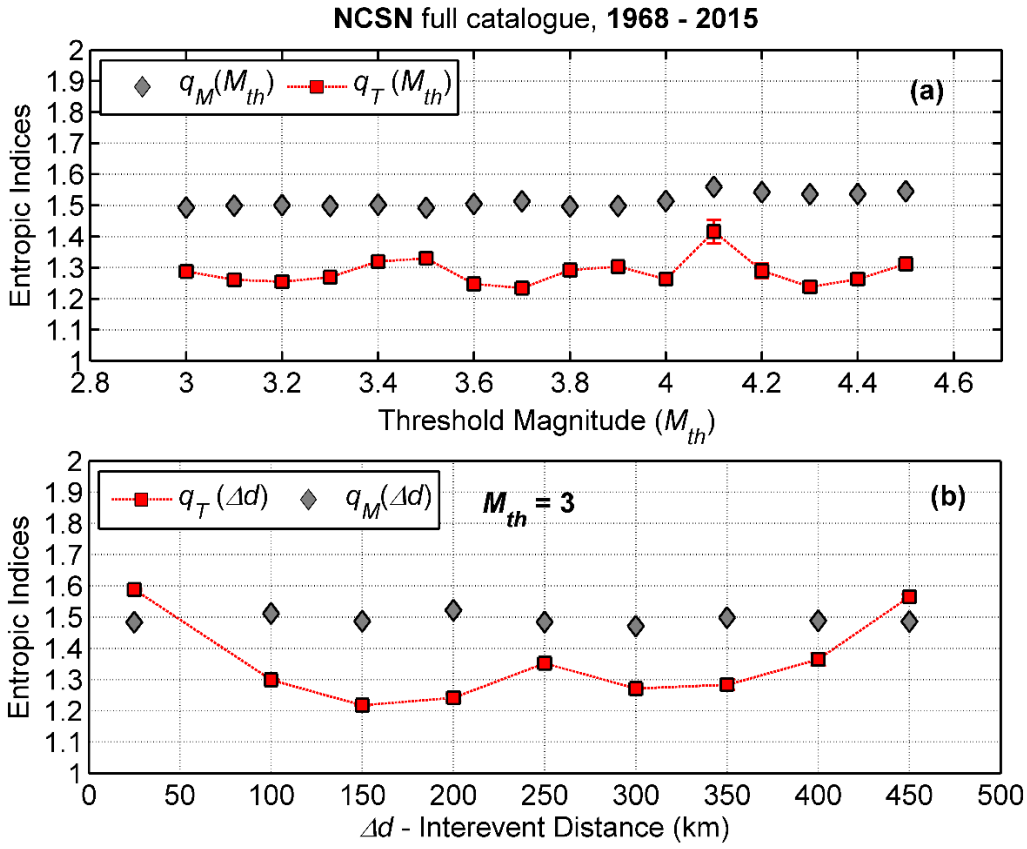

Figure 3.23 Analysis of the full NCSN catalogue for the 47-year period 1968 – 2015. **(a)** Dependence of entropic indices on threshold magnitude (M_{th}). **(b)** Dependence of entropic indices on interevent distance (Δd); earthquakes are groupped in bins of 50km and symbols are plotted at the midpoint of each bin. In all cases error bars represent 95% confidence intervals.

The “surprise” is that the temporal entropic indices estimated for the period 1968 – 2015 are generally *higher* than those estimated for the period 1984 – 2011, with particular reference to their variation with respect to interevent distance. Evidently, the differences result from the inclusion (exclusion) of earthquakes observed during the interval 1968 – 1984. This, in turn, indicates that earthquakes prior to mid to late 80’s occurred in a (long-range) correlated seismogenetic system and that this correlation was, somehow, relaxed in the years thereafter. Thus, and because correlation implies SOC dynamics, the question reduces to whether it is possible for the seismogenetic system to have switched from the more organized (non-equilibrating) state indicated by Fig. 3.23 to the less organized state indicated by Figs. 3.21 and 3.22. A probable single “turning” point for such a transition to have taken place may have been the M7 Loma Prieta earthquake of 17/10/1989. In order to test this hypothesis, two full NCSN sub-catalogues are analyzed, the first of which comprises 8289 events and extends from 1968 to 31/12/1988, prior to the Loma Prieta event, and the second of which comprises 4677 events and extends from 1/1/1990, almost 2½ months after the event, to 31/12/2015. The results of this experiment are summarized in Tables 3.2.2 and 3.2.3, illustrated in Fig. 3.24 and discussed below.

To begin with, the determination of the magnitude entropic index is *absolutely consistent* between the two periods, so much with respect to threshold magnitude, as with respect to interevent distance: For the period 1968–1988 $q_M(M_{th})$ varies between 1.49 and 1.51 and $q_M(\Delta d)$ between 1.47 and 1.54, while for 1990–2015 $q_M(M_{th})$ varies between 1.48 and 1.5 and $q_M(\Delta d)$ between 1.47 and 1.52. On the other hand, the temporal entropic indices exhibit markedly different behaviour between the two periods. During the interval 1968-1988 $q_T(M_{th})$ fluctuates between 1.30 and 1.45, indicating moderate overall correlation (Fig. 3.24a), while $q_T(\Delta d)$ is generally larger than 1.38 and exhibits a persistent upward trend for Δd > 200km, thereby indicating *increasingly higher* correlation at longer interevent distances so that $q_T(\Delta d) > 1.6$ at Δd > 300km (Fig. 3.24b).

Conversely, in the period 1990-2015 $q_T(M_{th})$ decreases gradually from just above **1.2** at M_{th} = 3.4-3.5 to only **1.09** at M_{th} = 4, indicating very weak overall correlation and near randomness at the larger magnitude thresholds (Fig. 3.24c). Moreover, $q_T(\Delta d)$ is higher than 1.45 at Δd < 100km and indicates high correlation at short interevent distances due to the effect of near-field interactions and aftershock sequences (Fig. 3.24d); nevertheless, it drops to approx. 1.12 for 100km < Δd < 200km (randomness) and gradually rises to 1.3 at Δd greater than 200km indicating weak to moderate correlation.

The results presented above seem to support the hypothesis that the Loma Prieta event has been a “turning point” in the evolution of North Californian seismicity. Before this earthquake, the regional seismogenetic system appears to have been characterized by a highly organized state involving long range interactions (stress-stress correlations), whereas after the event the level of organization appears to have dropped significantly, with some elements (e.g. larger faults subsystem, intermediate range interactions) having transited to an almost completely disorganized (random) state. It is also noteworthy that long-range correlation, albeit weakened, appears to have persisted even in the disorganized post Loma Prieta era, as attested to by the increasing trend of $q_T(\Delta d)$ at long interevent distances (ranges): this is an effect characteristic of SOC dynamics.

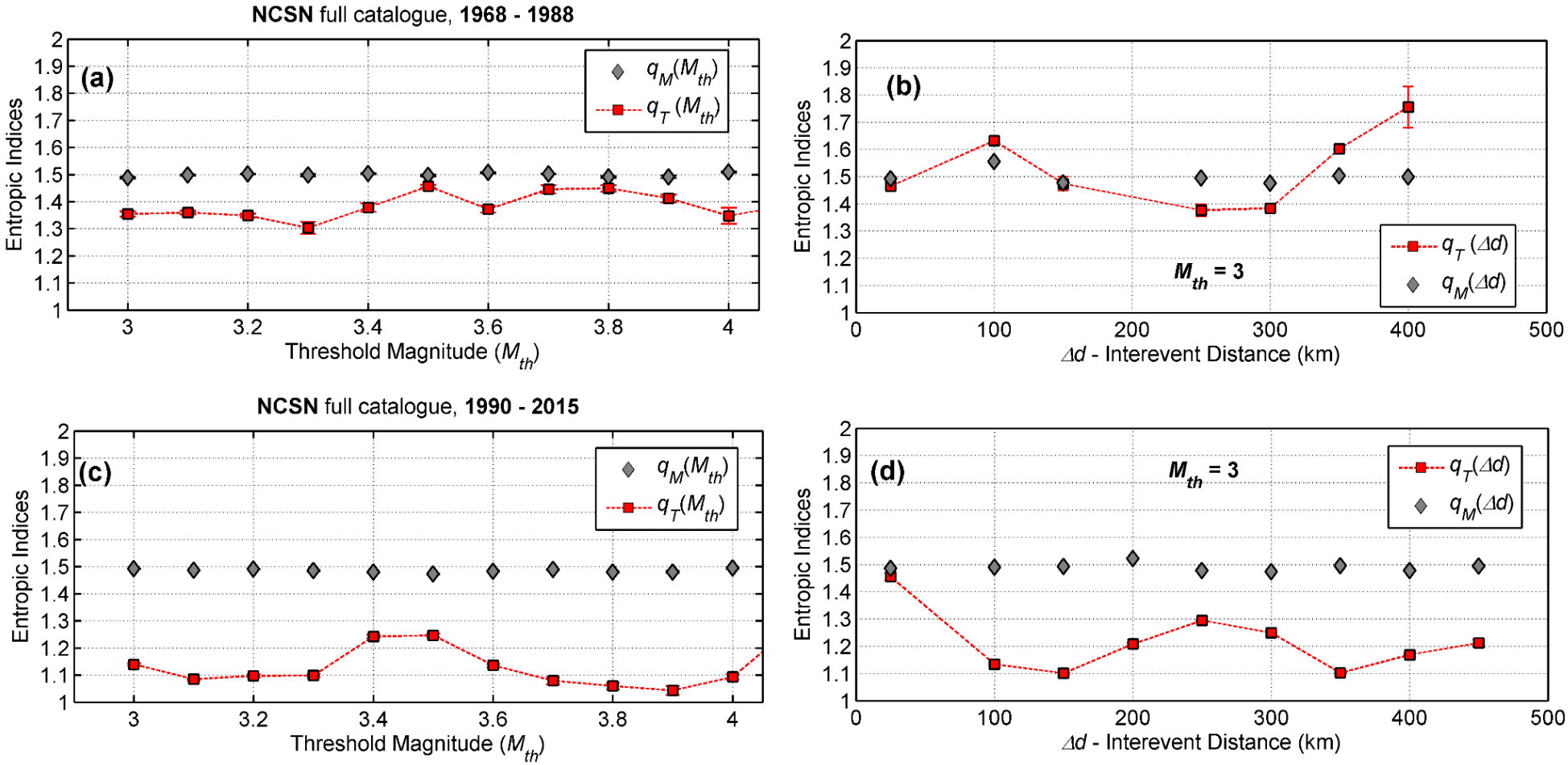

Figure 3.24 Analysis of the full NCSN catalogue for the periods 1968 – 1988 (top row) and 1990-2015 (bottom row). Panels **(a)** and **(c)** illustrate the dependence of the entropic indices on threshold magnitude (M_{th}). Panels **(b)** and **(d)** illustrate the dependence of the entropic indices on interevent distance (Δd), where earthquakes with groupped in bins of breadth Δd = 50km and symbols are plotted at the midpoint of each bin. Error bars represent 95% confidence intervals

iii.The north segment of San Andreas Fault and Sierra Nevada Range (1968-2015)

The next step in is to compare the geographically distinct clustering of seismicity along the San Andreas Fault (nSAF) and the Sierra Nevada Range/ Walker Lane belt (SNR). To this effect, I first analyse two subsets of the full NCSN catalogue corresponding to the nSAF and SNR areas, separated as shown in Fig. 3.15.

Let us, first, consider the results from the analysis of the nSAF sub-catalogue (Fig. 3.25). As can be seen in Fig. 3.25a, the magnitude entropic index $q_M(M_{th})$ exhibits a persistent linear trend from 1.47 at M_{th} = 3 to 1.58 at M_{th} =4.2, with $b_q(M_{th})$ respectively varying from 1.12 to 0.72: If taken at face value, this result would signify gradual change in the scaling of the San Andreas fault system as a function of fault size! The temporal entropic index $q_T(M_{th})$ is invariably larger than 1.15 and fluctuates around a mean value of 1.25 indicating low to moderate correlation. When earthquakes are grouped by interevent distance, $q_M(\Delta d)$ fluctuates slightly around a mean value of 1.5 (Fig. 3.25b). Conversely, the temporal entropic index $q_T(\Delta d)$ exhibits variability, being significant (> 1.6) for Δd up to 100 km (near-field effect), rapidly decaying to 1.15 – 1.26 for Δd between 100 and 350 km and, finally, increasing to 1.42 for Δd > 300 km.

Turning to the results from the SNR sub-catalogue (Fig. 3.25c and 3.25d), it is interesting to note that $q_M(M_{th})$ appears to exhibit a (very) low-rate linear trend towards higher values with increasing threshold magnitude, conceivably indicating corresponding changes in the scaling of the SNR fault system (Fig. 3.25c). As it appears that long interevent distances are very rare in the SNR system, the analysis is limited to no more than Δd = 300km (Fig. 3.25d); as can clearly be seen, $q_M(\Delta d)$ is stable around a mean value of 1.52 ($b_q(\Delta d)$ ~ 0.92). On the other hand, results for the temporal entropic index hold a surprise: as can be seen in Fig. 3.25c, $q_T(M_{th})$ varies from 1.41 at M_{th} = 3 to 1.51 at M_{th} = 4.2, exhibiting a clear quasi-linear tendency to increase with respect to threshold magnitude, which would be interpreted to signify a corresponding *increase* in the interdependence of earthquake occurrence (correlation) with magnitude and at least up to M = 4.2. Finally, with respect to interevent distances q_T shows moderate to high correlation (1.31-1.52) for all interevent distances up to 300km.

In taking the inquiry one step forward, I examine whether the “turning point” defined by the 1989 Loma Prieta earthquake has affected the nSAF and SNR sub-systems in (dis)similar ways. As per NCSN, the full nSAF and SNR sub-catalogues are analysed separately for the periods 1968-1988 and 1990-2015, that is prior to and after the event.

Prior to 1998, the full nSAF sub-catalogue contains 5738 events and the full SNR sub-catalogue 2615 events while after 1990, the corresponding numbers are 2549 and 2465 respectively. It straightforward to see, and certainly significant and worthy of further scrutiny, that during the first 20-year long period the full nSAF sub-catalogue contains almost double the number of events with respect to the second 25-year long period, meaning that there are significant differences in seismicity rates. Conversely, the corresponding numbers in the full SNR sub-catalogue are practically the same (constant seismicity rates?).

Results for the nSAF sub-catalogue are shown in Fig 3.26. As evident in Fig 3.26, for 1968 – 1988, $q_M(M_{th})$ exhibits a low-rate linear trend from 1.48 at M_{th} = 3 to 1.56 at M_{th} = 4.1; the trend is not apparent in the period 1990 – 2015, where $q_M(M_{th})$ appears to have stabilized just below the value of 1.5, so that at $b_q(M_{th}) > 1.1$ (Fig. 3.26c). Note, however, that because the number of earthquakes available for analysis at $M_{th} > 3.7$ is insufficient, it is not certain whether the "trend" has altogether ceased to exist, or it is simply unobservable. The estimation of magnitude entropic indices with respect to interevent distance is also hampered by the overall insufficient number of events at $\Delta d > 150$ km. Observations are necessarily limited to near and intermediate range interaction, where one may observe that $q_M(\Delta d)$ is rather stably determined for both periods, slightly fluctuating about 1.5 (Fig. 3,26b and 3.26d).

The temporal entropic index exhibits completely different behaviour between the two periods. For 1968 – 1988, $q_T(M_{th})$ displays an upward linear trend, changing from 1.4 at M_{th}=3 to higher than 1.6 at M_{th} = 4.1 and exhibiting high correlation, particularly at larger threshold magnitudes (Fig. 3.26a). Significant correlation is also observed in Fig. 3.26b, where $q_T(\Delta d)$ varies from 1.58 to 1.55 for Δd < 100km and consistently *increases* from 1.32 at Δd between 150-300km, to 1.66 at Δd between 300-450km, indicating high to very high correlation all ranges, with particular reference to long interevent distances (Fig. 3.26b).

For 1990 – 2015 completely different properties are observed: In Fig. 3.26c $q_T(M_{th})$ is generally lower than 1.1 and $\max[q_T(M_{th})] < 1.14$: this indicates general absence of significant correlation and a nearly random seismogenetic system. In Fig. 3.26d, $q_T(\Delta d)$ is *under* 1.2 throughout the catalogue, indicating very weak to no correlation at short and at long ranges.

Results for the full SNR sub-catalogue are presented in Fig. 3.27 and hold their own surprises. As can be seen in Fig. 3.27a, for the period 1968 – 1988, $q_M(M_{th})$ is very consistently determined at approx. 1.55 for all threshold magnitudes, yielding a correspondingly consistent $b_q(M_{th})$ of approx. 0.82. For the 1990 – 2015, and save for the last two threshold magnitudes, $q_M(M_{th})$ is also consistently determined but with values just below, or approximately equal to 1.5 so that $b_q \approx 1$ (Fig. 3.27c). Although it is not easy to make safe inferences, this might signify a change in the scaling of the active tectonic grain.

Turning to the analysis of the temporal entropic index, it is interesting to note that for the period 1968 – 1988, $q_T(M_{th})$ varies from 1.4 at M_{th} = 3.2 to 1.63 at M_{th} = 3.8 while decreases to 1.54 at M_{th} = 4, indicating significant to high correlation (Fig. 3.27a). Moreover, it exhibits an upward linear trend analogous to that observed in Fig. 3.26a for the corresponding analysis of the nSAF sub-catalogue. For the period 1990 – 2015, $q_T(M_{th})$ is consistently *higher* than 1.35 but is *no longer* increasing with threshold magnitude (Fig. 3.27c). Analogous observations can be made with respect to interevent distances. For the first period $q_T(\Delta d)$ exhibits persistent and strong increase from 1.49 at Δd < 100km to 1.72 at Δd > 150km, indicating *increasingly* strong correlation at intermediate and long ranges (Fig. 3.27b). For the second period (1990 – 2015) $q_T(\Delta d)$ varies from 1.73 at Δd < 50km to 1.75 at Δd > 300km indicating *persistently high* correlation at *all* ranges which, however, is *no longer* increasing with interevent distance (Fig. 3.27d). Overall, it appears that although something has changed, the SNR fault system remained highly correlated both prior to and after the Loma Prieta event and, more significantly, it is statistically *different* from the nSAF system.

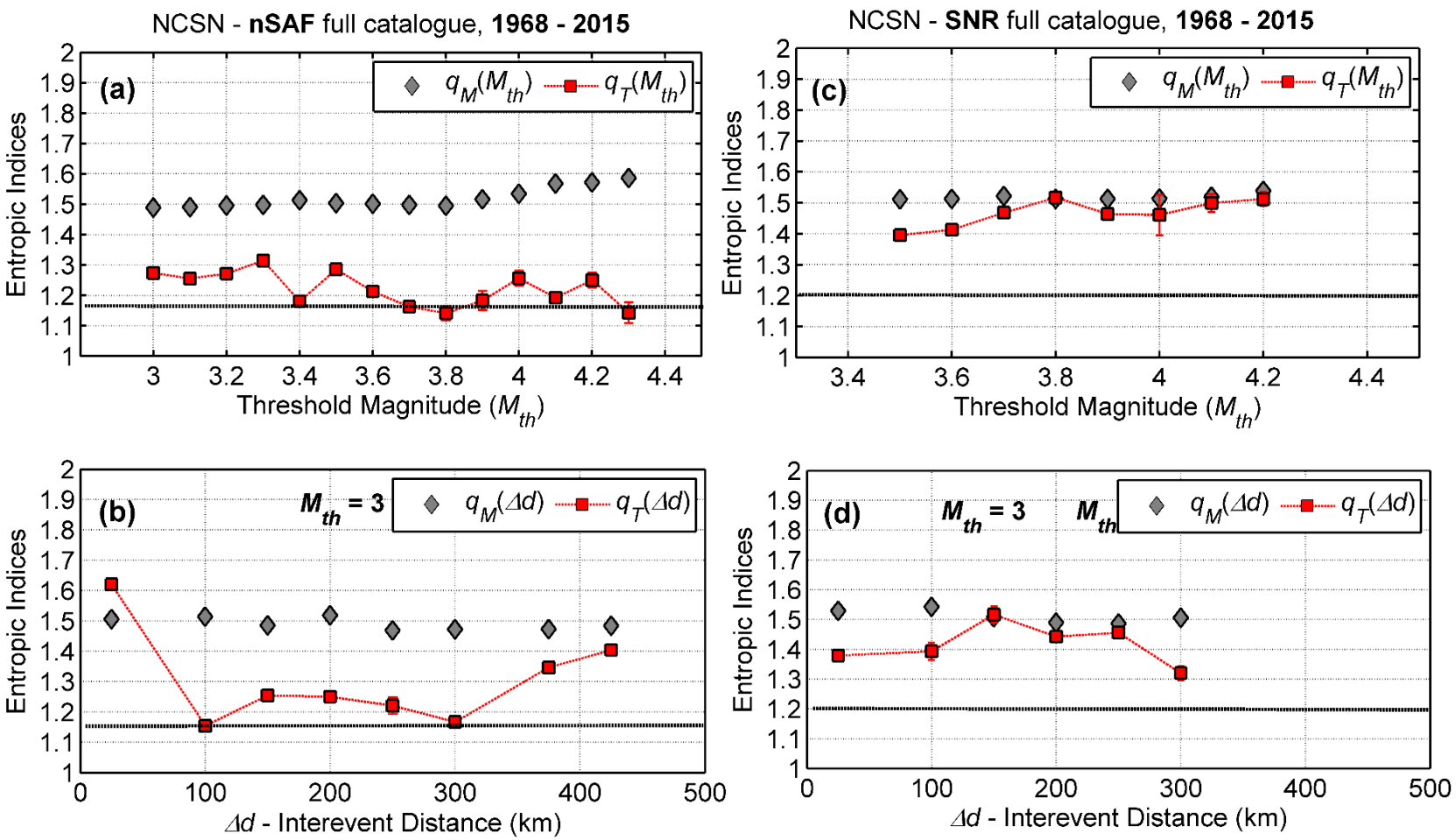

Figure 3.25 Analysis of the full nSAF catalogue (left column) and SNR catalogue (right column) for the 47-year period 1968-2015. Panels **(a)** and **(b)** illustrate the dependence of the entropic indices on threshold magnitude (M_{th}). Panels **(c)** and **(d)** illustrate the dependence on interevent distance (Δd); the horizontal double arrows indicate the breadth of interevent distance bins and symbols are plotted at the midpoint of each bin. Error bars represent 95% confidence intervals.

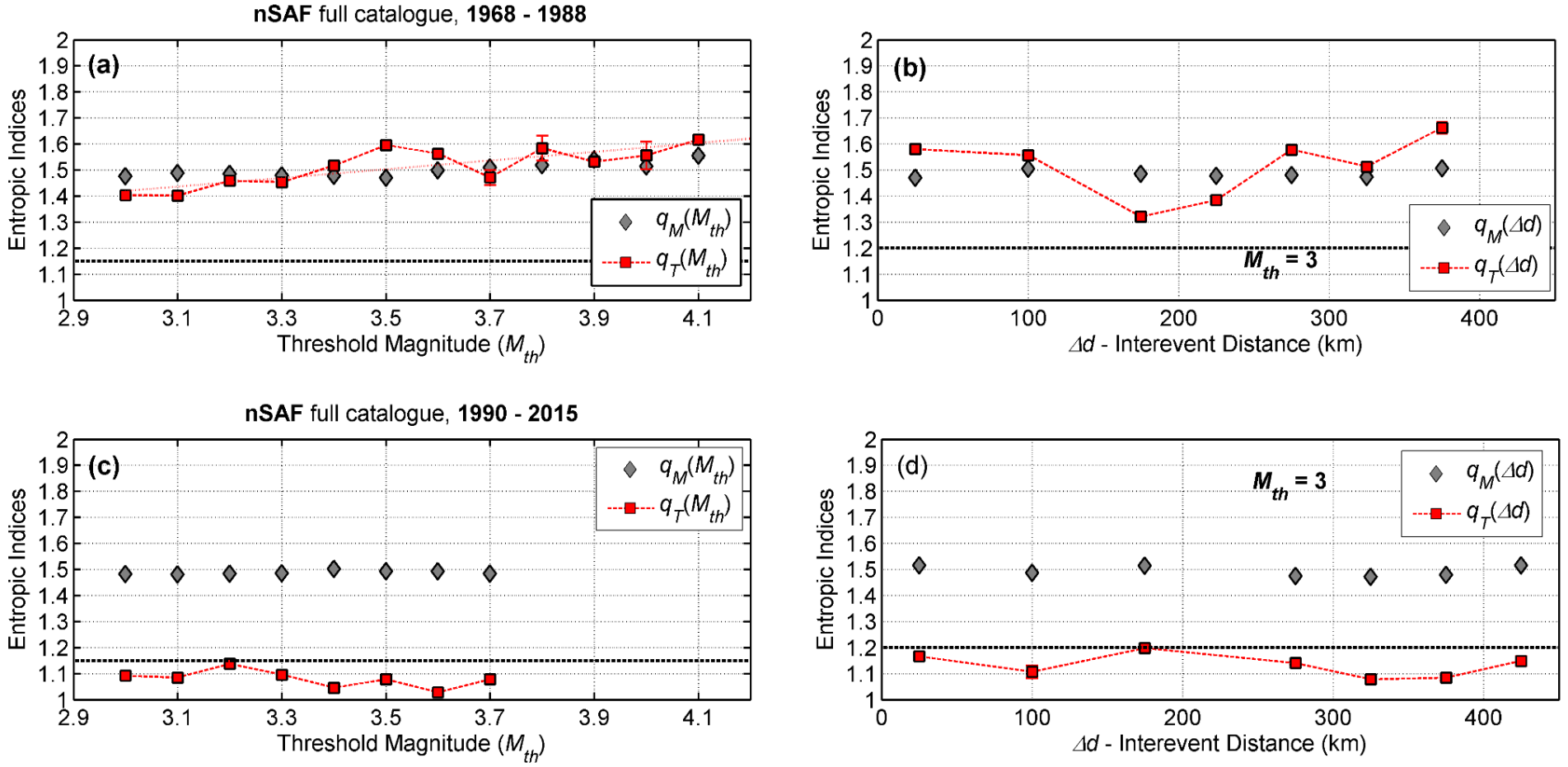

Figure 3.26 Analysis of the full nSAF catalogue for the periods 1968 – 1988 (top row) and 1990-2015 (bottom row). Panels **(a)** and **(c)** illustrate the dependence of the entropic indices on threshold magnitude (M_{th}). Panels **(b)** and **(d)** illustrate the dependence of the entropic indices on interevent distance (Δd); the horizontal double arrows indicate the breadth of interevent distance bins and symbols are plotted at the midpoint of each bin. Error bars represent 95% confidence intervals.

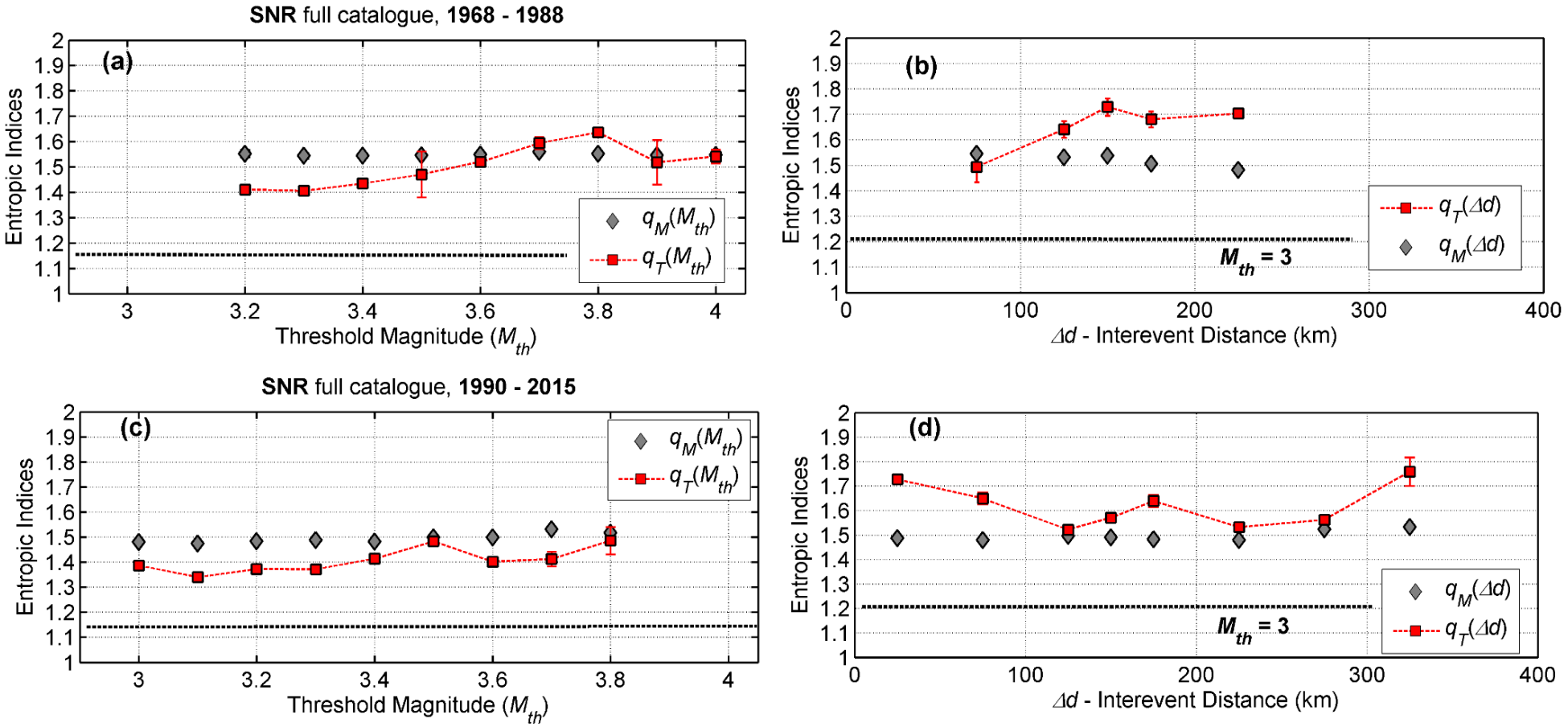

Figure 3.27 Analysis of the full SNR catalogue for the periods 1968 – 1988 (top row) and 1990-2015 (bottom row). Panels **(a)** and **(c)** illustrate the dependence of the entropic indices on threshold magnitude (M_{th}). Panels **(b)** and **(d)** illustrate the dependence of the entropic indices on interevent distance (Δd), where earthquakes with groupped in bins of breadth Δd = 50km and symbols are plotted at the midpoint of each bin. Error bars represent 95% confidence intervals.

iv.Analysis of North California Declustered Earthquake Catalogues 1968-2015

As has already been discussed, a primary objective of our study is to investigate whether background seismicity is generated by non-Poissonian dynamic processes. Accordingly, I shall now proceed to examine reduced versions of the NCSN, nSAF and SNR catalogues, in which aftershock sequences have been identified and removed by the stochastic declustering method of Zhuang et al (2002) at the $\phi_j(\geq 0.7)$, $\phi_j(\geq 0.8)$ and $\phi_j(\geq 0.9)$ probability levels (i.e. probability greater or equal to 70%, 80% and 90% for an event to belong to the background). The analysis of entropic indices is illustrated for the periods 1968-2015 where the catalogues were declustered at M_{th}=3.2. These results are compared to the results for the period 1968-2011 where the catalogues were declustered at M_{th}=3.0. As can be seen in Figs. 3.27 and 3.28 the results are almost identical. It is also important to note that with respect to interevent distance will be limited to the NCSN catalogue and only to the case $\phi_j(\geq 0.7)$. In all other realizations of the declustered catalogues, the analysis will focus on the study of $q_M(M_{th})$ and $q_T(M_{th})$ because the overall small populations of events at interevent distances longer than 50km may not warrant the statistical significance of $q_M(\Delta d)$ and $q_T(\Delta d)$.

Fig. 3.27 illustrates the results obtained from the NCSN catalogue, declustered at the ϕ_j (≥ 0.7) or 70% probability level. Specifically, Fig. 3.27a shows the variation of the entropic indices with threshold magnitude and Fig. 3.27b the analogous variation with interevent distance. It should be noted that for $\Delta d >$ 50km, the entropic indices had to be determined in variable-width Δd-bins so as to ensure their statistical significance. It is immediately apparent that $q_M(M_{th})$ changes smoothly from 1.51 to 1.55 and exhibits the familiar tendency to increase with threshold magnitude (Fig. 3.27a). However, $q_M(\Delta d)$ exhibits a peculiar albeit smooth oscillation with increasing interevent distance, which I will not endeavour to explain in physical terms (e.g. fault scaling) for lack of sufficient evidence. Next, it is interesting to note that with only one exception at M_{th} = 3.7, $q_T((M_{th})$ is consistently determined at values greater than 1.4, so that $\bar{q}_T(M_{th})$ = 1.45 $\pm$ 0.06; this is definitely higher than the corresponding value obtained for the full NCSN catalogue (1.33 $\pm$ 0.033). Given that for the most part aftershocks have been eliminated at the 70% probability level, this increase may be taken to indicate an overall correlated seismogenetic background. Analogous observations can be made on the behaviour of $q_T(\Delta d)$. Thus, for $\Delta d \leq$ 50km, q_T is 1.86, which is higher than the corresponding determination of the full NCSN catalogue by approx. 0.3. It is therefore conceivable that

this increase signifies the existence of strong short-range (near field) correlation in background seismicity. Likewise, for $\Delta d \geq 250$km q_T averages to 1.61 for the period 1968-2011 and to 1.48 which is higher by approximately 0.26 in comparison to the corresponding determination for the full NCSN catalogue. It is again conceivable that this increase signifies the existence of rather strong long-range (far field) correlation in the background.

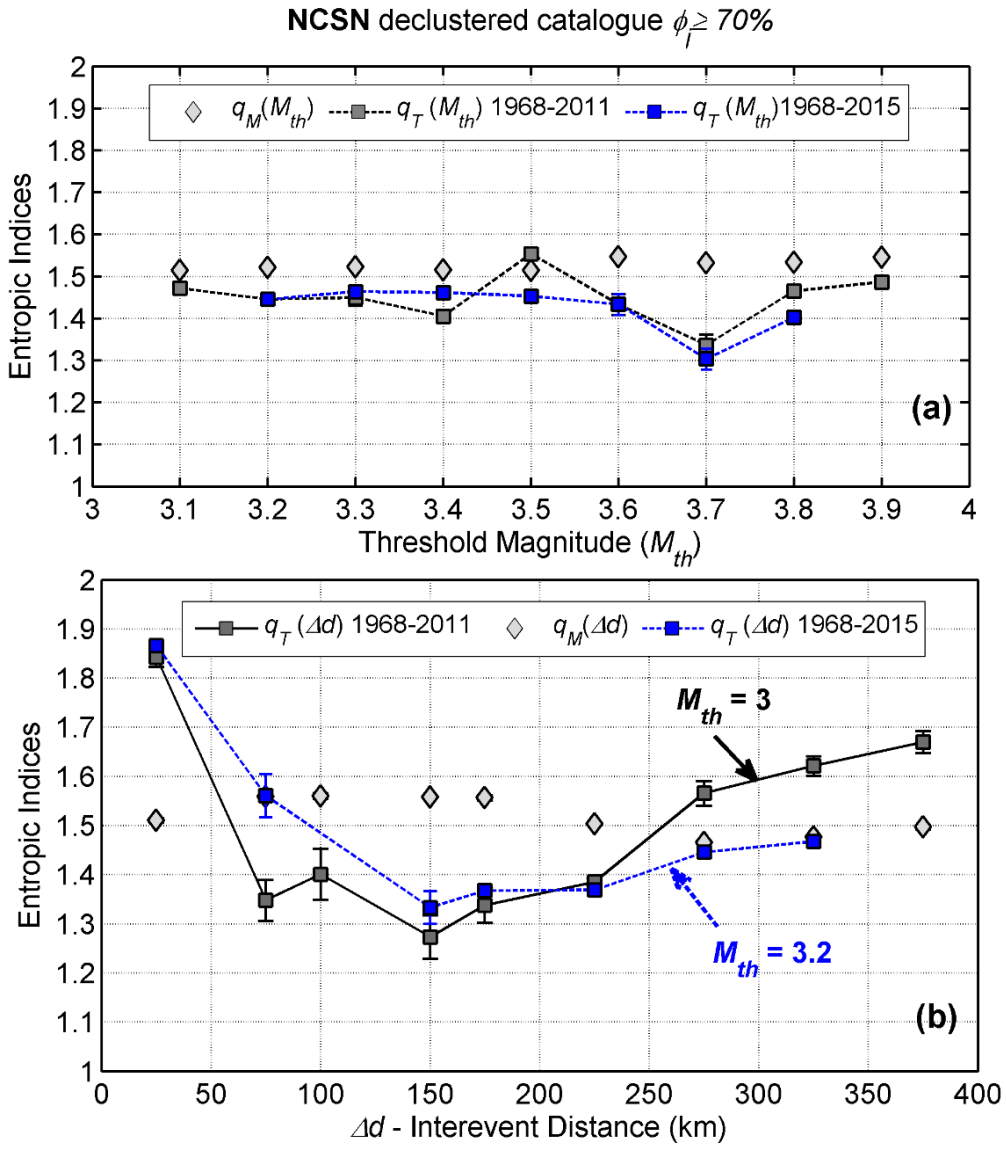

Figure 3.28 Analysis of declustered ($\phi \geq 70\%$) NCSN catalogue for the 47-year period 1968 – 2015. **(a)** Dependence of entropic indices on threshold magnitude (M_{th}). **(b)** Dependence of entropic indices on interevent distance (Δd); the horizontal double arrows indicate the breadth of interevent distance bins and symbols are plotted at the midpoint of each bin. Error bars represent 95% confidence intervals thoughout.

Let us, now, examine the nSAF and SNR catalogues declustered at the $\phi_j(\geq 0.7)$ level, for which results are shown in Fig 3.28a (nSAF) and Fig. 3.286b (SNR). It is apparent that $q_M(M_{th})$ determinations are very stable for both catalogues and exhibit minimal variation, so that for the declustered nSAF catalogue $\bar{q}_M(M_{th})$ = 1.51 $\pm$ 0.014 (b_q = 0.96) and for the SNR catalogue $\bar{q}_M(M_{th})$ = 1.54 $\pm$0.007 (b_q = 0.81): the two mean entropic indices stand apart of each other by more than two standard errors, which may indicate different scaling of earthquake (fault) sizes in the two areas. More interesting observations can be made in regard to the temporal entropic index. For the nSAF catalogue q_T varies between 1.41 and 1.60 with an average of 1.48 (for both declustering results), while for SNR q_T varies between 1.73 and 1.83 with an average of 1.78 when the catalogue is declustered at Mth=3, while q_T is slightly lower varying from 1.57 to 1.80 when the catalogue is declustered at Mth=3.2 (blue line). In spite of this difference, such values indicate that background processes at the respective seismogenetic systems are highly and very highly correlated and, more significantly, at levels higher than those estimated from the combined (NCSN) catalogue.

The hitherto analysis of the declustered catalogues yields temporal entropic indices which indicate correlation invariably higher than that inferred from the full catalogues, therefore strongly non-Poissonian background seismogenetic processes. Still, as already noted in CHAPTER 2, at the 70% probability level the declustered catalogues contain a certainly non-trivial number of leftover aftershocks. Accordingly, it is essential to show that the results obtained at this level hold, or even improve at higher probability thresholds.

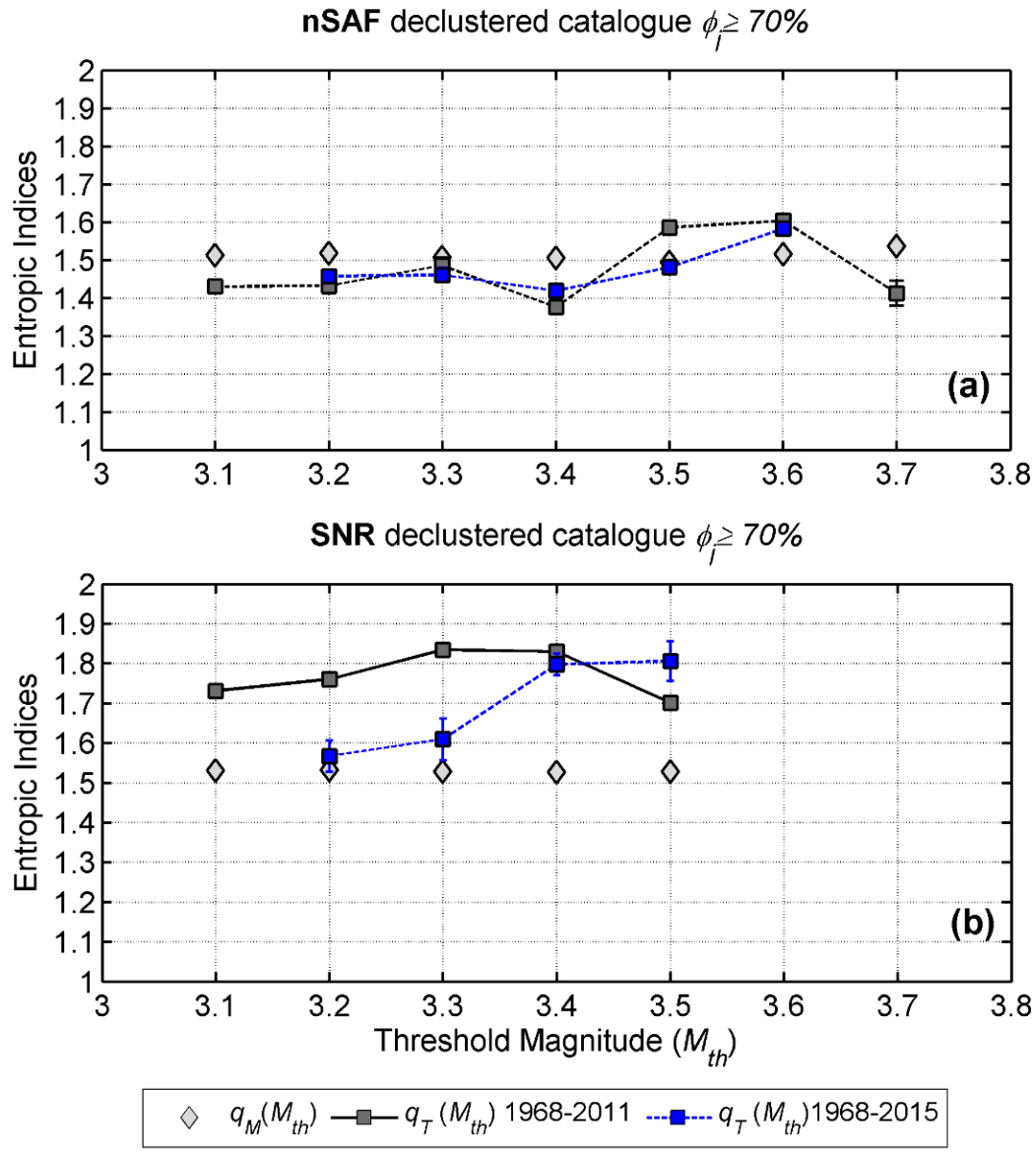

Figure 3.29 Dependence of entropic indices on threshold magnitude (M_{th}) over the 47-year period 1968 – 2015 for **(a)** the declustered ($\phi \geq 70\%$) nSAF catalogue and, **(b)** the declustered SNR catalogue. Error bars represent 95% confidence intervals.

The analysis of the NCSN and nSAF catalogues declustered at probability levels $\phi_j \geq 80\%$ and $\phi_j \geq 90\%$ to be background, as well as of the SNR catalogue declustered at probability $\phi_j \geq 80\%$ to be background, is summarized in Table 3.2.2. The nSAF catalogue declustered at at $\phi_j \geq 90\%$ contains only 370 events, while the SNR contains only 214 events thus they may not be reliably evaluated. In addition, the variations of $\bar{q}_M(M_{th})$ and $\bar{q}_T(M_{th})$ for the full and declustered NCSN, nSAF and SNR catalogues at different probabilities are shown in Fig. 3.29a and 3.29b respectively, with values corresponding to the full catalogues nominally plotted at the abscissa ϕ_j = 0.

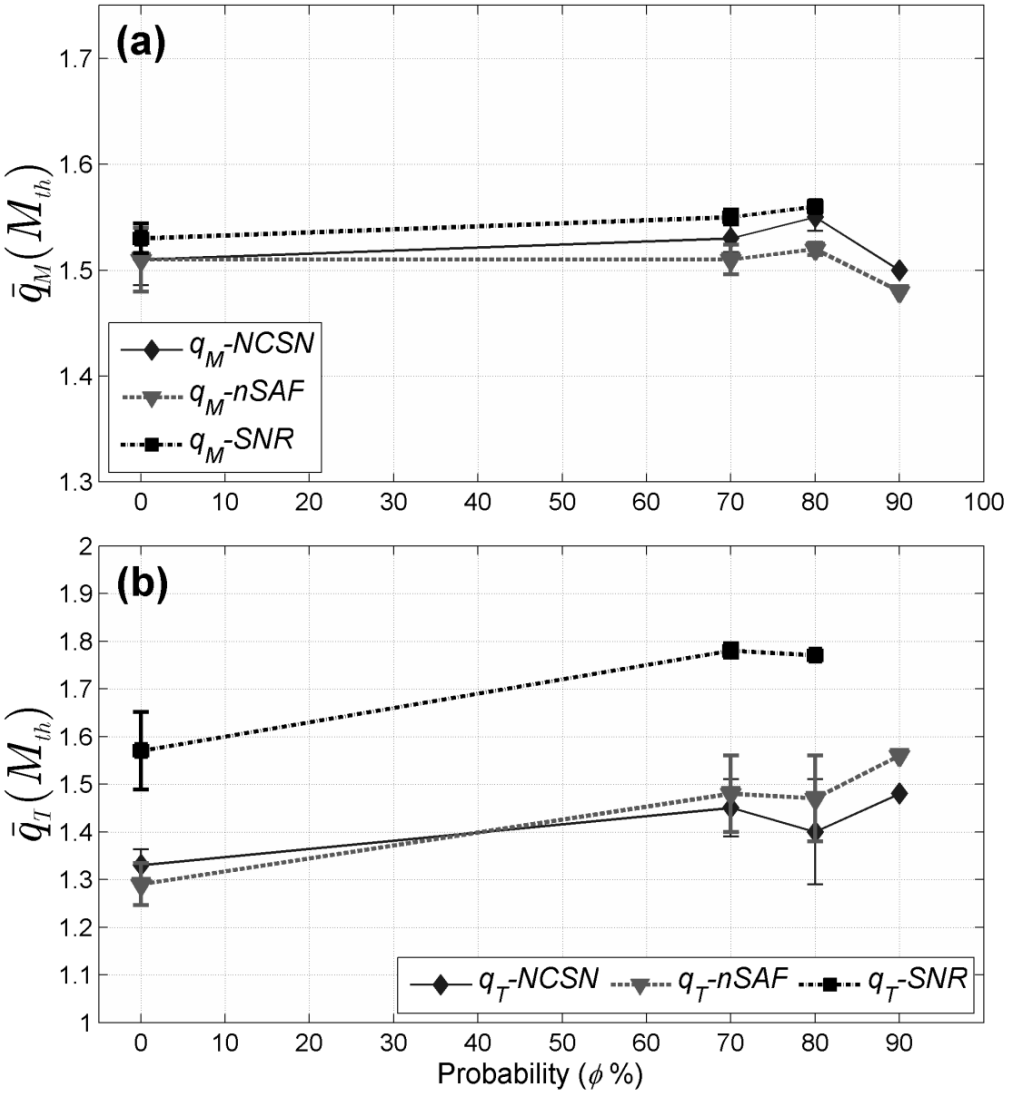

Figure 3.30 Variation of **(a)** the mean magnitude entropic index and **(b)** the mean temporal entropic index for the full and declustered (at different probability levels) NCSN, nSAF and SNR catalogues. Values corresponding to the full catalogues are nominally plotted at the abscissa ϕ_j = 0 (zero probability level).

Inspection of Table 3.2.2 and Fig. 3.29a shows that $\bar{q}_M(M_{th})$ exhibit very little variation with increasing probability. However, it is also interesting to note that results are distinctly different for the nSAF and SNR areas, possibly reflecting differences in the scaling of the respective active fault systems, with their combination (NCSN) comfortably plotting in between! Conversely, inspection of Table 3.2.2 and Fig. 3.29b clearly shows that $q_T(M_{th})$ and $\bar{q}_T(M_{th})$ in particular, exhibit *clear* increase with increasing probability to be background, with the nSAF and SNR areas being *significantly* different. Thus, $\bar{q}_T$-nSAF changes from 1.29 for full catalogue to 1.56 for the version declustered at the 90% probability level, while $\bar{q}_T$-SNR changes from 1.57 for the full catalogue to 1.77 for the version declustered at the 80% probability level. Their combination, reflected in the variation of $\bar{q}_T$-NCSN, changes from 1.33 for the full catalogue to 1.48 for the realization declustered at the 90% level and exhibits more “random” a nature, presumably in consequence of mixing two earthquake populations with distinctly different temporal dynamics.

Our analysis has shown that on removing aftershock sequences, increased correlation is observed! All catalogues considered herein yield q_T values that would render the seismogenetic system(s) of North California definitely non-Poissonian. Moreover, the dynamics of the nSAF and SNR sub-systems are distinctly different: The SNR system exhibits very high correlation (very long memory and very long-range interaction) to the point that any earthquake anywhere in the system would appear to influence the occurrence of future events. To a lesser degree, the same is true for the north segment of the San Andreas Fault system, with the difference that SNR appears to evolve in a perennial state of high correlation, while nSAF has demonstrated a dynamic transition from higher to lower non-equilibrating states in reference to the Loma Prietta event; this outcome also indicates that different driving (seismogenetic) mechanisms operate at those two areas.

TABLE 3.2.2 Summary of the variation of the entropic indices and *b*-values obtained from the analysis of North California full and declustered catalogues, as a function of threshold magnitude. $\bar{q}_T$ and $\bar{q}_M$ are the mean temporal and magnitude entropic indices respectively; $\sigma(q_T)$ and $\sigma(q_M)$ are the corresponding standard deviations. The last column lists *b*-values calculated with conventional techniques.

		Period	$\bar{q}_T$	$\sigma(q_T)$	q_T Range	$\bar{q}_M$	$\sigma(q_M)$	q_M Range	b_q range	*b* value
Comparative study	**NCSN**	1984-2011	1.26	0.042	1.19-1.34	1.52	0.024	1.49-1.57	1.04-0.75	1.0-0.91
	DD		1.18	0.086	1.04-1.33	1.52	0.026	1.49-1.58	1.04-0.72	1.1-0.96
Full NCSN		1968-2015	1.33	0.033	1.24-1.42	1.53	0.024	1.49-1.56	1.04-0.79	1.01-0.92
		1968-1988	1.38	0.038	1.35-1.44	1.50	0.006	1.49-1.51	1.04-0.96	1.01-0.91
		1990-2015	1.16	0.057	1.09-1.22	1.49	0.008	1.48-1.50	1.08–1.00	1.02-0.96
Full nSAF		1968-2015	1.22	0.044	1.15-1.28	1.53	0.030	1.47-1.58	1.12-0.72	1.15-0.95
		1968-1988	1.51	0.074	1.40-1.62	1.51	0.027	1.48-1.56	1.08-0.79	1.18-0.95
		1990-2015	1.09	0.043	1.05-1.13	1.48	0.012	1.46-1.49	1.12-1.01	1.13-0.99
Full SNR		1968-2015	1.46	0.081	1.41-1.51	1.52	0.014	1.51-1.53	0.96-0.88	0.92-0.84
		1968-1988	1.49	0.074	1.40-1.59	1.54	0.006	1.54-1.55	0.85-0.82	0.88-0.81
		1990-2015	1.44	0.046	1.37-1.51	1.50	0.019	1.49-1.52	1.04-0.92	1.00-0.87

Declustered NCSN	ϕ_j **≥70%**	1968-2015	1.40	0.060	1.31-1.49	1.53	0.013	1.51-1.55	0.96-0.82	0.95-0.75
	ϕ_j **≥80%**		1.40	0.110	1.23-1.52	1.55	0.013	1.53-1.57	0.89-0.75	0.93-0.72
	ϕ_j **≥90%**		1.45	0.040	1.41-1.48	1.50	0.006	1.49-1.50	1.04-1.00	1.02-0.77
Declustered nSAF	ϕ_j **≥ 70%**	1968-2015	1.48	0.080	1.41-1.60	1.51	0.014	1.49-1.54	1.04-0.85	0.99-0.78
	ϕ_j **≥ 80%**		1.47	0.09	1.37-1.58	1.52	0.006	1.51-1.52	0.96-0.92	0.99-0.75
	ϕ_j **≥ 90%**		1.56	0.025	1.49-1.63	1.48	NA	1.48	1.08	1.15
Declustered SNR	ϕ_j **≥ 70%**	1968-2015	1.69	0.045	1.58-1.80	1.55	0.007	1.54-1.56	0.85-0.78	1.08-0.79
	ϕ_j **≥ 80%**		1.76	0.015	1.75-1.78	1.56	0.006	1.55-1.56	0.82-0.79	0.97-0.74

TABLE 3.2.3 Summary of the variation of the entropic indices and *b*-values obtained from the analysis of North California full and declustered catalogues, as a function of interevent distance. $\bar{q}_M$ is the mean magnitude entropic index; $\sigma(qM)$ is the corresponding standard deviation.

Catalogue		**Period**	**q_T Range**		$\bar{q}_M$	**$\sigma(q_M)$**	**q_M Range**	**b_q Range**
			Δd < 100km	**Δd > 200km**				
Comparative Study	**NCSN**	1984-2011	1.58-1.62	1.10-1.30	1.50	0.013	1.48-1.51	1.08-0.96
	DD		1.58-1.62	1.10-1.30	1.49	0.016	1.46-1.51	1.17-0.96
NCSN full		1968-2015	~1.58	1.21-1.57	1.50	0.026	1.47-1.53	1.12-0.88
		1968-1988	1.40-1.70	~1.79	1.51	0.023	1.47-1.54	1.12-0.85
		1990-2015	1.48	1.12-1.30	1.49	0.021	1.47-1.52	1.12-0.92
NCSN, declustered, ϕ_j ≥70%		1968-2015	1.86-1.58	1.33-1.49	1.51	0.041	1.47-1.57	1.13-0.76
nSAF, full		1968-2015	1.60	1.15-1.42	1.50	0.017	1.48-1.53	1.08-0.88
		1968-1988	1.58-1.55	1.38-1.66	1.49	0.014	1.48-1.51	1.08-0.96
		1990-2015	1.11- 1.20 1.14-1.39		1.49	0.026	1.48-1.51	1.08-0.96
SNR full		1968-2015	1.31-1.52		1.51	0.012	1.50-1.53	1.00-0.92
		1968-1988	1.33-1.84		1.54	0.03	1.54-1.55	0.85-0.82
		1990-2015	1.52-1.73		1.49	0.026	1.48-1.51	1.08-0.96

3.3 COMPARATIVE ANALYSIS OF SOUTH AND NORTH CALIFORNIA

The results of the nSAF /sSAF and SNR/ECSZ full catalogues are compared in Fig. 3.30 and Fig. 3.31 while their declustered counterparts are compared in Fig. 3.32. With respect to $q_M(M_{th})$ it is apparent that the results are very comparable; $q_M(M_{th})$ fluctuates around a mean value of 1.5 ($b_q \approx 1$), with an exception for sSAF full catalogue (Fig. 3.30a) where $q_M(M_{th})$ is characterized by a distinct upward trend reaching 1.6 at M_{th}=4.2. A similar trend can be also observed at nSAF for the period 1968-1988 where $q_M(M_{th})$ rises up to 1.57 at M_{th}=4.1.

With respect to the temporal entropic index, it is straightforward to see that the post-1990 dynamics of nSAF and the post-1980 dynamics of sSAF are very comparable, just as the post-1968 dynamics of sSAF also turn out to be. Notably, as of 1980 the sSAF system has not experienced any major earthquake northward of the US-Mexican border. The large Baja California event of 2010 (M7.1) ruptured the Laguna Salada fault (LSF) in the Sonora desert (Mexico), well to the south of sSAF. Although the LSF is a probable southward continuation of the Elsinore fault, it can easily be verified that any activity leading to, or following this event, does not appear to have influenced the dynamics of sSAF, which was demonstrably also not influenced by the Loma Prieta earthquake. Once again, one is tempted to ponder whether such “isolation” of the sSAF is effected by the Garlock and “Unnamed” seismic zones. When the analysis of the declustered nSAF catalogue (available only at the $\phi \geq 70\%$ probability level) is compared to the corresponding analysis of the declustered sSAF catalogue, it is easily verified that sSAF appears to be overall stronger correlated than nSAF, albeit not very significantly (Fig. 3.32a).

The results of the SNR and ECSZ full catalogues are compared in Fig. 3.31c and 3.31d. If only $q_T(M_{th})$ is considered, ECSZ appears to be significantly more correlated than the strongly correlated SNR. However, when $q_T(\Delta d)$ is only taken into consideration, SNR and ECSZ appear to be comparable with particular reference to the periods 1990-2015 for SNR and 1980-2017 for ECSZ. The largest part of this apparent discrepancy is due to the extensive and populous aftershock sequences of the 1992 Landers and 1999 Hector Mine events; the two systems turn out to be absolutely comparable when declustered realizations of the catalogues are considered, as in Fig. 3.32b which illustrates results for the $\phi \geq 70\%$ probability level. The two sibling systems can also be shown to be comparable at the $\phi \geq 80\%$ level: a mean q_T of 1.76 in SNR was determined for the period 1968-2011 while for the period 1968-2015 an average of 1.86 for the period is determined.

Accordingly, the two subsystems of the Walker Lane zone are comparable although ECSZ appear to be somewhat stronger correlated than SNR.

The differences in the expression of seismicity between the sSAF/ICB and ECSZ fault networks, and for that matter between nSAF/sSAF/ICB and SNR/ECSZ, apparently reflect their niche in the geodynamic setting of the broader area: On the one hand is the proper transformational boundary between the North American and Pacific plates (nSAF/sSAF/ICB subsystems) which is open to the west and accommodates more than half of the total plate motion in Southern California (Becker et al., 2005; Liu et al., 2010, Dorsey et al., 2012). On the other hand, is the SNR/ECSZ subsystem, a *landlocked* shear zone in which approximately 25% of the total plate motion takes place (Plattner et al., 2009). It certainly stands to reason that the differences in the geodynamic setting of the respective fault networks affect the dynamic expression of seismicity. It is beyond the scope of this work to explore this rather intriguing problem.

The evidence presented above indicates that the seismogenetic systems of South California and North California are certainly non-Poissonian of nature. Foreground/background, as well as background seismicity is correlated, and correlation increases with declustering in the northern and southern segment of the San Andreas Fault system regions or remains unabated in the Eastern California Shear Zone and Sierra Nevada Range respectively. This is a point of significance as it demonstrates that on muting the contribution of the correlated time-local foreground activity, the existence of long-range interaction in the background process becomes evident, as can be explicitly studied in Figs. 3.30, 3.31 and 3.32. It should also be noted that even with full (clustered) earthquake catalogues, correlation observed at interevent distances longer than 100km can hardly be explained in terms of aftershock sequences, as such ranges transcend the lengths of aftershock zones associated with M_w 7-7.3 earthquakes (e.g. Kagan, 2002).

In concluding, it becomes clear that there are different mechanisms by which complexity and sub-extensivity may arise. The above results may assist in understanding the origin of complexity in the fault systems of California.

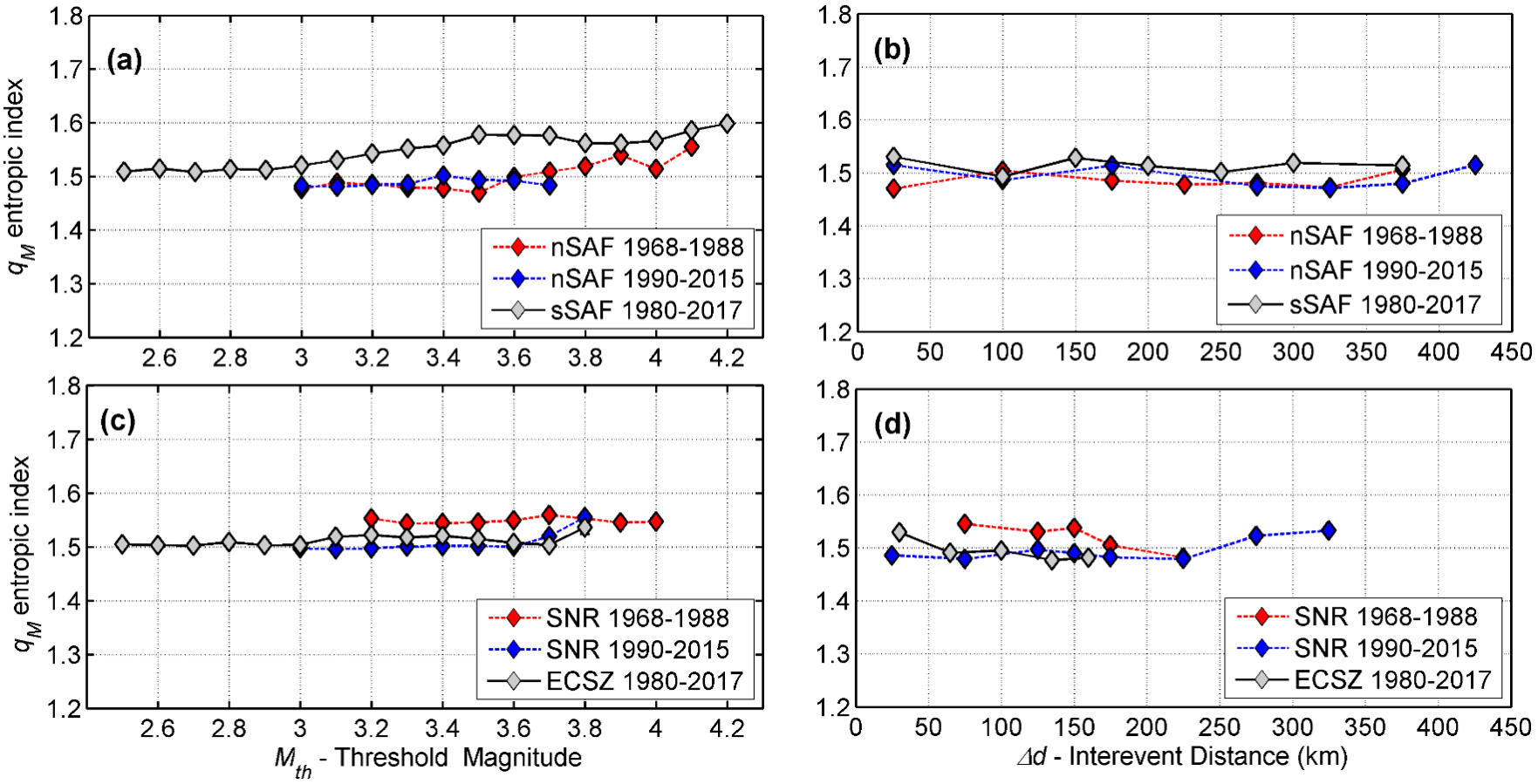

Figure 3.31 Comparison of $q_M(M_{th})$ and q_M (Δd) for the full catalogues of the seismogenetic systems in northern California with those obtained herein for southern California. **(a)** Comparison of q_M (M_{th}) for the northern (nSAF) and southern (sSAF) segments of the San Andreas Fault. **(b**) Comparison of q_M (Δd) for nSAF and sSAF. **(c)** Comparison of $q_T(M_{th})$ for the Walker Lane – Sierra Nevada Range (SNR) and Eastern California Shear Zone (ECSZ). **(d)** Comparison of q_M (Δd) for SNR and ECSZ

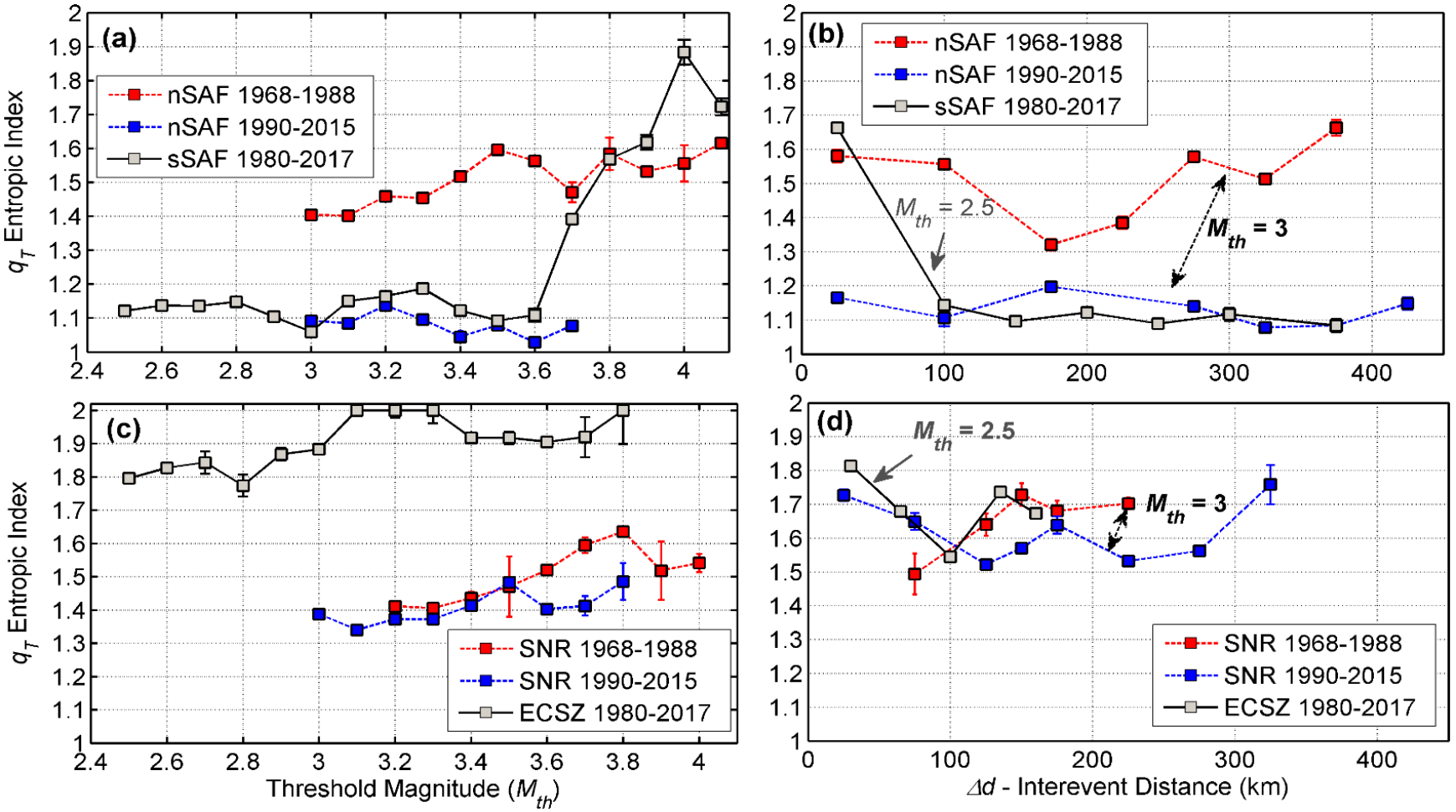

Figure 3.32 Comparison of $q_T(M_{th})$ and $q_T(\Delta d)$ for the full catalogues of the seismogenetic systems in northern California with those obtained herein for southern California. **(a)** Comparison of $q_T(M_{th})$ for the northern (nSAF) and southern (sSAF) segments of the San Andreas Fault. **(b)** Comparison of $q_T(\Delta d)$ for nSAF and sSAF. **(c)** Comparison of $q_T(M_{th})$ for the Walker Lane – Sierra Nevada Range (SNR) and Eastern California Shear Zone (ECSZ). **(d)** Comparison of $q_T(\Delta d)$ for SNR and ECSZ

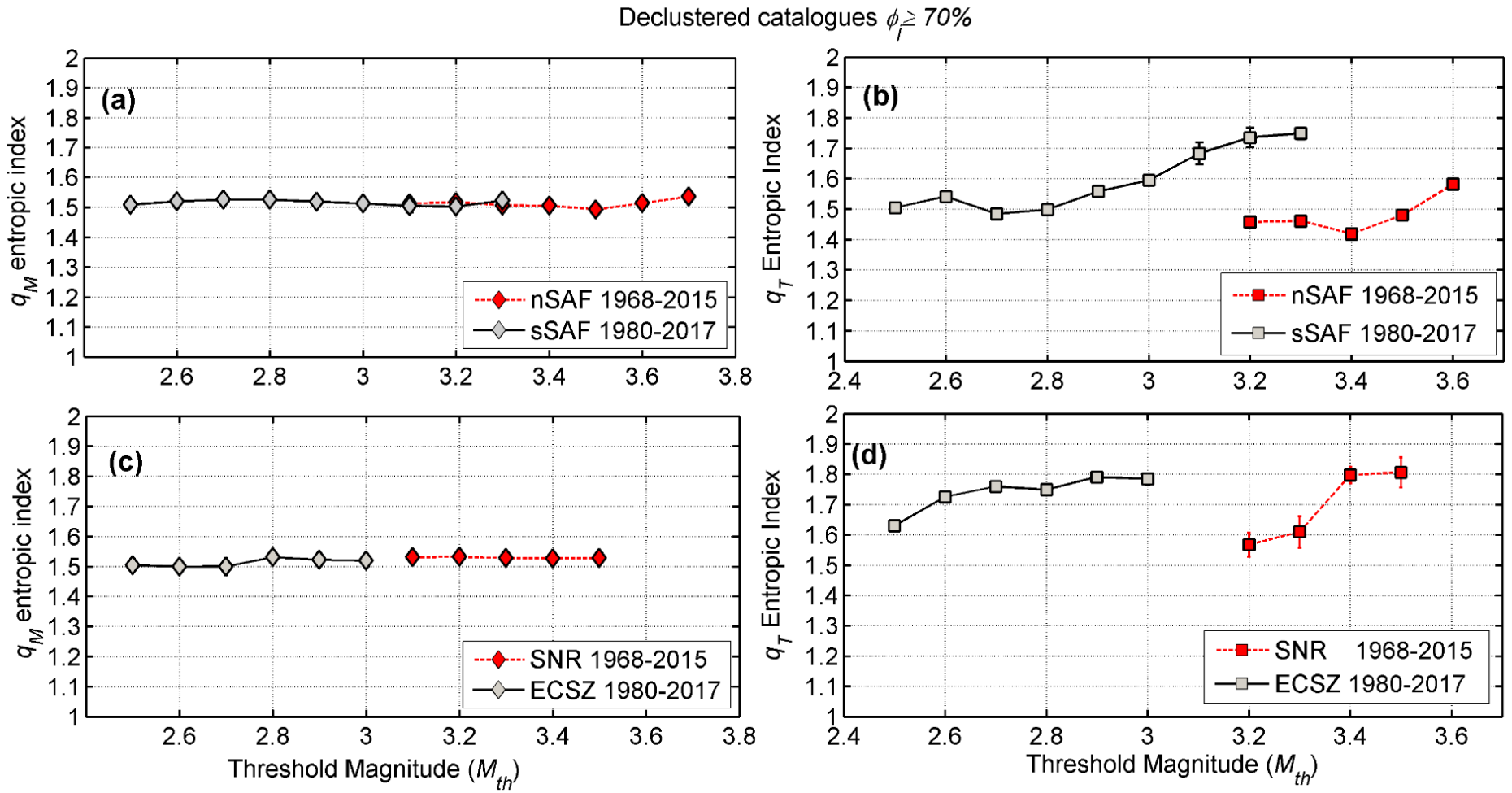

Figure 3.33 Comparison of $q_T(M_{th})$ obtained for *declustered* catalogues of the seismogenetic systems in northern California with those obtained herein for southern California ($\phi \geq 70\%$ probability level). **(a)** Comparison of the northern (nSAF) and southern (sSAF) segments of the San Andreas Fault. **(b)** Comparison of the Walker Lane – Sierra Nevada Range (SNR) and Eastern California Shear Zone (ECSZ).

3.3.1 EVOLUTION OF THE TEMPORAL ENTROPIC INDEX WITH TIME

So far, the nature of Californian seismogenetic process was examined via *multivariate* cumulative frequency distributions of earthquake magnitudes, interevent time and interevent distance in the context of Non-Extensive Statistical Physics. To take one step further, I shall investigate the time dependence with particular reference to periods preceding large ($M_L > 7$) earthquakes. To do this, F-M-T distributions are constructed over consecutive overlapping windows and are solved for the parameters a, α, q_M, c and q_T of Eq. 2.17. The procedure is applied to the full and declustered nSAF / SNR catalogues starting at the year 1968 and ending at the year 2015 and full and declustered sSAF/ ECSZ catalogues starting at the year 1980 and ending at the year 2017.

The F-M-T distributions are formed in the natural time of the respective seismogenetic processes: each window comprises 600 consecutive events while the overlap distance is 40 events; for the declustered catalogues, each window comprises 450 consecutive events while the overlap distance is 20 events. The differences in window sizes and overlap distances are a necessary adaptation to the different number of events left after declsutering the catalogues. In general, excellent approximations of the observed F-M-T distributions are obtained but for the sake of experimental rigour, this presentation will only consider models associated with a goodness of fit *better* than 0.97. The discussion focuses on the values and variation of the entropic indices, which are plotted as a function of time from Fig. 3.33 to Fig 3.38 and summarized in Table 3.3.1.

As is apparent in Fig. 3.34, the analysis of the nSAF full and declustered catalogues shows that the entropic index q_M, is quite consistently determined. For the full nSAF catalogue, q_M generally varies between 1.54 and 1.46 (Fig. 3.34a). It exhibits small fluctuations after the Loma Prieta main shock (M_L 7.0), first decreasing and, after approx. 1994, increasing slowly but persistently until the San Simeon and Parkfield earthquakes (M_L 6.6 and 6.0 respectively); a small increase can also be observed after approx. 2004.8. For the declustered nSAF catalogue q_M generally varies between 1.47 and 1.55 (Fig. 3.34a); it exhibits a small but persistent increase before the Loma Prieta event and remains stable after 1989. The application of Eq. 2.18 leads to b_q estimates that vary from 0.85 to 1.17 for the full catalogue and 0.76 to 1.11 for its declustered counterpart; it may be verified that these are remarkably consistent with corresponding determinations of *b*-values based on conventional methods (see Table 3.3.1). The entropic index q_M, like the

b-value to which it is related, represents the scaling of the size distribution of earthquakes and clearly indicates a correlated, scale-free process, possibly exhibiting a small-time dependence.

The temporal entropic index q_T exhibits significant variation for both the full and declustered catalogues. As can be seen in Fig. 3.33b, for the full nSAF catalogue q_T behaves "erratically", being generally very low (< 1.1) prior to large earthquakes (M > 5.7) and attains significant values (> 1.4 with a q_{Tmax} at 1.79)immediately after their occurrence, indicating very high correlation that can be easily explained as a consequence of their aftershock sequences. This explanation is further corroborated by the observation that the high correlation observed after the 1989 Loma Prieta earthquake gradually decays to oblivion after year 2000, reaching a value of 1.04 which clearly indicates randomness. It is evident that this pattern is recurrent: after a series of large earthquakes (e.g. the 2003 Central Coast earthquake, and 2007 San Francisco South Bay earthquake), q_T exhibits strong correlation and then it decays reaching values <1.1 (near randomness) right before the next large earthquake.

Conversely, the declustered nSAF (Fig.3.34c) catalogue reserves a surprise: q_T generally varies between 1.87 and 1.32, quasi-linearly increasing before the Loma Prieta earthquake from approx. 1.31 to 1.61 and remaining at high levels (> 1.62) up to year 2008; thereafter, it decreases to the level 1.32 – 1.44. These results strongly corroborate with the results obtained for the nSAF catalogue declustered at M_{th}=3.0 for the period 1968-2011.

As can be seen for the period 1968-2011 at probability level 70%, q_T exhibits strong correlation and also increases quasi-linearly before the Loma Prieta earthquake from 1.31 to 1.46 while after the large earthquake q_T remains stable at approx. 1.55 – 1.60 (q_{Tmax} =1.65) up to 2005 and decreases gradually to 1.39 in 2011. The same pattern is observed at probability 90% (Figure 3.33c – blue rectangles) where q_T values are increased after the large event at a mean range of 0.3 (q_{Tmax} =1.94). In all cases moderate to very high correlation is observed as a function of time indicating that the background process is *not* random at the 70% probability level and highly correlated at 90% level.

The analysis of the full and declustered sSAF catalogues also yields stable and consistent determination of q_M as a function of time. For the full catalogue q_M varies between 1.43 and 1.56, exhibiting fluctuations that are localized in time and clearly associated with the occurrence of significant earthquakes (Fig. 3.35a). For the declustered catalogue, q_M

varies between 1.42 and 1.56, exhibiting small and slow variation with time, clearly not associated with significant events. Respectively, b_q varies between 1.32 and 0.79 for the full catalogue and between 1.38 and 0.79 for the declustered catalogue; these are also verifiably consistent with corresponding determinations of *b*-values based on conventional methods (Table 3.3.1).

The temporal entropic index exhibits intense variations with time. Fig. 3.35b clearly shows that for the full sSAF catalogue q_T behaves as per the full nSAF catalogue; q_T is generally low (1.1 – 1.3) prior to large earthquakes but exhibits a persistent increasing trend from the lower to the higher end of this range prior to their occurrence; the index jumps to very high values (> 1.85) immediately after the incidence of large events, presumably reflecting the very high correlation associated with their aftershock sequences. Also, as per the nSAF analysis, the high correlation of the aftershock sequences decays to near oblivion (< 1.1) with time, but a rate *significantly* faster than the corresponding effect associated with the Loma Prieta event (see Fig. 3.35b). Such behaviour indicates that quite different dynamics operate to the north and south of the Garlock Fault, as well as the possibility that nSAF seismicity is expressed with a series of rapidly building up and decaying cycles. The validity of these preliminary observations and inferences remains to be tested.

The analysis of the declustered sSAF catalogue holds its own surprises analogous to its nSAF counterpart: as shown in Fig. 3.35c, at 70% probability level, q_T varies between 1.78 and 1.46. Although, some earthquake swarms (clusters) remain, especially in periods of large earthquakes (i.e. Baja event in 2010) where q_T indicates extremely high correlation as a consequence of the aftershock sequences, it is clear that in general the temporal entropic index is stably determined above 1.46. By increasing the probability of an event to belong to the background at 90%, q_T varies from 1.48 to 1.89. Such behaviour clearly indicates very high correlation for the background process and possibly SOC dynamics.

With respect to the full SNR and ECSZ catalogues, the magnitude entropic index is again consistently determined. For the SNR catalogue q_M, varies from 1.58 to 1.45 while for the ECSZ catalogue it varies from 1.58 to 1.42 (Fig. 3.35). Respectively, b_q varies from 0.72 to 1.22 for SNR, while for ECSZ it varies from 0.72 to 1.38. These are also verifiably consistent with corresponding determinations of *b*-values based on conventional methods (Table 3.3.1). The temporal entropic index, as in the case of nSAF and sSAF, exhibits significant fluctuations with time. For SNR catalogue, q_T is generally low (<1.3) prior to a

large earthquake and attains high correlation (>1.6) after the occurrence of a significant event. This behaviour is similar to nSAF; q_T decays after the expression of a large earthquake *(M_L>5.5*) however it does not reach near randomness. It is also noteworthy that after 2004 q_T is persistently stable around a value of 1.45-1.55 indicating strong correlation (Fig. 3.36). With respect to ECSZ full catalogue, q_T is very high (> 1.5) up to the Landers event of 1992.5; after 1992 q_T becomes unstable and behave erratically due to the overwhelming effect of the tightly spaced aftershock sequences (Fig. 3.36). After a three-year period, q_T increases persistently to 1.5 before the Hector Mine earthquake of 1999. It is interesting to notice that after Hector Mine event and up to the next significant earthquake of 5.6, q_T is very high (1.86-1.65) while after 2009 it decays gradually to 1.35 indicating overall very high correlation for the foreground process and possibly SOC dynamics. These results are strongly corroborated with the results obtained in Sections 3.1 and 3.2 and indicate that different levels of self-organization, namely between nSAF, SNR, sSAF and ECSZ might be developed and different mechanisms by which complexity and sub-extensivity may arise in the fault systems of California.

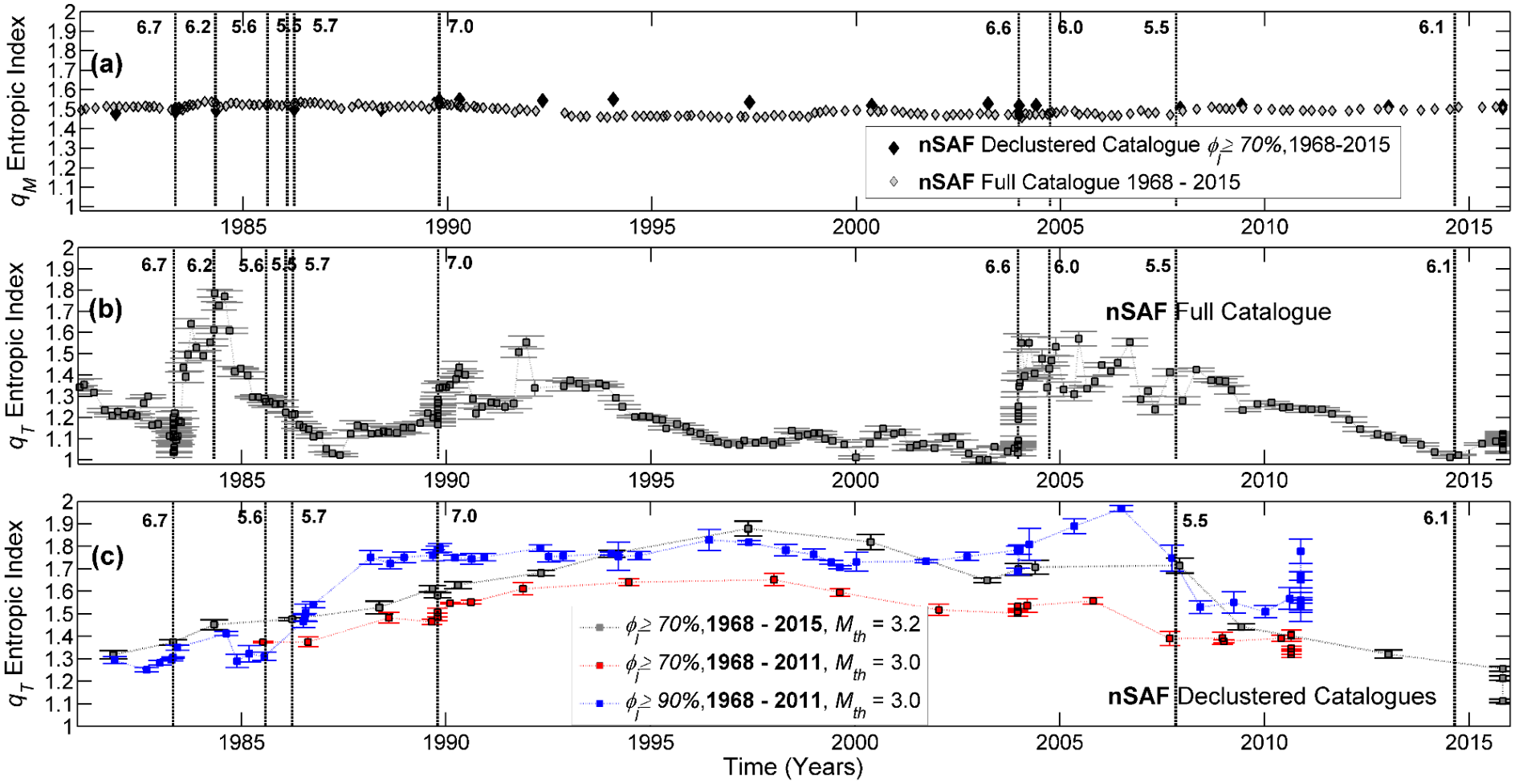

Figure 3.34 The entropic indices obtained for the nSAF full and declustered catalogue. Estimates are based on F–M–T distributions compiled over sliding windows of 600 events in the natural time of the seismogenetic process. Error bars refer to 95% confidence intervals. The vertical dashed lines indicate the occurrence of earthquakes with $M_L \geq 5.5$. The entropic indices obtained for the declustered nSAF catalogue at $\phi \geq 70\%$ probability level and compared with the results obtained for period 1968-2011, $M_{th}=3.0$ at $\phi \geq 70\%$ and $\phi \geq 90\%$ probability level.

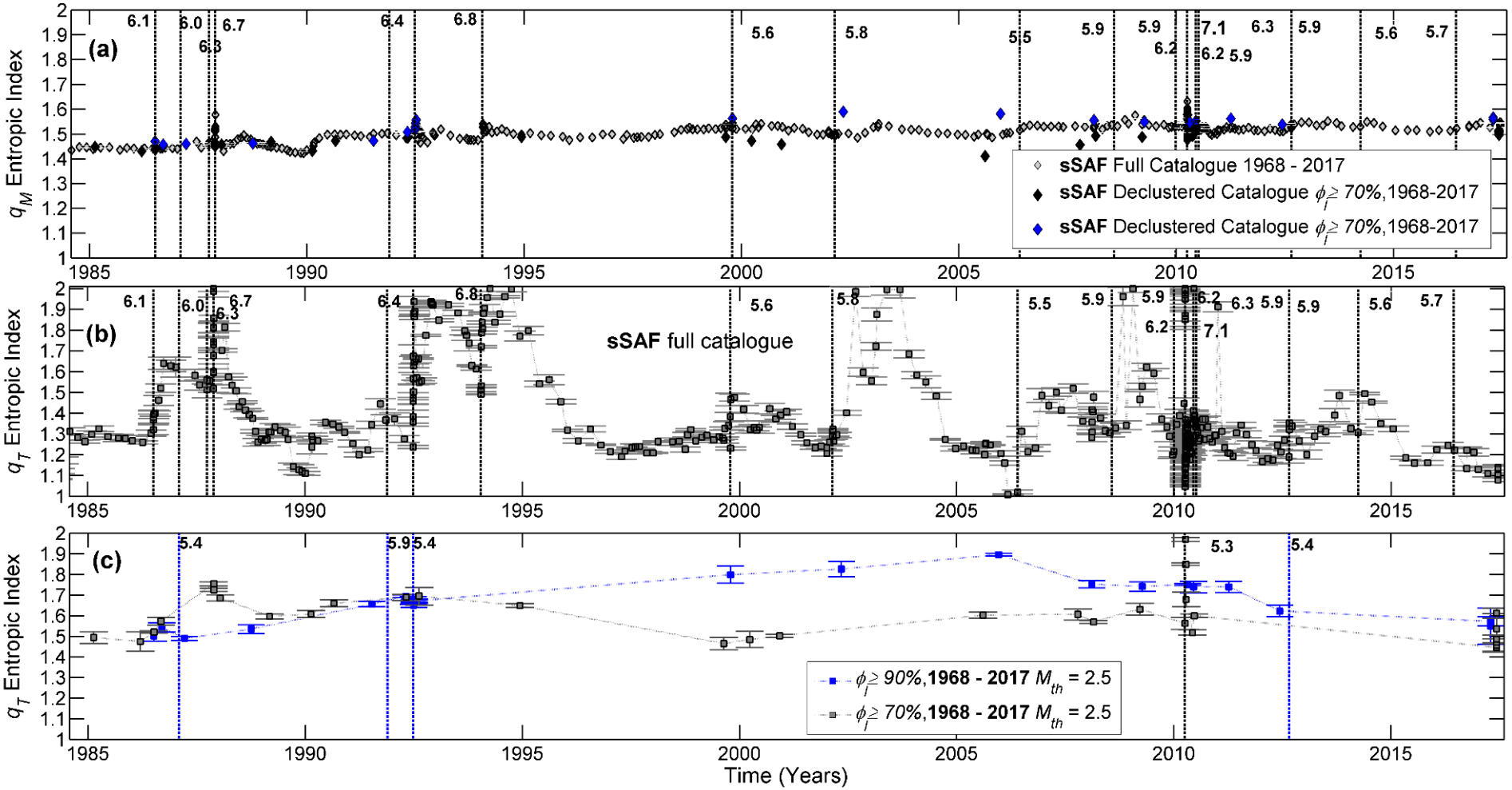

Figure 3.35 The entropic indices obtained for the sSAF full and declustered catalogue. Estimates are based on F–M–T distributions compiled over sliding windows of 600 events in the natural time of the seismogenetic process. Error bars refer to 95% confidence intervals. The vertical dashed lines indicate the occurrence of earthquakes with $M_L \geq 5.3$. The entropic indices obtained for the declustered nSAF catalogue at $\phi \geq 70\%$ and $\phi \geq 90\%$ probability level.

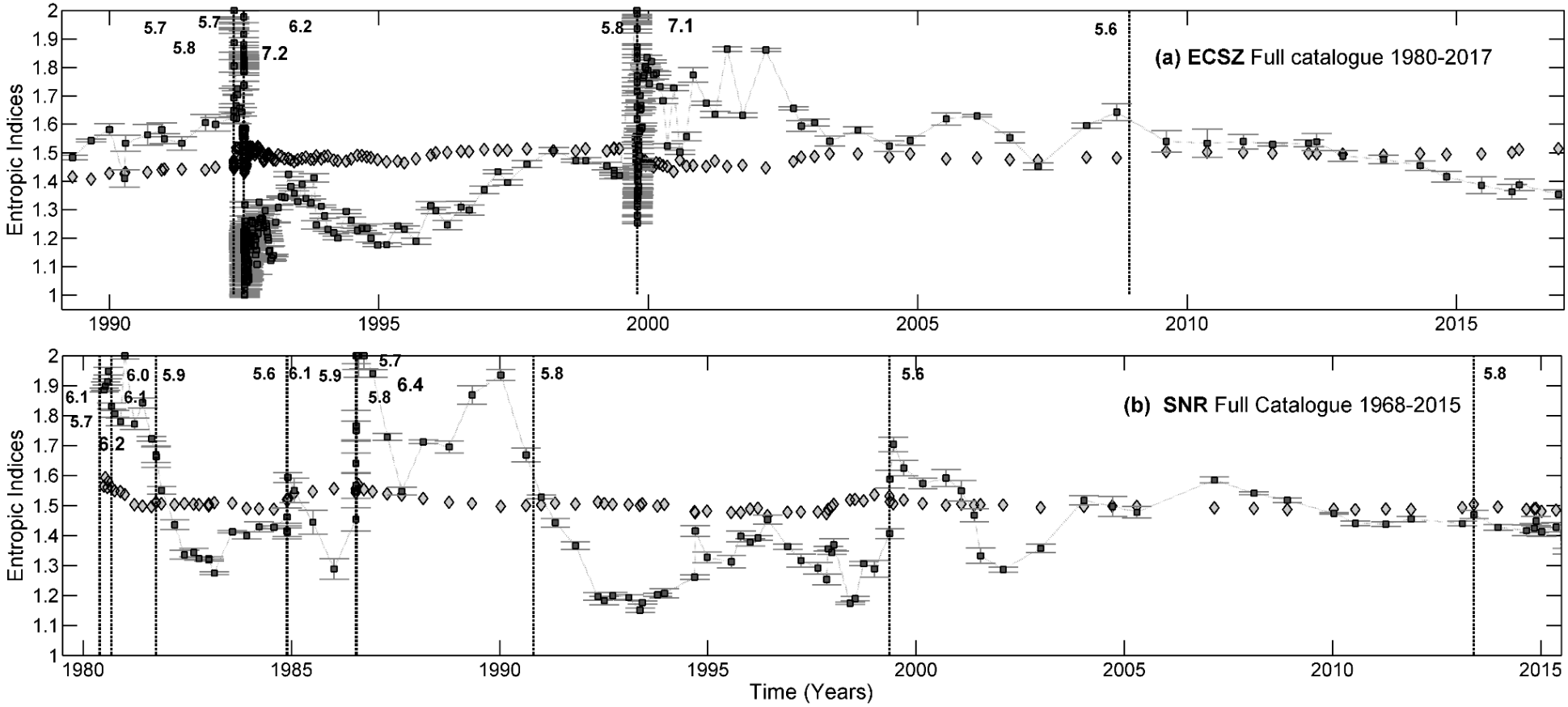

Figure 3.36 The entropic indices obtained for the full SNR and ECSZ catalogue. Estimates are based on F–M–T distributions compiled over sliding windows of 600 events in the natural time of the seismogenetic process. Error bars refer to 95% confidence intervals. The vertical dashed lines indicate the occurrence of earthquakes with $M_L \geq 5.5$.

TABLE 3.3.1 Summary of the entropic indices ans *b*-values obtained for the nSAF, sSAF, SNR and ECSZ catalogues.

Parameter variation	**Full nSAF Catalogue**	**Declustered nSAF Catalogue 70%**	**Declustered nSAF Catalogue 90%***	**Full sSAF Catalogue**	**Declustered sSAF Catalogue 70%**	**Declustered sSAF Catalogue 90%**	**Full SNR catalogue**	**Full ECSZ catalogue**
q_M	1.46-1.54	1.47 - 1.55	1.47 - 1.55	1.43 - 1.56	1.42 - 1.56	1.42 - 1.56	1.45-1.58	1.42-1.58
q_T	1.00 – 1.79	1.32 - 1.87	1.26-1.94	1.01 - 1.98	1.46 - 1.78	1.48-1.89	1.18 - 1.98	1.19-
b_q	1.17-0.85	1.11-0.76	1.11-0.76	1.32 - 0.79	1.38 - 0.79	1.38 - 0.79	1.22-0.72	1.38-0.72
***b* (conventional)**	—	1.1 - 0.78	1.1 - 0.78	—	1.25 - 0.86	1.25 - 0.86	1.25-0.78	1.32-0.85

3.4 MENDOCINO TRIPLE JUNCTION/ FRACTURE ZONE

The Mendocino Fracture zone is a part of northern California and the most seismically active in California state. An important factor is the history of the triple junction. The Mendocino Triple Junction formed 29–30 Ma at latitude 31º N in the modern North America reference frame, at the time the Pacific–Farallon spreading center first reached the subduction zone at the western edge of North America. The triple junction and the Mendocino Fracture Zone have subsequently migrated northwest with respect to North America and are presently at latitude 40.5º N. At the same time, the Rivera Triple Junction has migrated southeast to its present position relative to North America at latitude 23º N. After the Pacific and North America plates first came into contact, and because the Pacific Plate is moving northwest with respect to the North America Plate, the plate boundary was established as a right-lateral transform fault that has been growing both to the northwest and southeast for the past 29–30 million years. The SAF is the principal tectonic displacement zone, but additional faults with lower displacement rates are found both east and west of the SAF.

The Mendocino fault or Mendocino Fracture Zone (MFZ) lies at the base of the 1.5-km-high north-facing Gorda Escarpment (Godfrey et al., 1998) and extends from the triple junction westward 260 km to the southern end of the Gorda Ridge and spreading center. Further west, where the Pacific Plate is on bothsides, the Mendocino fault is inactive. The north coastal region of California accounted for about 25% of the seismic energy released in California in a 50-year period. The largest earthquake clearly associated with the Mendocino fault occurred at longitude, 125.8º W, on 01/09/1994 of Mw 6.9. An earlier earthquake of ML 6.6 struck the Mendocino fault at longitude 126.8º W, on 10/09/1980 (Dengler et al., 1995). Larger earthquakes (ML 7.3-7.6) may have struck MFZ in the past (first two decades of the 20th century), although their location uncertainty is due to the possibility of sources in the internally deforming Gorda Plate and a large location error because the first seismograph in the North Coast region was not set up until 1932.

3.4.1 Mendocino Fracture Zone Earthquake Data

The Mendocino Fracture zone (MFZ) broader area is bounded by the coordinates 40°N to 43°N and 123°W to 128°W (Figure 3.36). The earthquake data utilized for MFZ source area, was also extracted from the regional earthquake catalogue of the North California

Seismic Network (NCSN @ http://www.NCSN.org). Details are given in Tables 3.4.1 and 3.4.2. As in the case of nSAF and SNR, duration (M_d) and amplitude (M_x) scales have been exhaustively calibrated against the M_L scale, while M_w magnitudes were also converted to M_L using the empirical formula of Uhrhammer et al (1996). Thus, the MFZ catalogue is homogenous and complete for $M_L \geq 3.0$ (Fig. 3.37).

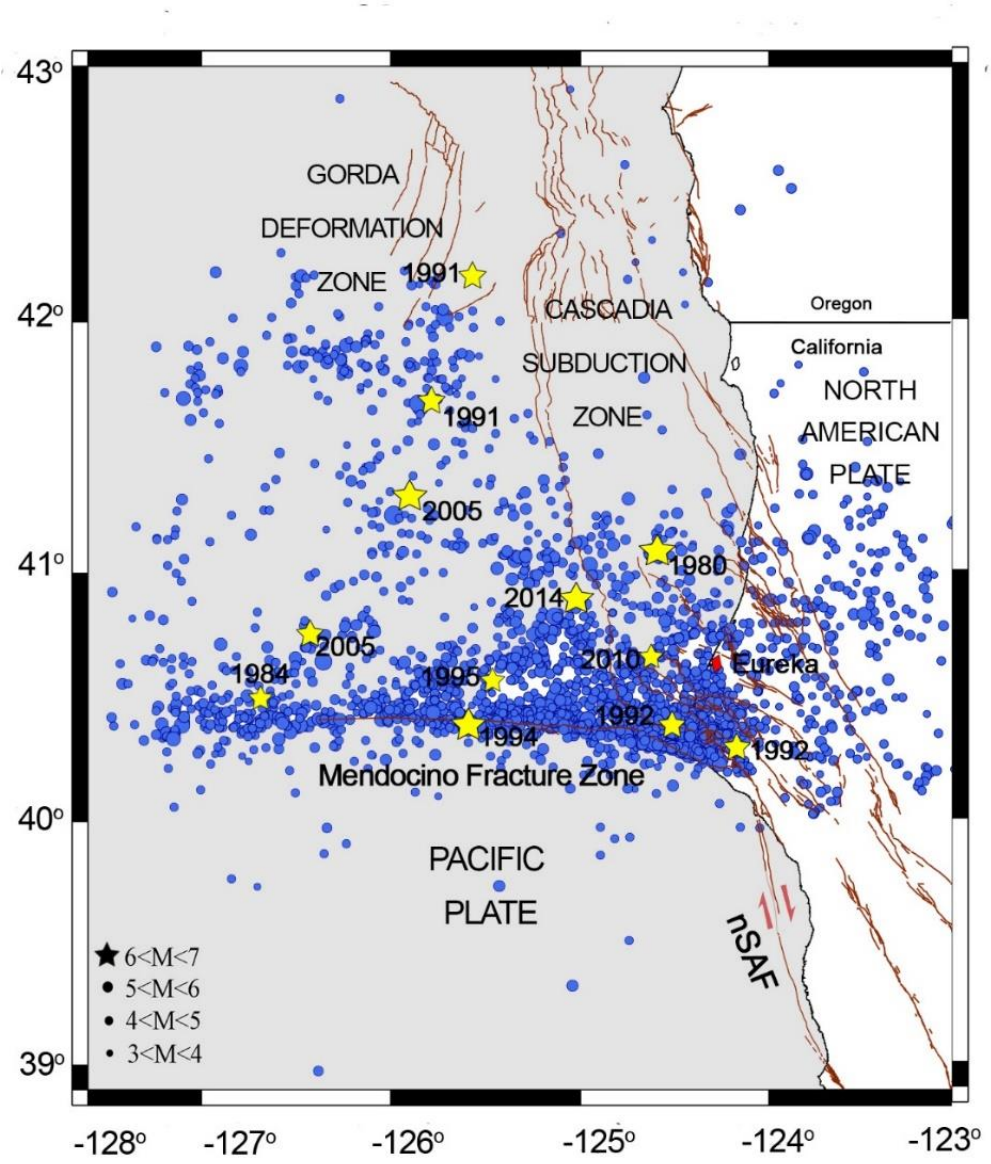

Figure 3.37 Map of seismicity in the Mendocino Triple Junction broader area reporting the earthquakes from 1/1/1968 to 31/12/2015, with M > 3 (blue circles): the epicentre of the main shock is outlined with the yellow star, while the main faults are depicted as light brown lines.

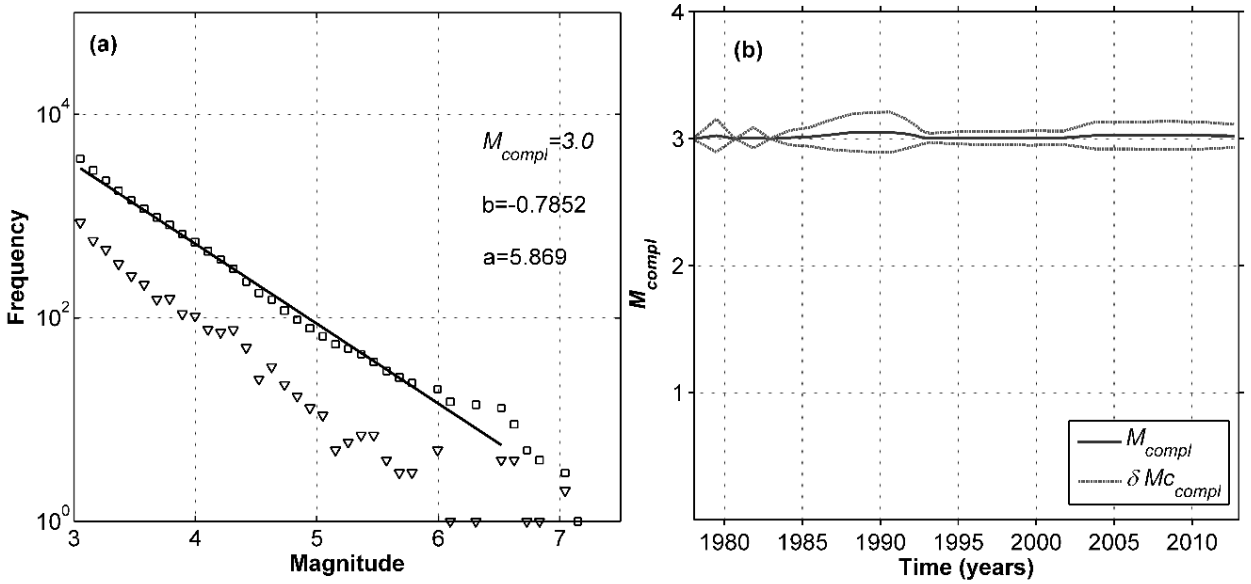

Figure 3.38 a) Incremental (down triangles) and cumulative (open squares) F-M distributions of the MFZ catalogue above the magnitude of completeness **b)** Variation of the magnitude of completeness (Mcompl) with time in the MFZ catalogue with 95% confidence limits

Figures 3.38 and 3.39 illustrate the results after declustering the full MFZ catalogue. Fig. 3.41 shows the cumulative earthquake count of the full MFZ catalogue for the period 1968-2015 (thick black line) and its declustered versions with probability $\phi_j \geq 70\%$ (thin black line), $\phi_j \geq 80\%$ (solid grey line) and $\phi_j \geq 90\%$ (dashed grey line). The catalogue declustered at the $\phi_j \geq 70\%$ level is almost free of the time-local rate surges (jerks) that indicate the presence of aftershock sequences. Nevertheless, it is not completely smooth and exhibits small fluctuations because a portion of the remaining events are foreground residuals. Consequently, in dealing with the MFZ catalogue, we will endeavour to confirm the results obtained at the 70% probability level by studying declustered realizations with probability $\phi_j \geq 80\%$ and $\phi_j \geq 90\%$ to be background. Fig. 3.39 illustrates background earthquake epicentres at different probability levels.

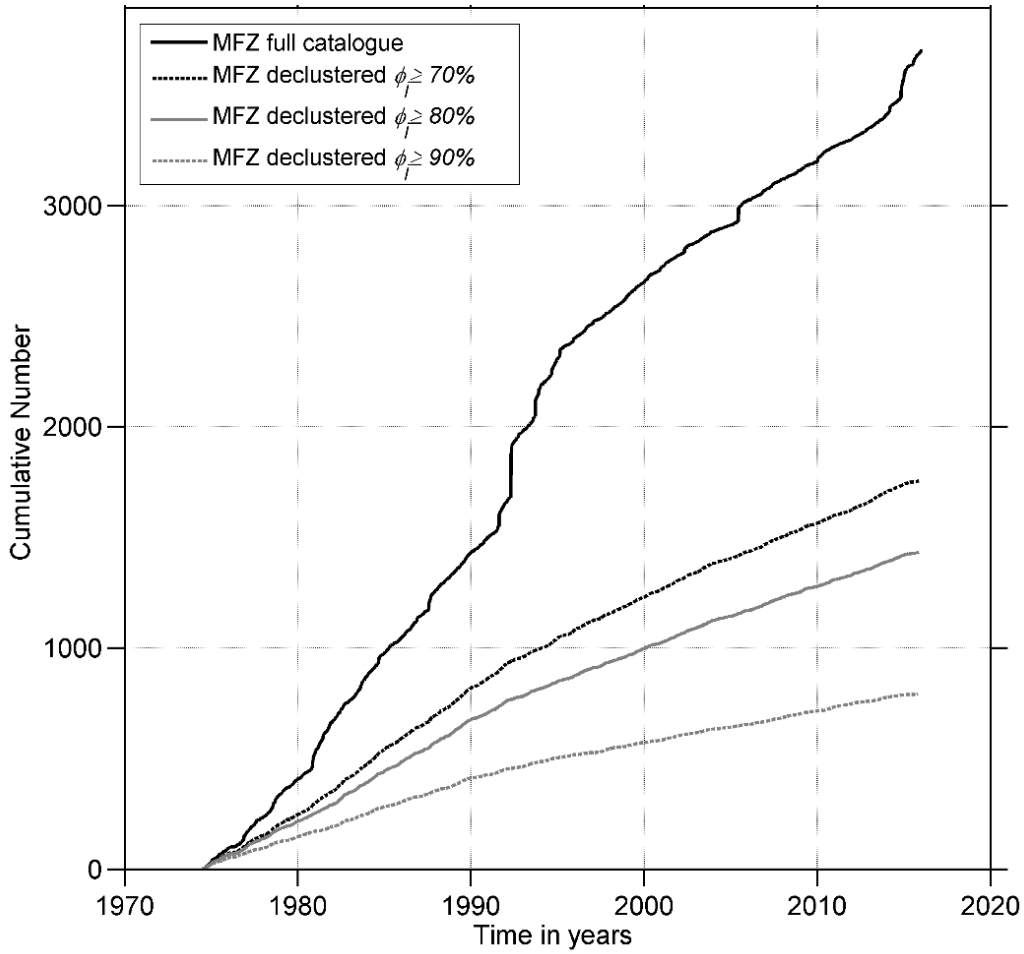

Figure 3.39. The cumulative earthquake count of the observed (full) and declustered realizations of the MFZ catalogue.

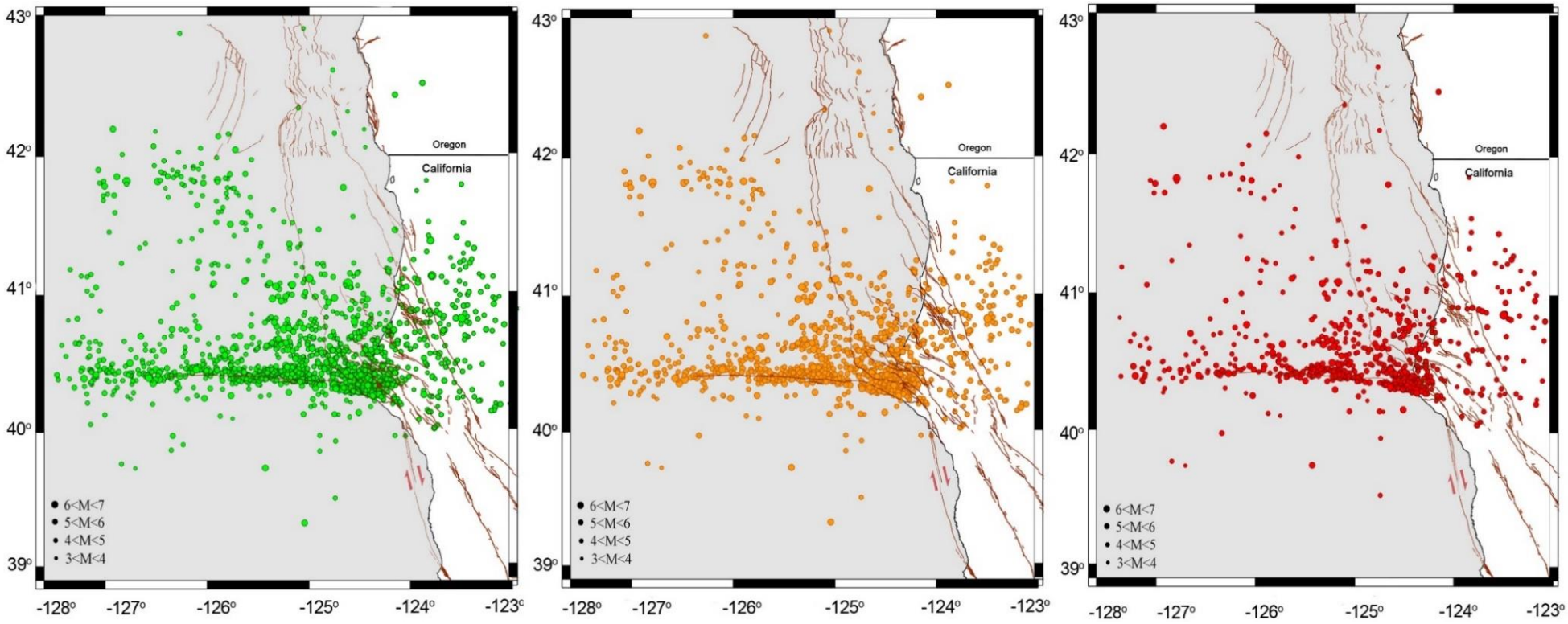

Figure 3.40 Map of seismicity in the Mendocino Triple Junction for the period 1/1/1968 to 31/12/2015, for the declustered catalogue at $\phi \geq 70\%$ probability level (green circles), at $\phi \geq 80\%$ probability level (orange circles) and at $\phi \geq 90\%$ probability level (red circles) respectively.

3.4.2 NESP results for Mendocino Fracture Zone Earthquake Catalogue

As can be seen in Figure 3.40 for the full MFZ catalogue q_M (M_{th}) is estimated at the markedly higher level of 1.56 – 1.60 with a mean of $\langle q_M \rangle$-MFZ = 1.57 $\pm$ 0.01, so that and $b_q(M_{th}) \in (0.78, 0.67)$. With respect to interevent distances $q_M(\Delta d)$ is again higher than in all previous areas, as it varies between 1.57 and 1.53, so that $b_q(\Delta d) \in (0.75, 0.89)$. Such q_M and b_q values indicate a rather high level of clustering in the MFZ active fault network while also shows that the high level of clustering inferred for the MFZ fault network persists over distances of at least 400 km.

The temporal entropic is also rather consistently determined. As can be seen, for the full MFZ catalogue $q_T(M_{th})$ fluctuates around 1.2 so that $\langle q_T(M_{th}) \rangle = 1.2 \pm 0.067$ but increases to 1.3 at larger threshold magnitudes ($M_{th} \geq 4.1$) exhibiting weak albeit persistent overall correlation. Finally, $q_T(\Delta d)$ is only moderate (1.3 – 1.35) at short interevent distances, increasing to 1.46 in the interval 50km–150km, only to decrease again to the level of 1.25 for Δd > 250km (moderate long-range correlation).

On removing the dependent events (Fig. 3.41) the $q_M(M_{th})$ determined for MFZ reduces to a mean value of 1.51 $\pm$ 0.008 indicating that the high level of active fault clustering observed in the full catalogue reduces to average levels. With respect to interevent distance $q_M(\Delta d)$ determinations fluctuate rather significantly, so that $\langle \bar{q}_M \ (\Delta d) \rangle$ = 1.54 $\pm$0.022 (b_q = 0.85). Interesting observations can be made in regard to the temporal entropic index: almost opposite to the North and South California analysis the declustered MFZ catalogue exhibits an upward quasi-linear trend from no correlation (q_T = 1.06) at M_{th} =3.0, to weak correlation $\langle q_T \rangle \approx 1.28$ at $M_{th} \geq 3.6$.

Finally, and presumably due to population statistics, $q_T(\Delta d)$ determinations from the declustered MFZ catalogue are limited to Δd < 250km; they do not exhibit some pattern and behaves erratically, fluctuating around a mean value of 1.15 $\pm$ 0.153 and possibly indicating a system weakly correlated over short and intermediate ranges, while at longer distances (Δd > 200km) ($q_T(\Delta d)$ rises to 1.48 indicating moderately high correlation.

Overall, it is noteworthy that the MFZ catalogue has shown evidence of significantly lower correlation in comparison to the other fault networks of California, especially at small cut-off magnitudes and short ranges. Another interesting observation is the rather higher values of the magnitude entropic index which may indicate increased clustering and of the fault network, and lower crustal heterogeneity in that area.

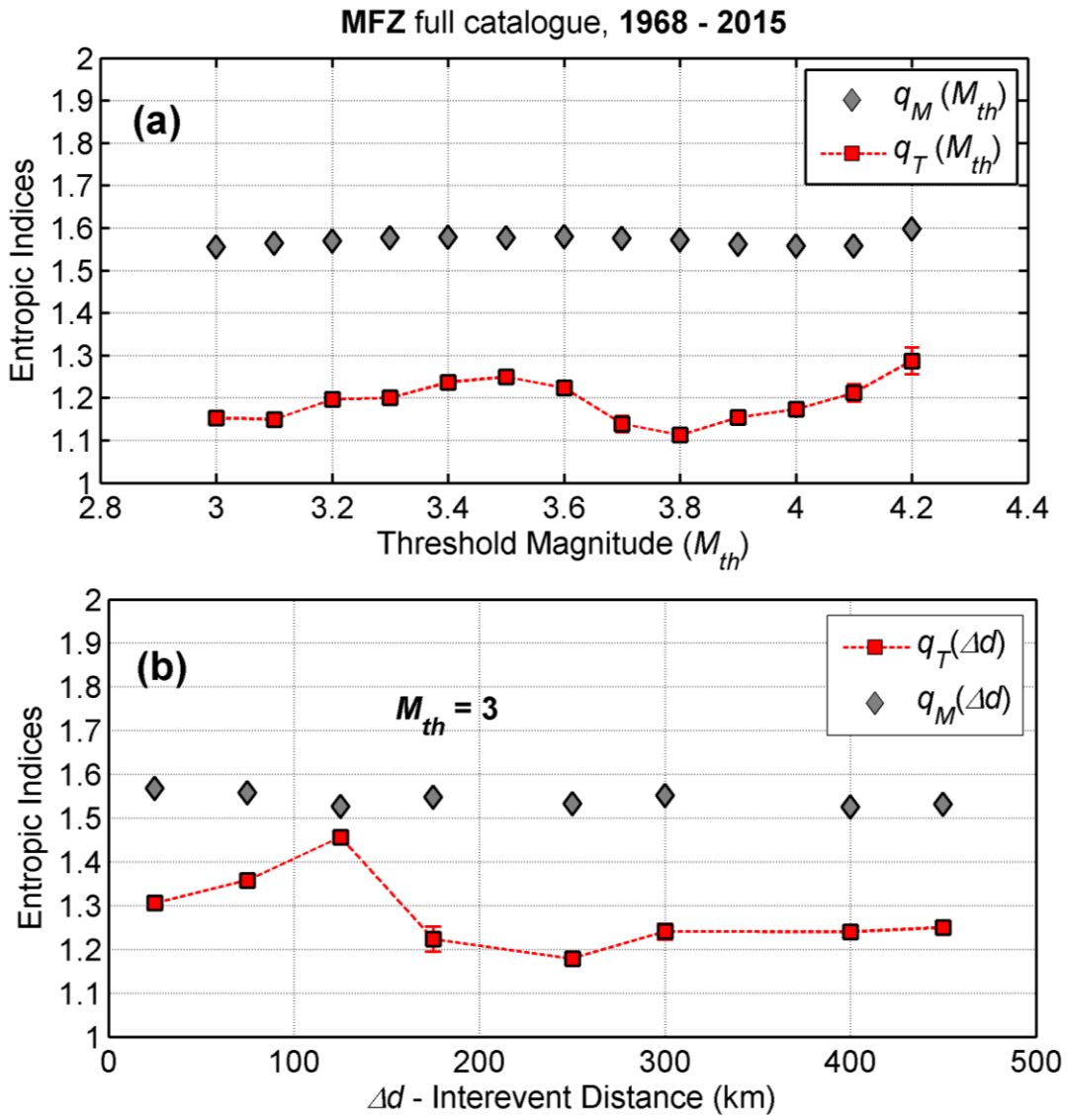

Figure 3.41 Analysis of the full MFZ catalogue for the 47-year period 1968 – 2015. **(a)** Dependence of entropic indices on threshold magnitude (M_{th}). **(b)** Dependence of entropic indices on interevent distance (Δd).

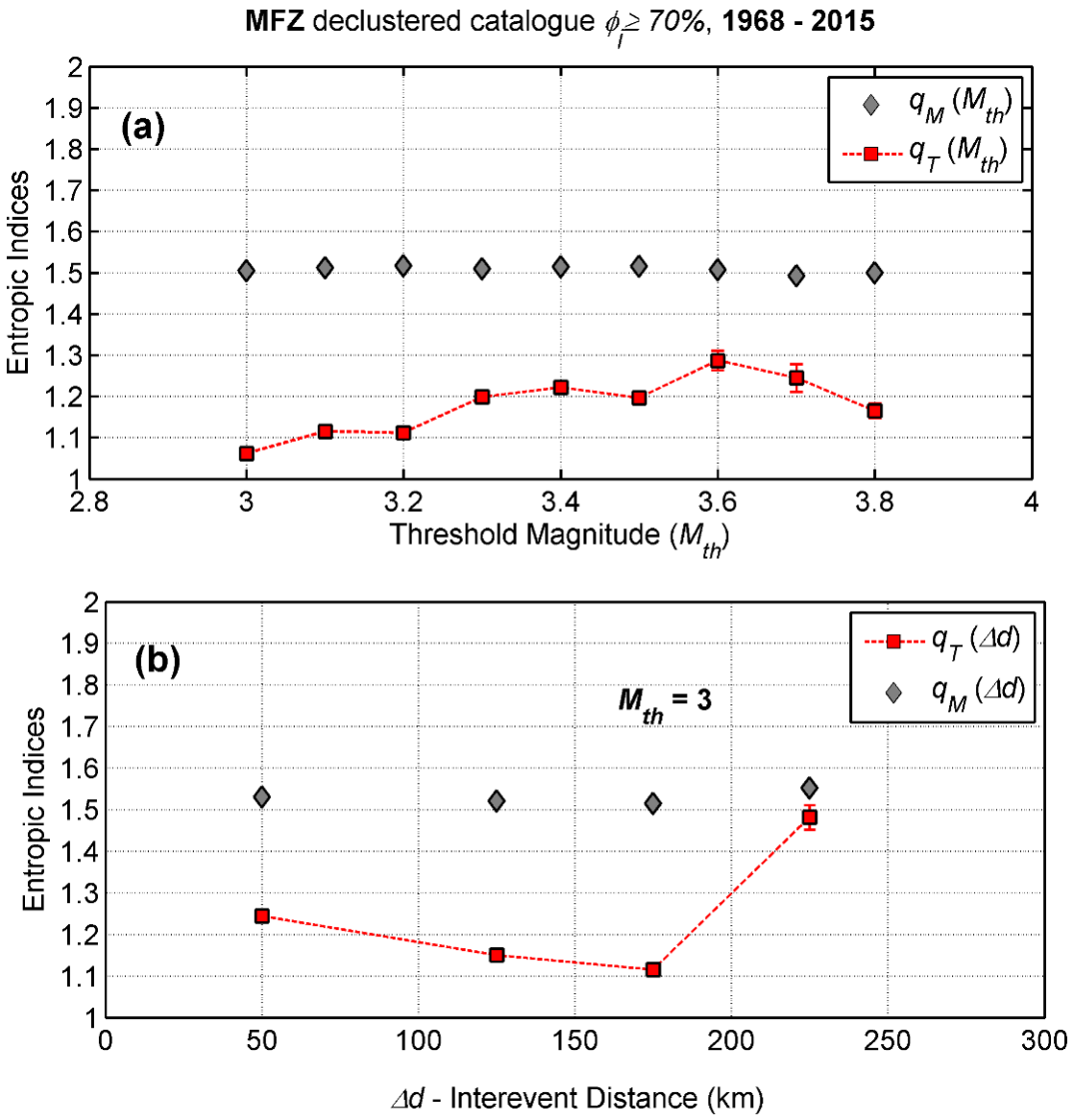

Figure 3.42 Analysis of the declustered MFZ catalogue for the 47-year period 1968 – 2015. **(a)** Dependence of entropic indices on threshold magnitude (M_{th}). **(b)** Dependence of entropic indices on interevent distance (Δd).

TABLE 3.4.1 Summary of the variation of the entropic indices and *b*-values obtained from the analysis of Mendocino full and declustered catalogues, as a function of threshold magnitude. $\bar{q}_T$ and $\bar{q}_M$ are the mean temporal and magnitude entropic indices respectively; $\sigma(q_T)$ and $\sigma(q_M)$ are the corresponding standard deviations. The last column lists *b*-values calculated with conventional techniques.

		Period	No. events	$\bar{q}_T$	$\sigma(q_T)$	q_T Range	$\bar{q}_M$	$\sigma(q_M)$	q_M Range	b_q range	*b* value
Full MFZ		1968-2015	3706	1.21	0.002	1.12-1.30	1.57	0.01	1.55-1.6	0.82-0.66	0.81-0.64
Declustered MFZ	**ϕ_j ≥70%**		1755	1.15	0.006	1.06-1.28	1.51	0.003	1.49-1.52	1.04-0.92	1.1-0.82
	ϕ_j ≥ 80%		1432	1.2	0.08	1.10-1.28	1.5	0.025	1.50-1.52	1.00-0.92	1.16-0.82
	ϕ_j ≥ 90%		792	1.2	0.025	1.16-1.24	1.53	0.03	1.52-1.54	0.92-0.85	1.19-0.79

TABLE 3.4.2 Summary of the variation of the entropic indices and *b*-values obtained from the analysis of Mendocino Fracture Zone full and declustered catalogues, as a function of interevent distance. $\bar{q}_M$ is the mean magnitude entropic index; $\sigma(qM)$ is the corresponding standard deviation.

Catalogue		Period	No.	q_T Range		$\bar{q}_M$	$\sigma(q_M)$	q_M Range	b_q Range
				Δd < 100km	**Δd > 100km**				
Full MFZ		1968-2015	3706	1.30-1.35	1.17-1.46	1.55	0.0035	1.52-1.57	0.92-0.75
Declustered MFZ	**ϕ_j ≥70%**		1755	1.24	1.11-1.48	1.52	0.004	1.51-1.54	0.96-0.85
	ϕ_j ≥ 80%		1432	1.25	1.11-1.44	1.53	0.025	1.52-1.54	0.92-0.85
	ϕ_j ≥ 90%		792	N/A	N/A	N/A	N/A	N/A	N/A

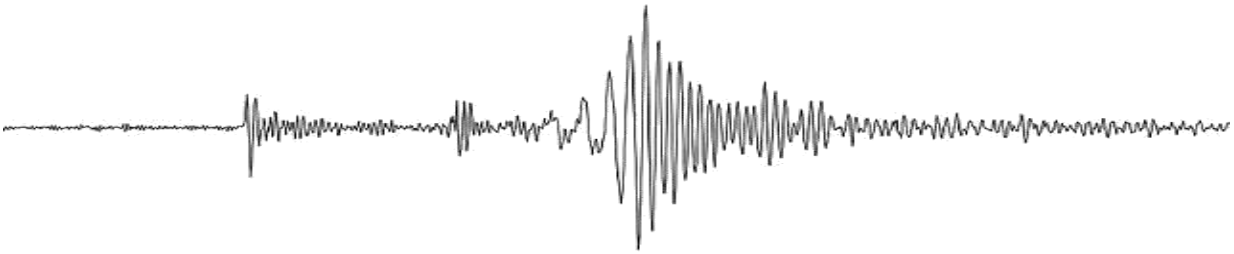

CHAPTER 4

CASE STUDY 2: CONTINENTAL ALASKA & ALEUTIAN ARC-TRENCH SYSTEM

THE SEISMOGENETIC SYSTEM OF ALEUTIAN – ALASKAN SYSTEM

Alaska and the Northern Cordillera were relatively unexplored geologically before the 1950's as they were sparsely populated. The growth of mining and oil companies during the second half of the 20th century led to a better understanding of geological features of the broader area but the great Gulf of Alaska earthquake of 27 March 1964 of Mw 9.2 led to an additional focus on earthquake hazards. For more than four decades after this super-quake most scientists still regard their research as work in progress. However, several recent publications including those of Ridway et al., (2007), Freymueller et al., (2008) and most recently Li et al., (2013) have enabled to summarize previous studies for a general readership. Moreover, the studies of the 1964 earthquake stimulated new research into the broader area including the Cascadia subduction zone, which had not been considered as a major earthquake hazard because of its low instrumental seismicity. At present, Cascadia is perceived as having the potential for a great Mw 9 earthquake, and the earthquake history of the Aleutian subduction zone, which has experienced three super-quakes in the twentieth century, including the 1964 event in the Gulf of Alaska, is a foretaste of the earthquake future of the area.

The Aleutian Arc and Continental (mainland) Alaska source areas are bounded by the coordinates 50°N to 70°N and 196°W to 126°W. The principal structural and geodynamic feature of this area –which also defines the geographical borderline of the north Pacific Rim– is the boundary between North American and Pacific plates (Fig. 4.1). The eastern plate boundary is defined by the Queen Charlotte – Fairweather (QCF) dextral transform fault system, parallel to which the Pacific plate moves N-NW relative to the North American plate at a rate of approx. 50 mm/year. The plate boundary transits from transformational to convergent along a zone extending between (57.5°N 137°W) and 59°N 145.5°W, in which the Yakutat terrane accretes to the North American plate and complicates the interaction between the two plates; the boundary then continues westwards as the Aleutian Arc and Trench system. Landward of the QCF system, and apparently related to the plate boundary, lays the right-lateral Denali transform fault. This is an arcuate feature running in a northwesterly direction for approx. 750km, from about (59°N, 135.3°W) to about (63.5°N 147°W); it then bends westwards and continues almost parallel to the plate boundary for an additional 500km, to approx. (63°N, 155.2°W). The Aleutian Arc and Trench extends for approx. 3400km, from the northern end of the QCF

system in the east (near 58.5°N, 137°W), to a triple junction with the Ulakhan Fault and the northern end of the Kuril-Kamchatka Trench in the west (near 56°N, 196°W). Westward of the Alaska Peninsula (Unimak Pass, 55.7°N, 164°W), it transits from continental in the east to intra-oceanic in the west. Subduction along the Arc generates the Aleutian Volcanic Arc that extends as far as 182°W. The motion of the Pacific plate is always to the N-NW but due to the arcuate geometry of the trench, the relative velocity vector of the convergence changes from almost trench-normal in the east (Gulf of Alaska) to almost trench-parallel in the west. Along the continental part of the subduction the rate of convergence varies from 56mm/year in the east (Gulf of Alaska), to 63mm/year in the west (near Unimak Pass); along the oceanic part of the subduction the rate varies from 63mm/year in the east to 74 cm/year in the west (e.g. DeMets and Dixon, 1999).

For the most part, seismicity in Alaska can be attributed to the plate boundary between the Pacific and North American plates. Most of the seismic energy is released by large events that rupture large segments of the boundary and accommodate most of the motion between the two plates. Earthquakes in the Aleutian subduction zone include bending-moment normal-faulting events near and seaward of the trench, interplate earthquakes with a maximum depth of seismic coupling of 35–41 km (Tichelaar and Ruff, 1993), earthquakes within the downgoing slab, and earthquakes within the upper plate between the aseismic accretionary wedge and the volcanic arc. Earthquakes are recorded in the subducted slab to depths greater than 200 km in the central Aleutians but only to 150 km beneath the Gulf of Alaska where the slab is younger and hotter

Within the North American plate (Continental Alaska), the highest seismicity rates are observed in southern Alaska, parallel to the plate boundary and decrease northwards, away from it. Fault-plane solutions of moderate earthquakes in south-central, central, and northern Alaska typically exhibit strike-slip kinematics with northwesterly to northerly compressional axes, whereas solutions in west-central Alaska generally exhibit normal faulting with northerly oriented tensional axes. Thus, with the exception of west-central Alaska, both the distribution of earthquake activity and the available focal mechanisms are qualitatively consistent with the hypothesis that the seismicity of Continental Alaska originates in the interaction of the Pacific Plate and North American plates (e.g. Page et al., 1991 and references therein). Moreover, it appears that the plate boundary is not composed of a single fault system but involves several secondary faults both seaward and landward of the primary boundary, which accommodate a small fraction of the relative plate motion. The Aleutian Arc and Trench system generates large numbers of

earthquakes in the crust, as well as in the subducting and overriding plates. Additionally, many earthquakes are associated with the activity of the Aleutian Volcanic Arc. Most large earthquakes in the region have thrust mechanisms indicating that they occur on the plate interface. However, some shallow (< 30km) events have either strike–slip or normal faulting mechanisms.

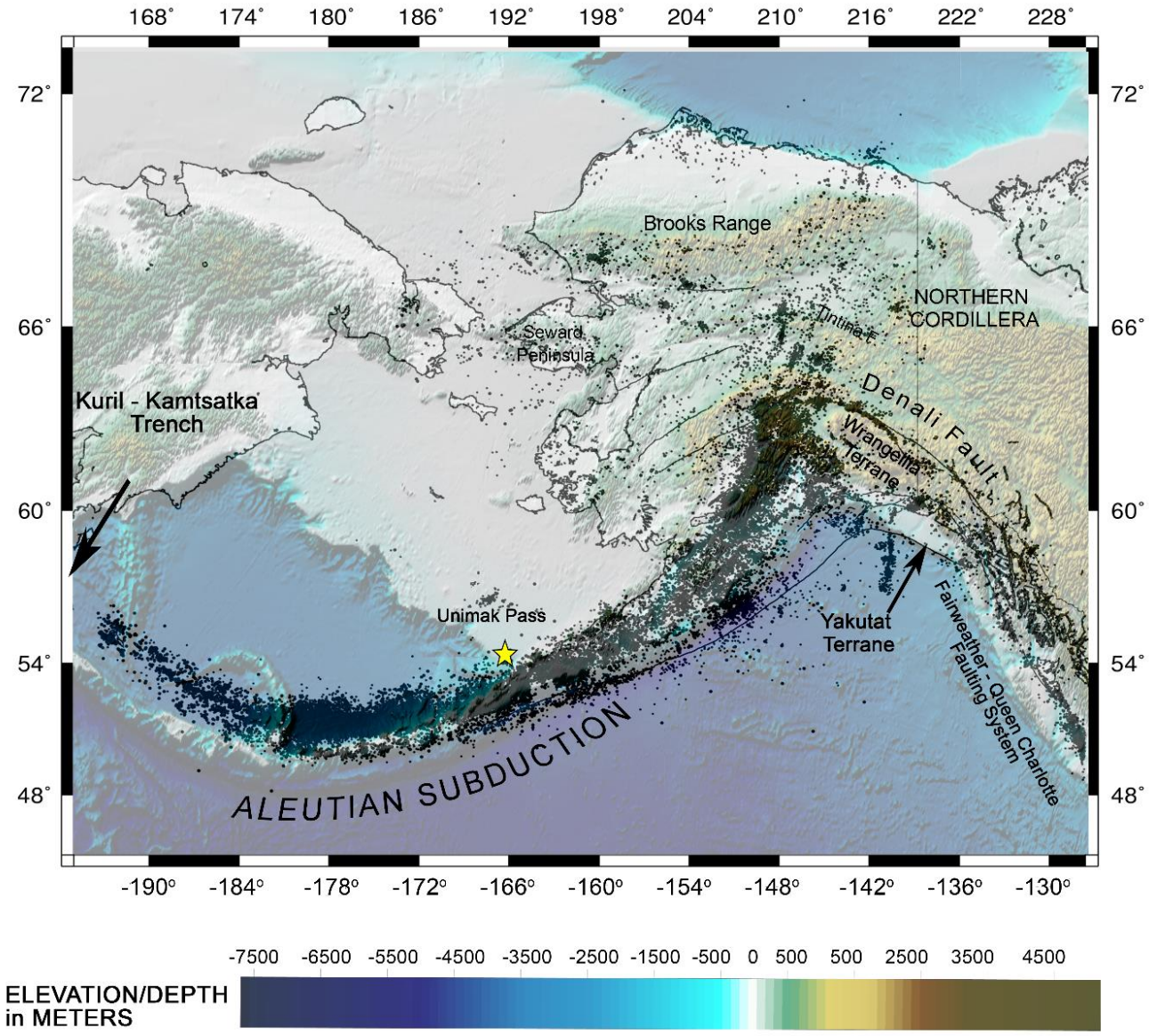

Figure 4.1 The seismicity of Continental Alaska as illustrated by mapping the epicentres of earthquakes included in the full AEIC catalogues for the period 1968–2015.

4.1 ALASKAN- ALEUTIAN CRUSTAL AND SUBCRUSTAL SEISMICITY

4.1.1 Aleutian zone

The Aleutian Arc Trench system is best known for generating great earthquakes and associated tsunamis, and for producing numerous volcanic eruptions. The Aleutian region produces thousands of earthquakes each year that manifest the subduction zone processes. The earthquakes are associated with faulting along the Aleutian megathrust, as well as faulting within both the subducting and overriding plates. Additionally, hundreds of earthquakes associated with Aleutian volcanic activity occur every year. Many of the regional earthquakes have identified source models, which makes it possible to differentiate between interplate and intraplate events. Most of the events have thrust mechanisms indicating that they occur on the plate interface. However, some shallow (depths less than 30 km) events have either strike–slip or normal faulting mechanisms. Most of the normal faulting events occur in the Aleutian outer rise region and are caused by bending of the plate as it enters the trench, while most of the shallow strike–slip events are concentrated along the island axis. Lu and Wyss (1996) studied tectonic stresses along the Aleutian subduction zone based on associated earthquakes' focal mechanisms. They concluded that directions of maximum compressive stress change along the Arc and identified several segments with homogeneous stress conditions. The boundaries between the identified blocks are most strongly correlated with the fracture zones and ends of rupture zones of great earthquakes. In the Aleutian region, the maximum horizontal stress direction is not perpendicular to the trench, but parallel to plate motion (Cross and Freymueller, 2007, 2008; Lu and Wyss, 1996). Ruppert et al., (2011) computed stress directions from source parameters of crustal earthquakes in the central Aleutian Arc. Stress directions in the overriding plate differ from those computed for the subduction interface.

Prior to expansion of the Aleutian seismic network at the end of the 1990s, earthquakes in the region were located and reported by the National Earthquake Information Center (NEIC). Only larger events (magnitude 4 or greater) were located, and all had large location uncertainties due to the absence of recordings at regional distances. Some of these events were large enough (magnitude 5.5 or greater) to be identified by the Global CMT project (Dziewonski et al., 1981).

4.1.2 Alaskan crustal faults

Although crustal faults are a secondary effect of subduction and collision zones, especially those close to the plate boundary, some are large enough to constitute their own independent seismic hazard (Plafker et al., 1994, Wesson et al., 2007). Continental Alaska could be divided into four microplates based on GPS velocities. As defined by Freymueller et al. (2008), and earlier by Lahr and Plafker (1980), these include: **a) the Southern Alaska** Microplate, rotating counter-clockwise about a pole in the Gulf of Alaska, **b) the subducting Yakutat Microplate** moving northwestward parallel to the c) **QC**-**Fairweather fault** at 40–49 mm/yr, and d) **the Bering Microplate** including the Bering Sea and possibly much of western Alaska, rotating slowly clockwise about a pole in eastern Siberia, moving southwestward parallel to the Aleutian Islands, with a diffuse, poorly defined boundary with the Southern Alaska Microplate (Freymueller et al., 2008). The Southern Alaska Microplate is rotating at a rate as high as 7 mm/yr, an average rate for the central Denali fault that fits a small circle about the pole of rotation in the Gulf of Alaska.

Herein the crustal seismicity of the Continental Alaska is examined in accordance to the following subset areas (see also Fig.4.2 and 4.3):

a) SOUTH ALASKA – Wrangelia terrane – Yakutat microplate.

Southern Alaska is dominated by the Wrangellia composite terrane (superterrane or microcontinent). The term “Wrangelia” is applied to a number of terranes and comprises Wrangell Terrane, Peninsular Terrane, and other rock units that were not originally part of the North American craton. It also comprises a composite terrane which also includes the Alexander Terrane. The Wrangelia superterrane extends along the Pacific margin of North America, from Vancouver Island, British Columbia, to south-central Alaska and is characterized throughout by similar rock sequences.

Another distinct South Alaskan block is the Yakutat microplate. This is a small composite oceanic-continental terrane that has migrated north-westward with the Pacific plate along the North America western margin and has been colliding obliquely with the continent in the corner of the Gulf of Alaska since the Miocene (e.g., Lahr and Plafker, 1980; Bruns, 1983; Plafker et al., 1994). The block acts as an indenter, resulting in crustal thickening, rapid uplift and intense seismicity in the adjacent Saint Elias and Chugach Mountains. The Yakutat block is being forced to the west around the corner of the Gulf of Alaska along a series of strike-slip and thrust faults. The Yakutat microplate is bounded on the

east by the Fairweather strike-slip fault, on the north by the Chugach–St. Elias thrust belt, on the west by the Kayak Island structural zone, and on the south by the Transition fault system. The Yakutat–Pacific plate boundary is found where the northeast-striking Aleutian megathrust changes strike eastward to the Transition fault. Fletcher and Freymueller (2003) and Haeussler (2008) pointed out that the Pacific Plate subducts beneath Alaska at a rate of 53 mm/yr whereas the Yakutat Microplate collides with and subducts beneath Alaska at a rate of 40–49 mm/yr in a more northwesterly direction (Figure 2.6). The difference represents convergence between the Yakutat and Pacific plates. However, this convergence has not been accommodated across the Chugach–St. Elias thrust faults for the past million years (Wallace, 2008), indicating that convergence during that time has been taken up across more diffuse structures, as supported by thermochronology (Berger and Spotila, 2008).

b) NORTH EAST ALASKA – Northern Cordillera

North-East Continental Alaska is bounded by 61^{o} to 68^{o} N/ 135^{o} to 150^{o} E and comprises a part of the broader area of Northern Cordillera. NE Alaska exhibits considerable current tectonic activity evidenced by strong seismicity, as a result of the continental collision between the composite oceanic Yakutat terrane and North America plate in the corner of the Gulf of Alaska (e.g., Plafker et al., 1994). To the west, the Pacific plate subducts beneath North America along the Aleutian-Alaskan trench at 60 mm/a, and to the SE lies the Queen Charlotte/Fairweather Pacific–North America transform boundary. Oceanic crust of the western Yakutat terrane is currently subducting beneath N. America to the NW (e.g., Plafker, 1987).

Intense seismicity occurs not only in the region of the Chugach–St. Elias thrust fault system (e.g., 1979 Mw 7.3 event), which forms the northern boundary of the Yakutat block with North., but also in the region north of Denali Fault. Earthquakes occur mainly along NE trending zones (Figure 4.3); left-lateral strike-slip focal mechanisms are consistent with the inferred Tertiary motion on subparallel faults to the SE (Page et al. 1995). Distributed seismicity continues northward at decreasing rates over a NE trending band through the NE Brooks Range of Alaska and extending slightly offshore to the Beaufort Sea (Figure 4.3). Earthquake mechanisms suggest a change from the NE-SW sinistral transpressional regime to the south to NE-SW sinistral transtension (Leonard et al, 2007).

c) TRANSFORM BOUNDARIES

Denali and Tintina Faults

The Denali Fault is a major intracontinental dextral (right lateral) strike-slip fault that extends from the central continental Alaska to the northwestern British Columbia Canada. The Denali fault may be divided into three sections based on its slip rate: a central section (CDF) with a slip rate of 10.5 ± 5.0 mm/yr, a western section (WDF) with a slip rate of 1.5 ± 0.5 mm/yr, and an eastern section (EDF), well to the east of the junction with the Totschunda fault, of 3.8 ± 1.4 mm/yr (Freymueller et al., 2008; Haeussler, 2008), although Matmon et al. (2006) found a slip rate 8 km east of the Totschunda intersection as high as 8 mm/yr. All of these rates are much lower than the Pacific–North America plate rate, the slip rate on the Fairweather fault, and the convergence rate of the Yakutat Microplate. The highest mountains in Alaska are the Alaska Range, close to the central Denali fault, north of the Chugach and Talkeetna mountains. Thermochronological data show that that major uplift and exhumation of the Alaska Range occurred during the Pliocene, starting around 6 Ma. However, there is increasing evidence for an earlier phase of deformation and exhumation starting at 25 Ma (Ridgway et al., 2007; Haeussler et al., 2008).

There, the Denali right-lateral strike-slip fault curves westward in a northward-convex syntaxis that is not predicted by the Pacific–North America plate vector. The curvature of the Denali fault was already in place by the Early Tertiary, placing the Alaska Range in a restraining bend relative to Pacific–North America plate motion and producing shortening and uplift. Another factor might be the buoyant Yakutat Microplate, undergoing flat-slab subduction unaccompanied by active volcanism and pushing existing terranes out of the way, principally southwestward. The Yakutat Microplate might account for the presence of earthquakes at 180 km depth beneath Mt. McKinley (Denali). The low dip of the subduction zone might produce greater coupling between the plates than expected in normal subduction, and this might produce higher mountains, as it does in the Cordillera Blanca of northern Perú

The Denali fault is considered an active fault despite the relatively low seismicity during the last decades (Ratchkovski et al., 2004). The 3 November 2002 Denali fault earthquake of Mw 7.9 was one of the largest strike-slip earthquakes in North America in the past century and a half (Eberhart-Phillips et al., 2003; Haeussler, 2008). The earthquake rupture began with 48 km of surface faulting on the previously unknown Susitna Glacier reverse fault, with displacement as high as 11m (Croneet al., 2004),

although InSAR indicated a smaller average slip of 7.3 m (Wright et al., 2004a). This was followed by 226 km of surface rupture on the central Denali fault to its intersection with the Totschunda fault, and another 66 km of surface rupture on the Totschunda fault (Eberhart-Phillips et al., 2003; Haeussler et al., 2004). Last time a similar earthquake of such magnitude (Mw 7.2–7.4) did occur on or near the fault on 6 July 1912 (Carver et al., 2004; Doser, 2004).

The Denali fault is clearly active, as discussed above, but the Tintina fault is not. The Tintina fault sustained a right-lateral strike-slip earthquake of ML 5.3 on 28 November 1972. However, the Tintina fault is interpreted by Haeussler (2008) as the northern margin of the seismically active zone of rotating blocks rather than being a thorough going active right lateral fault like the Denali fault. The Tintina fault does not curve into the west-trending Kaltag fault that is on trend with it to the west. The Kaltag fault was the source of a strike-slip earthquake of M 5.6 on 3 February 2000. Other earthquakes north of the Kaltag fault are the M 4.6 event of 6 October 1980 on the Kobuk fault and the Huslia earthquake of M 7.3 on 7 April 1958, a normal-fault event that is one of the largest earthquakes of Alaska's far north. These earthquakes are evidence that a large part of northern Alaska is seismically active (Ruppert et al., 2008).

Between the Denali and Tintina faults, instrumental seismicity aligns along northeast-striking zones, with left-lateral fault-plane solutions (Page et al., 1995; Ruppert et al., 2008; Figures 4.5a and 4.5b). From west to east, the northeast-trending seismic zones include the Dall Creek zone with an earthquake of Mw 6.1 on 9 March 1985, the Rampart zone with an earthquake of M 7.1 on 29 October 1968, the Minto Flat zone with an earthquake of Mw 6.0 on 6 October 1995 and another earthquake of Mw 5.8 on 29 November 2000, the Fairbanks zone with an earthquake of M 6.1 on 21 June 1967, and the Salcha zone with an earthquake of M 7.3 on 22 July 1937, the largest on any of the northeast-trending seismic zones. In addition, the Kantishna seismic cluster, with the largest event M 5.2, is located southwest of the Minto Flat zone close to the Denali fault (Ruppert et al., 2008). The Fairbanks seismic zone is close to the city of Fairbanks and is a seismic hazard to that city. If the region between the Denali and Tintina faults is in a broad right-lateral shear couple, tabular blocks bounded by northeast-striking faults should rotate clockwise and produce left-lateral strike-slip fault-plane solutions, another example of bookshelf tectonics.

Although the seismic zones are well expressed and follow northeast-striking left-lateral faults, these zones show no surface evidence of Holocene tectonic rupture, and linear earthquake zones tend to lie northwest of mapped faults (Page et al., 1995).

Queen Charlotte- Fairweather Transform Boundary

The Queen Charlotte-Fairweather (QCF) system extends 1200 km between Vancouver Island and southern Alaska. The northernmost 200 km of the fault are onshore, and this part of the fault forms the eastern boundary of the Yakutat block and strikes N34°W. Queen Charlotte-Fairweather Fault, is a transform boundary that accommodates most of the Pacific – North America (PA/NA) relative plate motion and thus it is considered as the northern cousin of the San Andreas Fault[8]. To the south right-lateral shear produced by the northwestward motion of the Pacific Plate with respect to the North American Plate is concentrated on the Queen Charlotte fault, whereas to the north it is distributed among the Queen Charlotte – Fairweather fault system, the Chatham Strait – Denali fault system, and the Transition fault zone (Lahr and Plafker, 1980). Both the geologic evidence for the displacement rate along the Fairweather fault (Plafker et al, 1978) and the historical record of large earthquakes support the view that the Queen Charlotte – Fairweather fault zone is the principal plate boundary (Tobin and Sykes, 1968; Page, 1973). The historical record of earthquakes with M≥ 7 includes 4 events along the Queen Charlotte – Fairweather fault zone (1927, 1949, 1958, and 1972), all of which involved dextral slip (Stauder, 1959; Rogers, 1986; Stauder, 1960; Perez and Jacob, 1980). The 1927 shock of M 7.1 was located near latitude 57.7°N; this event was followed by an Mw 8.1 shock in 1949 on the Queen Charlotte fault, which nucleated south of the areas ruptured a segment totaling 470 km in length (Rogers, 1986). In 1958, an M 7.9 earthquake broke about 350 km of the Fairweather fault (Ben-Menahem and Toksoz, 1963; Tobin and Sykes, 1968) with as much as 6.6 m of dextral surface slip measured onshore (Tocher, 1960). The 1972 M, 7.4 Sitka earthquake ruptured a 190-km segment of the fault system between the northern limit of the 1949 fault break and the southern limit of the 1958 break (Page, 1973), with inferred slip of 7 m in the epicentral region (Schell and Ruff, 1989).

[8] The SAF, like the Queen Charlotte–Fairweather fault to the north, is part of the transform boundary between the Pacific Plate and North America Plate. Its north end is a triple junction involving the Pacific, North America, and Gorda plates; the west-striking boundary between the Pacific and Gorda plates is the Mendocino Transform fault. North of the Mendocino Transform, the Gorda Plate is subducting beneath North America with a dip of 9º–11º, and south of it, the Pacific Plate is sliding past North America along a boundary that strikes approximately N 40º W.

Prior to 1972, this plate-boundary segment had been identified as a seismic gap and a likely site for an earthquake (Tobin and Sykes, 1968; Kelleher, 1970; Sykes, 1971).

WESTERN ALASKA – Seward Peninsula

The western part of Continental Alaska (west of 153ºW) which includes the Seward Peninsula and a part of the Bering block is characterized by progressively diffused seismic activity. The historical record of seismicity includes four earthquakes of magnitude 6.0 or greater in western Alaska, of which the largest was the 1958 Huslia earthquake and four in the Chukchi Sea. The Ms 7.3 Huslia shock produced extensive failures in surficial unconsolidated deposits within an elongate northeast-striking zone that possibly betrays a buried culprit fault (Davis, 1960). Predominantly normal slip on a plane subparallel to the trend of the failure zone is inferred from the published fault-plane solutions (Wickens and Hodgson, 1967; Estabrook et al, 1988). Two magnitude 6 aftershocks followed. The second largest shock was the M, 6.9 Chukchi Sea earthquake of 1928; three magnitude 6 shocks followed this event. All three of these events were poorly located. The remaining magnitude 6 earthquake occurred on the southern Seward Peninsula in 1950; little is known about this shock. Regional seismic monitoring in the vicinity of the Seward Peninsula from 1977 to 1982 (Biswas et al, 1986b) affords a more detailed view of the seismicity in western Alaska. In the magnitude range 2.0 to 5.0, activity seems to be widespread throughout this part of Alaska and the adjacent offshore regions and confined to shallow depths. The most complete and accurate data are from the area 64 to 67°N, 161 to 168°W. The mapped seismicity forms a diffuse cloud punctuated by several clusters; no prominent linear trends are apparent (Fig.4.3). The broad distribution of activity suggests that seismic deformation is distributed over many active faults and not concentrated on one or two major fault systems. To some degree, location errors contribute to the apparent scatter in the mapped epicenters. The Bendeleben and Kigluaik faults are the principal mapped active faults on the Seward Peninsula, both of which exhibit Holocene normal displacement (Hudson and Plafker, 1978). However, activity does not concentrate along these faults; diffuse seismicity is mapped both north and south of the Kigluaik fault; it is not clear whether any of this activity actually centers on the fault.

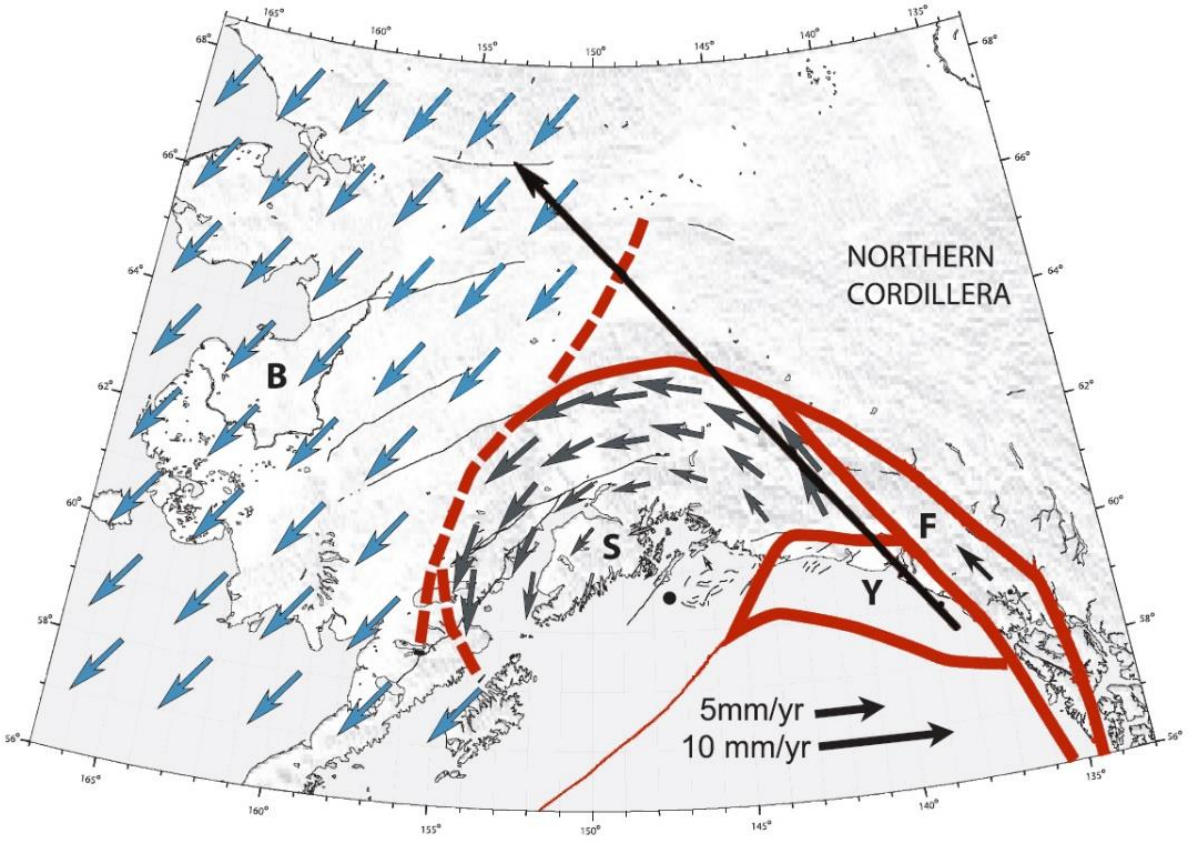

Figure 4.2 Subdivision of Alaska into microplates based on GPS, with motion vectors relative to stable North America. Microplate names: **B**, Bering; **F**, Fairweather; **S**, Southern Alaska; **Y**, Yakutat; block boundaries in thick red lines. Southern Alaska–Bering microplate boundary uncertain; more than one solution shown. Eastern boundary of Fairweather microplate follows eastern Denali, Duke River, and Chatham Strait fault, even though Chatham Strait fault is not known to be active. Western boundary assumes a “Connector” fault between Totschunda and Fairweather faults, although such a fault has not been documented, and the slip rate on the Fairweather fault is very high in comparison to that on the Totschunda fault. Solid dot is pole of rotation of Southern Alaska Microplate. Thinner gray lines: active faults modified from Plafker et al. (1994b). Pacific–North America vector not shown but would be longer than the Yakutat–North America vector. From Freymueller et al. (2008)

The above outlined seismotectonic setting results in the following earthquake source areas:

a) **The Aleutian Arc- Trench System** (ATC- ATD) extending from the Gulf of Alaska to the NW end of the Kuril-Kamtsatka Trench

b) The Continental Alaska divided in various microplates:

Subset area A: From South to North the Wrangelia Terrane extending up to the Alaskan Cordillera up to Brooks Range

Subset area B: Queen Charlotte – Fairweather and Denali Fautling systems to the East

Subset area C: Western Part of Continental Alaska including the Seward Peninsula

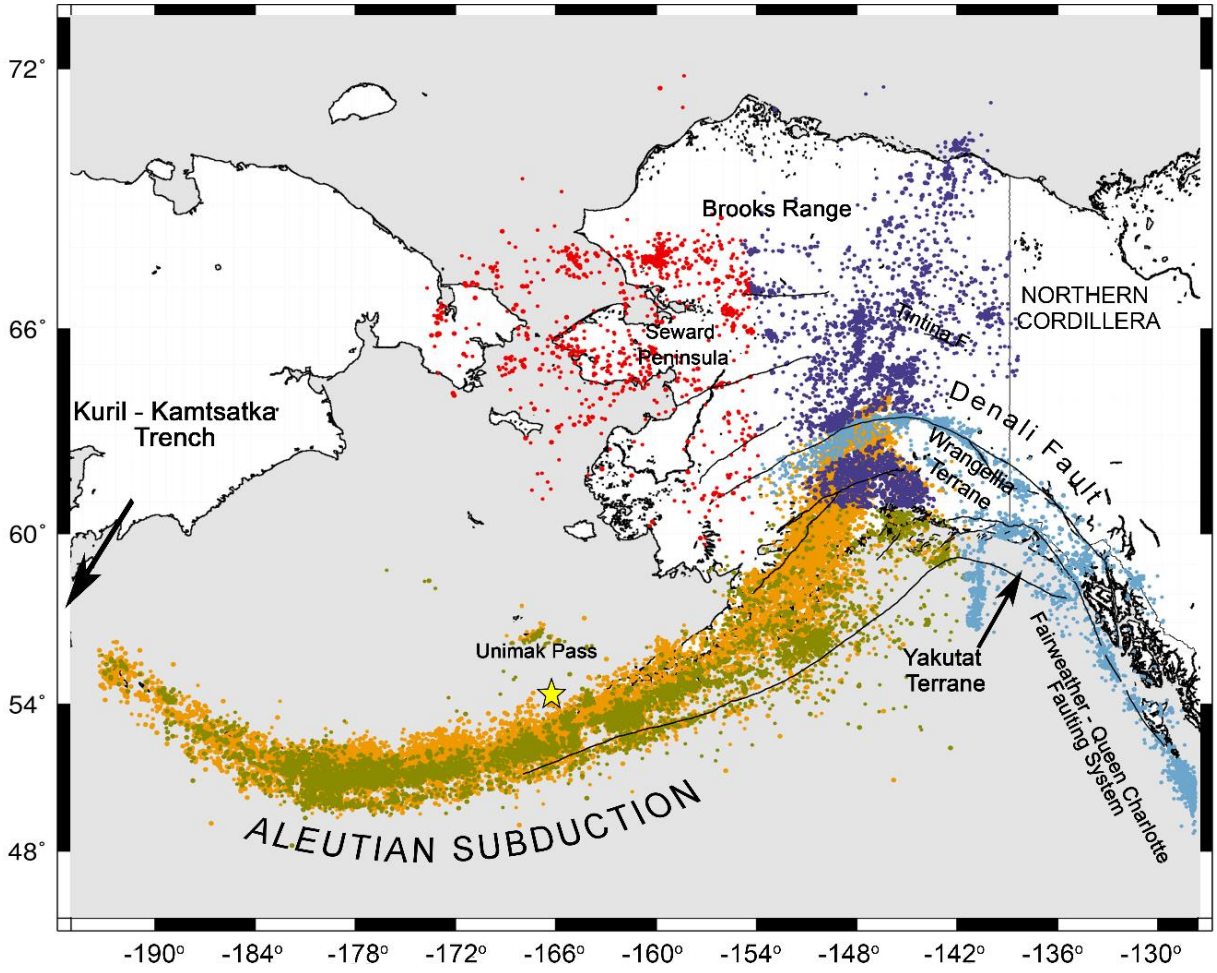

Figure 4.3 Alaskan earthquake epicenters and major faults. Different subset areas are illustrated with different colors:

4.2 EARTHQUAKE DATA

The earthquake data utilized for the source areas of Continental Alaska and the Aleutian Arc was extracted from the regional earthquake database of the Alaska Earthquake Centre (http://www.aeic.alaska.edu/html_docs/db2catalog.html) and comprises a total of 48,995 events recorded in the area 50°N to 70°N and 196°W to 126°W over the period 1968–2015. In the AEC catalogue the overwhelming majority of events is reported in the M_L magnitude scale. However, a significant number is reported *only* in the surface (M_S) and body wave (m_b) magnitude scales. On the bright side, another significant number is reported in multiple magnitude scales and of these, 1715 are jointly reported in the M_L, M_S and m_b scales. It is, therefore, straightforward to generate calibration tables by which to convert M_S and m_b to M_L. This exercise was carried out by robust re-weighted linear regression with a re-descending bisquare influence function. The $M_L - M_S$ relationship is shown in Fig. 4.4Aa and the resulting regression (calibration) formula is

$$M_L = (1.074 \pm 0.018) \times m_b - (0.4099 \pm 0.0942), \qquad 4 \leq m_b \leq 7.2.$$

The $M_L - m_b$ relationship is shown in Fig. 4.4Ab and the corresponding regression formula is

$$M_L = (0.712 \pm 0.013) \times M_S + (1.651 \pm 0.066), \qquad 3.5 \leq M_S \leq 7.5.$$

The relationships between $M_L - m_b$ and $M_L - M_S$ are obviously linear so that the regression coefficients rather precisely determined. Thus, acknowledging the problems associated with the saturation of the local and body wave scales at the large magnitude end of the spectrum, and assuming that both relationships can be linearly extrapolated to smaller magnitude scales, it is possible to construct a homogeneous version of the AEC catalogue with all events reported in the local magnitude scale.

The AEC catalogue presents a conundrum: Fig. 4.4A.c clearly shows that F–M distribution of seismicity recorded along the Aleutian Arc is bimodal, a feature not present in the seismicity of Continental Alaska (Fig. 4.4A.d). For magnitude scales between M_L =3 and 4.3 the b value is 0.47 and for $M_L \geq 4.4$ increases, almost abruptly, to 1.1. The origin of this bimodal distribution might be natural, (different physical mechanisms operating at small and intermediate-large magnitude scales), although b values as low as 0.47 over so broad an area are not easy to explain. On the other hand, as can be seen in the incremental distribution (downward pointing triangles in Fig. 4.4Ac) the escalation of frequency is faltering between M_L = 3.9 and 4.3 (events missing) and there is a rather

suspicious leap of about 5500 events between M_L = 3.0 and 3.1 (event surplus), which is also difficult to explain naturally. Given, also, is the relative sparsity and almost one-dimensional geometry of the monitoring network along the Aleutians (see https://earthquake.alaska.edu/network) and the difficulties associated thereof, with the detection of small earthquakes. Finally, it is not difficult to verify that bimodality is definitely more pronounced in the western (oceanic) part of the convergence (west of Unimak Pass), where the network is sparsest. As a result, one cannot be certain that the differences between the small and intermediate-large magnitude scales are natural and therefore it is difficult to investigate this rather non-trivial issue in the space available herein. From Figs. 4.4A and 4.4B it is apparent that the homogenized version of the AEC catalogue is complete for $M_L \geq 3.5$ up to Unimak Pass while for the entire area of the Arc-trench system the catalogue is complete for $M_L \geq 4.4$. In consequence, and as far as the Aleutian Arc and Trench is concerned, I shall consider earthquake populations with $M_L \geq 3.5$ only for the area up to Unimak Pass, while for the broader area I will consider only the intermediate and large earthquake population ($M_L \geq 4.4$), for which the F-M distribution, albeit imperfect, does raise concerns about its constitution. Conversely, in Continental Alaska I shall consider all earthquakes with magnitudes $M_L \geq 3$, for which the catalogue appears to be complete (Fig 4.4Ad).

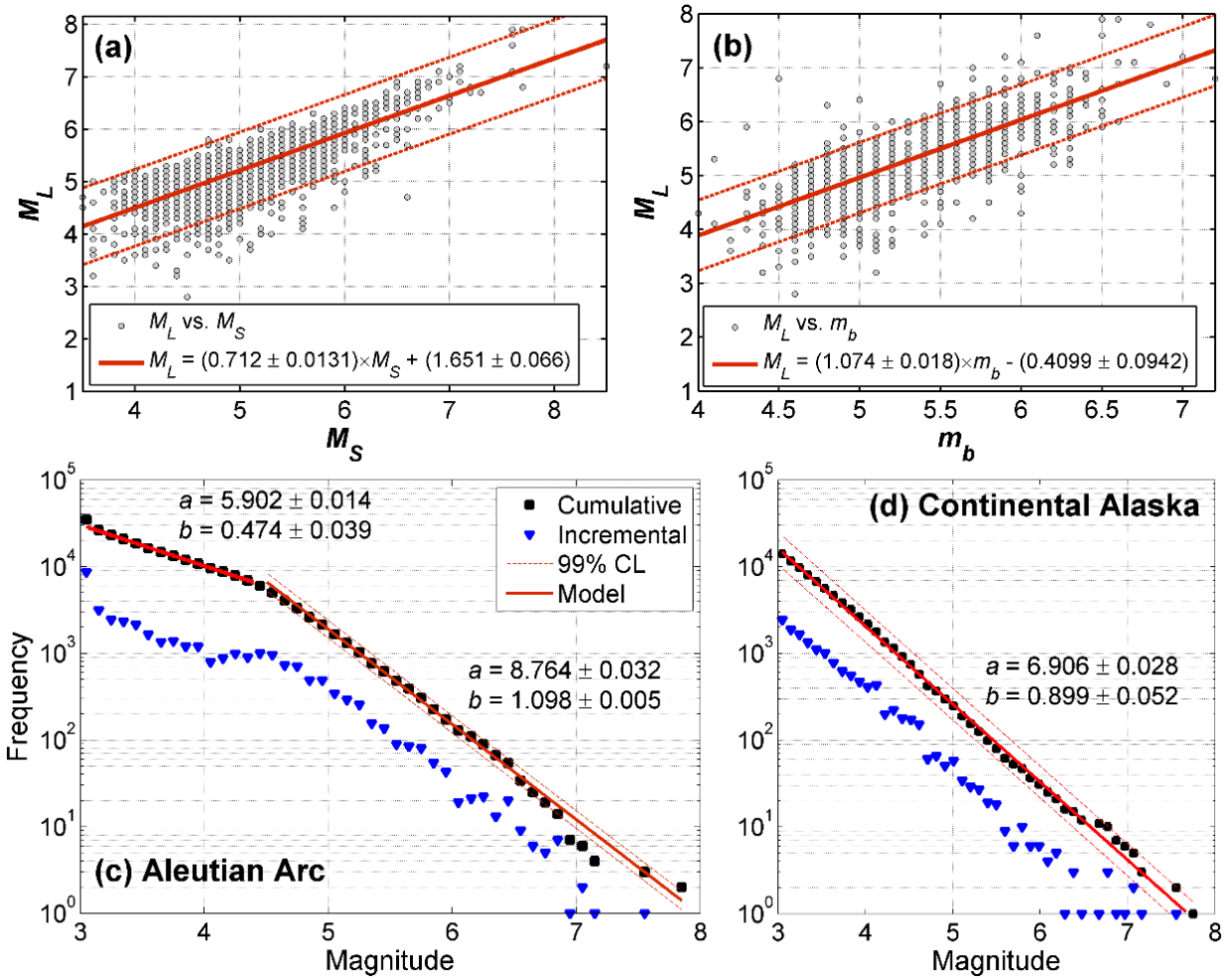

Figure 4.4A (a) Relationship between local and surface wave magnitude scales and **(b)** between the local and body wave magnitude scales, for the area of Alaska and the Aleutian Arc. Analysis based on 1715 events jointly reported in the M_L, M_S and m_b magnitude scales, in the catalogue of the Alaska Earthquake Centre. The regression lines were fitted with robust linear least squares; broken lines mark the 95% confidence limits. **(c)** The frequency – magnitude distribution of seismicity along the Aleutian Arc and Trench. **(d)** As per 4.4Ac for continental Alaska. Down pointing solid triangles represent the incremental distribution; solid squares represent the cumulative distribution; broken lines are 99% confidence limits.

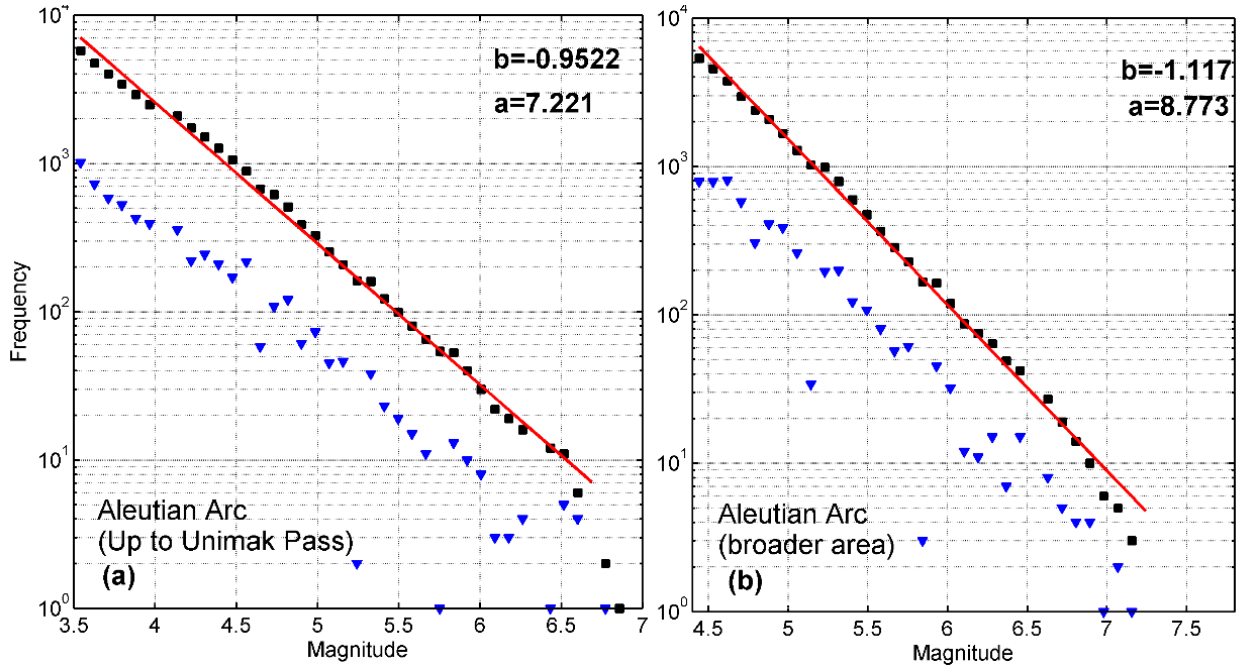

Figure 4.4B (a) The frequency – magnitude distribution of seismicity along the Aleutian Arc and Trench system up to Unimak Pass. **(b)** As per Fig. 4.4Ba for the broadr area of the Aleutian Arc and Trench system . Down pointing solid triangles represent the incremental distribution; solid squares represent the cumulative distribution; broken lines are 99% confidence limits.

As evident in the foregoing, seismogenesis in Alaska and the Aleutian Arc develops in a rather complex tectonic background, extends over a very large area and range of depths and exhibits regional variation. For these reasons, it is not feasible to thorough examine the entire area of Continental Alaska and the Aleutian Arc. In this area it is possible to distinguish three classes of earthquake activity: a) crustal earthquakes in Continental Alaska primarily associated with the eastern transformational plate margin, b) crustal earthquakes along the Alaskan – Aleutian Arc primarily associated with the convergent plate margin and, c) sub-crustal earthquakes along the Alaskan – Aleutian Arc associated with the subducting slab. This provides an opportunity to study and compare the statistics of earthquakes generated in different seismotectonic settings, environmental (crust vs. subducting slab) and boundary conditions (free in the crust vs. fixed in the slab), and to inquire whether said differences affect the dynamic expression of the fault network.

Following the above reasoning, I will inquire the statistical nature of crustal seismicity:

a) along the eastern transformational plate boundary defined by the Queen Charlotte – Fairweather and Denali faults; this area will henceforth to be referred to as Queen Charlotte - Denali zone, or QCD

b) Along the transitional zone spanned by the Wrangelia Composite terrane including the seismicity north of Denali fault at the Alaskan part of Northern Cordillera; this area will henceforth to referred to as Wrangelia zone or WNG, and

c) The western part of continental Alaska or the Bering microplate henceforth referred to as ALW

The statistical nature of seismicity observed along the convergent plate boundary will be also inquired but in this case, a separate analysis of crustal and sub-crustal earthquakes is conducted; As crustal earthquakes are considered those which nucleate in the brittle domain, i.e. the schizosphere (less than 20 km depth), while the subcrustal earthquakes are distinguished according to the depth of the Mohorovičić discontinuity, which varies beneath the Yakutat – Wrangelia terrane and along the Aleutian Arc (see Figures 4.5a, 4.5b and 4.6).The crustal seismicity and earthquake catalogues will henceforth be referred to as ATC (Aleutian Trench Crustal), while their sub-crustal counterpart will be referred to as ATD (Aleutian Trench Deep). The epicentral distributions of the QCD, WNG, ALW, ATC and ATD earthquakes are illustrated in Fig. 4.3; information about the respective catalogues is summarized in Table 4.1.

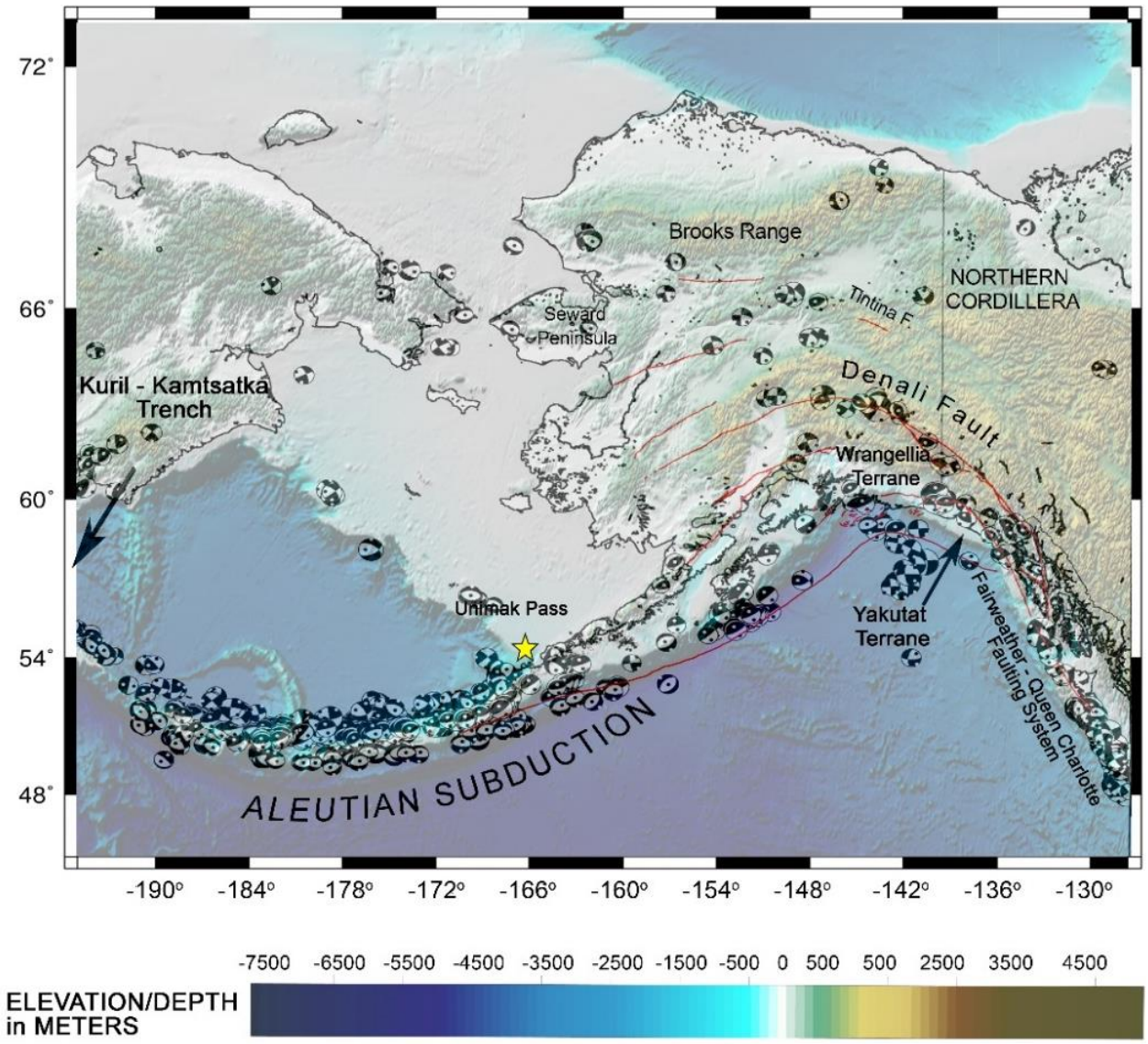

Figure 4.5a Faults and focal mechanisms of crustal earthquakes in the broader area of Continental Alaska – Aleutian Arc; the beach balls mechanisms are plotted on their ISC primary coordinates.

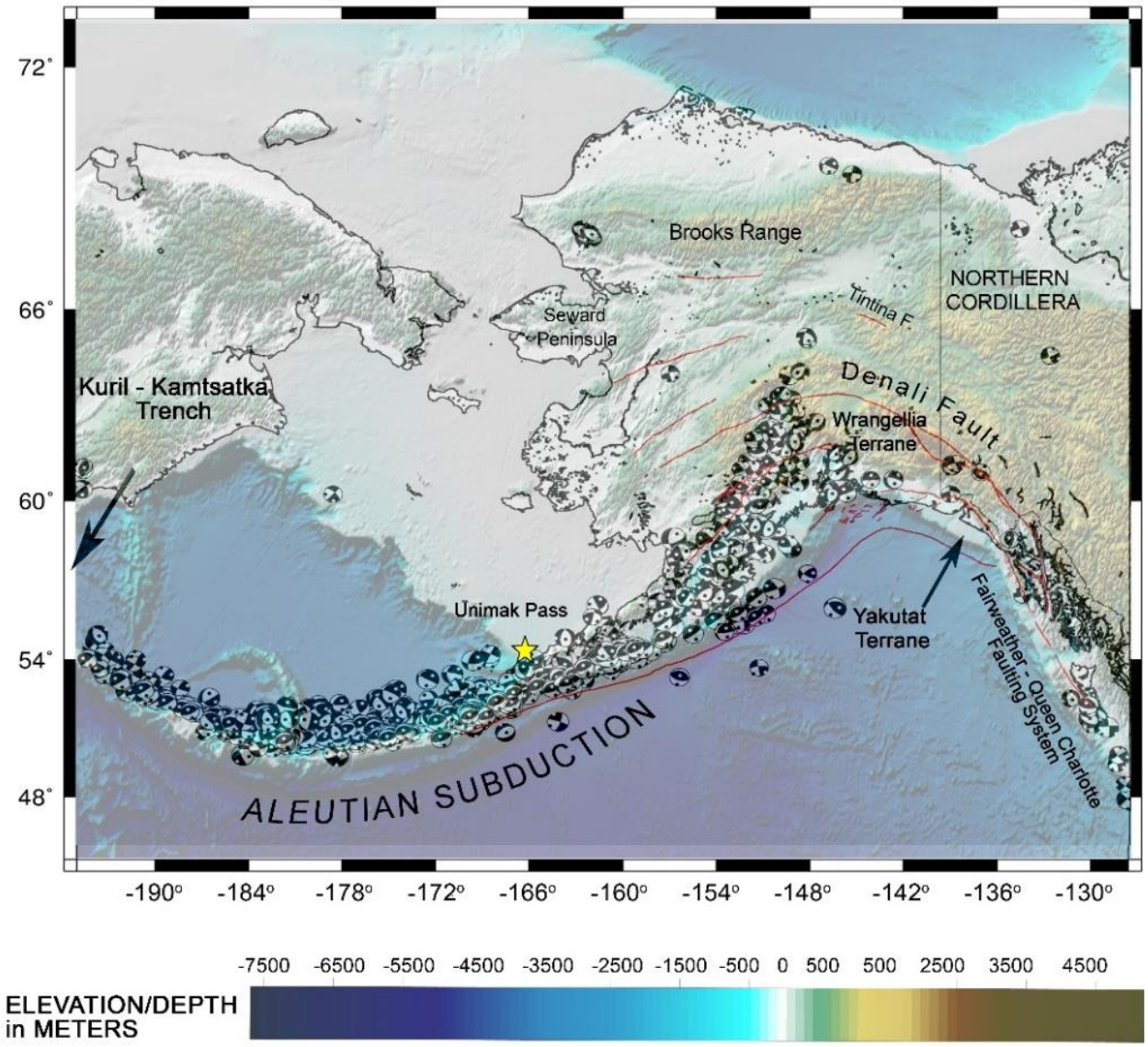

Figure 4.5b Faults and focal mechanisms of sub-crustal earthquakes in the broader area of Continental Alaska – Aleutian Arc; the beach balls mechanisms are plotted on their ISC primary coordinates.

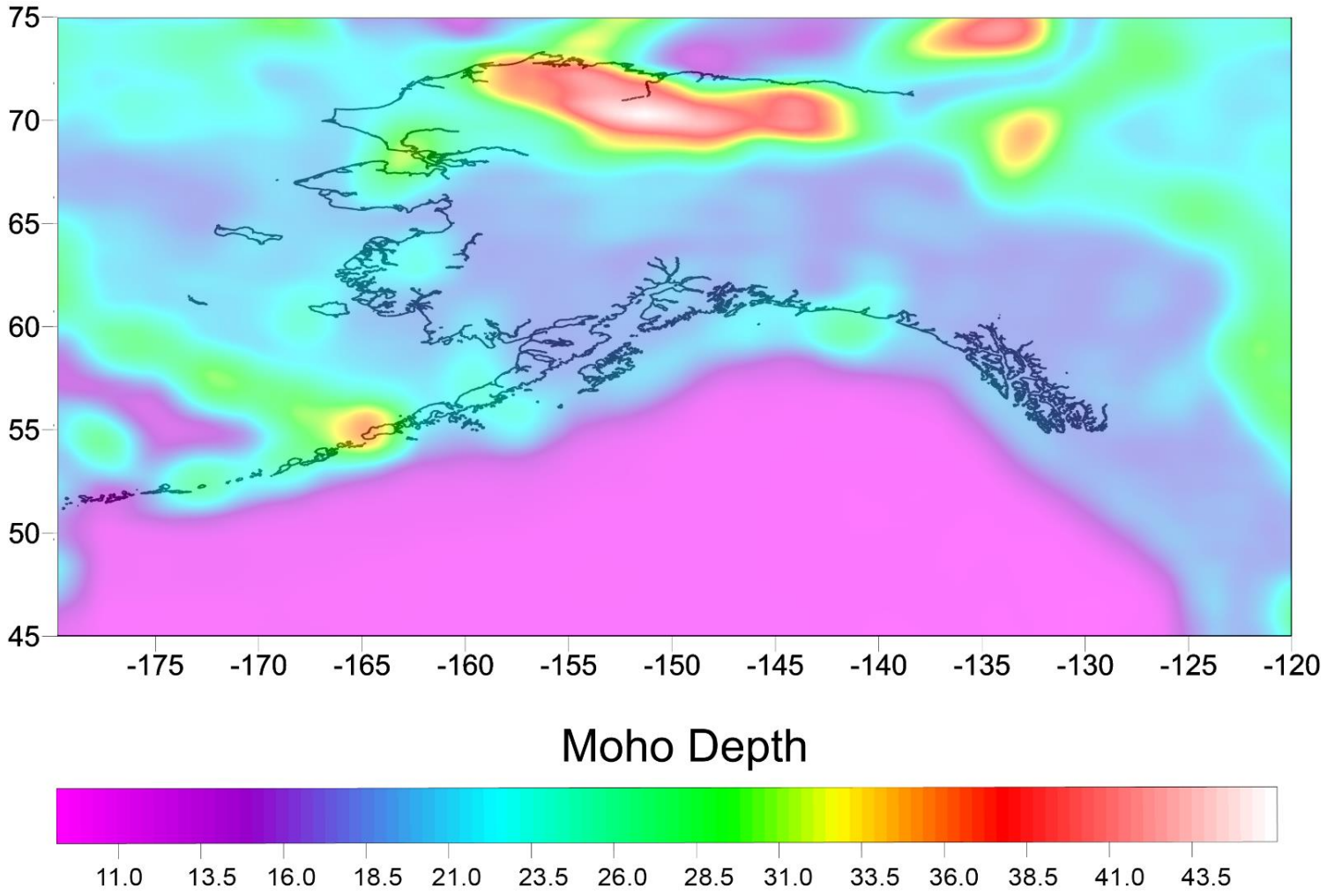

Figure 4.6 Estimated Moho surface for Alaska and Aleutian Arc. The Moho depth ranges from 11 km (fixed minimum) under the Pacific plate to 48 km beneath Cook Inlet (Saltus et al., 2007).

TABLE 4.1. Summary of Alaskan system earthquake catalogues used in the present analysis.

Source Area	**Source Area Code**	**Period**	**M_{comp}**	**depth (km)**	**Full catalogues**	**Declustered catalogues** ($\phi_i \geq 70\%$)	**Declustered catalogues** ($\phi_i \geq 80\%$)	**Declustered catalogues** ($\phi_i \geq 90\%$)
					№ events	№ events	№ events	№ events
Aleutian system (subcrustal) up to Unimak Pass	**ATD**	1968-2015	3.5	Moho	4767	3981	3735	3165
Aleutian system (subcrustal) complete data set			4.4		5367	1381	1294	1092
Aleutian system (crustal) up to Unimak Pass	**ATC**	1968-2015	3.5	<20	3263	1563	1374	1015
Aleutian system (crustal) complete data set			4.4		1278	947	860	693
Queen Charlotte – Fairweather – Denali Fault	**QCD**	1968-2015	3.0	<20	4332	1639	1380	899
Wrangelia terrane and NE Continental Alaska	**WNG**	1968-2015	3.0	<20	4164	2563	2245	1578
Western Continental Alaska – Seward Peninsula	**ALW**	1968-2015	3.0	<20	1089	487	470	395

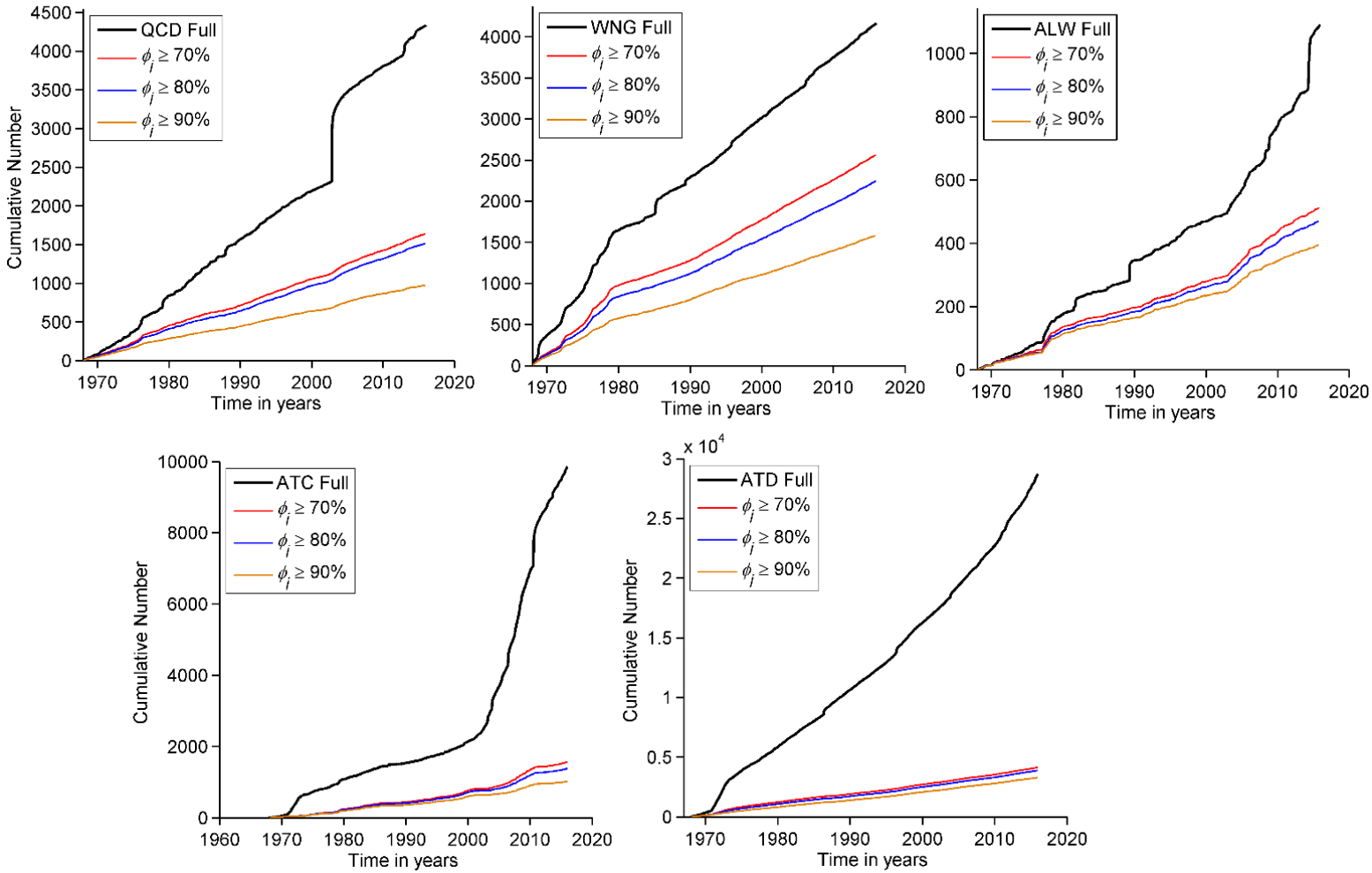

Figure 4.7 Cumulative event count of the full and declustered AEIC catalogues for the period 1968 – 2015

4.3 NESP RESULTS FOR ALASKAN EARTHQUAKE CATALOGUES

4.3.1. Analysis of Full earthquake catalogues for 1968 – 2015

Let us now conduct a comparative analysis of the seismicity observed: **a)** along the two major microplates of the continental Alaska, i.e the Wrangelia – North Alaska microplate and the Bering (West Alaska) microplate, **b)** along the major transform boundary between the North American and Pacific plates: Queen Charlotte – Fairweather and Denali zone of transform faults (QCD) and **c)** the Aleutian Arc and Trench system (AT) formed by the northerly subduction of the Pacific Plate under the North American plate. The earthquakes caused by the first two systems occur primarily in the schizosphere. The earthquakes caused by the latter system occur both in the crust and below the crust in association to the Aleutian Wadati-Benioff zone. In such a regional tectonic setting, let us take our enquiry one step farther by attempting to examine whether the environment in which seismogenesis occurs, (pressure, material homogeneity, boundary conditions etc.), has an effect on the dynamic expression of the seismogenetic system. Accordingly, the Aleutian Arc and Trench seismicity is divided into *crustal* and *sub-crustal* based on published estimates of the Mohorovičić discontinuity and conduct our analysis on two data subsets henceforth to be referred to as ATC (crustal seismicity) and ATD (sub-crustal seismicity). Full catalogues are examined, as well as versions of all catalogues declustered at the 70% and 80% level (Figure 4.7). The results are summarily presented in Tables 4.2 and 4.3 and Figures 4.8 - 4. 15.

Fig. 4.8 illustrates the variation of the magnitude entropic index q_M and temporal entropic index q_T with respect to threshold magnitude. Focusing first on the QCD full catalogue (Fig. 4.8a) it is straightforward to observe that $q_M(M_{th})$ is stable and exhibits minimal variation fluctuating around a mean value of 1.60 ± 0.008 ($b_q = 0.67$). For the WNG full catalogue $q_M(M_{th})$ is also stably determined albeit at a smaller scale, around a mean value of 1.51 ± 0.001 while $b_q = 0.96$ (Fig. 4.8b) while for the ALW catalogue $q_M(M_{th})$ is characterized by a distinct linear decreasing trend and varies from 1.58 ($b_q = 0.72$) at M_{th} =3.0 to 1.49 ($b_q = 1.04$) at M_{th} =3.9, indicating a possible decrease in earthquake clustering.

The analysis of the temporal entropic index with respect to threshold magnitude is shown in Fig. 4.8 with red rectangles. Starting again from QCD Fig. 4.8a illustrates the variation of $q_T(M_{th})$ for the full data set. It is apparent that the temporal entropic index starts off low, ($q_T \sim 1.1$), but demonstrates a steady linear increasing trend; it transcends the threshold

of randomness at M_{th} = 3.2 and climbs to 1.44 at $M_{th} \geq 4.5$ (significant correlation); this variation can be fitted with a linear trend line giving an average a rate of 0.22 per magnitude unit. A quasi-linear increasing trend is also evident for the WNG full catalogue; $q_T(M_{th})$ is again very low (~1.1) at smaller magnitude thresholds while indicates significant correlation (~ 1.35-1.37) at M_{th} = 4.1-4.2. For the ALW catalogue $q_T(M_{th})$ behaves in a different way: overall it exhibits moderate correlation throughout the catalogue varying from 1.31 to 1.2 with an exception at M_{th} =3.6 where it drops at 1.05 indicating very low correlation.

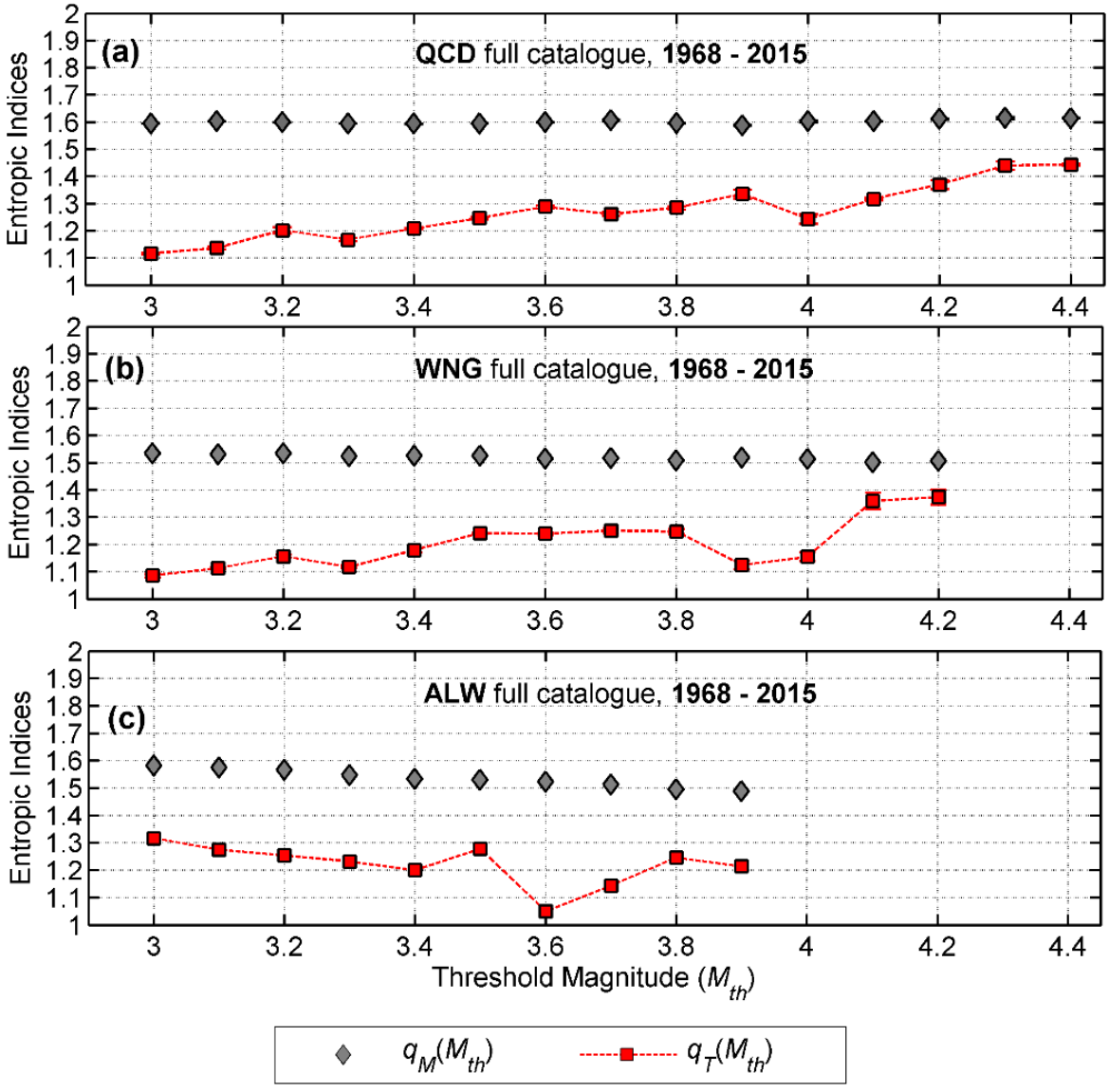

Figure 4.8 Variation of the magnitude (q_M) and temporal entropic indices (q_T) with threshold magnitude (M_{th}) for the full earthquake catalogues of: (a) the QDC; (b) WNG and, (c) ALW. 95% confidence limits are also drawn but are not always visible as they usually are smaller than the symbols.

Figs. 4.9.a and 4.9c illustrate the variation of q_M with respect to interevent distance – q_M (Δd). It is straightforward to see that the full QCD, WNG and ALW catalogues yield results analogous to those shown for $q_M(M_{th})$ in Fig. 4.1. For the full QCD catalogue $q_M(\Delta d)$ is rather consistent over interevent distances of up to 800km and varies between 1.56 and 1.61; respectively, b_q varies in the range 0.62 to 0.77. For the full WNG and ALW catalogues $q_M(\Delta d)$ is stably determined over interevent distances of up to 500km and varies between 1.51 and 1.56 (b_q ~0.96 to 0.78) and between 1.57-1.59 (b_q ~075 to 0.69) respectively.

The variation of the temporal entropic index with interevent distance is illustrated in Fig. 4.9 with red rectangles. To begin with the results from the full QCD catalogue, it is apparent that $q_T(\Delta d)$ exhibits a strong correlation throughout the catalogue: it remains always above the threshold of randomness, maximizing at ranges of the order 300km to 600km (q_T > 1.45), and thereafter slowly declining to moderate ranges of the order of 700km (q_T > 1.3). This may indicate that aftershocks are rather broadly spread out along the QCD fault zones.

For the full WNG catalogue, $q_T(\Delta d)$ exhibits strong increase from 1.74 at Δd < 100km to 1.4 at Δd > 300km, indicating *increasingly* strong correlation not only at shorter interevent distances but also at long ranges (Fig. 4.2b), while intermediate ranges are characterized by moderately low correlation (1.24-1.09). For the full ALW $q_T(\Delta d)$ decreases gradually from 1.77 at Δd < 150km to 1.29 at Δd = 300km, while at longer distances it reaches to 1.47indicating *persistently high* correlation at *all* ranges which, however, is *no longer* increasing with interevent distance.

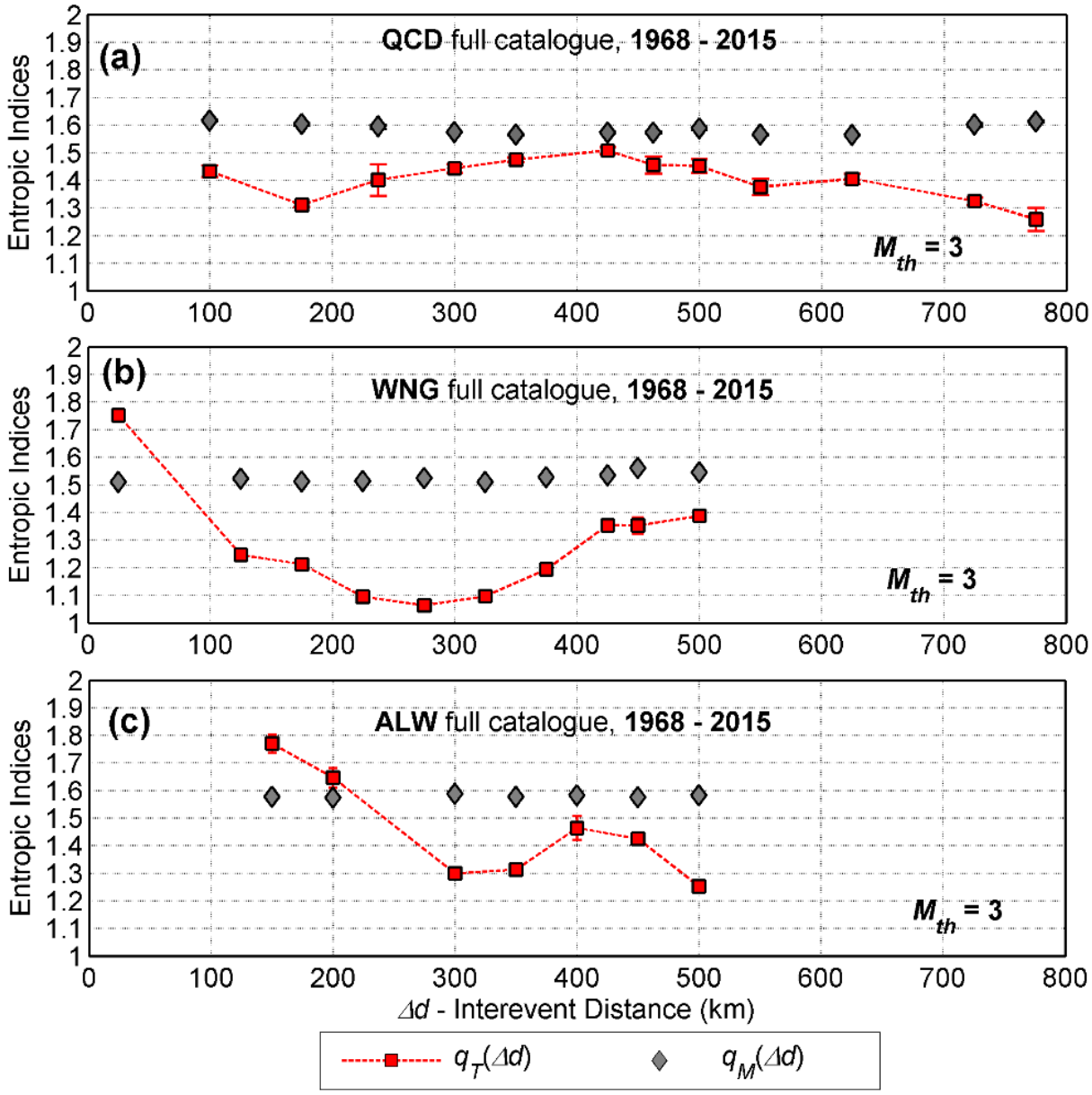

Figure 4.9. Variation of the magnitude (q_M) and temporal entropic indices (q_T) with interevent distance (Δ_d) for the full earthquake catalogues of: (a) the QDC; (b) WNG and, (c) ALW. 95% confidence limits are also drawn but are not always visible as they usually are smaller than the symbols.

Let us now turn our attention to the results for the Aleutian Arc and Trench catalogues. As already mentioned above, the Aleutian system presents a bimodality which cannot be explained in physical terms. In consequence, the analysis is conducted as follows: crustal and subcrustal seismicity is examined **a)** for $M_L \geq 4.4$ in the borader area of Aleutian Arc-trench system **b)** for $M_L \geq 3.5$ in the Aleutian Arc and Trench up to Unimak Pass where the network is denser.

The analysis of the ATC and ATD catalogues are shown in Figs. 4.10 and 4.11. For the ATC data up to Unimak Pass $q_M(M_{th})$ decreases smoothly from approx. 1.62 at M_{th} = 3.5,

to approx. 1.54 at M_{th} = 4.5, so that $\langle q_M(M_{th})\rangle$ = 1.58 ± 0.006 (Fig. 4.10a); respectively, $b_q(M_{th})$ varies between 0.62 and to 0.85. For the full ATC data, $q_M(M_{th})$ fluctuates slightly above 1.5 so that $\langle q_M(M_{th})\rangle$ = 1.54 ± 0.002 (Fig. 4.10c); respectively, $b_q(M_{th})$ varies between 0.81 and to 0.92. In Figs. 4.3b and 4.3d, stable and mutually consistent determination of $q_M(M_{th})$ is evident in both the full ATD and ATD up to Unimak Pass catalogues: q_M fluctuates slightly about 1.5 so that the mean q_M is 1.51 ± 0.024 for the full catalogue and 1.49 ± 0.01 for the ATD data up to Unimak Pass.

Focusing now on the results obtained for the temporal entropic index, $q_T(M_{th})$ shows variation for the data sets of crustal (ATC) and (ATD) subcrustal earthquakes. For the ATC data set up to Unimak Pass, $q_T(M_{th})$ decreases smoothly from 1.5 at M_{th} =3.5 to 1.26 at M_{th} =4.1, while for M_{th} > 4.1 it varies from 1.29 to 1.55, indicating significant correlation. For the ATC full data set (Figure 4.10c) the temporal entropic index behaves in similar manner: it slowly decays from 1.59 at M_{th} =3.5 to 1.35 at M_{th} =4.9 and then rises up to 1.56 at 5.1, showing overall high correlation. Exactly the opposite behaviour is observed in sub-crustal seismicity (ATD). As evident in Fig. 4.10b and Fig 4.10d, q_T is generally lower than 1.18 so that $\langle q_T(M_{th})\rangle$ =1.12± 0.003, with an exemption for M> 4.6 at the Unimak data set where $q_T(M_{th})$ rises up to 1.28 indicating moderate correlation at greater magnitude thresholds.

Fig. 4.11 illustrates the variation of q_M with respect to interevent distance – $q_M(\Delta d)$. It is straightforward to see that both the complete and up to Unimak Pass earthquake data sets yield results analogous to those shown for $q_M(M_{th})$ in Fig. 4.10. In crustal seismicity (ATC), for the data set up to Unimak Pass $q_M(\Delta d)$ is rather consistent over interevent distances of up to 600km and varies between 1.56 and 1.61, so that $\langle q_T(\Delta d)\rangle$ = 1.58 ± 0.02; respectively, b_q varies in the range 0.62 to 0.77. For the complete ATC data set $q_M(M_{th})$ is stably determined around 1.51-1.54, so that b_q varies between 0.96 and 0.85 (Fig.4.4c). In sub-crustal seismicity (ATD) for the complete data set $q_M(\Delta d)$ is stably determined over interevent distances longer than 800km and fluctuates around a mean value of 1.6 (1.56 and 1.62), so that b_q varies in between 0.79 and 0.61 (Fig. 4.11d). In the ATD data set up to Unimak Pass (Fig.4.11b) $q_M(\Delta d)$ is characterised by a quasi-linear upward trend and increases from shorter to longer distances (from 1.52 to 1.59), so so that b_q varies from 0.92 to 0.69.

.

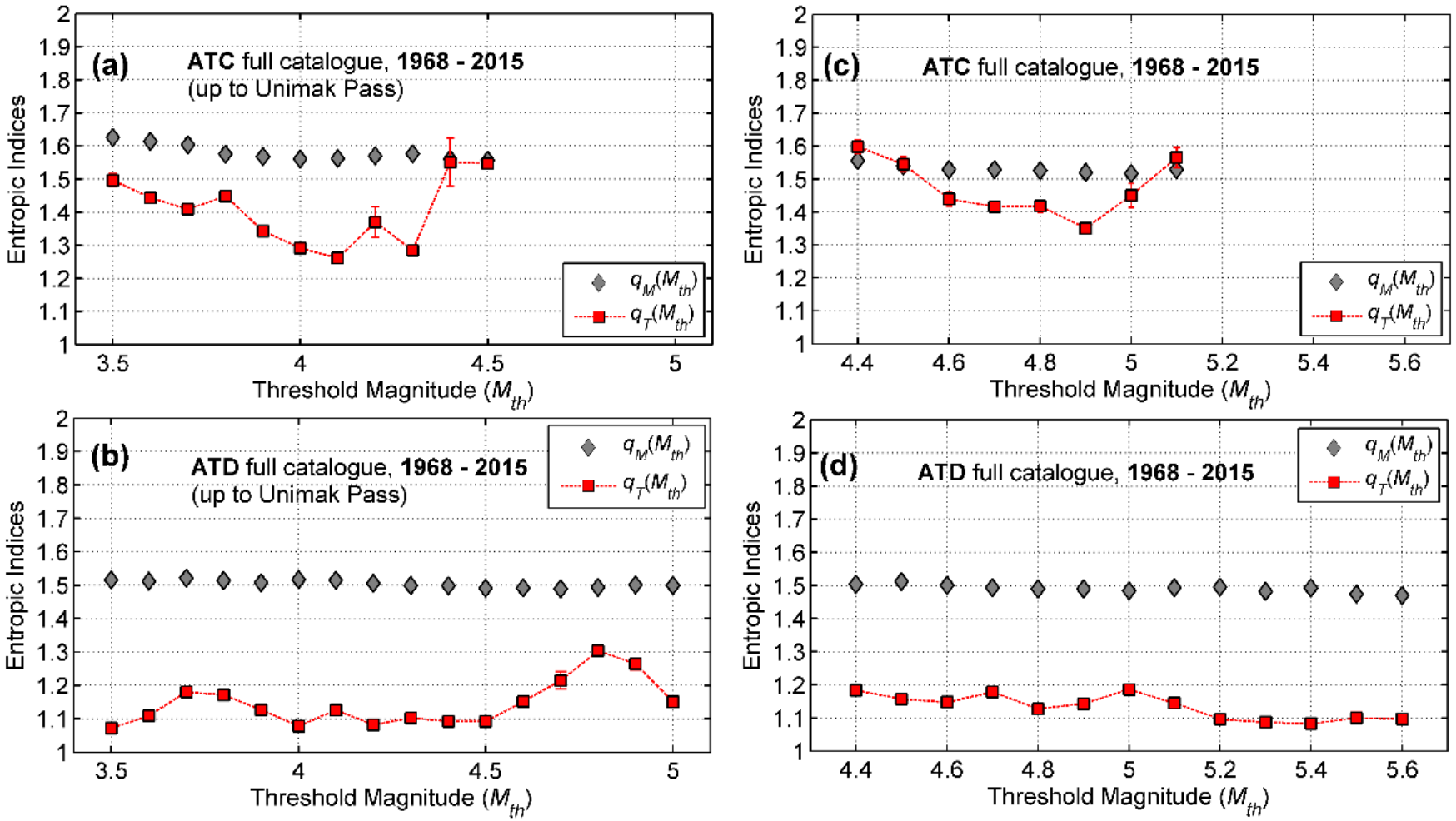

Figure 4.10 Variation of the magnitude (q_M) and temporal entropic indices (q_T) with threshold magnitude (M_{th}) for the full earthquake catalogues of: (a) ATC up to Unimak Pass with magnitude completeness M ≥3.5; (b) ATD up to Unimak Pass with magnitude completeness M ≥3.5, (c) ATC broader area with magnitude completeness M ≥4.4 and d) ATD broader area with magnitude completeness M ≥4.4. 95% confidence limits are also drawn but are not always visible as they usually are smaller than the symbols.

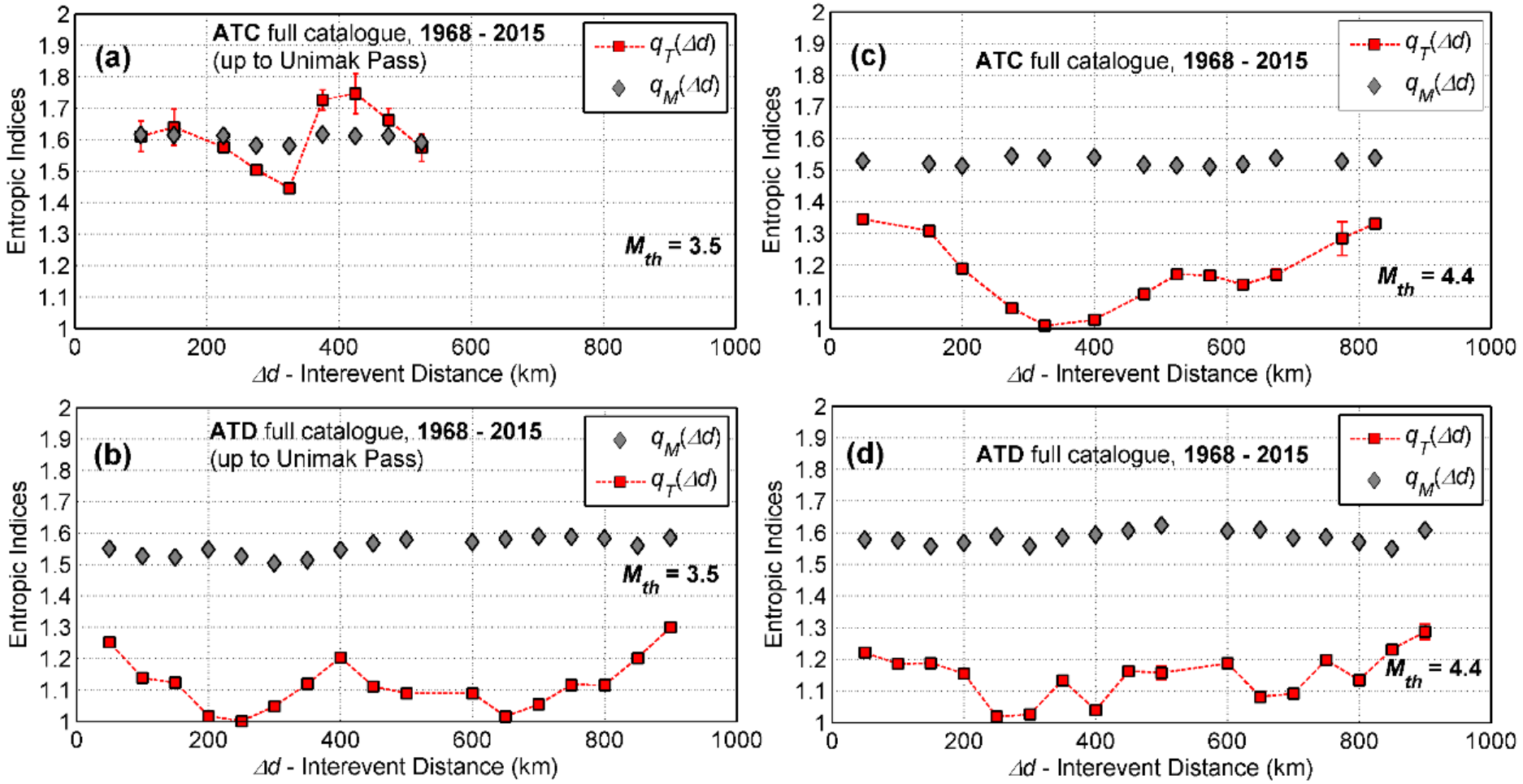

Figure 4.11 Variation of the magnitude (q_M) and temporal entropic indices (q_T) with interevent distance (Δ_d)) for the full earthquake catalogues of: (a) ATC up to Unimak Pass with magnitude completeness M ≥3.5; (b) ATD up to Unimak Pass with magnitude completeness M ≥3.5, (c) ATC broader area with magnitude completeness M ≥4.4 and d) ATD broader area with magnitude completeness M ≥4.4. 95% confidence limits are also drawn but are not always visible as they usually are smaller than the symbols.

In concluding the presentation of the results for the full ATC and ATD catalogues, Fig. 4.11 demonstrates the analysis of the temporal entropic index with respect to interevent distance with red rectangles. Turning our attention to the analysis of the crustal seismicity along the Aleutian Arc and Trench, we note that for the complete ATC data set (at M_{th} = 4.4 level), weak to moderate correlation can be observed only at interevent distances shorter than 200km and longer than 700km; in all other cases q_T is lower than the threshold of 1.2 (Fig. 4.4b). However, the ATC data set at the M_{th} = 3.5 level appears to unveil *strong* background correlation not only at short ranges but also at long interevent ranges, (100km < Δd < 550km), where q_T varies between 1.44 and 1.72 (Fig. 4.11a). The analysis of sub-crustal seismicity (ATD) shows nihil to marginal correlation over all interevent distances and up to 900km. Both at the M_{th} = 3.5 and at the M_{th} = 4.4 levels, the ATD catalogues yield very comparable results. For the former, $q_T(\Delta d)$ determinations vary between 1.29 and 1.01 with a mean of 1.15 $\pm$ 0.07; for the latter they vary between 1.27 and 1.01 with a mean of 1.13 $\pm$ 0.05. As per Figs. 4.11b and 4.11d, sub-crustal seismicity appears to be Poissonian also with respect to interevent distance.

4.3.2. Analysis of Declustered earthquake catalogues for 1968 – 2015

Turning our attention to the declustered counterparts of AEC catalogues, in Figure 4.12a it can be clearly seen for QDC that while the full catalogue yielded a mean value of $q_M(M_{th})$ at 1.60 $\pm$ 0.008 (b_q = 0.67), the declustered catalogue yields 1.52 $\pm$ 0.012 (b_q = 0.92). Analogous reduction of q_M with declustering has also been observed in SCSR and MFZ (California). As in those, activity in QCD is localized near the fault zones. Therefore, it is plausible that the reduction of q_M levels between the full and declustered catalogues implies a corresponding reduction in the level of activity localization from very high (b_q = 0.67) to nearly “average” (b_q = 0.92), in direct consequence of clustered aftershock removal. This reduction appears to take place without effects of the scaling (hierarchical distribution) of the faults that does not change with magnitude. For the declustered WNG catalogue show that $q_M(M_{th})$ fluctuates around a mean value of 1.47$\pm$ 0.008 (b_q = 1.12) while for the ALW declustered counterpart $q_M(M_{th})$ behaves in a similar manner as in the full catalogue and decreases albeit smoothly with magnitude threshold from 1.58 to 1.54 (b_q = 0.72 to 0.85).

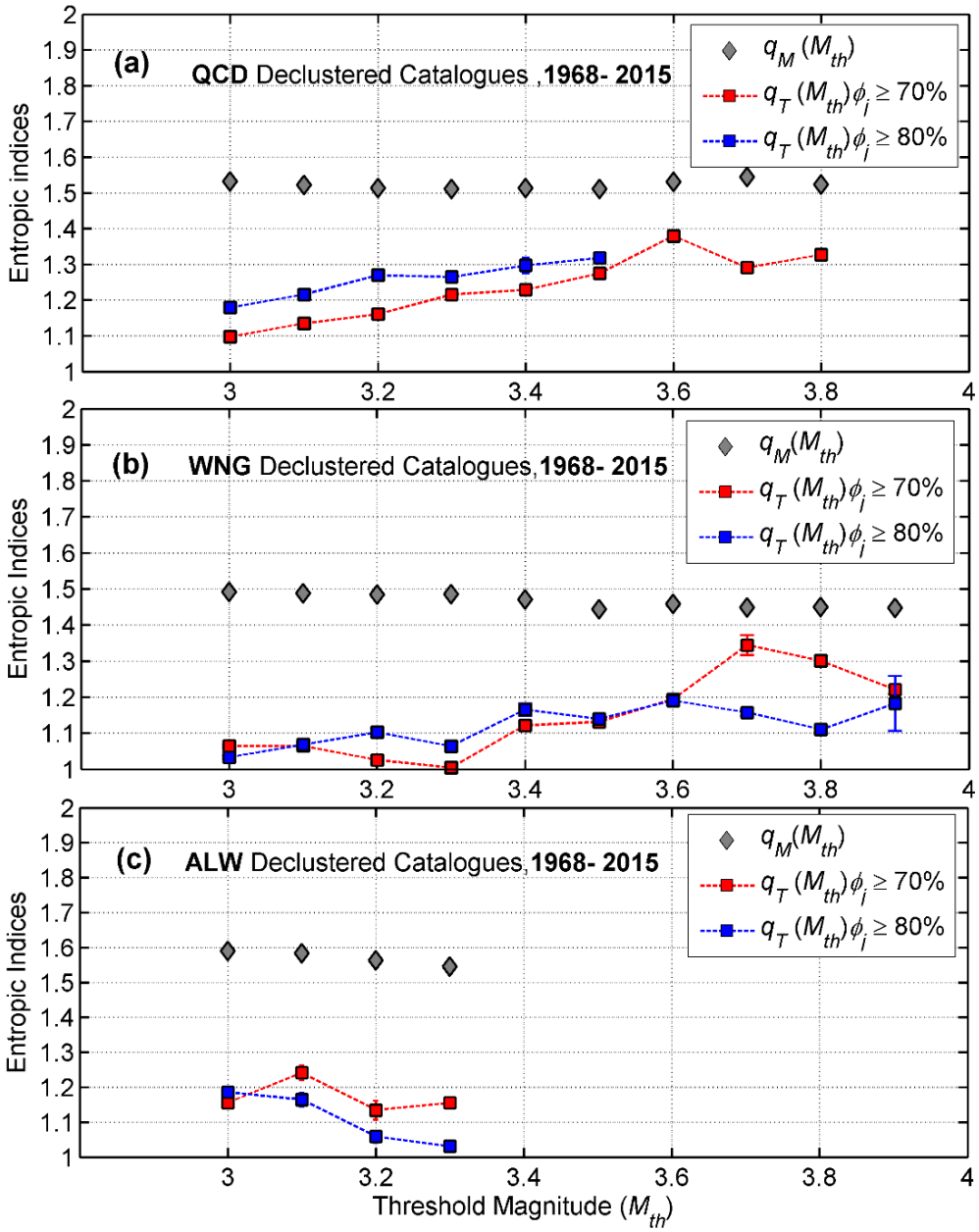

Figure 4.12 Variation of the magnitude (q_M) and temporal entropic indices (q_T) with magnitude threshold (M_{th}) for the declustered at 70% and 80% probability level earthquake catalogues of: (a) QCD; (b) WNG, (c) ALW. 95% confidence limits are also drawn but are not always visible as they usually are smaller than the symbols.

Focusing now on the results obtained for the temporal entropic index at 70% and 80% probability levels, $q_T(M_{th})$ shows variation for the subset areas of continental Alaska. For the declustered QCD catalogue (Fig.4.12a), as in the case of the full catalogue, $q_T(M_{th})$also transcends the randomness threshold at M_{th} = 3.2 and climbs to 1.33 at M_{th} =3.8; the linear trend in this case has a rate of 0.29 per magnitude unit, noticeably higher than that of the full catalogue. It can also be seen that for all M_{th} > 3.2, the declustered

catalogue q_T is consistently higher than the full catalogue q_T indicating more correlated background process. By increasing the probability level at 80% one can see that this linear trend remains while the $q_T(M_{th})$ values are consistently higher than in the 70% declustered version by approx. 0.05 units; at M_{th} = 3.2 q_T is 1.17 (1.1 at 70%) and climbs to 1.32 at M_{th} =3.5 (1.27 at 70%).It is also worth reminding that quasi-linear increase of q_T with magnitude has been observed in the SCSR, SNR and pre-1989 nSAF catalogues and has been attributed to operational long-range correlation; therefore, the same interpretation should apply in the case of QCD.

An analogous behaviour is also observed for the 70% declustered WNG catalogue; $q_T(M_{th})$ fluctuates near randomness threshold at $M_{th} \leq 3.4$ and increases up to 1.34 at M_{th} = 3.7 (Fig.4.12b). In general, the declustered WNG catalogue at 70% level shows that for all $M_{th} > 3.5$ q_T is consistently higher than the full catalogue indicating a correlated background process. However, upon removing aftershocks and increasing the probability at 80% q_T decays to very low near randomness thresholds throughout the catalogue. Finally, for the ALW declustered catalogue $q_T(M_{th})$ varies from 1.13 to 1.24 indicating very low correlation at 70% probability level throughout the catalogue (Fig. 4.12c), though at higher probability levels (φ_j>80%) $q_T(M_{th})$ decays to randomness threshold (1.05-1.03). Fig. 4.13 demonstrates the analysis of the entropic indices with respect to interevent distance. As can be seen, for both QCD and WNG catalogues the analysis yield very consistent $q_M(\Delta d)$, which varies between 1.51 and 1.53, so that $\langle q_M(\Delta d)\rangle = 1.52 \pm 0.008$ and $b_q(\Delta d)$ that varies between 0.94 and 0.87. It is again possible to observe a statistically significant reduction in the value of q_M, which can be interpreted in terms of a corresponding reduction in the level of activity localization upon aftershock removal.

A rather unexpected outcome is also that inadequate earthquake populations prohibited the generation of dependable estimation of q_T at short interevent distances (less than 75–100 km). In the case of QCD this applies even for the full catalogue; it appears that even aftershocks are rather broadly spread out along the QCD fault zones. In the declustered QCD and WNG catalogues, earthquake populations sufficient for statistically significant results exist only for interevent distances between 100 and 450 km. Inadequate populations also did not allow determination of $q_T(\Delta d)$ from the ALW declustered catalogue (at φ_j>70% only 512 events were left). Inadequate populations also did not allow determination of $q_T(\Delta d)$ from the declustered catalogue at distances shorter than 75km and longer than 450km. Yet, within this range for the QCD declustered at 70% and 80% probability level $q_T(\Delta d)$ is consistently determined at the level 1.27–1.45 and 1.19-

1.41 respectively, indicating moderate correlation. Given also the results obtained for $q_T(M_{th})$ in Fig. 4.11a, it can be concluded that within the period of observation, the QCD zone has existed in a persistent state of non-equilibrium. ,Analogous observations can be made upon the WNG declustered catalogue: significant results were produced for interevent distances greater than 100 km. In Fig. 4.13b one can see that for $\Delta d \leq 150$ km at 70% level, $q_T(\Delta d)$ is determined around 1.34-1.38, while for 150km $> \Delta d \geq 150$ km $q_T(\Delta d)$ decays near randomness threshold while at longer distances it indicates moderately low correlation. When the probability for an event to belong to the background increases to 80%, it can be clearly seen that $q_T(\Delta d)$ indicates very low correlation to near randomness process throughout the catalogue [$q_T(\Delta d)$ = 1.05 – 1.23].

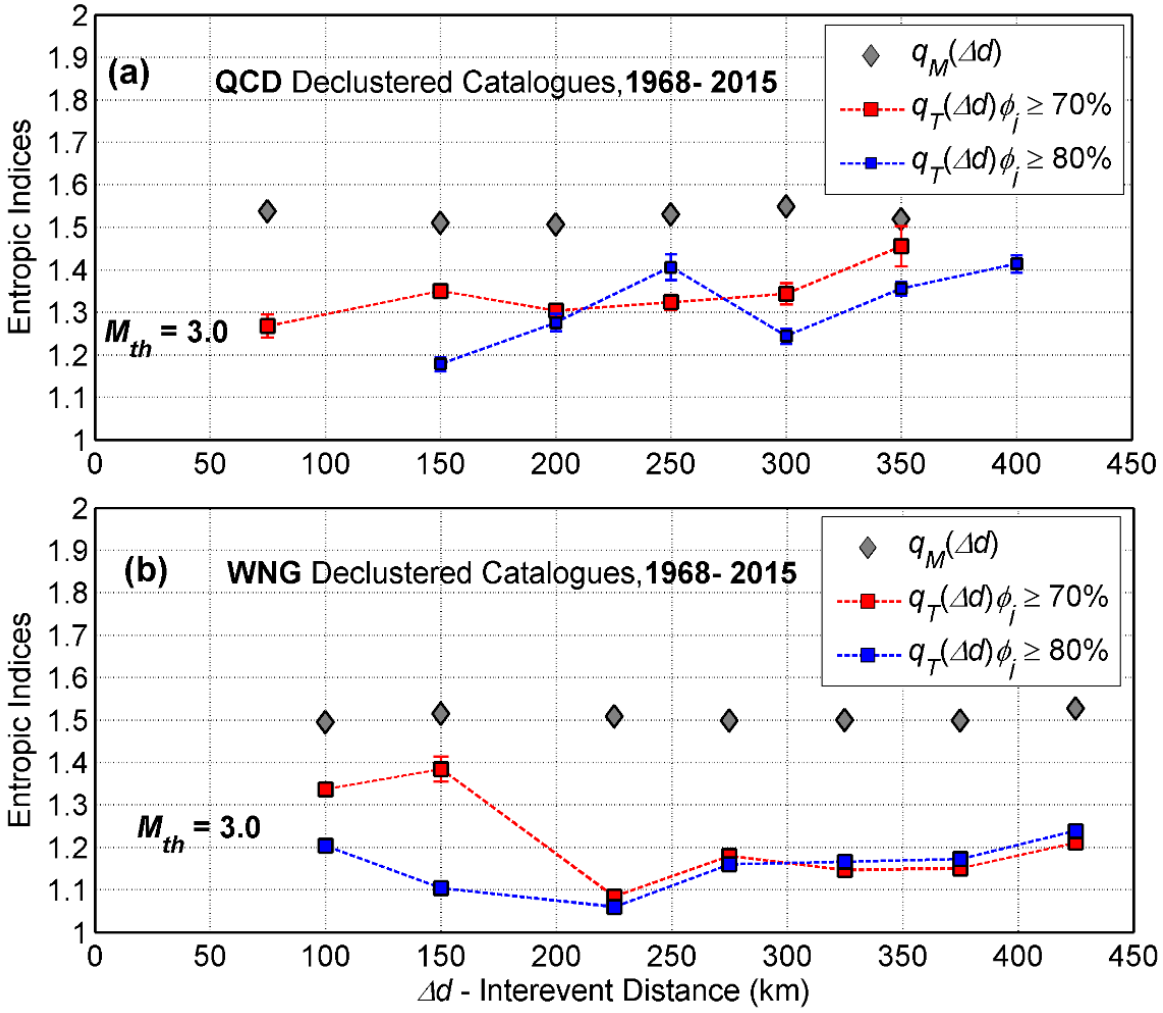

Figure 4.13 Variation of the magnitude (q_M) and temporal entropic indices (q_T) with interevent distance (Δ_d) for the declustered at 70% and 80% probability level earthquake catalogues of: (a) QCD; (b) WNG, (c) ALW. 95% confidence limits are also drawn but are not always visible as they usually are smaller than the symbols.

Focusing now on the Aleutian system, Fig. 4.14 shows the variation of entropic indices with magnitude threshold (M_{th}). For the declustered ATC - Unimak data, $q_M(M_{th})$ decreases smoothly from approx. 1.6 at M_{th} = 3.5, to approx. 1.55 at M_{th} = 4, so that $\langle q_M(M_{th})\rangle$ = 1.58 ± 0.002 (Fig. 4.14a); respectively, $b_q(M_{th})$ varies between 0.67 and to 0.81. The small reduction of q_M between the full and declustered catalogues might signify a corresponding reduction in the level of activity localization as per QCD but to a lesser degree. In Figs. 4.14b, 4.14c and 4.14d, stable and mutually consistent determination of $q_M(M_{th})$ is evident in both the declustered ATC and ATD complete data sets as well the declustered ATC complete data set: q_M fluctuates slightly about 1.5 so that the mean q_M shows no statistical difference.

The analysis of the temporal entropic index with respect to threshold magnitude is shown with red rectangles for 70% probability level and blue rectangles for 80% probability level. For the complete ATC data set, $q_T(M_{th}70\%)$ increases steadily from about 1.45 at M_{th} = 4.4 to over 1.5 for $M_{th} \geq 4.6$, while at the ATC up to Unimak Pass $q_T(M_{th}70\%)$) decreases from 1.51 at M_{th} = 3.5 to 1.32 at M_{th} = 4.0. At $q_T(M_{th}80\%)$ the correlation is even higher for the complete and up to Unimak Pass ATC data sets; q_T varies from 1.58-1.69 and 1.57 -1.32 respectively(Fig.4.14c). This implies a correlated background and points toward long-range interaction. Exactly the opposite behaviour is observed in sub-crustal seismicity (ATD). As evident in Fig. 4.14b and 4.14d, q_T is generally lower than 1.18. An exception can be made for at $q_T(M_{th}$ 80%) at M_{th} 4.7 and 4.8 where q_T is estimated at 1.28-1.23 indicating low to moderate correlation. On the basis of this evidence alone, the sub-crustal fault network of the subduction zone would appear to be Poissonian.

In concluding the presentation of our results, Fig. 4.15 demonstrates the analysis of entropic indices with respect to interevent distance. With respect to magnitude entropic index it can be clearly seen that for ATC and ATD data sets up to Unimak Pass (Figs 4.15a and 4.15b), $q_M(\Delta d)$ increases smoothly with interevent distance. For the ATC $q_M(\Delta d)$ increases from 1.49 at Δd=100km up to 1.57 at Δd=450km; respectively, $b_q(\Delta d)$ varies between 1.04 and to 0.75. For the ATD data set (up to Unimak Pass) and up to 400km $\langle q_M((\Delta d)\rangle$ = 1.53±0.0008 (b_q= 0.88), while for $\Delta d \geq$ 600km $\langle q_M((\Delta d)\rangle$ = 1.57±0.002 (b_q= 0.75). For the corresponding ATC and ATD complete data sets $q_M(\Delta d)$ is rather stably determined around a mean value of 1.5 and as in the case of magnitude threshold shows no statistical difference.

Unfortunately for the ATC data sets results were obtained only at the 70% probability level. ATC declustering appears to unveil *strong* background correlation at long interevent ranges, (400km < Δd < 800km), where q_T varies between 1.45 and 1.65 and, notably, mirrors the variation of q_T in the full catalogue (Fig. 4.8c). For the complete ATC data set, at short and intermediate ranges (Δd < 400km) q_T cannot be estimated due to dwindled earthquake populations (and consequent loss of statistical robustness). However, for the crustal seismicity up to Unimak Pass q_T was estimated not only at longer distances but also at short ranges; q_T varies from 1.19 to 1.36 indication moderate background correlation.

The analysis of sub-crustal seismicity (ATD) shows at 70% probability level nihil to marginal correlation over all interevent distances (Fig. 4.15b and 4.15d). Both at M_{th} = 3.5 the M_{th} = 4.4 level (ATD Unimak and complete data set), declustered catalogues yield very comparable results. For the former, $q_T(\Delta d)$ determinations vary between 1.17 and 1.05 with a mean of 1.11 $\pm$ 0.007; for the latter they vary between 1.17 and 1.03 with a mean of 1.11 $\pm$ 0.02. As per Fig. 4.14b, q_T (M_{th} 80%) reveals a moderate correlation for Δd > 600km where the temporal entropic index varies from 1.21 to 1.34, while as per 4.14d, sub-crustal seismicity appears to be Poissonian also with respect to interevent distance.

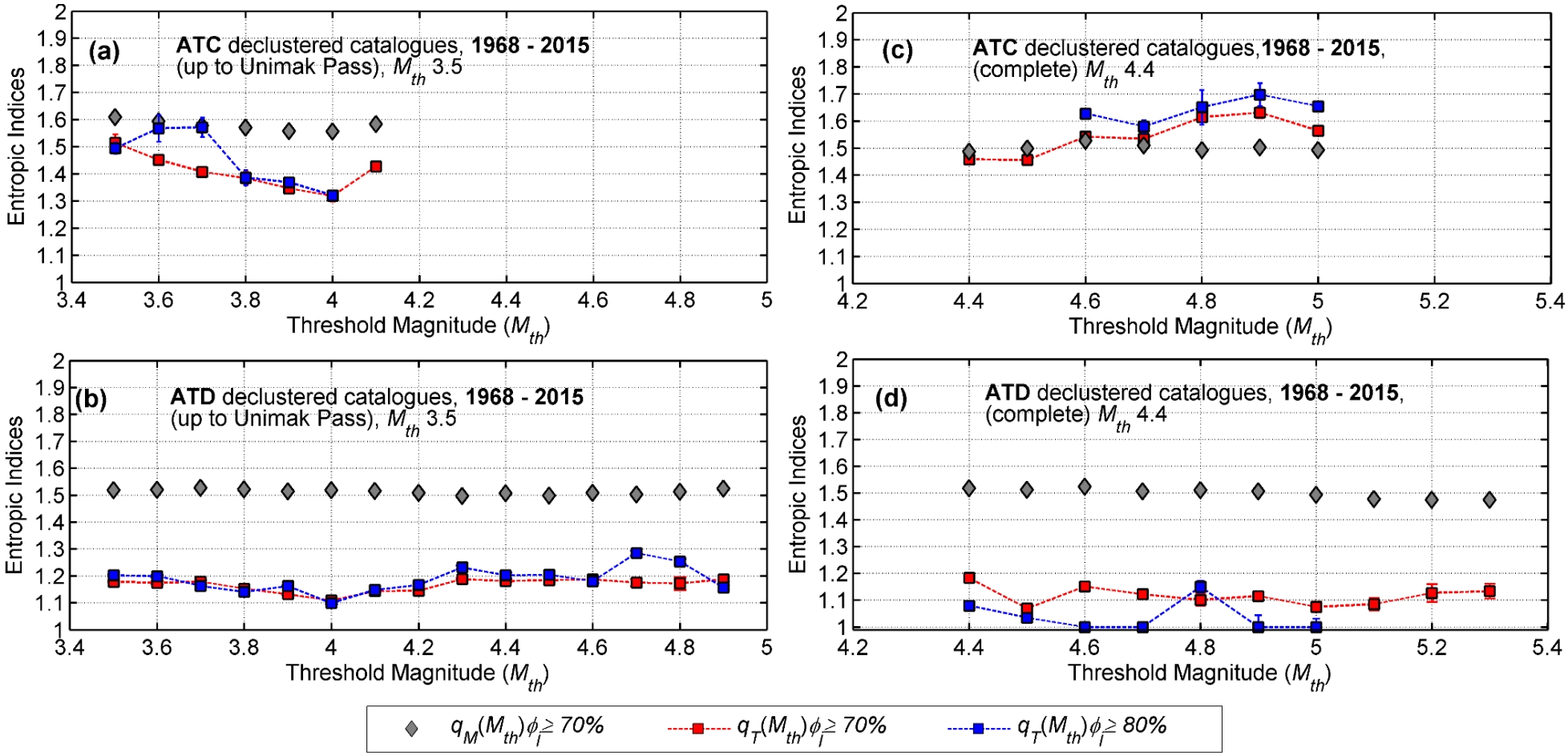

Figure 4.14 Variation of the magnitude (q_M) and temporal entropic indices (q_T) with threshold magnitude (M_{th}) for the declustered earthquake catalogues at 70% probability level of: (a) ATC up to Unimak Pass with magnitude completeness M ≥3.5; (b) ATD up to Unimak Pass with magnitude completeness M ≥3.5, (c) ATC broader area with magnitude completeness M ≥4.4 and d) ATD broader area with magnitude completeness M ≥4.4. 95% confidence limits are also drawn but are not always visible as they usually are smaller than the symbols.

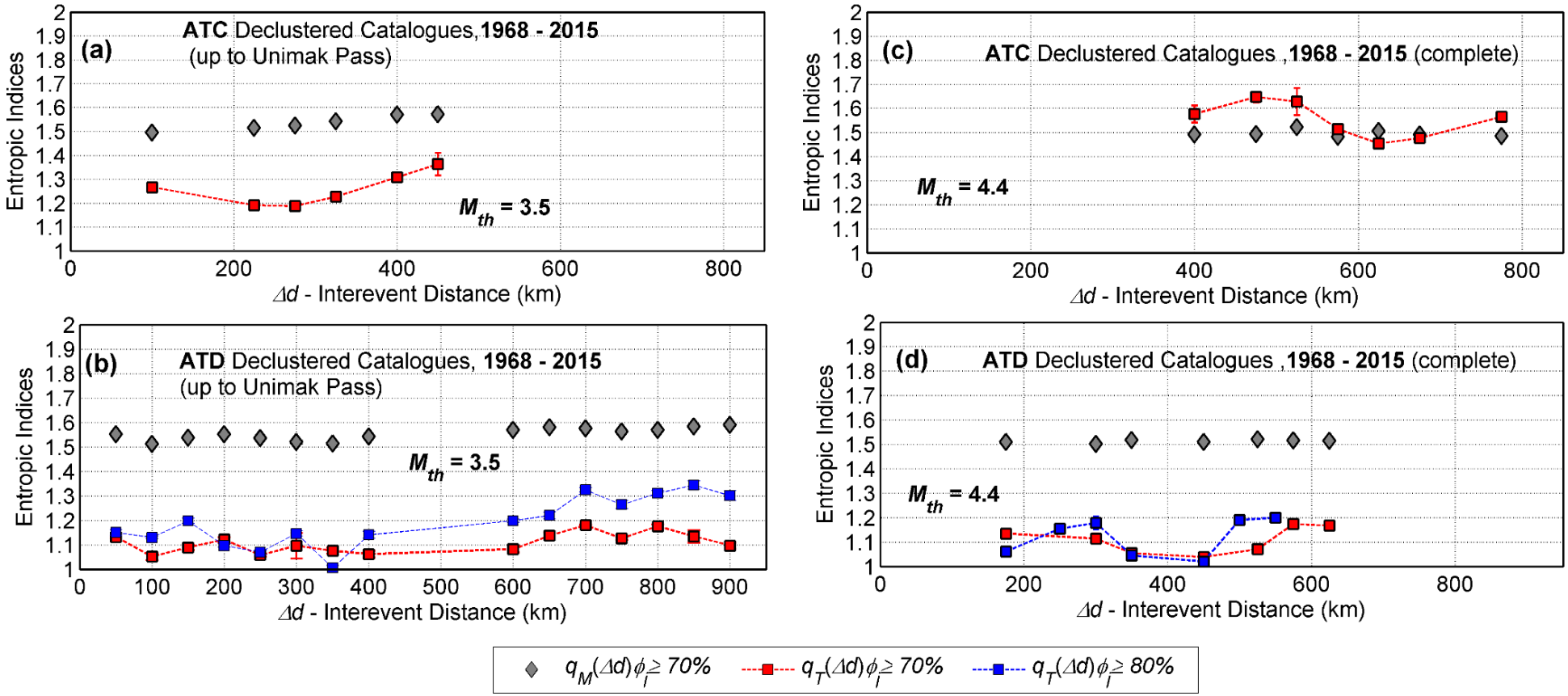

Figure 4.15 Variation of the magnitude (q_M) and temporal entropic indices (q_T) with interevent distance (Δ_d) for the declustered earthquake catalogues at 70% probability level of: (a) ATC up to Unimak Pass with magnitude completeness M ≥3.5; (b) ATD up to Unimak Pass with magnitude completeness M ≥3.5, (c) ATC broader area with magnitude completeness M ≥4.4 and d) ATD broader area with magnitude completeness M ≥4.4. 95% confidence limits are also drawn but are not always visible as they usually are smaller than the symbols.

TABLE 4.2 Summary of the variation of the entropic indices and *b*-values obtained from the analysis of Alaskan full and declustered catalogues, as a function of threshold magnitude. $\bar{q}_T$ and $\bar{q}_M$ are the mean temporal and magnitude entropic indices respectively; $\sigma(q_T)$ and $\sigma(q_M)$ are the corresponding standard deviations. The last column lists *b*-values calculated with conventional techniques.

	Period	$\bar{q}_T$	$\sigma(q_T)$	q_T **Range**	$\bar{q}_M$	$\sigma(q_M)$	q_M **Range**	b_q **range**	***b* value**
Full QCD	1968-2015	1.30	0.05	1.16-1.44	1.60	0.008	1.59-1.61	0.69-0.64	0.65-0.60
Declustered 70%		1.23	0.01	1.1-1.37	1.52	0.0008	1.51-1.54	0.98-0.85	0.88-0.79
Declustered 80%		1.25	0.002	1.18-1.31					
Full WNG	1968-2015	1.21	0.008	1.05-1.37	1.52	0.001	1.51-1.54	0.98-0.85	0.88-0.79
Declustered 70%		1.17	0.0034	1.00-1.34	1.47	0.001	1.45-1.49	1.22-1.04	1.19-1.11
Declustered 80%		1.14	0.006	1.03-1.18					
Full ALW	1968-2015	1.16	0.004	1.05-1.27	1.55	0.0025	1.58-1.49	0.72-1.04	0.66-1.12
Declustered 70%		1.19	0.027	1.13-1.24	1.56	0.001	1.54-1.58	0.98-0.72	0.89-0.71
Declustered 80%		1.11	0.007	1.05-1.18					

	Period	$\bar{q}_T$	$\sigma(q_T)$	q_T Range	$\bar{q}_M$	$\sigma(q_M)$	q_M Range	b_q range	b value
Full ATC (M_{th} 3.5)	1968-2015	1.40	0.07	1.26-1.55	1.58	0.001	1.56-1.62	0.78-0.61	0.72-0.59
Declustered 70%		1.42	0.011	1.34-1.49	1.58	0.001	1.55-1.60	0.82-0.66	0.80-0.61
Declustered 80%		1.45	0.035	1.32-1.57					
Full ATC (M_{th} 4.4)	1968-2015	1.47	0.009	1.35-1.59	1.54	0.001	1.51-1.56	0.96-0.78	1.06-0.69
Declustered 70%		1.54	0.007	1.46-1.63	1.50	0.001	1.48-1.52	1.08-0.92	1.12-0.97
Declustered 80%		1.64	0.04	1.58-1.69					
Full ATD (M_{th} 3.5)	1968-2015	1.19	0.14	1.07-1.30	1.50	0.0008	1.48-1.52	1.08-0.92	1.14-0.86
Declustered 70%		1.14	0.02	1.09-1.18	1.51	0.0007	1.50-1.52	1.00-0.92	1.1-0.84
Declustered 80%		1.19	0.008	1.09-1.28					
Full ATD (M_{th} 4.4)	1968-2015	1.13	0.005	1.08-1.18	1.50	0.00046	1.48-1.51	1.08-0.96	1.16-0.88
Declustered 70%		1.12	0.01	1.06-1.18	1.49	0.0003	1.47-1.51	1.12-0.96	1.16-0.90
Declustered 80%		1.07	0.03	1.00-1.14					

TABLE 4.3 Summary of the variation of the entropic indices and *b*-values obtained from the analysis of Alaskan full and declustered catalogues, as a function of interevent distance. $\bar{q}_M$ is the mean magnitude entropic index; σ(*qM*) is the corresponding standard deviation.

	Period	**q_T Range**					
		Δd < 200km	**Δd > 200km**	$\bar{q}_M$	**$\sigma(q_M)$**	**q_M Range**	**b_q range**
Full QCD	1968-2015	1.31-1.43	1.26-1.50	1.58	0.003	1.56-1.61	0.78- 0.63
Declustered 70%		1.26-1.34	1.30-1.45	1.52	0.0039	1.50-1.54	1.00-0.85
Declustered 80%		N/A	1.17-.141				
Full WNG	1968-2015	1.21-1.75	1.06-1.38	1.53	0.005	1.51-1.56	0.96-0.78
Declustered 70%		1.33-1.38	1.08-1.21	1.50	0.001	1.50-1.51	1.00-0.96
Declustered 80%		1.10-1.20	1.05-1.23				
Full ALW	1968-2015	1.64-1.76	1.26-1.46	1.57	0.005	1.56-1.58	0.78-0.72
Declustered 70%		N/A		N/A			
Declustered 80%		N/A					
	Period	**q_T Range**					

		Δd < 100km	Δd > 200km	$\bar{q}_M$	$\sigma(q_M)$	q_M Range	b_q range
Full ATC (Mth 3.5)	1968-2015	1.61-1.63	1.44-1.75	1.60	0.002	1.59–1.61	0.69-0.63
Declustered 70%		1.26	1.19-1.36	1.54	0.0022	1.50-1.57	1.00-
Declustered 80%		N/A	N/A				
Full ATC (Mth 4.4)	1968-2015	1.19-1.34	1.09-1.33	1.53	0.0006	1.51-1.54	0.96-0.85
Declustered 70%		N/A	1.45-1.65	1.50	0.001	1.49-1.50	1.04-1.00
Declustered 80%		N/A	N/A				
Full ATD (Mth 3.5)	1968-2015	1.01-1.25	1.00-1.29	1.54	0.0002	1.50-1.58	1.00-0.72
Declustered 70%		1.05-1.14	1.06-1.17	1.55	0.0006	1.51-1.58	0.96-0.72
Declustered 80%		1.09-1.19	1.01-1.32				
Full ATD (Mth 4.4)	1968-2015	1.15-1.22	1.01-1.28	1.58	0.001	1.56-1.62	0.78-0.61
Declustered 70%		1.13	1.04-1.16	1.51	0.004	1.50-1.51	1.00-0.96
Declustered 80%		1.06	1.02-1.19				

4.4 TEMPORAL EVOLUTION OF ALEUTIAN ARC – TRENCH SYSTEM SEISMICITY

As in the case of the Californian seismogenetic system, let us now investigate the time dependence of the Aleutian Arc – Trench system (crustal and subcrustal seismicity) with particular reference to periods preceding large earthquakes ($M_L > 7$). F-M-T distributions are compiled over consecutive overlapping windows and solved for the parameters a, α, q_M, c and q_T of Eq. 2.17 (see Chapter 2). The procedure is applied to the full and declustered Alaskan catalogues with completeness magnitude M_{th} =4.4 starting at the year 1978 and ending at the year 2015.

The F-M-T distributions are formed in the natural time of the respective seismogenetic processes: each window comprises 400 consecutive events while the overlap distance is 20 events for both full and declustered catalogues. In general, excellent approximations of the observed F-M-T distributions are obtained but for the sake of experimental rigour, this presentation will only consider models associated with a goodness of fit better than 0.97. The discussion focuses on the values and variation of the temporal entropic index, which is plotted as a function of time from Fig. 4.16 and Fig 4.17 and summarized in Table 4.4.

As is apparent in Fig. 4.16, the analysis of the ATC (crustal) full and declustered catalogues shows that the temporal entropic index exhibits significant variation for the full catalogue. As in the case of the full nSAF catalogue, q_T behaves “erratically”, being generally very low (up to 1.1) prior to large earthquakes (M > 7.9) and attains significant values (> 1.4 with a q_{Tmax} at 1.92) immediately after their occurrence, indicating very high correlation that can be easily explained as a consequence of their aftershock sequences. This explanation is further corroborated by the observation of the high correlation observed after the 1986 Andreanof earthquake; then q_T becomes unstable and decays to levels near randomness thresholds (1.1). It is evident that this pattern is recurrent: after a series of large earthquakes, for instance the 1996 earthquake of M=7.9[9], q_T exhibits strong correlation and then it becomes unstable and behaves erratically due to the

[9] At 8:03 p.m. ADT (04:03 6/10 UTC) on Sunday evening, June 9, 1996, a major earthquake occurred in the Andreanof Islands region of Aleutian Islands. The magnitude 7.9 earthquake, the largest earthquake to occur in North America in the previous ten years, was preceded by several foreshocks the day before; the largest of which had moment magnitude 6.5. One hundred and ninety-four aftershocks (open circles), magnitude 4.0 or larger, had occurred through the end of June 1996, the largest of which occurred eleven hours after the main shock and had a magnitude of 7.2. (*UAF, Alaska Earthquake Center*)

overwhelming effect of the tightly spaced aftershock sequences reaching values <1.1 (near randomness) right before the next large earthquake.

Conversely, the declustered ATC catalogue reserves a surprise: for the period 1980 to 2005 q_T generally exhibits very low correlation near randomness threshold not only after the expression of large earthquakes but also prior to significant events (e.g. the 1986 and the 1996 earthquake of M=7.9). However, from 2005 q_T increases from approximately 1.16 to 1.36 and remains at moderate levels (> 1.21) up to year 2015.

The analysis of the subcrustal seismicity (ATD catalogues) is presented in Figure 4.17. It can be clearly seen that for the full ATD catalogue q_T behaves as per the full ATC catalogue up until 1988; q_T fluctuates around 1.16 – 1.3 prior to the large 1986 earthquake (ML=7.9) and exhibits a persistent increasing trend from the lower to the higher end of this range prior to their occurrence; the index jumps to very high values (> 1.9) immediately after the incidence of the large event, presumably reflecting the very high correlation associated with their aftershock sequences. Also, as per the ATC analysis, the high correlation of the aftershock sequences decays gradually to near oblivion (< 1.1). An interesting observation can be made for the period 1990 – 2010: despite the existence of large events we do not observe a series of rapidly building up and decaying cycles, as in the ATC full catalogue; q_T is stably determined around a mean value of 1.25-1.30 indicating moderate correlation. After 2010, it decays rapidly to oblivion.

The analysis of the declustered ATD catalogue holds its own surprise, as shown in Fig. 4.17b; q_T is generally lower than 1.1 indicating very low correlation. However, after the 1986 earthquake and for a five-year period q_T increases from 1.16 to 1.45 indicating moderate to highly correlated background process. A similar behaviour can be observed after a ten-year period, after the 1996 earthquake; the temporal index rises up to 1.33 and then decays gradually at a faster rate to randomness thresholds.

Based on the above observations, it becomes clear that the crustal and subcrustal seismicity of the Aleutian Arc – Trench system reveal a different behaviour. On the one hand, ATC exhibits significant long-range correlation over the entire period of 47 years since 1968 observable in the full and declustered catalogues; this reveals itself both implicitly, as an increase in the value of q_T with threshold magnitude, and explicitly. This quasi-stationary state of high correlation has attributes of Self-Organized Criticality. To the contrary, the sub-crustal system of the Alaskan – Aleutian subduction, is definitely Poissonian. Because it is the only one, it cannot serve as a basis for generalizations. The

behaviour of q_M is also clearly different between ATD and the crustal systems, possibly indicating different dynamics, gross earthquake productivity rates and large-scale domain heterogeneities are *not* dramatically dissimilar. Accordingly, the absence of temporal correlation in ATD may not have to do with the material properties of the subducting slab and should be sought elsewhere.

The contrast with the crustal systems is rather impressive nonetheless, and may comprise a piece of information useful in the course of shaping up some preliminary understanding of the statistical (and physical) nature of seismogenesis

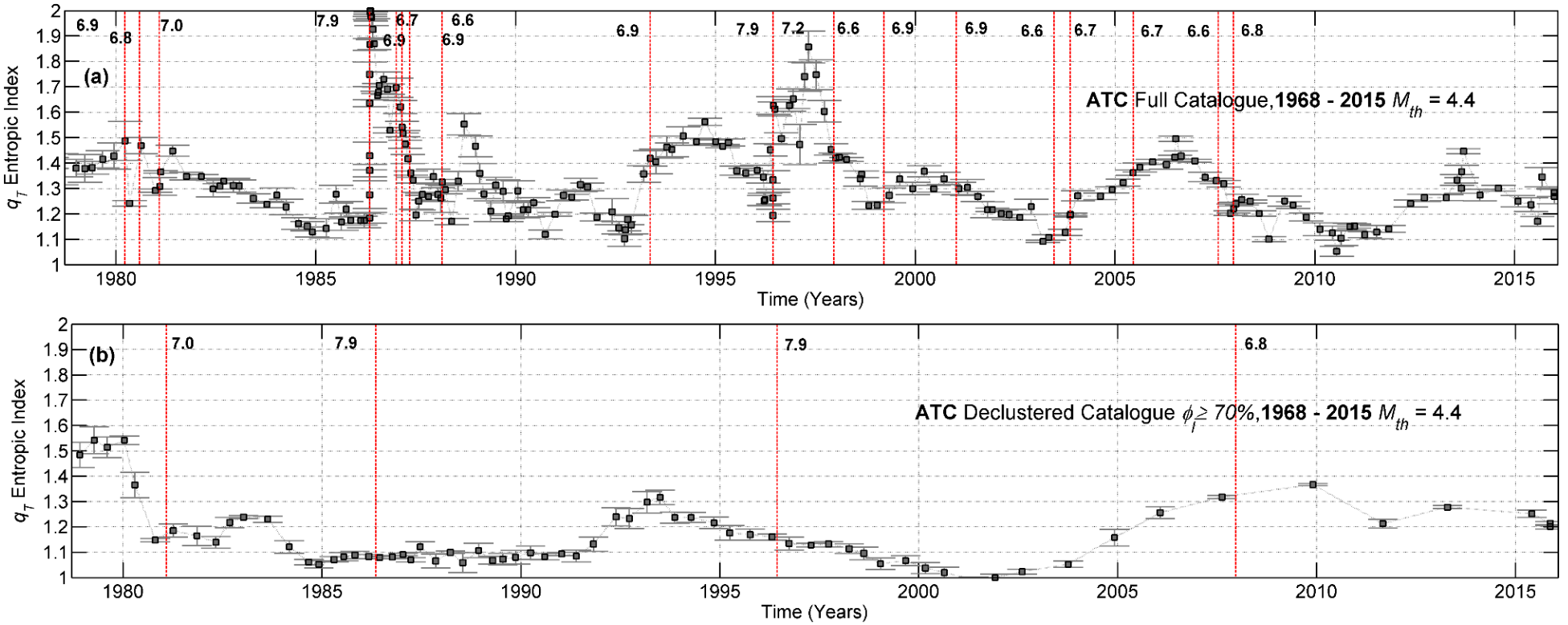

Figure 4.16 The entropic indices obtained for the ATC (complete) full and declustered catalogue with Mth=4.4. Estimates are based on F–M–T distributions compiled over sliding windows of 400 events in the natural time of the seismogenetic process. Error bars refer to 95% confidence intervals. The vertical dashed lines indicate the occurrence of earthquakes with $M_L \geq 6.6$.

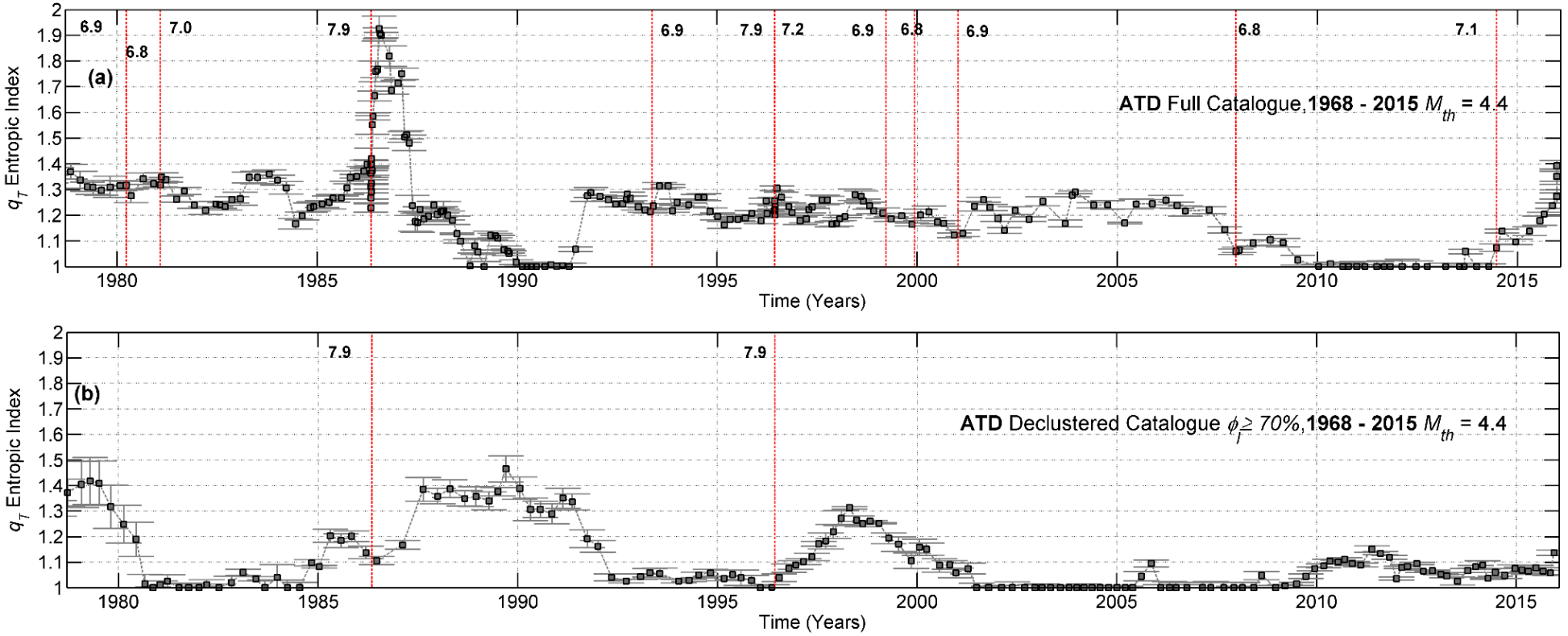

Figure 4.17 The entropic indices obtained for the ATD (complete) full and declustered catalogue with Mth=4.4. Estimates are based on F–M–T distributions compiled over sliding windows of 400 events in the natural time of the seismogenetic process. Error bars refer to 95% confidence intervals. The vertical dashed lines indicate the occurrence of earthquakes with $M_L \geq$ 6.9.

CHAPTER 5

CASE STUDY 3: THE SEISMOGENETIC SYSTEM OF GREECE & WESTERN TURKEY

THE EASTERN MEDITERRANEAN SEISMOGENETIC SYSTEM

The seismotectonic framework of the broader eastern Mediterranean area is dominated by the collision of the Arabian and African Plates with Eurasia (McKenzie, 1972, 1978; Jackson and McKenzie, 1988; Papazachos and Kiratzi, 1996; Papazachos et al., 1998; McClusky et al., 2000). Various plate motion models indicate that the Arabian plate is moving northwards relative to Eurasia at a rate of _18–25 mm/year, averaged over 3 Ma. The African plate is also moving northwards relative to Eurasia at a rate of 10 mm/year (DeMets et al., 1990). Its leading edge is being subducted along the Hellenic Trench. As the rate of subduction is higher than the relative motion of Africa relative to Eurasia, it requires a southward movement of the arc relative to Eurasia. A major role in the seismotectonic framework of the Aegean area plays the motion of two other smaller plates: the Anatolian and the Aegean microplates.

The Anatolian block is moving southwestwards, and this motion is facilitated by the presence of the subduction where the Aegean plate can easily override the subducting slab of the African plate (Kiratzi and Louvari, 2003). The Aegean Plate is moving rapidly towards the SW relative to Eurasia at a rate of 30 mm/year (McClusky et al., 2003). This westward escape of the Anatolian Plate is facilitated by the presence of the North and East major strike slip faults. The Anatolia Plate extends from eastern Anatolia to the Aegean coastal region of Turkey, where it breaks up into highly deformed crust as far west as the Ionian Sea (Jolivet and Faccenna, 2000; McClusky et al., 2000). The northern boundary, or principal tectonic displacement zone, is the North Anatolian right-lateral strike-slip fault (NAF), extend in from eastern Turkey in a broadly northward-convex curve across the Anatolian Peninsula through the Sea of Marmara into the northern Aegean Sea. From the Sea of Marmara westward, the NAF is expressed as three individual strike-slip fault traces with a component of normal displacement. In the Aegean Sea north of these strike-slip faults, the Anatolia Plate is not rigid, and its northern boundary is more diffuse, including normal faults in the northern Aegean Sea and as far north as Bulgaria, south of the stable Moesian Platform. The Dinarides extend southeastward from the Alps along the Croatian coast into Albania and into Epirus and the Ionian Islands in northwestern coastal Greece, characterized by faults and earthquakes with evidence of reverse faulting close to the Eurasia (Hellenic)–Nubia plate boundary (Copley et al., 2009). This zone is the remnant of a much broader southeast-trending Alpine zone formerly including all of Greece (Underhill, 1989). Except for this zone of reverse faulting along the west coast and strike-slip faulting in the northern Aegean Sea, the rest of

Greece is characterized by normal faulting through the Peloponnesus Peninsula to the island of Crete (Kokkalas et al., 2006), related to subduction-zone rollback. Normal faulting also characterizes the southwestern coastal regions of Anatolia, whereas central and eastern Anatolia, a more rigid plate, is dominated by strike-slip faulting.

The broad curvature of the NAF in Turkey means that the Anatolia Plate is rotating counterclockwise; the plate ends southwestward where oceanic crust of the Africa (Nubia) Plate is subducting north-northeast beneath southwestern Greece and Turkey. The convergence rate at the Hellenic trench is ~ 40 mm/yr, as compared with the convergence rate farther west between Nubia and Eurasia of 8.1 mm/yr. However, the GPS-derived convergence rate between Eurasia and Nubia at the longitude of Greece, comparing stations in the lower Nile with those in stable Eurasia to the north, is 5–6mm/yr (McClusky et al., 2000), indicating that the high rate at the plate boundary is due to southward spreading caused by Aegean normal faulting and slab rollback. It is a full-fledged subduction zone, marked by deep-focus earthquakes in the downg oing slab and by active volcanism, including the Santorini caldera of the southern. Earthquakes on the subduction zone are rare compared with crustal earthquakes and are found mainly at shallow depths (Shaw and Jackson, 2010). The normal faulting in the upper plate is similar to that in the Calabrian subduction zone in the Tyrrhenian Sea and the dying Carpathian subduction zone in the Balkans, both attributed to slab rollback. Greece has the highest instrumental seismicity in Europe.

Based on the above, it becomes clear that the seismotectonic setting of the Eastern Mediterranean is undisputedly complex. In order to implement the generalised NESP formalism I will attempt to identify seismic source areas and address the seismotectonic framework by examining the stress field of the Hellenic and Western Turkey system. The present analysis is an attempt to better underpin the validity of the NESP approach by investigating the dynamics of the Hellenic – Westen Turkey and searching for signs of randomness or self-organization as a function of time.

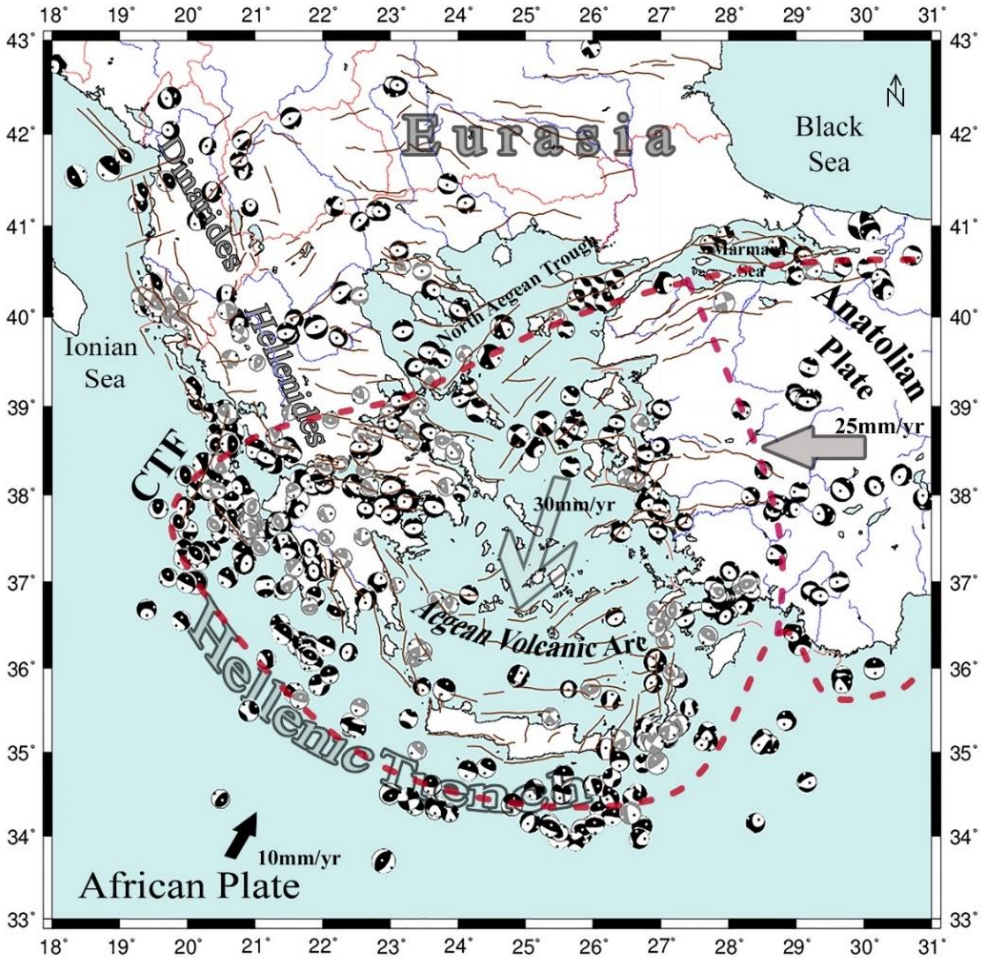

Figure 5.1 Fault plane solutions for major shallow earthquakes (depths<40km); the illustrated black and white beachballs are conducted by Harvard CMT solutions, the grey-white beachballs by Konstantinou et al, 2010. The dashed blue line represents the boundaries of the Aegean micorplate. The active faults are illustrated with dark red lines.

5.1 CONTEMPORARY STRESS FIELD

Geological and tectonic mapping does not always produce direct evidence of the contemporary stress field in a given area. The stress field may be assessed from data such as the fault plane solutions of the earthquakes occurring in a region; however, thus reliable earthquake focal mechanisms are essential for the study of the source characteristics of an earthquake. Here, I attempt to determine the stress field of the Hellenic and Western Turkey system.

A paradigmatic example of stress inversion obtained for the area of NE Peloponnesus is illustrated in Fig. 5.2a and is presented as follows: Let the stress field be defined in the standard geological/geophysical sense with $\sigma1 > \sigma2 > \sigma3 > 0$ representing the principal stress axes. Then, the relative magnitude and orientation of the stress axes can be computed from focal mechanisms by formal inversion, i.e. by finding the stress tensor

that optimally reproduces the observed focal mechanisms. The stress field inversion method implemented herein is the SATSI algorithm of Hardebeck and Michael (2006), as redesigned and recast into the MSATSI software package by Martínez-Garzón et al., (2014). In fact, SATSI is an upgraded version of the method of Michael (1984, 1987) and uses a bootstrap resampling method for misfit calculations and homing into the optimal solution. According to Hardebeck and Haucksson (2001) this approach is more accurate for noisy data sets and provides a more appropriate estimate of uncertainty. The inversion also returns a measure of the misfit between the optimal (best fit) solution and the data, given by the angle $\bar{\beta}$ which is the mean of the angles β formed between the calculated slip vector from stress tensor inversion and the observed slip vector from fault plane solutions. A synthetic control study also showed that the amount of heterogeneity in the stress field could be characterized by $\bar{\beta}$: For focal mechanism data with errors of the order 10°-30°, $\bar{\beta}$ varies in the range 30°-45° when the spatially uniform and variable parts of the stress field have equal sizes (Michael, 1991). Thus, misfit angles significantly lower that these values can be taken to indicate satisfactory solutions and approximately homogeneous stress fields.

Conditions for the results of formal inversion to be meaningful are: (a) the stress should be uniform in the study area, at least during the interval in which the data was acquired, (b) the earthquakes under consideration should be shear dislocations on pre-existing faults, (c) similar shear stress magnitude should be present at each fault and, (d) the slip should occur in the direction of the resolved shear stress on the fault plane.

Accordingly, the inversion was carried out on the basis of 930 crustal events (depth ≤ 40km) from Konstantinou et al., (2010) database and Harvard CMT catalogue. A representation of the expected crustal stress result is shown in Fig. 5.2b. As can be seen, four subset areas can be distinguished (Fig.5.3): a) North Anatolian Fault and North Aegean Trough (henceforth referred as NAF-NAT) characterized by WNW-ESE normal faulting, b) the area of Central Greece and South Aegean (henceforth referred as HEL) characterized by normal faults, c) the broader area of Cephalonia Transform Fault (henceforth referred as CTF) characterized by dextral strike-slip faults and thrust faults and d) Hellenic Subduction Zone (henceforth referred as SUB) which exhibits complex faulting patterns, with an overlapping of the sinistral strike-slip faulting of the Pliny and Strabo trenches with the thrust faulting of the outer eastern Hellenic Arc. A more detailed description of their seismotectonic characteristics is given in the following sections.

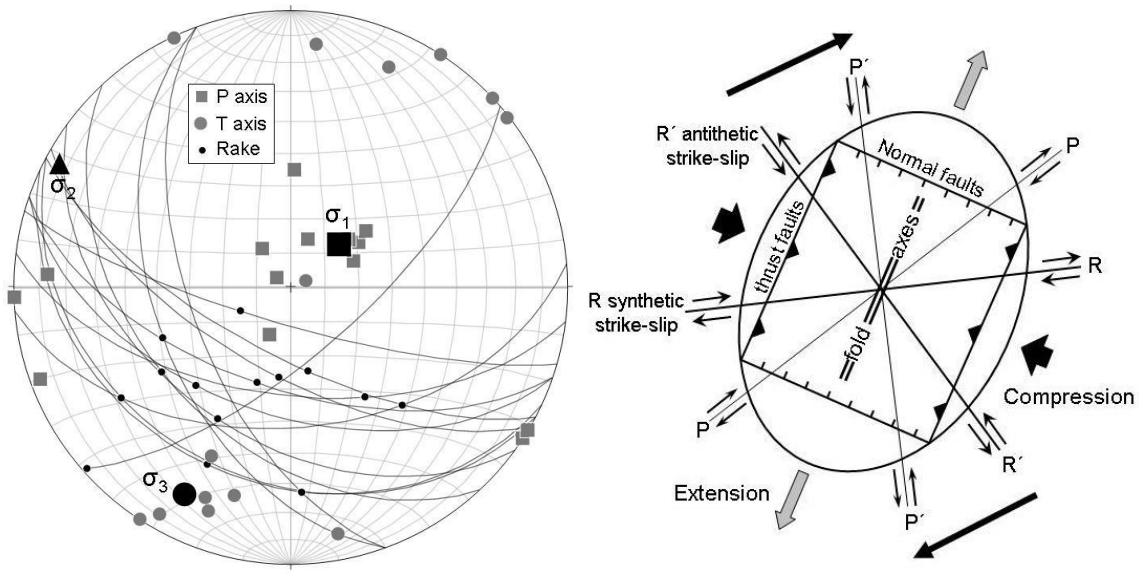

Figure 5.2a. Schmidt projection of the stress field obtained by inversion of 22 post-2002 mechanisms with *M*w between 3.8 and 4.9 in the area of NE Peloponnesus. Grey squares and circles indicate estimates produced by bootstrap resampling and the expanse of the 95% confidence area for σ_1 and σ_3 respectively. The expected "typical" faulting mechanisms and the schematics of the faulting pattern expected from Riedel shear theory are also projected.

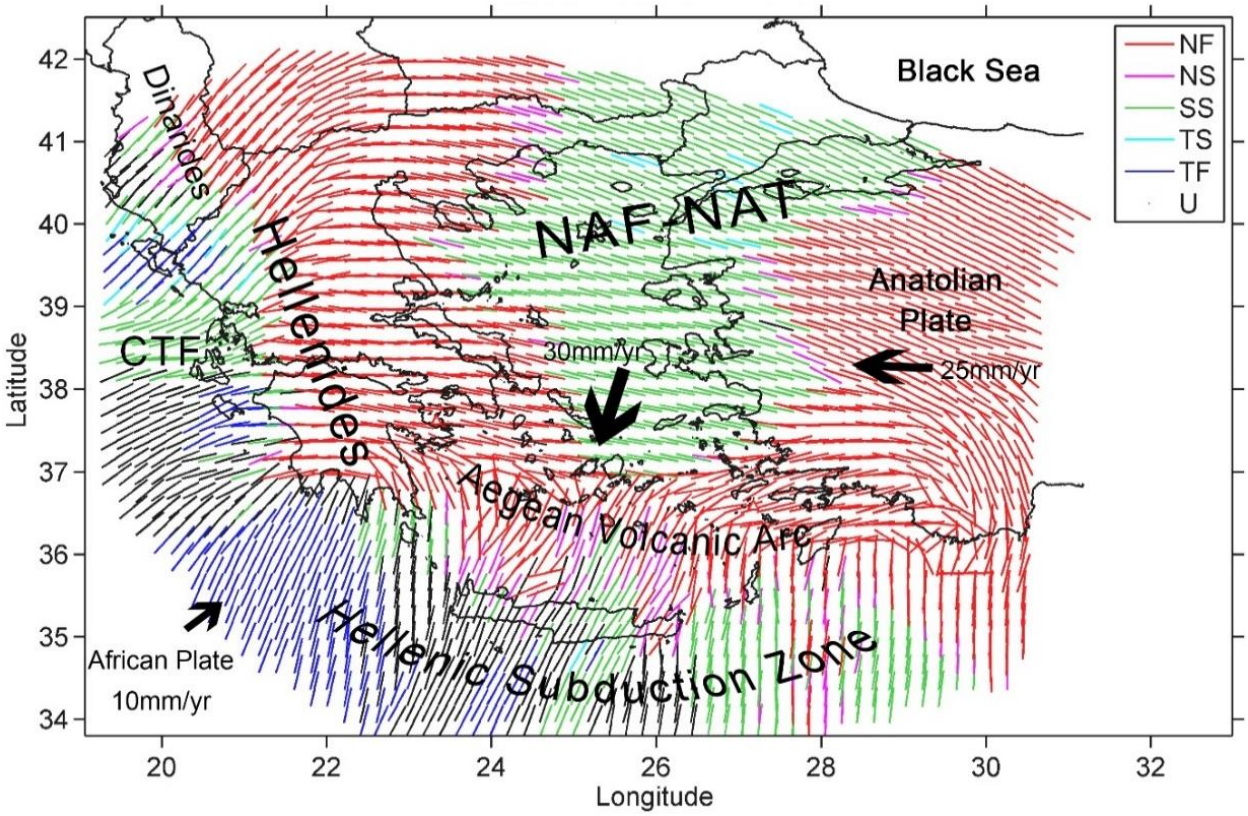

Figure 5.2b Stress tensor map of Greece compiled from Harvard CMT and Konstantinou et al., (2010) solutions for the period 1977-2013 and depths <40 km.

5.2 HELLENIC SEISMOTECTONIC SETTING

North Anatolian Fault in the North Aegean Sea

The North Anatolian is a right-lateral strike-slip fault (NAF) extending from eastern Turkey across the Anatolian Peninsula through the Sea of Marmara into the Northern Aegean Sea. It is the northern boundary of the internally deforming Anatolian Plate. Evidence through GPS measurements have shown that fault strike changes from west-southwest at the Turkish coast to southwest closer to the Greek mainland, reflecting the counterclockwise rotation of the Anatolia Plate. The fault in Turkey expresses more strike-slip, whereas the fault in the Northern Aegean Sea expresses transtension. Extensional component to predominantly strike-slip focal mechanisms are considered to be responsible for the presence of linear basins such as North Aegean Trough and Skyros Basin. In the particular area large earthquakes include strike-slip events (*Ms* 7.2 - 17/02/1968; *Ms* 6.9- 18/01/1982 and *Ms* 6.9-06/08/1983) and a normal fault event *Ms* 6.5 on 04/03/1967. Regarding the continuation of NAF into the Greek Mainland, it is unclear how right slip decreases westward across the Aegean and how it is accommodated on the Greek mainland (Goldsworthy et al., 2002).

Greek mainland (Hellenides) and South Aegean normal faults

Based on the focal mechanisms the Greek mainland can be divided into the following areas:

1. Northwestern Greece (including Bulgaria, Thessaly, and Greek Macedonia) which is dominated by normal faulting trending predominantly northwest–southeast and east–west, with normal-fault focal mechanisms and south-oriented velocities ranging from 2-3mm/yr (Kahle et al., 2000; McClusky et al., 2000; Sella et al., 2002) to 5–10 mm/yr relative to Eurasia (Nyst and Thatcher, 2004). The eastern area of the North Aegean is dominated by the western extension of the North Anatolian fault, with predominantly strike-slip focal mechanisms. GPS measurements suggest a north–south extension across Bulgaria which does not exceed 1 mm/yr (Kotzev et al., 2001, 2006; Dimitrov et al., 2006), and that Bulgaria is still within the area of Aegean extension. The most recent large earthquakes within the particular area is the M 6.4 in Thessaloniki on 20/07/19784 (Papazachos et al., 1979) and the M6.0 in Skopje on 26/07/1963 (mentioned but not described).
2. At N-NE Peloponnesus and particularly the deformation zone of the Gulf of Corinth, the GPS velocities for the past 20 years show that an extension is almost accommodated

offshore the internal part of the rift in a band as narrow as 10km near the area of Aigion. The present extension (in Xilocastro) is calculated to about 11mmyr and oriented at N185°, while in the western part at 16mmyr to the same direction. Southern and northern blocks behave as small tectonic units and are affected by rotations rates7 ± 0.5◦ Myr−1 for the northern block, 2.8±0.8◦ Myr−1 for the southern block (Avallone et al., 2004). According to large scale surveys (McClusky et al., 2000) Peloponnesus moves at 30 mmyr−1 towards N215°. The given values of velocity and their accuracy establish this estimation of rotation rate of Peloponnesus as reliable, based also on paleomagnetic data. Corinth Rift opens more rapidly in the west than in the east (Taymaz et al., 1991). Based on tectonic and seismological analysis, the northern part of the rift is deforming at a relative slow north–south rate of 120 ±50 nstrain yr−1, while the internal deformation of the southern part of the rift is less than 20 nstrain·yr−1, (Goldsworthy et al., 2002) The slow rate of deformation across the major faults of the southern part of the Gulf (<1 nstrain·yr−1) implies long recurrence periods for large earthquakes (Ms =6.5 to 7) on these faults, 500–1000 years or more. Therefore, the smaller structures located in the inner part of the rift (like the 1995 fault) accommodate most of the rift extension probably with relatively frequent earthquakes of lower magnitude (Ms = 5.5 to 6.5).

3. The southern Peloponnesus as well as the islands of Crete and Karpathos east of Crete are marked by normal faults striking slightly east of north in Crete and the islands between Crete and the Peloponnesus and north-northwest farther north in the Peloponnesus (Figures 7.5, 7.6). The pattern of east–west extension, about 5 mm/yr in the Peloponnesus based on GPS (Nyst and Thatcher, 2004), is south of the volcanic arc, where extension is north–south (Figure 7.4). The faults cut across Miocene and older bedrock structures, including the east–west orientation of the island of Crete itself. On the other hand, faults have been in place long enough to occupy positions at range fronts, like the American Basin and Range. Armijo et al. (1992) pointed out the similarity between the orientation of normal faults in the southern Aegean and Peloponnesus and those in Tibet (Armijo et al., 1986), where extension also takes place at right angles to the direction of plate convergence. An important recent earthquake of this subprovince was the 1986 Kalamata earthquake of Ms 5.8 on the west side of the Taygetos Mountains (Lyon-Caen et al., 1988). According to Armijo et al., (1991) a slip rate of 1 mm/yr and a recurrence interval for large earthquakes of 3000 years is estimated. Focal-mechanism solutions indicate almost pure extension. Lyon-Caen et al., (1988) also included source parameters of an offshore normal-fault earthquake north of western Crete on 27 April 1965 of mb 5.7

at a depth of 13 ± 5 km, and essentially east–west extension, adding information about this sub-province of north-striking faults.

Reverse faulting in Ionian Sea

One of the most seismically active parts of Greece is westernmost of Gulf of Corinth, the Ionian island of Cephalonia (Kefallinia). This area has experienced some of the greatest earthquakes in the past five decades (M>7 in 1953, 1972 and 1983). Cephalonia is located at the northwestern end of the Hellenic subduction zone, and a scarp marking the northeast-striking Cephalonia Transform Fault (CTF) is the boundary between subducting oceanic crust to the southeast, and a continental collision zone between the Dinarides fold-thrust belt and the Adriatic (Apulian) platform (Underhill, 1989; Clément et al., 2000; Sachpazi et al., 2000; Shaw and Jackson, 2010). Cephalonia is crossed by thrust faults. A fault plane solution of an event Ms5.8 on 23/01/1992 is believed to be consistent with displacement on one of these thrust faults (Tselentis et al., 1997), although these relations would also be consistent with an earthquake on the subduction zone. An earthquake of *Ms* 7 on 17 January 1983 may have occurred on a secondary transform fault striking northeast directly beneath Kefallinia (Scordilis et al., 1985).

Hellenic Subduction Zone

The Hellenic Subduction Zone is marked by Western Hellenic NW-striking trenches and the NE striking trenches SE of Crete and Rhodes (Pliny and Strabo). These trenches represent outer-arc basins with parts of them at depths > 4km and other areas at depths < 3km. Its NW ending is abrupt at the right-lateral CTF. The Hellenic subduction zone is characterized by high seismicity that follows the Hellenic arc. Examples of outstanding historical events around Crete are the earthquakes near the southwestern coast of Crete in 365 with *Ms* 8.3 and north of eastern Crete in 1856 with *Ms* 8.2 (Papazachos, 1996).

The Benioff zone has been studied extensively (Papazachos and Comnikakis, 1971; Comninakis and Papazachos, 1980; Makropoulos and Burton, 1984; Papazachos, 1990; Hatzfeld and Martin, 1992; Hatzfeld, 1994; Knapmeyer, 1999; Papazachos et al, 2000, Shaw and Jackson, 2010). Intermediate depth earthquakes (approx. 60-160 km depth) allowed to define the Benioff zone and indicate a descending slab with a very low dip south of the Ionian Sea trench (Matapan Trench) to depths of 50–80 km and a dip up to 45° to depths of 100-160 km beneath the volcanic arc which formed by the Cyclades and the Dodecanese. The Benioff zone steepens from the western towards the eastern part of the Hellenic subduction zone. In the eastern part of the Hellenic subduction zone, the

maximum depth of the events is about 160 km; north of western Crete no hypocenters are found deeper than 100 km. The slab has been using tomography to depths up to 600 km (Jonge et al., 1994), although some models consider the deeper part a detached slab (Spakman et al., 1993; Jiménez-Munt et al., 2003) rather than part of a continuous subduction zone.

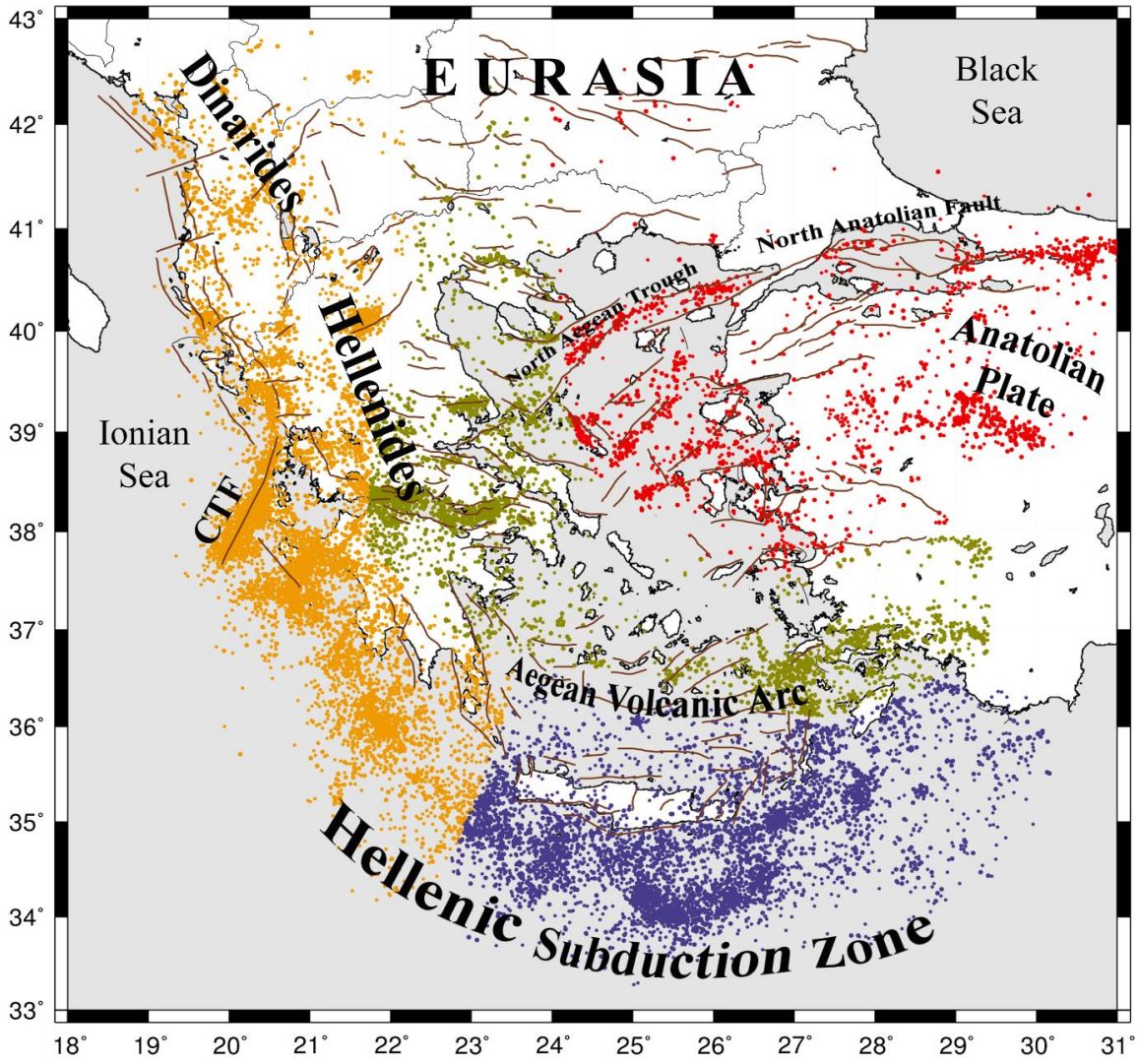

Figure 5.3 Earthquake epicenters and major faults for the subset areas of the Hellenic – Western Turkey seismogenetic system for the period 1964-2015 and $M_{th} \geq 3.8$. **CTF** subset area is illustrated with orange colored epicenters; **HEL** subset area is illustrated with green colored epicenters; **NAF-NAT** subset area is illustrated with red colored epicenters; **SUB** subset area is illustrated with purple colored epicenters;

5.3 EARTHQUAKE DATA

The earthquake data utilized for Greece and Western Turkey was extracted by the ISC data base which is homogenous by construction with consistently determined hypocenters and magnitude (http://www.isc.ac.uk, Internatl. Seis. Cent., Thatcham, United Kingdom, 2011). The full catalogue comprises 18625 events reported in body-wave *Mb* (magnitude scale) and recorded within the area 33°N/43°N and 18°E/31°E over the period 01/01/1964- 31/08/2015, while its declustered counterpart at 70% probability level comprises 3341 events.

The ISC catalogue presents a puzzling situation: Fig. 5.4a clearly shows two periods based on the computation of magnitude completeness: the period 1964-1996 where M_c varies from 4.1 to 4.4 and the period (1997-2015) where M_c decreases to approximately 3.5-3.8. Moreover, the F-M distribution of seismicity –as this is outlined in Fig. 5.4b– is bimodal. For magnitude scales between ML =3.5 and 4.1 the b value is 0.24 and for ML > 4 increases, almost abruptly, to 1.17 – 1.3. The origin of bimodal distributions might sometimes be natural, (different physical mechanisms operating at small and intermediate-large magnitude scales), although b values as low as 0.24 over such a broad area are not easy to explain. In this case, it is not difficult to verify that that bimodality is definitely due to the relative sparsity of the monitoring network up until the mid-1990s. This observation is strongly corroborating with the analysis of the seismic parameters for the two distinct periods. Figures 5.5 to 5.8 show the results of mapping various seismic parameters such us the minimum magnitude of completeness[10], earthquake density[11], resolution map[12] and b-value map[13] via ZMAP software tool.

According also to a research conducted by Mignan and Chouliaras (2014) with respect to NOA network within the period 1964-2013, it was shown that the number of seismic

[10] We examine the spatial variations by creating dense spatial grids, in order to evaluate the minimum magnitude of completeness. The map was computed with a constant number of samples using a regularly spaced grid set at dx = 0.25/dy = 0.25-degree intervals. The minimum number of events for each sample was set to 250.

[11] This map can be used to investigate the reporting history of the seismic network. The earthquake density map represents a spatial distribution of earthquakes and works as a further option of quality control.

[12] we determine the range of radii with respect to the selected number of events; this provides an approximate assessment of the radius we could choose in case we want to calculate a *b-value* map with constant radius, from which a local recurrence time map or, equivalently, a local probability map can be constructed.

[13] The specific map represents an initial estimation of *b-value*, but it should not be examined independently from the other parameters.

stations increased with time; during the first three decades the number of the stations was approx. 30 and only during the mid-00's the network and its products improved. The development took place gradually from the end of 2007 to 2011 where more than 100 additional stations were installed. With denser network and modern data processing, the minimum magnitude of completeness (M_c) decreased from 4.1-4.6 to < 3.8 thresholds.

It is apparent that for the period 1964-1996, the homogenized version of the ISC catalogue, is complete for ML > 4.1 (Figs. 5.4; 5.5 and 5.9a & 5.9b). Conversely, for the period 1997-2015 I shall consider all earthquakes with magnitudes ML ≥ 3.6-3.8, for which the catalogue appears to be complete.

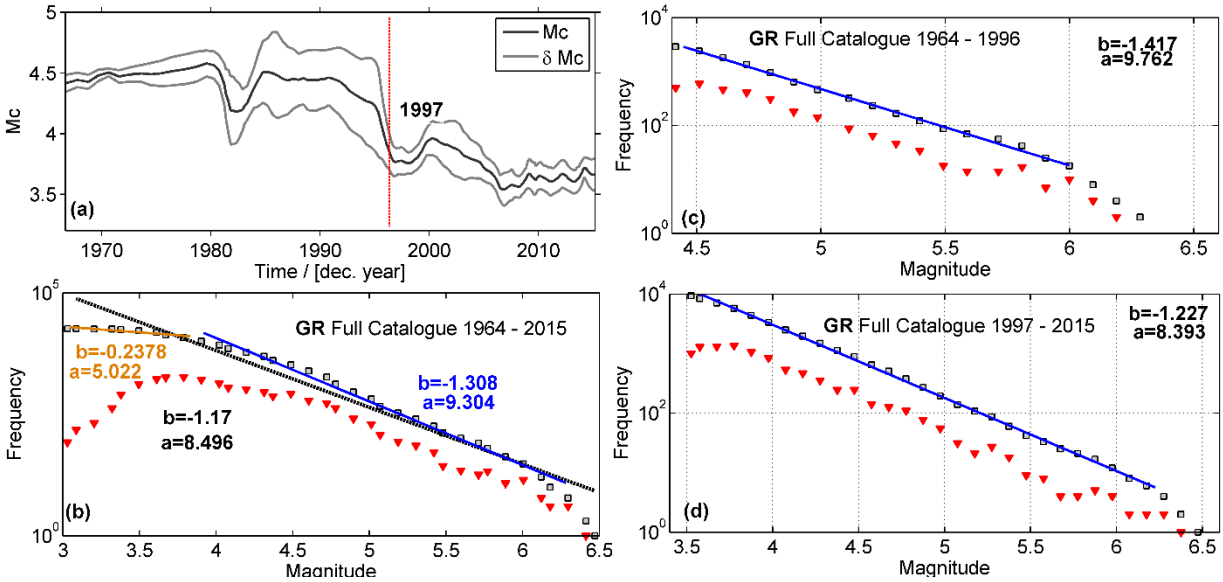

Figure 5.4 a) Estimation of magnitude of completeness with time for full GR catalogue b) estimation of a and b-value period 1964 – 2015 c) as per b for the period 1964 – 1996 d) as per b for the period 1997 – 2015.

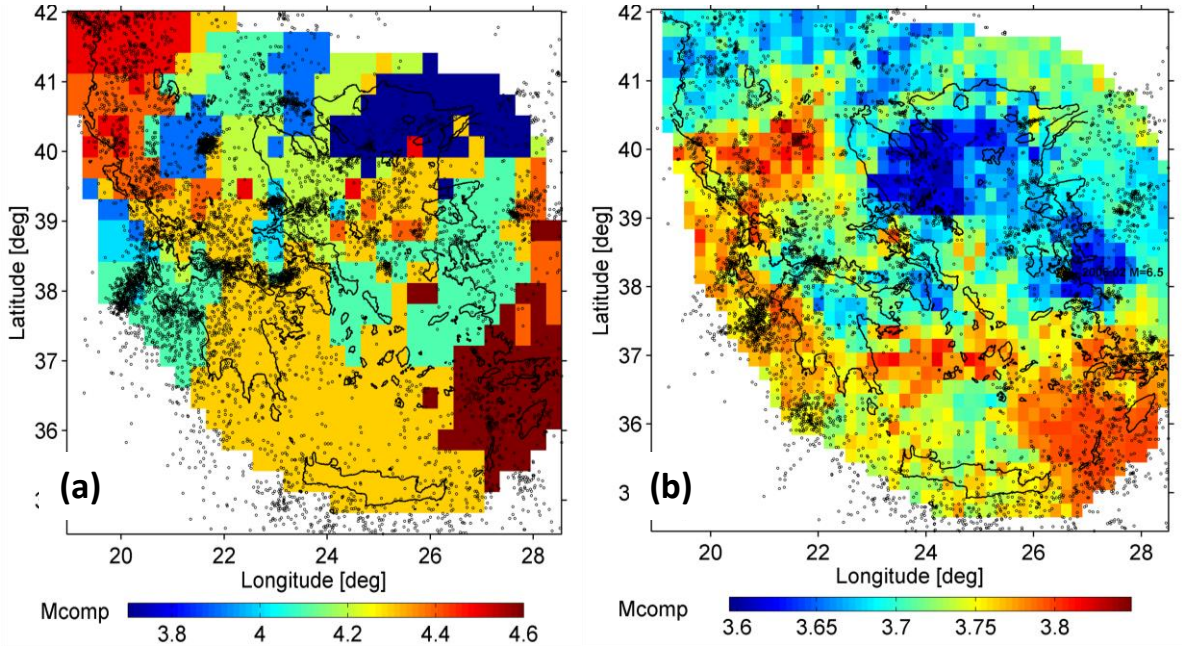

Figure 5.5 Spatial mapping of minimum magnitude of completeness Mc for the periods: a)1964-1996 and b) 1997-2011

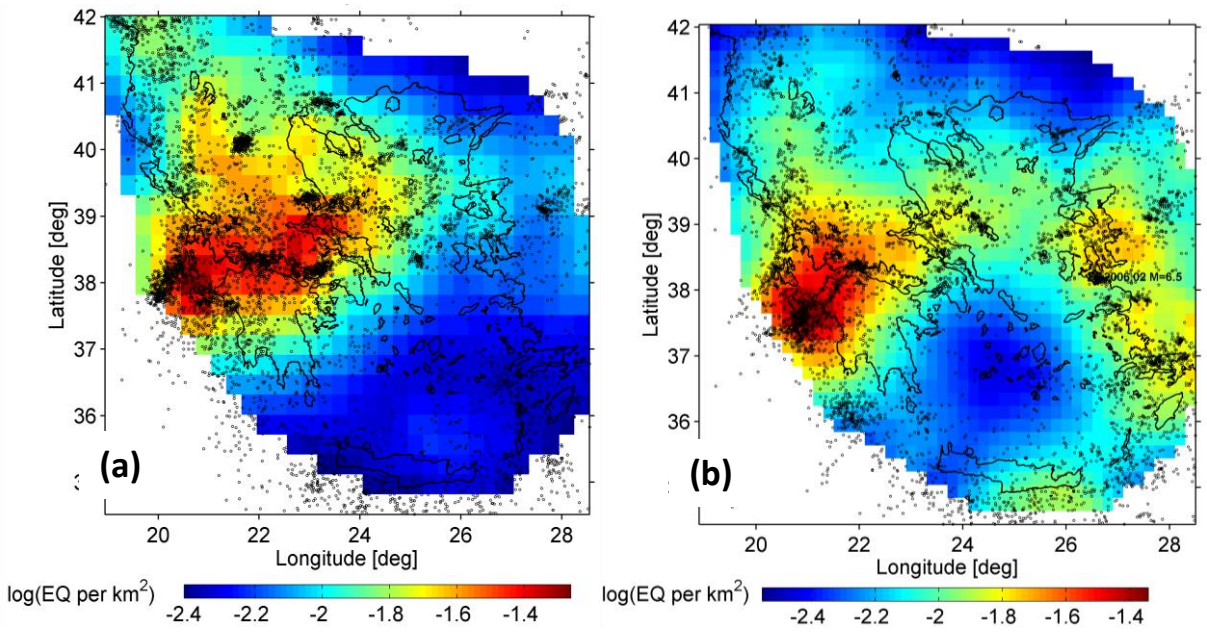

Figure 5.6 Earthquake density map for the periods: 1964-1996 and 1997-2011.

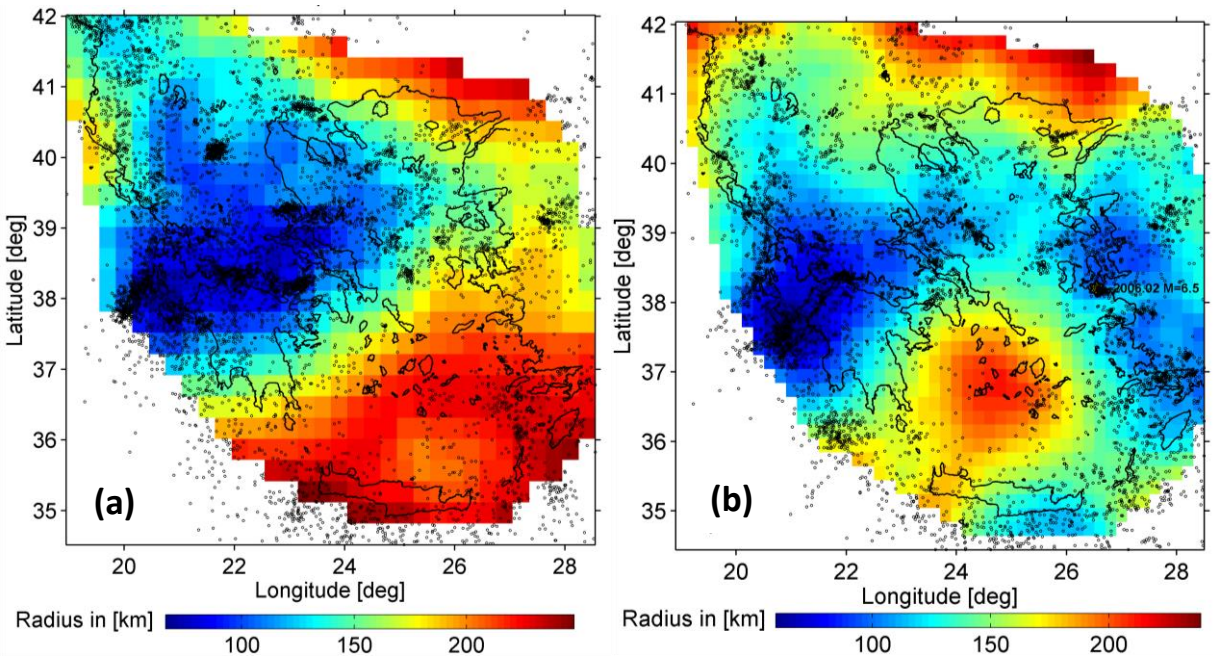

Figure 5.7 Resolution map for the periods: 1964-1996 and 1997-2015.

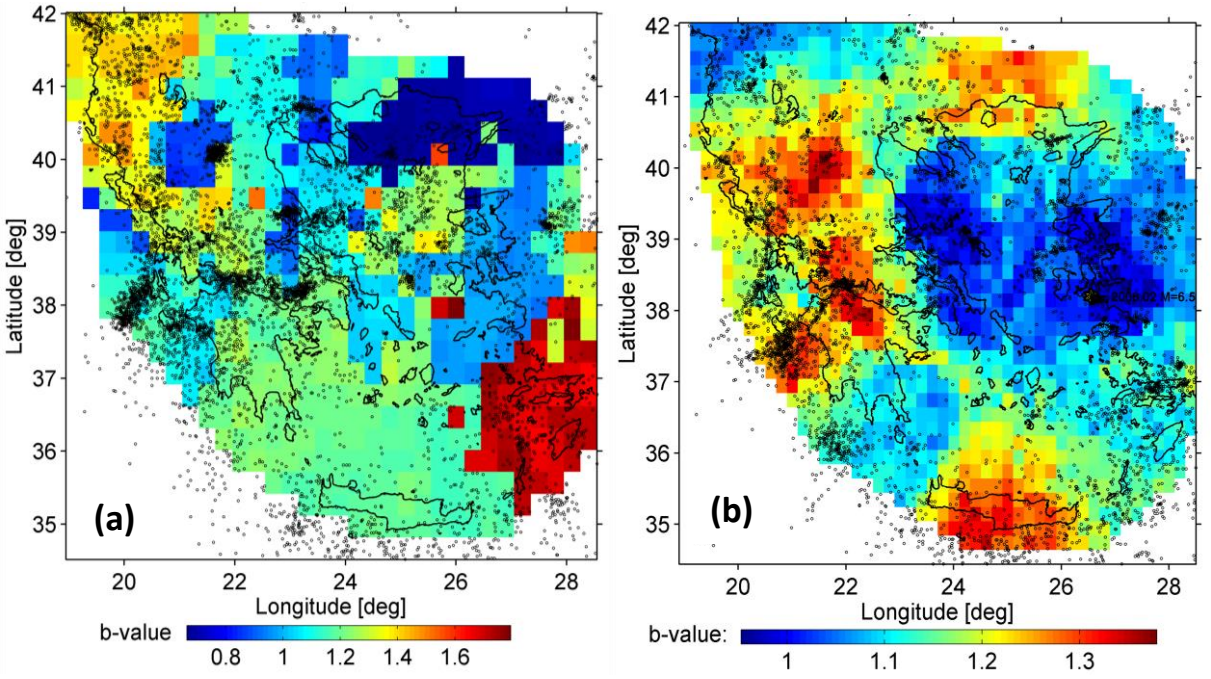

Figure 5.8 *b-value* map for the periods: 1964-1996 and 1997-2011.

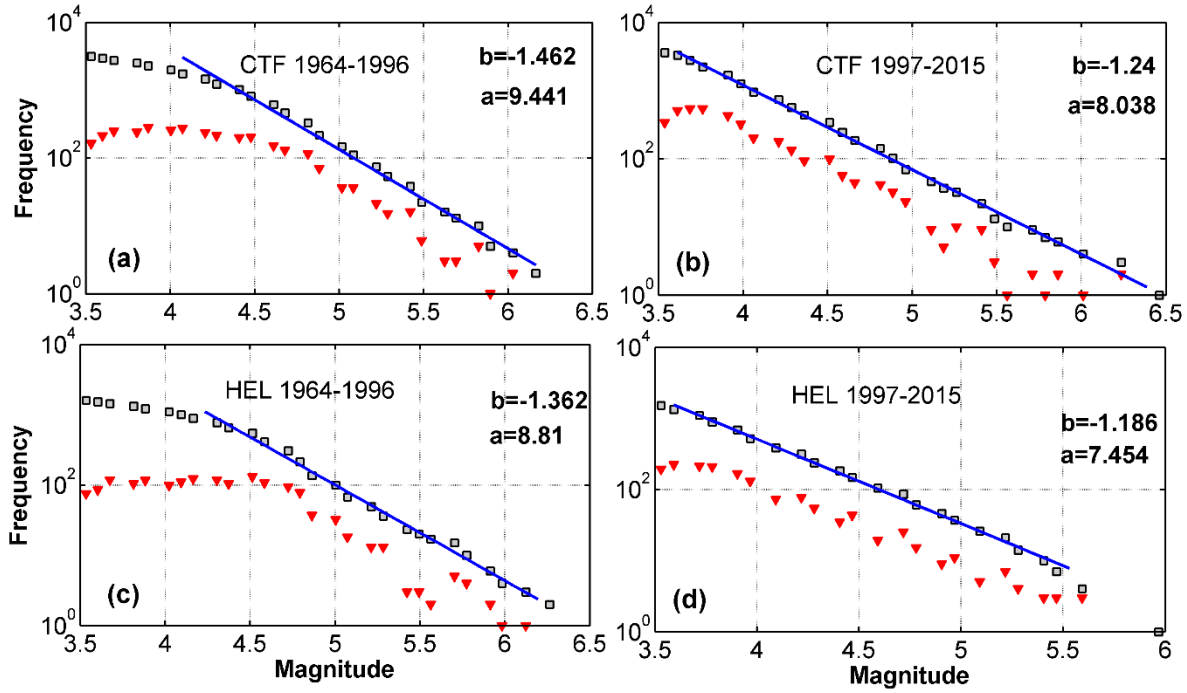

Figure 5.9a Maximum likelihood estimates of the subset areas CTF and HEL for the periods 1964-1996 and 1997-2015

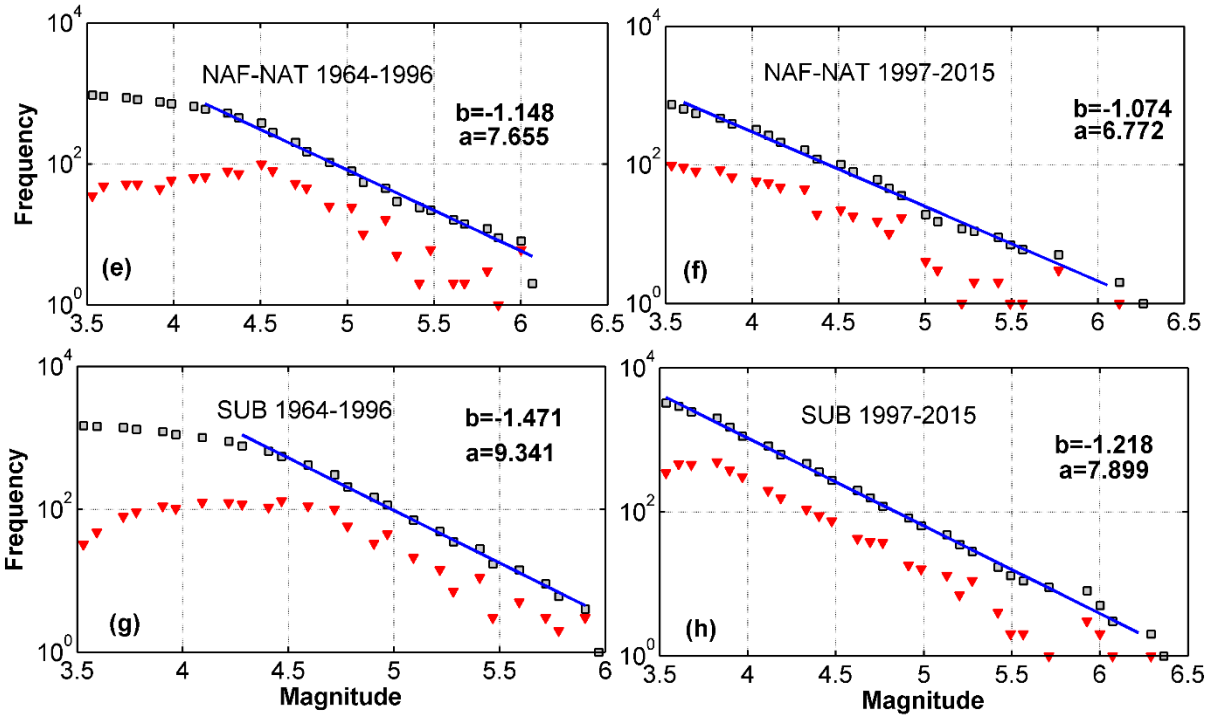

Figure 5.9b Maximum likelihood estimates of the subset areas NAF-NAT and SUB for the periods 1964-1996 and 1997-2015

TABLE 5.1 Summary of ISC earthquake catalogue for Greek seismicity.

Source Area	**Source Area Code**	**Period**	M_{comp}	**Full catalogues**	**Declustered catalogues** ($\phi_i \geq 70\%$)	**Declustered catalogues** ($\phi_i \geq 80\%$)	**Declustered catalogues** ($\phi_i \geq 90\%$)
				№ events	№ events	№ events	№ events
Cephalonia Transform Fault – Hellenic Trench	**CTF**	1964-2015	4.0	3250	871	507	477
		1964-1996	4.0	1990	*<300*	*<300*	*<300*
		1997-2015	3.6	3266	*<300*	*<300*	*<300*
Internal Hellenides and South Aegean Sea	**HEL**	1964-2015	4.1	1387	519	425	>300
		1964-1996	4.1	998	*<300*	*<300*	*<300*
		1997-2015	3.6	1333	*<300*	*<300*	*<300*
Source Area	**Source Area Code**	**Period**	M_{comp}	**Full catalogues**	**Declustered catalogues** ($\phi_i \geq 70\%$)	**Declustered catalogues** ($\phi_i \geq 80\%$)	**Declustered catalogues** ($\phi_i \geq 90\%$)

				№ events	№ events	№ events	№ events
North Anatolian Fault - Trough	**NAF-NAT**	1964-2015	4.1	925	511	*<300*	*<300*
		1964-1996	4.1	658	*<300*	*<300*	*<300*
		1997-2015	3.5	744	*<300*	*<300*	*<300*
Hellenic Trench (Subduction Zone)	**SUB**	1964-2015	4.1	1833	*<300*	*<300*	*<300*
		1964-1996	4.3	767	*<300*	*<300*	*<300*
		1997-2015	3.7	2452	*<300*	*<300*	*<300*
Central Hellenic Shear Zone	**SHR**	1964-2015	4.1	6259	1075	819	406

5.4 NESP RESULTS

As already discussed above, the content of the ISC catalogue has improved significantly in response to improvements in the detection threshold of the seismological network and in analytical procedures, especially after 1997. In order to conduct a comprehensive as possible study and ensure the significance of results, a comparative analyses of full earthquake catalogues for the individual source areas defined in Sections 5.1 and 5.2 is conducted, for: **a)** the complete period 1964-2015 with a threshold magnitude $M_{th} \geq 4.1$, **b)** as well as for the two overlapping periods: 1964-1996 with a threshold magnitude $M_{th} \geq 4.1$, and 1997-2015 with a threshold magnitude $M_{th} \geq 3.6\text{-}3.8$. As in the case of California and Alaska, the analysis focuses on the variation of the entropic indices with respect to threshold magnitude, (M_{th}) and interevent distance (Δd). The results are summarized in Table 5.2 and illustrated in Figures 5.10 to 5.19. Once again, in order to maintain experimental rigour, estimation of the entropic indices is *not* performed for catalogue subsets containing *less than* 300 events and results are *not* considered and displayed *unless* associated with a goodness of fit (R^2) *better* than 0.97.

5.4.2. Analysis of Full earthquake catalogues for 1964-2015, 1964-1996 and 1997-2015

The analysis of the full CTF catalogue returns stable determinations of $q_M(M_{th})$ which vary from 1.43 to 1.47 (Fig. 5.10a) and yield b_q in the interval (1.32, 1.12), with larger the q_M (lower b_q) observed at the smaller magnitude scales. As can also be seen in Fig. 5.10b, $q_M(\Delta d)$ determinations are stable in the interval (1.47, 1.43), respectively yielding b_q in the interval (1.12, 1.32). The temporal entropic indices $q_T(M_{th})$ are rather consistently determined and found to vary between 1.08 and 1.28 indicating *low to moderate correlation* (Fig. 5.10a). Moreover, as evident in Fig.5.10b, $q_T(\Delta d)$ is rather stably determined with highly moderate correlation at short and intermediate interevent distances (1.38- 1.2), while for Δd > 400km, $q_T(\Delta d)$ rises up to 1.60 indicating high correlation at longer interevent distances.

As can be seen, the temporal entropic indices estimated for the period 1964 – 2015 and 1964-1996 are pretty much similar and generally *lower* than those estimated for the period 1997 – 2015, with particular reference to their variation with respect to magnitude threshold. To begin with, the determination of the magnitude entropic index, is *inconsistent* between the two periods, so much with respect to threshold magnitude, as with respect to interevent distance: for the period 1964–1996 $q_M(M_{th})$ varies between 1.40

and 1.45 and $q_M(\Delta d)$ between 1.44 and 1.47, while for 1997–2015 $q_M(M_{th})$ varies between 1.44 and 1.48 and $q_M(\Delta d)$ between 1.47 and 1.50.

The temporal entropic indices exhibit a slightly different behaviour between the two periods. During the interval 1964-1996 $q_T(M_{th})$ fluctuates between 1.01 and 1.24, indicating very low overall correlation (Fig. 5.11a), while $q_T(\Delta d)$ is stably determined and generally lower than 1.27 throughout the catalogue, thereby indicating low correlation at all so that $q_T(\Delta d)$ ranges (Fig. 5.11c). Conversely, in the period 1997-2015 $q_T(M_{th})$ increases gradually from just above 1.13 at M_{th} = 3.6 to only 1.25 at M_{th} = 4.8, indicating moderate correlation at the larger magnitude thresholds (Fig. 5.11b). Moreover, $q_T(\Delta d)$ is higher than 1.26 at Δd < 100km and indicates moderate correlation at short interevent distances due to the effect of near-field interactions and aftershock sequences (Fig. 5.11d); nevertheless, it drops to approx. 1.12 for 100km < Δd < 200km (near randomness) and gradually rises to 1.3 at Δd greater than 400km indicating moderate correlation.

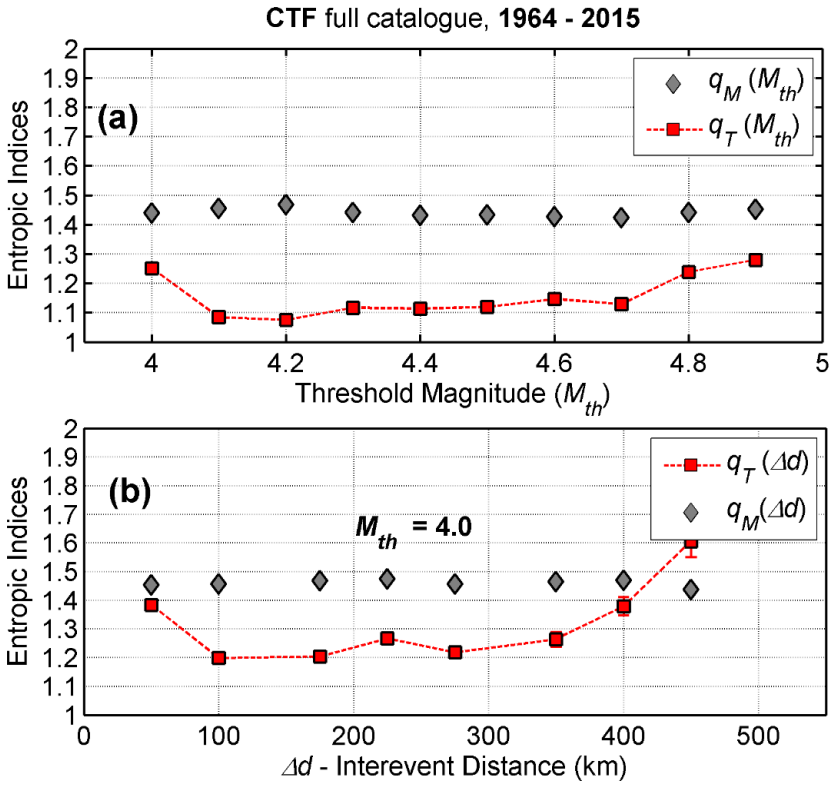

Figure 5.10 Analysis of the full CTF catalogue for the 51-year period 1964 – 2015. **(a)** Dependence of entropic indices on threshold magnitude (M_{th}). **(b)** Dependence of entropic indices on interevent distance (Δd); earthquakes are groupped in bins of 50km and symbols are plotted at the midpoint of each bin. In all cases error bars represent 95% confidence intervals.

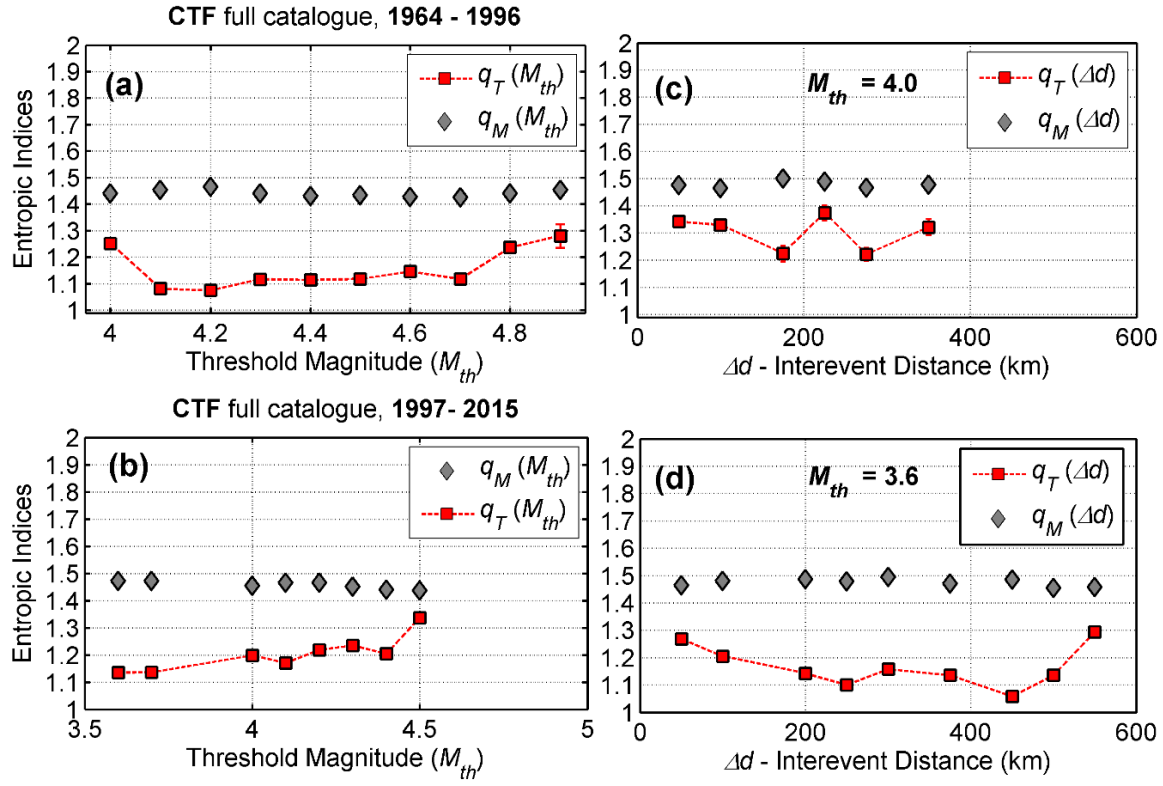

Figure 5.11 Analysis of the full CTF catalogue for the periods 1964 – 1996 (top row) and 1997-2015 (bottom row). Panels **(a)** and **(c)** illustrate the dependence of the entropic indices on threshold magnitude (M_{th}). Panels **(b)** and **(d)** illustrate the dependence of the entropic indices on interevent distance (Δd), where earthquakes with groupped in bins of breadth Δd = 50km and symbols are plotted at the midpoint of each bin. Error bars represent 95% confidence intervals

Proceeding to the the Internal Hellenides (Continental Greece), the analysis of the HEL full catalogue for the complete period 1964-2015, shows a linear downward trend of $q_M(M_{th})$ from 1.46 at M_{th}=4.1 to 1.40 at M_{th}=4.7, while $q_M(\Delta d)$ is stably determined around a mean value of 1.5 throughout the catalogue.

The temporal entropic index $q_T(M_{th})$ varies from 1.15 at M_{th} = 4.1 to 1.43 at M_{th} = 4.7, exhibiting a clear quasi-linear tendency to increase with respect to threshold magnitude, which would be interpreted to signify a corresponding *increase* in the interdependence of earthquake occurrence (correlation) with magnitude and at least up to M = 4.7 (Fig.5.12a). When the analysis is carried out with respect to interevent distances, it is expected that $q_T(\Delta d)$ will exhibit very high values at interevent distances shorter than 100km due to the dominant effect of near field interactions, with particular reference to aftershock sequences. However, such behaviour is not observed (Fig. 5.12b); for $\Delta d \leq$ 100km $q_T(\Delta d)$ varies from 1.17 to 1.25 indicating weakly moderate correlation. To the contrary, for intermediate distances 250km $\leq \Delta d <$ 400km the results of the HEL catalogue indicate

moderate to high correlation (1.33 <q_T < 1.41), while for longer distances $q_T(\Delta d)$ drops to 1.13 (Δd>400km). Note, however, that because the number of earthquakes available for analysis at 200km ≤Δd < 400km is insufficient, it is not certain whether the moderately high correlation does altogether exist for intermediate distances, or it is simply unobservable.

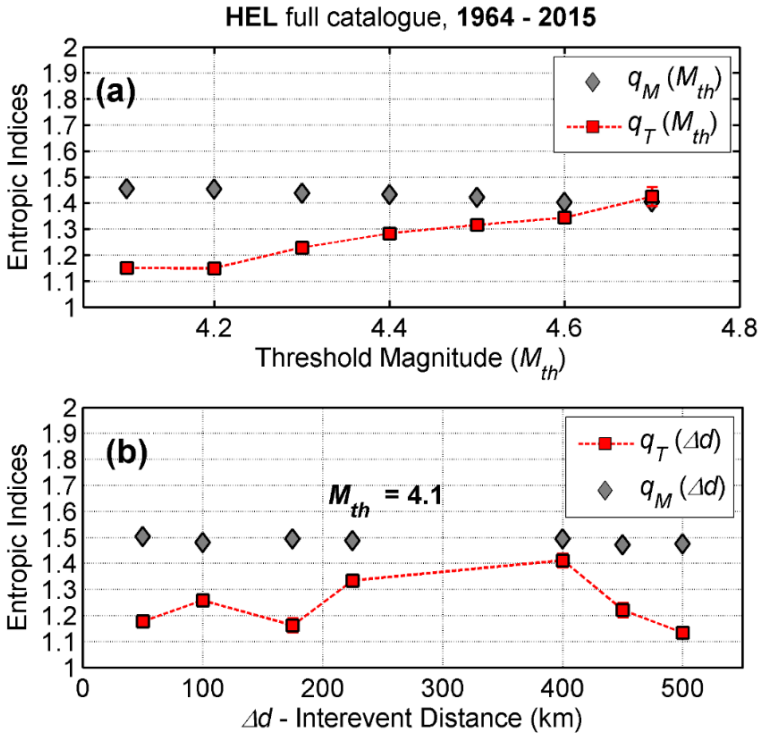

Figure 5.12 Analysis of the full HEL catalogue for the 51-year period 1964 – 2015. **As per Fig. 5.10**

Results for the HEL sub-catalogues are shown in Fig.5.13. As evident in Fig 5.13a, for 1964-1996, $q_M(M_{th})$ exhibits a low-rate linear trend from 1.45 at M_{th} = 4.1 to 1.41 at M_{th} = 4.7; the trend is not apparent in the period 1997 – 2015, where $q_M(M_{th})$ appears to have stabilized just below the value of 1.5, so that at $b_q(M_{th})$ > 1.1 (Fig.5.13b). The estimation of magnitude entropic indices with respect to interevent distance is also hampered by the overall insufficient number of events at 200km≤Δd<400km. Observations are necessarily limited to near and long-range interaction, where one may observe that $q_M(\Delta d)$ is rather stably determined for both periods, slightly fluctuating about 1.5 (Fig.5.13c and Fig.5.13d). The temporal entropic index exhibits strong fluctuations for both periods. For 1964 – 1996, $q_T(M_{th})$ behaves erratically fluctuating from 1.14 to 1.19 at smaller magnitudes while it rises up to 1.39 at larger threshold magnitudes. For 1997-2015,

$q_T(M_{th})$ displays an upward linear trend changing from 1.1 at M_{th}=3.6 to higher than 1.2 at M_{th} = 3.9 and exhibiting higher correlation, particularly at larger threshold magnitudes. Overall, $q_T(M_{th})$ indicates general absence of significant correlation at smaller magnitudes. This erratic behaviour is also observed for interevent distances. For 1964-1996 $q_T(\Delta d)$ varies from 1.25 to 1.48 for Δd < 200km and then consistently *decreases* from 1.32 at Δd between 250-400km, to 1.1-1.23 at Δd >400km (Fig.5.13c). For 1997 – 2015 $q_T(\Delta d)$ decreases from 1.53 (Δd < 100km) to 1.10 (Δd>350km) indicating high correlation at short ranges and very weak to no correlation at intermediate ranges. An interesting observation is that $q_T(\Delta d)$ increases Δd >400km to 1.37 indicating high long-range correlations.

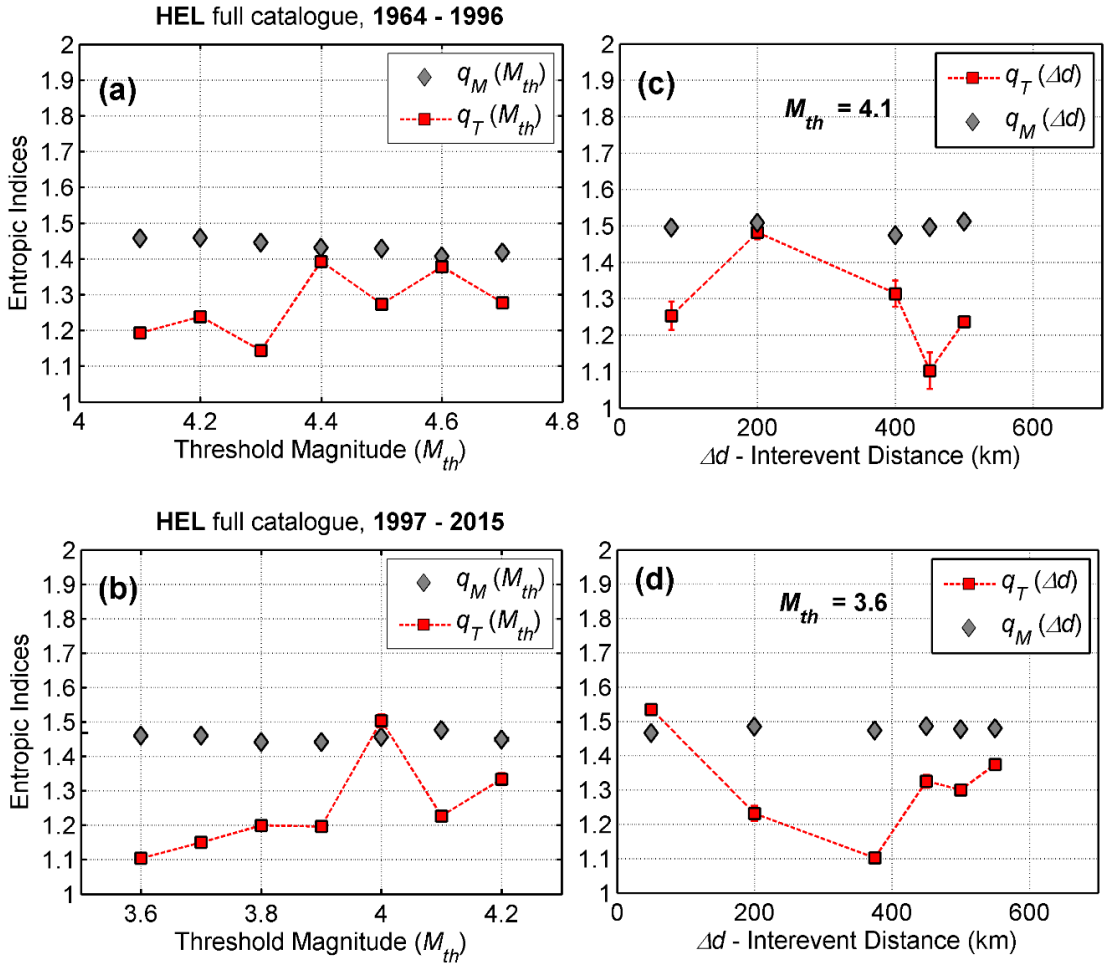

Figure 5.13 Analysis of the full HEL catalogue for the periods 1964 – 1996 (top row) and 1997-2015 (bottom row). **As per Fig.5.11**

Results for the full 1964-2015 NAF-NAT sub-catalogue are presented in Fig. 5.14. As can be seen, $q_M(M_{th})$ is very consistently determined at approx. 1.5 for all threshold magnitudes, yielding a correspondingly consistent $b_q(M_{th})$ of approx. 1.00. Analogous

observations can be made with respect to interevent distance for ; q_M (Δd) is also stably determined with values just below, or approximately equal to 1.5 so that $b_q \approx 1$. The temporal entropic index is also consistently determined with values above the randomness threshold 1.2 (with max $q_T(M_{th})$ = 1.30 and max $q_T(\Delta d)$ = 1.35) indicating moderate to high correlation at all ranges which however is not increasing with interevent distance.Turning our attention to the analysis of NAF-NAT sub-catalogues for the two periods, it is important to note that results are shown only for magnitude threshold, as the declustered 1964-1996 and 1997-2015 catalogues respectively contain 658 and 744 events and cannot be reliably evaluated for the analysis of interevent distance. As can be seen in Fig. 5.15, for both periods $q_M(M_{th})$ is once again very consistently determined at approx. 1.5 for all threshold magnitudes. The temporal entropic index holds its own "surprise": for both periods $q_T(M_{th})$ varies from 1.51 to 1.59 (1964-1996) and from 1.67 to 1.49 (1997-2015). Overall, it appears that NAF-NAT system remains highly correlated at *all* ranges, and more significantly, it is statistically *different* from the CTF and HEL systems.

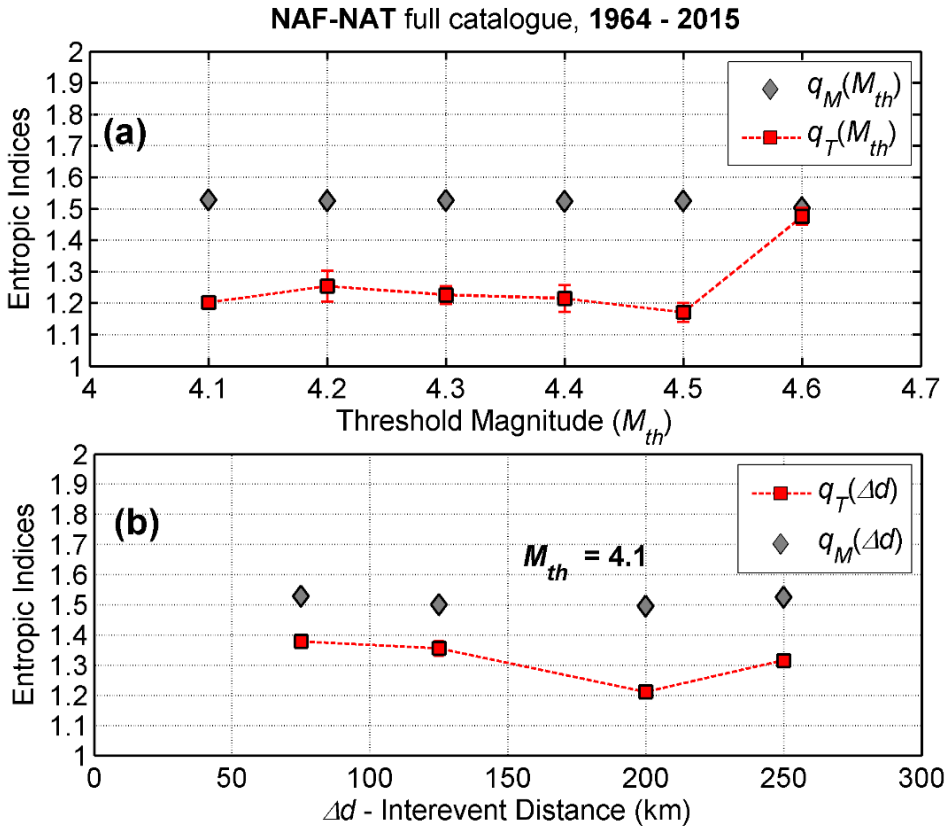

Figure 5.14 Analysis of the full NAF catalogue for the 51-year period 1964 – 2015. **As per Figure 5.12**

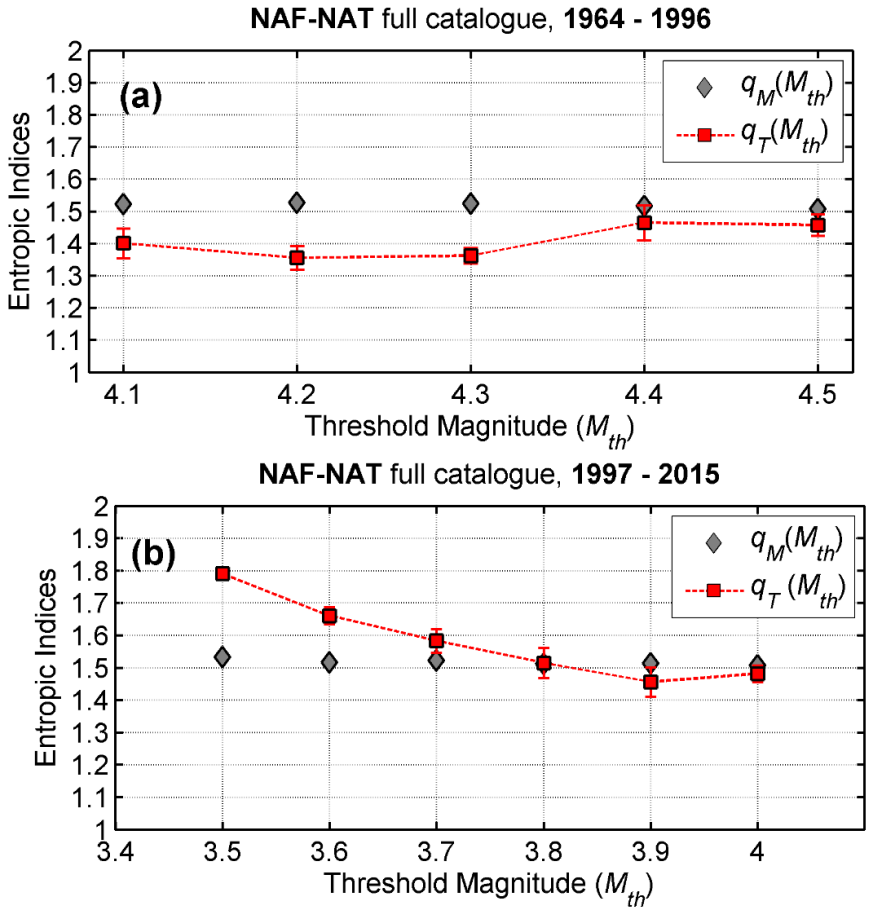

Figure 5.15 Analysis of the full NAF-NAT catalogue for the periods 1964 – 1996 (top row) and 1997-2015 (bottom row). Panels **(a)** and **(b)** illustrate the dependence of the entropic indices on threshold magnitude (M_{th}). Error bars represent 95% confidence intervals

Finally, the area of Hellenic Trench (Subduction Zone) is examined. The analysis of the SUB catalogues is conducted for M_{th} ≥4.4 for which the catalogue appears to be complete (see section 5.3). The analysis of the full SUB catalogue for 1964-2015, returns stable determinations of $q_M(M_{th})$ which vary from 1.44 to 1.41 (Fig.5.16a) and yield b_q in the interval (1.27, 1.43), with larger the q_M (lower b_q) observed at the smaller magnitude scales. As can also be seen in Fig. 5.16b, $q_M(\Delta d)$ determinations are stable in the interval (1.43, 1.47), respectively yielding b_q in the interval (1.32, 1.12). The temporal entropic index $q_T(M_{th})$ is rather consistently determined and found to vary between 1.09 and 1.26 indicating *very weak correlation – near randomness thresholds*. Moreover, as evident , $q_T(\Delta d)$ is also consistently determined at 1.09-1.00 (100≤Δd<300km) indicating randomness for shorter and intermediate interevent distances, while for Δd>300km, $q_T(\Delta d)$ rises up to 1.29 indicating moderate correlation at longer interevent distances.

Results for the 1964-1996 and 1997-2015 SUB -catalogue are presented in Fig. 5.17. As can be seen, $q_M(M_{th})$ and $q_M(\Delta d)$ are very consistently determined at approx. 1.5 for all threshold magnitudes, yielding a correspondingly consistent $b_q(M_{th})$ of approx. 1.00. An exception is made for $q_M(M_{th})$ where the values are very low at approx. 1.4 ($b_q(M_{th})$=1.5). The temporal entropic index $q_T(M_{th})$ is also consistently determined indicating in general low correlations with magnitude thresholds for both periods. With respect to interevent distance $q_T(\Delta d)$ shows higher correlations at short distances (1.34 – 1.41) due to the overwhelming effect of aftershock sequences, while at large ranges $q_T(\Delta d)$ decays to oblivion.

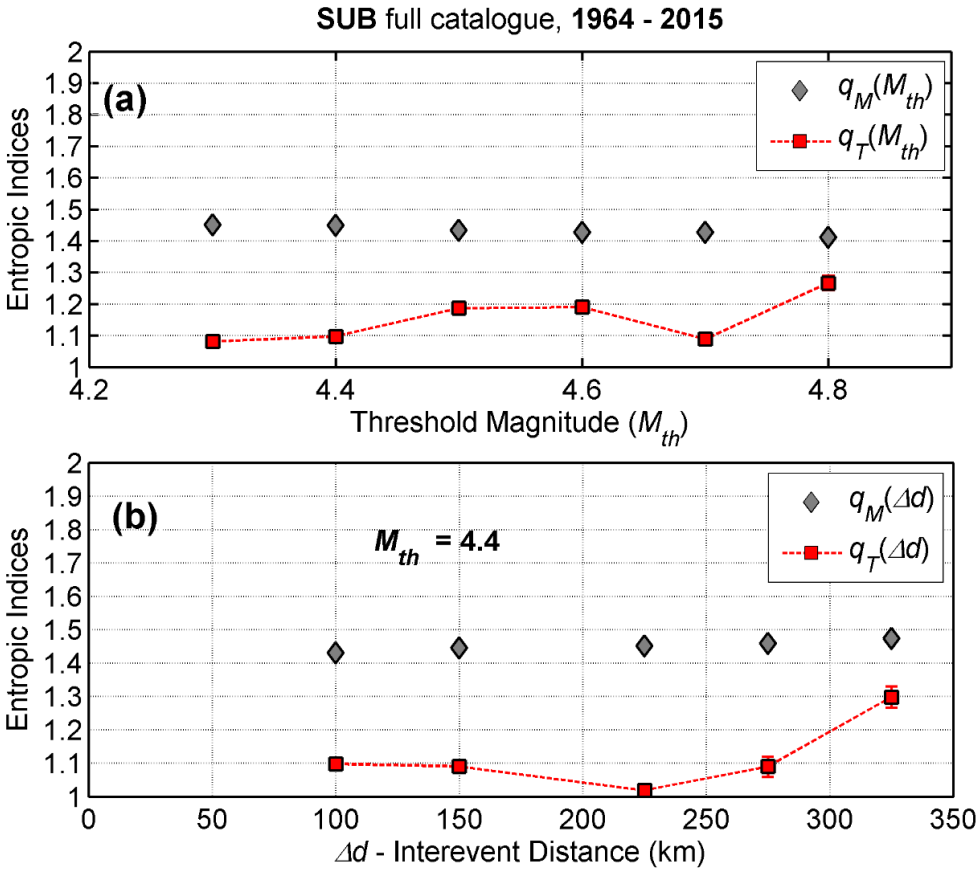

Figure 5.16 Analysis of the full SUB catalogue for the 51-year period 1964 – 2015. **As per Fig. 5.14**

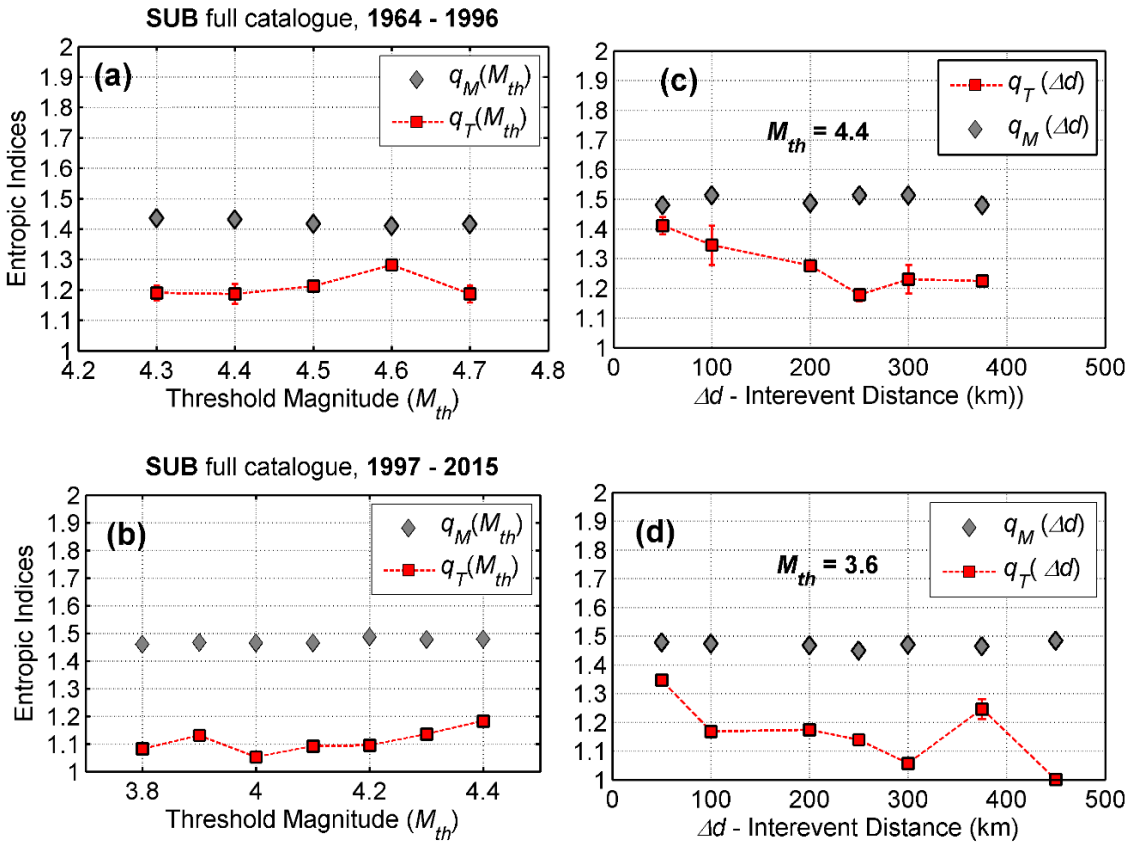

Figure 5.17 Analysis of the full SUB catalogue for the periods 1964 – 1996 (top row) and 1997-2015 (bottom row). As per Figure 5.15.

5.4.3. Analysis of the Declustered earthquake catalogues for 1964-2015

Let us proceed to the examination of the reduced versions of sub-catalogues, in which aftershock sequences have been identified and removed by the stochastic declustering method of Zhuang et al (2002) at the $\phi \geq 0.7$ and $\phi \geq 0.8$ probability levels (i.e. probability greater or equal to 70% and 80% for an event to belong to the background). Due to small populations of events left which do not guarantee a statistical significance and also due to a high M_c completeness, our analysis will be limited to the CTF and HEL declustered catalogues (Fig. 18) and will focus on the study of $q_M(M_{th})$ and $q_T(M_{th})$.

Fig. 5.19 demonstrates the analysis of the CTF catalogue declustered at 70% (red coloured symbols) and 80% (blue coloured symbols) probability level with respect to magnitude threshold. As can be seen, the analysis yield very low $q_M(M_{th})$, which varies between 1.41 and 1.38, so that $b_q(M_{th})$ varies between 1.44 and 1.63. It is again possible to observe a statistically significant reduction in the value of q_M, which might be interpreted in terms of a corresponding reduction in the level of activity localization upon aftershock

removal or as an artefact due to the impact of catalogue incompleteness. A rather unexpected outcome is the analysis of the temporal entropic index; at 70% probability level q_T varies from 1.05 to 1.24 indicating a low correlation which may be probably due to the existence of remaining aftershocks. When the probability for an event to belong to the background increases to 80%, it can be clearly seen that q_T indicates high correlation throughout the catalogue [$q_T(M_{th})$ = 1.36 – 1.51]. Analogous observations can be made upon the HEL declustered catalogue. In Fig. 5.20a one can see that $q_M(M_{th})$ is again very low and determined around 1.43-1.40, so that $b_q(M_{th})$ varies between 1.32 and 1.50. The temporal entropic index (Fig. 5.21), unlike in the CTF declustered catalogue, is stably determined for both 70% and 80% probability levels at 1.43-1.31 indicating moderate to high correlation.

Overall, the analysis of the temporal entropic indices for the different source area points toward a weakly correlated seismogenetic system verging on the limit of randomness, at least during the period 1964-1996. An exception can be made for the area of North Anatolian Trough - northern Aegean Sea seismogenetic system where the correlation is overall high. Moreover, the analysis of the declustered catalogues has shown that where the events are given 80% probability to belong to the background, the CTF and HEL sub-systems are moderately correlated. Once again it should be noted that the above analysis marks a first approach in the examination of the dynamics of the Hellenic seismogenetic system and is an attempt to better validate our method.

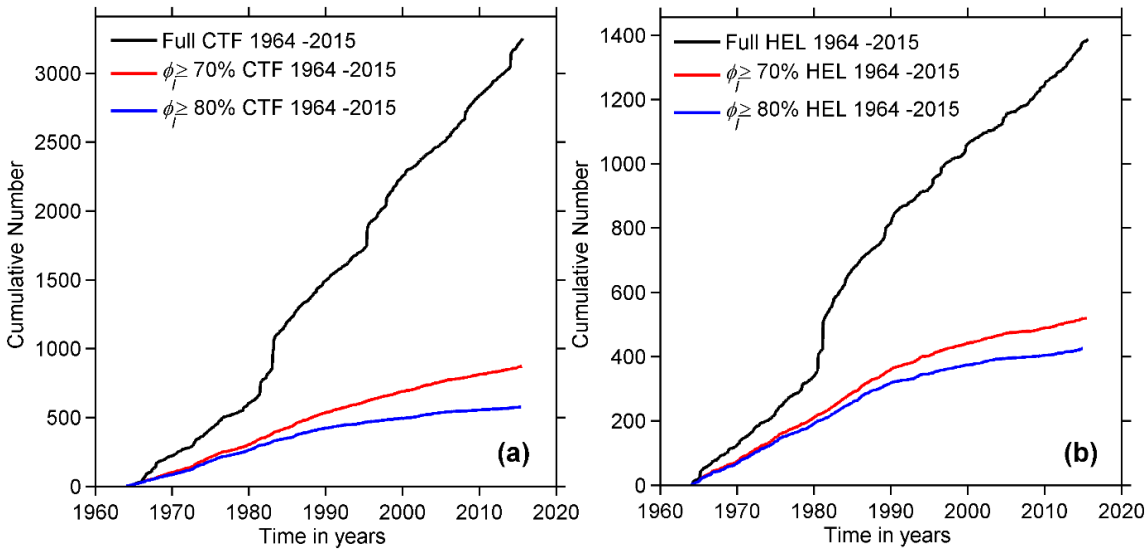

Figure 5.18 Cumulative event count of the full and declustered CTF and HEL catalogues for the period 1964 – 2015 (magnitude of completeness $M_c \geq 4.0$ and 4.1 respectively).

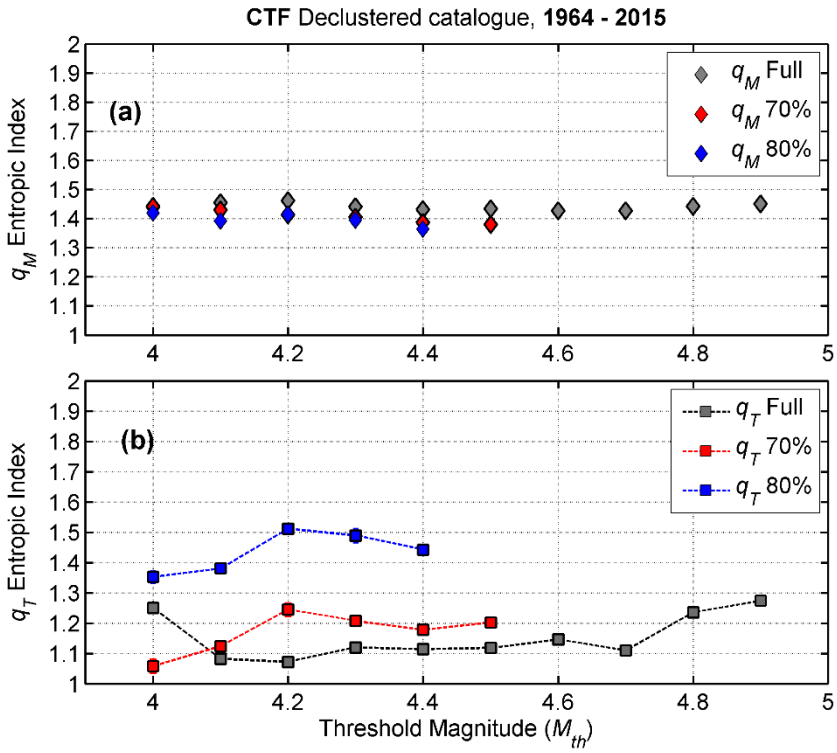

Figure 5.19 Analysis of the declustered CTF catalogue for the periods 1964 – 2015 Panel **(a)** illustrates the dependence of the *qM* entropic index on threshold magnitude (M_{th}). Panel **(b)** illustrates the dependence of the *qT* entropic index on threshold magnitude (M_{th}).

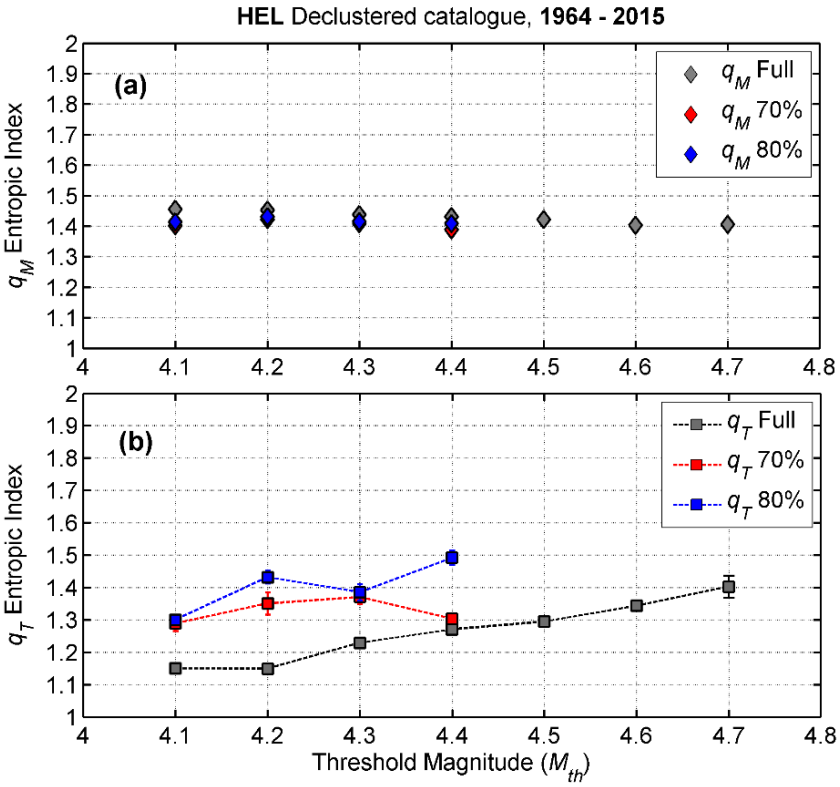

FIGURE 5.20 Analysis of the declustered HEL catalogue for the periods 1964 – 2015 As per Figure 5.19

5.5 NESP APPLICATION TO THE NNE-SSW HELLENIC SHEAR ZONE

Recent studies have been advocated that the Hellenides were separated during Pliocene period into northern and southern parts by an ENE trending zone which includes the Cephalonia-Corinth– North Anatolian fault systems (Papanikolaou and Royden, 2007; Papanikolaou 2009; 2013). The existence of such NNE-SSW shear zone comprising these faulting systems has been strongly corroborated by a number of studies which indicated a correlation between large events within this area. For example, in their study Tzanis & Makropoulos (2001) demonstrated that the two devastating earthquakes of Ismit 17/08/1999 M=7.4 and Athens 7/9/1999 M=5.9 may be linked through long range interactions. In particular, the study has shown that power-law changes in the seismic release rates began immediately after the 17/8/99 M7.4 Izmit earthquake (Turkey) and culminated with the 7/9/99 M5.9 Athens event disappearing soon afterwards. However, they could be clearly observed over the entire North Aegean, the Sporadhes, Evia, Attica and through the Central and SW Peloponnese.

These observations fit very well into the concept of a (self) organised system with long range interactions and clearly indicate the influence of the enormous Turkish event over the entire Aegean region. Based on the above information, I shall investigate the nature of this seismogenetic zone which has been considered as a southwestern propagation of the NAF (hereinafter referred to as SHR), by searching for evidence of complexity and non-extensivity in the earthquake record.

The earthquake data was extracted once again by the ISC data base which is homogenous by construction with consistently determined hypocenters and magnitude. The full catalogue comprises 6259 events reported in body-wave *Mb* (magnitude scale) and recorded within the area 36.8°N/41.3°N and 20.8°E/31°E (see orange shaded area in Fig.5.21) over the period 01/01/1964- 31/08/2015, while its declustered counterpart at 70% and 80% probability level comprises 1075 and 819 events respectively.

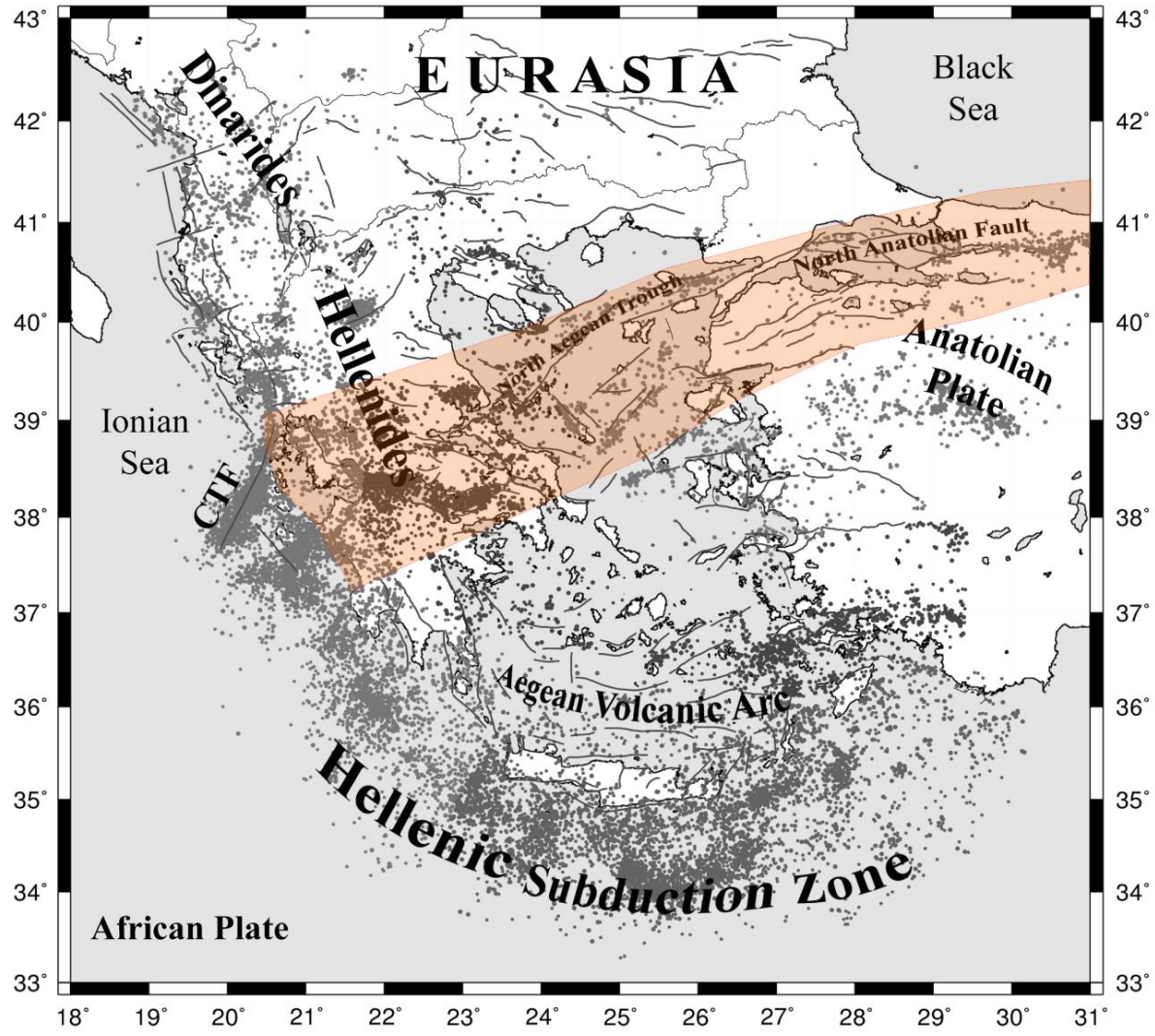

Figure 5.21 Earthquake epicenters and major faults of Greece – Western Turkey for the period 1964-2015 and $M_{th} \geq 4.1$. The NNE-SSW shear zone (SHR) is illustrated with orange shading

5.5.1 Analysis of the Full and Declustered SHR earthquake catalogue for 1964-2015

The results of this exercise are illustrated in Figures 5.22 and 5.23. As can be seen in Fig. 5.22, $q_M(M_{th})$ determinations from both full and declustered catalogues are stably determined; for the full catalogue $q_M(M_{th})$ varies from 1.45 to 1.49 while for the declustered counterparts it is lower varying from 1.37 to 1.41. The application of Eq. (18) yields $b_q(M_{th})$ estimates that respectively vary from 1.22 to 1.04 and 1.63 to 1.43. The entropic index q_M, like the b-value to which it is related, represents the scaling of the size distribution of earthquakes and clearly indicates a correlated, scale-free process, possibly associated with a gradual change in the size distribution of active faulting. As can be seen in Table 5.2, the determinations of $b_q(M_{th})$ are consistent with the corresponding determinations of

$b(M_{th})$ which have been computed with conventional (robust least squares) methods and vary in the interval 1.30 to 0.92 and 1.69 to 1.2 respectively.

More interesting observations can be made in regard to the temporal entropic index. The temporal entropic index $q_T(M_{th})$ computed from the full SHR catalogue is in general terms, rather stable and for the most part remain consistently greater than the "randomness threshold" of 1.2. It varies smoothly from 1.1 at M_{th} = 4.1 to 1.39 at the M_{th} = 4.8 and exhibiting steady, quasi-linear increase with increasing threshold magnitude. For the declustered catalogue at 70% probability level, q_T varies between 1.08 at M_{th} = 4.1 while for M_{th} > 4.1 it rises to 1.21-1.33. Analogous behaviour is observed when the catalogue is declustered at 80% probability level: q_T varies between 1.1 at M_{th} = 4.1 while for M_{th} > 4.1 it rises to 1.28-1.33, indicating weak to moderate correlation at larger threshold magnitudes. The variation of entropic indices with interevent distance is shown in Fig. 5.23. As before, the magnitude entropic indices $q_M(\Delta d)$ obtained from both full and declustered catalogues are stably determined $\overline{q}_M$ *-full* = 1.49 $\pm$ 0.001 and $\overline{q}_M$ *- declustered* = 1.45 $\pm$ 0.002. Turning now to the results for the temporal entropic index, q_T varies from 1.12 at Δd =100km to 1.27 -1.42 for $\Delta d \geq$ 200km. It is apparent that q_T exhibits upward trend with increasing interevent distance signifying the existence of long-range correlation (far-field). Overall, the analysis of the temporal entropic indices points toward a weakly correlated seismogenetic system verging on the limit of randomness. The behaviour of q_T with threshold magnitude and interevent distance is rather similar in *both* full and declustered catalogues: this indicates a present albeit weak long-range effect underlying the temporal expression of earthquake occurrence which, in turn, is taken to imply non-Poissonian dynamics.

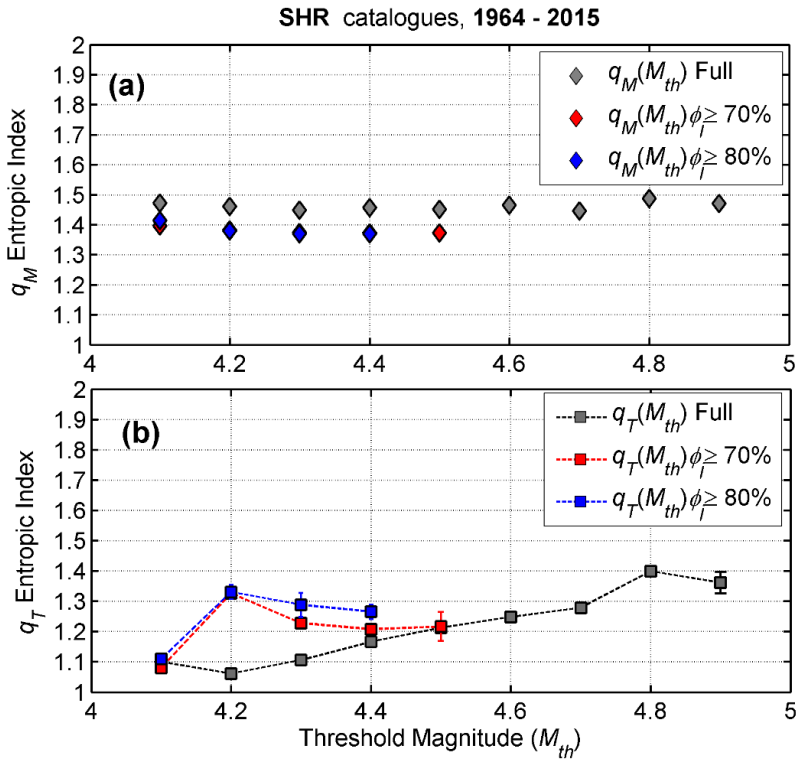

Figure 5.22 Analysis of the SHR full and declustered catalogues for the periods 1964 – 2015 Panel **(a)** illustrates the dependence of the *qM* entropic index on threshold magnitude (M_{th}). Panel **(b)** illustrates the dependence of the *qT* entropic index on threshold magnitude (M_{th}).

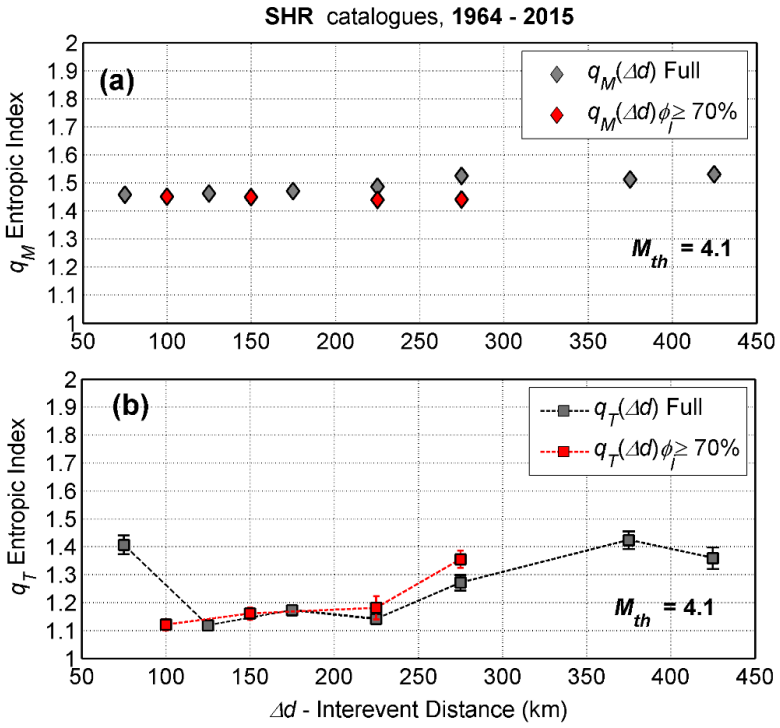

Figure 5.23 As per figure 5.22 Panel **(a)** illustrates the dependence of the *qM* entropic index on interevent distance (*Δd)*. Panel **(b)** illustrates the dependence of the *qT* entropic index on interevent distance (*Δd)*.

TABLE 5.2 Summary with the range of variation of the entropic indices obtained from the earthquake source areas of Greece – Western Turkey.

		No. events	$q_T(M_{th})$ Range	$q_T(\Delta d)$ Range		$q_M(\Delta d)$ Range	$q_M(M_{th})$ Range	$b_q(M_{th})$ Range	*b-value*
				Δd<100km	Δd>100km				
FULL 1964-2015	**CTF**	3250	1.08-1.28	1.19-1.38	1.20-1.60	1.43-1.47	1.43-1.47	1.32-1.12	1.59-1.01
	HEL	1387	1.15-1.42	1.17-1.25	1.16-1.41	1.47-1.49	1.43-1.45	1.32-1.22	1.61-0.95
	NAF-NAT	925	1.17-1.47	1.37	1.21-1.35	1.49-1.53	1.50-1.51	1.00-0.96	1.15- 0.90
	SUB	1833	1.08-1.26	1.09	1.01-1.29	1.43-1.47	1.41-1.45	1.43-1.22	1.54-1.02
FULL 1964-1996	**CTF**	1990	1.07-1.28	1.33-1.34	1.22-1.37	1.47-1.50	1.43-1.47	1.32-1.12	1.66-0.92
	HEL	998	1.14-1.39	1.25	1.10-1.50	1.47-1.51	1.40-1.45	1.5-1.22	1.55-0.91
	NAF-NAT	658	1.35-1.46	N/A		N/A	1.50-1.52	1.0-0.92	1.34-0.85
	SUB	767	1.19-1.28	1.34-1.41	1.18-1.27	1.48-1.51	1.41-.144	1.43-1.27	1.61-0.92
FULL 1997-2015	**CTF**	3266	1.13-1.33	1.20-1.27	1.05-1.29	1.45-1.49	1.43-1.47	1.32-1.12	1.45-1.05
	HEL	1333	1.10-1.50	1.53	1.10-1.37	1.46-1.48	1.44-1.47	1.27-1.12	1.54-1.03
	NAF-NAT	744	1.45-1.79	N/A		N/A	1.50-1.52	1.0-0.92	1.36-0.81
	SUB	2452	1.08-1.18	1.18-1.34	1.01-1.24	1.45-1.47	1.46-1.48	1.17-1.08	1.31-1.15
DECLUSTERED ϕ ≥ 70%	**CTF**	871	1.08-1.24	N/A		N/A	1.38-1.44	1.63-1.27	1.68-0.99
	HEL	519	1.30-1.49				1.41-1.43	1.43-1.32	1.67-0.97

DECLUSTERED ϕ ≥ 80%	**CTF**	575	1.29-1.39	N/A		N/A	1.38-1.44	1.63-1.27	1.69-0.94
	HEL	425	1.35-1.51				1.41-1.43	1.43-1.32	1.66-0.91
SHR FULL	**SHR**	6259	1.1-1.39	1.40	1.16-1.42	1.45-1.52	1.45-1.49	1.22-1.04	1.30-0.92
SHR DECLUSTERED ϕ ≥ 70%		1075	1.08-1.33	1.12	1.16-1.36	1.44-1.45	1.38-1.41	1.63-1.44	1.61-1.27
SHR DECLUSTERED ϕ ≥ 80%		819	1.-1.33	N/A		N/A	1.38-1.41	1.63-1.44	1.69-1.2

DISCUSSION AND CONCLUSIONS

Recapitulation

The question as to whether seismogenetic systems are random or organized, has been a subject of an ongoing debate. The question originates in a long-standing discourse between the two principal schools of thought (and epistemological paradigms) developed in the process of studying earthquake occurrence and quantifying the expectation of seismic activity. Accordingly, far from being purely academic the problem of understanding the proper statistical nature of seismicity is also practical: the answer can have significant repercussions on forecasting intermediate term earthquake hazard.

Seismicity comprises the superposition of a background process expressing the continuum of tectonic deformation, and a foreground process of prolific short-term activity associated with earthquake swarms or/and aftershock sequences. The first and historic school (doctrine) posits that background seismicity is produced by a self-excited conditional Poisson (point) process whose entropy is assumed to obey the Boltzmann-Gibbs formalism; background earthquakes are spontaneously and independently generated in the fault network and there is no interaction between faults, such that would influence their time and place of occurrence [Epidemic-Type Aftershock Sequence, (e.g. Ogata, 1988, 1998; Zhuang et al, 2002; Helmstetter and Sornette, 2003; Touati et al, 2009; Segou et al, 2013), and Proxy-ETAS models (e.g. Console and Murru, 2001), as well as EEPAS (Each Earthquake is a Precursor According to Scale, e.g. Rhoades & Evison, 2006; Rhoades 2007) and PPE (Proximity to Past Earthquakes, e.g. Marzocchi and Lombardi, 2008) models].

The second and more recent doctrine posits that background seismicity is generated by a non-equilibrating fault network (system) in which background events are dependent due to correlations (interactions) developing and evolving between faults, which may extend over long spatiotemporal distances and influence their time and place of occurrence. Correlation effectively confers memory to the system and manifests itself in the form of power laws governing the temporal and spatial statistics of seismicity ((e.g. Bak and Tang, 1989; Sornette and Sornette, 1989; Olami et al., 1992; Sornette and Sammis, 1995; Rundle et al., 2000; Bak et al, 2002; Bakar and Tirnakli, 2009, etc.). Both Poisson and Complex/Critical doctrines, albeit from different vantage points, consider that the foreground process i.e. the

earthquakes of an aftershock sequence to be dependent, but the former assigns only local significance to this dependence, while Criticality considers them to be an integral part of the regional seismogenetic process.

Herein, I attempt to explore the statistical nature of seismicity by using the generalized formalism of Non-Extensive Statistical Physics (described in Chapters 1 and 2) as a universal context for the statistical description of earthquake occurrence and trying to ascertain the existence and degree of correlation in active fault networks (or, equivalently, the level of non-equilibrium). The existence of correlation is assessed by evaluating the entropic index q appearing in the q-exponential distribution predicted by NESP for the dynamic parameters of non-equilibrating systems; q is bounded as $0 \leq q \leq 2$, with $q = 1$ corresponding to the pure exponential distribution expected for conservative Poissonian processes and $q > 1$ indicating Complexity/Criticality in non-conservative systems. Specifically, I evaluate an entropic index associated with the distribution of earthquake magnitudes, which conveys information about the size and space distribution of fault activity and is genetically related to the *b-value* of the Gutenberg-Richter law, and an entropic index associated with the distribution of the lapse between consecutive events (interevent time), which indicates the extent of interaction in a fault network. I refer to these as the magnitude (q_M) and temporal (q_T) indices respectively and compute them by modelling bivariate empirical distributions of earthquake frequency vs. magnitude *and* interevent time, or F-M-T for short; such distributions express the joint probability of observing earthquakes larger than a given magnitude after a given lapse time.

The present work has focused on:

a) the transformational plate boundaries of the north-eastern circum-Pacific belt, i.e the Californian San Andreas, Sierra Nevada – Walker Lane, Mendocino faulting systems and Queen Charlotte – Fairweather – Denali faulting systems in Alaska, as well as the large transformational zone of Greece and Western Turkey which runs from the North Anatolian Fault – North Aegean Trough into Evia, Attica, NW Peloponnesus ending up to the Cephalonia Transform Fault, and **b)** the convergence plate boundary that of the Aleutian Arc – Trench System in the NE Pacific Rim.

Of these, the divergent, transformational and inland seismogenetic systems are mainly *crustal*: earthquakes occur mostly in *schizosphere*, i.e. in the rigid, brittle part of the upper lithosphere. On the other hand, the convergent systems are both crustal and *sub-crustal*.

With reference to the latter I attempt to inquire into whether environmental conditions (temperature, pressure) or/and boundary conditions (free at the surface, fixed at depth) affect the dynamic expression of fault networks. In consequence, I examine crustal earthquakes (generated in the cold schizoshere) and sub-crustal earthquakes (generated in the warm, high-pressure Wadati-Benioff zones) separately by winnowing them according to the local depth of the Mohorovičić discontinuity. The results are compared to the analysis conducted by Tzanis & Tripoliti (2018, *in press*) which focused on a broad area of the NW Circum-Pacific Belt and particularly on three convergence plate boundaries: the Ryukyu Arc, the Izu – Bonin Arc and the Honshu Arc (south segment of the Okhotsk Plate comprising the Pacific–Okhotsk) and Okhotsk–Amur plate convergences. In their study only one transformational continental tectonic domain was taken into considerations (south-western Honshu on the Amurian Plate). Such an exercise may provide evidence as to the existence of differences in the dynamics of crustal and sub-crustal seismogenesis and the origin these differences thereof.

Finally, the analysis is applied to homogeneous earthquake catalogues and the author examines not only full (complete) catalogues in which aftershocks sequences are included, but also the respective declustered versions of the catalogues in which aftershocks have been removed by the efficient stochastic declustering method of Zhuang et al (2002). The premise for conducting this analysis is simple. If background seismicity is Poissonian, then the elimination of aftershocks should reduce the catalogue to a set of uncorrelated events ($qT \rightarrow 1$). If it does not, the argument in favour of Complexity and against Poissonian seismicity would be compelling.

Full Catalogues

Turning now to the discussion of the results, it might be said that they comprise “expected” and “interesting” parts. The “expected” part is the behaviour of the magnitude entropic index q_M. As demonstrated in chapters 3, 4 and 5 (see also respective Tables) experimental b_q values determined with the procedure described in Chapter 2 are consistent with b values computed with conventional methods. This is important because the G-R law *cannot* be derived in the context of point (Poisson) processes but *can* be derived from first principles in the generalized context of NESP.

Naturally, *b-value* exhibits differences between seismogenetic systems (Wiemer & Wyss, 2002). Respectively, the q_M (b_q) analysis of full catalogues shows that some seismogenetic systems, (e.g. MFZ, QCD), exhibit rather high clustering of faulting activity, while some others (e.g. CTF, HEL) exhibit rather low clustering of faulting activity. In some cases (SCSR, nSAF, SNR) the degree of clustering (q_M) increases with threshold magnitude, i.e. extends over long ranges. At any rate, in the general context of NESP, the Gutenberg-Richter law can be almost naturally derived from the *q*-exponential distribution. Accordingly, a most significant outcome of q_M analysis is that it demonstrates that active fault networks may be classified as *sub-extensive* with a high degree of self-organization.

Since as demonstrated herein, there can be little doubt that the time-honoured frequency-magnitude distribution of Gutenberg and Richter emerges from non-extensive fault networks, the rest of the discussion concentrates on the temporal dynamics of seismicity, as indicated by the temporal entropic index q_T. To that end, the threshold value above which it is safe to conclude that q_T indicates non-extensive seismogenetic processes, was determined by applying the NESP analysis as described in Chapter 2, to several background catalogues generated on the basis of the ETAS model. The results established that the systematic observation of experimental values $q_T\,(M_{th}) \geq 1.15$ and $q_T\,(\Delta d) \geq 1.2$ would be compelling evidence of non-extensive seismogenetic dynamics.

Figs. 6.1 to 6.6 are a compact presentation and colour-coded classification of all $q_T(M_{th})$ and $q_T(\Delta d)$ functions shown in Chapters 3, 4 and 5, and summarized in the respective Tables. In the classification scheme, all values of $q_T < 1.15$ are shown in red and are considered to indicate *nihil correlation*. Values higher than 1.15 generally indicate statistically significant correlation that is rated as "*weak*" (orange, $1.15 \leq q_T \leq 1.25$), "*moderate*" (light green, $1.26 \leq q_T \leq 1.4$), "*significant*" (green, $1.41 \leq q_T \leq 1.5$), "*strong*" (light blue, $1.51 \leq q_T \leq 1.6$) and "*very strong*" (purple, $1.6 < q_T$). The pie charts of Fig. 6.7 and 6.8 summarize the proportions of q_T classes determined from the full and declustered catalogues and provides a succinct picture of the existence, extent and relative strength of correlation in the crustal and subcrustal seismogenetic systems studied herein. Note that for crustal seismicity the results used in the compilation of the pie charts refer only to proper transformational plate boundaries and no other inland seismogenetic systems, i.e only the ALW and WNG systems were not included. Moreover, for the SAF and SNR the results used in the compilation of the pie chart refer to

the *entire* period 1968-2015; the results obtained from the analysis of the ante and post Loma Prieta sub-catalogues have *not* been separately included.

Mere inspection of Figs. 6.7 and 6.8 should suffice to satisfy one that different seismogenetic systems may exhibit very different attributes and degrees of complexity. Characteristic example is the stark contrast between the weakly correlated crustal system of convergent plate boundaries (**CPBCr**), the strongly correlated crustal system of transformational plate boundaries (**TPBCr**) and the uncorrelated *sub-crustal* system of convergent plate boundaries (**CPBsub**).

Let us first concentrate on the “full” process: As a general rule, full earthquake catalogues yield moderate to strong correlation throughout. For **TPBCr** systems definite increase of correlation with magnitude is observed in North and South California (nSAF, SNR and ICB/sSAF, ECSZ), the transformational Queen Charlotte – Fairweather Fault (QCD), the transformational zone of North Anatolia Fault – North Aegean Trough (NAF-NAT) in Greece, as well as minor faulting systems in Continental Alaska (ALW). This could be attributed to the fact that small earthquakes, whose numbers overwhelm the catalogues, may be uncorrelated because they have limited interaction radii and their majority is spawned by different parental earthquakes at distal locations of the seismogenetic area. Accordingly, distal small earthquakes belonging to filial generations of localized activity have no causal relationship and when mixed and chronologically ordered in a catalogue, randomize the statistics of interevent times. In this view, the increase of correlation with magnitude can be interpreted as an effect of the ever-increasing interaction radii (connectivity) of progressively larger events, as well as of the nature of the fault network. The same effect is also observed in other crustal seismogenetic systems such of the north-west circum – Pacific belt (Tzanis & Tripoliti, *personal communication 2018*).

It is worth noting that the pattern of lower correlation at smaller magnitude scales although repeats in the crustal seismogenetic systems of Sierra Nevada range – Walker Lane (SNR) and the East California Shear Zone (ECSZ) albeit it is more stable with a mean $q_T(M_{th})$ at 1.89 for ECSZ and 1.51 for SNR. This suggests profound differences between ECSZ and ICB/sSAF (South California) and nSAF/SNR (North California) which may also have to do with the nature, dynamic state and even the size of the fault network.

The above observation is strongly corroborated by the results from the analysis of the nature and dynamics of SNR / nSAF which provided strong evidence of sub-extensivity albeit with different characteristics. The nSAF exhibited different behaviour with respect to the powerful (M7.2) Loma Prieta event of 1989: prior to that earthquake, nSAF was strongly correlated over all magnitude scales and interevent distances; *after* the earthquake it was found to be weakly correlated over all magnitude scales and all but the shortest and longest interevent distances. In this respect, nSAF exhibits evolutionary (self-o*rganizing*) Criticality without evident acceleration or deceleration of seismic release rates. The SNR system was found to be highly correlated over all analysable magnitude scales and interevent distances and to exhibit attributes of quasi-stationary self-organized criticality. When the results of the nSAF and sSAF full catalogues are compared, it is straightforward to see that the post-1990 dynamics of nSAF and the post-1980 dynamics of sSAF are very comparable, just as the post-1968 dynamics of sSAF also turn out to be. This implies that sSAF system has not experience any major earthquake so as to influence its dynamics in such way as Loma Prieta event in nSAF, nor has been influenced by the Loma Prieta earthquake itself. One might be tempted to ponder whether such “isolation” of the sSAF is effected by the Garlock and “Unnamed” seismic zones.

The differences in the expression of seismicity between the nSAF/sSAF/ICB and SNR/ECSZ fault networks, apparently reflect their niche in the geodynamic setting of the broader area: On the one hand is the proper transformational boundary between the North American and Pacific plates (nSAF/sSAF/ICB subsystems) which is open to the west and accommodates more than half of the total plate motion in Southern California (Becker et al., 2005; Liu et al., 2010, Dorsey et al., 2012). On the other hand, is the SNR/ECSZ subsystem, a *landlocked* shear zone in which approximately 25% of the total plate motion takes place (Plattner et al, 2009). It certainly stands to reason that the differences in the geodynamic setting of the respective fault networks affect the dynamic expression of seismicity.

Very strong correlation in **TPBCr** systems is generally observed at short (<100km) interevent distances, which can be easily explained as an effect of internal dynamics of in aftershock and swarm clusters. Correlation levels drop to weak–moderate at longer interevent distances (>200km), although a low-rate but clear increase with interevent distance is observed. Correlation at very long ranges (>300km) can hardly be explained in terms of aftershocks

because these are several times the characteristic dimensions of aftershock zones associated with M_w 6.7 earthquakes and significantly larger than those of zones associated with M_w 7-7.3 earthquakes (e.g. Kagan, 2002). This implies that at interevent distances longer that 150km a persistent degree of long-range interaction exists, which also implies a persistent degree of long-range connectivity in the fault network. Once again it is evident that ECSZ / SNR systems are characterized by long range interactions throughout the catalogue, an attribute which differentiates them from the proper transformational nSAF/ sAF/ICB sub systems.

Moving on to the crustal seismicity of convergence plate boundaries (**CPBCr** systems), strong correlation is observed in the crustal plate convergence in the Aleutian Arc (ATC) where the temporal entropic index indicated definite increase of correlation with magnitude. Analogous results were observed at the NW Pacific convergence plates and specifically, the Ryukyu Arc, the Izu – Bonin Arc, the Honshu Arc and Okhotsk–Amur plate convergences. Conversely, the Philippine Sea – Pacific plate convergence indicated weak correlation over all magnitude ranges (no increase) in the crust (Tzanis & Tripoliti, *personal communication 2018*). It is worth noting, that the crustal seismogenetic systems of California and Alaska develop in thicker continental crust, as also the systems of the NW Pacific belt. Conversely, the crustal system of Philippine Sea – Pacific plate convergence develops in thin oceanic crust. It is therefore tempting to contemplate that the thickness of the crust may have a role in the development and evolution of internal dynamics (self-organization) in a seismogenetic system. Once again, very strong correlation is observed at shorter distances in all convergence crustal subsystems, which can be easily explained as an effect of tightly spaced aftershocks and swarm clusters. Correlation levels drop to weak – near randomness thresholds at longer interevent distances (>200km) and rises to moderate levels at very long distances.

Finally, the internal dynamic of sub-crustal seismicity (**CPBsub** systems) yield insignificant to weak correlation with respect to threshold magnitude as well as interevent distance: the temporal entropic index will generally not exceed 1.15, except at short ranges (<100km) where it is weak to moderate in Aleutian Arc (ATD), as well as in the NW Pacific Belt (weak in RKU, PSP and OKH, but strong in SJP).

Declustered Catalogues

A primary objective of this study is to investigate whether background seismicity is generated by non-Poissonian dynamic processes. Accordingly, I proceed to review the results obtained for the declustered versions of the catalogues, in which aftershock sequences have been identified and removed by the stochastic declustering method of Zhuang et al (2002) at the $\phi \geq 0.7$ and $\phi \geq 0.8$ probability levels (i.e. probability greater or equal to 70% and 80% for an event to belong to the background).). It must be noted that because of the small population of events left after declustering, the analysis of entropic indices is limited to catalogues which guarantee the statistical significance of $q_T(M_{th})$and $q_T(\Delta d)$. Figures 6.2-6.3 and 6.5-6.6 illustrate the results obtained for $q_T(M_{th})$ and $q_T(\Delta d)$ respectively. It is immediately apparent that on removing the aftershock sequences the crustal transformational boundaries (**TPBCr**) are clearly correlated and the correlation either increases with declustering or remains unscathed.

In particular, it can be easily verified that South California (sSAF/ICB) appears to be overall stronger correlated than North California (nSAF), albeit not very significantly. Another interesting observation is that once again the ECSZ and SNR systems turn out to be absolutely comparable at $\phi \geq 70\%$ and $\phi \geq 80\%$ probability level although ECSZ appear to be somewhat stronger correlated than SNR (Chapter 3,). The persistence of correlation (observed in full-catalogue analyses) is also evident in the transformational QCD system in Alaska, the SHR system in Greece and the SJP system in SW Japan, as well as the crustal seismicity in convergence plate boundaries (CPBCr) of the north -east (ATC) and the north-west circum (RKU, PSP and OKH)– Pacific belt (Tzanis & Tripoliti, *personal communication 2018*).

This is a point of significance in that it demonstrates that removal of the clutter effected by the large numbers of time-local foreground events uncovers the existence of long-range interaction in the global background process. The extent of long-range correlation can be explicitly studied in Figures. 6.5 and 6.6, where it becomes apparent that at intermediate and long interevent distances, (Δd > 150km), crustal seismicity is generally correlated and that declustering, either does not affect the degree of correlation, or causes it to increase. Another point of significance is that ETAS-based stochastic declustering *fails* to reduce earthquake catalogues to sequences of independent events. van Stiphout et al (2012) presented a study

in which they compared declustering algorithms by applying the χ^2 goodness of fit test to determine whether the "background" recovered by some declustering algorithm obeys a Poisson distribution in time. They found at the 5% significance level, that catalogues declustered by the methods of Zhuang et al. (2002) and Marsan and Lengliné (2008) follow a Poisson distribution in time; accordingly, they suggest that Poisson processes are in control of the background seismicity. It could be contended that this (and analogous) tests may be misleading because the distribution of occurrence times is *not* a measure of interrelationship between distal successive events *whatsoever* and does not relate the occurrence of an earthquake to its predecessor and successor events. On the other hand, the distribution of interevent times does, as adequately explained in the foregoing.

Let us now review the correlation in the *sub-crustal* convergence plate boundaries (CPBsub) and particularly the seismogenetic system of (eastern) Aleutian Wadati-Benioff zone (ATD). When the earthquake catalogue is declustered it becomes clear that the level of correlation drops significantly but does not disappear. When evaluated as a function of threshold magnitude long range correlations are weak to insignificant. When evaluated as a function of interevent distance, short-range correlations disappear while at very long distances the correlation is weak. Analogous results have been obtained for the sub-crustal systems of NW Pacific Belt. All three CPBsub systems that were examined remain at weak-moderate levels while long range correlation is generally insignificant (Tzanis & Tripoliti, *personal communication 2018*).

The decrease of correlation in the declustered catalogues of CPBsub systems comes into stark contrast with results obtained in the transformational plate boundaries, where correlation was observed to either increase, or to remain unscathed. Note, that the long-term statistical behaviour of all sub-crustal seismogenetic systems referred herein appears to be predominantly Poissonian although it should be emphasized it is *not* exactly Poissonian as evident by the evolutionary characteristics of correlation (see below). To the contrary, the crustal seismogenetic systems appears to involve long range interactions, although there are different mechanisms by which complexity may arise. Inasmuch as power-law distributions and long-range effects are hallmarks of critical phenomena, Self-Organized Criticality and Self-Organizing Criticality, (which naturally emerge from the inherent non-linear dynamics of the fault system), are by far the principal candidates. Based on the above

it is tempting to suggest that the regional the geodynamic setting is of great significance to the development of correlation.

Evolution of Correlation

So far, the results related to long term properties of the studied seismogenetic systems over the whole period of observations. It is equally, if not more interesting, to examine the evolution (time-dependence) of their dynamic states also as imaged by the time-dependent changes of the temporal entropic index. As it turns out, the evolution of correlation is very dynamic.

As far as crustal full processes are concerned, very strong correlations are always observed immediately following the occurrence of significant events; this is a time/local effect that gradually dies away as aftershock sequences die away and the systems relax to states of lower correlation, in which they remain until the next large event. In the *relaxed* state, correlation is generally moderate and corresponds to q_T of the order of 1.2 - 1.3 or higher. More precisely, the above behaviour has been observed in the crustal convergence plate boundary of Alaska (ATC), as well as in both south and north stretches of SAF (nSAF and sSAF).

However, there is significant qualitative difference between nSAF and sSAF: Correlation is much stronger in the south (q_T > 1.7) immediately after large earthquakes, followed by relatively fast recovery to quasi-randomness, whereas it appears to be weaker and decay at a significantly slower pace in the north. An additional difference is that in the south SAF, systematic return to a weak non-equilibrium (correlated) state is consistently observed prior to large events, with q_T gradually increasing from the level of 1.1 – 1.2 (uncorrelated – weakly correlated) to approx. 1.3 and higher (moderately correlated).These fluctuations are also evident in the “isolated” SNR/ECSZ subsystems, where q_T is generally low (<1.3) prior to a large earthquake and attains high correlation (>1.6) after the occurrence of a significant event. Moreover, it is interesting to notice that both SNR/ECSZ systems become very stable after 2000 indicating overall very high correlation (1.35- 1.6) for the foreground process and possibly SOC dynamics. These results are strongly corroborated with the results obtained from the analysis of the long-term properties and may changes in the mode of deformation between the southern and northern stretches of the SAF. Moreover, they indicate that different levels of self-organization, namely between nSAF, SNR, sSAF and ECSZ might

develop and different mechanisms by which complexity and sub-extensivity may arise in the fault systems of California. Such behaviour is also comparable to that observed in the seismogenetic systems of the NW Pacific belt (Tzanis & Tripoliti, *personal communication 2018*).

Analogous observations can be made in regard to sub-crustal full processes albeit with two significant differences. The first is that the time-local increase of correlation after significant earthquakes is generally no higher than “strong” and decays rather faster than in the crust (apparently due to the lower intensity and shorter duration of sub-crustal aftershock sequences). The second is that in the relaxed states, correlation is *considerably* lower than that of the corresponding crustal relaxed states: it is generally weak and very frequently insignificant, or even *nihil*!

Additional insight is obtained by studying the evolution of correlation in background (global) seismogenetic processes. In **TBCr** systems (California, USA), the background evolutionary correlations are found to be *significantly* increased in comparison to that of full process. It is evident that by removing aftershock sequences, increased the correlation is observed throughout! An interesting observation is that the variation of q_T remains the same in shape and time dependence, however, q_T amplitudes depend on the probability level. In higher probability levels ($\phi j \geq 90\%$) q_T amplitudes are slightly higher by approximately 0.1-0.2. These differences are obviously related to the different content of the declustered catalogues and deserve further scrutiny. In any case, it is clear that on removing aftershock sequences, increased the correlation is observed providing strong evidence of complexity in the expression of background seismicity in Californian TBCr subsystems

The above results come into contrast with corresponding results from **CPBCr** and **CPBsub** (Chapter 4) where the background evolutionary correlation is found to be significantly lower in comparison with the full processes. In the crust q_T appears to linger about the level of 1.1 -1.2 (weak to nihil correlation) and is generally stable or slowly changing with time. A notable case of evolutionary changes in the crust is the state of correlation in the Aleutian plate system (ATC), in which correlation is practically nihil right before the occurrence of large earthquakes and thereafter increases, albeit at a slow rate to weak-moderate levels during the period preceding the next large earthquake (the 1986 and 1996 M7.9 Andreanof Islands). A rather important observation is that the level of sub-crustal background correlation appears

to vary dynamically with time: it is generally insignificant to weak and may even drop to nihil ($q_T \rightarrow 1$) for extended time intervals, but it can also dynamically transition to moderate levels for extended periods that are generally associated with temporal clusters of large earthquakes. The latter effect is very important because it shows that Wadati-Benioff zones may transition between states of high and low non-equilibrium, for reasons that cannot as yet be specified but are apparently related to the geo-dynamic evolution of the sub-crustal fault network. In this respect, the Aleutian system presents a particular interest in that both crustal and sub-crustal background appear a built-up stress (moderate correlation) ahead of Andreanof mega-earthquakes and relax (nihil correlation) after their occurrence. The above results are comparable to the analysis conducted by Tzanis & Tripoliti, (*personal communication 2018)* for the Okhotsk plate system; in particular, they observed that both crustal and sub-crustal background activity appear to evolve from low to moderately correlated states ahead of Tōhoku mega-earthquake, (albeit for brief periods and at a faster rate than in ATC-ATD system), whose source area also appears to have undergone a rapid transition from quasi-Poissonian (quasi-equilibrating) to moderately sub-extensive (non-equilibrating).

CONCLUSIONS

Overall, the results obtained from the present work, may be of some use in the course of understanding the origin and nature of complexity in the seismogenetic systems studied herein. First, let us make a list of some points that should be considered significant:

a) To begin with, different fault systems may exhibit radically different attributes and degrees of complexity. Characteristic example is the adjacent/related Mendocino Fracture Zone and Sierra Nevada – Walker Lane systems in California, in which the first is partly accommodating the deformation effected by the second. Yet, the former exhibits marginal correlation while the second strong or very strong. Another example is the Continental west Alaska (ALW) and Wrangelia – North Alaskan Cordillera (WNG) systems as well as the various subsystems of the Greek mainland (HEL, SUB) where the correlation is marginal and bounds from moderate - weak to nihil.

b) Crustal seismogenetic systems are undisputedly complex. Some (SCSR, SNR, ECSZ, NAF-NAT) exhibit persistent and significant to strong long-range correlation over the entire period of observations; other exhibit a distinct increase in the value of q_T with threshold

magnitude (sSAF, ICB, SHR, QCD and ATC); these is also observable in the full and declustered catalogues. Far from suggesting that the state of strong correlation may endure "forever", it should, nevertheless, pointed out that this quasi-stationary state of high correlation has attributes of Self-Organized Criticality.

c) *Self-Organized* Criticality is not a general rule. This is evident in nSAF undergoing enormous changes with respect to the large Loma Prieta earthquake and switching from a state of high correlation with strong attributes of Criticality during the period leading up to the event (1968-1989), to practically Poissonian in the period following the event (1990-present). This shows that Criticality may be cyclic and possibly evolving in association with earthquake cycles. It also has attributes of the *Self-Organizing* variety, albeit without evident acceleration of seismic release rates as predicted by some models (e.g. Sammis and Sornette, 2001). It is very possible that the plain designation "Criticality" would suffice to characterize this case, or maybe all cases for that matter.

d) A last important point is the stark contrast between the weakly correlated seismogenetic backgrounds of convergent plate boundaries and the strongly correlated backgrounds of transformational plate boundaries. The only sub-crustal system studied herein, i.e. the Alaskan – Aleutian subduction (ATD) as well as sub-crustal systems of NW Circum-Pacific Belt which verge on randomness (Tzanis & Tripoliti, personal communication 2018*)*, appear to be predominantly Poissonian although it should be emphasized, they are *not* exactly Poissonian. This contrast with the crustal systems is rather impressive nonetheless and may comprise a piece of information useful in the course of shaping up some preliminary understanding of the statistical (and physical) nature of seismogenesis. It should be also noted that, the behaviour of q_M is clearly different between ATD and the crustal systems, possibly indicating different dynamics, gross earthquake productivity rates and large-scale domain heterogeneities are *not* dramatically dissimilar. Accordingly, the absence of temporal correlation in ATD may not have to do with the material properties of the subducting slab and should be sought elsewhere.

Based on the above observations useful conclusion emerge:

Complexity may arise by several different mechanisms. Inasmuch as power-law distributions and long-range interaction are hallmarks of critical phenomena, the persistent correlation of

crustal background processes points toward *Self-Organized Criticality* which, however, is certainly neither uniform across the crust, nor stationary as initially thought. On the other hand, Complexity and Criticality do not always go together and there are non-critical mechanisms that may generate power-laws, (e.g. Sornette, 2004; Sornette and Werner, 2009), some of which may apply to deep-focus seismicity. In one such example, Celikoglu et al. (2010) demonstrated that the Coherent Noise Model (CNM) can generate q-exponential distributions of interevent times, although their simulation as incomplete in the sense that it did not include some spatial (geometric) configuration of interacting faults and could not assess the differences with an actual fault network.

It becomes clear that we can put together the basics of a plausible interpretation for our results, which will be based on fault networks with *small-world* topologies (e.g. Abe and Suzuki, 2004, 2007; Caruso et al., 2005, 2007). Given that active fault networks are *non-conservative* systems –friction is a non-conservative force– and therefore susceptible to non-linearity, we are pointed to this direction by the documented existence of long-range interaction and (possible) criticality, fruitful studies based on non-conservative small-world Olami-Feder-Christensen models (Caruso et al., 2005; Caruso et al., 2007), and suggestive evidence of small-worldness in the seismicity of California by Abe and Suzuki (2004, 2007). In such networks each fault is a node that belongs to a local cluster where it occupies some hierarchical level according to its size and interacts with local or distal faults (nodes) according to the respective connectivity and range of its hierarchical level. Upon excitation by some (slow or fast) stress perturbation, a node responds by storing (accumulating) energy in the form of strain and subsequently transmitting it to *connected* nodes or/and releasing it at various rates; in other words, it operates as a delayed feedback loop inducing heterogeneity in the distribution of stress transfer and release rates. Finally, and more importantly, crustal fault networks are subject to free boundary conditions at the Earth-Atmosphere interface; top-tier faults, (which in transformational and convergent tectonic settings generally break at the surface), comprise primary boundary elements of the network.

It is documented that in Olami-Feder-Christensen networks, free boundary conditions compel the boundary elements to interact at a different (delayed) frequency with respect to the bulk of elements buried deeper in the network and that this inhomogeneity induces partial synchronization of the boundary elements, building up long range spatial correlations and

facilitating the development of a critical state (e.g. Lise and Paszucki, 2002; Caruso et al., 2005; Hergarten and Krenn, 2011). This effect should also be accentuated by heterogeneity and delayed feedback across the entire network, which also appear to be important for the development of criticality in small-world networks (Yang, 2001; Caruso et al., 2007). In the particularly interesting study of Hergarten and Krenn (2011), the dynamics of the network are governed by two competing mechanisms: Synchronization, which pushes the system toward criticality, and de-synchronization which prevents it from becoming overcritical and generates foreshocks and aftershocks. Once the system has reached the critical state, synchronized failure transfers more stress to connected nodes and this causes them to fail early, de-synchronizing with the rest of the system. If, however, time lag between de-synchronized failures is short, the system can re-synchronize and repeat the cycle. This mechanism generates sequences of foreshocks, main shocks and aftershocks. Notably, the notion that aftershocks are generated by the de-synchronization caused by large earthquakes is quite different –and more SOC– than that of spontaneous triggering advocated by the ETAS model.

In consequence of the above, it is plausible that the small-world character and sub-extensive critical state of the hitherto examined crustal fault networks, is induced by the high connectivity of synchronised top-tier faults, for instance the contiguous segments of the large transform faults. These may operate as “hubs” that facilitate longitudinal interactions (transfer of stress) between distal clusters but inhibit interactions between distal or unconnected networks that operate quasi-independently and develop different levels of self-organization, as for instance between nSAF and SNR, or nSAF and MFZ. In addition, the intensity of the longitudinal interactions may vary in response to time-dependent changes in the external driving force and connectivity (stress transfer) between hubs, as for instance may have happened to nSAF before and after the Loma Prieta event. In crustal systems and upper sub-crustal fault networks of convergent plate boundaries along the NE and NW circum-Pacific belt, top-tier faults are essentially low-angle to sub-horizontal mega-thrusts, whose contiguous segments do *not* push against each other and thus are not as strongly connected as large transform faults, thereby keeping the network in a state of weak to moderate correlation.

This interpretation posits that free boundary conditions are central to the development of complexity and criticality. By inference, it also implies that deep-seated fault networks of Wadati-Benioff zones, should be kept away from criticality as they are subject to fixed boundary conditions that inhibit synchronization. Moreover, the absence of synchronization may partially explain the low-intensity and short life of aftershock sequences associated with intermediate and deep-focus earthquakes (in addition to environmental conditions and material properties).

It also appears that deep-seated fault networks may transition between correlated (complex) and uncorrelated (quasi-Poissonian) states. With the limited evidence at hand, it is rather difficult to decide if such correlated states are generated internally, i.e. are self-organized critical, or are induced externally (possibly non-critical). As mentioned above there are complexity mechanisms that do not involve criticality yet may maintain a fault system in a state of apparent non-equilibrium; a list can be found in in Sornette (2004) and a comprehensive discussion in Sornette and Werner (2009). In a more recent development, Celikoglu et al., (2010) applied the Coherent Noise Model (Newman, 1996) based on the notion of external stress acting coherently onto all agents of the system without having any direct interaction with them. The CNM was shown to generate power-law behaviour in interevent time distributions but has a weak point in that it does not include some geometric configuration of the agents and it is not known how this would influence the behaviour of the system. At any rate, the fault networks of Wadati-Benioff zones appear to lack long-range interaction –a crucial hallmark of Criticality– and the transitions into and out of the correlated states appear to be associated with temporal clusters of large events. Accordingly, one might suggest that deep-seated networks, being “incapable” of synchronization and lacking crucial characteristics of criticality, may become correlated through non-critical mechanisms such as the CNM, i.e. by external geodynamic forcing. It follows that a lot of additional experimental and theoretical work is needed before any sound conclusions can be reached.

In a final comment, the present work has been based on statistical physics for which the designation “statistical” may not have the same meaning as that in “statistical seismology”. As eloquently pointed out by Sornette and Werner (2009), statistical seismology is “*a field that has developed as a marriage between probability theory, statistics and the part of seismology concerned with empirical patterns of earthquake occurrences … but not with*

physics". On the other hand, statistical physics endeavours to generate the statistical models from first principles, respecting the laws of thermodynamics and taking into account physical laws such as those of friction, rupture etc. In other words, it uses physics to support stochastic models, a quality often missing from traditional statistical seismology (Dieterich, 1994). A set of questions such as "how can the collective properties of a set formed by all earthquakes in a given region, be derived", "how does the structure of seismicity depend on its elementary constituents – the earthquakes", "What are these properties", could be answered when considering the use of statistical physics in understanding the collective properties of earthquakes. In this respect, NESP formalism, appears to be an effective and insightful tool in the investigation of seismicity and its associated complexity. NESP-based approach is constrained by physics and as such, it is analogously significant.

It becomes clear that the application of such modern tools of complexity theory will give strong impact to understand the basic rules, governing seismogenesis. The key scientific challenge on how to use this information in favour of earthquake forecasting lies ahead and hopefully in near future will be a topic of more rigorous investigation.

		FULL catalogues		$q_T(M_{th})$																																				
			PERIOD	2.5	2.6	2.7	2.8	2.9	3	3.1	3.2	3.3	3.4	3.5	3.6	3.7	3.8	3.9	4	4.1	4.2	4.3	4.4	4.5	4.6	4.7	4.8	4.9	5	5.1	5.2	5.3	5.4	5.5	5.6	5.7
NE PACIFIC RIM	South California	SCSR	1968-2017	1.15	1.16	1.15	1.18	1.16	1.18	1.17	1.15	1.06	1.08	1.24	1.23	1.34	1.37	1.45	1.65	1.6																				
		sSAF	1968-2017	1.12	1.13	1.14	1.14	1.1	1.05	1.15	1.16	1.18	1.12	1.09	1.1	1.39	1.56	1.61	1.88	1.72	1.79																			
		ICB	1968-2017	1.14	1.09	1.12	1.22	1.31	1.35	1.28	1.52																													
		ECSZ	1968-2017	1.79	1.82	1.84	1.77	1.86	1.88	1.95	1.95	1.95	1.91	1.92	1.9	1.92	1.95																							
	North California	NCSN	1968-2015						1.28	1.26	1.25	1.27	1.31	1.32	1.24	1.23	1.29	1.3	1.26	1.41	1.29	1.23	1.26	1.31																
		NCSN	1968-1988						1.35	1.36	1.3	1.34	1.37	1.45	1.37	1.44	1.45	1.41	1.34																						
		NCSN	1990-2015						1.13	1.08	1.09	1.09	1.24	1.24	1.13	1.07	1.05	1.04	1.09																						
		nSAF	1968-2015						1.27	1.25	1.27	1.31	1.17	1.28	1.21	1.16	1.14	1.18	1.25	1.19	1.24	1.15																		
		nSAF	1968-1988						1.4	1.4	1.45	1.45	1.51	1.59	1.56	1.47	1.58	1.53	1.56	1.61																				
		nSAF	1990-2015						1.09	1.08	1.13	1.09	1.04	1.07	1.02	1.077																									
		SNR	1968-2015											1.39	1.41	1.46	1.51	1.46	1.46	1.5	1.51																			
		SNR	1968-1988									1.41	1.4	1.43	1.47	1.51	1.59	1.63	1.51	1.54																			
		SNR	1990-2015						1.38	1.34	1.37	1.37	1.41	1.48	1.41	1.41	1.48																								
		MFZ	1968-2015						1.15	1.15	1.19	1.2	1.23	1.24	1.22	1.13	1.11	1.15	1.17	1.21	1.28																			
	Alaska & Aleutian Arc-	QCD	1968-2015						1.16	1.13	1.2	1.16	1.2	1.24	1.28	1.26	1.28	1.33	1.24	1.31	1.36	1.44	1.44																	
		WNG	1968-2015						1.09	1.11	1.15	1.11	1.17	1.24	1.23	1.25	1.24	1.12	1.15	1.35	1.37																			
		ALW	1968-2015						1.31	1.27	1.25	1.23	1.19	1.27	1.04	1.14	1.24	1.21																						
		ATC (Unimak)	1968-2015											1.49	1.44	1.41	1.44	1.34	1.29	1.26	1.36	1.28	1.55	1.54															
		ATC (complete)	1968-2015																				1.59	1.54	1.43	1.41	1.41	1.35	1.45	1.56								
		ATD (Unimak)	1968-2015											1.07	1.11	1.18	1.17	1.12	1.07	1.12	1.08	1.1	1.09	1.09	1.15	1.21	1.3	1.26	1.15								
		ATD (complete)	1968-2015																				1.18	1.15	1.14	1.17	1.12	1.14	1.18	1.14	1.09	1.09	1.08	1.08	1.09	1.09
NW PACIFIC BELT	Ryukyu Izu-Bonin and Honshu Arcs	RKUC	2002-2016						1.38	1.39	1.4	1.43	1.42	1.46	1.58	1.66	1.64	1.61	1.67		1.73	1.8																
		RKUS	2002-2016							1.19	1.14	1.11	1.09	1.08	1.12	1.13	1.13	1.12	1.1	1.13	1.17	1.12	1.12	1.21	1.15	1.1	1.18											
		PSPC	2002-2016						1.22	1.21	1.26	1.24	1.24	1.26	1.28	1.24	1.28	1.28	1.23	1.21	1.14	1.16	1.15																
		PSPS	2002-2016						1.2	1.18		1.13	1.12	1.1	1.07	1.06	1.08	1.05	1.03	1.04	1.05	1.07	1.09	1.05	1.09	1	1.08											
		OKHC	2002-2010						1.36	1.32	1.32	1.44	1.52	1.61	1.63	1.67	1.81	1.87	1.79	1.77	1.67	1.76																
		OKHS	2002-2010						1.18	1.19	1.17	1.17	1.17	1.15	1.16	1.13	1.15	1.21	1.19	1.16	1.12	1.16	1.16	1.07	1.12	1.17	1.25											
		SJPC	2002-2016						1.18	1.24	1.24	1.26	1.29	1.44	1.5	1.6																							
		SJPS	2002-2016						1.03	1.05	1.07	1.06	1.08	1.14	1.17	1.31																							
HELLENIC SEISMOGENETIC SYSTEM	Greece & Western Turkey	CTF	1964-2015																	1.25	1.08	1.07	1.11	1.11	1.11	1.14	1.14	1.12	1.23	1.27							
		CTF	1964-1996																	1.25	1.08	1.07	1.11	1.11	1.14	1.12	1.23	1.24								
		CTF	1997-2015												1.13	1.14	1.19	1.16	1.22	1.23	1.2	1.33															
		HEL	1964-2015																	1.15	1.14	1.22	1.28	1.31	1.34	1.42										
		HEL	1964-1996																	1.19	1.23	1.15	1.39	1.27	1.37	1.27										
		HEL	1997-2015												1.1	1.15	1.2	1.2	1.5	1.22	1.33																
		NAF-NAT	1964-2015																	1.2	1.25	1.22	1.21	1.17	1.47											
		NAF-NAT	1964-1996																	1.4	1.36	1.36	1.46	1.45												
		NAF-NAT	1997-2015											1.79	1.66	1.58	1.51	1.46	1.48																		
		SUB	1964-2015																			1.08	1.09	1.18	1.19	1.08	1.27									
		SUB	1964-1996																			1.19	1.18	1.21	1.28	1.18										
		SUB	1997-2015														1.08	1.13	1.05	1.09	1.09	1.13	1.18														
		SHR	1964-2015																	1.1	1.06	1.1	1.16	1.21	1.24	1.27	1.39	1.36								

Figure 6.1 Summarization and classification of all q_T vs. M_{th} determinations for the full catalogues of the NE Pacific Belt, NW Pacific Belt and Hellenic Seismogenetic system.

		DECLUSTERED 70% catalogues		$q_T(M_{th})$																												
			PERIOD	2.5	2.6	2.7	2.8	2.9	3	3.1	3.2	3.3	3.4	3.5	3.6	3.7	3.8	3.9	4	4.1	4.2	4.3	4.4	4.5	4.6	4.7	4.8	4.9	5	5.1	5.2	5.3
NE PACIFIC RIM	South California	SCSR	1968-2017	1.46	1.42	1.41	1.43	1.46	1.50	1.57	1.68	1.71	1.80	1.78																		
		sSAF	1968-2017	1.50	1.54	1.48	1.55	1.59	1.68	1.73	1.74																					
		ICB	1968-2017	1.71	1.70	1.81																										
		ECSZ	1968-2017	1.62	1.72	1.75	1.74	1.79	1.78																							
	North California	NCSN	1968-2015								1.44	1.46	1.46	1.45	1.43	1.30	1.40															
		nSAF	1968-2015								1.45	1.46	1.42	1.48	1.58																	
		SNR	1968-2015								1.56	1.60	1.79	1.80																		
		MFZ	1968-2015						1.06	1.11	1.11	1.19	1.22	1.19	1.28	1.24	1.16															
	Alaska & Aleutian Arc-Trench	QCD	1968-2015						1.09	1.13	1.16	1.21	1.22	1.27	1.37	1.29	1.32															
		WNG	1968-2015						1.06	1.06	1.02	1.00	1.12	1.13	1.19	1.34	1.30	1.22														
		ALW	1968-2015						1.16	1.24	1.13	1.16																				
		ATC (Unimak)	1968-2015											1.51	1.45	1.40	1.38	1.34	1.31	1.42												
		ATC (complete)	1968-2015																				1.45	1.46	1.54	1.53	1.61	1.63	1.56			
		ATD (Unimak)	1968-2015											1.18	1.17	1.18	1.15	1.13	1.10	1.14	1.14	1.19	1.18	1.18	1.19	1.17	1.17	1.19				
		ATD (complete)	1968-2015																				1.18	1.06	1.15	1.12	1.10	1.11	1.07	1.08	1.13	1.13
NW PACIFIC BELT	Ryukyu Izu-Bonin and Honshu Arcs	RKUC	2002-2016						1.17	1.18	1.19	1.17	1.22	1.13	1.21	1.13																
		RKUS	2002-2016						1.15		1.13	1.08	1.06	1.09	1.07	1.07	1.08	1.01	1.05	1.04	1.12	1.10	1.07	1.10								
		PSPC	2002-2016						1.22	1.17	1.13	1.11	1.14	1.09	1.12	1.15	1.14	1.18	1.22	1.00												
		PSPS	2002-2016						1.21	1.20	1.19	1.18	1.17	1.12	1.10	1.05	1.06	1.06	1.04	1.00	1.01	1.03	1.04	1.07	1.03	1.03	1.08					
		OKHC	2002-2010						1.09	1.05	1.09	1.06	1.06	1.10																		
		OKHS	2002-2010						1.20	1.14	1.13	1.10	1.16	1.14	1.13	1.16	1.11	1.07	1.10	1.14	1.19	1.10	1.11	1.07								
		SJPC	2002-2016						1.09	1.17	1.28	1.31	1.34																			
		SJPS	2002-2016						1.15	1.08	1.00	1.03																				
HELLENIC SEISMOGENETIC SYSTEM	Greece & Western Turkey	CTF	1964-2015																	1.05	1.12	1.24	1.20	1.17	1.20						
		HEL	1964-2015																		1.28	1.35	1.37	1.30								
		SHR	1964-2015																		1.08	1.33	1.23	1.21	1.22							

Figure 6.2 Summarization and classification of all q_T vs. M_{th} determinations for the declustered at 70% catalogues of the NE Pacific Belt, NW Pacific Belt and Hellenic Seismogenetic system.

		DECLUSTERED 80% catalogues		$q_T(M_{th})$																												
			PERIOD	2.5	2.6	2.7	2.8	2.9	3	3.1	3.2	3.3	3.4	3.5	3.6	3.7	3.8	3.9	4	4.1	4.2	4.3	4.4	4.5	4.6	4.7	4.8	4.9	5	5.1
NE PACIFIC RIM	South California	SCSR	1968-2017	1.62	1.62	1.7	1.69	1.65	1.65	1.63	1.69	1.69																		
		sSAF	1968-2017	1.65	1.62	1.62	1.64	1.71	1.72	1.72	1.72																			
		ICB	1968-2017	1.82	1.88	1.88	1.84																							
		ECSZ	1968-2017																											
	North California	NCSN	1968-2015							1.38	1.34	1.46	1.48	1.52	1.23															
		nSAF	1968-2015							1.37	1.42	1.5	1.59																	
		SNR	1968-2015							1.77	1.8	1.75																		
		MFZ	1968-2015						1.1	1.19	1.15	1.27	1.21	1.21	1.23	1.23														
	Alaska & Aleutian Arc-Trench	QCD	1968-2015						1.17	1.22	1.27	1.26	1.3	1.32																
		WNG	1968-2015						1.03	1.06	1.1	1.06	1.16	1.13	1.19	1.15	1.11	1.18												
		ALW	1968-2015						1.18	1.16	1.05	1.03																		
		ATC (Unimak)	1968-2015											1.49	1.56	1.57	1.38	1.36	1.32											
		ATC (complete)	1968-2015																				1.62	1.57	1.65	1.69	1.65			
		ATD (Unimak)	1968-2015											1.20	1.19	1.16	1.14	1.16	1.09	1.15	1.16	1.23	1.20	1.20	1.18	1.28	1.25	1.16		
		ATD (complete)	1968-2015																					1.07	1.03	1.00	1.00	1.14	1.00	1.00
NW PACIFIC BELT	Ryukyu Izu-Bonin and Honshu Arcs	RKUC	2002-2016						1.12	1.15	1.19	1.16	1.15	1.14	1.23	1.19														
		RKUS	2002-2016						1.13		1.09	1.06	1.05	1.06	1.08	1.07	1.08	1.03	1.11	1.09	1.1	1.13	1.13	1.14						
		PSPC	2002-2016						1.14	1.12	1.09	1.08	1.14	1.14	1.17	1.14	1.11	1.15	1.22											
		PSPS	2002-2016						1.18	1.15	1.14	1.15	1.14	1.08	1.06	1.05	1.03	1.02	1.02	1	1.05	1.04	1.09	1.14	1.08	1.07	1.11			
		OKHC	2002-2010						1.09	1.05	1.09	1.06	1.06	1.1																
		OKHS	2002-2010						1.15	1.15	1.14	1.11	1.11	1.14	1.13	1.18	1.11	1.08	1.09	1.19	1.15	1.12	1.16							
		SJPC	2002-2016						1.09	1.15	1.28	1.3	1.33																	
HELLENIC SEISMOGENETIC SYSTEM	Greece & Western Turkey	CTF (64-15)	1964-2015																1.35	1.38	1.51	1.49	1.44							
		HEL (64-15)	1964-2015																	1.3	1.43	1.39	1.49							
		SHR	1964-2015																	1.11	1.33	1.29	1.27							

Figure 6.3 Summarization and classification of all q_T vs. M_{th} determinations for the declustered at 80% catalogues of the NE Pacific Belt, NW Pacific Belt and Hellenic Seismogenetic system.

		FULL catalogues		q_T (Δd) km									
			PERIOD	0-100	100-200	200-300	300-400	400-500	500-600	600-700	700-800	800-900	900-1000
NE PACIFIC RIM	South California	SCSR	1968-2017	1.59	1.23	1.05	1.15	1.23					
		sSAF	1968-2017	1.57	1.15	1.13	1.08						
		ICB	1968-2017	1.47	1.12	1.28							
		ECSZ	1968-2017	1.85	1.69								
	North California	NCSN	1968-2015	1.44	1.22	1.31	1.27	1.46					
		NCSN	1968-1988	1.56	1.47	1.38	1.72						
		NCSN	1990-2015	1.45	1.1	1.25	1.11	1.17					
		nSAF	1968-2015	1.62	1.25	1.25	1.24	1.4					
		nSAF	1968-1988	1.57	1.32	1.47	1.58						
		nSAF	1990-2015	1.12	1.18	1.14	1.08	1.15					
		SNR	1968-2015	1.38	1.47	1.38							
		SNR	1968-1988	1.54	1.69	1.7							
		SNR	1990-2015	1.68	1.58	1.55	1.76						
		MFZ	1968-2015	1.32	1.34	1.19	1.24	1.25					
	Alaska & Aleutian Arc-Trench	QCD	1968-2015		1.39	1.41	1.47	1.49	1.37	1.41	1.28		
		WNG	1968-2015	1.75	1.22	1.07	1.13	1.35					
		ALW	1968-2015		1.76	1.64	1.29	1.38					
		ATC (Unimak)	1968-2015		1.61	1.53	1.44	1.69	1.57				
		ATC (complete)	1968-2015	1.34	1.21	1.1	1	1.1	1.17	1.15	1.28	1.33	
		ATD (Unimak)	1968-2015	1.25	1.08	1.04	1.14	1.13	1.08	1.05	1.12	1.25	
		ATD (complete)	1968-2015	1.22	1.17	1.01	1.08	1.15	1.16	1.1	1.14	1.25	
NW PACIFIC BELT	Ryukyu Izu-Bonin and Honshu Arcs	RKUC	2002-2016	1.82	1.2	1.12	1.15	1.08	1.06	1.16	1.22	1.22	
		RKUS	2002-2016	1.32	1,12-1,06	1.05	1.11	1.05	1.06	1.1	1.13	1.06	1.03
		PSPC	2002-2016	1.96	1.15	1.21	1.12	1.24	1.31				
		PSPS	2002-2016	1.44	1.15	1.07	1.11	1.1	1.12	1.09	1.07		
		OKHC	2002-2010	1.81	1.24	1.32	1.26	1.18	1.23				
		OKHS	2002-2010	1.3	1.14	1.11	1.15	1.09	1.1	1.17			
		SJPC	2002-2016	1.91	1.12	1.18	1.15	1.18	1.16				
		SJPS	2002-2016	1.74	1.4	1.12							
HELLENIC SEISMOGENETIC SYSTEM	Greece & Western Turkey	CTF	1964-2015	1.28	1.2	1.24	1.26	1.58					
		CTF	1964-1996	1.34	1.23	1.3	1.32						
		CTF	1997-2015	1.27	1.16	1.14	1.14	1.05	1.29				
		HEL	1964-2015	1.22	1.16	1.33		1.41	1.17				
		HEL	1964-1996	1.25	1.48			1.1	1.23				
		HEL	1997-2015	1.53	1.23		1.1	1.32	1.35				
		NAF-NAT	1964-2015	1.37	1.35	1.31							
		SUB	1964-2015		1.09	1.01	1.29						
		SUB	1964-1996	1.38	1.27	1.18	1.22						
		SUB	1997-2015	1.34	1.17	1.12	1.24	1.01					
		SHR	1964-2015	1.41	1.17	1.27	1.42	1.36					

Figure 6.4 Summarization and classification of all q_T vs. Δd determinations for the full catalogues of the NE Pacific Belt, NW Pacific Belt and Hellenic Seismogenetic system.

		DECLUSTERED 70% catalogues		q_T (Δd) km									
			PERIOD	0-100	100-200	200-300	300-400	400-500	500-600	600-700	700-800	800-900	900-1000
NE PACIFIC RIM	South California	SCSR	1968-2017	1.63	1.73	1.69							
		sSAF	1968-2017	1.61	1.63	1.72							
	North California	NCSN	1968-2015	1.71	1.36	1.41	1.46						
		MFZ	1968-2015	1.24	1.12	1.48							
	Alaska & Aleutian Arc-Trench	QCD	1968-2015	1.26	1.33	1.33	1.46						
		WNG	1968-2015		1.36	1.13	1.14	1.21					
		ATC (Unimak)	1968-2015		1.26	1.18	1.32	1.36					
		ATC (complete)	1968-2015					1.57	1.47	1.45	1.56		
		ATD (Unimak)	1968-2015	1.08	1.10	1.12	1.07		1.08	1.14	1.14	1.15	
		ATD (complete)	1968-2015	1.13	1.13	1.11	1.04	1.04	1.19				
NW PACIFIC BELT	Ryukyu Izu-Bonin and Honshu Arcs	RKUC	2002-2016	1.77	1,23-1,28	1.22	1.27	1.12	1.15	1.27	1.26	1.38	
		RKUS	2002-2016	1.17	1.06	1.09	1.07	1.15	1.09	1.07	1.13	1.09	
		PSPC	2002-2016	1.16		1.14		1.34	1.36	1.27	1.16		
		PSPS	2002-2016	1.25	1.12	1.08	1.11	1.09	1.15	1.1	1.11		
		OKHC	2002-2010			1.25	1.37	1.33	1.27				
		OKHS	2002-2010	1.18	1.1	1.1	1.05	1.11	1.17	1.18	1.16		
		SJPC	2002-2016	1.31	1.16	1.14	1.1						
HELLENIC SEISMOGENETIC SYSTEM	Greece & Western Turkey	SHR	1964-2015		1.12	1.18	1.36						

Figure 6.5 Summarization and classification of all q_T vs. Δd determinations for the declustered at 70% catalogues of the NE Pacific Belt, NW Pacific Belt and Hellenic Seismogenetic system.

		DECLUSTERED 80% catalogues		q_T (Δd) km									
			PERIOD	0-100	100-200	200-300	300-400	400-500	500-600	600-700	700-800	800-900	900-1000
NE PACIFIC RIM	South California	SCSR	1968-2017	1.56	1.75	1.84	1.89						
		sSAF	1968-2017	1.72	1.85								
	North California	MFZ	1968-2015	1.25	1.16	1.44							
	Alaska & Aleutian Arc-Trench	QCD	1968-2015		1.22	1.40	1.38						
		WNG	1968-2015		1.15	1.11	1.17	1.23					
		ATD (Unimak)	1968-2015	1.13	1.09	1.08	1.08		1.20	1.25	1.28	1.32	
		ATD (complete)	1968-2015		1.06	1.15	1.04	1.02	1.19				
NW PACIFIC BELT	Ryukyu Izu-Bonin and Honshu Arcs	RKUC	2002-2016	1.78	1.11	1.18	1.2	1.12	1.18	1.29	1.19		
		RKUS	2002-2016	1.11	1,12-1,04	1.12	1.08	1.12	1.09	1.12	1.14	1.11	
		PSPC	2002-2016	1.19	1.21	1.16		1.27	1.23	1.27	1.3		
		PSPS	2002-2016	1.22	1.16	1.2	1.11	1.11	1.08	1.09	1.04		
		OKHC	2002-2010			1.18	1.3	1.34	1.31				
		OKHS	2002-2010	1.26	1.14	1.05	1.11	1.09	1.2	1.22	1.18		
		SJPC	2002-2016		1.15	1.12	1.07						

Figure 6.6 Summarization and classification of all q_T vs. Δd determinations for the declustered at 80% catalogues of the NE Pacific Belt, NW Pacific Belt and Hellenic Seismogenetic system.

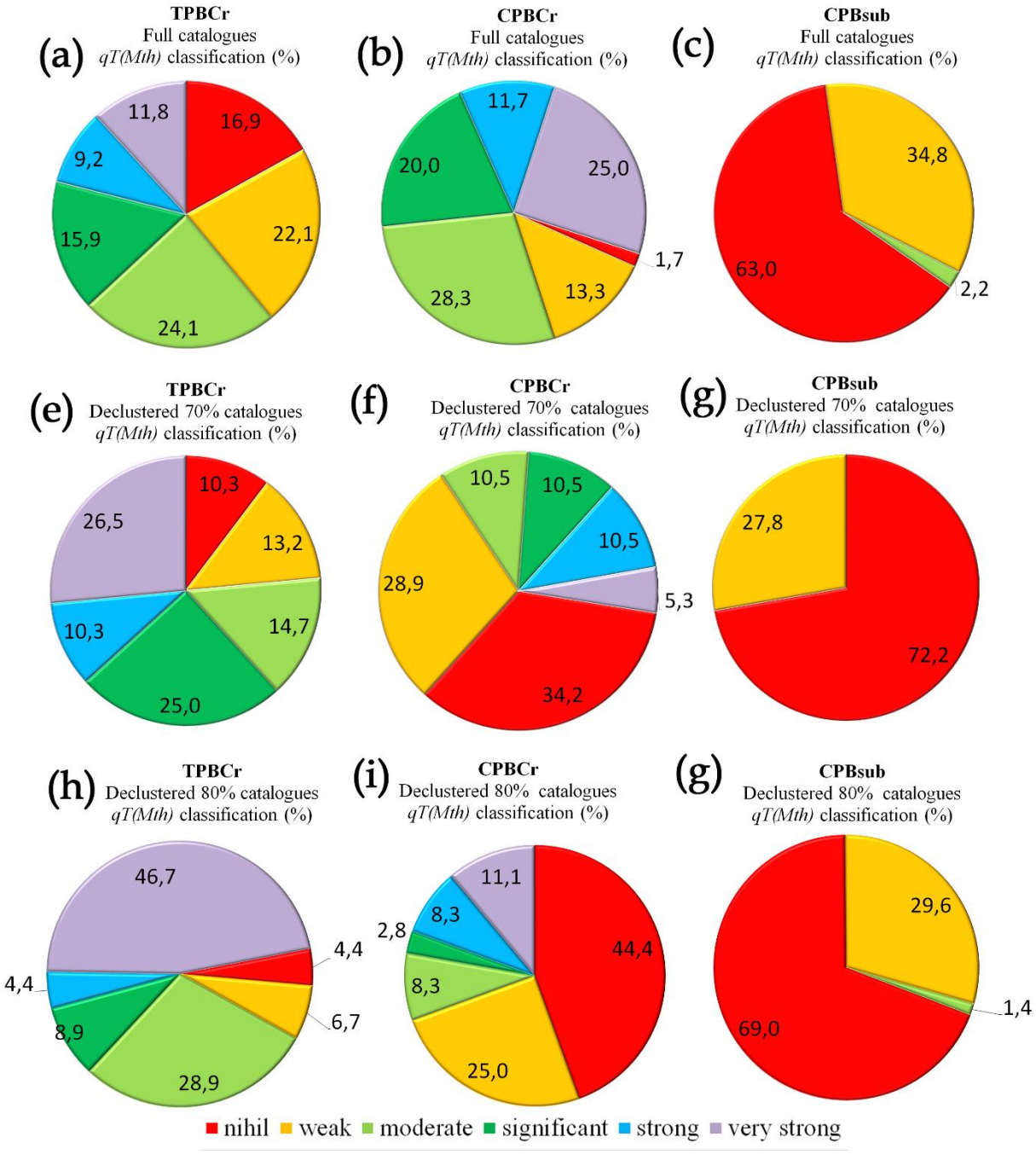

Figure 6.7 Proportions of $q_T(M_{th})$ classes determined from the analysis of *full* and *declustered* TPBCr, CPBCr and CPBsub systems.

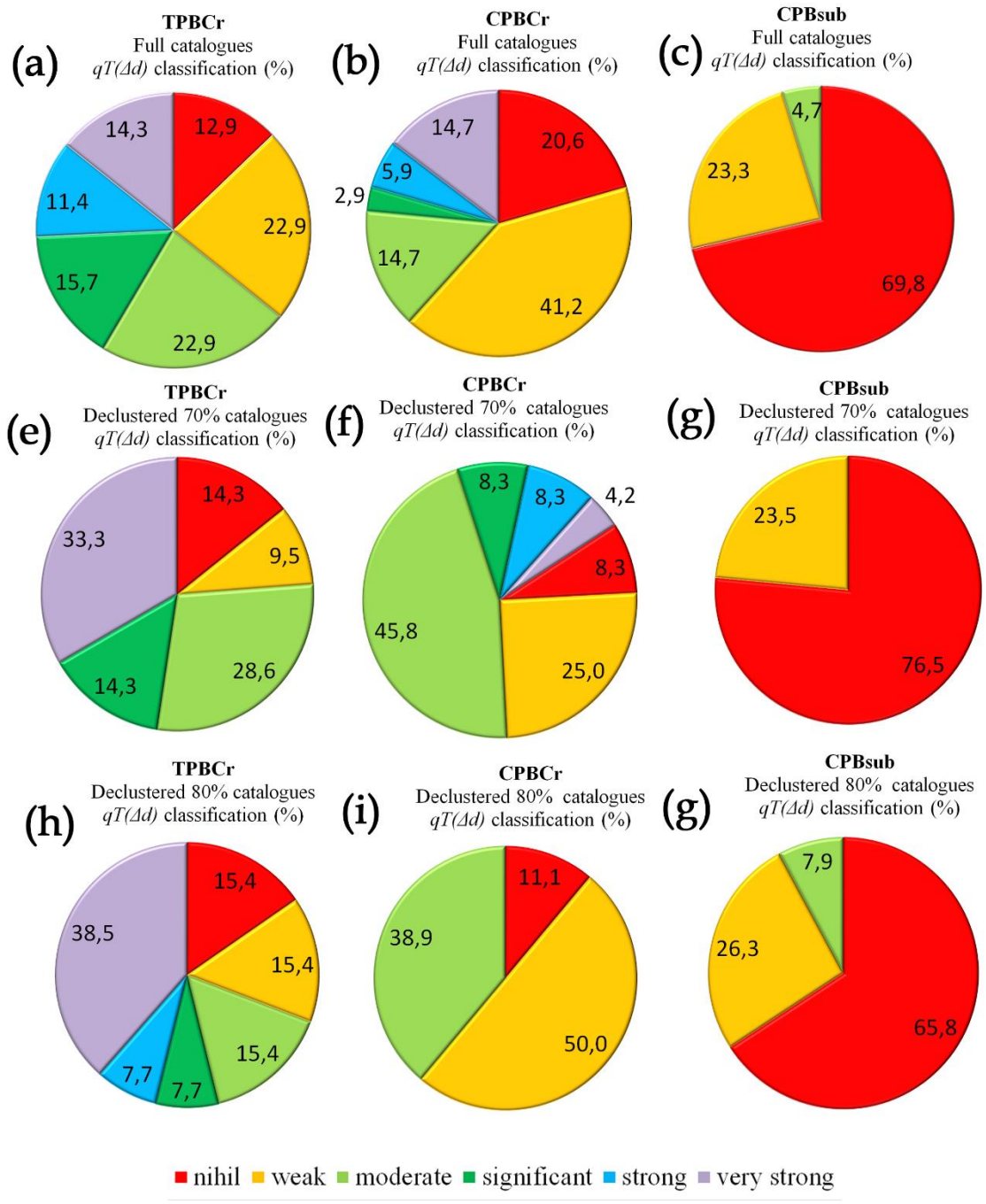

Figure 6.8 Proportions of $q_T(\Delta d)$ classes determined from the analysis of *full* and *declustered* TPBCr, CPBCr and CPBsub systems.

REFERENCES

[1] Abaimov S.G., 2009. General formalism of non-equilibrium statistical mechanics, path approach., Cornell University Library, Statistical Mechanics, arXiv:0906.0190v4

[2] Abe S. and Suzuki N., 2003. Law for the distance between successive earthquakes, J. Geophys. Res. (Solid Earth) 108, B2, 2113.

[3] Abe S., and Suzuki N., 2004. Complex Network of Earthquakes. In: Bubak M., van Albada G.D., Sloot P.M.A., Dongarra J. (eds) Computational Science - ICCS 2004. ICCS 2004. Lecture Notes in Computer Science, vol 3038. Springer, Berlin, Heidelberg; doi: 10.1007/978-3-540-24688-6_135

[4] Abe, S., and Suzuki N., 2005. Scale-free statistics of time interval between successive earthquakes. Physica A, 350, 588-596.

[5] Abe, S., and Suzuki, N., 2007. Dynamical evolution of clustering in complex network of earthquakes, Eur. Phys. J. B 59, 93–97; doi: 10.1140/epjb/e2007-00259-3

[6] Aki, K. 1965. Maximum likelihood estimate of b in the formula log N a bM and its confidence limits, Bull. Earthq. Res. Inst. Tokyo Univ. 43, 237–239

[7] Allègre C.J. Le Mouel J.L, Provost A., 1982. Scaling rules in rock fracture and possible implications for earthquake prediction Nature, 297 (1982), pp.47-49

[8] Amelung F. and King G., 1997; Earthquake scaling laws for creeping and non-creeping faults. Geophysical Research Letters, VOL. 24, No. 5, Pages 507-510, March 1, 1997, Paper number 97GL00287. 094-8534/97/97GL-00287505.00

[9] Antonopoulos C.G., Michas G., Vallianatos F. and Bountis T., 2014. Evidence of q-exponential statistics in Greek seismicity. Physica A: Statistical Mechanics and its Applications, 409, 71-77; doi: 10.1016/j.physa.2014.04.042

[10] Armijo, R., Lyon-Caen, H., and Papanastassiou, D., 1991. A possible normal-fault rupture for the 464 BC Sparta earthquake. Nature 351: 137–139.

[11] Armijo, R., Lyon-Caen, H., and Papanastassiou, D., 1992. East–west extension and Holocene normal-fault scarps in the Hellenic arc. Geology 20: 491–494.

[12] Armijo, R., Tapponnier, P., Mercier, J. L., and Han T.-L., 1986. Quaternary extension in southern Tibet: field observations and tectonic implications. J. Geophys. Res. 91: 13 803–13 872.

[13] Astiz L. and Shearer M. P., 2000. Earthquake Locations in the Inner Continental Borderland, Offshore Southern California, Bulletin of the Seismological Society of America, 90 (2), 425–449.

[14] Avallone A., Briole P., Agatza – Balodimou A. et al., 2004. Analysis of eleven years of deformation measured by GPS in the Corinth Rift Laboratory area. C. R. Geoscience 336 301–311.

[15] Bak P, Tang C and Wiesenfeld K., 1987. Self-organized criticality: An explanation of the 1/f noise. Phys. Rev. Lett. 59, 381. DOI: https://doi.org/10.1103/PhysRevLett.59.381

[16] Bak P, Tang C and Wiesenfeld K., 1988. Self-organized ciritcality. Phys. Rev. A 38, 364. DOI: https://doi.org/10.1103/PhysRevA.38.364

[17] Bak, P. and Tang C., 1989. Earthquakes as a self-organized critical phenomenon. J. Geophys. Res., 94, 15635-15637.

[18] Bak, P., Christensen, K., Danon, L. and Scanlon, T., 2002. Unified scaling law for earthquakes, Phys. Rev. Lett., 88, 178501; doi:10.1103/PhysRevLett.88.178501.

[19] Bakar, B. and Tirnakli, U., 2009. Analysis of self-organized criticality in Ehrenfest's dog-flea model, Phys. Rev. E, 79, 040103; doi:10.1103/PhysRevE.79.040103.

[20] Balasis G., Daglis I.A., Papadimitriou C., Kalimeri M., Anastasiadis A. and Eftaxias K., 2008. Dynamical complexity in Dst time series using non-extensive Tsallis entropy, Geophys. Res. Lett. 35, L14102.

[21] Baldovin F. and Robledo A., 2002. Sensitivity to initial conditions at bifurcations in one dimensional nonlinear maps: Rigorous nonextensive solutions, Europhys. Lett. 60, 518
[22] Baldovin F. and Robledo A., 2002. Universal renormalization-group dynamics at the onset of chaos in logistic maps and nonextensive statistical mechanics, Phys. Rev. E 66, R045104
[23] Baldovin F. and Robledo A. 2004. Nonextensive Pesin identity – Exact renormalization group analytical results for the dynamics at the edge of chaos of the logistic map., Phys. Rev. E 69, 045202(R)
[24] Baldovin F., Tsallis C. and Schulze B., 2003. Nonstandard entropy production in the standard map, Physica A 320, 184.
[25] Barlow H. 1990. Conditions for versatile learning, Helmholtz's unconscious inference, and the task of perception, Vision Research, Volume 30, Issue 11,1990, Pages 1561-1571, https://doi.org/10.1016/0042-6989(90)90144-A
[26] Barriere B. and Turcotte D.L., 1991. A scale-invariant cellular-automata model for distribited seismicity. Geophysical Research Letters, VOL. 18, NO. 11, PAGES 2011-2014, November 1991. https://doi.org/10.1029/91GL02415
[27] Batak R. C and Kantz H., 2014. Observing spatio-temporal clustering and separation using interevent distributions of regional earthquakes, Nonlin. Processes Geophys. 21, 735–744; doi: 10.5194/npg-21-735-2014.
[28] Beck, C. and Schloegl, F., 1993. Thermodynamics of Chaotic Systems: An Introduction, Cambridge University Press, Cambridge University Press, pp. 88-93.
[29] Becker T.W., Hardebeck J.L. and Anderson G., 2005. Constraints on fault slip rates of the southern California plate boundary from GPS velocity and stress inversions, Geophys. J. Int., 160 (2), 634–650.
[30] Bender B., 1983. Maximum likelihood estimation of b values for magnitude grouped data. Bulletin of the Seismological Society of America (1983) 73 (3): 831-851.
[31] Ben-Menahem A. and Toksöz M.N., 1963. Source mechanism form spectrums of long-period surface waves. J. Geoph. Res. 68, 5207-5222.
[32] Bennet R.A., Davis J.L. and Wernicke B.P., 1999. Present-day pattern of Cordilleran deformation in the western United States. Geology (1999) 27 (4): 371-374. https://doi.org/10.1130/0091-7613(1999)027<0371:PDPOCD>2.3.CO;2
[33] Berger A.L. and Spotila J.A., 2008. Denudation and deformation in a glaciated orogenic wedge: The St. Elias orogen, Alaska. Geology (2008) 36 (7): 523-526.https://doi.org/10.1130/G24883A.1
[34] Biswas N.N., Aki K., Pulpan H., Tytgat G., 1986b. Characteristics of regional stresses in Alaska and neighboring areas. GEOPHYSICAL RESEARCH LETTERS, VOL. 13, NO. 3, PAGES 177-180, MARCH 1986. https://doi.org/10.1029/GL013i003p00177
[35] Boltzmann L., 1877. Bemerkungen über einige Probleme der mechanischen Wärmetheorie, 1877 Wien. Ber. 75 62
[36] Boltzmann L, Über die Beziehung zwischen dem zweiten Hauptsatzes der mechanischen Wärmetheorie und der Wahrscheinlichkeitsrechnung respektive den Sätzen über das Wärmegleichgewicht, 1877 Wien. Ber. 76 373
[37] Boltzmann L, Weitere studien über das Wärmegleichgewicht unter Gasmolekulen, 1872 Wien. Ber. 66 275
[38] Borges E.P., Tsallis C., Ananos G.F.J, and de Oliveira P.M.C., 2002. Nonequilibrium probabilistic dynamics at the logistic map edge of chaos, Phys. Rev. Lett. 89, 25

[39] Borovkov, K. and Bebbington M.S., 2003. A Stochastic Two-node Stress Transfer Model Reproducing Omori's Law. M. Pure appl. geophys. (2003) 160: 1429. https://doi.org/10.1007/s00024-003-2354-8

[40] Bottiglieri, M., Lippiello E., Godano C., and de Arcangelis L., 2011. Comparison of branching models for seismicity and likelihood maximization through simulated annealing, J. Geophys. Res., 116, B02303, doi: 10.1029/2009JB007060.

[41] Bountzis P., Papadimitriou E. and Tsaklidis G., 2018: Estimating the earthquake occurrence rates in Corinth Gulf (Greece) through Markovian arrival process modeling, Journal of Applied Statistics, DOI: 10.1080/02664763.2018.1531977.

[42] Bowman D. D., Ouillon G., Sammis C., G Sornette A., Sornette D., 1998. An observational test of the critical earthquake concept Journal of Geophysical Research: Solid Earth Volume 103, Issue B10 https://doi.org/10.1029/98JB00792

[43] Brodsky, E.E., 2006. Long-Range Triggered Earthquakes that Continue after the Wave Train Passes, Geophysical Research Letters, V. 33, paper L15313, 5 pp.

[44] Brodsky E.E., Karakostas V., and Kanamori H., 2000. A New Observation of Dynamically Triggered Regional Seismicity: Earthquakes in Greece Following the August 1999 Izmit, Turkey Earthquake. GEOPHYSICAL RESEARCH LETTERS, VOL. 27, NO. 17, PAGES 2741-2744, SEPTEMBER 1, 2000.

[45] Bruns T.R., 1983. Model for the origin of the Yakutat block, an accreting terrane in the northern Gulf of Alaska. Geology (1983) 11 (12): 718-721. doi.org/10.1130/0091-7613(1983)11<718: MFTOOT>2.0.CO;2

[46] Burridge R, Knopoff, L. 1967. Model and theoretical seismicity. Bulletin of the Seismological Society of America (1967) 57 (3): 341-371.

[47] Carbone, V., Sorriso-Valvo, L., Harabaglia, P. and Guerra, I., 2005. Unified scaling law for waiting times between seismic events, Europhys. Lett. 71 (6), 1036; doi: 10.1209/epl/i2005-10185-0.

[48] Carlson J. M. and Langer J. S., 1989. Mechanical model of an earthquake fault Phys. Rev. A 40, 6470 https://doi.org/10.1103/PhysRevA.40.6470

[49] Caruso, F., Latora, V., Rapisarda, A. and Tadić, B., 2005. The Olami-Feder-Christensen model on a small-world topology, arXiv: cond-mat/0507643v1.

[50] Caruso, F., Pluchino, A., Latora, V., Vinciguerra, S. and Rapisarda, A., 2007. Analysis of self-organized criticality in the Olami-Feder-Christensen model and in real earthquakes, Phys. Rev. E, 75, 055101; doi: 10.1103/PhysRevE.75.055101.

[51] Carver G, Plafker G., Metz M., Cluff L., Slemmons B., Johnson E., Roddick J., Sorensen S., 2004. Surface Rupture on the Denali Fault Interpreted from Tree Damage during the 1912 Delta River Mw 7.2–7.4 Earthquake: Implications for the 2002 Denali Fault Earthquake Slip Distribution. Bulletin of the Seismological Society of America (2004) 94 (6B): S58-S71. https://doi.org/10.1785/0120040625

[52] Celikoglu, A., Tirnakli, U., and Duarte Queirós, S., 2010. Analysis of return distributions in the coherent noise model, Phys. Rev. E, 82, 021124; doi:10.1103/PhysRevE.82.021124.

[53] Chen C-c., 2003. Accelerating seismicity of moderate-size earthquakes before the 1999 Chi-Chi, Taiwan, earthquake: Testing time-prediction of the self-organizing spinodal model of earthquakes. *Geophysical Journal International*, Volume 155, Issue 1, 1 October 2003, Pages F1–F5,https://doi.org/10.1046/j.1365-246X.2003.02071.x

[54] Cho N. F., Tiampo K. F., Mckinnon S. D., Vallejos J. A., Klein W., and Dominguez R., 2010, A simple metric to quantify seismicity clustering, Nonlin. Processes Geophys. 17, 293–302, 2010 www.nonlin-processes-geophys.net/17/293/2010/ doi: 10.5194/npg-17-293-2010 © Author(s) 2010. CC Attribution 3.0 License.

[55] Christensen K and Olami Z., 1992. Variation of the Gutenberg-Richter b values and nontrivial temporal correlations in a Spring-Block Model for earthquakes Journal of Geophysical Research: Solid Earth Volume 97, Issue B6 https://doi.org/10.1029/92JB00427
[56] Christensen K and Olami Z., 1992. Scaling, phase transitions, and nonuniversality in a self-organized critical cellular-automaton model Phys. Rev. A 46, 1829 https://doi.org/10.1103/PhysRevA.46.1829
[57] Christensen K, Hamon D, Jensen J.H, and Lise S. 2001 Comment on “Self-Organized Criticality in the Olami-Feder-Christensen Model” Phys. Rev. Lett. 87, 039801 https://doi.org/10.1103/PhysRevLett.87.039801
[58] Christeson, G. L., Van Avendonk H. J. A., Gulick S. P. S., Reece R. S., Pavlis G. L., and Pavlis T. L., 2013. Moho interface beneath Yakutat terrane, southern Alaska, J. Geophys. Res. Solid Earth, 118, 5084–5097, doi:10.1002/jgrb.50361.
[59] Clausius R. 1872. The Mechanical Theory of Heat with its Application to the Steam Engine and to Physical Properties of Body John Van Voorst, London
[60] Clément, C., Hirn, A., Charvis, P., Sachpazi, M., and Marnelis, F., 2000. Seismic structure and the active Hellenic subduction in the Ionian Islands. Tectonophysics 329: 141–156.
[61] Cliff Frohlich C. and Davis S.D. 1993. Teleseismic b values; Or, much ado about 1.0 Journal of Geophysical Research: Solid Earth Volume 98, Issue B1 https://doi.org/10.1029/92JB01891
[62] Comninakis P.E. and Papazachos B.C, 1980. Space and time distribution of the intermediate focal depth earthquakes in the Hellenic arc. Tectonophysics, 70 (1980) T35-T47. https://doi.org/10.1016/0040-1951(80)90278-4
[63] Console R. and Murru, M., 2001. A simple and testable model for earthquake clustering, J. Geoph. Res., 106, B5, 8699-8711.
[64] Console R., Murru M., Catalli F., Falcone G., 2007. Real Time Forecasts through an Earthquake Clustering Model Constrained by the Rate-and-State Constitutive Law: Comparison with a Purely Stochastic ETAS Model Seismological Research Letters (2007) 78 (1): 49-56. https://doi.org/10.1785/gssrl.78.1.49
[65] Copley A., Boait, F., Hollingsworth, J., Jackson, J., andMcKenzie, D., 2009. Subparallel thrust and normal faulting in Albania and the rates of gravitational potential energy and rheology contrasts in mountain belts. J. Geophys. Res. 114, B05407, doi: 10.1029/2008JB005931.
[66] Cornell C. A., 1968. Engineering seismic risk analysis, Bull. Seism. Soc. Am. 58, 1583–1606
[67] Corral A., 2004. Long-term clustering, scaling, and universality in the temporal occurrence of earthquakes, Phys. Rev. Lett., 92, 108501.
[68] Costa U.M.S. Lyra M.L., Plastino A.R. and Tsallis C., 1997. Power-law sensitivity to initial conditions within a logistic-like family of maps: Fractality and nonextensivity, Phys. Rev. E 56, 245.
[69] Cross R.S and Freymueller J.T, 2007. Plate coupling variation and block translation in the Andreanof segment of the Aleutian arc determined by subduction zone modeling using GPS data. GEOPHYSICAL RESEARCH LETTERS, VOL. 34, L06304, doi:10.1029/2006GL028970, 2007
[70] Cross R.S and Freymueller J.T, 2008. Evidence for and implications of a Bering plate based on geodetic measurements from the Aleutians and western Alaska. JOURNAL OF GEOPHYSICAL RESEARCH, VOL. 113, B07405, doi:10.1029/2007JB005136, 2008
[71] da Silva C.R, da Cruz H.R. and Lyra M.L., 1999. Low-dimensional non-linear dynamical systems and generalized entropy, Braz. J. Phys. 29, 144

[72] Daley, D., and Vere-Jones, D., 2003. An Introduction to the Theory of Point Processes (2nd ed), New York: Springer Verlag
[73] Darooneh A.H. and Dadashinia C., 2008. Analysis of the spatial and temporal distributions between successive earthquakes: Nonextensive statistical mechanics viewpoint, Physica A 387, 3647
[74] Davidsen, J. and Goltz, C., 2004. Are seismic waiting time distributions universal? Geophys. Res. Lett., 31, L21612; doi 10.1029/2004GL020892.
[75] de Carvalho J. X. and Prado C. P. C P. C., 2000. Self-Organized Criticality in the Olami-Feder-Christensen Model Phys. Rev. Lett.84, 4006 https://doi.org/10.1103/PhysRevLett.84.4006
[76] de Carvalho J. X. and Prado C. P. C., 2001. de Carvalho and Prado Reply: Phys. Rev. Lett.87, 039802 https://doi.org/10.1103/PhysRevLett.87.039802
[77] DeMets C., Gordon R. G., Argus D. F., and Stein, S., 1990. Current plate motions. Geophys. J. Internat. 101: 425–478.
[78] DeMets C., and Dixon T., 1999. New kinematic models for Pacific-North America motion from 3 Ma to present, 1: Evidence for steady motion and biases in the NUVEL-1A model, Geophys. Res. Lett., 26, 1921-1924.
[79] Dengler L., Moley K., McPherson R., Pasyanos M., Dewey J.W. and Murray M.H., 1995. The September 1, 1994 Mendocino fault earthquake, California Geology 48, 43 – 53.
[80] Dickinson W.R., and Snyder W. S., 1979a. Geometry of triple junctions related to San Andreas transform. J. Geophys. Res. 84: 561-572.
[81] Dieterich J., 1994. A constitutive law for rate of earthquake production and its application to earthquake clustering, J. Geophys. Res., 99, 2601-2618.
[82] Dimitrov D., Camelbeek T., Ruegg J.-C., Georgiev I., and Bogev E., 2006. Surface seismic deformations in the Plovdiv region (Bulgaria) by space geodesy and seismology data. SENS 2006: Second Scientific Conference with International Participations, Space, Ecology, Nanotechnology, Safety, 14–16 June 2006, Varna, Bulgaria, 8 pp.
[83] Dimri V., 2005. Fractals in Geophysics and Seismology: An Introduction. In: Dimri V.P. (eds) Fractal Behaviour of the Earth System. Springer, Berlin, Heidelberg.
[84] Dixon, T.H., Miller, M., Farina, F., Wang, H., and Johnson, D., 2000. Present-day motion of the Sierra Nevada block and some tectonic implications for the Basin and Range province, North American Cordillera, Tectonics, 19, 1–24; doi: 10.1029/1998TC001088.
[85] Donner R.V and Barbarosa M.S., 2008. Nonlinear Time Series Analysis in the Geosciences. Applications in Climatology, Geodynamics and Solar-Terrestrial Physics. Earth and Environmental Science, Springer-Verlag Berlin Heidelberg 2008. Print ISBN 978-3-540-78937-6, https://doi.org/10.1007/978-3-540-78938-3
[86] Doser D.I, 2004. Seismicity of the Denali-Totschunda Fault Zone in Central Alaska (1912–1988) and Its Relation to the 2002 Denali Fault Earthquake Sequence. Bulletin of the Seismological Society of America (2004) 94 (6B): S132-S144. https://doi.org/10.1785/0120040611
[87] Drossel B., 2002. Complex Scaling Behavior of Nonconserved Self-Organized Critical Systems Phys. Rev. Lett. 89, 238701 https://doi.org/10.1103/PhysRevLett.89.238701
[88] Dziewonski A.M, Chou T.A., Woodhouse J.H., 1981. Determination of earthquake source parameters from waveform data for studies of global and regional seismicity. JOURNAL OF GEOPHYSICAL RESEARCH, VOL. 86, NO. B4, PAGES 2825-2852, doi.org/10.1029/JB086iB04p02825

[89] Eaton J.P., 1992. Determination of amplitude and duration magnitudes and site residuals from short-period seismographs in Northern California, Bull. Seism. Soc. Am., 82 (2), 533-579.

[90] Eberhart-Phillips D. and other. 2003. The 2002 Denali Fault Earthquake, Alaska: A Large Magnitude, Slip-Partitioned Event. 16 MAY 2003 VOL 300 SCIENCE. www.sciencemag.org.

[91] Ellsworth W.L., Matthews M.V, Nadeau R.M, Stuart P. Nishenko S.P, Reasenberg P.A and Simpson R.W 1999. A Physically Based Earthquake Recurrence Model for Estimation of Long-Term Earthquake Probabilities U.S. DEPARTMENT OF THE INTERIOR U.S. GEOLOGICAL SURVEY Open-File Report 99-522

[92] Enescu B., Mori J., Masatoshi Miyazawa M., 2007. Quantifying early aftershock activity of the 2004 mid-Niigata Prefecture earthquake (M_w6.6) Journal of Geophysical Research: Solid Earth Volume 112, Issue B4 https://doi.org/10.1029/2006JB004629

[93] Eneva M. and Pavlis L. G, 1991. Spatial Distribution of Aftershocks and Background Seismicity in Central California, Pure and Applied Geophysics, 137 (1), 35-61.

[94] Esquivel, F.J. and Angulo, J.M., 2015. Non-extensive analysis of the seismic activity involving the 2011 volcanic eruption in El Hierro, 2015, Spatial Statistics**,** 14 (B), 208–221; doi: http://dx.doi.org/10.1016/j.spasta.2015.08.001.

[95] Estabrook C.H., Stone D. B. and Davies J. N., 1988. Seismotectonics of Northern Alaska. JOURNAL OF GEOPHYSICAL RESEARCH, VOL. 93, NO. B10, PAGES 12,026-12,040, OCTOBER 10, 1988

[96] Faulds J.E, Henry C.D., Hinz N.H., Drakos P.S and Delwiche B., 2005. Transect across the northern Walker Lane, northwest Nevada and northeast California: An incipient transform fault along Pacific – North American plate boundary. Geological Society of America, Field Guide 6. 2005

[97] Felzer K.R, Becker T.W., Abercrombie R.E., Ekström G., Rice J.R., 2002. Triggering of the 1999 MW 7.1 Hector Mine earthquake by aftershocks of the 1992 MW 7.3 Landers earthquake Journal of Geophysical Research: Solid Earth Volume 107, Issue B9 https://doi.org/10.1029/2001JB000911

[98] Felzer, K. R. and Brodsky, E. E. 2006. Evidence for dynamic aftershock triggering from earthquake densities, Nature, 441, 735-738.

[99] Felzer, K. R., 2007. Stochastic ETAS Aftershock Simulator Program (AFTsimulator), available at http://pasadena.wr.usgs.gov/office/kfelzer/AftSimulator.html; last access 20 October 2014.

[100] Felzer, K. R., Becker, T. W., Abercrombie, R. E., Ekstrom, G. and Rice J. R., 2002. Triggering of the 1999 Mw 7.1 Hector Mine earthquake by aftershocks of the 1992 Mw 7.3 Landers earthquake, J. Geophys. Res., 107, 2190; doi: 10.1029/2001JB000911.

[101] Felzer, K.R., and E.E. Brodsky 2006. “Decay of Aftershock Density with Distance Indicates Triggering by Dynamic Stress”, Nature, Vol. 441, p. 735-737.

[102] Fialko Y., 2006. Interseismic strain accumulation and the earthquake potential on the South San Andreas Fault system, Nature, 441; doi: 10.1038/nature04797, 968-971.

[103] Field, E. H., 2007. A summary of previous Working Groups on California Earthquake Probabilities, 389 Bull. Seismol. Soc. Am., 97 (4), 1033–1053, doi:10.1785/0120060048

[104] Fisher M.E and Ruelle D. 1966. The Stability of Many-Particle Systems, J. Math. Phys. 7, 260

[105] Fisher M.E. 1965. Arch. Rat. Mech. Anal. 17, 377 (1964), J. Chem. Phys. 42, 3852 (1965) andJ. Math. Phys. 6, 1643

[106] Fisher. And. Lebowitz J.L. 1970. Commun. Math. Phys. 19, 251
[107] Fletcher H. J., and Freymueller J. T., 2003. New constraints on the motion of the Fairweather fault, Alaska, from GPS observations. GEOPHYSICAL RESEARCH LETTERS, VOL. 30, NO. 3, 1139, doi:10.1029/2002GL016476, 2003
[108] Franca G.S, Vilar C.S, Silva R. and. Alcaniz J.S. 2007. Nonextensivity in geological faults? Physica A 377, 285
[109] Freymueller Jeffrey T, Woodard Hilary, Cohen Steven C, Cross Ryan, Elliott Julie, Larsen Christopher F, Hreinsdóttir Sigrún and Zweck Chris 2008. Active Deformation Processes in Alaska, Based on 15 Years of GPS Measurements. Active Tectonics and Seismic Potential of Alaska. (2008), Geophys. Monogr. Ser., vol. 179, edited by J. T. Freymueller et al., pp. vii-viii, AGU, Washington, D. C.
[110] Furlong, K.P., Schwartz, S. Y., 2004. Influence of the Mendocino triple junction on the tectonics of coastal California. Annu. Rev. Earth Planet. Sci. 32:403–33 doi: 10.1146/annurev.earth.32.101802.120252
[111] Gardner, J. K., and Knopoff, L., 1974. Is the sequence of earthquakes in Southern California, with aftershocks removed, Poissonian? Bull. Seism. Soc. Am., 64 (5), 1363-1367.
[112] Gell-Mann, M. and Tsallis, C. (eds.), 2004. Nonextensive Entropy – Interdisciplinary Applications. Oxford University Press, New York.
[113] Gerstenberger, M., Wiemer, S. and Giardini, D., 2001. A systematic test of the hypothesis that b varies with depth in California. Geophysical Research Letters, 28(1), 57-60. Gibbs J W, On the equilibrium of heterogeneous substances, 1876 Trans. Conn. Acad. 3 108
[114] Gibbs J W 1878. On the equilibrium of heterogeneous substances, 1878 Trans. Conn. Acad. 3 343
[115] Gibowicz S.J. and Lasocki, S., 2001. Seismicity induced by mining: Ten years later. In: Dmowska, R. and Saltzman, B., Eds., Advances in Geophysics, Academic Press, Academic Press, 39-181ibowicz and Lasocki, 2001
[116] Gisiger, T. 2001. Scale Invariance in Biology: Coincidenceor Footprint of a Universal Mechanism? Biol. Rev., 76, 161–209
[117] Goldsworthy, M., Jackson, J., and Haines, J., 2002. The continuity of active fault systems in Greece. Geophys. J. Internat. 148: 596–618.
[118] Gomberg, J. and Felzer K.R., 2011. Reply to Comment on „A Model of Earthquake Triggering Probabilities and Application to Dynamic Deformations Constrained by Ground Motion Observations", Journal of Geophysical Research, Vol. 116, Paper B03313, 3 pp.
[119] Goter, S.K., Oppenheimer, D.H., Mori, J.J., Savage, M.K., and Masse, R.P., 1994. Earthquakes in California and Nevada, U.S. Geological Survey Open-File Report 94-647, scale 1:1,000,000, 1 sheet.
[120] Grandy W T, 1988. Foundations of Statistical Mechanics vol II: Non-equilibrium Phenomena (Dordrecht: D. Reidel Publishing Company)
[121] Grandy W T, 2008. Entropy and the Time Evolution of Macroscopic Systems (Oxford: Oxford University Press)
[122] Grassberger P., 1994. Efficient large-scale simulations of a uniformly driven system. Phys. Rev. E 49, 2436. DOI: https://doi.org/10.1103/PhysRevE.49.2436
[123] Guest, B., Niemi, N. and Wernicke, B., 2007. Stateline fault system: A new component of the Miocene-Quaternary Eastern California shear zone, Geol. Soc. Am. Bull., 119 (11–12), 1337-1347; doi: 10.1130/0016-7606(2007)119[1337: SFSANC]2.0.CO;2
[124] Guo, Z., Ogata, Y., 1997. Statistical relations between the parameters of aftershocks in time, space and magnitude. J. Geophys. Res. 102, 2857 – 2873Gutenberg, B.,

and C. F. Richter (1944). Frequency of earthquakes in California, Bull. Seismol. Soc. Am. 34, 185–188

[125] Gutenberg, B., and Richter C. F., 1954. Seismicity of the Earth, Second Ed., Princeton University Press, Princeton, New Jersey, 310 pp

[126] Haeussler P. J., 2008. An Overview of the Neotectonics of Interior Alaska: Far-Field Deformation from the Yakutat Microplate Collision. Active Tectonics and Seismic Potential of Alaska Geophysical Monograph Series 179 This paper is not subject to U.S. copyright. Published in 2008 by the American Geophysical Union. 10.1029/179GM05

[127] Haeussler P.J., O' Sullivan P., Berger A.L., Spotila J.A., 2008. Neogene Exhumation of the Tordrillo Mountains, Alaska, and Correlations with Denali (Mount Mckinley). Active Tectonics and Seismic Potential of Alaska Geophysical Monograph Series 179 This paper is not subject to U.S. copyright. Published in 2008 by the American Geophysical Union. 10.1029/179GM15

[128] Hainzl, S., Scherbaum, F. and Beauval, C., 2006. Estimating background activity based on interevent-time distribution, Bull. Seismol. Soc Am., 96 (1), 313–320; doi: 10.1785/0120050053.

[129] Hamilton R.M., 1967. Mean magnitude of an earthquake sequence. Bulletin of the Seismological Society of America (1967) 57 (5): 1115-1116.

[130] Hammond W. C. Blewitt G., Li Z., Plag H.-P. And Kreemer C., 2012. Contemporary uplift of the Sierra Nevada, western United States, from GPS and InSAR measurements, Geology, 40 (7), 667-770; doi:10.1130/G32968.1.

[131] Hanken H., 1983. Advanced synergetics: Instability hierarchies of self-organizing systems and devices, Springer, Berlin Heidelberg New York

[132] Hardebeck, J. L., and. Hauksson E., 2001. Crustal stress field in southern California and its implications for fault mechanics, J. Geophys. Res., 106, 21,859–21,882.

[133] Hardebeck, J. L., and A. J. Michael., 2006. Damped regional-scale stress inversions: Methodology and examples for Southern California and the Coalinga aftershock sequence, J. Geophys. Res., 111, B11310, doi:10.1029/2005JB004144

[134] Hatzfeld D. and Martin C. 1992. Intermediate depth seismicity in the Aegean defined by teleseismic data. Earth and Planetary Sctence Letters, 113 (1992) 267-275. https://doi.org/10.1016/0012-821X(92)90224-J

[135] Hatzfeld D., 1994. On the shape of the subducting slab beneath the Peloponnese, Greece. Geophys. Res. Lett., 21 (1994), pp. 173–176

[136] Hauksson, E., Yang, W. and Shearer, P.M., 2012. Waveform Relocated Earthquake Catalog for Southern California (1981 to 2011), Bull. Seismol. Soc. Am., 102 (5), 2239-2244; doi:10.1785/0120120010

[137] Hauksson E., 2010. Spatial Separation of Large Earthquakes, Aftershocks, and Background Seismicity: Analysis of Interseismic and Coseismic Seismicity Patterns in Southern California. In: Savage M.K., Rhoades D.A., Smith E.G.C., Gerstenberger M.C., Vere-Jones D. (eds), Seismogenesis and Earthquake Forecasting: The Frank Evison Volume II. Pure and Applied Geophysics, 167, 979-997; doi: 10.1007/s00024-010-0083-3.

[138] Hawkes, A.G. 1972. Spectra of some mutually exciting point processes with associated variables, in P.A.W. Lewis (ed), Stochastic Point Processes, Wiley, 261-271.

[139] Hawkes, A.G. and Adamopoulos, L., 1973. Cluster models for earthquakes - regional comparisons, Bull Internat. Stat. Inst., 45, 454-461.

[140] Hawkes, A.G. and Oakes, D., 1974. A cluster representation of a self-exciting process, Journal Apl. Prob., 11, 493-503.

[141] Helmstetter A., Hergaten S., and Sornette D., 2004. Properties of foreshocks and aftershocks of the nonconservative self-organized critical Olami-Feder-Christensen model. Phys. Rev. E 70, 046120 – Published 28 October 2004. DOI: https://doi.org/10.1103/PhysRevE.70.046120

[142] Helmstetter A., Kagan Y., Jackson D.D, 2006. Comparison of Short-Term and Time-Independent Earthquake Forecast Models for Southern California. Bulletin of the Seismological Society of America (2006) 96 (1): 90-106. https://doi.org/10.1785/0120050067

[143] Helmstetter, A. and Sornette, D., 2003. Predictability in the Epidemic-Type Aftershock Sequence model of interacting triggered seismicity, J. Geophys. Res., 108 (B10), 2482; doi: 10.1029/2003JB002485.

[144] Hergarten S. and Neugebauer H.J., 2002. Foreshocks and Aftershocks in the Olami-Feder-Christensen Model. Phys. Rev. Lett. 88, 238501 –DOI: https://doi.org/10.1103/PhysRevLett.88.238501

[145] Hergarten, S. and Krenn, R., 2011. Synchronization and desynchronization in the Olami-Feder-Christensen earthquake model and potential implications for real seismicity, Nonlin. Processes Geophys. 18, 635–642; doi:10.5194/npg-18-635-2011.

[146] Herrera C., Nava F.A., Lomnitz C., 2016. Time-dependent earthquake hazard evaluation in seismogenic systems using mixed Markov Chains: An application to the Japan area. Earth Planets Space, 58, 973–979, 2006.

[147] Hirata T. 1989. Fractal Dimension of Fault Systems in Japan: Fractal Structure in Rock Fracture Geometry at Various Scales. In: Scholz C.H., Mandelbrot B.B. (eds) Fractals in Geophysics. Pure and Applied Geophysics. Birkhäuser, Basel. DOI https://doi.org/10.1007/978-3-0348-6389-6_9

[148] Hohenberg PC and Halperin B.I., 1977. Theory of dynamic critical phenomena. Rev. Mod. Phys. 49, 435 – Published 1 July 1977

[149] Holliday J.R., Turcotte D.L., Rundle J.B. 2008. A Review of Earthquake Statistics: Fault and Seismicity-Based Models, ETAS and BASS. In: Camacho A.G., Díaz J.I., Fernández J. (eds) Earth Sciences and Mathematics. Pageoph Topical Volumes. Birkhäuser Basel. DOI https://doi.org/10.1007/978-3-7643-8907-9_2

[150] Hough, S.E., and Jones L.M., 1997. “Aftershocks: Earthquakes or Afterthoughts”, EOS, Transactions of the American Geophysical Union, November 11.

[151] Hudson, Travis, and Plafker, George, 1978. Kigluaik and Bendeleben faults, Seward Peninsula, in Johnson, K. M., ed., The United States Geological Survey in Alaska Accomplishments during 1977: U.S. Geological Survey Circular 772-B, p. B47-B50.

[152] Ishimoto, M. and Iida, K., 1939. Observations sur les seismes enregistres par le microsismographe construit dermerement. Bull.Earthquake Res. Inst., Tokyo Univ., 17: 443-478.

[153] Ito K.and Matsuzaki M., 1990. Earthquakes as self-organized critical phenomena. JOURNAL OF GEOPHYSICAL RESEARCH, VOL. 95, NO. B5, PAGES 6853-6860, MAY 10, 1990, https://doi.org/10.1029/JB095iB05p06853

[154] Iwata T, 2010. Effect of secondary aftershocks on aftershock decay in the rate- and state-friction model. EGU General Assembly 2010, held 2-7 May 2010 in Vienna, Austria, p.7920

[155] Iwata T. and Young R.P., 2005. Tidal Stress/Strain and the b-values of Acoustic Emissions at the Underground Research Laboratory, Canada, Pure appl. geophys. 162 (2005) 1291–1308 0033 – 4553/05/071291 – 18 DOI 10.1007/s00024-005-2670-2

[156] Jackson J. and McKenzie D., 1988. The relationship between plate motions and seismic moment tensors, and the rates of active deformation in the Mediterranean and Middle East. Geophysical Journal (1988) 93, 45-73

[157] Jackson, D.D., and Kagan, Y.Y., 1999. “Testable earthquake forecasts for 1999,” Seism. Res. Lett., 70(4), 393-403

[158] Janiszewski, H. A., Abers G. A., Shillington D. J., and Calkins J. A., 2013. Crustal structure along the Aleutian island arc: New insights from receiver functions constrained by active-source data, Geochem. Geophys. Geosyst. 14, doi:10.1002/ggge.20211.

[159] Jánosi M.I., and Kertész J., 1993. Self-organized criticality with and without conservation. Physica A: Statistical Mechanics and its Applications. Volume 200, Issues 1–4, 15 November 1993, Pages 179-188. https://doi.org/10.1016/0378-4371(93)90516-7.

[160] Jaumé and Sykes, 1999. Evolving towards a critical point: a review of accelerating seismic moment/energy release prior to large and great earthquakes. Pure Appl. Geophys., 155 (1999), pp. 279-306

[161] Jensen H.J. 1998. Self-Organized Criticality: Emergent Complex Behavior in Physical and Biological Systems. Cambridge University Press. Vol. 10 Cambridge Lecture Notes in Physics. ISBN 1107393485, 9781107393486

[162] Jennings, C.W., 1994, Fault activity map of California and adjacent areas, with locations of recent volcanic eruptions: California Division of Mines and Geology Geologic Data Map 6, 92 p., 2 pls., scale 1:750,000.

[163] Jiménez-Munt, I., Sabadini, R., Gardi, A., and Bianco, G., 2003. Active deformation in the Mediterranean from Gibraltar to Anatolia inferred from numerical modeling and geodetic and seismological data. J. Geophys. Res. 108(B1), doi: 10.1029/2001JB001544.

[164] Jolivet L and Faccenna C., 2000. Mediterranean extension and the Africa-Eurasia collision. TECTONICS, VOL. 19, NO. 6, PAGES 1095-1106 DECEMBER 2000

[165] Jolly A.D and McNutt S.R, 1999. Seismicity at the volcanoes of Katmai National Park, Alaska; July 1995–December 1997. Journal of Volcanology and Geothermal Research. Volume 93, Issues 3–4, 30 November 1999, Pages 173-190, https://doi.org/10.1016/S0377-0273(99)00115-8

[166] Jones L.M, 1988. Focal Mechanisms and the state of San Andreas Fault in Southern California, J. Geophys. Res., 93 (B8), 8869-8891.

[167] Jonge, M. R., Wortel, M. J. R., and Spakman, W., 1994. Regional scale tectonic evolution and the seismic velocity structure of the lithosphere and upper mantle: the Mediterranean region. J. Geophys. Res. 99: 12 091–12 108.

[168] Kagan, Y. Y. and Jackson, D. D., 1991, Long-term earthquake clustering, Geophys. J. In: (1991) 104, 117-133

[169] Kagan, Y. Y. and Jackson, D. D. 1995. New seismic gap hypothesis: Five years after. JOURNAL OF GEOPHYSICAL RESEARCH, VOL. 100, NO. B3, PAGES 3943-3959, MARCH 10, 199. https://doi.org/10.1029/94JB03014

[170] Kagan, Y. Y. and Jackson, D. D., 2000. Probabilistic forecasting of earthquakes, Geophys J Int 143(2), 438–453.

[171] Kagan, Y.Y., 2002. Aftershock zone scaling, Bull. Seismol. Soc. Am., 92 (2), 641-655.

[172] Kahle, H.S., Cocard, M., Peter, Y., et al., 2000. GPS derived strain rate field within the boundary zones of the Eurasian, African, and Arabian plates. J. Geophys. Res. 105: 353–370.

[173] Kalimeri M., Papadimitriou C., Balasis G. and Eftaxias K., 2008. Dynamical complexity detection in pre-seismic emissions using nonadditive Tsallis entropy, Physica A 387, 1161

[174] Kelleher J.A, 1970. Space-Time Seismicity of the Alaska-Aleutian Seismic Zone. JOURNAL OF GEOPHYSICAL RESEARCH. VOL. 75, NO. 29, OCTOBER 10, 1970

[175] Kijko, A., and Sellevoll M. A., 1989. Estimation of earthquake hazard parameters from incomplete data files, Part I, Utilization of extremeand complete catalogues with different threshold magnitudes, Bull. Seismol. Soc. Am. 79, 645–654.

[176] King G.C.P and Bowman D.D., 2003. The evolution of regional seismicity between large earthquakes. JOURNAL OF GEOPHYSICAL RESEARCH, VOL. 108, NO. B2, 2096, doi:10.1029/2001JB000783, 2003

[177] Kiratzi A. & Louvari E., 2003. Focal mechanisms of shallow earthquakes in the Aegean Sea and the surrounding lands determined by waveform modelling: a new database. Journal of Geodynamics, 36, 251–274.

[178] Kissel, C. & Laj, C. 1988. Tertiary geodynamical evolution of the Aegean arc: a palaeomagnetic reconstruction. Tectonophysics, 146, 183–201.

[179] Knapmeyer M., 1999. Geometry of the Aegean Benioff zones. Ann. Geofis., 42 (1999), pp. 27–37.

[180] Kokkalas S, Xyploias P., Koukouvelas I., Doutsos T, 2006. Postcollisional contractional and exensional deformation in the Aegean region. Geological Society of America, Special Paper 409.

[181] Konstantinou, K. I., Melis N. S., and Boukouras K., 2010. Routine regional moment tensor inversion for earthquakes in the Greek region: The National Observatory of Athens (NOA) database (2001—2006), Seismol. Res. Lett., 81, 750–760, doi:10.1785/gssrl.81.5.738, 2010

[182] Kotzev, V., Nakov, R., Burchfiel, B. C., King, R., and Reilinger, R., 2001. GPS study of active tectonics in Bulgaria: results from 1996 to 1998. J. Geodynamics 31: 189–200.

[183] Kotzev, V., Nakov, R., Georgiev, T., Burchfiel, B. C., and King, R.W., 2006. Crustal motion and strain accumulation in western Bulgaria. Tectonophysics 413: 127–145.

[184] Lahr J.C and Plafker G., 1980. Holocene Pacific–North American plate interaction in southern Alaska: Implications for the Yakataga seismic gap. Geology (1980) 8 (10): 483-486. https://doi.org/10.1130/0091-7613(1980)8<483:HPAPII>2.0.CO;2

[185] Landau L.D. and Lifshitz E.M. 1980. Statistical physics by L. D. Landau and E. M. Lifshitz Course of Theoretical Physics. Vol. 9. Statistical Physiscs Part.2. Translated from the Russian by J.B. Sykes and M.J. Kearsely. (1980). Pergamon Press Ltd. Headington Hill Hall Oxford OX3 0BW, England

[186] Lay, T. and Wallace, T. C., 1995. Modern Global Seismology, Academic Press, New York, pp. 383-387.

[187] Leonard L., Hyndman R.D., Mazzoti S., Nykolaishen L., Schmidt M., Hippchen S. 2007. Current deformation in the northern Canadian Cordillera inferred from GPS measurements. JOURNAL OF GEOPHYSICAL RESEARCH, VOL. 112, B11401, doi:10.1029/2007JB005061

[188] Li J., Aberbs G.A, Kim Y., Christensen D. 2013. Alaska megathrust 1: Seismicity 43 years after the great 1964 Alaska megathrust earthquake. JOURNAL OF GEOPHYSICAL RESEARCH: SOLID EARTH, VOL. 118, 4861–4871, doi:10.1002/jgrb.50358, 2013

[189] Li, Q., and M. Liu 2006. Geometrical impact of the San Andreas Fault on stress and seismicity in California, Geophys. Res. Lett., 33, L08302, doi:10.1029/2005GL025661.
[190] Lise S. and Paczuski M., 2000. Self-organized criticality and universality in a nonconservative earthquake model. PHYSICAL REVIEW E, VOL 63, 036111. DOI: 10.1103/PhysRevE.63.036111
[191] Lise S. and Paczuski M., 2001. Scaling in a nonconservative earthquake model of self-organized criticality. PHYSICAL REVIEW E, VOLUME 64, 046111. DOI:10.1103/PhysRevE.64.046111
[192] Lise, S. and Paczuski, M., 2002. A Nonconservative Earthquake Model of Self-Organized Criticality on a Random Graph, Phys. Rev. Lett., 88 (22), 228301; doi:10.1103/PhysRevLett.88.228301
[193] Liu M., Wang H. and Li Q., 2010. Inception of the Eastern California Shear Zone and evolution of the Pacific-North American plate boundary: From kinematics to Geodynamics; J. Geophys. Res., 115, B077401; doi: https://doi.org/10.1029/2009JB007055.
[194] Lockner D. A. and Byrlee JD, 1991. Precursory AE Patterns Leading to Rock Fracture. 5TH Conference; 5th, Acoustic emission/microseismic activity in geologic structures and materials; 1991; University Park; PA. SERIES ON ROCK AND SOIL MECHANICS. Vol. 19, pp 45-58.
[195] Lu Z. and Wyss M., 1996. Segmentation of the Aleutian plate boundary derived from stress direction estimates based on fault plane solutions. JOURNAL OF GEOPHYSICAL RESEARCH, VOL. 101, NO. B1, PAGES 803-816, JANUARY 10, 1996
[196] Lyon-Caen, H., Armijo, R., Drakopoulos, J., et al., 1988. The 1986 Kalamata (South Peloponnesus) earthquake: detailed study of a normal fault, evidences for east–west extension in the Hellenic arc. J. Geophys. Res. 93: 14 967–15 000.
[197] Lyra M. L. and Tsallis C., 1998. Nonextensivity and multifractality in low-dimensional dissipative systems, Phys. Rev. Lett. 80, 53.
[198] Main, I. G 1995. Earthquakes as critical phenomena: Implications for probabilistic seismic hazard analysis. Bulletin of the Seismological Society of America (1995) 85 (5): 1299-1308.
[199] Main, I. G, 1996. Statistical Physics, seismogenesis and seismic hazard. Reviews of Geophysics, 34, 4/ November 1996, pages 433-462, Paper number 96 RG02808
[200] Main, I. G. and Naylor M., 2008.Maximum entro py production andearthquake dynamics, Geophys. Res. Lett., 35, L19311, doi: 10.1029/2008GL035590.
[201] Main, I. G. and Naylor M., 2010. Entropy production and self-organized (sub) criticality in earthquake dynamics. Phil. Trans. R. Soc. A (2010) 368, 131–144 doi:10.1098/rsta.2009.0206
[202] Makropoulos K.C & Burton P.W, 1984. Greek tectonics and seismicity. Tectonophysics, 106 (1984), pp. 275–304.
[203] Mandelbrot, B. 1967. Statistical Self-Similarity and Fractional. Dimension. Science, New Series, Vol. 156, No. 3775. (May 5, 1967), pp. 636-638.
[204] Mangira O., Vasiliadis G., and Papadimitriou E., 2017. Application of a linked stress release model in Corinth Gulf and Central Ionian Islands (Greece). Acta Geophys. DOI 10.1007/s11600-017-0031-z.
[205] Mangira O., Console R., Papadimitriou E., Vasiliadis G., 2018. A restricted Linked Stress Release Model (LSRM) for the Corinth gulf (Greece). Tectonophysics Volume 723, 16 January 2018, Pages 162-171.
[206] Marsan, D. and Lengliné, O., 2008. Extending earthquakes's reach through cascading, Science, 319, 1076; doi: 10.1126/science.1148783.

[207] Marsan, D., and Lengline O., 2010. “A New Estimation of Decay of Aftershock Density with Distance to the Mainshock”. Journal of Geophysical Research, Vol. 115, Paper B09302, 16 pp.
[208] Martinez, M.D., Lana, X., Posadas, A.M. and Pujades, L., 2005. Statistical distribution of elapsed times and distances of seismic events: the case of the Southern Spain seismic catalogue, Nonlinear Proc. Geophys., 12, 235–244.
[209] Martínez-Garzón, P., Kwiatek, G., Ickrath, M. and M. Bohnhoff 2014. MSATSI: A MATLAB© package for stress inversion combining solid classic methodology, a new simplified user-handling and a visualization tool. Seismol. Res. Lett. 85 (4), 896-904. DOI:10.1785/0220130189.
[210] Marzocchi W. and Lombardi A., 2009. Real-time forecasting following a damaging earthquake. GEOPHYSICAL RESEARCH LETTERS, VOL. 36, L21302, doi:10.1029/2009GL040233, 2009
[211] Marzocchi, W. and Lombardi, A. M., 2008. A double branching model for earthquake occurrence, J. Geophys. Res., 113, B08317; doi: 10.1029/2007JB005472.
[212] Marzocchi, W., Garcia-Aristizabal, A., Gasparini, P. et al 2012. Basic principles of multi-risk assessment: A case study in Italy. Nat Hazards (2012) 62: 551. https://doi.org/10.1007/s11069-012-0092-x
[213] Matmon A., Schwartz D.P., Haeussler P.J, Finkel R. 2006. Denali Fault slip rates and Holocene–late Pleistocene kinematics of central Alaska. Geology 34(8) ·August 2006, DOI: 10.1130/G22361.1
[214] Matthews M.V, Ellsworth W.L., Reasenberg P.A., 2002. A Brownian Model for Recurrent Earthquakes. Bulletin of the Seismological Society of America (2002) 92 (6): 2233-2250. https://doi.org/10.1785/0120010267
[215] McCaffrey, R., 2005. Block kinematics of the Pacific-North America plate boundary in the southwestern United States from inversion of GPS, seismological, and geologic data, J. Geophys. Res., 110, B07401, doi: 10.1029/2004JB003307.
[216] McClusky S., Reilinger R., Mahmoud S., Ben Sari D., Tealeb A., 2003. GPS constraints on Africa (Nubia) and Arabia plate motions. Geophysical Journal International. Volume 155, Issue 1, pages 126–138, October 2003. doi:10.1046/j.1365-246X. 2003.02023.x
[217] McClusky, S., Balassanian, S., Barka, A., et al., 2000. Global positioning system constraints on plate kinematics and dynamics in the eastern Mediterranean and Caucasus. J. Geophys. Res. 105: 5695–5719.
[218] McCrory P.A., Wilson D S., Stanley R.G 2009. Continuing evolution of the Pacific–Juan de Fuca–North America slab window system —A trench–ridge–transform example from the Pacific Rim. Tectonophysics 464 (2009) 30–42
[219] McKenzie D, 1972, Active Tectonics of the Mediterranean Region. Geophys. J. R. ustr. SOC. (1972) 30, 109-185
[220] McKenzie D., 1978. Active tectonics of the Alpine-Himalayan belt: the Aegean Sea and surrounding regions. Geophys. J. R. astr. SOC. (1978) 55, 217-254
[221] McKim Malville John, 1999. Pilgrimage and Complexity, Indira Gandhi National Centre for the Arts, New Delhi, Jan 5-9, 1999.
[222] McQuarrie D. A. and Simon J. D 1997. Physical Chemistry: A Molecular Approach (University Science Books, Sausalito, CA, 1997).
[223] Michael A.J., 1984. Determination of stress from slip data: Faults and folds. JOURNAL OF GEOPHYSICAL RESEARCH, VOL. 89, NO. B13, PAGES 11,517-11,526, DECEMBER 10, 1984
[224] Michael A.J., 1987. Use of focal mechanisms to determine stress: A control study. JOURNAL OF GEOPHYSICAL RESEARCH, VOL. 92, NO. B1, PAGES 357-368, JANUARY 10, 1987. https://doi.org/10.1029/JB092iB01p00357

[225] Michas, G., Vallianatos, F. and Sammonds, P., 2015. Statistical mechanics and scaling of fault populations with increasing strain in the Corinth Rift, Earth and Planetary Science Letters, 431, 150–163; doi: 10.1016/j.epsl.2015.09.014.
[226] Michas, G., Vallianatos, F. and Sammonds, P., 2013. Non-extensivity and long-range correlations in the earthquake activity at the West Corinth rift (Greece), Nonlin. Proc. Geoph., 20, 713-724.
[227] Mignan A. 2008. Non-Critical Precursory Accelerating Seismicity Theory (NC PAST) and limits of the power-law fit methodology. Tectonophysics 452 (2008) 42–50. https://doi.org/10.1016/j.tecto.2008.02.010
[228] Mignan A., King G.C.P., Bowman D., 2007. A mathematical formulation of accelerating moment release based on the stress accumulation model. JOURNAL OF GEOPHYSICAL RESEARCH, VOL. 112, B07308, doi:10.1029/2006JB004671, 2007
[229] Miller G. and Boulter C.J, 2003. Crossover behavior in the event size distribution of the Olami-Feder-Christensen model. PHYSICAL REVIEW E 67, 046114. DOI: 10.1103/PhysRevE.67.046114
[230] Miller G. and Boulter C.J., 2002. Measurements of criticality in the Olami-Feder-Christensen model. PHYSICAL REVIEW E 66, 016123. DOI: 10.1103/PhysRevE.66.016123
[231] Mogi K. 1968. Sequential Occurrences of Recent Great Earthquakes. JOURNAL OF PHYSICS OF THE EARTH, Vol. 16, No. 1
[232] Mogi, 1962. Magnitude-Frequency Relation for Elastic Shocks Accompanying Fractures of Various Materials and Some Related Problems in Earthquakes. Bull.Earthq.Res.Inst. 40, 831-853, 1962
[233] Mogi, 1962. Study of elastic shocks caused by the fracture of heterogeneous materials and its relation to earthquake phenomena. Bull. Earthq. Res. Inst., Univ. Tokyo 40, 125-173, 1962
[234] Molchan, G., 2005. Interevent time distribution in seismicity: A theoretical approach, Pure appl. Geophys. 162, 1135–1150; doi: 10.1007/s00024-004-2664-5. Monograph Series 179, edited by J.T. Freymueller, P.J. Haeussler, R.L. Wesson, and G. Ekström (2008).
[235] Moré, J.J. and Sorensen, D.C., 1983. Computing a Trust Region Step, SIAM Journal on Scientific and Statistical Computing, 3, 553–572.
[236] Mori J. and Abercrombie R.E., 1997. Depth dependence of earthquake frequency-magnitude distributions in California: Implications for rupture initiation/ JOURNAL OF GEOPHYSICAL RESEARCH, VOL. 102, NO. B7, PAGES 15,081-15,09
[237] Mosca I., Console R., D' Addezio G.D, 2012. Renewal models of seismic recurrence applied to paleoseismological and historical observations TectonophysicsVolumes 564–565, 5 September 2012, Pages 54-67. https://doi.org/10.1016/j.tecto.2012.06.028
[238] Musmeci, F., and D. Vere-Jones. 1986. A variable-grid algorithm for smoothing clustered data, Biometrics, 42, 483-494.
[239] Nakanishi H. 1991. Statistical properties of the cellular-automaton model for earthquakes. PHYSICAL REVIEW A VOLUME 43, NUMBER 12.
[240] Nakanishi H., 1990. Cellular-automaton model of earthquakes with deterministic dynamics. Phys. Rev. A 41, 7086(R). DOI: https://doi.org/10.1103/PhysRevA.41.7086
[241] Nanjo K.Z 2011. Earthquake forecasts for the CSEP Japan experiment based on the RI algorithm. Earth Planet Sp (2011) 63: 9. https://doi.org/10.5047/eps.2011.01.001.

[242] Nanjo K.Z, Hirata N., Obara K., Kasahara K., 2012. Decade-scale decrease inb value prior to the M9-class 2011 Tohoku and 2004 Sumatra quakes. GEOPHYSICAL RESEARCH LETTERS, VOL. 39, L20304, doi:10.1029/2012GL052997

[243] Nanjo K.Z. 2010. Earthquake forecast models for Italy based on the RI algorithm. ANNALS OF GEOPHYSICS, 53, 3, 2010; doi: 10.4401/ag-4810

[244] Newman, M. E. J., 1996. Self-Organized Criticality, Evolution and the Fossil Extinction Record, Proc. Roy. Soc. Lond. B, 263, 1605–1610.

[245] Nishenko S.P and Buland R. 1987. A generic recurrence interval distribution for earthquake forecasting. Bulletin of the Seismological Society of America, 77 (4) (1987), pp. 1382-1399

[246] Nishenko S.P and Sykes L.R. 1993. Comment on 'Seismic gap hypothesis: ten years after' by Y.Y. Kagan and D.D. Jackson Journal of Geophysical Research, 98 (1993), pp. 9909-9916

[247] Nyst, M. and Thatcher W., 2004. New constraints on the active tectonic deformation of the Aegean. J. Geophys. Res. 109: B11406, doi: 10.1029/2003JB002830.

[248] Ogata Y. and Shimazaki K., 1984. Transition from aftershock to normal activity: The 1965 Rat Islands earthquake aftershock sequence. Bulletin of the Seismological Society of America (1984) 74 (5): 1757-1765.

[249] Ogata Y. et al., 1991. Some Statistical Features of the Long-Term Variation of the Global and Regional Seismic Activity. International Statistical Review / Revue Internationale de Statistique Vol. 59, No. 2 (Aug. 1991), pp. 139-161. DOI: 10.2307/1403440

[250] Ogata Y., 1983. Estimation of the parameters in the Modified Omori Formula for Aftershock Frequencies by the Maximum Likelihood Procedure. Journal of Physics and Earth Vol 31 (1983) Issue 2 Pages 115-124. https://doi.org/10.4294/jpe1952.31.115

[251] Ogata Y., Jones L.M., Shinji T., 2003a. When and where the aftershock activity was depressed: Contrasting decay patterns of the proximate large earthquakes in southern California. JOURNAL OF GEOPHYSICAL RESEARCH, VOL. 108, NO. B6, 2318, doi:10.1029/2002JB002009

[252] Ogata Y.and Katsura, 1993. Analysis of temporal and spatial heterogeneity of magnitude frequency distribution inferred from earthquake catalogues. Geophys. J. Int. (1993) 113,727-738

[253] Ogata, Y., 1998. Space-time point-process models for earthquake occurrences, Annals of the Institute of Statistical Mathematics, 50, 379-402.

[254] Ogata, Y., 1988. Statistical models for earthquake occurrences and residual analysis for point processes, J. Am. Stat. Assoc., 83 (401), 9-27.

[255] Okuda S., Ouchi T. and Terashima T. 1992. Deviation of magnitude frequency distribution of earthquakes from the Gutenberg—Richter law: detection of precursory anomalies prior to large earthquakes. Physics of the Earth and Planetary Interiors, 73 (1992) 229—238

[256] Olami Z., Feder H.J.S, Christensen K., 1992. Self-organized criticality in a continuous, nonconservative cellular automaton modeling earthquakes. Phys. Rev. Lett. 68, 1244 – Published 24 February 1992

[257] Omori, F., 1894a. On Aftershocks, Rep. Imp. Earthq. Inv. Com. 2, 103–138 (in Japanese).

[258] Omori, F, 1894b. On Aftershocks of Earthquakes, J. Coll. Sci. Imp. Univ. Tokyo 7, 111–200 (in Japanese)

[259] Onsager L, Reciprocal relations in irreversible processes. I, 1931 Phys. Rev. 37 405 41

[260] Onsager L, Reciprocal relations in irreversible processes. II, 1931 Phys. Rev. 38 2265

[261] Orfanogiannaki K., Karlis D., and Papadopoulos G., 2010. Identifying seismicity levels via Poisson hidden Markov models, Pure Appl. Geophys. 167 (2010), pp. 919–931.
[262] Otsuka M., 1972. A simulation of earthquake occurrence. Phys. Earth Planet. Interiors 6, 311—3 15
[263] Otsuka M., 1972. A chain-reaction-type source model as a tool to interpret the magnitude-frequency relation of earthquakes. Journal of Physics of the Earth. 1972 Volume 20 Issue 1 Pages 35-45. https://doi.org/10.4294/jpe1952.20.35
[264] Page R., 1968. Focal Depths of Aftershocks. JOURNAL OF GEOPHYSICAL RESEARCH VOL. 73, NO. 12, https://doi.org/10.1029/JB073i012p03897
[265] Page R.A., Plakfer G. and Pulpan H. 1995. Block rotation in east-central Alaska: A framework for evaluating earthquake potential? Geology (1995) 23 (7): 629-632. https://doi.org/10.1130/0091-7613(1995)023<0629: BRIECA>2.3.CO;2
[266] Page R. A., Biswas, N. N., Lahr, J. C., and Pulpan, H., 1991, Seismicity of continental Alaska, in Slemmons, D. B., Engdahl, E. R., Zoback, M. D., and Blackwell, D. D., eds., Neotectonics of North America: Boulder, Colorado, Geological Society of America, Decade Map Volume l.
[267] Page R.A., 1973. The Sitka, Alaska, earthquake of 1972; An expected visitor: Earthquake Information Bulletin, v. 5, no. 5, p. 4 – 9. –, 1975, Evaluation of seismicity and earthquake shaking at otTshore sites: Houston, Texas, 7th Offshore Technology Conference, Proceedings, v. 3, p. 179 – 190.
[268] Panorias C., Papadopoulou A., & Tsapanos T. (2016). On the earthquake occurrences in Japan and the surrounding area via semi Markov modeling. Bulletin of the Geological Society of Greece, 50(3), 1535-1542. doi: http://dx.doi.org/10.12681/bgsg.11866
[269] Papadakis G., Vallianatos F. and Sammonds P., 2013. Evidence of Nonextensive Statistical Physics behaviour of the Hellenic Subduction Zone seismicity, Tectonophysics, 608, 1037-1048.
[270] Papadakis G. Vallianatos F. and Sammonds P., 2015. A Nonextensive Statistical Physics Analysis of the 1995 Kobe, Japan Earthquake, Pure and Applied Geophysics, 172 (7), 1923-1931.
[271] Papadimitriou C. Kalimeri M. and. Eftaxias K., 2008. Nonextensivity and universality in the earthquake preparation process, Phys. Rev. E 77, 036101 (2008).
[272] Papadopoulos G.A, Skafida H.G and Vassiliou I.T., 1993. Nonlinearity of the magnitude-frequency relation in the Hellenic Arc-Trench System and the characteristic earthquake model. JOURNAL OF GEOPHYSICAL RESEARCH, VOL. 98, NO. B10, PAGES 17,737-17,744. https://doi.org/10.1029/93JB00559
[273] Papanikolaou D. 2009. Timing of tectonic emplacement of the ophiolites and terrane paleogeography in the Hellenides. Lithos 108 (2009) 262–280. doi: 10.1016/j.lithos.2008.08.003
[274] Papanikolaou D. 2013, Tectonostratigraphic models of the Alpine terranes and subduction history of the Hellenides. Tectonophysics 595–596 (2013) 1–24. https://doi.org/10.1016/j.tecto.2012.08.008
[275] Papanikolaou D.J. and Royden L. H., 2007. Disruption of the Hellenic arc: Late Miocene extensional detachment faults and steep Pliocene-Quaternary normal faults—Or what happened at Corinth? TECTONICS, VOL. 26, TC5003, doi:10.1029/2006TC002007, 2007
[276] Papazachos B.C, 1996. Large seismic faults in the Hellenic arc. Annali Di GEOFISICA, VOL. XXXIX, N. 5, October 1996.
[277] Papazachos B.C, Papadimitriou E, Kiratzi A., Papazachos C.B, Louvari E. 1998. Fault plane solutions in the Aegean Sea and the surrounding area and their tectonic

implication. Bolletino di Geofisica Teorica ed Applicata. Vol. 39, N.3, pp. 199-218, September 1998.

[278] Papazachos C., 1990. Seismicity of the Aegean and surrounding area. Tectonophysics, 178 (1990), pp. 287–308

[279] Papazachos C, Karakostas V.G, Papazachos C.B, Scordilis E.M., 2000. The geometry of the Wadati–Benioff zone and lithospheric kinematics in the Hellenic arc. Tectonophysics, 319 (2000), pp. 275–300.

[280] Papazachos C. & Comnikakis P. 1971. Geophysical and tectonic features of the Aegean Arc. J. Geophys. Res., 76 (1971), pp. 8517–8533

[281] Papazachos C. & Kiratzi A., 1996. A detailed study of the active crustal deformation in the Aegean and surrounding area. Tectonophysics 253, 129-153.

[282] Papazachos, B. C., Mountrakis, A., Psilovikos, V., and Leventakis, G., 1979. Surface fault traces and fault plane solutions of the May June 1978 shocks in the Thessaloniki area, north Greece. Tectonophysics 53: 171–183.

[283] Parsons T. and Geist E.L., 2009. Is There a Basis for Preferring Characteristic Earthquakes over a Gutenberg–Richter Distribution in Probabilistic Earthquake Forecasting? Bulletin of the Seismological Society of America (2009) 99 (3): 2012-2019.https://doi.org/10.1785/0120080069

[284] Patanè D., De Miguel F., Ibanez J.M., 1992. A basic program based on the Wadati diagram to calculate earthquakes focal depth and P and S waves velocities: application in the Etnean area. CNR Istituto Internazionale di Vulcanologia, Open File Report No. 3/91, 5 pp.

[285] Peixoto T. P. and Davidsen J., 2008. Network of recurrent events for the Olami-Feder-Christensen model. PHYSICAL REVIEW E 77, 066107. DOI: 10.1103/PhysRevE.77.066107.

[286] Peng, Z., Aiken C., Hill D.P. and Shelly D.R., 2010. “Remotely Triggered Microearthquakes and Tremor in Central California Following the 2010 Mw 8.8 Chile Earthquake”, Geophysical Research Letters, 10.1029/2020GL045462.

[287] Pepke S. L. and Carlson J.M., 1994. Predictability of self-organizing systems. Phys. Rev. E 50, 236 – Published 1 July 1994. DOI: https://doi.org/10.1103/PhysRevE.50.236.

[288] Pérez C.J., Corral A., Diaz – Guilera A., Christensen K and Arenas A., 1996. On self-organized criticality and synchronization in lattice models of coupled dynamical systems. International Journal of Modern Physics BVol. 10, No. 10, pp. 1111-1151 (1996)Review. https://doi.org/10.1142/S0217979296000416

[289] Pérez O.J. and Jacob K. H., 1980. St. Elias, Alaska, earthquake of February 28, 1979: Tectonic setting and precursory seismic pattern. Bulletin of the Seismological Society of America (1980) 70 (5): 1595-1606.

[290] Pérez O.J. and Jacob K. H., 1980. Tectonic model and seismic potential of the Eastern Gulf of Alaska and Yakataga seismic gap. Journal of Geophysical Research, vol. 85, no. B12, pages 7132-715

[291] Pertsinidou C. E., Tsaklidis G., Papadimitriou E. & Limnios N. 2017. Application of hidden semi-Markov models for the seismic hazard assessment of the North and South Aegean Sea, Greece, Journal of Applied Statistics, 44:6, 1064-1085, DOI:10.1080/02664763.2016.1193724.

[292] Pertsinidou C. E., Tsaklidis G., Papadimitriou E., 2017. Study of the seismic activity in central Ionian Islands via semi-Markov modelling. Acta Geophys. DOI 10.1007/s11600-017-0040-y.

[293] Plafker G., 1987. Regional geology and petroleum potential of the northern Gulf of Alaska continental margin. Circum-Pacific Council for Energy and Mineral

Resources 2009 – Geology and Resource Potential of the Western North America and Adjacent Ocean Basins--Beaufort Sea to Baja California, Volume 6, 1987.

[294] Plafker G., Hudson T., Bruns T., Rubin M., 1978. Late Quaternary offsets along the Fairweather fault and crustal plate interactions in southern Alaska. Canadian Journal of Earth Sciences, 1978, 15(5): 805-816, https://doi.org/10.1139/e78-085

[295] Plafker, George, Moore, J.C., and Winkler, G.R., 1994. Geology of the southern Alaska margin, in Plafker, George, and Berg, H.C., eds., The geology of Alaska, v. G–1 of the geology of North America: Boulder, Colo., Geological Society of America, p. 389–449.

[296] Plattner, C., Malservisi, R., Furlong K.P., Govers, R., 2010. Development of the Eastern California Shear Zone – Walker Lane belt: The effects of microplate motion and pre-existing weakness in the Basin and Range, Tectonophysics 485, 78–84; doi: https://doi.org/10.1016/j.tecto.2009.11.021.

[297] Prejean, S.G., D.P. Hill, E.E. Brodsky, S.E. Hough, M.J.S. Johnston, S.D. Malone, D.H. Opppenheimer, A.M. Pitt, and K.B. Richards-Dinger 2004. Remotely Triggered Seismicity on the United States West Coast Following the Mw 7.9 Denali Fault Earthquake, Bulletin of the Seismological Society of America, V. 94, p. S348-S359.

[298] Ramos O., 2010. Criticality in earthquakes. Good or bad for prediction? Tectonophysics 485 (2010) 321–326. doi: 10.1016/j.tecto.2009.11.007

[299] Ramos O., Altshuler E. and Ma˚løy K. J.., 2006. Quasiperiodic Events in an Earthquake Model. PRL 96, 098501 (2006) PHYSICAL REVIEW LETTERS. DOI: 10.1103/PhysRevLett.96.098501

[300] Ratchkovski N.A., Wiemer S., Hansen R.A., 2004. Seismotectonics of the Central Denali Fault, Alaska, and the 2002 Denali Fault Earthquake Sequence. Bulletin of the Seismological Society of America, Vol. 94, No. 6B, pp. S156–S174, December 2004

[301] Rau C., Mahavadi P., and Lu M., 1993. Magnetic order and critical behavior at surfaces of ultrathin Fe (100) p(1×1) films on Pd (100) substrates, J. Appl. Phys. 73No. 10 (1993) 6757-6759 (DOI:10.1063/1.352476).

[302] Reasenberg P.A. and Jones L. M., 1989. Earthquake Hazard after a Mainshock in California. Science 03 Mar 1989: Vol. 243, Issue 4895, pp. 1173-1176DOI: 10.1126/science.243.4895.1173

[303] Reasenberg, P.A. 1985. Second-order moment of central California seismicity, 1969-82, J. Geophys. Res., 90, 5479, 5495.

[304] Reid H. F. 1910. The mechanism of the earthquake, in The California Earthquake of April 18, 1906, Report of the State Earthquake Investigation Commission, Vol. 2, pp. 16–28, Carnegie Institute of Washington, Washington, D.C., 1910

[305] Rhoades, D. A. and F. F. Evison, 2006. The EEPAS forecasting model and the probability of moderate-to-large earthquakes in central Japan, Tectonophysics, 417(1/2), 119–130, 2006.

[306] Rhoades, D. A., 2007. Application of the EEPAS model to forecasting earthquakes of moderate magnitude in Southern California, Seismol. Res. Lett., 78 (1), 110–115.

[307] Rhoades, D.A. and Evison, F. F. 2004. Long-range earthquake forecasting with every earthquake a precursor according to scale, Pure Appl. Geophys. 161, 47-71.

[308] Ridgway K.D. Trop J.M. Jones D.E., 1999. Petrology and provenance of the Neogene Usibelli Group and Nenana Gravel: Implications for the denudation history of the central Alaska Range: Journal of Sedimentary Research, v. 69, no. 6, p. 1262–1275

[309] Ridgway K.D. Trop J.M. Jones D.E., 1999. Petrology and provenance of the Neogene Usibelli Group and Nenana Gravel: Implications for the denudation history of the

central Alaska Range: Journal of Sedimentary Research, v. 69, no. 6, p. 1262–1275

[310] Rogers G.C., 1986. Seismic gaps along the Queen Charlotte fault: Earthquake Prediction Research, v. 4, p. 1 – 11. Rothe, J. P., 1969, The seismicity of the Earth, 1953-1965: Paris, UNESCO, 336 p.

[311] Rundle J.B, 1988. A physical model for earthquakes: 1. Fluctuations and interactions. JOURNAL OF GEOPHYSICAL RESEARCH, VOL. 93, NO. B6, PAGES 6237-6254, JUNE 10, 1988. https://doi.org/10.1029/JB093iB06p06237

[312] Rundle J.B, Klein W., Tiampo K, Gross S., 2000. Linear pattern dynamics in nonlinear threshold systems. PHYSICAL REVIEW E VOLUME 61, NUMBER 3, 1063-651X/2000/61 (3)/2418(14)

[313] Rundle J.B., Tiampo K.F., Klein W and Sa. Martins J.S. 2002. Self-organization in leaky threshold systems: The influence of near-mean field dynamics and its implications for earthquakes, neurobiology, and forecasting. PNAS February 19, 2002 99 (suppl 1) 2514-2521; https://doi.org/10.1073/pnas.012581899

[314] Rundle, J.B., Klein, W., Turcotte, D.L. and Malaud, B.D., 2000. Precursory seismic activation and critical point phenomena, Pure appl. Geophys. 157, 2165-2182.

[315] Ruppert N.A. Ridgway K.D. Freymueller J.T. Cross R.S. Hansen R.A., 2008. Active tectonics of interior Alaska: Seismicity, GPS geodesy, and local geomorphology, in Freymueller, J.T., Haeussler, P.J., Wesson, R., and Ekström, G., eds., Active Tectonics and Seismic Potential of Alaska: Washington, D.C., American Geophysical Union Geophysical Monograph Series 179, p. 109–133.

[316] Ruppert N.A., 2008. Stress map for Alaska from earthquake focal mechanisms, in Freymueller, J.T., Haeussler, P.J., Wesson, R., and Ekström, G., eds., Active Tectonics and Seismic Potential of Alaska: Washington, D.C., American Geophysical Union Geophysical Monograph Series 179, p. 351–367.

[317] Ruppert N.A., Prejean S., Hansen R.A. 2011. Seismic swarm associated with the 2008 eruption of Kasatochi Volcano, Alaska: Earthquake locations and source parameters. JOURNAL OF GEOPHYSICAL RESEARCH, VOL. 116, B00B07, doi: 10.1029/2010JB007435.

[318] Sachpazi, M., Hirn, A., Clément, C., et al., 2000. Western Hellenic subduction and Cephalonia Transform: local earthquakes and plate transport and strain. Tectonophysics 319: 301–319.

[319] Saichev, A. and Sornette, D., 2013. Fertility Heterogeneity as a Mechanism for Power Law Distributions of Recurrence Times, Physical Review E, 97, 022815; also available at arXiv:1211.6062 [physics.geo-ph] (last access 20 October 2014).

[320] Saleeby, J., Saleeby, Z., Nadin, E. and Maheo, G., 2009. Step-over in the structure controlling the regional west tilt of the Sierra Nevada microplate: eastern escarpment system to Kern Canyon system, International Geology Review, 51 (7-8), 634-669.

[321] Saltus R.W., Hudson T.L. and Wilson F.H., 2007. The geophysical character of southern Alaska – Implications for crustal evolution. The Geological Society of America, Special Paper 431 in Tectonic Growth of a Collisional Continental Margin: Crustal Evolution of Southern Alaska by Kenneth D. Ridgway, Jeffrey M. Trop, Jonathan M.G. Glen, J. Michael O'Neill. DOI: https://doi.org/10.1130/2007.2431(01)

[322] Sammis, C.G. and Sornette, D., 2001. Positive feedback, memory and the predictability of earthquakes, e-print at http://arXiv.org/abs/cond-mat/0107143v1; last accessed December 2015.

[323] Schell, M. M., and Ruff, L. J., 1989. Rupture of a seismic gap in southeastern Alaska; The Sitka earthquake (Ms 7.6): Physics of the Earth and Planetary Interiors, v. 54, p. 241 – 257

[324] Shen-Tu, B., W. E. Holt, and A. J. Haines (1999). Deformation kinematics in the western United States determined from Quaternary fault slip ratesand recent geodetic data, J. Geophys. Res. 104, no. B12, 28,927–28,955, doi: 10.1029/1999JB900293.

[325] Scherrer T.M, França G.S., Silva R., de Freitas D.B., Vilar C.S., 2015. Nonextensivity at the Circum-Pacific subduction zones – Preliminary studies, Physica A: Statistical Mechanics and its Applications, 426 63–71; doi: 10.1016/j.physa.2014.12.038.

[326] Schoenball, M., N. C. Davatzes, and J. M. G. Glen, 2015. Differentiating induced and natural seismicity using space-time-magnitude statistics applied to the Coso Geothermal field, Geophys.Res. Lett. 42, 6221–6228; doi: 10.1002/2015GL064772.

[327] Scholz C.H., 1968. The frequency-magnitude relation of microfracturing in rock and its relation to earthquakes. Bulletin of the Seismological Society of America (1968) 58 (1): 399-415.

[328] Scholz C.H., 1991. Earthquakes and faulting: Self-Organized critical phenomena with a characteristic dimension, pp 41-56. Proceedings of the NATO Advanced Study Institute on Spontaneous formation of Space – Time Structures and Criticality, 2-12 April 1991, Edited by Riste T & Sherrington D., 1991ISBN 978-94-010-5551-2.

[329] Scholz, C., 2002. The mechanics of earthquakes and faulting, 2nd Edition, Cambrigde University Press, pp 198-211.

[330] Schwartz D.P and Coppersmith K. J., 1984. Fault behavior and characteristic earthquakes: Examples from the Wasatch and San Andreas Fault Zones. JOURNAL OF GEOPHYSICAL RESEARCH, VOL. 89, NO. B7, PAGES 5681-5698, JULY 10, 1984. https://doi.org/10.1029/JB089iB07p05681

[331] Scordilis, E. M., Karakalsis, G. F., Karacostas, B. G., et al. 1985. Evidence for transform faulting in the Ionian Sea: the Cephalonia Island earthquake sequence of 1983. Pure and Applied Geophysics 123: 388–397.

[332] Segou, M., T. Parsons, and W. Ellsworth, 2013. Comparative evaluation of physics-based and statistical forecasts in Northern California, J. Geophys. Res. Solid Earth, 118, doi: 10.1002/2013JB010313.

[333] Sella, G. F., Dixon, T. H., and Mao, A. 2002. REVEL: a model for recent plate velocities from space geodesy. J. Geophys. Res. 107, doi: 10.1029/2000JB000033.

[334] Shaw B.E, 1995. Frictional weakening and slip complexity in earthquake faults. JOURNAL OF GEOPHYSICAL RESEARCH, VOL. 100, NO. B9, PAGES 18, 239-18,251. https://doi.org/10.1029/95JB01306

[335] Shaw, B. and Jackson, J., 2010. Earthquake mechanisms and active tectonics of the Hellenic subduction zone. Geophys, J. Internat. 181:966–984.

[336] Shcherbakov R. & Turcotte D.L. 2004. A Damage Mechanics Model for Aftershocks. Pure appl. geophys. (2004) 161: 2379. https://doi.org/10.1007/s00024-004-2570-x DOI https://doi.org/10.1007/s00024-004-2570-x

[337] Shcherbakov R., Turcotte D and Rundle J., 2004. A generalized Omori's law for earthquake aftershock decay. GEOPHYSICAL RESEARCH LETTERS, VOL. 31, L11613, doi:10.1029/2004GL019808

[338] Shcherbakov R., Turcotte D and Rundle J., 2005. Aftershock Statistics, Pure appl. geophys. 162, 1051–10760033 – 4553/05/071051 – 26 DOI 10.1007/s00024-004-2661-8.

[339] Shimazaki K. and Nakata T. 1980. Time-predictable recurrence model for large earthquakes, Geophys. Res. Lett., 7, 279-282, 1980. American Geophysical Union. Reproduced by permission of American Geophysical Union

[340] Silva, R., Franca, G., S., Vilar, C., S., Alcaniz, J., S., 2006. Nonextensive models for earthquakes, Physical Review E, 73, 026102; doi:10.1103/PhysRevE.73.026102.

[341] Sornette, A. and Sornette, D., 1989. Self-organized criticality and earthquakes, Europhys. Lett. 9, 197-202.

[342] Sornette A. and Sornette D., 1990. Earthquake rupture as a critical point: consequences for telluric precursors. Tectonophysics, 179 (1990) 327-334. https://doi.org/10.1016/0040-1951(90)90298-M

[343] Sornette D. 1991. Self-Organized Criticality in Plate Tectonics. In: Riste T., Sherrington D. (eds) Spontaneous Formation of Space-Time Structures and Criticality. NATO ASI Series (Series C: Mathematical and Physical Sciences), vol 349. Springer, Dordrecht. DOIhttps://doi.org/10.1007/978-94-011-3508-5_6

[344] Sornette D., and Sammis C.G., 1995. Complex critical exponents from renormalization group theory of earthquakes: Implications for earthquake predictions, J. Phys. 1, 5, 607-619.

[345] Sornette, D., 2004. Critical Phenomena in Natural Sciences: Chaos, Fractals, Self-organization and Disorder: Concepts and Tools, 2nd ed., 529 pp., Springer, Berlin.

[346] Sornette, D., and Werner, M.J., 2009. Statistical Physics Approaches to Seismicity, in Complexity in Earthquakes, Tsunamis, and Volcanoes, and Forecast, W.H.K. Lee (Ed), in the Encyclopedia of Complexity and Systems Science, R. Meyers (Editor-in-chief), 7872-7891, Springer, ISBN: 978-0-387-755888-6; available at arXiv:0803.3756v2 [physics.geo-ph] (last access 20 October 2014).

[347] Sotolongo-Costa O. and Posadas A., 2004. Fragment-asperity interaction model for earthquakes, Phys. Rev. Lett. 92, 048501.

[348] Sotolongo-Costa, O. and Posadas, A., 2004. Tsalli's entropy: A non-extensive frequency-magnitude distribution of earthquakes. Phys. Rev. Letters, 92 (4), 048501; doi:10.1103/PhysRevLett.92.048501.

[349] Spakman, W., van der Lee, S., and van der Hilst, R. D., 1993. Travel-time tomography of the European–Mediterranean mantle down to 1400 km. Phys. Earth Planet. Interiors 79: 3–74

[350] Stanley H.E, 1971. Introduction to phase transitions and critical phenomena. Introduction to Phase Transitions and Critical Phenomena, by H Eugene Stanley, pp. 336. Foreword by H Eugene Stanley. Oxford University Press, Jul 1987. ISBN-10: 0195053168. ISBN-13: 9780195053166 (First published in 1971).

[351] Stauder, W., 1959, A mechanism study; The earthquake of October 24, 1927: Geofisica Pura e Applicata, v. 44, p. 135 – 143. –, 1960, The Alaska earthquake of July 10, 1958; Seismic studies: Bulletin of the Seismological Society of America, v. 50, p. 293 – 322.

[352] Stauder W., 1960. The Alaska earthquake of July 10, 1958: Seismic studies. Bulletin of the Seismological Society of America (1960) 50 (2): 293-322.

[353] Steihaug, T., 1983. The Conjugate Gradient Method and Trust Regions in Large Scale Optimization, SIAM J. Numer. Anal., 20, 626–637.

[354] Sykes, L. R., 1971, Aftershock zones of great earthquakes, seismicity gaps, and earthquake prediction for Alaska and the Aleutians: Journal of Geophysical Research, v. 76, p. 8021-8041

[355] Sykes L.R and Jaumé S. C., 1990. Seismic activity on neighbouring faults as a long-term precursor to large earthquakes in the San Francisco Bay area. Nature volume348, pages 595–599, http://dx.doi.org/10.1038/348595a0

[356] Talbi, A. and Yamazaki, F., 2010. A mixed model for earthquake interevent times, J. Seismol, 14, 289–307; doi: 10.1007/s10950-009-9166-y.
[357] Taymaz, T., Jackson, J. A. & McKenzie, D. P. 1991a. Active tectonics of the North and Central Aegean Sea. Geophysical Journal International, 106, 433–490.
[358] Telesca, L., 2010a. Nonextensive analysis of seismic sequences, Phys. Stat. Mech. Appl. 389, 1911–1914.
[359] Telesca, L., 2010b. A nonextensive approach in investigating the seismicity of L'Aquila area (central Italy), struck by the 6 April 2009 earthquake (ML 5:8), Terra Nova, 22, 87–93.
[360] Telesca, L., 2011. Tsallis-based nonextensive analysis of the Southern California seismicity. Entropy, 13, 1267-1280.
[361] Telesca, L., 2012. Maximum Likelihood Estimation of the Nonextensive Parameters of the Earthquake Cumulative Magnitude Distribution, Bull. Seismol. Soc. Am., 102, 886-891.
[362] Telesca, L., and Chen, C-C., 2010. Nonextensive analysis of crustal seismicity in Taiwan, Nat. Hazards Earth Syst. Sci., 10, 1293–1297.
[363] Thatcher, W., G. R. Foulger, B. R. Julian, J. Savrc, E. Quilty, and G. W. Bawden, Present day deformation across the Basin and Range Province, Western United States, Science, 283,1714-1718, 1999
[364] Tichelaar B.W. and Ruff L.J., 1993. Depth of Seismic Coupling Along Subduction Zones. Journal of Geophysical Research, VOL. 98, NO. B2, Pages 2017-2037, FEBRUARY 10, 1993
[365] Tinti S., and Mulargia F., 1987. Confidence intervals of b values for grouped magnitudes, Bull. Seismol. Soc. Am. 77, 2125–2134
[366] Tirnakli U. and Abe S. 2004. Aging in coherent noise models and natural time, Phys. Rev. E 70, 056120
[367] Tirnakli U. 2004. Aging in earthquake models, in Complexity, Metastability and Nonextensivity, Proc. 31st Workshop of the International School of Solid-State Physics
[368] Tirnakli U. 2005. Aging in earthquake models, in Complexity, Metastability and Nonextensivity, Proc. 31st Workshop of the International School of Solid-State Physics (20 July 2004, Erice, Italy), eds. C. Beck, G. Benedek, A. Rapisarda and C. Tsallis (World Scientific, Singapore, 2005), page 350.
[369] Tirnakli U., Ananos G.F.J., and Tsallis C. 2001. Generalization of the Kolmogorov-Sinai entropy: Logistic -like and generalized cosine maps at the chaos threshold, Phys. Lett. A 289, 51.
[370] Tirnakli U., Tsallis C. and Lyra M.L. 1999. Circular-like maps: Sensitivity to the initial conditions, multifractality and nonextensivity, Eur. Phys. J. B 11, 309.
[371] Tobin, D. G., and Sykes, L. R., 1968. Seismicity and tectonics of the northeast Pacific Ocean: Journal of Geophysical Research, v. 73, p. 3821-3845.
[372] Tocher, D., 1960. The Alaska earthquake of July 10, 1958; Movement on the Fairweather fault and field investigation of southern epicentral region: Bulletin of the Seismological Society of America, v. 50, p 267 – 292
[373] Touati, S., Naylor, M. and Main, I.G., 2009. Origin and Nonuniversality of the Earthquake Interevent Time Distribution, Phys. Rev. Letters, 102, 168501; doi: 10.1103/PhysRevLett.102.168501
[374] Tsallis C., 1999. Possible generalization of Boltzmann-Gibbs statistics, J. Stat. Phys. 52, 479
[375] Tsallis C., Plastino A.R and Zheng W.-M. 1997. Chaos, Power-law sensitivity to initial conditions – New entropic representation, Chaos Sol. Fract. 8, 885

[376] Tsallis, C. and Tirnakli, U., 2010. Nonadditive entropy and nonextensive statistical mechanics – Some central concepts and recent applications, Journal of Physics: Conference Series 201 (2010) 012001; doi:10.1088/1742-6596/201/1/012001
[377] Tsallis, C., 1988. Possible generalization of Boltzmann-Gibbs statistics, J. Stat. Phys., 52, 479–487; doi: 10.1007/BF01016429.
[378] Tsallis, C., 2001. Nonextensive Statistical Mechanics and Thermodynamics: Historical Background and Present Status, in Abe, S. and Okamoto, Y (eds.), Nonextensive Statistical Mechanics and Its Applications, 3 – 98, Springer, Berlin, Heidelberg; doi: 10.1007/3-540-40919-X
[379] Tsallis, C., 2009. Introduction to Nonextensive Statistical Mechanics: Approaching a Complex World. Springer Verlag, Berlin, 378pp.
[380] Tsapanos T.M. and Papadopoulou A. 1999. A discrete Markov model for earthquake occurrences in Southern Alaska and Aleutian Islands, J. Balkan Geophys. Soc., 2 (3), 75–83.
[381] Tselentis, G.-A., Melis, N. S., Sokos, E., and Beltas, P. 1997. The winter 1991–1992 earthquake sequence at Cephalonia Island, western Greece. Pure and Applied Geophysics 150: 75–89.
[382] Tzanis A. and Makropoulos K., 2001. Did the 7/9/1999 M5.9 Athens Earthquake Come with a Warning? Natural Hazards 27: 85–103, 2002.
[383] Ünal S., Celebioglu S., and Özmen B., 2011. Seismic hazard assessment of Turkey by statistical approaches. TURKISH JOURNAL OF EARTH SCIENCES 23(11):350-360. DOI:10.3906/yer-1212-9
[384] Uhrhammer B. R. A., Loper S. J., and Romanowicz B., 1996. Determination of local magnitude using BDSN Broadband Records, Bull. Seism. Soc. Am., 86 (5), 1314-1330.
[385] Underhill, J. R., 1989. Late Cenozoic deformation of the Hellenides foreland, western Greece. Geol. Soc. America Bull. 101: 613–634.
[386] Utsu T., 1957. Magnitude of earthquakes and occurrence of their aftershocks, Zisin (J. Seismol. Soc. Jap.), 10, 35-45 (in Japanese).
[387] Utsu T., 1965. A method for determining the value of b in a formula log n = a – bM showing the magnitude-frequency relation for earthquakes, Geophys. Bull., Hokkaido Univ., Hokkaido, Japan, 13, 99-103 (in Japanese).
[388] Utsu T., 1982. Catalog of large earthquakes in the region of Japan from 1885 through 1980. Bull Earthq. Res. Inst. Univ. Tokyo 57, 401-463, 1982
[389] Utsu, T., 1992. On seismicity, in: Report of Cooperative Research of the Institute of Statistical Mathematics 34, Mathematical Seismology VII, Annals of the Institute of 'Statistical Mathematics, Tokyo, 139-157, 1992
[390] Utsu T.; Ogata Y.; Matsu'ura, R.S., 1995. The centenary of the Omori formula for a decay law of aftershock activity, J. Phys. Earth, 43, 1–33.
[391] Vallianatos F, Papadakis G, Michas G. 2016 Generalized statistical mechanics approaches to earthquakes and tectonics. Proc. R. Soc. A, 472: 20160497; doi: 10.1098/rspa.2016.0497.
[392] Vallianatos, F. and Sammonds, P., 2013. Evidence of non-extensive statistical physics of the lithospheric instability approaching the 2004 Sumatran- Andaman and 2011 Honshu mega-earthquakes, Tectonophysics, doi: 10.1016/j.tecto.2013.01.009.
[393] Vallianatos, F. and Telesca, L. (Eds.), 2012. Statistical Mechanics in Earth Physics and Natural Hazards, Acta Geophysica, 60, 499–501.
[394] Vallianatos, F., Benson, P., Meredith, P. and Sammonds, P., 2012a. Experimental evidence of a non-extensive statistical physics behaviour of fracture in triaxially

deformed Etna basalt using acoustic emissions, Europhy. Let. 97, 58002, doi: 10.1209/0295-5075/97/58002.

[395] Vallianatos, F., Michas, G., Papadakis, G. and Sammonds, P., 2012b. A non-extensive statistical physics view to the spatiotemporal properties of the June 1995, Aigion earthquake (M6.2) aftershock sequence (West Corinth Rift, Greece)", Acta Geophysica, 60 (3), 758-768.

[396] Vallianatos, F., Michas, G., Papadakis, G. and Tzanis, A., 2013a. Evidence of non-extensivity in the seismicity observed during the 2011–2012 unrest at the Santorini volcanic complex, Greece. Nat. Hazards Earth Syst. Sci., 13, 177–185; doi: 10.5194/nhess-13-177-2013.

[397] van Stiphout, T., Zhuang J, and Marsan D., 2012, Seismicity declustering, Community Online Resource for Statistical Seismicity Analysis, doi: 10.5078/corssa-52382934. Available at http://www.corssa.org.

[398] Vere-Jones, D. 1976. A branching model for crack propagation. PAGEOPH (1976) 114: 711. https://doi.org/10.1007/BF00875663

[399] Vere Jones D. (1977). Statistical theories of crack propagation. Math Geol (1977) 9: 455. https://doi.org/10.1007/BF02100959

[400] Votsi I., Limnios N., Tsaklidis G., and Papadimitriou E., 2012. Estimation of the expected number of earthquake occurrences based on semi-Markov models, Methodol. Comput. Appl. Probab. 14, pp. 685–703.

[401] Votsi I., Limnios N., Tsaklidis G., and Papadimitriou E., 2013. Hidden markov models revealing the stress field underlying the earthquake generation, Phys. A 392, pp. 2868–2885.

[402] Votsi I., Limnios N., Tsaklidis G., and Papadimitriou E., 2014. Hidden semi-Markov modeling for the estimation of earthquake occurrence rates, Commun. Statist. Theory Methods 43, pp. 1484–1502.

[403] Wallace W.K., 2008. Yakataga Fold-and-Thrust Belt: Structural Geometry and Tectonic Implications of a Small Continental Collision Zone. Active Tectonics and Seismic Potential of Alaska Geophysical Monograph Series 179 Copyright 2008 by the American Geophysical Union. 10.1029/179GM13

[404] Warren, N.W., and G.V. Latham. 1970. An Experimental Study of Thermally Induced Microfracturing and its Relation to Volcanic Seismicity. J. Geophys Res., 75, 4455-4464.

[405] Watanabe S., 1969. Knowing and Guessing: Quantitative Study of Inference and Information. Published by John Wiley & Sons Inc ISBN 10: 0471921300 ISBN 13: 9780471921301

[406] Weibull W. (1951). A statistical distribution function of Wide Applicability. ASME Journal of Applied Mechanics, Transactions of the American Society of Mechanical Engineers, September 1951, pages 293-297.

[407] Wernicke, B., Axen, G.J. and Snow J.K., 1988. Basin and Range extensional tectonics at the latitude of Las Vegas, Nevada, Geol. Soc. Am. Bull., 100 (11), 1738-1757; doi: 10.1130/0016-7606(1988)100<1738: BARETA>2.3.CO;2

[408] Wesnousky, S., 1994. The Gutenberg Richter or Characteristic Earthquake Distribution, which is it? Bulletin of the Seismological Society of America, 84 (1994), pp. 1940-1959

[409] Wesnousky, S., 2005. Active faulting in the Walker Lane, Tectonics, 24 (3), TC3009; doi: 10.1029/2004TC001645.

[410] Wesson R.L and Boyd O.S., 2007. Stress before and after the 2002 Denali fault earthquake. GEOPHYSICAL RESEARCH LETTERS, VOL. 34, L07303, doi:10.1029/2007GL029189

[411] Wickens, A. J. and Hodgson, J. H., 1967. Computer re-evaluation of earthquake mechanisms solutions 1922 – 1962: Ottawa, Canada, Publications of the Dominion Observatory, v. 33, no. 1, 560 p

[412] Widom B., 1965. Equation of State in the Neighborhood of the Critical Point. The Journal of Chemical Physics 43, 3898 (2004); https://doi.org/10.1063/1.1696618

[413] Wiemer, S. and J.P. Benoit 1996. Mapping the b-value anomaly at 100 km depth in the Alaska and New Zealand subduction zones, Geophys. Res. Lett., 23, 1557-1560.

[414] Wiemer, S. and K. Katsumata 1999. Spatial variability of seismicity parameters in aftershock zones, J. Geophys. Res., 104, 13135-13151

[415] Wiemer, S. and S.R. McNutt 1997. Variations in frequency-magnitude distribution with depth in two volcanic areas: Mount St. Helens, Washington, and Mt. Spurr, Alaska, Geophys. Res. Lett., 24, 189-192

[416] Wiemer, S. and M. Wyss 1997.Mapping the frequencymagnitude distribution in asperities: an improved technique to calculate recurrence times, J. Geophys. Res., 102, 15115-15128

[417] Wiemer S, McNutt S.R., and Wss M., 1998. Temporal and three-dimensional spatial analysis of the frequency-magnitude distribution neal Long Valley caldera, California. Geophys. J. Int.134, 409-421.

[418] Wissel F.and Drossel B., 2006. Transient and stationary behavior of the Olami-Feder-Christensen model. Phys. Rev. E 74, 066109 – Published 15 December 2006

[419] Wyss M. and Lee W.H.K., 1973. Time variations of the average earthquake magnitude in central California. In proceedings of the Conference on Tectonic Problems of the San Andreas Fault system. Pp 24-42. Stanford University Geol.Sci.

[420] Wyss, M., 1973. Towards a physical understanding of the earthquake frequency distribution, Geophys. J. R. Astron. Soc., 31, 341-359

[421] Wyss M. and Wiemer S, 2000. Change in the probabilities for earthquakes in Southern California due to the Landers M7.3 earthquake. Science 290, 1334-1338.

[422] Wyss M., Shimazaki K. and Wiemer S. 1997. Mapping active magma chambers by b values beneath the off-Ito volcano, Japan. JOURNAL OF GEOPHYSICAL RESEARCH, VOL. 102, NO. B9, PAGES 20,413-20, 42. https://doi.org/10.1029/97JB01074

[423] Wyss M., Schorlemmer D and Wiemer S. 2000. Mapping asperities by minima of local recurrence time: The San-Jacinto – Elsinore fault zones. J.Geophys.Res.102, 20, 413-20,422.

[424] Wyss M., Klein F., Nagamine K., Wiemer S. 2001. Anomalously high b-values in the South Flank of Kilauea volcano, Hawaii: evidence for the distribution of magma below Kilauea's East rift zone. Journal of Volcanology and Geothermal Research 106 (2001) 23±37. doi.org/10.1016/S0377-0273(00)00263-8

[425] Yang, X. S., 2001. Chaos in small-world networks, Phys. Rev. E, 63, 046206; DOI: 10.1103/PhysRevE.63.046206.

[426] Yeats R., 2013. Active Faults of the World, Cambridge University Press.

[427] Zechar J.D. and Jordan T.H., 2010. Simple smoothed seismicity earthquake forecasts for Italy. ANNALS OF GEOPHYSICS, 53, 3, 2010; doi: 10.4401/ag-4845

[428] Zechar J.D., Jordan T.H., 2010The Area Skill Score Statistic for Evaluating Earthquake Predictability Experiments. In: Savage M.K., Rhoades D.A., Smith E.G.C., Gerstenberger M.C., Vere-Jones D. (eds) Seismogenesis and Earthquake Forecasting: The Frank Evison Volume II. Pageoph Topical Volumes. Springer, Basel

[429] Zhuang J., Ogata Y. and Vere-Jones D., 2002. Stochastic declustering of space-time earthquake occurrences, J. Amer. Stat. Assoc., 97, 369-380.

[430] Zhuang, J., D. Harte, M.J. Werner, S. Hainzl, and S. Zhou, 2012. Basic models of seismicity: temporal models, Community Online Resource for Statistical Seismicity Analysis, doi: 10.5078/corssa-79905851. Available at http://www.corssa.org.

[431] Zobin V.M., 1979. Variations of volcanic earthquake source parameters before volcanic eruptions. Journal of Volcanology and Geothermal Research, 6(1979) 279--293

[432] Zöller G. and Hainzl S., 2001. Detecting premonitory seismicity patterns based on critical point dynamics. Natural Hazards and Earth System Science, Copernicus Publications on behalf of the European Geosciences Union, 2001, 1 (1/2), pp. 93-98

[433] Zöller G., Hainzl S., Holschneider M., and Ben-Zion Y., 2005. Aftershocks resulting from creeping sections in a heterogeneous fault, Geophysical Research Letters, vol. 32, l03308, doi:10.1029/2004gl021871.

[434] Zuniga F.R. and Wyss M., 1995. Inadvertent changes in magnitude reported in earthquake catalogs: Their evaluation through b-value estimates. Bulletin of the Seismological Society of America (1995) 85 (6): 1858-1866